Hf, Sr, Nd and Pb isotope systematics and major and trace element compositions of the Archean subcratonic lithosphere beneath Somerset Island, Arctic Canada

by

STEFANIE SCHMIDBERGER

Department of Earth and Planetary Sciences
McGill University, Montréal
June 2001

A thesis submitted to
the Faculty of Graduate Studies and Research
in partial fulfilment of the requirements of the degree of

Doctor of Philosophy

© copyright
2001, Stefanie Schmidberger

Hf, Sr, Nd and Pb isotope systematics and major and trace element compositions of the Archean subcratonic lithosphere beneath Somerset Island, Arctic Canada

by

STEFANIE SCHMIDBERGER

Department of Earth and Planetary Sciences

McGill University, Montréal

June 2001

A thesis submitted to

the Faculty of Graduate Studies and Research

in partial fulfilment of the requirements of the degree of

Doctor of Philosophy

© copyright

2001, Stefanie Schmidberger

National Library
of Canada

Bibliothèque nationale
du Canada

Acquisitions and
Bibliographic Services

Acquisitions et
services bibliographiques

395 Wellington Street
Ottawa ON K1A 0N4
Canada

395, rue Wellington
Ottawa ON K1A 0N4
Canada

Your file Votre référence

Our file Notre référence

The author has granted a non-exclusive licence allowing the National Library of Canada to reproduce, loan, distribute or sell copies of this thesis in microform, paper or electronic formats.

L'auteur a accordé une licence non exclusive permettant à la Bibliothèque nationale du Canada de reproduire, prêter, distribuer ou vendre des copies de cette thèse sous la forme de microfiche/film, de reproduction sur papier ou sur format électronique.

The author retains ownership of the copyright in this thesis. Neither the thesis nor substantial extracts from it may be printed or otherwise reproduced without the author's permission.

L'auteur conserve la propriété du droit d'auteur qui protège cette thèse. Ni la thèse ni des extraits substantiels de celle-ci ne doivent être imprimés ou autrement reproduits sans son autorisation.

0-612-78765-6

Canada

Abstract

Hf, Sr, Nd and Pb isotopes, and major, trace and rare earth elements (REE) were determined for a suite of peridotite and pyroxenite xenoliths, constituent garnet and clinopyroxene and the host Nikos kimberlite (100 Ma) from Somerset Island, in order to constrain the chemical and isotopic composition of the lithosphere beneath the northern Canadian craton. The refractory Nikos peridotites are characterized by high olivine forsterite contents (avg. Fo=92.3) and depletions in incompatible major elements (Fe, Al, Ca), but are enriched in incompatible trace elements, such as large ion lithophile elements (LILE) and light rare earth elements (LREE), while having approximately chondritic heavy rare earth element (HREE) contents. Mass balance calculations using REE contents of clinopyroxene and garnet indicate that calculated LREE abundances for the Nikos xenoliths are significantly lower (e.g. Nd ~50%) than those of the analyzed whole-rocks. These results suggest the presence of small amounts of a kimberlite-related LREE-rich interstitial component (i.e. ~1% kimberlite liquid and/or ~0.01% apatite) to account for the excess LREE abundances, with little effect on the HREE budgets of the xenoliths.

The $^{143}Nd/^{144}Nd_{(0.1Ga)}$ (0.51249-0.51276) isotopic compositions of the Nikos peridotites are little variable and overlap those of the Nikos kimberlite at the time of sample transport. The low-temperature peridotites (<1100°C) that sample the shallow lithosphere are characterized by more radiogenic $^{176}Hf/^{177}Hf_{(0.1Ga)}$ (0.28296-0.28419) and Pb ($^{206}Pb/^{204}Pb_{(0.1Ga)}$=17.82-19.03), but lower $^{87}Sr/^{86}Sr_{(0.1Ga)}$ (0.7047-0.7066) isotopic ratios than those of the high-temperature peridotites (>1100°C; 0.28265-0.28333; 17.18-18.30; 0.7064-0.7085, respectively). Incompatible trace element compositions of the xenoliths confirm this depth stratification indicating that shallow and deep (>160 km) Somerset lithosphere are characterized by distinct chemical and isotopic characteristics.

The Lu-Hf isotope compositions of the low-temperature peridotites plot along a 2.8 Ga reference isochron, which is consistent with an interpretation that the shallow Somerset lithosphere stabilized in the Archean to depth of ~150 km. The deep lithospheric mantle, which is probably younger, does not share the same petrogenetic history and may contain recycled material (altered oceanic crust and sedimentary component?). The Hf isotope compositions for the shallow low-temperature peridotites

indicate that part of the lithosphere beneath the Canadian craton is characterized by more radiogenic Hf isotope signatures than estimates for “depleted” mantle.

Résumé

Les compositions isotopiques en Hf, Sr, Nd et Pb et les teneurs en éléments majeurs et traces (incluant les éléments des terres rares, REE) ont été analysées pour des xénolites de péridotite et de pyroxénite, des grenats et des clinopyroxènes provenant de la kimberlite Nikos sur l'Île Somerset (Arctique canadien). Le but était de mieux cerner la composition chimique et isotopique du manteau lithosphérique sous-continental dans la partie nord du craton canadien. Les péridotites sont de nature réfractaire et caractérisées par des olivines ayant de forts contenus en forstérite (moyenne=92.3) et un appauvrissement en éléments majeurs incompatibles (Fe, Al, Ca); cependant elles sont enrichies en éléments traces incompatibles (LILE) et en terres rares légères (LREE), tout en ayant des teneurs en terres rares lourdes (HREE) approximativement chondritiques. Des calculs de bilan de masse utilisant les abondances des REE dans le clinopyroxène et le grenat livrent des teneurs en LREE pour les xénolites (roches totales) qui sont significativement plus faibles (e.g. Nd ~50%) que les concentrations mesurées. Ces résultats suggèrent la présence d'une composante intersticielle riche en LREE reliée à la kimberlite (~1% de liquide kimberlitique et/ou ~0.01% d'apatite) pour expliquer l'excès en LREE, ce qui n'influencera pas les budgets des HREE.

Les rapports isotopiques de $^{143}Nd/^{144}Nd_{(0.1Ga)}$ (0.51249-0.51276) des péridotites sont peu variables et identiques à ceux de la kimberlite au moment de la mise en place. Les péridotites de basse température (<1100°C), qui échantillonnent la partie supérieure de la lithosphère sous-continentale, sont caractérisées par des rapports $^{176}Hf/^{177}Hf_{(0.1Ga)}$ (0.28296-0.28419) et Pb ($^{206}Pb/^{204}Pb_{(0.1Ga)}$=17.82-19.03) plus radiogéniques, mais des rapports $^{87}Sr/^{86}Sr_{(0.1Ga)}$ (0.7047-0.7066) plus faibles, quand on les compare à ceux des péridotites de haute température (>1100°C; 0.28265-0.28333; 17.18-18.30; 0.7064-0.7085). La stratification en profondeur du manteau lithosphérique sous-continental de l'Île Somerset est également confirmée par les teneurs très distinctes des éléments traces incompatibles dans les xénolites de basse température versus ceux de haute température.

Les rapports isotopiques de Lu-Hf des péridotites de basse température tracent une isochrone de référence de 2.8 milliards d'années, suggérant que le manteau lithosphérique supérieur sous l'Île Somerset s'est stabilisé durant l'Archéen. La partie plus profonde de

ce manteau, qui est probablement plus jeune, n'est pas cogénétique du précédent et pourrait contenir du matériel recyclé (croûte océanique altérée et composante sédimentaire subductée?). Les rapports isotopiques de Hf des péridotites de basse température indiquent qu' une partie de la lithosphère sous-continentale du craton canadien est plus radiogénique que la compositions isotopique de Hf du manteau appauvri.

ACKNOWLEDGEMENTS

I am grateful for financial support in the form of a NSERC doctoral scholarship and NSERC research funds for isotope, major and trace element analyses made available from Dr. Don Francis' operating grant.

I am extremely appreciative of my supervisor's, Dr. Don Francis, constant advice and support, discussions on mantle xenoliths and kimberlites and editorial skills.

I thank Dr. Tariq Ahmedali and Glenna Keating for performing the whole rock X-ray fluorescence analyses and George Panagiotidis for producing thin sections for microprobe analysis. I would like to thank Glenn Poirier for assistance in obtaining the electron microprobe results. Fabien Rasselet is thanked for assistance in the field, handpicking separates of magmatic kimberlite for major and trace element and isotope analysis, and performing the CO_2 analyses with the assistance of Constance Guignard. I am grateful to Dr. Nobu Shimizu from Woods Hole Oceanographic Institution and Dr. Tony Simonetti for their help with ion microprobe analyses. I would also like to thank Dr. Janne Blichert-Toft for introducing me to the secrets of Lu-Hf chemistry.

I am especially appreciative for countless discussions and the help and support provided by my husband Tony. Most of all, I am grateful of Tony and Patrick for their encouragement, friendship and love.

Table of Contents

Extended Abstract ii
Résumé iv
Acknowledgements vi
Table of Contents vii
List of Tables ix
List of Figures x
List of Appendices xii
Preface xiii
Contributions of Authors xv

CHAPTER 1 1

- Introduction 2
- References 5

CHAPTER 2: Nature of the Mantle Roots Beneath the North American Craton: Mantle Xenolith Evidence From Somerset Island Kimberlites 8

- Abstract 9
- 1. Introduction 11
- 2. Geology 12
- 3. Kimberlite Host 13
- 4. Mantle Xenoliths 14
- 5. Analytical Data 15
- 6. Discussion 20
- 7. Conclusions 26
- Acknowledgements 26
- References 28
- Figure Captions 32
- Tables 34
- Figures 41

CHAPTER 3: Constraints on the Trace Element Composition of the Archean Mantle Root Beneath Somerset Island, Arctic Canada 53

- Abstract 54
- Introduction 55
- Samples and Procedures 56
- Analytical Data 59
- Discussion 63
- Conclusions 73
- Acknowledgements 75
- References 76
- Figure Captions 82
- Tables 85

Figures 94

CHAPTER 4: Sr-Nd-Pb Isotope Systematics of Mantle Xenoliths From Somerset Island Kimberlites: Evidence for Lithosphere Stratification Beneath Arctic Canada 107

Abstract 108
1. Introduction 110
2. Samples 111
3. Analytical Methods 115
4. Results 116
5. Discussion 121
6. Conclusions 129
Acknowledgements 130
References 132
Figure Captions 136
Tables 138
Figures 141

CHAPTER 5: Probing Archean Lithosphere Using the Lu-Hf Isotope Systematics of Peridotite Xenoliths Form Somerset Island Kimberlites, Canada 149

Abstract 150
1. Introduction 152
2. Samples 154
3. Analytical Methods 156
4. Results 160
5. Discussion 163
6. Conclusions 170
Acknowledgements 171
References 172
Figure Captions 177
Tables 179
Figures 181

CHAPTER 6: GENERAL CONCLUSIONS 189

APPENDIX A 192

APPENDIX B 199

List of Tables

Table

2-1 Major and trace element analyses of kimberlites 34

2-2 Representative analyses of bulk xenoliths 35

2-3 Representative analyses of olivines 36

2-4 Representative analyses of orthopyroxenes 37

2-5 Representative analyses of clinopyroxenes 38

2-6 Representative analyses of garnets 36

2-7 Temperature and pressure estimates 40

3-1 Major, trace and rare earth element analyses for kimberlites 85

3-2 Major element analyses and calculated mineral modes for bulk xenoliths 86

3-3 Trace and rare earth element analyses for bulk xenoliths 88

3-4 Major, trace and rare earth element analyses of clinopyroxenes 90

3-5 Major, trace and rare earth element analyses of garnets 91

3-6 Calculated rare earth element contents for bulk xenoliths 92

3-7 Rare earth element contents for calculated interstitial liquid 93

4-1 Rb, Sr, Sm and Nd abundances and Sr and Nd isotope compositions for Nikos kimberlites and xenoliths 138

4-2 Pb, U and Th abundances and Pb isotopic compositions for Nikos kimberlites and xenoliths 140

5-1 Lu-Hf isotope data for Nikos peridotites and kimberlite 179

5-2 Lu-Hf isotope data for Nikos garnets 180

List of Figures

Figure	Description	
2-1	Geological map of Somerset Island	41
2-2	Photomicrographs of xenoliths from the Nikos kimberlite showing a) coarse texture in peridotite, b) porphyroclastic texture in peridotite and c) coarse texture in pyroxenite	42
2-3	Histogram of whole rock magnesium numbers of peridotites, and high-Mg and low-Mg pyroxenites	45
2-4	Variations of major elements a) Al_2O_3, b) CaO, c) NiO with MgO (wt.%) of Nikos peridotites	46
2-5	Histogram of Al_2O_3 content (wt.%) of Nikos peridotites	47
2-6	Modal mineral proportions of Nikos xenoliths	48
2-7	Pressures and temperatures of last equilibration of the Nikos xenoliths ...	49
2-8	Modal olivine content (wt.%) versus $Mg^{\#}$ in olivine of the Nikos peridotites	50
2-9	Variation of FeO and SiO_2 (wt.%) of the Nikos peridotites	51
2-10	NiO (wt.%) in olivine versus modal orthopyroxene content (wt.%) of the Nikos peridotites	52
3-1	Geological map of Somerset Island	94
3-2	(a) Primitive mantle-normalized trace element and (b) chondrite-normalized rare earth element patterns for Nikos kimberlites	95
3-3	(a) Primitive mantle-normalized trace element and (b) chondrite-normalized rare earth element patterns for Nikos peridotites	96
3-4	(a) Primitive mantle-normalized trace element and (b) chondrite-normalized rare earth element patterns for Nikos pyroxenites	97
3-5	Chondrite-normalized rare earth element patterns for coexisting clinopyroxene and garnet in (a) high temperature and (b) low temperature Nikos peridotites	98
3-6	Chondrite-normalized rare earth element patterns for Nikos (a) clinopyroxene and (b) garnet compared to high and low temperature peridotites from the Kaapvaal and Siberian cratons	99
3-7	Rare earth element mass balance results for (a) high temperature peridotite NK1-7 and (b) low temperature peridotite NK1-4	100
3-8	Calculated chondrite-normalized rare earth element patterns for (a) high temperature peridotite NK1-7 and (b) low temperature peridotite NK1-4	101

3-9 Calculated chondrite-normalized rare earth element patterns for possible interstitial liquids in equilibrium with constituent mineral phases of the Nikos peridotites 102

3-10 Calculated chondrite-normalized rare earth element patterns for (a) high temperature peridotite NK1-7 and (b) low temperature peridotite NK1-4 before and after the addition of interstitial kimberlite liquid 103

3-11 Clinopyroxene-garnet partition coefficients in Nikos peridotites 104

3-12 Temperature dependence of clinopyroxene-garnet Ce partitioning in the Nikos peridotites 105

3-13 Depth distribution of (a) La and (b) Sr abundances in clinopyroxenes and (c) Zr and (d) Sr abundances (ppm) in garnets of low and high temperature peridotites 106

4-1 Geological map of Somerset Island 141

4-2 Initial Nd and Sr isotopic compositions for Nikos kimberlites 142

4-3 Initial Pb isotopic compositions for Nikos kimberlites 143

4-4 Nd and Sr isotopic compositions for Nikos xenoliths 100 Ma ago 144

4-5 Pb isotopic compositions for Nikos xenoliths 100 Ma ago 145

4-6 Nd and Sr isotopic compositions for Nikos clinopyroxenes and garnets 100 Ma ago 146

4-7 Sr and Pb isotopic compositions versus 1/Sr and 1/Pb for low and high-temperature Nikos peridotites 100 Ma ago 147

4-8 Sr isotopic compositions for Nikos clinopyroxenes plotted versus depth of last equilibration 148

5-1 Geological map of Somerset Island 181

5-2 ^{176}Lu/^{177}Hf versus (a) initial $\varepsilon_{Hf(T)}$ for Nikos kimberlites and (b) $\varepsilon_{Hf(0.1Ga)}$ for Nikos peridotites at the time of kimberlite emplacement 182

5-3 ^{176}Lu/^{177}Hf versus ^{176}Hf/^{177}Hf diagram for Nikos peridotites 183

5-4 ^{176}Lu/^{177}Hf versus ^{176}Hf/^{177}Hf diagram for Nikos garnets 184 ....

5-5 Hf-Nd variation diagram for Nikos peridotites 100 Ma ago................. 185

5-6 Lu (ppm) versus Al_2O_3 contents (wt%) for Nikos peridotites 186

5-7 $\varepsilon_{Hf(0.1Ga)}$ versus ^{87}Sr/^{86}Sr$_{(0.1Ga)}$ for Nikos peridotites 187

5-8 Lu-Hf and Sm-Nd internal isochron “dates” versus temperature of last equilibration for low-temperature garnet-whole rock pairs 188

List of Appendices

A ^{180}Hf isotope tracer calibration 192

B Whole-rock and mineral compositions of Nikos peridotites 199

Preface

This thesis consists of four papers, three of which are already published or in press and the last of which has been submitted to Earth and Planetary Science Letters. Each chapter is self-contained with an abstract, introduction, analytical techniques, presentation of results, discussion and conclusions. References, tables and figures are placed at the end of each chapter and are in the format of the journal.

The extended abstract provides an integrated summary of the major and trace element and Hf, Sr, Nd and Pb isotope results for the Nikos peridotites and pyroxenites, constituent minerals and the host kimberlite. Chapter 1 presents an introduction, which states the rationale and objectives of the research and contains a comprehensive review of the literature. The major element chemistry of the xenoliths, mineral phases and kimberlites, modal mineralogy, and geothermobarometric calculations (i.e. temperature and pressure estimates) are presented in Chapter 2. The trace and rare earth element (REE) compositions of the Nikos xenoliths and constituent clinopyroxene and garnet are documented in Chapter 3, with a discussion of their implications for the incompatible element budgets of the Somerset lithosphere. The Sr, Nd and Pb isotope data for the Nikos xenoliths, minerals and host kimberlite are reported in Chapter 4 and shown to indicate an isotopic stratification with depth in the underlying Somerset lithosphere. The Lu-Hf isotope systematics of the peridotites and constituent garnets are discussed in Chapter 5 along with their constraints on the age of stabilization of the Somerset lithosphere, and the petrogenetic history of shallow and deep subcontinental mantle. To date, these results are the first Lu-Hf isotope data ever reported for a kimberlite-hosted mantle xenolith suite. Chapter 6 ends the thesis with a more general discussion of the implications of the results.

The following is an excerpt from the “Guidelines Concerning Thesis Preparation” as required by the Faculty of Graduate Studies and Research at McGill University:

»Candidates have the option of including, as part of the thesis, the text of one or more papers submitted, or to be submitted, for publication, or the clearly-duplicated text of one or more published papers. These must be bound together as an integral part of the thesis and connecting texts that provide logical bridges between the different papers are mandatory.

The thesis must conform to all other requirements of the “Guidelines Concerning Thesis Preparation” and should be in a literary form that is more than a mere collection of manuscripts published or to be published. The thesis must include: A table of contents, a general abstract in English and French, an introduction which clearly states the rational and objectives of the research, a comprehensive review of the literature, and a general conclusion and summary.

Additional material must be provided when appropriate (e.g., in appendices) and in sufficient detail to allow a clear and precise judgement to be made of the importance and originality of the research reported in the thesis.

In the case of manuscripts co-authored by the candidate and others, the candidate is required to make an explicit statement in the thesis as to who contributed to such work and to what extent. The supervisor must attest to the accuracy of this statement at the doctoral oral defense. Since the task of the examiners is made more difficult in these cases, it is in the candidate's interest to clearly specify the responsibilities of all the authors of the co-authored papers.«

Contributions of Authors

During 1997 to 2001, I obtained the Hf, Sr, Nd and Pb whole rock and Hf, Sr and Nd mineral isotope data, which included sample preparation and analysis by thermal ionization (TIMS) and multicollector inductively coupled plasma mass spectrometry (MC-ICP-MS) using the Micromass IsoProbe at GEOTOP-UQAM-McGill. For Lu-Hf isotope analysis, the chemical procedure for the separation of Lu and Hf was set up by myself in collaboration with Tony Simonetti. This involved the calibration of a ^{180}Hf tracer in order to obtain high-precision Hf concentration determinations (see Appendix A). For my thesis work, I acquired the ability to conduct electron microprobe analysis and obtained the major element compositions of constituent peridotite minerals (i.e. olivine, orthopyroxene, clinopyroxene, garnet) for all xenolith samples (n=55) at McGill University. I have also carried out ion microprobe analyses with the assistance of Dr. Nobu Shimizu at Woods Hole Oceanographic Institution, an analytical technique capable of measuring the trace element and REE abundances in clinopyroxene and garnet. The major element X-ray fluorescence analyses were obtained by Dr. Tariq Ahmedali and Glenna Keating at McGill University and the trace element ICP-MS analyses at the CRPG (Nancy), France and Université de Montréal. The thesis author, Stefanie Schmidberger, is responsible for the preparation and writing of the four scientific manuscripts and acknowledges the critical reviews of the co-authors Don Francis, Tony Simonetti and Clément Gariépy. Interpretations of the analytical data are the result of numerous discussions with, and input from the various co-authors.

The current status of the papers contained in this thesis is as follows:

Chapter 2: PUBLISHED. Schmidberger S. S. and Francis D. (1999) Nature of the mantle roots beneath the North American craton: Mantle xenolith evidence from Somerset Island kimberlites. *Lithos* **48**, 195-216.

Chapter 3: PUBLISHED. Schmidberger S. S. and Francis D. (2001) Constraints on the trace element composition of the Archean mantle root beneath Somerset Island, Arctic Canada. *J. Petrol.* **42**, 1095-1117.

Chapter 4: PUBLISHED. Schmidberger S. S., Simonetti A. and Francis D. (2001) Sr-Nd-Pb isotope systematics of mantle xenoliths from Somerset Island kimberlites: Evidence for lithosphere stratification beneath Arctic Canada. *Geochim. Cosmochim. Acta.* **65**, 4243-4255.

Chapter 5: Schmidberger S. S., Simonetti A., Francis D. and Gariépy C. Probing Archean lithosphere using the Lu-Hf isotope systematics of peridotite xenoliths from Somerset Island kimberlites, Canada. SUBMITTED TO: *Earth Planet. Sci. Lett.*

CHAPTER 1

Introduction

Archean cratons are underlain by cold, refractory mantle roots (e.g.; Nixon et al., 1981; Boyd and Mertzman, 1987) that extend to depths greater than 200 km (Jordan, 1988; Grand, 1994). The low density of the subcratonic mantle, which is thought to be the residue of extensive partial melting (e.g.; Boyd, 1989; Herzberg, 1993, Walter, 1998), can explain its long-term stability and isolation from the convecting asthenosphere (Jordan, 1978; Pollack, 1986; Shapiro et al., 1999). Peridotite xenoliths that are sampled by kimberlites and alkali basalts are a unique window into the subcratonic mantle and provide invaluable insights into its chemical composition (e.g.; Menzies, 1990). Many of these peridotites are strongly depleted in incompatible major elements such as Fe, Al and Ca and have higher mg-numbers (mg-number=Mg/[Mg+Fe] >0.92) than peridotites that sample oceanic or post-Archean lithospheric mantle (e.g.; Nixon, 1987; Boyd, 1989; Herzberg, 1993) and fertile mantle compositions such as pyrolite or primitive mantle (mg-numbers=0.88-0.92; Ringwood, 1975; McDonough, 1990). Experimental results at high pressure show that extensive melting of peridotite produces picritic to komatiitic melts and a residue characterized by highly refractory major element compositions (e.g.; Takahashi and Scarfe, 1985; Baker and Stolper, 1994). Investigations of mantle xenolith suites from the South African Kaapvaal and the Siberian cratons, which dominate the available dataset, have indicated that the subcratonic lithosphere could be characterized by low olivine/orthopyroxene (avg. orthopyroxene >20 wt.%) and low Mg/Si (1.1-1.5) ratios compared to that beneath oceanic terranes (e.g.; Boyd et al., 1997; Griffin et al., 1999). The most extreme orthopyroxene-rich mineralogies, however, cannot be explained by single-stage melt extraction from fertile mantle and require that either post-formational processes modified the composition of the lithosphere (e.g.; Kelemen et al. 1992; Boyd et al., 1997), or that parts of the mantle are significantly more silica-rich compared to primitive mantle models (Herzberg, 1993). Samples of the lithospheric mantle under other Archean cratons (e.g.; Canadian craton) are still rare, and the chemical composition and evolution of the deep cratonic mantle roots have yet to be clearly established.

Determining the age of the subcontinental lithosphere is important in order to constrain its stabilization history and evolution, and its role in the formation of the Archean cratons. The isotopic diversity found in continental basalts, and to a lesser extent in cratonic peridotite xenoliths (Zindler and Hart, 1986 and references therein), first suggested the antiquity and long-term stability of the deep subcontinental mantle roots (Brooks et al., 1976; Pearson, 1999). These peridotite xenoliths are frequently enriched in incompatible trace elements such as large ion lithophile elements (LILE) and light rare earth elements (LREE) relative to compositions for primitive mantle and chondrites (McDonough and Sun, 1995) suggesting that the subcontinental lithosphere has been infiltrated by small volume metasomatic melts or fluids over time (Erlank et al., 1987; Menzies et al., 1987; McDonough, 1990; Shimizu, 1999). Dating these peridotites using the conventional isotope techniques such as Rb-Sr or Sm-Nd is thus difficult, since they are highly susceptible to metasomatic alteration of the whole-rock trace element abundances and isotopic compositions (Pearson, 1999). Re-Os systematics appear to be less affected by metasomatism and have provided valuable age constraints for the subcratonic mantle (Pearson, 1999). Re depletion ages range from 3.5 to 2.7 Ga for the lithosphere beneath South Africa, Siberia and North America (Carlson and Irving, 1994;

Pearson et al., 1995a,b; Irvine et al., 1999), and indicate that these cratonic mantle roots stabilized in the Archean.

The Lu-Hf isotopic system is characterized by both refractory and relatively immobile elements that are hosted by silicate minerals (Bedini and Bodinier, 1999). The distinct chemical properties (i.e. different mineral-melt partition coefficient, e.g.; Hart and Dunn, 1993; Fujimaki et al., 1984) of the parent (Lu) and daughter (Hf) elements in the presence of mineral phases such as garnet and zircon result in their fractionation during igneous processes, indicating an important potential for the Lu-Hf system in geochronology and tracing geological processes (e.g.; Duchêne et al., 1997; Blichert-Toft and Albarède, 1997; Blichert-Toft et al., 1997; Vervoort and Blichert-Toft, 1999; Scherer et al., 2000).

This thesis focuses on the investigation of the Hf, Sr, Nd and Pb isotope systematics and major, trace and rare earth element (REE) compositions of a suite of peridotite and pyroxenite xenoliths from the Cretaceous (100 Ma) Nikos kimberlite on Somerset Island in the Canadian Arctic (NWT; Heaman, 1989; Smith et al., 1989; Pell, 1993). The modal mineralogy and major element compositions of the xenoliths provide constraints on the chemical nature of the lithosphere beneath the Canadian craton and enable a comparison with data for South African, Siberian and other Canadian xenolith suites. Incompatible trace element abundances of peridotite minerals (i.e. clinopyroxene and garnet) and whole-rock compositions are used to model the trace element budgets of the Somerset lithosphere. The Hf, Sr, Nd and Pb isotopic compositions of the Nikos xenoliths and kimberlite provide insight into the isotopic stratification of the subcratonic lithosphere with depth and enable to evaluate petrogenetic models for the shallow and deep subcratonic mantle. The Lu-Hf isotope systematics of the Nikos peridotites provide information on the age of stabilization of the Somerset lithosphere.

References

Baker M. B. and Stolper E. M. (1994) Determining the composition of high-pressure mantle melts using diamond aggregates. *Geochim. Cosmochim. Acta* **58**, 2811-2827.

Bedini R. M. and Bodinier J.-L. (1999) Distribution of incompatible trace elements between the constituents of spinel peridotite xenoliths: ICP-MS data from the East African Rift. *Geochim. Cosmochim. Acta* **63**, 3883-3900.

Blichert-Toft J. and Albarède F. (1997) The Lu-Hf isotope geochemistry of chondrites and the evolution of the mantle-crust system. *Earth Planet. Sci. Lett.* **148**, 243-258.

Blichert-Toft J., Chauvel C. and Albarède F. (1997) Separation of Hf and Lu for high-precision isotope analysis of rock samples by magnetic sector-multiple collector ICP-MS. *Contrib. Mineral. Petrol.* **127**, 248-260.

Brooks C., James D. E. and Hart S. R. (1976) Ancient lithosphere: its role in young continental volcanism. *Science* **139**, 1086-1094.

Boyd F. R. (1989) Compositional distinction between oceanic and cratonic lithosphere. *Earth Planet. Sci. Lett.* **96**, 15-26.

Boyd F. R. and Mertzman S. A. (1987) Composition and structure of the Kaapvaal lithosphere, southern Africa. In *Magmatic processes: physiochemical principles* (ed. B. O. Mysen). Geochem. Soc. Spec. Publ. pp. 13-24.

Boyd F. R., Pokhilenko N. P., Pearson D. G., Mertzman S. A., Sobolev N. V. and Finger L. W. (1997) Composition of the Siberian cratonic mantle: evidence from Udachnaya peridotite xenoliths. *Contrib. Mineral. Petrol.* **128**, 228-246.

Carlson R. W. and Irving A. J. (1994) Depletion and enrichment history of subcontinental lithospheric mantle: Os, Sr, Nd and Pb evidence for xenoliths from the Wyoming Craton. *Earth Planet. Sci. Lett.* **126**, 457-472.

J. Dalmasso, G. Barci-Funel, G.J. Ardisson, Reinvestigation of the decay of the long-lived odd-odd ^{176}Lu nucleus, Appl. Radiat. Isot. 43 (1992) 69-76

Duchêne S., Blichert-Toft J., Luais B., Télouk P., Lardeaux J.-M. and Albarède F. (1997) The Lu-Hf dating of garnets and the ages of the Alpine high-pressure metamorphism. *Nature* **387**, 586-589.

Erlank A. J., Waters F. G., Hawkesworth C. J., Haggerty S. E., Allsopp H. L., Rickard R. S. and Menzies M. A. (1987) Evidence for mantle metasomatism in peridotite nodules from the Kimberley pipes, South Africa. In *Mantle metasomatism* (eds. M. A. Menzies and C. J. Hawkesworth). Academic Press, London. pp. 221-311.

Fujimaki H., Tatsumoto M. and Aoki K. I. (1984) Partition coefficients of Hf, Zr, and REE between phenocrysts and groundmasses. *J. Geophys. Res.* **89**, B662-B672.

Grand S. P. (1994) Mantle shear structure beneath the Americas and surrounding oceans. *J. Geophys. Res.* **99**, 11.591-11.621.

Griffin W. L., O'Reilly S. Y. and Ryan C. G. (1999) The composition and origin of sub-continental lithospheric mantle. In *Mantle petrology: field observations and high pressure experimentation* (eds. Y. Fei, C. M. Bertka and B. O. Mysen). Geochem. Soc. Spec. Publ. 6. pp. 13-45.

Hart S. R. and Dunn T. (1993) Experimental clinopyroxene-melt partitioning of 24 trace elements. *Contrib. Mineral. Petrol.* **113**, 1-8.

Heaman L. H. (1989) The nature of the subcontinental mantle from Sr-Nd-Pb isotopic studies on kimberlite perovskite. *Earth Planet. Sci. Lett.* **92**, 323-334.

Herzberg C. T. (1993) Lithosphere peridotites of the Kaapvaal craton. *Earth Planet. Sci. Lett.* **120**, 13-29.

Irvine G. J., Kopylova M. G., Carlson R. W., Pearson D. G., Shirey S. B. and Kjarsgaard B. A. (1999) Age of the lithospheric mantle beneath and around the Slave craton: a Rhenium-Osmium isotopic study of peridotite xenoliths from the Jericho and Somerset Island kimberlites. *Ninth Annual V. M. Goldschmidt Conference*. LPI Contribution No. 971, 134-135.

Jordan T. H. (1978) Composition and development of the continental tectosphere. *Nature* **274**, 544-548.

Jordan T. H. (1988) Structure and formation of the continental tectosphere. *J. Petrol.*, Spec. Lithosphere Issue, 11-37.

Kelemen P. B., Dick H. J. B. and Quick J. E. (1992) Formation of harzburgite by pervasive melt/rock reaction in the upper mantle. *Nature* **358**, 635-641.

McDonough W. F. (1990) Constraints on the composition of the continental lithospheric mantle. *Earth Planet. Sci. Lett.* **101**, 1-18.

McDonough W. F. and Sun S. S. (1995) The composition of the earth. *Chem. Geol.* **120**, 223-253

Menzies M. A. (1990) Archean, Proterozoic, and Phanerozoic lithospheres. In *Continental mantle* (ed. M. A. Menzies). Oxford Univ. Press, Oxford. pp. 67-86.

Menzies M. A., Rogers N., Tindle A. and Hawkesworth C. J. (1987) Metasomatic and enrichment processes in lithospheric peridotites, an effect of asthenosphere-lithosphere interaction. In *Mantle metasomatism* (eds. M. A. Menzies and C. J. Hawkesworth). Academic Press, London. pp. 313-361.

Nixon P. H. (1987) Kimberlitic xenoliths and their cratonic setting. In *Mantle Xenoliths* (ed. P. H. Nixon). John Wiley & Sons, Chichester. pp. 215-239.

Nixon P. H., Rogers N. W., Gibso, I. L. and Grey A. (1981) Depleted and fertile mantle xenoliths from southern African kimberlites. *Annu. Rev. Earth Planet. Sci.* **9**, 285-309.

Pearson D. G. (1999) The age of continental roots. *Lithos* **48**, 171-194.

Pearson D. G., Carlson R. W., Shirey S. B., Boyd F. R. and Nixon P. H. (1995a) Stabilisation of Archean lithospheric mantle: a Re-Os isotope study of peridotite xenoliths from the Kaapvaal craton. *Earth Planet. Sci. Lett.* **134**, 341-357.

Pearson D. G., Shirey S. B., Carlson R. W., Boyd F. R., Pokhilenko N. P. and Shimizu N. (1995b) Re-Os, Sm-Nd, and Rb-Sr isotope evidence for thick Archean lithospheric mantle beneath the Siberian craton modified by multistage metasomatism. *Geochim. Cosmochim. Acta* **59**, 959-977.

Pell J. (1993) New kimberlite discoveries on Somerset Island. In *Exploration Overview 1993*. NWT Geology Division, Department of Indian and Northern Affairs, Yellowknife. pp. 47.

Pollack H. N. (1986) Cratonization and thermal evolution of the mantle. *Earth Planet. Sci. Lett.* **80**, 175-182.

Ringwood A. E. (1975) *Composition and petrology of the Earth's mantle*. McGraw-Hill, New York, pp.618.

Scherer E. E., Cameron K. L. and Blichert-Toft J. (2000) Lu-Hf garnet geochronology: Closure temperature relative to the Sm-Nd system and the effects of trace mineral inclusions. *Geochim. Cosmochim. Acta* **64**, 3413-3432.

Shapiro S. S., Hager B. H. and Jordan T. H. (1999) Stability and dynamics of the continental tectosphere. *Lithos* **48**, 115-133.

Shimizu N. (1999) Young geochemical features in cratonic peridotites from Southern Africa and Siberia. In *Mantle petrology: field observations and high pressure experimentation* (eds. Y. Fei, C. M. Bertka and B. O. Mysen). Geochem. Soc. Spec. Publ. 6. pp. 47-55.

Smith C. B., Allsopp H. L., Garvie O. G., Kramers J. D., Jackson P. F. S. and Clement C. R. (1989) Note on the U-Pb perovskite method for dating kimberlites: examples from the Wesselton and DeBeers mines, South Africa, and Somerset Island, Canada. *Chem. Geol. (Isot. Sect.)* **79**, 137-145.

Takahashi E. and Scarfe C. M. (1985) Melting of peridotite to 14 GPa and the genesis of komatiite. *Nature* **315**, 566-568.

Vervoort J. D. and Blichert-Toft J. (1999) Evolution of the depleted mantle: Hf isotope evidence from juvenile rocks through time. *Geochim. Cosmochim. Acta* **63**, 533-556.

Walter M. J. (1998) Melting of garnet peridotite and the origin of komatiite and depleted lithosphere. *J. Petrol.* **39**, 29-60.

Zindler A. and Hart S. R. (1986) Chemical Geodynamics. *Ann. Rev. Earth Planet. Sci.* **14**, 493-571.

CHAPTER 2

Nature of the mantle roots beneath the North American craton: mantle xenolith evidence from Somerset Island kimberlites

Abstract

The recently discovered Nikos kimberlite on Somerset Island, in the Canadian Arctic, hosts an unusually well preserved suite of mantle xenoliths dominated by garnet-peridotite (lherzolite, harzburgite, dunite) showing coarse and porphyroclastic textures, with minor garnet-pyroxenite. The whole rock and mineral data for fifty-four Nikos xenoliths indicate a highly refractory underlying mantle with high olivine forsterite contents (ave. Fo = 92.3) and moderate to high olivine abundances (ave. 80 wt.%). These characteristics are similar to those reported for peridotites from the Archean Kaapvaal and Siberian cratons (ave. olivine Fo = 92.5), but are clearly distinct from the trend defined by oceanic peridotites and mantle xenoliths in alkaline basalts and kimberlites from post-Archean continental terranes (ave. olivine Fo = 91.0). The Nikos xenoliths yield pressures and temperatures of last equilibration between 20 to 55 kb and 650 to 1300 °C, and a number of the peridotite nodules appear to have equilibrated in the diamond stability field. The pressure and temperature data define a conductive paleogeotherm corresponding to a surface heat flow of 44 mW/m^2. Paleogeotherms based on xenolith data from the central Slave province of the Canadian craton require a lower surface heat flow (~40 mW/m^2) indicating a cooler geothermal regime than that beneath the Canadian Arctic. A large number of kimberlite-hosted peridotites from the Kaapvaal craton in South Africa and parts of the Siberian craton are characterized by high orthopyroxene contents (ave. Kaapvaal 32 wt.%, Siberia 20 wt.%). The calculated modal mineral assemblages for the Nikos peridotites show moderate to low contents of orthopyroxene (ave. 12 wt.%), indicating that the orthopyroxene-rich mineralogy characteristic of the

Kaapvaal and Siberian cratons is not a feature of the cratonic upper mantle beneath Somerset Island.

Keywords: Canadian craton, kimberlite, mantle roots, mantle xenolith, peridotite, Somerset Island

1. Introduction

Global seismic tomography has shown that cold mantle roots with high seismic velocities underlie most Archean cratons to depths of at least 350 to 400 km (Jordan, 1988; Grand, 1994). Kimberlite-hosted mantle xenoliths are the only direct samples of these mantle roots beneath Archean cratonic areas and thus provide constraints on their composition and structure. Studies of such xenoliths in kimberlites from South Africa have shown the highly refractory nature of the mantle roots beneath the Archean Kaapvaal craton, with high olivine forsterite contents (Mg/(Mg+Fe) greater than 0.91; e.g. Cox et al, 1973; Nixon et al., 1981; Boyd, 1987). A large number of these mantle nodules are characterized by high modal orthopyroxene (up to 45 wt.%; Boyd and Canil, 1997) and low Mg/Si ratios (Boyd et al., 1997). The occurrence of orthopyroxene-rich mineral assemblages has also been reported for the Siberian craton (ave. Opx = 20 wt.%; Boyd et al., 1997). These compositional characteristics indicate that the deep-seated mantle roots of Archean cratons are chemically distinct from the upper mantle beneath oceanic and post-Archean crustal terranes (Boyd, 1989; Boyd et al., 1997; Shi et al., 1998). Whether the orthopyroxene-rich character reported for the mantle roots beneath the Kaapvaal and Siberian cratons is characteristic of cratonic mantle roots in general, however, has yet to be established.

In this paper, we present geochemical data for a suite of mantle xenoliths from the Nikos kimberlite on Somerset Island in the Canadian Arctic. Mineral chemistry and modal mineral analysis provide constraints on the nature of the mantle roots beneath the Canadian craton and enable a comparison with the compositional characteristics reported for the Archean Kaapvaal and Siberian cratons.

2. Geology

Somerset Island is part of the Innuitian tectonic province on the northern margin of the North American continent (Trettin et al, 1972). The local stratigraphy comprises middle Proterozoic to early Paleozoic sedimentary sequences that overlie the crystalline Precambrian basement of the Boothia Uplift (Steward, 1987). The Precambrian basement represents a northward salient of the Canadian shield that was deformed and faulted in the late Proterozoic to early Paleozoic, possibly related to compression associated with the Caledonian Orogeny in northern Europe and Greenland (Okulitch and Trettin, 1991). Granulite facies gneisses from the crystalline basement of the Boothia Uplift yield zircon dates between 2.5 and 2.2 Ga for their protoliths, while Sm-Nd model ages of 3.0 to 2.2 Ga suggest the presence of reworked Archean crustal material in these gneisses (Frisch and Hunt, 1993).

Other kimberlite occurrences on Somerset Island and their mantle xenoliths have been previously described (e.g. Mitchell, 1977; Jago and Mitchell, 1987; Fig. 1). The kimberlite pipes were emplaced during the Cretaceous along a major fault system related to the development of the Boothia Uplift (Mitchell, 1975). U-Pb dates on perovskite indicate kimberlite formation ages between 88 and 105 Ma (Heaman, 1989; Smith et al., 1989). Kimberlite emplacement coincides with major compressive deformation in the southeastern Arctic Islands induced by rifting that preceded sea-floor spreading in the Labrador Sea and Baffin Bay and the associated rotation of Greenland away from the North American continent that began in the early Cretaceous (Okulitch and Trettin, 1991). The timing of kimberlite emplacement on Somerset Island coincides with a world wide period of kimberlite activity in the Cretaceous (Nixon, 1987).

3. Kimberlite host

Previous field work and petrographic studies have shown that the majority of the Somerset kimberlites are brecciated diatremes or hypabyssal root zones (Mitchell and Meyer, 1980), consisting of fragments of kimberlite host, country rock, and mantle-derived xenocrysts. Establishing the compositions of the liquids for such kimberlites is problematic because of the difficulty of accounting for the country rocks and xenocrysts present in the kimberlite breccia. Magmatic kimberlite, containing less than 15 vol% of clasts larger than 4 mm, is rare on Somerset Island (Mitchell and Meyer, 1980; Mitchell, 1986).

The recently discovered Nikos kimberlite (Pell, 1993) outcrops along a steep cliff on the eastern coast of Somerset Island (73°28'N and 90°58'W; Fig. 1) and consists of three individual pipes that were sampled during the summer of 1996. Petrographic observations of the kimberlite samples indicate that one of these pipes (NK3) is characterized by a non-brecciated, magmatic texture. The magmatic kimberlite exhibits a porphyritic microcrystalline texture containing phenocrysts of olivine, phlogopite, and spinel in a very fine-grained carbonate-rich matrix. Two generations of olivine can be identified, rounded olivine phenocrysts (>1 mm) that most probably crystallized prior to the intrusion of the kimberlite and small euhedral to subhedral olivines (<1 mm). Garnet megacrysts (up to 5 mm) may represent xenocrysts derived by fragmentation of garnet peridotite xenoliths or be a liquidus phase at high pressure in the kimberlite magma (Mitchell, 1978; Mitchell and Meyer, 1980). The microcrystalline groundmass consists of calcite, serpentine, perovskite, and apatite. Calcite occurs as aggregates of tabular euhedral crystals or as sub-parallel laths, which are deflected around large olivine crystals, indicating their primary magmatic nature. Serpentine occurs as spherical microcrystalline segregations and as an alteration product of olivine marginally replacing these phenocrysts.

The whole rock analyses of kimberlite NK3 (n = 5) indicate an extremely carbonate rich composition, with $CaCO_3$ contents between 27 to 39 wt.% (ave. 31 wt.%), low SiO_2 abundances (20-25 wt.%), and a strong enrichment in incompatible trace element contents (Ba = 2200-3000 ppm; Sr = 1100-2200 ppm; Table 1). The high carbonate contents of the kimberlitic liquid indicate compositions intermediate between kimberlite (ave. $CaCO_3$ = 14 wt.%; Mitchell, 1986; Ringwood et al., 1992) and carbonatite ($CaCO_3$ = 50-80 wt.%; Woolley and Kempe, 1989), in keeping with recent experimental studies that have shown that a continuous spectrum of melt compositions from carbonatite to kimberlite can be produced by increasing degree of melting at pressures on the order of 60 kb (Dalton and Presnall, 1997).

4. Mantle xenoliths

The Nikos kimberlite hosts an unusually well preserved suite of large (10-20 cm) mantle-derived xenoliths, fifty-four of which were collected and analyzed in this study. The Nikos xenolith suite is dominated by garnet-peridotites (about 90%) comprising lherzolites, harzburgites, and lesser dunites. Also present are small numbers of pyroxene-rich nodules that are classified as garnet-pyroxenite rather than eclogite (Dawson, 1980; Hatton and Gurney, 1987) because of their low modal garnet (10-15 wt.%) and Al_2O_3 contents (5-10 wt.%), and the low jadeite component in clinopyroxene (Na_2O <1.6 wt.%).

The majority of the peridotite nodules have textures ranging from coarse equant to coarse tabular (Fig. 2a), based on the textural classification for mantle-derived rocks of Harte (1977). Large subhedral crystals of well preserved and relatively strain-free olivine (up to 10 mm) and orthopyroxene (ave. 2-5 mm) dominate the mineral assemblage. Clinopyroxene occurs as emerald green anhedral crystals with smooth grain boundaries (1-3 mm). Purple red garnet occurs as large porphyroclasts (ave. 5 mm) and is variably surrounded by kelyphitic rims of phlogopite and small spinel crystals. A small number of peridotite xenoliths exhibit porphyroclastic textures (<10%; Fig. 2b), characterized by large porphyroclasts (up to 10 mm) of strained olivine with undulose extinction surrounded by strain-free olivine neoblasts (0.1-0.5 mm) with tabular to polygonal equant habits. In these rocks, orthopyroxene occurs as porphyroclasts (2-5 mm) with irregular habit, and clinopyroxene and garnet are optically similar to those found in the coarse peridotites. The pyroxenite nodules show coarse equant textures (Fig. 2c) with large subhedral crystals (2-5 mm) of clinopyroxene and orthopyroxene, and smaller crystals (1 mm) of pale red garnet with a polygonal habit.

5. Analytical data

5.1. Whole rock chemistry

Whole rock analyses indicate that the Nikos peridotites are strongly depleted in fusible elements such as Fe, Ti, Ca, Al, and Na compared to estimated primitive mantle compositions (McDonough, 1990; Table 2). The whole rock magnesium numbers ($Mg^{\#}$ = Mg/(Mg+Fe); Fig. 3) for the lherzolites (ave. $Mg^{\#}$ = 0.91), harzburgites (ave. $Mg^{\#}$ = 0.92), and dunites (ave. $Mg^{\#}$ = 0.92) indicate a shift toward higher values for the harzburgites and dunites consistent with their larger degree of depletion. The Nikos nodules are significantly more refractory than oceanic peridotites and mantle xenoliths derived from beneath post-Archean continental crust ($Mg^{\#}$ = 0.89-0.91; Boyd, 1989). There is a good negative correlation between Al and Ca, and Mg (Fig. 4a, b), and a rough positive correlation between Ni and Mg (Fig. 4c). Compared to spinel-lherzolites from the

Canadian Cordillera (Shi et al., 1998), the late Phanerozoic orogenic belt that borders the western margin of the Canadian shield, the Nikos peridotites contain much lower Al_2O_3 contents (Fig. 5) and higher $Mg^{\#}$'s (Fig. 8). This indicates that the mantle roots beneath the Canadian shield are significantly more refractory than the lithopheric mantle beneath the Phanerozoic Cordillera. Spinel-harzburgites occurring in some of the Cordilleran xenolith suites from the southwestern Yukon and northern British Columbia, however, exhibit Al_2O_3 contents indistinguishable from those for the Nikos xenoliths (Fig. 5). These refractory harzburgites are associated with a seismically-detected hot mantle anomaly (Shi et al., 1998).

The pyroxenites, on the other hand, show a large variation in $Mg^{\#}$'s. The pyroxenites having high $Mg^{\#}$'s between 0.88 to 0.92 (high-Mg pyroxenites) overlap those of the peridotites. The $Mg^{\#}$'s for the other group of pyroxenites, however, are significantly lower ($Mg^{\#} = 0.84\text{-}0.85$; low-Mg pyroxenites), indicating that they are more Fe-rich than the coexisting peridotite xenoliths (Fig. 3).

5.2. Mineral chemistry

5.2.1. Olivine

Olivine in the peridotites is magnesium-rich and ranges in $Mg^{\#}$ from 0.91 to 0.93 (ave. 0.921) in the lherzolites and 0.92 to 0.93 (ave. 0.925) in the harzburgites, indicating higher values for the more refractory nodules (Table 3 for representative analyses). Individual olivine crystals do not exhibit chemical zoning and are homogeneous on thin section scale. There is no compositional difference between the olivines of the coarse and porphyroclastic peridotites. The Somerset olivine $Mg^{\#}$'s (ave. 0.923) are similar to those for peridotites from the Kaapvaal and Siberian cratons (ave. 0.925), but somewhat higher than the values reported for the Jericho (ave. 0.913; Kopylova et al., 1999) and the Torrie xenoliths (ave. 0.920; MacKenzie and Canil, 1999) from the Slave province of the Canadian craton. This suggests that parts of the mantle root beneath the center of the Slave Province are slightly less refractory than the mantle underlying the cratonic margin beneath Somerset Island. The NiO contents of the olivine (ave. 0.38 wt.%) in both the lherzolites and harzburgites are, however, similar to those reported for the Slave craton (Jericho xenoliths ave. 0.39 wt.%, Kopylova et al., 1999; Torrie xenoliths ave. 0.36 wt.%, MacKenzie and Canil, 1999).

5.2.2. Orthopyroxene

The $Mg^{\#}$'s of orthopyroxene in the peridotites range between 0.92 and 0.94 (ave. 0.930; Table 4), and are slightly higher than those of coexisting olivine suggesting equilibrated mineral parageneses (Gurney et al, 1979). The coarse and the porphyroclastic peridotites can not be distinguished in terms of their orthopyroxene $Mg^{\#}$'s. Orthopyroxenes in the pyroxenites exhibit a larger variation in $Mg^{\#}$'s, with an average value of 0.90 for high-Mg pyroxenites and 0.85 for low-Mg pyroxenites. Low Al_2O_3 abundances in both the peridotite and pyroxenite orthopyroxenes, ranging between 0.69 to 1.42 wt.%, reflect the presence of coexisting garnet.

5.2.3. Clinopyroxene

The clinopyroxenes are chromium-rich diopsides (Table 5) and exhibit $Mg^{\#}$'s in the peridotites (ave. 0.929) that are similar to those of the coexisting orthopyroxene (Table 4). The $Mg^{\#}$'s of high-Mg pyroxenite clinopyroxene (0.92-0.94) overlap those of the clinopyroxene in the peridotites, whereas $Mg^{\#}$'s of low-Mg pyroxenites (0.91) are considerably lower. The clinopyroxene Cr_2O_3 contents in the peridotites and the high-Mg pyroxenites range between 0.9 and 3.3 wt.% while the clinopyroxene of the low-Mg pyroxenites exhibits lower Cr_2O_3 abundances (0.4 wt.%). The chromium-diopsides of the

Nikos peridotites have slightly higher Cr_2O_3 contents than those reported for the Jericho (0.6-2.2 wt.%; Kopylova et al., 1999) and the Torrie xenoliths (0.3-1.5 wt.%; MacKenzie and Canil, 1999) in the Slave province.

5.2.4. Garnet

The garnet in the peridotites and the high-Mg pyroxenites is a chromium-pyrope with high magnesium contents and $Mg^{\#}$'s ranging between 0.79 and 0.86 (Table 6). $Mg^{\#}$'s of garnet in the low-Mg pyroxenites are significantly lower (0.64). The garnets exhibit no chemical zoning and are homogeneous on the scale of a thin section. The pyrope-rich garnet of the Nikos xenoliths has high Cr_2O_3 contents ranging between 1.5 and 7.7 wt.%, with the highest values observed in the harzburgites (4.0-7.7 wt.%). CaO abundances in garnet are low and indistinguishable in peridotites and pyroxenites (4.5-6.4 wt.%). The garnets in the peridotites and high-Mg pyroxenites would be classified as Group 9 garnets in the statistical classification of garnets of Dawson and Stephens (1975), in agreement with previous results for garnets in peridotite xenoliths from other Somerset Island kimberlites (Kjarsgaard and Peterson, 1992). The garnets in the low-Mg pyroxenites would be classified as Group 3 garnets because of their higher FeO and lower MgO contents.

5.3. Mineral modes

The modal mineral proportions of all Nikos xenoliths were calculated using a high-pressure peridotite norm calculation that determines the modal proportions of olivine, orthopyroxene, clinopyroxene, and garnet or spinel based on the whole rock compositions (Table 2). As a cross calibration, the normative mineralogy of twenty samples was calculated by reconstructing the bulk xenoliths from their mineral analyses using a least-squares technique. Both methods yield similar results, with modal mineral proportions differing by 3.0±1.8 wt.% (1 SD) for olivine, 3.0±2.5 wt.% (1 SD) for orthopyroxene, 1.3±0.6 wt.% (1 SD) for clinopyroxene, and 3.3±1.4 wt.% (1 SD) for garnet for all samples. The peridotite nodules range from garnet-lherzolites and garnet-harzburgites to garnet-dunites (ave. of all peridotites: olivine, 80 wt.%; orthopyroxene, 12 wt.%; chrome-diopside, 5 wt.%; pyrope-rich garnet, 3 wt.%). The majority of lherzolites fall rather close to the harzburgite field with only slightly more than 5 wt.% clinopyroxene (Fig. 6). These lherzolites exhibit major element compositions that are continuous with those of the harzburgites (Fig. 4a-c) and their division in two different rock types is somewhat artificial. The pyroxenites exhibit mineral assemblages consisting of clinopyroxene and orthopyroxene (ave. >80 wt.%), and garnet (ave. 12 wt.%). The high-Mg pyroxenites contain 5-10 wt.% olivine, while the low-Mg pyroxenites contain no olivine. Traces of spinel and minor amounts of phlogopite (less than 1 vol%) can be observed in individual xenolith samples.

5.4. Temperature and pressure

Temperatures and pressures of last equilibration were calculated for the Somerset xenoliths using geothermometers and barometers based on the compositions of coexisting pyroxenes and the solubility of Al_2O_3 in orthopyroxene in the presence of garnet. Temperatures were determined using the thermometers of Finnerty and Boyd (1987) and Brey and Köhler (1990). That of Finnerty and Boyd (1987) uses an empirical data fit to the miscibility gap between coexisting orthopyroxene and clinopyroxene and has been cross calibrated with the diamond/graphite transition (Kennedy and Kennedy, 1976) and the phlogopite stability field at upper mantle conditions. The thermometer of Brey and Köhler (1990) is based on a thermodynamic model for the solubility of orthopyroxene in clinopyroxene and was calibrated in reversed experiments between 900 to 1400 °C and 10 to 60 kb using natural fertile lherzolite compositions. These more recent experiments avoid Fe loss problems by using olivine crystals as sample containers.

MacGregor (1974) showed that the solubility of Al_2O_3 in orthopyroxene in the presence of garnet decreases with increasing pressure. Perkins and Newton (1980) used the same empirical method, but different thermodynamic parameters. The pressures calculated for the Nikos xenoliths using their calibration, however, were significantly lower than those obtained with the barometer of MacGregor (1974). The aluminum in enstatite (Al-in-en) barometer of MacGregor (1974) was evaluated by Finnerty and Boyd (1987) and found to yield results that are the most consistent with the diamond/graphite transition.

The pressures and temperatures for the Nikos xenoliths (Table 7) are shown in Figure 7. The method of Finnerty and Boyd (1987) combined with the Al-in-en barometer of MacGregor (1974) yields temperatures and pressures (Table 7) that are on average about 100 °C and 5 kb lower than the thermometer of Brey and Köhler (1990). The calculated pressures and temperatures, however, define similar trends in P-T space for both thermometers. In the following discussion, only the results using the thermometer of Brey and Köhler (1990) will be used.

6. Discussion

6.1. Paleogeothermal regime

The Nikos xenoliths record a wide range of equilibration conditions in the upper mantle, indicating that they were derived over a depth range between 55 and 170 km (Fig. 7). Although the pressure and temperature estimates for the harzburgites and lherzolites overlap, the harzburgites tend to plot at the higher end of the P-T array. This suggests that the upper part of the mantle sampled by the Nikos kimberlites tends to be more fertile than the lower portion of the mantle. A number of the peridotite samples plot to the right of the diamond/graphite transition (Kennedy and Kennedy, 1976) and appear to have equilibrated within the diamond stability field. The pyroxenites yield the lowest pressures and temperatures, indicating that they may be derived from shallower depths.

The calculated pressure and temperature data were fitted to a conductive geotherm using the approach of Pollack and Chapman (1977) assuming a lower crustal heat production of 0.25 $\mu W/m^3$ for the Canadian shield and a heat production of 10^{-2} $\mu W/m^3$ for the underlying mantle. The paleogeotherm for the Nikos xenoliths corresponds to a surface heat flow of 44 mW/m^2 at the time of last equilibration in the mantle (Fig. 7). These results are similar to recently reported pressure and temperature results for other xenoliths from the Nikos kimberlite (Zhao et al., 1997; Fig. 7) and those reported for the Batty Bay kimberlite, located 35 km to the southwest on Somerset Island (Kjarsgaard and Peterson, 1992). Boyd and Canil (1997) report a conductive geotherm of 40 mW/m^2 for a peridotite suite from the Grizzly kimberlite pipe in the Slave province, consistent with pressure and temperature conditions obtained for peridotites from the Jurassic Jericho kimberlite in the Slave province (Fig. 7; Kopylova et al., 1999). These results suggest that the geothermal gradient is cooler beneath the center of the Slave craton than towards its margin beneath Somerset Island, or that the thermal conditions have changed from the Jurassic to the Cretaceous. The latter possibility is supported by the higher present day heat flow measurements at Yellowknife in the Slave province (51 mW/m^2; Lewis and

Wang, 1992) and at Resolute Bay in the Canadian Arctic (52 mW/m^2; Lachenbruch, 1957).

Above ~1100 °C the pressure and temperature estimates for the Nikos peridotites deviate from the 44 mW/m^2 geotherm and are shifted towards slightly higher temperatures. This inflection is not correlated with any textural change in the xenoliths, as coarse peridotites are present at both the low and high temperature ends of the array. The inflection in the P-T array suggests the existence of a thermal boundary and may possibly represent the transition from lithospheric to asthenospheric mantle. This inflection would indicate a minimum thickness for the lithosphere of ~140 km beneath Somerset Island. The lithosphere boundary beneath the center of the Slave province has been estimated to be at depths between 195 and 200 km on the basis of both seismic studies (Bostock, 1997) and xenolith evidence (Boyd and Canil, 1997). The 140 km depth of the inflection in the Nikos P-T array may suggest that the transition from the base of the lithosphere shallows from the center of the Slave craton to its margin beneath Somerset Island. This interpretation is consistent with results for the Kaapvaal craton, where the lithosphere-asthenosphere transition has been reported to shallow away from the cratonic center (200 km) to its margins (~140 km; Boyd, 1987).

Porphyroclastic peridotites from the Kaapvaal craton in South Africa have been interpreted to represent asthenospheric mantle, whereas coarse peridotites are interpreted to represent lithospheric mantle (Boyd, 1987). Although a similar relationship apparently exists in the Jericho pipe of the Slave province (Kopylova et al., 1999), porphyroclastic xenoliths are rare in the Nikos pipe and do not give consistently higher P-T results. The lack of a correlation between texture and equilibration conditions observed for the Nikos peridotites is consistent with findings for the xenoliths from the Batty Bay kimberlite (Kjarsgaard and Peterson, 1992).

6.2. Nature of the Canadian mantle roots

Peridotite represents the dominant rock type (>90%) of the Nikos xenolith suite, indicating a peridotitic composition for Canadian mantle roots similar to that reported for the Kaapvaal and Siberian cratons (Nixon, 1987; Boyd et al, 1997). The chemical compositions of the Nikos peridotites are depleted in fusible elements compared to primitive mantle compositions (McDonough, 1990) and fertile spinel-lherzolites from beneath the Canadian Cordillera (Shi et al., 1998). The high olivine forsterite contents (ave. Fo = 92.3) and moderate to high modal abundances of olivine (ave. 80 wt.%) indicate the highly refractory nature of the Nikos peridotites and suggest that they represent the residues of large degree partial melting. The spectrum from lherzolite to harzburgite can be modeled using fractional melting equations based on Yb contents of the xenoliths. The results indicate an average of ~30% melt extraction from the most fertile lherzolite to refractory harzburgite.

The chemical signatures of the Nikos peridotites are similar to the compositions reported for the Archean Kaapvaal and Siberian cratons (ave. olivine Fo = 92.5; Boyd et al., 1997) and clearly distinct from the trend defined by peridotites from oceanic domains (ave. olivine Fo = 91.0; Boyd, 1989) and spinel-peridotites from the Canadian Cordillera (Shi et al., 1998) that represent the mantle beneath Phanerozoic accreted terranes along the western margin of the Canadian shield (Fig. 8). Spinel-harzburgites associated with a mantle thermal anomaly beneath the southwestern Yukon (Shi et al., 1998), however, have intermediate compositions with higher modal olivine and olivine forsterite contents compared to the more fertile spinel-lherzolites, and trend towards the more depleted compositions of the Nikos peridotites. These spinel-harzburgites were interpreted to represent the residue of ~20-25 % partial melting of lherzolite mantle (Francis, 1987; Shi et al., 1998).

Many peridotite xenoliths from the Kaapvaal craton are anomalously enriched in orthopyroxene, with average modal orthopyroxene contents of 32 wt.% (Boyd et al., 1997). Minor occurrences of such orthopyroxene-rich mineral assemblages have been reported from the Siberian craton (Boyd et al., 1997), however, these peridotites have an average orthopyroxene content of only 20 wt.% and are thus less enriched in orthopyroxene than the Kaapvaal xenoliths. This orthopyroxene-rich nature can not be attributed solely to the extraction of basaltic components from primitive mantle by extensive partial melting (Herzberg, 1993). Such processes would induce depletion in both clinopyroxene and orthopyroxene content, and a shift of the residual mineral assemblage to higher olivine, but lower orthopyroxene abundances. A recent experimental study on depleted cratonic harzburgite by Kinzler and Grove (1998), however, has shown that the majority of the orthopyroxene enriched mineral assemblages from the Kaapvaal and Siberian cratons can be produced by polybaric, near fractional melting of primitive mantle at >2 GPa. The most extreme orthopyroxene enriched peridotites, however, cannot be explained by such processes and these require that either parts of the mantle are significantly enriched in silica compared to primitive mantle models (Herzberg, 1993) or that post melt-extraction processes have modified the composition of the Kaapvaal mantle roots (e.g. Boyd et al., 1997: Kelemen et al., 1997). Igneous separation of orthopyroxene-rich cumulate layers or metamorphic segregation of the residual mantle into orthopyroxene-rich and olivine-rich layers have been proposed by Boyd et al. (1997) as possible explanations for the orthopyroxene-rich nature of cratonic mantle roots. Such processes would induce a negative correlation between Si and Fe, opposite to the trend observed in melting experiments on fertile garnet-peridotite (Hirose and Kushiro, 1993; Baker and Stolper, 1994). In the Nikos xenolith suite, however, a negative correlation between Si and Fe (Fig. 9) that has been reported for Siberian and Kaapvaal peridotites (Boyd et al., 1997) is not observed. Kelemen et al. (1997) interpreted a positive correlation between NiO in olivine and modal orthopyroxene contents in some cratonic mantle xenolith suites to be indicative of metasomatic infiltration of residual mantle by Fe-poor silicic melts, possibly originating from subducted oceanic lithosphere. This would induce the formation of orthopyroxene at the expense of olivine, resulting in increased NiO in the residual olivine associated with high orthopyroxene abundances. This trend between modal orthopyroxene and olivine NiO contents is not well developed in the Nikos peridotites (Fig. 10).

Compared to xenolith suites from the Kaapvaal and Siberian cratons, the Nikos peridotites are characterized by lower orthopyroxene abundances (ave. 12 wt.%). The chemical and modal signatures of the Nikos peridotites are similar to those recently reported for the Grizzly kimberlite peridotites in the Slave province (Boyd and Canil, 1997), which also have high magnesium numbers (ave. $Mg^{\#} = 0.927$), but mineral assemblages characterized by relatively low orthopyroxene (ave. ~11 wt.%; MacKenzie and Canil, 1999). The trend towards higher olivine and lower orthopyroxene abundances exhibited by the Nikos peridotites suggests an origin by large degree partial melting of primitive mantle compositions. This interpretation is supported by continuous trends in major element variations, in particular the negative correlation of MgO and Al_2O_3 (Fig. 4a), suggesting that the Nikos peridotites are related by partial melting. It is also consistent with an overall positive correlation between modal olivine abundance and olivine forsterite content (Fig. 8).

7. Conclusions

The Nikos peridotites define a hotter paleogeotherm than that reported for the mantle beneath the central Slave province. An inflection in the pressure and temperature array may indicate that the transition from lithospheric to asthenospheric mantle is shallower under Somerset Island (140 km) than under the center of the Slave craton (200 km).

The high forsterite contents associated with moderate to high olivine abundances of the Nikos peridotites are characteristic of peridotite xenolith suites derived from subcontinental mantle beneath Archean cratons. These characteristics clearly indicate that they are distinctly more refractory than oceanic peridotites and post-Archean mantle xenolith suites. The modal abundances of the Nikos xenoliths suggest that they formed by extensive degrees of partial melting of primitive mantle. However, the high orthopyroxene abundances that characterize the Kaapvaal craton and parts of the Siberian craton are not characteristic of the Nikos peridotite suite. More studies of mantle xenolith suites from other Archean cratons are needed to determine whether the orthopyroxene-rich mantle roots beneath the Kaapvaal craton are an exception, or a general feature of cratonic mantle roots.

Acknowledgements

We would like to thank Tariq Ahmedali for performing the bulk rock X-ray fluorescence analyses and Glenn Poirier for his help in obtaining the electron microprobe results. We also thank Fabien Rasselet for assistance in the field, hand picking separates of magmatic kimberlite for major and trace element analysis, and performing the CO_2

analyses with the assistance of Constance Guignard. Tony Simonetti is thanked for discussions and earlier revisions of the manuscript.

References

Baker, M.B. and Stolper, E.M., 1994. Determining the composition of high-pressure mantle melts using diamond aggregates. Geochim. Cosmochim. Acta, 58: 2811-2827.

Bostock, M.G., 1997. Anisotropic upper-mantle stratigraphy and architecture of the Slave craton. Nature, 390: 392-395.

Boyd, F.R., 1987. High- and low-temperature garnet peridotite xenoliths and their possible relation to the lithosphere-asthenosphere boundary beneath southern Africa. In: P. H. Nixon (Editor), Mantle Xenoliths. John Wiley & Sons, Chichester, pp. 403-412.

Boyd, F.R., 1989. Compositional distinction between oceanic and cratonic lithosphere. Earth Planet. Sci. Lett., 96: 15-26.

Boyd, F.R. and Canil, D., 1997. Peridotite xenoliths from the Slave craton, Northwest Territories. In: Seventh annual V.M. Goldschmidt Conference, Houston, 34-35.

Boyd, F.R. and Mertzman, S.A., 1987. Composition and structure of the Kaapvaal lithosphere, southern Africa. In: B. O. Mysen (Editor), Magmatic processes: physiochemical principles. Geochem. Soc. Spec. Publ., pp. 13-24.

Boyd, F.R., Pokhilenko, N.P., Pearson, D.G., Mertzman, S.A., Sobolev, N.V. and Finger, L.W., 1997. Composition of the Siberian cratonic mantle: evidence from Udachnaya peridotite xenoliths. Contrib. Mineral. Petrol., 128: 228-246.

Brey, G.P. and Köhler, T., 1990. Geothermobarometry in four-phase lherzolites II. New thermobarometers, and practical assessment of existing thermobarometers. J. Petrol., 31: 1353-1378.

Carswell, D.A., Clarke, D.B. and Mitchell, R.H., 1979. The petrology and geochemistry of ultramafic nodules from Pipe 200, northern Lesotho. In: F. R. Boyd and H. O. A. Meyer (Editors), Proceedings of the Second International Kimberlite Conference. AGU, Washington, pp. 127-144.

Cox, K.G., Gurney, J.J. and Harte, B., 1973. Xenoliths from the Matsoku pipe. In: P. H. Nixon (Editor), Lesotho Kimberlites. Lesotho National Development Corporation, Maseru, Lesotho, pp. 76-100.

Cox, K.G., Smith, M.R. and Beswetherick, S., 1987. Textural studies of garnet lherzolites: evidence of exsolution origin from high-temperature harzburgites. In: P. H. Nixon (Editor), Mantle Xenoliths. John Wiley & Sons, Chichester, pp. 537-550.

Dalton, J.A. and Presnall, D.C., 1997. Phase relations in the system $CaO\text{-}MgO\text{-}Al_2O_3\text{-}SiO_2\text{-}CO_2$ from 3.0 to 7.0 GPa: carbonatites, kimberlites and carbonatite-kimberlite relations. In: GAC/MAC annual meeting, Ottawa, A-34.

Danchin, F.R., 1979. Mineral and bulk chemistry of garnet lherzolite and garnet harzburgite from the Premier mine, South Africa. In: F. R. Boyd and H. O. A. Meyer (Editors), Proceedings of the Second International Kimberlite Conference. AGU, Washington, pp. 104-126.

Dawson, J.B., 1980. Kimberlites and their xenoliths. Springer-Verlag, Berlin, 252 pp.

Dawson, J.B. and Stephens, W.E., 1975. Statistical classification of garnets from kimberlite and associated xenoliths. J. Geol., 83: 589-607.

Finnerty, A.A. and Boyd, F.R., 1987. Thermobarometry for garnet peridotites: basis for the determination of thermal and compositional structure of the upper mantle. In: P. H. Nixon (Editor), Mantle Xenoliths. John Wiley & Sons, Chichester, pp. 381-402.

Francis, D., 1987. Mantle-melt interaction recorded in spinel lherzolite xenoliths from the Alligator Lake volcanic complex, Yukon, Canada. J. Petrol., 28: 569-597.

Frisch, T. and Hunt, P.A., 1993. Reconnaissance U-Pb geochronology of the crystalline core of the Boothia Uplift, District of Franklin, Northwest Territories. In: Radiogenic age and isotope studies: Report 7. Geological Survey of Canada, Paper, pp. 3-22.

Grand, S.P., 1994. Mantle shear structure beneath the Americas and surrounding oceans. J. Geophys. Res., 99: 11.591-11.621.

Gurney, J.J., Harris, J.W. and Rickard, R.S., 1979. Silicate and oxide inclusions in diamonds from the Finsch kimberlite pipe. In: F. R. Boyd and H. O. A. Meyer (Editors), Kimberlites, diatremes and diamonds: their geology and petrology and geochemistry. AGU, Washington, pp. 1-15.

Harte, B., 1977. Rock nomenclature with particular relation to deformation and recrystallization textures in olivine-bearing xenoliths. J. Geol., 85: 279-288.

Hatton, C.J. and Gurney, J.J., 1987. Roberts Victor eclogites and their relation to the mantle. In: P. H. Nixon (Editor), Mantle Xenoliths. John Wiley & Sons, Chichester, pp. 453-463.

Heaman, L.H., 1989. The nature of the subcontinental mantle from Sr-Nd-Pb isotopic studies on kimberlite perovskite. Earth Planet. Sci. Lett., 92: 323-334.

Herzberg, C.T., 1993. Lithosphere peridotites of the Kaapvaal craton. Earth Planet. Sci. Lett., 120: 13-29.

Hirose, K. and Kushiro, I., 1993. Partial melting of dry peridotites at high pressures: Determination of compositions of melts segregated from peridotite using aggregates of diamond. Earth Planet. Sci. Lett., 114: 477-489.

Jago, B.C. and Mitchell, R.H., 1987. Ultrabasic xenoliths from the Ham kimberlite, Somerset Island, Northwest Territories. Canadian Mineral., 25: 515-525.

Jordan, T.H., 1988. Structure and formation of the continental tectosphere. J. Petrol., Spec. Lithosphere Issue: 11-37.

Kelemen, P.B., Bernstein, S. and Hart, S.R., 1997. SiO_2 addition to cratonic mantle via melt/rock reaction above subduction zones. In: Workshop on Continental Roots, Harvard University and MIT.

Kennedy, C.S. and Kennedy, G.C., 1976. The equilibrium boundary between graphite and diamond. J. Geophys. Res., 81: 2467-2470.

Kinzler, R.J. and Grove, T.L., 1998. Origin of depleted cratonic harzburgite by deep fractional melt extraction and shallow olivine cumulate infusion. Proceedings of the Seventh International Kimberlite Conference: in press.

Kjarsgaard, B.A. and Peterson, T.D., 1992. Kimberlite-derived ultramafic xenoliths from the diamond stability field: a new Cretaceous geotherm for Somerset Island, Northwest Territories. In: Current Research, 1992-B. Geological Survey of Canada, pp. 1-6.

Kopylova, M.G., Russell, J.K. and Cookenboo, H., 1999. Petrology of peridotite and pyroxenite xenoliths from the Jericho kimberlite: implications for the thermal state of the mantle beneath the Slave craton, Northern Canada. J. Petrol. 40, 79-104.

Lachenbruch, A.H., 1957. Thermal effects of the ocean on permafrost. Geol. Soc. Am. Bull. 68: 1515-1529.

Lewis, T.J. and Wang, K., 1992. Influence of terrain on bedrock temperatures. Palaeogeography, Palaeoclimatology, Palaeoecology, 98: 87-100.

MacGregor, I.D., 1974. The system $MgO-Al_2O_3-SiO_2$: solubility of Al_2O_3 in enstatite for spinel and garnet peridotite compositions. American Mineralog., 59: 110-119.

MacKenzie, J.M. and Canil, D., 1999. Composition and thermal evolution of cratonic mantle beneath the central Archean Slave Province, NWT, Canada. Contrib. Mineral. Petrol. 134, 313-324.

McDonough, W.F., 1990. Constraints on the composition of the continental lithospheric mantle. Earth Planet. Sci. Lett., 101: 1-18.

Mitchell, R.H., 1975. Geology, magnetic expression, and structural control of the central Somerset Island kimberlites. Can. J. Earth Sci., 12: 757-764.

Mitchell, R.H., 1977. Ultramafic xenoliths from the Elwin Bay kimberlite: the first Canadian paleogeotherm. Can. J. Earth Sci., 14: 1202-1210.

Mitchell, R.H., 1978. Mineralogy of the Elwin Bay kimberlite, Somerset Island, N.W.T., Canada. American Mineralog., 63: 47-57.

Mitchell, R.H., 1986. Kimberlites: Mineralogy, Geochemistry, and Petrology. Plenum Press, New York, 442 pp.

Mitchell, R.H. and Meyer, H.O.A., 1980. Mineralogy of micaceous kimberlite from the Jos dyke, Somerset Island. Canadian Mineralog., 18: 241-250.

Nixon, P.H., 1987. Kimberlitic xenoliths and their cratonic setting. In: P. H. Nixon (Editor), Mantle Xenoliths. John Wiley & Sons, Chichester, pp. 215-239.

Nixon, P.H. and Boyd, F.R., 1973. Petrogenesis of the granular and sheared ultrabasic nodule suite in kimberlites. In: P. H. Nixon (Editor), Lesotho Kimberlites. Lesotho National Development Corporation, Maseru, Lesotho, pp. 48-56.

Nixon, P.H., Rogers, N.W., Gibson, I.L. and Grey, A., 1981. Depleted and fertile mantle xenoliths from southern African kimberlites. Annu. Rev. Earth Planet. Sci., 9: 285-309.

Okulitch, A.V. and Trettin, H.P., 1991. Late Cretaceous - Early Tertiary deformation, Artic Islands. In: H. P. Trettin (Editor), Geology of the Innuitian Orogen and Artic Platform of Canada and Greenland. Geological Survey of Canada, pp. 469-489.

Pell, J., 1993. New kimberlite discoveries on Somerset Island. In: Exploration Overview 1993, NWT Geology Division, Department of Indian and Northern Affairs, Yellowknife, 47 pp.

Perkins, D. and Newton, R.C., 1980. The compositions of coexisting pyroxenes and garnet in the system $CaO-MgO-Al_2O_3-SiO_2$ at 900° -1100° C and high pressures. Contrib. Mineral. Petrol., 75: 291-300.

Pollack, H.N. and Chapman, D.S., 1977. On the regional variation of heat flow, geotherms and lithospheric thickness. Tectonophysics, 38: 279-296.

Ringwood, A.E., Kesson, S.E., Hibberson, W. and Ware, N., 1992. Origin of kimberlites and related magmas. Earth Planet. Sci. Lett., 113: 521-538.

Shi, L., Francis, D., Ludden, J., Frederiksen, A. and Bostock, M., 1998. Xenolith evidence of lithospheric melting above anomalously hot upper mantle under the northern Canadian Cordillera. Contrib. Mineral. Petrol., 131: 39-53.

Smith, C.B., Allsopp, H.L., Garvie, O.G., Kramers, J.D., Jackson, P.F.S. and Clement, C.R., 1989. Note on the U-Pb perovskite method for dating kimberlites: examples from the Wesselton and DeBeers mines, South Africa, and Somerset Island, Canada. Chem. Geol. (Isotope Geos.), 79: 137-145.

Steward, W.D., 1987. Late Proterozoic to Early Tertiary stratigraphy of Somerset Island and northern Boothia Peninsula, District of Franklin. Geological Survey of Canada Paper, 83-26: 78 pp.

Trettin, H.P., Frisch, T.O., Sobczak, L.W., Weber, J.R., Niblett, E.R., Law, L.K., DeLaurier, I. and Witham, K., 1972. The Innuitian Province. In: R. A. Price and R. J. W. Douglas (Editors), Variations in tectonic styles in Canada. Geological Association of Canada, Special Paper, pp. 83-179.

Woolley, A.R. and Kempe, D.R.C., 1989. Carbonatites nomenclature, average chemical compositions, and elemental distribution. In: K. Bell (Editor), Carbonatites; genesis and evolution. Unwin Hyman Inc., London, pp. 1-14.

Zhao, D., Essene, E.J., Zhang, Y., Hall, C.M. and Wang, L., 1997. Newly discovered kimberlites and mantle xenoliths from Somerset Island and Brodeur Peninsula, Canada: Pressure, temperature, oxygen fugacity, volatile content and age. In: NWT Geology Division, Department of Indian and Northern Affairs, Yellowknife, pp. 1-105.

Figure Captions

Figure 2-1. Geological map of Somerset Island (after Steward, 1987) showing kimberlite locations. Legend: light gray, Paleozoic cover rocks; striped, Late Proterozoic cover rocks; dark gray, Precambrian basement; bold lines, normal faults.

Figure 2-2. Photomicrographs of xenoliths from the Nikos kimberlite showing a) coarse texture in peridotite, b) porphyroclastic texture in peridotite and c) coarse texture in pyroxenite. Upper photographs with plane polars, lower photographs with crossed polars.

Figure 2-3. Histogram of whole rock magnesium numbers ($Mg^{\#} = Mg/(Mg+Fe)$) of peridotites, and high-Mg and low-Mg pyroxenites.

Figure 2-4. Variations of major elements a) Al_2O_3, b) CaO, c) NiO with MgO (wt.%) of Nikos peridotites. Primitive mantle composition after McDonough (1990).

Figure 2-5. Histogram of Al_2O_3 content (wt.%) of Nikos peridotites compared to data for the bi-modal northern Cordilleran spinel-harzburgite and spinel-lherzolite suite and the uni-modal southern Cordilleran spinel-lherzolite suite (Shi et al., 1998). Primitive mantle composition after McDonough (1990).

Figure 2-6. Modal mineral proportions of Nikos xenoliths compared to data for kimberlite-hosted mantle xenoliths from the Kaapvaal craton in South Africa (Cox et al., 1973; Nixon and Boyd, 1973; Carswell et al., 1979; Danchin, 1979; Boyd and Mertzman, 1987; Cox et al., 1987). Primitive mantle composition after McDonough (1990).

Figure 2-7. Pressures and temperatures of last equilibration of the Nikos xenoliths using the thermometer of Brey and Köhler (1990) combined with the Al-in-en barometer of MacGregor (1974). Diamond/graphite transition after Kennedy and

Kennedy (1976). Model conductive geotherms representing a surface heat flow of 40 mW/m^2 and 44 mW/m^2 after Pollack and Chapman (1977). Data for peridotites from the Jericho kimberlite (Kopylova et al., 1999) in the Canadian Slave province and other xenolith data from the Nikos kimberlite on Somerset Island (Zhao et al., 1997) are shown for comparison.

Figure 2-8. Modal olivine content (wt.%) versus Mg$^\#$ in olivine of the Nikos peridotites. Field for the Kaapvaal and Siberian cratons (Boyd, 1989; Boyd et al., 1997) and data for the Canadian Cordillera (Shi et al., 1998; lherzolites, open circles; harzburgites, open triangles) are shown for comparison. Trend defined by oceanic peridotites after Boyd (1989).

Figure 2-9. Variation of FeO and SiO_2 (wt.%) of the Nikos peridotites indicating no correlation of these elements in the xenoliths.

Figure 2-10. NiO (wt.%) in olivine versus modal orthopyroxene content (wt.%) of the Nikos peridotites.

Table 2-1

Major and trace element analyses of kimberlites

The major and trace elements were analyzed by X-ray fluorescence analysis at McGill University with a Philips PW 2400 spectrometer. The major elements and Ba, V, Co, Cr, and Ni were analyzed on fused discs using a α-coefficient technique with an analytical precision of less than 0.06 wt.% (1 SD). Total Fe is given as FeO. Other trace elements were analyzed on pressed pellets using a Rh Kb Compton scatter matrix correction with an analytical precision of 5%.

Sample Rock	NK3-K1 Kimberlite	NK3-K2 Kimberlite	NK3-K3 Kimberlite	NK3-K4 Kimberlite	NK3-K5 Kimberlite
Major elements in wt.%					
SiO_2	19.85	25.05	23.21	22.72	23.62
TiO_2	2.06	2.15	1.62	1.73	1.51
Al_2O_3	2.20	2.81	2.03	1.90	1.64
FeO	7.06	8.13	6.99	7.32	7.26
MnO	0.14	0.16	0.15	0.14	0.15
MgO	19.97	26.12	23.07	23.03	25.59
CaO	21.58	15.34	17.57	18.90	16.61
Na_2O	0.19	0.14	0.06	0.09	0.10
K_2O	1.00	0.66	0.55	0.30	0.59
P_2O_5	0.64	0.64	0.92	0.83	0.85
H_2O	1.43	5.00	5.07	8.55	0
CO_2	22.78	12.68	17.10	13.19	20.96
Total	98.90	98.88	98.35	98.71	98.88
$CaCO_3$	38.52	27.38	31.36	30.00	29.65
Trace elements in ppm					
Ba	2694	2231	2972	3007	2445
Rb	72	46	30	22	38
Sr	1299	1072	1647	2233	1418
Th	18.2	17.4	22.3	23.1	18.7
U	0	1.4	0	0	0
Zr	139	162	163	146	147
Nb	166	169	198	190	179
Y	9.3	11.3	11.8	9.5	10.4
Cr	1366	1586	1721	1526	1362
Ni	672	817	861	855	917
Co	52	64	59	64	65
V	153	151	136	140	126
Sc	28	16	15	19	23

Table 2-2

Representative analyses of bulk xenoliths

LOI: loss on ignition. Total Fe is given as FeO and Mg$^{\#}$=Mg/(Mg+Fe). Lherz: lherzolite, Harz: harzburgite, Pyrox: pyroxenite, porphyr: porphyroclastic. Modes were calculated using the whole rock compositions and a high-pressure peridotite norm recipe. Analytical procedure as in Table 2-1.

Sample	NK1-5	NK2-3	NK2-10	NK3-20	NK3-25	NK1-2	NK1-3	NK1-6	NK1-7	NK1-17	NK1-18	NK2-7	NK3-1	NK3-17
Rock	Lherz	Lherz	Lherz	Lherz	Lherz	Harz	Harz	Harz	Harz	Harz	Harz	Pyrox	Pyrox	Pyrox
Texture	coarse	coarse	coarse	coarse	coarse	coarse	coarse	coarse	porphyr	coarse	coarse	coarse	coarse	coarse
Major elements in wt.%.														
SiO_2	42.28	42.46	41.54	43.19	41.42	41.77	40.81	40.37	41.24	41.22	42.94	48.95	50.97	50.15
TiO_2	0.07	0.09	0.03	0.10	0.21	0.03	0.03	0.02	0.03	0.01	0.03	0.13	0.18	0.18
Al_2O_3	1.95	2.90	1.25	3.21	4.28	1.31	1.33	1.25	1.57	0.81	0.79	8.05	4.71	4.89
FeO	7.74	7.21	7.43	7.58	7.41	7.39	7.42	7.10	7.06	7.05	6.97	4.93	6.04	6.01
MnO	0.12	0.13	0.11	0.13	0.13	0.11	0.11	0.10	0.10	0.11	0.10	0.18	0.15	0.15
MgO	41.49	41.87	45.53	37.50	39.46	44.44	44.03	43.41	43.55	45.40	44.93	23.69	19.44	19.48
CaO	1.44	1.98	1.22	3.21	2.13	1.11	0.82	0.41	0.72	0.49	0.54	9.45	16.46	16.91
Na_2O	0.06	0.15	0.07	0.35	0.09	0.10	0.01	0.00	0.00	0.08	0.05	0.90	0.46	0.28
K_2O	0.08	0.19	0.05	0.14	0.52	0.03	0.04	0.03	0.02	0.03	0.03	0.11	0.11	0.09
P_2O_5	0.01	0.02	0.04	0.02	0.04	0.02	0.02	0.01	0.01	0.03	0.01	0.01	0.02	0.01
Cr_2O_3	0.85	1.04	0.53	0.67	1.09	0.52	0.60	0.68	0.70	0.68	0.51	1.69	0.79	0.73
NiO	0.30	0.31	0.32	0.28	0.25	0.32	0.33	0.33	0.31	0.31	0.35	0.38	0.09	0.09
LOI	3.50	1.77	1.84	3.30	2.81	2.71	3.89	5.85	4.31	3.88	2.75	1.90	0.52	0.58
Total	99.89	100.13	99.97	99.68	99.85	99.85	99.42	99.57	99.62	100.10	100.00	100.37	99.94	99.55
Mg$^{\#}$	0.905	0.912	0.916	0.898	0.905	0.915	0.914	0.916	0.917	0.920	0.920	0.895	0.852	0.852
Calculated modes in wt.%.														
Oliv	71.0	69.0	87.8	56.9	60.9	83.5	84.1	82.5	79.2	87.9	80.6	4.4	0	0
Opx	18.1	15.8	4.2	22.5	19.5	8.8	9.1	12.3	13.8	7.7	15.1	41.0	23.6	22.2
Cpx	6.1	8.6	5.1	14.2	9.8	4.7	3.4	1.7	2.9	2.3	2.3	39.2	67.0	67.6
Garn	4.8	6.6	3.0	6.4	9.9	3.0	3.5	3.5	4.1	2.2	2.0	15.4	9.4	10.3

Table 2-3
Representative analyses of olivines
The mineral compositions (wt.%) were determined using a JEOL 8900L electron microprobe at McGill University. The mineral phases were analyzed by wavelength dispersive spectroscopy with an acceleration voltage of 20 kV, beam current of 20 nA, and a beam diameter of 5 μm. On-peak counting times were 20 s, and the background counting times 10 s.

Sample Rock	NK1-5 Lherz	NK2-3 Lherz	NK2-10 Lherz	NK3-20 Lherz	NK3-25 Lherz	NK1-2 Harz	NK1-3 Harz	NK1-6 Harz	NK1-7 Harz	NK1-17 Harz	NK1-18 Harz
SiO_2	40.75	41.43	40.78	41.26	41.29	41.02	41.03	40.81	41.01	40.94	41.26
FeO	8.15	7.07	7.43	8.59	8.47	7.48	7.37	7.15	7.35	7.09	7.21
MnO	0.12	0.10	0.10	0.09	0.11	0.10	0.10	0.10	0.10	0.10	0.10
MgO	49.43	51.04	50.83	50.27	50.48	50.20	50.43	51.30	50.67	51.04	50.88
CaO	0.04	0.01	0.01	0.01	0.05	0.01	0.01	0.02	0.05	0.02	0.03
Cr_2O_3	0.04	0.00	0.01	0.00	0.02	0.01	0.01	0.02	0.04	0.01	0.04
NiO	0.35	0.40	0.36	0.38	0.36	0.35	0.35	0.38	0.37	0.36	0.43
Total	98.94	100.08	99.56	100.63	100.83	99.19	99.33	99.79	99.62	99.58	99.99
$Mg^{\#}$	0.915	0.928	0.924	0.912	0.914	0.923	0.924	0.927	0.925	0.928	0.926
Formulae based on three cations											
Si	1.004	1.003	0.993	1.000	0.998	1.004	1.002	0.989	1.004	0.995	1.001
Fe	0.168	0.143	0.151	0.174	0.171	0.153	0.151	0.145	0.150	0.144	0.146
Mn	0.003	0.002	0.002	0.002	0.002	0.002	0.002	0.002	0.002	0.002	0.002
Mg	1.815	1.843	1.845	1.816	1.819	1.832	1.837	1.854	1.835	1.850	1.840
Ca	0.001	0.000	0.000	0.000	0.001	0.000	0.000	0.000	0.001	0.000	0.001
Cr	0.001	0.000	0.000	0.000	0.000	0.000	0.000	0.000	0.001	0.000	0.001
Ni	0.007	0.008	0.007	0.007	0.007	0.007	0.007	0.007	0.007	0.007	0.008
O	4.001	4.003	3.992	4.000	3.997	4.004	4.002	3.989	3.999	3.995	4.001

Table 2-4
Representative analyses of orthopyroxenes (analytical procedure as in Table 2-3)

Sample	NK1-5	NK2-3	NK2-10	NK3-20	NK3-25	NK1-2	NK1-3	NK1-6	NK1-7	NK1-17	NK1-18	NK2-7	NK3-1	NK3-17
Rock	Lherz	Lherz	Lherz	Lherz	Lherz	Harz	Harz	Harz	Harz	Harz	Harz	Pyrox	Pyrox	Pyrox
SiO_2	56.69	56.66	56.78	57.04	56.79	57.11	57.18	56.35	56.50	56.56	56.34	57.02	56.16	55.64
TiO_2	0.09	0.08	0.06	0.00	0.09	0.04	0.05	0.04	0.06	0.01	0.03	0.06	0.03	0.02
Al_2O_3	1.22	0.96	1.04	1.01	1.24	0.95	0.97	1.14	1.35	0.90	1.20	0.95	1.11	1.17
FeO	5.00	4.58	5.01	4.95	5.34	4.72	4.65	4.53	4.57	4.46	4.48	4.97	9.68	9.66
MnO	0.13	0.11	0.11	0.12	0.12	0.12	0.13	0.11	0.11	0.12	0.11	0.11	0.14	0.12
MgO	35.00	35.97	35.27	35.35	34.78	35.80	35.89	35.82	35.62	36.18	35.18	35.70	32.66	32.55
CaO	0.71	0.23	0.34	0.53	0.68	0.34	0.30	0.38	0.83	0.34	0.72	0.22	0.20	0.22
Na_2O	0.14	0.04	0.09	0.01	0.13	0.09	0.08	0.15	0.15	0.09	0.13	0.03	0.01	0.00
Cr_2O_3	0.49	0.27	0.35	0.29	0.35	0.38	0.34	0.47	0.56	0.33	0.61	0.18	0.18	0.17
NiO	0.10	0.09	0.11	0.07	0.10	0.08	0.08	0.10	0.09	0.07	0.12	0.08	0.15	0.15
Total	99.59	99.00	99.18	99.37	99.64	99.63	99.69	99.09	99.84	99.06	98.95	99.34	100.34	99.72
$Mg^{\#}$	0.926	0.933	0.926	0.927	0.921	0.931	0.932	0.934	0.933	0.935	0.933	0.928	0.857	0.857
Formulae based on four cations														
Si	1.952	1.953	1.961	1.962	1.956	1.959	1.960	1.940	1.934	1.946	1.948	1.963	1.955	1.948
Ti	0.002	0.002	0.002	0.002	0.002	0.001	0.001	0.001	0.002	0.000	0.001	0.002	0.001	0.001
Al	0.049	0.039	0.043	0.040	0.050	0.038	0.039	0.046	0.054	0.037	0.049	0.039	0.045	0.048
Fe	0.144	0.132	0.145	0.165	0.154	0.135	0.133	0.130	0.131	0.128	0.130	0.143	0.282	0.283
Mn	0.004	0.003	0.003	0.003	0.004	0.003	0.004	0.003	0.003	0.003	0.003	0.003	0.004	0.004
Mg	1.797	1.849	1.816	1.810	1.787	1.831	1.834	1.839	1.818	1.856	1.814	1.832	1.695	1.699
Ca	0.026	0.008	0.013	0.008	0.025	0.012	0.011	0.014	0.030	0.012	0.027	0.008	0.008	0.008
Na	0.009	0.002	0.006	0.001	0.009	0.006	0.005	0.010	0.010	0.006	0.009	0.002	0.000	0.000
Cr	0.013	0.007	0.010	0.006	0.010	0.010	0.009	0.013	0.015	0.009	0.017	0.005	0.005	0.005
Ni	0.003	0.002	0.003	0.002	0.003	0.002	0.002	0.003	0.002	0.002	0.003	0.002	0.004	0.004
O	5.979	5.977	5.984	5.989	5.983	5.980	5.981	5.966	5.965	5.965	5.976	5.984	5.979	5.975

Table 2-5
Representative analyses of clinopyroxenes (analytical procedure as in Table 2-3)

Sample	NK1-5	NK2-3	NK2-10	NK3-20	NK3-25	NK1-2	NK1-3	NK1-6	NK1-7	NK1-17	NK1-18	NK2-7	NK3-1	NK3-17
Rock	Lherz	Lherz	Lherz	Lherz	Lherz	Harz	Harz	Harz	Harz	Harz	Harz	Pyrox	Pyrox	Pyrox
SiO_2	53.68	53.45	53.44	54.08	54.14	53.89	54.19	54.07	54.11	54.11	53.65	53.65	53.99	53.02
TiO_2	0.16	0.21	0.17	0.20	0.17	0.13	0.13	0.13	0.08	0.04	0.07	0.16	0.08	0.09
Al_2O_3	2.48	2.89	3.08	2.67	2.61	2.74	2.98	3.70	2.36	2.26	2.25	2.70	1.73	1.80
FeO	2.64	1.96	2.34	2.28	2.70	2.25	2.31	2.35	2.34	2.08	2.32	1.95	3.12	3.04
MnO	0.10	0.05	0.09	0.06	0.10	0.08	0.09	0.07	0.08	0.07	0.07	0.05	0.06	0.05
MgO	17.46	15.80	15.58	16.15	17.74	16.07	15.84	14.91	18.07	16.39	17.46	16.02	16.82	16.60
CaO	18.79	20.91	19.23	21.74	19.12	19.67	19.14	17.20	18.68	20.51	19.06	21.86	23.61	23.59
Na_2O	1.79	2.06	2.40	1.65	1.66	2.20	2.46	3.36	1.61	1.85	1.78	1.58	0.63	0.50
Cr_2O_3	1.99	1.96	2.30	1.46	1.52	2.22	2.27	3.26	1.77	1.87	2.34	1.15	0.45	0.37
NiO	0.05	0.04	0.04	0.04	0.06	0.04	0.04	0.04	0.06	0.04	0.08	0.05	0.08	0.09
Total	99.17	99.34	98.68	100.33	99.86	99.32	99.46	99.11	99.22	99.26	99.13	99.19	100.59	99.17
$Mg^{\#}$	0.922	0.935	0.922	0.927	0.921	0.927	0.924	0.919	0.932	0.934	0.931	0.936	0.906	0.907
Formulae based on four cations														
Si	1.947	1.936	1.951	1.947	1.949	1.954	1.961	1.960	1.958	1.965	1.947	1.952	1.949	1.943
Ti	0.004	0.005	0.005	0.005	0.005	0.004	0.004	0.004	0.002	0.001	0.002	0.004	0.002	0.003
Al	0.106	0.117	0.132	0.113	0.111	0.117	0.127	0.158	0.101	0.097	0.096	0.116	0.074	0.078
Fe	0.080	0.061	0.071	0.069	0.081	0.068	0.070	0.071	0.071	0.063	0.070	0.059	0.094	0.093
Mn	0.003	0.002	0.003	0.002	0.003	0.003	0.003	0.002	0.003	0.002	0.002	0.002	0.002	0.002
Mg	0.944	0.865	0.848	0.867	0.952	0.869	0.855	0.806	0.975	0.887	0.945	0.869	0.905	0.907
Ca	0.730	0.822	0.752	0.839	0.737	0.764	0.742	0.668	0.724	0.798	0.741	0.852	0.913	0.926
Na	0.126	0.137	0.170	0.115	0.116	0.155	0.172	0.236	0.113	0.131	0.125	0.111	0.044	0.036
Cr	0.057	0.053	0.066	0.042	0.043	0.064	0.065	0.094	0.051	0.054	0.067	0.033	0.013	0.011
Ni	0.001	0.001	0.001	0.001	0.002	0.001	0.001	0.001	0.002	0.001	0.002	0.001	0.002	0.003
O	5.967	5.961	5.970	5.971	5.969	5.970	5.973	5.970	5.976	5.973	5.965	5.973	5.971	5.970

Table 2-6
Representative analyses of garnets (analytical procedure as in Table 2-3)

Sample Rock	NK1-5 Lherz	NK2-3 Lherz	NK2-10 Lherz	NK3-20 Lherz	NK3-25 Lherz	NK1-2 Harz	NK1-3 Harz	NK1-6 Harz	NK1-7 Harz	NK1-17 Harz	NK1-18 Harz	NK2-7 Pyrox	NK3-1 Pyrox	NK3-17 Pyrox
SiO_2	41.35	41.34	41.42	42.01	41.84	41.91	41.65	41.51	41.46	41.38	41.05	41.67	40.67	40.53
TiO_2	0.25	0.08	0.09	0.07	0.32	0.09	0.09	0.08	0.14	0.02	0.13	0.04	0.05	0.09
Al_2O_3	18.92	21.44	21.27	22.56	20.76	20.04	19.70	20.58	20.29	20.78	18.51	23.35	22.00	22.49
FeO	6.89	7.85	7.57	9.38	7.23	7.15	7.27	6.86	6.24	7.01	6.36	8.11	14.89	14.88
MnO	0.38	0.48	0.41	0.46	0.33	0.45	0.48	0.38	0.30	0.42	0.32	0.48	0.60	0.56
MgO	20.52	19.53	20.01	19.03	20.11	20.48	20.23	20.66	20.67	19.88	19.79	20.11	14.63	14.97
CaO	5.11	5.28	5.07	4.80	5.02	5.05	5.22	4.62	5.22	5.45	5.94	4.65	5.88	6.07
Na_2O	0.03	0.03	0.03	0.01	0.03	0.02	0.02	0.03	0.02	0.04	0.02	0.01	0.01	0.01
Cr_2O_3	4.78	3.21	3.74	1.92	3.71	3.99	4.29	4.42	4.76	4.12	6.77	1.49	1.32	1.27
NiO	0.01	0.01	0.02	0.01	0.01	0.00	0.00	0.01	0.02	0.01	0.02	0.00	0.00	0.00
Total	98.22	99.27	99.63	100.27	99.38	99.18	98.97	99.16	99.12	99.14	98.92	99.93	100.05	100.89
$Mg^\#$	0.842	0.816	0.825	0.783	0.832	0.836	0.832	0.843	0.855	0.835	0.847	0.815	0.637	0.642
Formulae based on eight cations														
Si	3.012	2.978	2.971	3.001	3.009	3.017	3.011	2.985	2.983	2.983	2.990	2.960	2.991	2.950
Ti	0.014	0.004	0.005	0.004	0.017	0.005	0.005	0.004	0.008	0.001	0.007	0.002	0.003	0.005
Al	1.624	1.821	1.798	1.900	1.760	1.701	1.679	1.745	1.720	1.766	1.589	1.955	1.907	1.929
Fe	0.419	0.473	0.454	0.561	0.435	0.431	0.440	0.413	0.375	0.423	0.387	0.482	0.916	0.906
Mn	0.023	0.029	0.025	0.028	0.020	0.028	0.030	0.023	0.018	0.026	0.020	0.029	0.037	0.034
Mg	2.228	2.098	2.140	2.027	2.156	2.198	2.181	2.216	2.217	2.137	2.149	2.131	1.604	1.625
Ca	0.399	0.408	0.390	0.367	0.387	0.389	0.404	0.356	0.402	0.421	0.464	0.354	0.463	0.474
Na	0.005	0.004	0.004	0.002	0.004	0.003	0.003	0.004	0.003	0.005	0.003	0.002	0.001	0.001
Cr	0.275	0.183	0.212	0.108	0.211	0.227	0.245	0.251	0.271	0.235	0.390	0.083	0.077	0.073
Ni	0.000	0.001	0.001	0.000	0.001	0.000	0.000	0.001	0.001	0.000	0.001	0.000	0.000	0.000
O	11.972	11.981	11.979	12.007	12.008	11.983	11.976	11.985	11.982	11.976	11.984	11.978	11.983	11.955

Table 2-7
Temperature and pressure estimates

Sample	Rock	Texture	Two-Pyrox Brey &Köhler (1990)	Al-in-Opx MacGregor (1974)	Two-Pyrox Finnerty & Boyd (1987)	Al-in-Opx MacGregor (1974)
			Temp (°C)	P (kb)	Temp (°C)	P (kb)
NK1-5	Lherz	coarse	1261	54.5	1125	46.3
NK1-14	Lherz	coarse	1026	42.5	933	36.7
NK1-23	Lherz	coarse	632	18.3	670	20.7
NK2-3	Lherz	coarse	761	26.6	710	23.4
NK2-10	Lherz	coarse	1001	40.8	901	34.5
NK3-4	Lherz	coarse	1237	51.7	1124	44.9
NK3-15	Lherz	coarse	1218	51.1	1103	44.2
NK3-20	Lherz	coarse	819	31.0	638	19.5
NK3-22	Lherz	porphyr	762	22.6	651	16.1
NK3-24	Lherz	coarse	738	23.1	646	17.5
NK3-25	Lherz	coarse	1260	53.9	1121	45.5
NK1-1	Harz	coarse	1186	49.2	1080	44.0
NK1-2	Harz	coarse	1045	44.7	935	37.7
NK1-3	Harz	coarse	1070	46.1	962	39.3
NK1-4	Harz	coarse	878	33.9	832	31.1
NK1-6	Harz	coarse	1144	48.8	1029	41.8
NK1-7	Harz	porphyr	1293	54.8	1162	46.9
NK1-9	Harz	coarse	1132	48.0	1058	43.5
NK1-12	Harz	coarse	1054	45.3	980	40.6
NK1-13	Harz	coarse	1267	63.8	1147	55.9
NK1-15	Harz	coarse	1132	48.4	1022	41.6
NK1-17	Harz	coarse	1007	43.2	926	38.1
NK1-18	Harz	coarse	1215	52.0	1103	45.2
NK3-18	Harz	coarse	1197	56.1	1067	47.7
NK2-7	Pyrox	coarse	713	23.8	606	17.0
NK3-19	Pyrox	coarse	1033	44.3	949	38.9
NK3-1	Pyrox	coarse	739	23.2	-	-
NK3-17	Pyrox	coarse	657	18.4	-	-

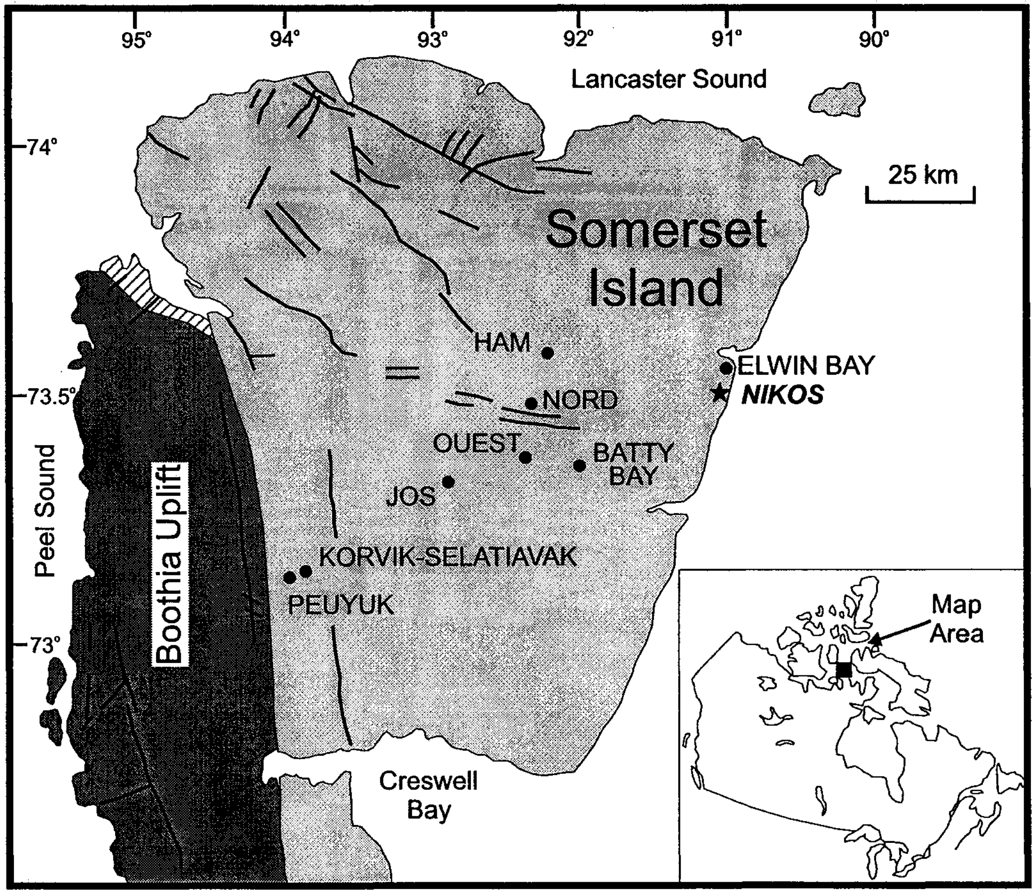
95°
94°
93°
92°
91°
90°
Lancaster Sound
74°
25 km
Somerset Island
HAM
ELWIN BAY
NIKOS
73.5°
NORD
OUEST
BATTY BAY
JOS
Peel Sound
Boothia Uplift
KORVIK-SELATIAVAK
PEUYUK
73°
Map Area
Creswell Bay

Figure 2-1

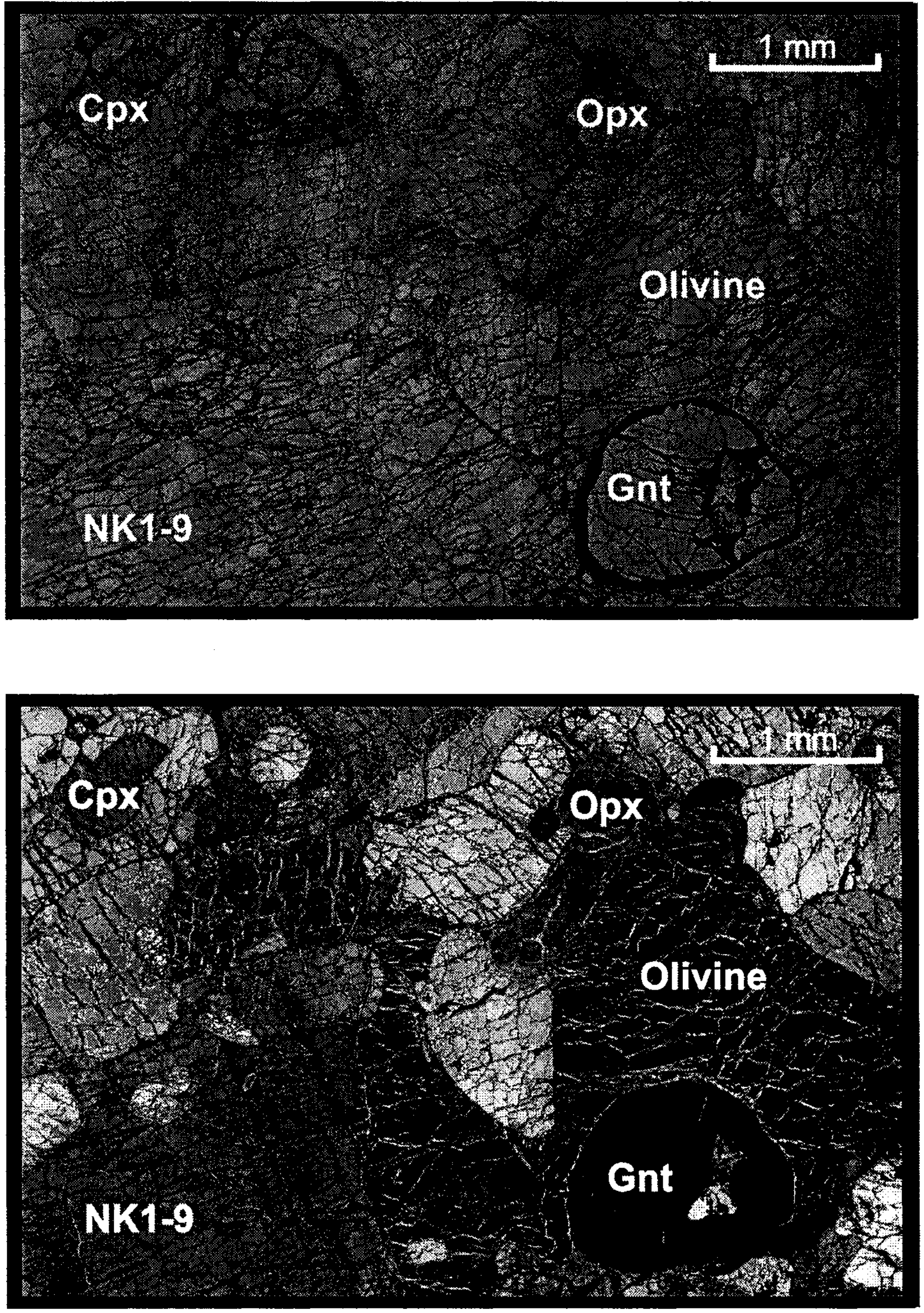

Figure 2-2a

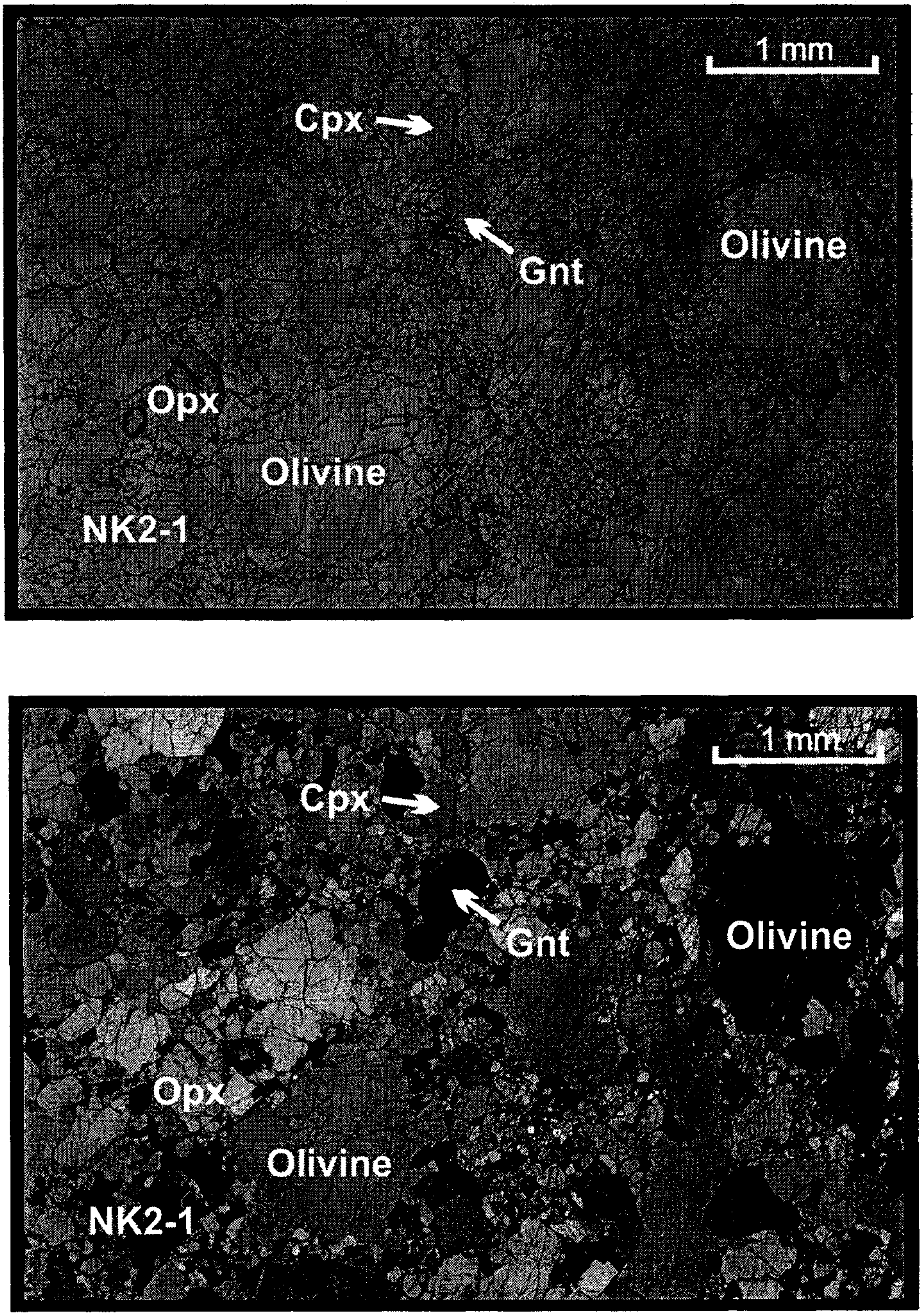
1 mm
Cpx
Gnt
Olivine
Opx
Olivine
NK2-1
1 mm
Cpx
Gnt
Olivine
Opx
Olivine
NK2-1

Figure 2-2b

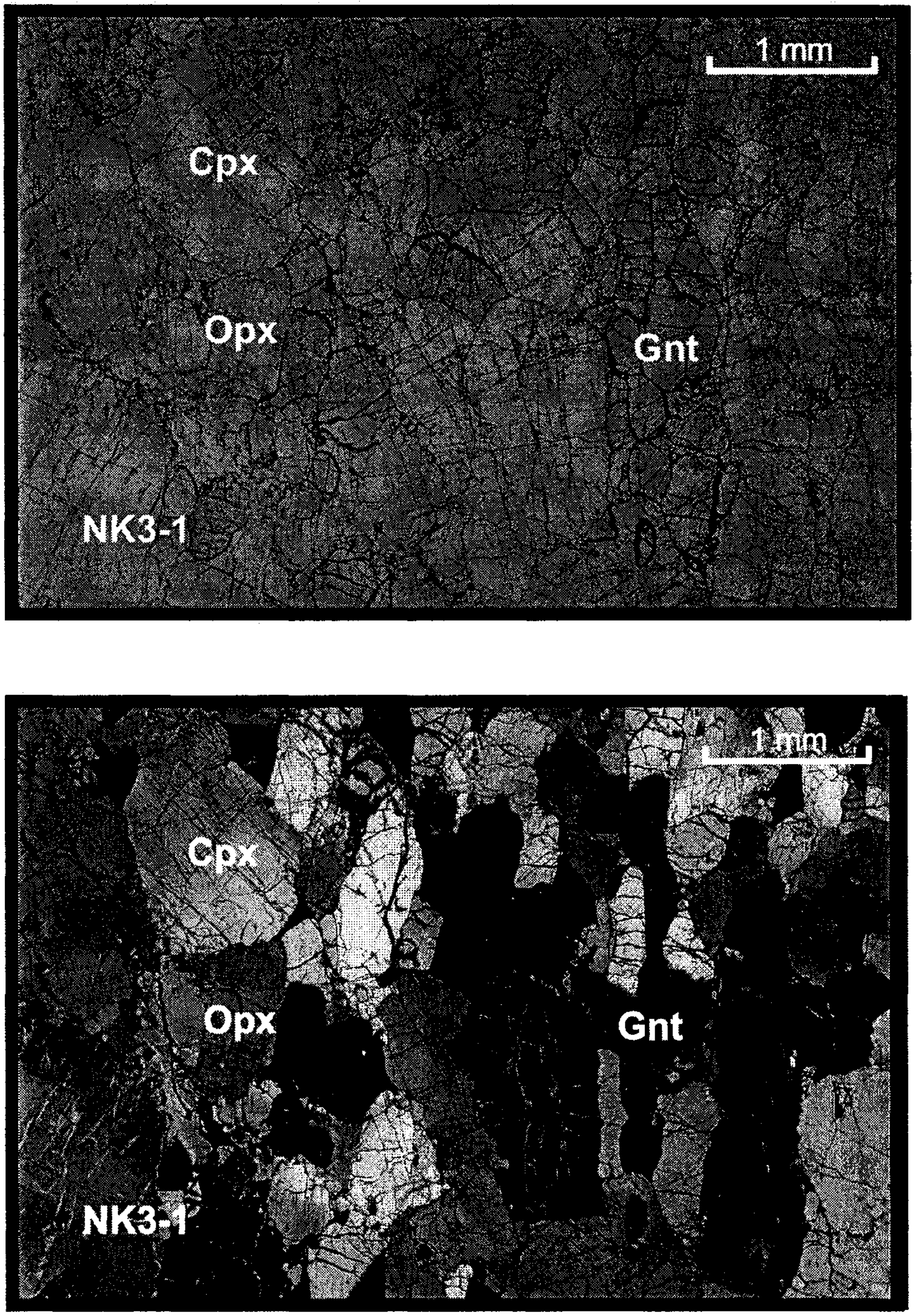

Figure 2-2c

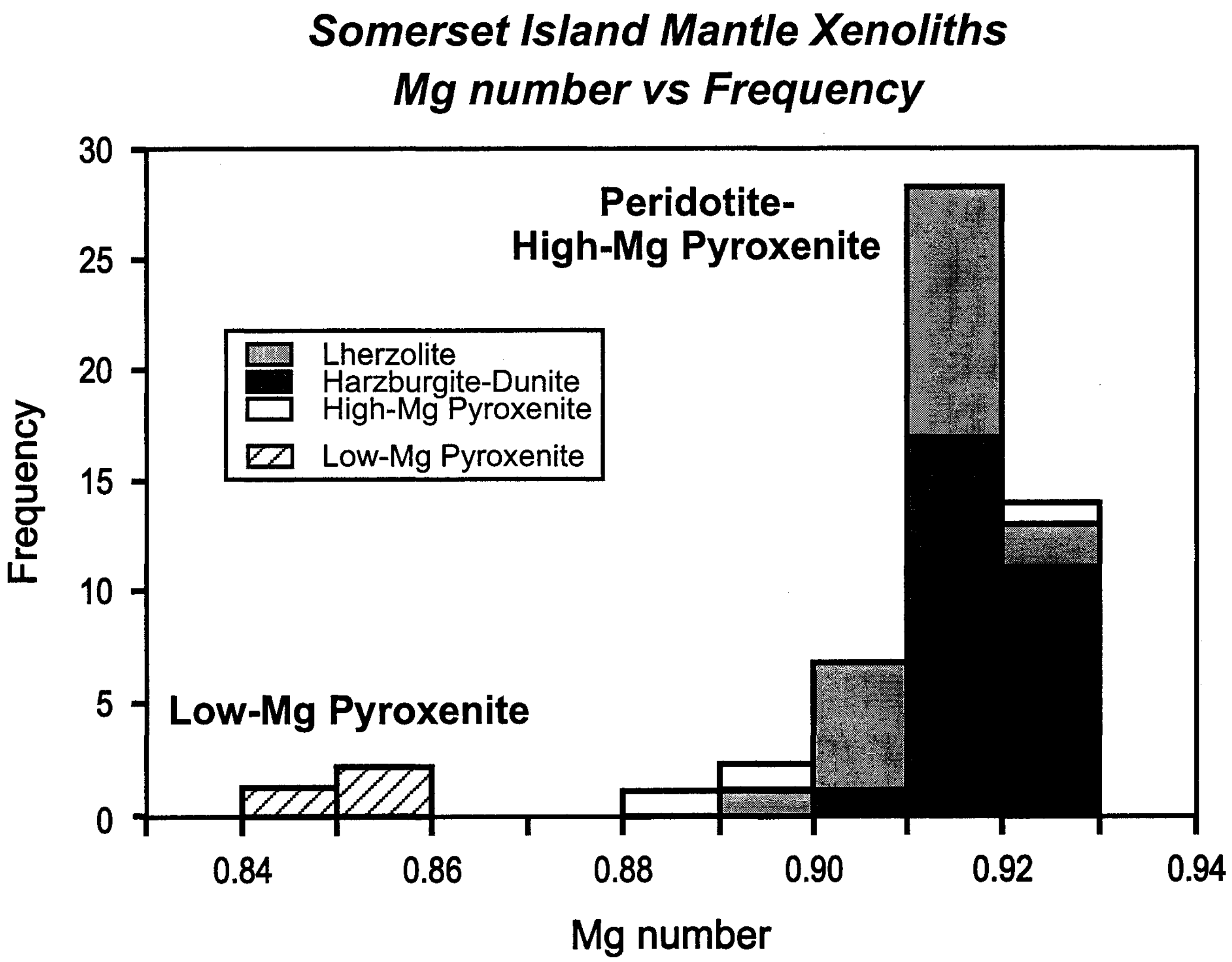

Somerset Island Mantle Xenoliths
Mg number vs Frequency
Peridotite-
High-Mg Pyroxenite
Lherzolite
Harzburgite-Dunite
High-Mg Pyroxenite
Low-Mg Pyroxenite
Low-Mg Pyroxenite
Frequency
0
5
10
15
20
25
30
0.84
0.86
0.88
0.90
0.92
0.94
Mg number

Figure 2-3

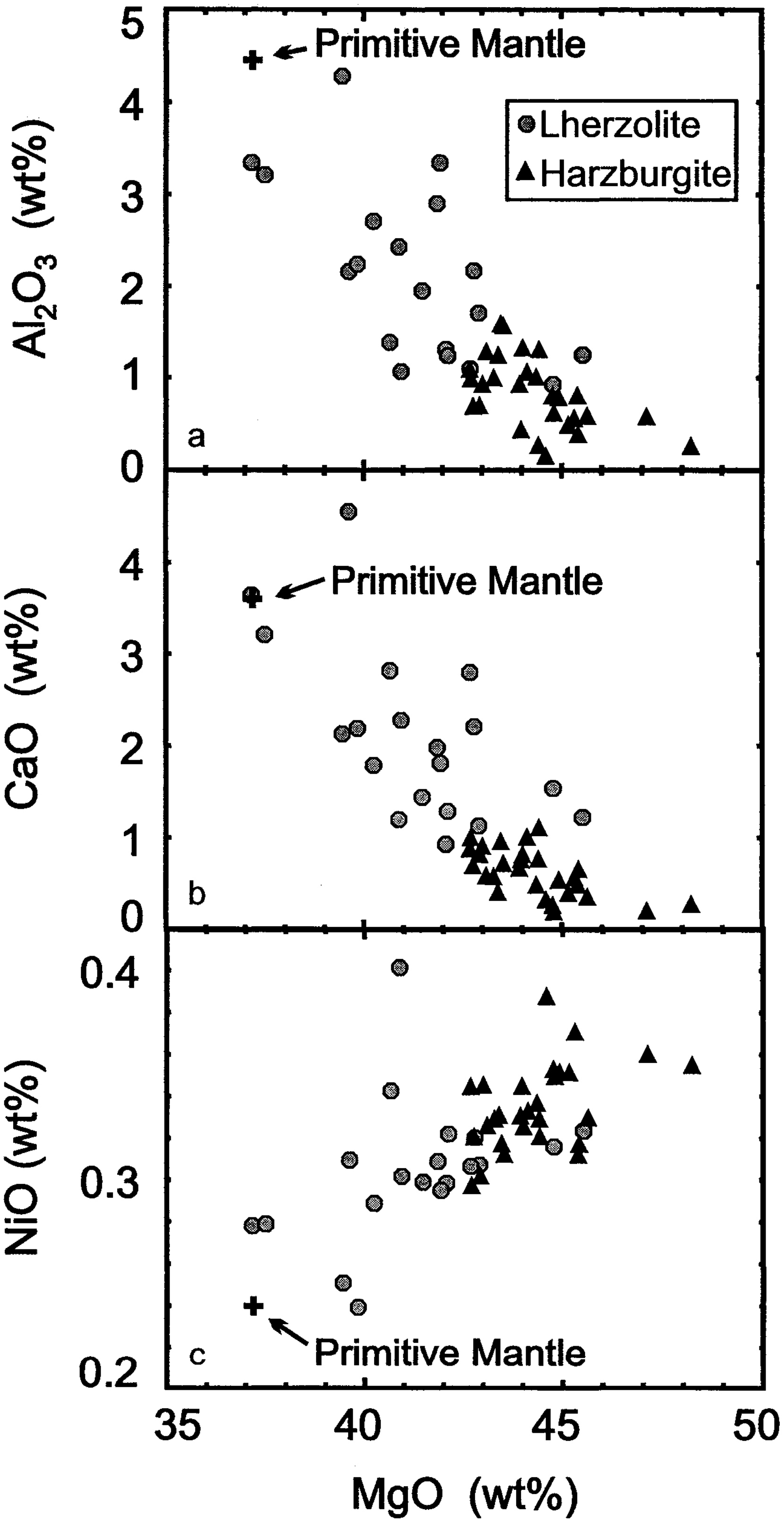
Primitive Mantle
Lherzolite
Harzburgite
Al$_2$O$_3$ (wt%)
5
4
3
2
1
0
a
Primitive Mantle
CaO (wt%)
4
3
2
1
0
b
Primitive Mantle
NiO (wt%)
0.4
0.3
0.2
c
35
40
45
50
MgO (wt%)

Figure 2-4

Somerset Island and Cordilleran Peridotite Mantle Xenoliths

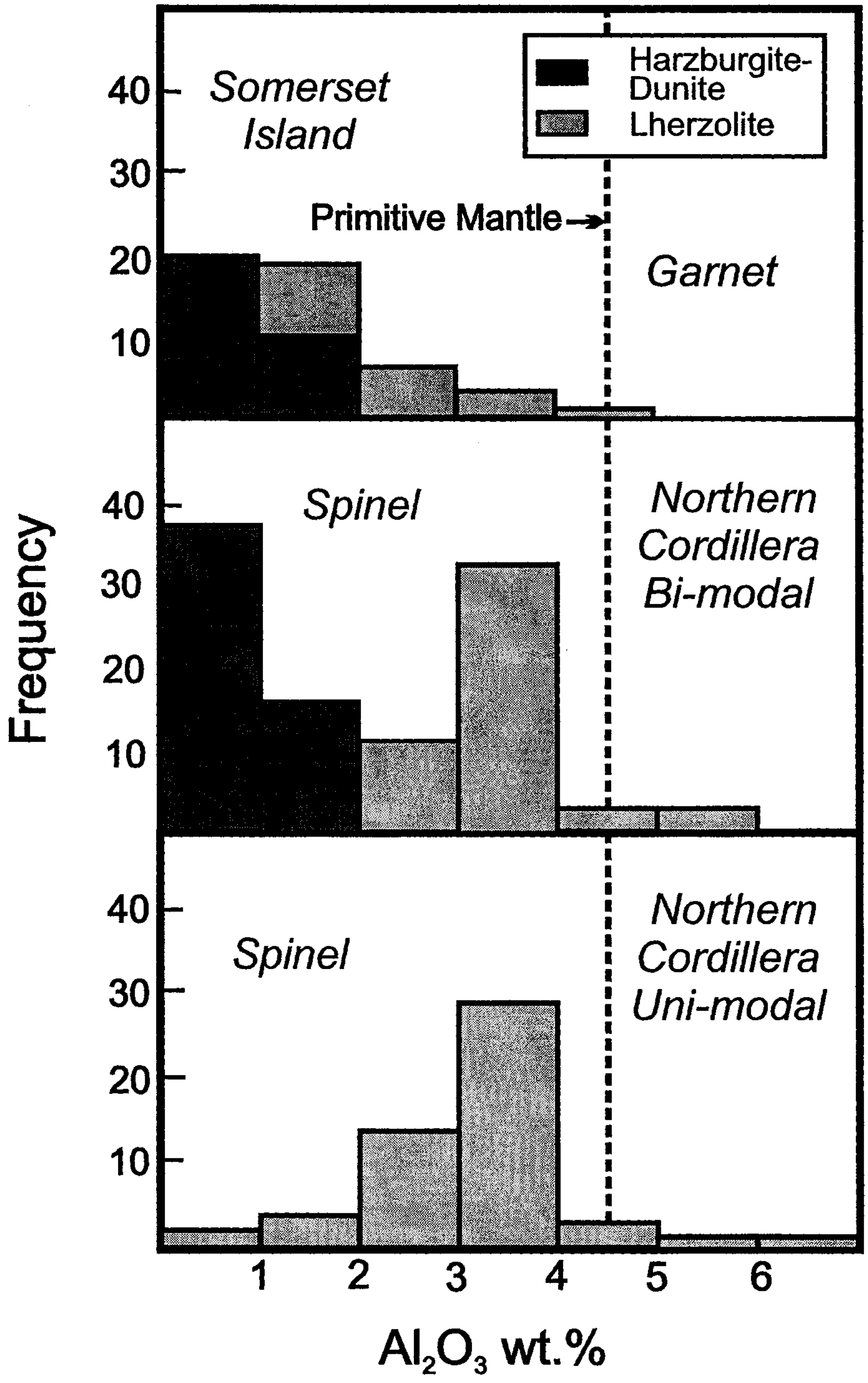

Figure 2-5

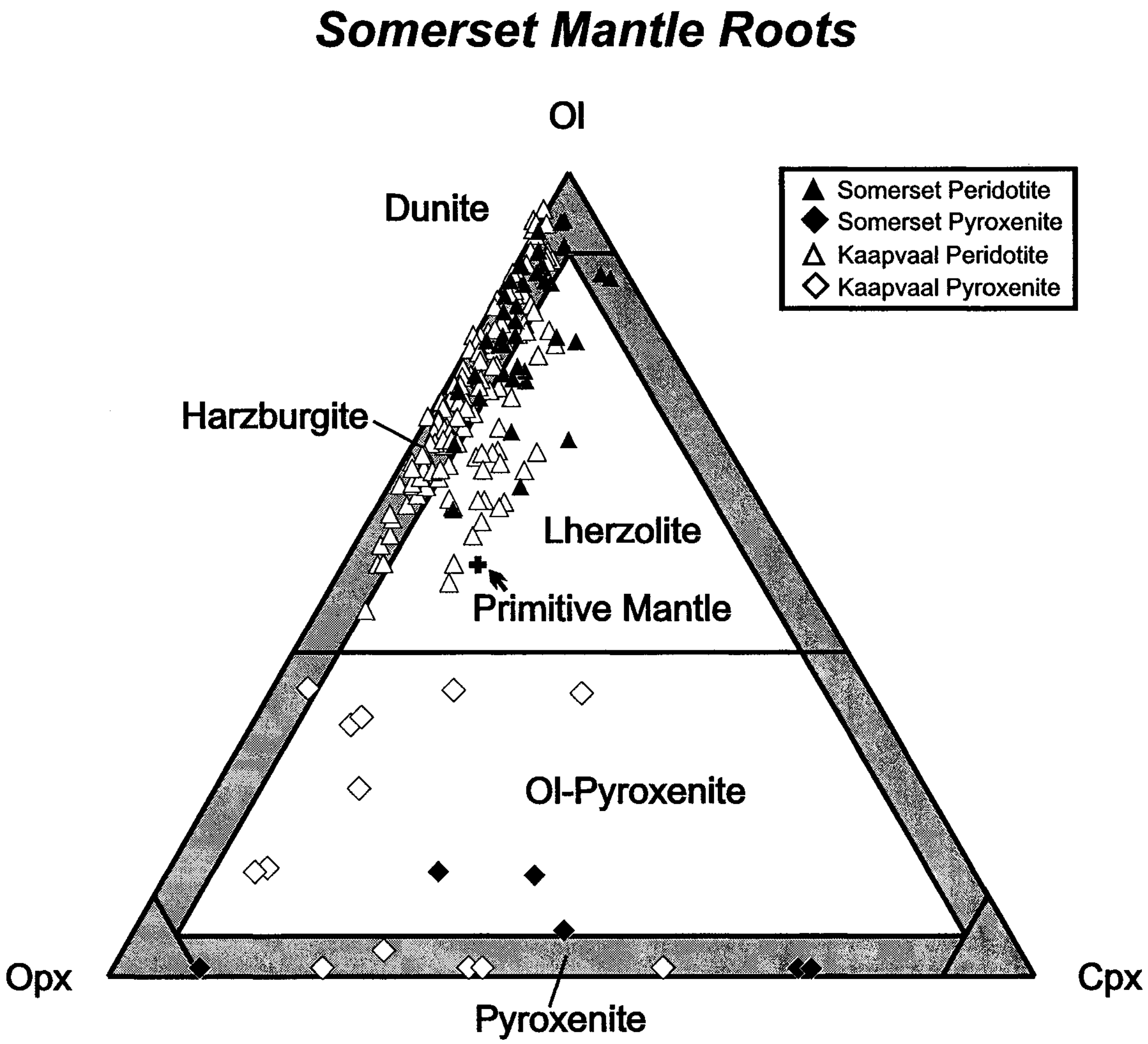
Somerset Mantle Roots
Ol
Dunite
Harzburgite
Lherzolite
Primitive Mantle
Ol-Pyroxenite
Pyroxenite
Opx
Cpx
▲ Somerset Peridotite
◆ Somerset Pyroxenite
△ Kaapvaal Peridotite
◇ Kaapvaal Pyroxenite

Figure 2-6

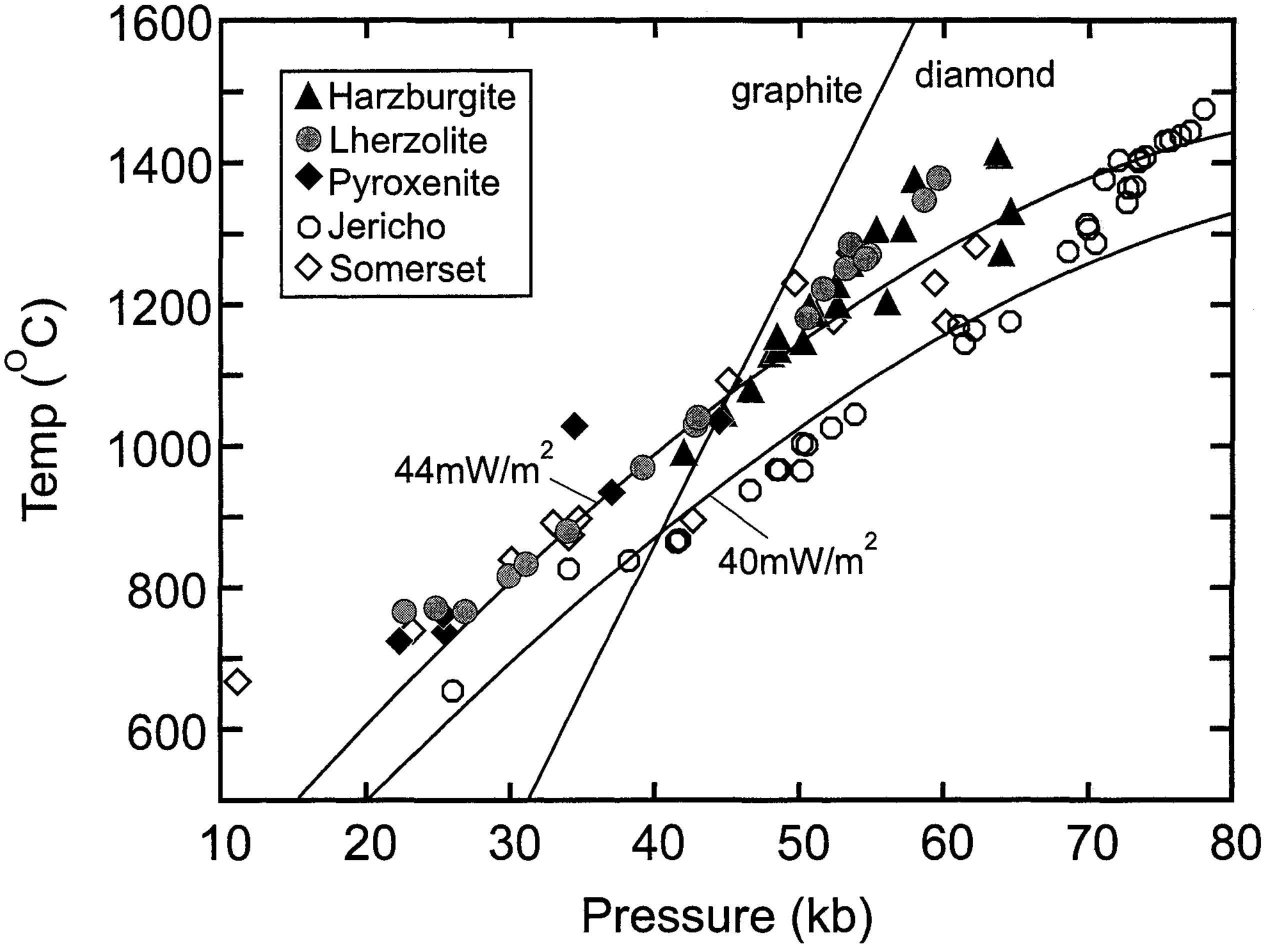

▲ Harzburgite
● Lherzolite
◆ Pyroxenite
○ Jericho
◇ Somerset
graphite
diamond
44mW/m²
40mW/m²
Temp (°C)
Pressure (kb)
1600
1400
1200
1000
800
600
10
20
30
40
50
60
70
80

Figure 2-7

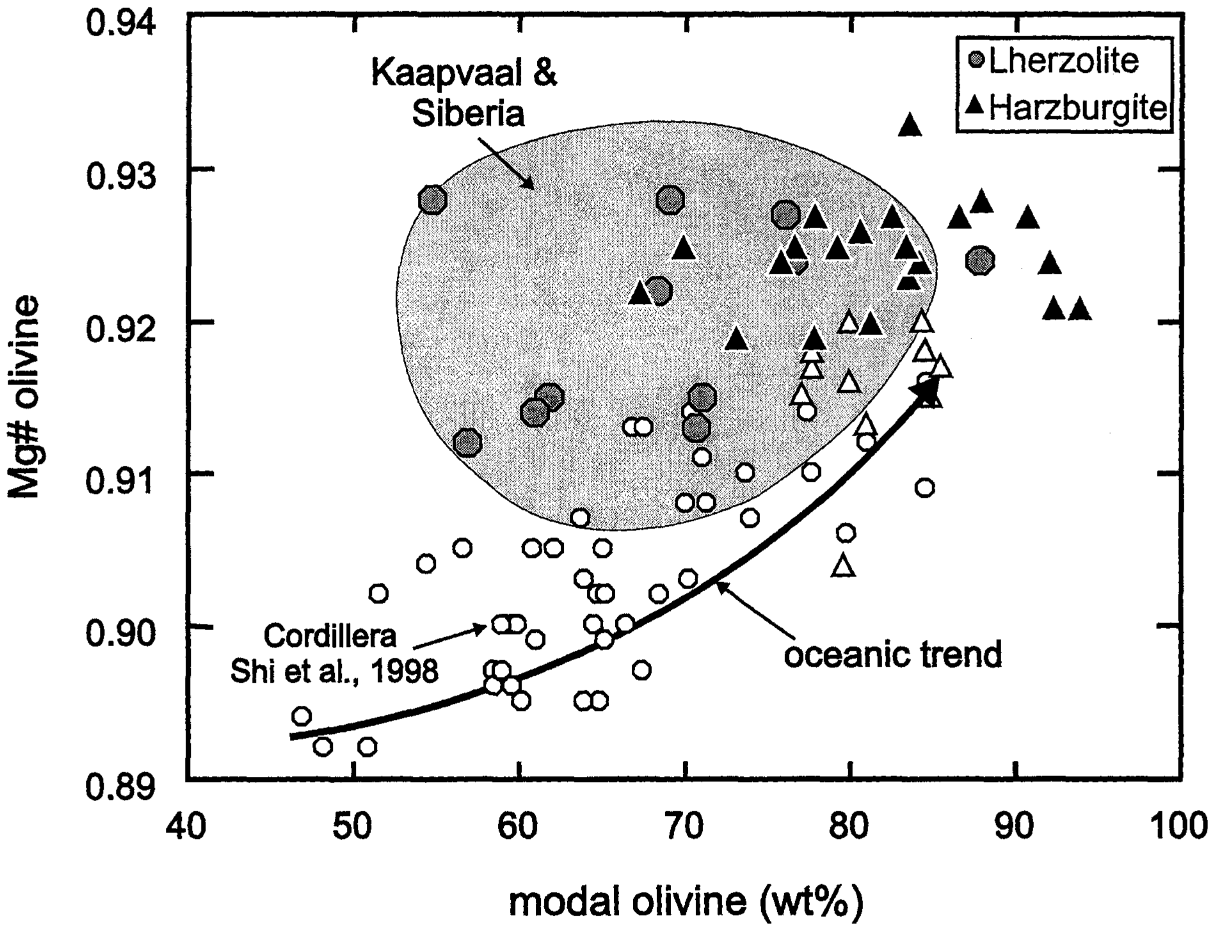

0.94
0.93
0.92
0.91
0.90
0.89
Mg# olivine
40
50
60
70
80
90
100
modal olivine (wt%)
Lherzolite
Harzburgite
Kaapvaal & Siberia
Cordillera Shi et al., 1998
oceanic trend

Figure 2-8

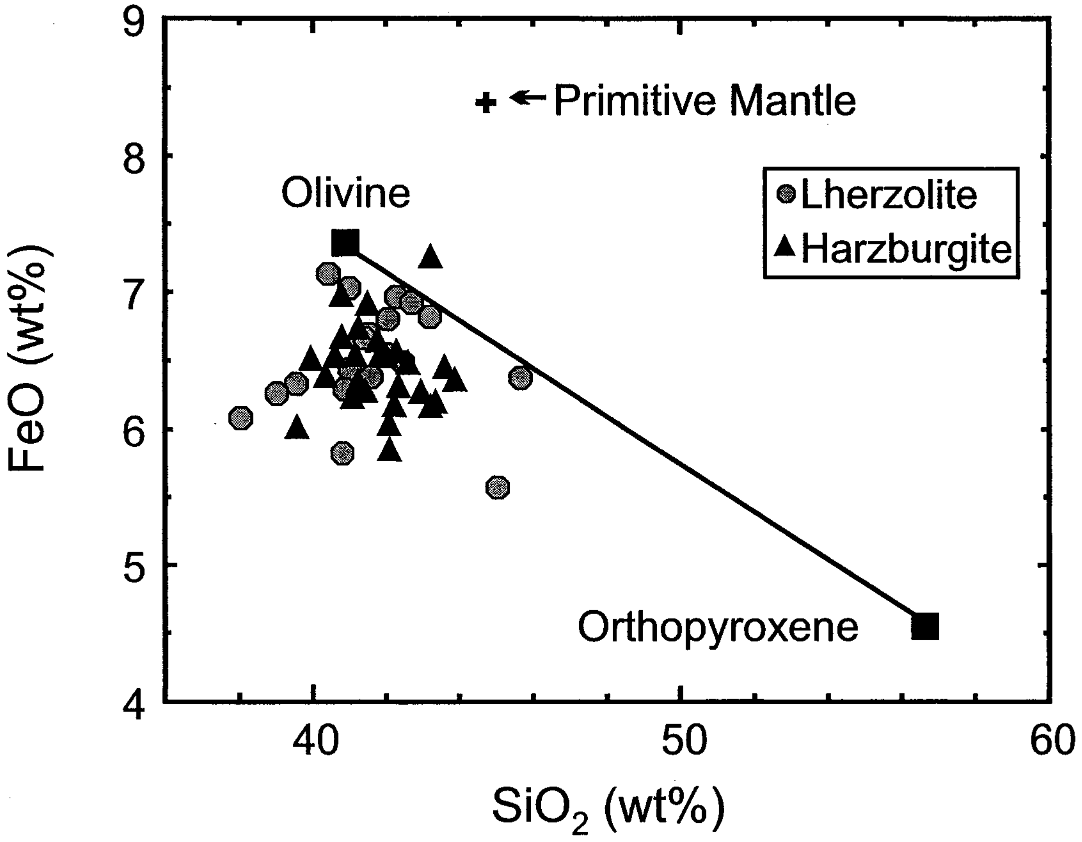
9
8
7
6
5
4
FeO (wt%)
40
50
60
SiO$_2$ (wt%)
Primitive Mantle
Olivine
Orthopyroxene
Lherzolite
Harzburgite

Figure 2-9

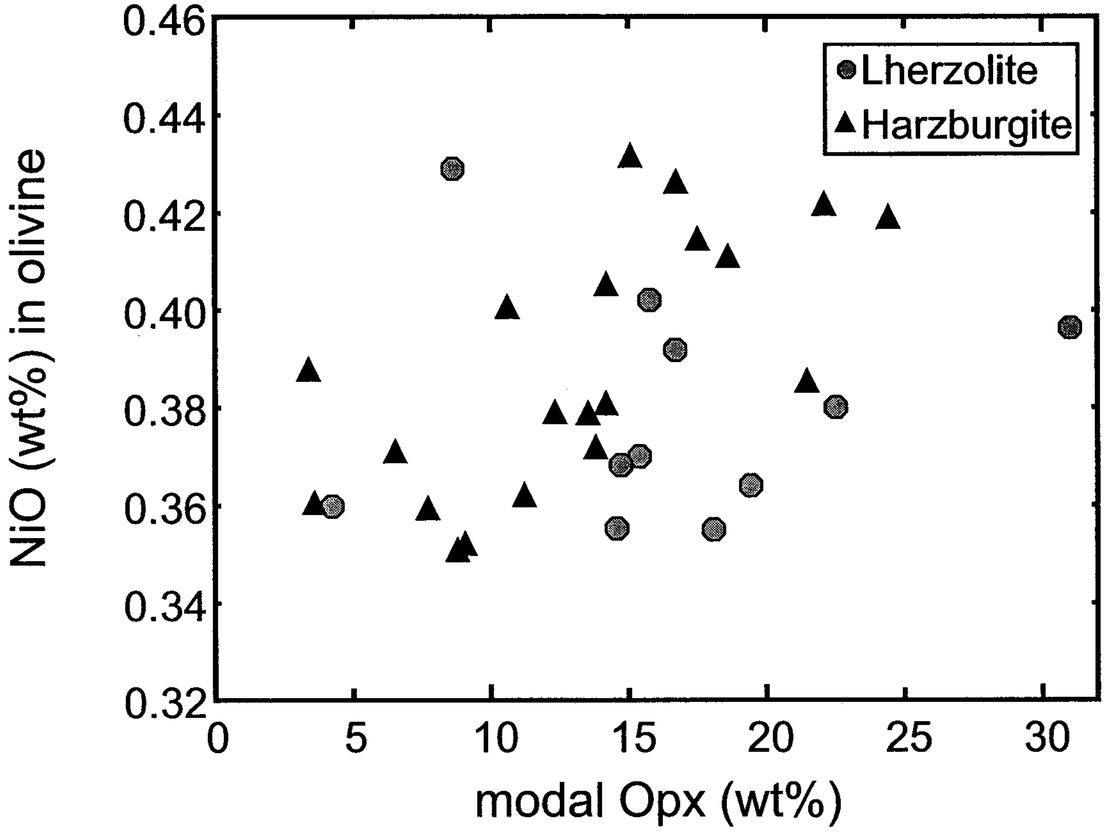
0.46
0.44
0.42
0.40
0.38
0.36
0.34
0.32
NiO (wt%) in olivine
0
5
10
15
20
25
30
modal Opx (wt%)
Lherzolite
Harzburgite

Figure 2-10

CHAPTER 3

Constraints on the trace element composition of the Archean mantle root beneath Somerset Island, Arctic Canada

ABSTRACT

Peridotites that sample Archean mantle roots are frequently incompatible trace element enriched despite their refractory major element compositions. To constrain the trace element budget of the lithosphere beneath the Canadian craton, trace element and rare earth element (REE) abundances were determined for a suite of garnet-peridotites and garnet-pyroxenites from the Nikos kimberlite pipe on Somerset Island, Canadian Arctic, their constituent garnet and clinopyroxene, and the host kimberlite. These refractory mantle xenoliths are depleted in fusible major elements, but enriched in incompatible trace elements, such as large ion lithophile elements (LILE), Th, U and light rare earth elements (LREE). Mass balance calculations based on modal abundances of clinopyroxene and garnet and their respective REE contents yield discrepancies between calculated and analyzed REE contents for the Nikos bulk rocks that amount to LREE deficiencies of 70 to 99%, suggesting the presence of small amounts of interstitial kimberlite liquid (0.4 to 2 wt%) to account for the excess LREE abundances. These results indicate that the peridotites had in fact depleted or flat LREE patterns before contamination by their host kimberlite. LREE and Sr enrichment in clinopyroxene and low Zr and Sr abundances in garnet in low temperature peridotites (800 to 1100 °C) compared to high temperature peridotites (1200 to 1400 °C) suggest that the shallow lithosphere is geochemically distinct from the deep lithosphere beneath the northern margin of the Canadian craton. The Somerset mantle root appears to be characterized by a depth zonation that may date from the time of its stabilization in the Archean.

Key words: Canada; mantle; metasomatism; peridotite; trace elements

INTRODUCTION

The mantle underlying many Archean cratons has anomalously high seismic velocities to depths of 350 to 400 km (Jordan, 1988; Grand, 1994), indicating the presence of cold refractory roots, depleted in the fusible major elements compared to fertile mantle (Boyd & Mertzman, 1987; McDonough, 1990). These deep residual peridotite roots probably contribute to the stability of Archean continental lithosphere because of their lower density and higher viscosity compared to that of the surrounding asthenospheric mantle (Boyd & McCallister, 1976; Jordan, 1979; Pollack, 1986). Mantle xenoliths that are hosted by kimberlites and alkaline basalts are our only window into the subcontinental lithosphere. They provide essential evidence on the chemical composition and evolution of the upper mantle to depths of greater than 200 km. Studies of these mantle xenoliths enable us to characterize the abundance and distribution of major, minor and trace elements in peridotites and between their constituent minerals. Most subcratonic peridotite samples have undergone a complex history of melt extraction that has changed their chemical composition and resulted in depletion of the residual mantle in fusible major elements such as Fe, Al and Ca (e.g. Nixon, 1987; Herzberg, 1993; Boyd *et al.*, 1997). In contrast to their depletion in incompatible major elements, however, many peridotite xenoliths have unexpectedly high abundances of incompatible trace elements, such as large ion lithophile elements (LILE) and light rare earth elements (LREE; Erlank *et al.*, 1987; Menzies *et al.*, 1987). Although these findings have been widely interpreted to indicate that the lithospheric mantle has been affected by interaction with incompatible element enriched percolating melts or fluids over time (Hawkesworth *et al.*, 1983; Menzies & Hawkesworth, 1987), it is important to establish the chemical nature of these metasomatic agents and whether metasomatism is an ancient feature or associated with the kimberlite magmatic event itself.

Previous studies on Somerset Island peridotites have shown that Re-Os isotope systematics for these xenoliths yield Re depletion ages of up to 2.7 Ga (Irvine *et al.*, 1999), indicating the existence of Archean lithospheric mantle underneath the northern margin of the Canadian craton. In this study, we present trace element and rare earth element (REE) data for a suite of garnet-peridotites and garnet-pyroxenites, constituent garnet and clinopyroxene, and the host kimberlite from the Nikos kimberlite pipes on Somerset Island, in the southern Canadian Arctic (Fig. 1). The geochemical data provide information on mantle depletion and constraints on incompatible trace element enrichment during metasomatism following melt extraction. REE distribution patterns for constituent garnet and clinopyroxene give insights into trace element partitioning and are used to constrain the change in chemical composition of the refractory mantle root with depth. Models of trapped liquid compositions along grain boundaries indicate that the Nikos kimberlite probably acted as the metasomatic agent during sample entrainment.

SAMPLES AND PROCEDURES

Kimberlite

The recently discovered Cretaceous (100 Ma) Nikos kimberlite (Heaman, 1989; Smith *et al.*, 1989; Pell, 1993; Fig. 1) consists of three individual pipes that are described in more detail in Schmidberger & Francis (1999). The Nikos kimberlites were emplaced into late Archean crystalline basement overlain by Paleozoic cover rocks of the northern margin of the Canadian craton (Steward, 1987; Frisch & Hunt, 1993). Although it has been argued that Somerset Island is part of the Proterozoic Innuitian tectonic province (Trettin *et al.*, 1972), late Archean Re depletion ages for other Somerset Island peridotite xenoliths (Irvine *et al.*, 1999) indicate the presence of an Archean mantle root beneath the southern Canadian Arctic.

The southernmost Nikos kimberlite pipe (NK3) is characterized by a non-brecciated, magmatic texture, and appears to represent kimberlite liquid (Schmidberger & Francis, 1999). The magmatic kimberlite exhibits a porphyritic microcrystalline texture, consisting of phenocrysts of olivine, phlogopite and spinel in a very fine-grained carbonate-rich matrix of calcite, serpentine, perovskite and apatite. Calcite occurs as aggregates of tabular sub-parallel crystals showing flow texture around larger olivine phenocrysts, which has been interpreted to be a primary magmatic feature (Schmidberger & Francis, 1999). Crushed whole-rock kimberlite samples were carefully handpicked under the binocular microscope prior to grinding to eliminate contamination from xenocrysts and country rock fragments.

Mantle xenoliths

The mantle xenolith suite for this study consists of large (10 to 30 cm), well-preserved garnet-peridotites and lesser garnet-pyroxenites, thirty of which were analyzed for their major and trace element and REE contents in this study (Tables 2 and 3). The majority of the Nikos peridotites show coarse textures, typical of mantle xenoliths, with large crystals of olivine, orthopyroxene, clinopyroxene and garnet, although a few xenoliths with porphyroclastic textures are observed. Small differences in modal clinopyroxene contents do not justify dividing the suite according to the IUGS classification into harzburgitic (clinopyroxene <5 wt%) and lherzolitic (clinopyroxene >5 wt%) rock types, and the more general term peridotite is preferred for the xenoliths in the present study. A detailed description of mineralogy and petrology of the mantle xenoliths can be found in Schmidberger & Francis (1999). Whole-rock analyses of the peridotite xenoliths are strongly depleted in fusible major elements such as Fe, Al and Ca when compared to primitive mantle compositions (McDonough, 1990; Schmidberger & Francis, 1999; Table 2). High magnesium numbers (mg-number=Mg/(Mg+Fe)) between 0.90 to 0.93 and their refractory olivine-rich mineralogy confirm the depleted nature of these peridotites (Table 2). The Somerset whole-rock characteristics are similar to those for kimberlite-hosted peridotites from the Canadian Slave province (Kopylova *et al.*, 1999; MacKenzie & Canil, 1999), and a detailed comparison of both xenolith suites can be found in Schmidberger & Francis (1999). Temperature and pressure estimates of last equilibration for the Nikos xenoliths (800 to 1400 °C and 25 to 60 kb) suggest that the peridotites were entrained from depths between 80 to 190 km (Schmidberger & Francis, 1999; Table 2).

The pyroxenites contain large crystals of clinopyroxene and orthopyroxene, and smaller crystals of garnet. These pyroxene-rich rocks have a range of mg-numbers (Schmidberger & Francis, 1999; Table 2). The high-Mg pyroxenites contain olivine and abundant garnet (15 to 25 wt%) and have mg-numbers (0.88 to 0.90; NK2-7, NK3-14) that overlap those of the peridotites. The low-Mg pyroxenites (mg-number: 0.85; NK3-1, NK3-17), on the other hand, are less garnet-rich (9 to 10 wt%) and have higher modal amounts of clinopyroxene (67 to 68 wt%) compared to the high-Mg pyroxenites (22 to 39 wt%).

Clinopyroxene and garnet

The emerald green clinopyroxene of the Somerset peridotites is a chromian diopside (Schmidberger & Francis, 1999), while the garnets are chromian pyrope, the majority of which are purple in color (Table 5). A small number of samples contain blood red garnets (NK1-5, NK2-2, NK3-4). These garnets tend to have higher MgO, SiO_2 and Al_2O_3, but lower CaO, Cr_2O_3 and MnO contents, compared to the purple garnets (Table 5). The high temperature estimates of 1200 to 1400 °C (Schmidberger & Francis, 1999) for samples with red garnet possibly suggest that these xenoliths were derived from deep lithospheric mantle, whereas the temperatures calculated for xenoliths with purple garnet are much more variable (800 to 1400 °C). Major element analyses of garnet and clinopyroxene indicate that these minerals are not chemically zoned and are compositionally homogeneous on the scale of a thin section. Inclusion-free crystals of clinopyroxene and garnet were handpicked under the binocular microscope from ten peridotites and one low-Mg pyroxenite sample, and were analyzed for their REE and trace element (Ti, V, Cr, Sr, Y, Zr) contents with a Cameca IMS 3f ion microprobe at Woods Hole Oceanographic Institution. The major elements of these separates were determined using electron microprobe analysis at McGill University, as described in Schmidberger & Francis (1999).

ANALYTICAL DATA

Kimberlite

The kimberlite whole-rock analyses are extremely high in $CaCO_3$ (27 to 39 wt%; Table 1), indicating liquid compositions intermediate between kimberlite and carbonatite (Woolley & Kempe, 1989; Ringwood *et al.*, 1992). Primitive-mantle normalized trace element patterns for the Nikos kimberlites (Table 1; Fig. 2a) show a strong enrichment in LILE (e.g. Ba, Sr) and Nb, Th, U and Pb, typical of small-degree partial melts such as kimberlites (Mitchell, 1986; Dalton & Presnall, 1998). The REE patterns for the Nikos kimberlites exhibit steep slopes with $(La/Sm)_N$ of 7 and relative depletion in heavy rare earth elements (HREE; Fig. 2b). Although LREE characteristics are similar to those for kimberlites from South Africa, Zaire, North America and India (Mitchell & Brunfelt, 1975; Paul *et al.*, 1975; Cullers *et al.*, 1982; Wedepohl & Muramatsu, 1979; Muramatsu, 1983; Fieremans *et al.*, 1984; Mitchell, 1986; Fig. 2b), HREE levels are distinctly lower in the Nikos kimberlites, particularly from Er to Lu. With the exception of Ba and Pb, which are strongly enriched, the levels of most other trace elements in the Nikos kimberlites overlap the fields for kimberlites from South Africa, Zaire, North America and India (Fig. 2b).

Mantle xenoliths

Incompatible trace element patterns for the bulk peridotites are subparallel and indicate that LILE (e.g. Ba, Sr), Nb, Th and U concentrations are enriched when compared to primitive mantle abundances (Sun & McDonough, 1989; McDonough & Sun, 1995; Table 3; Fig. 3a). Their trace element patterns are, however, clearly distinct from those of the Nikos kimberlites, which have much higher LILE, Nb, Th, U and Pb contents (Fig. 3a). Chondrite-normalized HREE patterns for the peridotites are flat, whereas the LREE are fractionated with $(La/Sm)_N$ of 4 to 6, resulting in concave-upward LREE patterns. The kimberlites, on the other hand, have much steeper slopes for LREE and, in particular, HREE compared to the peridotites (Fig. 3b).

The pyroxenites also contain high concentrations of incompatible trace elements such as LILE, Nb, Th and U, compared to values for primitive mantle (Table 3; Fig. 4a). The high-Mg pyroxenites (NK2-7, NK3-14), however, are considerably more enriched in incompatible trace elements than the low-Mg pyroxenites (NK3-1, NK3-17), and have trace element patterns that overlap those for peridotites showing the highest abundances of these elements (Fig. 4a). Incompatible trace element patterns for the low-Mg pyroxenites, on the other hand, are similar to those for peridotites with the lowest trace elements levels. Furthermore, the high-Mg pyroxenites have strongly fractionated LREE patterns ($(La/Sm)_N$ = 4 to 14), whereas low-Mg pyroxenites exhibit much less LREE fractionation ($(La/Sm)_N$ = 2). The HREE abundances for both the high and low-Mg pyroxenites tend to be higher than those for the peridotites (Fig. 4b), probably reflecting their higher modal abundance of garnet (av. 15 wt%) compared to that of the peridotites (av. 7 wt%; Table 2).

Clinopyroxene and garnet

The clinopyroxenes show convex-upward chondrite-normalized REE patterns with enriched LREE compared to chondrites (1 to 100 times) and relatively depleted HREE, with approximately chondritic abundances (Table 4; Fig 5a, b). The clinopyroxenes from peridotites yielding high temperatures of equilibration (1200 to 1400 °C) are only moderately enriched in LREE abundances (1 to 10 times chondrite; Fig. 5a). In comparison, clinopyroxenes from low temperature peridotites (800 to 1100 °C; NK1-3, NK1-4, NK1-14, NK2-3) exhibit significantly greater LREE enrichment (up to 100 times chondrite; Fig. 5b) and high Sr contents (>100 ppm; Table 4). In contrast, HREE patterns for both high temperature and low temperature peridotites are indistinguishable.

The clinopyroxenes in high temperature Nikos peridotite xenoliths have LREE contents that overlap those of clinopyroxenes in high temperature peridotites (>1100 °C) from the Kaapvaal craton in South Africa, although the HREE concentrations of the Kaapvaal clinopyroxenes tend to be higher (Shimizu, 1975; Boyd, 1987; Fig. 6a). Unlike many of the high temperature Kaapvaal xenoliths (Boyd, 1987), the high temperature Somerset peridotites are not characterized by strong deformation textures. In comparison, clinopyroxenes from high temperature Siberian peridotites (Shimizu *et al.*, 1997) have LREE contents that are intermediate between those of the low and high temperature Nikos clinopyroxenes, and overlapping HREE contents (Fig. 6a).

The low temperature Nikos peridotites have clinopyroxenes with LREE contents that overlap those of clinopyroxenes from low temperature Kaapvaal peridotites (<1100 °C), although the latter have considerably lower HREE contents (Fig. 6a). Clinopyroxenes from low temperature Siberian peridotites appear to exhibit highly variable REE patterns.

The REE patterns for garnets are HREE enriched and LREE depleted compared to those of coexisting clinopyroxene, crossing the latter between Sm and Eu (Table 5; Fig 5a, b). Garnet REE patterns for low temperature xenoliths are indistinguishable from those for high temperature peridotites. Strong depletion in LREE compared to HREE is consistent with garnet/liquid REE partition coefficients (Hauri *et al.*, 1994; Halliday *et al.*, 1995 and references therein) and has been interpreted to represent equilibrium REE distribution between garnet and a coexisting liquid (Shimizu, 1999). Sinusoidal patterns, characterized by an enrichment in the middle rare earth elements (MREE) compared to LREE and HREE (that have been interpreted to reflect recent, non-equilibrated melt-mineral reactions in other xenolith suites; Hoal *et al.*, 1994; Shimizu, 1999), are not observed in the Nikos garnets. The LREE contents of garnet in the low-Mg pyroxenite NK3-1 (Fig. 5a) are extremely low, indicating the highly depleted nature of this sample.

The REE patterns for the Nikos garnets are subparallel to those for garnets from high temperature Kaapvaal peridotites, although the latter contain higher overall REE abundances (Shimizu, 1975; Fig. 6b). Garnets from low temperature Kaapvaal peridotites have sinusoidal, non-equilibrated REE patterns with higher LREE and considerably lower HREE contents than those in the Nikos garnets (Fig. 6b). The LREE concentrations in the Nikos garnets are lower than those of garnets from Siberian high temperature peridotites, but their HREE contents overlap (Shimizu *et al.*, 1997; Fig. 6b).

DISCUSSION

Mantle composition

Late Archean Re depletion ages for other Somerset Island peridotites (up to 2.7 Ga; Irvine *et al.*, 1999) indicate that the northern margin of the Canadian craton is underlain by an Archean lithospheric mantle root, which may be only slightly younger than the Archean subcontinental lithosphere beneath the central Slave province, whose kimberlite xenoliths yield Re depletion ages of up to 3 Ga (Irvine *et al.*, 1999). In comparison, peridotite xenoliths in kimberlites on the Kaapvaal and Siberian cratons yield Re depletion ages (3.3 to 3.5 Ga; Pearson *et al.*, 1995a; Pearson *et al.*, 1995b), indicating that their mantle roots stabilized by the mid Archean.

Pressure and temperature estimates for the Nikos peridotites suggest the existence of a lithospheric mantle root to a depth of at least 190 km beneath Somerset Island, significantly deeper than the lithospheric mantle beneath Proterozoic mobile belts surrounding the Archean cratons (<160 km; Finnerty & Boyd, 1987; Nixon, 1987). High mg-numbers and depletion in fusible major elements, typical of Archean mantle xenolith suites (e.g. Boyd, 1987; Boyd *et al.*, 1997), indicate the refractory nature of the Nikos peridotites, that have been interpreted to represent the residues of large degree partial melting in the mantle (~30% melt extraction; Schmidberger & Francis, 1999). These results are supported by experimental studies (Walter, 1998) on the melting of pyrolitic mantle at high pressures and temperatures, which indicate that the most refractory Nikos peridotites would require a minimum of 30% melt extraction from a primitive mantle source.

Melt extraction should also result in the depletion in incompatible trace elements of the residual mineral assemblages (Harte, 1983; Carlson & Irving, 1994). Trace element patterns for the Nikos peridotites, however, are enriched in LILE, Th, U and LREE compared to those estimated for primitive mantle compositions (McDonough & Sun, 1995). These signatures suggest that interaction with melts or fluids during metasomatism has resulted in incompatible trace element enrichment of the mantle beneath Somerset Island. Metasomatism and partial melt extraction may have been related to a single magmatic event (e.g. Shi *et al.*, 1998) or incompatible trace element enrichment could reflect the infiltration of a metasomatic agent into lithospheric mantle that had previously been depleted in fusible major elements, as proposed for the mantle beneath the Kaapvaal craton in South Africa (e.g. Menzies & Hawkesworth, 1987; Hoal *et al.*, 1994; Pearson *et al.*, 1995a).

Depleted subcontinental lithosphere

It is important to establish the chemical composition of cratonic mantle roots because their refractory nature preserves a record of the large degree of partial melting involved in their formation during stabilization of the continents (Boyd & McCallister, 1976; Jordan, 1979; Walter, 1998). High pressure melting experiments show that the incipient melting of a carbonate-bearing garnet-peridotite produces alkalic liquids such as carbonatites and kimberlites and then picritic to komatiitic melts at larger degrees of partial melting, leaving a refractory residue that is highly depleted in fusible major elements such as Fe, Al and Ca (e.g. Takahashi & Scarfe, 1985; Baker & Stolper, 1994; Dalton & Presnall, 1998). Experimental data suggest that melting at pressures between 4.5 to 6 GPa (depths of up to 200 km), and temperatures between about 1500 to 1700 °C, produces harzburgitic residues because of the preferential melting of clinopyroxene (Canil, 1992; Walter, 1998). Loss of clinopyroxene, the main LREE carrier in peridotites, to the liquid phase depletes the residue in these elements, whereas the stability of garnet in the restite favors the retention of HREE in the residual mineral assemblage (Frey, 1969; Nagasawa et al., 1969; Hauri *et al.*, 1994). Progressive melting should result in chondrite-normalized bulk-rock REE patterns characterized by smooth LREE depleted profiles (Navon & Stolper, 1987). The Somerset peridotites are, however, characterized by enrichment in LILE and LREE compared to the HREE, despite their refractory major element signatures, as are peridotite xenolith suites from cratonic areas in South Africa and Siberia (Erlank *et al.*, 1987; Menzies *et al.*, 1987). These presumed metasomatic effects make it difficult to establish the chemical composition of the mantle roots prior to their interaction with metasomatic agents.

Previous studies have shown that bulk REE contents in peridotites are controlled by clinopyroxene and garnet, whereas orthopyroxene and olivine contribute little to REE budgets (e.g. Shimizu, 1975; Eggins *et al.*, 1998). The whole-rock REE compositions can, therefore, be modeled by quantitative mass balance calculations using the modal abundances of clinopyroxene and garnet and their respective REE contents. These mass balance calculations indicate that, in contrast to the analyzed whole-rock compositions, the calculated whole-rocks have much lower LREE abundances, while having similar

HREE contents (Table 6; Fig. 7). In particular, La and Ce are deficient in the calculated peridotite compositions by 99 to 90% for the high temperature peridotites (e.g. NK1-7; Fig. 7a) and 80 to 70% for the low temperature peridotites (e.g. NK1-4; Fig. 7b). Nd, Sm and Eu deficiencies in the calculated whole-rocks of both low temperature and high temperature peridotites range from 70 to 40%, but decrease for Dy, Er and Yb to less than 20% (Fig. 7). The calculated whole-rock REE patterns for the low temperature peridotites are approximately chondritic (e.g. NK1-4; Fig. 8b) or only slightly enriched (NK2-3). In contrast, the calculated LREE of high temperature peridotites are depleted compared to chondrites (e.g. NK1-7; Fig. 8a) and the calculated whole-rock patterns correspond to those expected for refractory mantle, with a residual mineral assemblage of olivine + orthopyroxene + garnet ± clinopyroxene, that has been depleted by a large degree of partial melting (~30 to 40 %; Navon & Stolper, 1987; Walter, 1998).

The large discrepancy for the LREE between the calculated and analyzed whole-rock compositions that was obtained for all xenoliths suggests that an interstitial phase(s) is present, either a trapped melt, or an accessory mineral phase, that contributes significantly to the LREE budget of the peridotites.

Interstitial kimberlite liquid

To account for the excess LREE contents of the whole-rock analyses, we modeled the possible presence of interstitial melt along grain boundaries of the peridotites. The calculations are based on bulk-rock trace element analyses and mineral modes, determined using a high-pressure norm calculation described in Schmidberger & Francis (1999), and a trapped melt in equilibrium with them (Bédard, 1994). The distribution of REE between minerals and trapped liquid in these calculations is determined using mineral-melt partition coefficients for the constituent peridotite phases (olivine, orthopyroxene, clinopyroxene, garnet) and a kimberlitic melt (Fujimaki *et al.*, 1984). The mass balance calculations indicate that the discrepancies can be explained by the presence of 0.1 to 2.5 wt% trapped liquid with a composition overlapping that of the Nikos kimberlite (Table 7; Fig. 9). The similarity of the trapped liquid trace element composition to that of the kimberlite suggests the presence of interstitial kimberlitic melt or a kimberlite-derived phase(s) to account for the excess LREE in the analyzed whole-rocks. The addition of 0.4 to 2 wt% kimberlite liquid to the calculated whole-rock compositions yields REE patterns that are remarkably similar to those of the analyzed bulk rocks (Table 6; Fig. 10).

Accessory minerals

The mineral apatite is known to be a major carrier for LREE with elemental abundances up to several thousand ppm (e.g. Ce: 2600 to 3000 ppm; Kramers *et al.*, 1983; Irving & Frey, 1984; O'Reilly *et al.*, 1991) and accessory apatite has been described in peridotite xenoliths (Dawson, 1980; Kramers *et al.*, 1983; O'Reilly *et al.*, 1991). Even if present in only trace amounts, apatite can play a major role in the LREE budget of mantle rocks (O'Reilly *et al.*, 1991).

We modeled the presence of apatite as a possible accessory mineral phase in the Nikos peridotites using an apatite REE composition determined by isotope dilution analysis (Kramers *et al.*, 1983) from a metasomatized South African xenolith suite. Similar REE abundances have been reported for apatite from metasomatized Australian spinel-lherzolites using proton microprobe analysis (O'Reilly *et al.*, 1991). The inclusion of small modal amounts of apatite (0.01 to 0.15 wt%) in the mass balance calculations also yields whole-rock REE patterns that are similar to the bulk-rock analyses (Table 6). Minor amounts of apatite could, therefore, also account for the LREE surplus in the Nikos whole-rock analyses. Although apatite is as yet undetected in thin sections, the presence of 0.1 wt% apatite along grain boundaries would be hard to observe optically. The presence of apatite in the Nikos peridotites could have resulted from interaction of the xenoliths with their host kimberlite, precipitating intergranular apatite during xenolith transport at 100 Ma. Whole-rock phosphorus abundances (Table 2), however, while consistent with mass balance calculations assuming the presence of a trapped interstitial kimberlite liquid in the Somerset bulk rocks (Tables 1 and 6), are 2 to 5 times lower for most xenoliths than those required by the apatite contents necessary to match the trace elements (Table 6).

Mineral phases such as phlogopite were also considered as possible LREE carriers, however, mass balance calculations indicate that more than 25 wt% mica would be required to account for the excess LREE contents. Although traces of phlogopite (maximum 1 wt%) are observed in some Nikos peridotite xenoliths, its modal abundance is completely insufficient to explain the discrepancy between calculated and analyzed whole-rock peridotite compositions.

The results of these mass balance calculations indicate that the shallow low temperature peridotites had in fact flat LREE patterns, whereas those of the deeper-seated high temperature peridotites were LREE depleted compared to chondrites before contamination by their host kimberlite.

Pyroxenites

The dominant rock type (over 90%) of the Nikos xenolith suite is peridotitic in composition, representing the Archean cratonic mantle root beneath Somerset Island, whereas pyroxenite appears to represent only a minor constituent (less than 10%; Schmidberger & Francis, 1999). The major element chemistry and mineralogy of the Nikos pyroxenites indicate that the division into high-Mg pyroxenites and low-Mg pyroxenites (Schmidberger & Francis, 1999) correlates with distinct incompatible traces element patterns. In contrast to their higher mg-numbers and a more refractory whole-rock composition, the high-Mg pyroxenites are more enriched in incompatible trace elements such as LILE and LREE than the low-Mg pyroxenites.

The major and trace element differences between high-Mg and low-Mg pyroxenites suggest that there is no direct genetic link between these two types of pyroxenites, an interpretation that is supported by their distinct Nd-Sr-Pb isotope systematics (Schmidberger & Francis, 1998). The low-Mg pyroxenites have REE profiles showing less fractionation between LREE and HREE compared to those of the peridotites and the high-Mg pyroxenites. The coarse textures, low mg-numbers and relatively depleted trace element signatures compared to the remaining samples suggest that they are cumulates, possibly representing veins in a peridotitic lithospheric mantle.

The similarity of the high-Mg pyroxenites to the peridotites in terms of their mg-numbers and high abundances of LILE and LREE is supported by their overlapping Nd-Sr-Pb isotope systematics (Schmidberger & Francis, 1998). These pyroxenites may constitute a pyroxene-rich component in the lithospheric mantle produced by small scale segregation of peridotite compositions into olivine and pyroxene-rich layers by metamorphic differentiation (Boyd et al., 1997).

Trace element partitioning

The significance of the distribution of incompatible elements between mineral pairs can be evaluated by comparing their trace element abundance ratios to experimentally determined trace element partition coefficients and to those reported in other natural systems (Iving & Frey, 1978; Irving & Frey, 1984, Harte & Kirkley, 1997; Shimizu *et al.*, 1997). The clinopyroxene/garnet REE partition coefficients for the Nikos xenoliths decrease from La to Yb, which is consistent with mineral-melt distribution coefficients for garnet that increase from the LREE to the HREE as those for clinopyroxene decrease (e.g. Halliday *et al.*, 1995 and references therein; Fig. 11). REE partitioning for clinopyroxene-garnet pairs from the high temperature peridotites (e.g. $La_{Cpx/Garn}$: 20 to 40) is consistent with experimental data for high temperature systems up to 1400 °C ($La_{Cpx/Garn}$: 20 to 80; Hauri *et al.*, 1994; Halliday *et al.*, 1995 and references therein; Fig. 11). These findings suggest that the distribution of REE between clinopyroxene and garnet equilibrated at high temperatures in these xenoliths. In contrast, clinopyroxene-garnet pairs from the low temperature peridotites and the low-Mg pyroxenite sample yield clinopyroxene/garnet partition coefficients that are significantly higher than those for the high temperature peridotites ($La_{Cpx/Garn}$: 200 to 840; Fig. 11). These partition coefficients overlap those observed in natural systems at temperatures between 800 to 1100 °C ($La_{Cpx/Garn}$: 60 to >1000; Griffin & Brueckner, 1985; Harte & Kirkley, 1997), suggesting that REE equilibration in the shallow lithosphere occurred at lower temperatures. These results confirm findings that clinopyroxene/garnet partition coefficients for the REE (e.g. $Ce_{Cpx/Garn}$; Fig. 12) vary significantly with temperature (Griffin & Brueckner, 1985).

Mantle stratification

Pressure estimates for the low temperature peridotites indicate entrainment from depths between 80 to 150 km in the lithospheric mantle. The clinopyroxenes in low temperature peridotites have REE patterns (Fig. 5b) that show strong enrichment in the LREE with abundances of up to 100 times chondrite (e.g. La: 6 to 27 ppm). These clinopyroxenes are also characterized by high Sr abundances (100 to 400 ppm; Fig. 13a, b). In contrast, the clinopyroxenes in the high temperature peridotites from depths estimated to be between 160 to 190 km have significantly lower LREE and Sr abundances than clinopyroxenes in the shallower low temperature peridotites (e.g. La up to 10 times chondrite; Figs. 5a and 13a, b).

Incompatible trace element abundances in the Nikos garnets range considerably and also correlate with temperature and pressure estimates for their xenoliths. Garnets in the low temperature peridotites are characterized by low Zr and Sr contents (9 to 60 ppm and 0.2 to 0.7 ppm, respectively), whereas garnets in the high temperature peridotites have Zr and Sr abundances (35 to 100 ppm and 0.4 to 1.1 ppm, respectively) that are significantly higher (Fig. 13c, d). Although this variation of Zr and Sr in garnet with depth could be interpreted as reflecting temperature dependent partitioning of these elements between clinopyroxene and garnet, Zr and Sr contents in the calculated whole-rocks using modal abundances of clinopyroxene and garnet and their respective Zr and Sr abundances also correlate with depth of derivation. The garnet in a peridotite from 150 km depth (NK1-3) has Zr and Sr contents overlapping those of garnets from the high temperature peridotites, but its coexisting clinopyroxene has trace element abundances and clinopyroxene/garnet partition coefficients similar to those of the low temperature peridotites (Fig. 13). The intermediate depth estimate (150 km) for this sample is consistent with it representing a transition between an upper and lower lithospheric mantle.

The correlation between incompatible trace element characteristics in clinopyroxene and garnet and estimated depth of entrainment for the Nikos peridotites is supported by calculated REE whole-rock patterns for the low temperature peridotites that are distinct from those of the high temperature peridotites, suggesting the existence of a vertically zoned lithospheric mantle root beneath Somerset Island. The strong LREE and Sr enrichment observed for clinopyroxenes in the low temperature peridotites compared to those in the high temperature peridotites suggests that the shallow lithospheric mantle beneath the Canadian craton is a significant reservoir for incompatible trace elements. The shallow lithospheric mantle could have been metasomatized by incompatible element-rich fluids or LREE enriched melts that intersected their solidus boundaries during passage through the lithosphere, originating from deeper levels of the subcontinental mantle (Wyllie, 1987). This, however, is difficult to reconcile with relatively low incompatible trace element abundances observed in the clinopyroxenes of underlying high temperature peridotites that appear to have been less affected by metasomatic melts of fluids ascending from depths. It, therefore, appears likely, that the subcontinental mantle root underneath Somerset Island is characterized by a vertical zonation in trace element distribution and that the shallow lithosphere is geochemically distinct from the deep lithosphere beneath the northern Canadian craton. The existence of this vertical layering may date from the time of its stabilization in the Archean.

Trace element systematics for clinopyroxene and garnet from Kaapvaal and Siberian peridotite xenoliths suggest that the continental lithosphere beneath these cratons is also chemically layered (e.g. Shimizu, 1975; Shimizu *et al.*, 1997). The shallow subcontinental lithospheric mantle is characterized by mineral compositions enriched in incompatible trace elements, whereas the deep lithospheric mantle has relatively low mineral incompatible trace element abundances (Shimizu, 1975; Shimizu *et al.*, 1997; Fig. 6). It is not likely that these trace element enriched signatures reflect interaction between mineral phases and the host kimberlite during sample transport, as this process should have equally affected both the low and high temperature peridotites. The trace element enriched clinopyroxene compositions of the shallow lithosphere beneath Somerset Island are similar to those observed for the Kaapvaal and the Siberian cratons, which may suggest that the upper portions of lithospheric mantle are generally enriched in incompatible trace elements compared to the deeper lithosphere.

CONCLUSIONS

Despite their high mg-numbers and refractory major element compositions, the Nikos peridotites exhibit whole-rock incompatible trace element patterns that are enriched in LILE, Th, U and LREE compared to primitive mantle compositions. The calculated whole-rock REE patterns of both the high and low temperature xenoliths have much lower LREE contents compared to the LREE enriched analyzed whole-rock compositions, while having similar HREE contents. The REE deficiency amounts to 99 to 70% for La and Ce, but 20% or less for the HREE, indicating the presence of an interstitial phase containing the excess LREE abundances observed in the analyzed peridotites. Models of an interstitial melt in equilibrium with constituent peridotite minerals yield REE patterns that are comparable to those of the Nikos kimberlites. Mass balance calculations indicate that small amounts of kimberlitic liquid (0.4 to 2 wt%) may account for excess REE contents that are observed in the Nikos peridotites. Trace amounts of apatite (0.01 to 0.15 wt%), crystallized from the host kimberlite, might also solve mass balance problems for the incompatible REE abundances. Whole-rock phosphorus contents, however, appear to be lower than those required by the apatite mass balance calculations. Most significantly, however, the calculated whole-rock compositions indicate that the shallow low temperature peridotites were characterized by flat LREE patterns, whereas the deeper-seated high temperature peridotites had depleted LREE patterns prior to contamination by their host kimberlite.

REE partitioning between garnet and clinopyroxene for high temperature xenoliths that sample the deep lithospheric mantle is consistent with high temperature experimental data indicating that these clinopyroxene-garnet pairs equilibrated at high temperatures and pressures in the lower lithosphere. REE clinopyroxene/garnet partition coefficients for the low temperature xenoliths are larger than those for the high temperature xenoliths and overlap data for mantle-derived rocks from natural systems at lower temperatures (800 to 1100 °C). These findings suggest that REE partitioning between constituent clinopyroxene and garnet in the subcontinental lithosphere is a function of temperature and thus depth.

The strong enrichment in REE and Sr in clinopyroxenes and low Zr and Sr contents in garnets observed for the low temperature peridotites compared to abundances of these elements in the high temperature peridotites suggest that the shallow subcontinental lithosphere beneath the northern Canadian craton is geochemically distinct from the underlying lower lithospheric mantle. The Somerset mantle root appears to be characterized by a depth zonation in incompatible elements that may date from the time of its stabilization in the late Archean.

ACKNOWLEDGEMENTS

We thank Tariq Ahmedali and Glenna Keating for performing the whole-rock X-ray fluorescence analyses and Glenn Poirier for assistance in obtaining the electron microprobe results. We are grateful to Nobu Shimizu from Woods Hole Oceanographic Institution and Tony Simonetti for their help with ion microprobe analyses. We also thank Fabien Rasselet for assistance in the field, hand picking separates of magmatic kimberlite for major and trace element analysis, and performing the CO_2 analyses with the assistance of Constance Guignard. We appreciate the comments of Roberta Rudnick, Bill Griffin and Graham Pearson that have significantly improved the manuscript.

REFERENCES

Baker, M. B. & Stolper, E. M. (1994). Determining the composition of high-pressure mantle melts using diamond aggregates. *Geochimica Cosmochimica Acta* **58**, 2811-2827.

Bédard, J. H. (1994). A procedure for calculating the equilibrium distribution of trace elements among the minerals of cumulate rocks, and the concentration of trace elements in the coexisting liquids. *Chemical Geology* **118**, 143-153.

Boyd, F. R. (1987). High- and low-temperature garnet peridotite xenoliths and their possible relation to the lithosphere-asthenosphere boundary beneath southern Africa. In: Nixon, P. H. (ed.) *Mantle Xenoliths*. Chichester: John Wiley & Sons, pp. 403-412.

Boyd, F. R. & McCallister, R. H. (1976). Densities of fertile and sterile garnet peridotites. *Geophysical Research Letters* **3**, 509-512.

Boyd, F. R. & Mertzman, S. A. (1987). Composition and structure of the Kaapvaal lithosphere, southern Africa. In: Mysen, B. O. (ed.) *Magmatic processes: physiochemical principles*: Geochemical Society Special Publications **1**, pp. 13-24.

Boyd, F. R., Pokhilenko, N. P., Pearson, D. G., Mertzman, S. A., Sobolev, N. V. & Finger, L. W. (1997). Composition of the Siberian cratonic mantle: evidence from Udachnaya peridotite xenoliths. *Contributions to Mineralogy and Petrology* **128**, 228-246.

Canil, D. (1992). Orthopyroxene stability along the peridotite solidus and the origin of cratonic lithosphere beneath southern Africa. *Earth and Planetary Science Letters* **111**, 83-95.

Carlson, R. W. & Irving, A. J. (1994). Depletion and enrichment history of subcontinental lithospheric mantle: an Os, Sr, Nd and Pb isotopic study of ultramafic xenoliths from the northwestern Wyoming Craton. *Earth and Planetary Science Letters* **126**, 457-472.

Cullers, L. R., Mullenax, J., Dimarco, M. J. & Nordeng, S. (1982). The trace element content and petrogenesis of kimberlites in Riley County, Kansas U.S.A. *American Mineralogist* **67**, 223-233.

Dalton, J. A. & Presnall, D. C. (1998). The continuum of primary carbonatitic-kimberlitic melt compositions in equilibrium with lherzolite: data from the system CaO-MgO-Al_2O_3-SiO_2-CO_2 at 6 GPa. *Journal of Petrology* **39**, 1953-1964.

Dawson, J. B. (1980). *Kimberlites and their xenoliths*. Berlin: Springer-Verlag.

Eggins, S. M., Rudnick, R. L. & McDonough, W. F. (1998). The composition of peridotites and their minerals: a laser-ablation ICP-MS study. *Earth and Planetary Science Letters* **154**, 53-71.

Erlank, A. J., Waters, F. G., Hawkesworth, C. J., Haggerty, S. E., Allsopp, H. L., Rickard, R. S. & Menzies, M. A. (1987). Evidence for mantle metasomatism in peridotite nodules from the Kimberley pipes, South Africa. In: Menzies, M. A. & Hawkesworth, C. J. (eds.) *Mantle metasomatism*. London: Academic Press, pp. 221-311.

Fieremans, M., Hertogen, J. & Demaiffe, D. (1984). Petrography, geochemistry and strontium isotopic composition of the Mbuji-Mayi and Kundelungu kimberlites. In: Kornprobst, J. (ed.) *Kimberlites I: Kimberlites and related rocks*. New York: Elsevier, pp. 107-120.

Finnerty, A. A. & Boyd, F. R. (1987). Thermobarometry for garnet peridotites: basis for the determination of thermal and compositional structure of the upper mantle. In: Nixon, P. H. (ed.) *Mantle Xenoliths*. Chichester: John Wiley & Sons, pp. 381-402.

Frey, F. A. (1969). Rare earth element abundances in a high-temperature peridotite intrusion. *Geochimica Cosmochimica Acta* **33**, 1429-1447.

Frisch, T. & Hunt, P. A. (1993). Reconnaissance U-Pb geochronology of the crystalline core of the Boothia Uplift, District of Franklin, Northwest Territories. In: *Radiogenic age and isotope studies: Report 7*. Geological Survey of Canada, Paper 93-2, pp. 3-22.

Fujimaki, H., Tatsumoto, M. & Aoki, K. (1984). Partition coefficients of Hf, Zr and REE between phenocrysts and groundmasses. Proceedings of the fourteenth lunar and planetary science conference, Part 2. *Journal of Geophysical Research* **89**, Suppl. B662-B672.

Grand, S. P. (1994). Mantle shear structure beneath the Americas and surrounding oceans. *Journal of Geophysical Research* **99**, 11.591-11.621.

Griffin, W. L. & Brueckner, H. K. (1985). REE, Rb-Sr and Sm-Nd studies of Norwegian eclogites. *Chemical Geology (Isotope Geoscience Section)* **52**, 249-271.

Halliday, A. N., Lee, D.-C., Tommasini, S., Davies, G. R., Paslick, C. R., Fitton, J. G. & James, D. E. (1995). Incompatible trace elements in OIB and MORB and source enrichment in the sub-oceanic mantle. *Earth and Planetary Science Letters* **133**, 379-395.

Harte, B. (1983). Mantle peridotites and processes - the kimberlite sample. In: Hawkesworth, C. J. & Norry, M. J. (eds.) *Continental basalts and mantle xenoliths*. Cheshire: Shiva Publishing Limited, pp. 46-91.

Harte, B & Kirkley, M. B. (1997) Partitioning of trace elements between clinopyroxene and garnet: data from mantle eclogites. *Chemical Geology* **136**, 1-24.

Hauri, E. H., Wagner, T. P. & Grove, T. L. (1994). Experimental and natural partitioning of Th, U, Pb and other trace elements between garnet, clinopyroxene and basaltic melts. *Chemical Geology* **117**, 149-166.

Hawkesworth, C. J., Erlank, A. J., Marsh, J. S., Menzies, M. A. & van Calsteren, P. W. (1983). Evolution of the continental lithosphere: evidence from volcanics and xenoliths in southern Africa. In: Hawkesworth, C. J. & Norry, M. J. (eds.) *Continental basalts and mantle xenoliths*. Cheshire: Shiva Publishing Limited, pp. 111-138.

Heaman, L. H. (1989). The nature of the subcontinental mantle from Sr-Nd-Pb isotopic studies on kimberlite perovskite. *Earth and Planetary Science Letters* **92**, 323-334.

Herzberg, C. T. (1993). Lithosphere peridotites of the Kaapvaal craton. *Earth and Planetary Science Letters* **120**, 13-29.

Hoal, K. E. O., Hoal, B. G., Erlank, A. J. & Shimizu, N. (1994). Metasomatism of the mantle lithosphere recorded by rare earth elements in garnets. *Earth and Planetary Science Letters* **126**, 303-313.

Irvine, G. J., Kopylova, M. G., Carlson, R. W., Pearson, D. G., Shirey, S. B. & Kjarsgaard, B. A. (1999). Age of the lithospheric mantle beneath and around the Slave craton: a rhenium-osmium isotopic study of peridotite xenoliths from the Jericho and Somerset Island kimberlites. Houston, Lunar and Planetary Institute, Contribution no. 971, *Ninth Annual V. M. Goldschmidt Conference*, 134-135.

Irving, A. J. & Frey, F. A. (1978). The distribution of trace elements between garnet megacrysts and volcanic liquids of kimberlitic to rhyolitic composition. *Geochimica Cosmochimica Acta* **42**, 771-787.

Irving, A. J. & Frey, F. A. (1984). Trace element abundances in megacrysts and their host basalts: constraints on partition coefficients and megacryst genesis. *Geochimica Cosmochimica Acta* **48**, 1201-1221.

Jordan, T. H. (1979). Mineralogies, densities and seismic velocities of garnet lherzolites and their geophysical implications. In: Boyd, F. R. & Meyer, H. O. A. (eds.) *The mantle sample: Inclusions in kimberlites and other volcanics.* Washington: American Geophysical Union, pp. 1-13.

Jordan, T. H. (1988). Structure and formation of the continental tectosphere. *Journal of Petrology,* Special Lithosphere Issue, 11-37.

Kopylova, M. G., Russell, J. K. & Cookenboo, H. (1999). Petrology of peridotite and pyroxenite xenoliths from the Jericho kimberlite: implications for the thermal state of the mantle beneath the Slave craton, Northern Canada. *Journal of Petrology* **40**, 79-104.

Kramers, J. D., Roddick, J. C. M. & Dawson, J. B. (1983). Trace element and isotope studies on veined, metasomatic and "MARID" xenoliths from Bultfontein, South Africa. *Earth and Planetary Science Letters* **65**, 90-106.

Lahaye, Y. & Arndt, N. (1996). Alteration of a komatiite flow from Alexo, Ontario, Canada. *Journal of Petrology* **37**, 1261-1284.

MacKenzie, J. M. & Canil, D. (1999). Composition and thermal evolution of cratonic mantle beneath the central Archean Slave Province, NWT, Canada. *Contributions to Mineralogy and Petrology* **134**, 313-324.

McDonough, W. F. (1990). Constraints on the composition of the continental lithospheric mantle. *Earth and Planetary Science Letters* **101**, 1-18.

McDonough, W. F. & Sun, S. S. (1995). The composition of the earth. *Chemical Geology* **120**, 223-253.

Menzies, M. A. & Hawkesworth, C. J. (1987). Upper mantle processes and composition. In: Nixon, P. H. (ed.) *Mantle Xenoliths.* Chichester: John Wiley & Sons, pp. 725-738.

Menzies, M. A., Rogers, N., Tindle, A. & Hawkesworth, C. J. (1987). Metasomatic and enrichment processes in lithospheric peridotites, an effect of asthenosphere-lithosphere interaction. In: Menzies, M. A. & Hawkesworth, C. J. (eds.) *Mantle metasomatism.* London: Academic Press, pp. 313-361.

Mitchell, R. H. (1986). *Kimberlites: Mineralogy, Geochemistry, and Petrology.* New York: Plenum Press.

Mitchell, R. H. & Brunfelt, A. O. (1975). Rare earth element geochemistry of kimberlites. *Physics and Chemistry of the Earth* **9**, 671-686.

Muramatsu, Y. (1983). Geochemical investigations of kimberlites from the Kimberley area, South Africa. *Geochemical Journal* **17**, 71-86.

Nagasawa, H., Wakita, H., Higuchi, H. & Onuma, N. (1969). Rare earths in peridotite nodules: an explanation of the genetic relationships between basalt and peridotite nodules. *Earth and Planetary Science Letters* **5**, 377-381.

Navon, O. & Stolper, E. (1987). Geochemical consequences of melt percolation: the upper mantle as a chromatographic column. *Journal of Geology* **95**, 285-307.

Nixon, P. H. (1987). Kimberlitic xenoliths and their cratonic setting. In: Nixon, P. H. (ed.) *Mantle Xenoliths.* Chichester: John Wiley & Sons, pp. 215-239.

O'Reilly, S. Y., Griffin, W. L. & Ryan, C. G. (1991). Residence of trace elements in metasomatized spinel lherzolite xenoliths: a proton-microprobe study. *Contributions to Mineralogy and Petrology* **109**, 98-113.

Paul, D. K., Potts, P. J., Gibson, G. L. & Harris, P. G. (1975). Rare earth element abundance in Indian kimberlites. *Earth and Planetary Science Letters* **15**, 151-158.

Pearson, D. G., Carlson, R. W., Shirey, S. B., Boyd, F. R. & Nixon, P. H. (1995a). Stabilisation of Archean lithospheric mantle: a Re-Os isotope study of peridotite xenoliths from the Kaapvaal craton. *Earth and Planetary Science Letters* **134**, 341-357.

Pearson, D. G., Shirey, S. B., Carlson, R. W., Boyd, F. R., Pokhilenko, N. P. & Shimizu, N. (1995b). Re-Os, Sm-Nd, and Rb-Sr isotope evidence for thick Archean lithospheric mantle beneath the Siberian craton modified by multistage metasomatism. *Geochimica Cosmochimica Acta* **59**, 959-977.

Pell, J. (1993). New kimberlite discoveries on Somerset Island. *Exploration Overview 1993.* Yellowknife: NWT Geology Division, Department of Indian and Northern Affairs, pp. 47.

Pollack, H. N. (1986). Cratonization and thermal evolution of the mantle. *Earth and Planetary Science Letters* **80**, 175-182.

Ringwood, A. E., Kesson, S. E., Hibberson, W. & Ware, N. (1992). Origin of kimberlites and related magmas. *Earth and Planetary Science Letters* **113**, 521-538.

Schmidberger, S.S. & Francis, D. (1998). Pb, Nd, Sr, and Hf isotope data for Somerset Island mantle xenoliths – Evidence for Archean deep mantle roots beneath Northern Canada. *Annual meeting GAC/MAC*, A-167.

Schmidberger, S. S. & Francis, D. (1999). Nature of the mantle roots beneath the North American craton: mantle xenolith evidence from Somerset Island kimberlites. *Lithos* **48**, 195-216.

Shi, L., Francis, D., Ludden, J., Frederiksen, A. & Bostock, M. (1998). Xenolith evidence of lithospheric melting above anomalously hot upper mantle under the nortern Canadian Cordillera. *Contributions to Mineralogy and Petrology* **131**, 39-53.

Shimizu, N. (1975). Rare earth elements in garnets and clinopyroxenes from garnet lherzolite nodules in kimberlites. *Earth and Planetary Science Letters* **25**, 26-32.

Shimizu, N. (1999). Young geochemical features in cratonic peridotites from Southern Africa and Siberia. In: Fei, Y., Bertka, C. M. & Mysen, B. O. (eds.) *Mantle petrology: field observations and high pressure experimentation: a tribute to Francis R. (Joe) Boyd*: The Geochemical Society, pp. 47-55.

Shimizu, N., Pokhilenko, N. P., Boyd, F. R. & Pearson, D. G. (1997). Geochemical characteristics of mantle xenoliths from the Udachnaya kimberlite pipe. *Russian Geology and Geophysics* **38**, 205-217.

Smith, C. B., Allsopp, H. L., Garvie, O. G., Kramers, J. D., Jackson, P. F. S. & Clement, C. R. (1989). Note on the U-Pb perovskite method for dating kimberlites: examples from the Wesselton and DeBeers mines, South Africa, and Somerset Island, Canada. *Chemical Geology (Isotope Geos.)* **79**, 137-145.

Steward, W. D. (1987). Late Proterozoic to Early Tertiary stratigraphy of Somerset Island and northern Boothia Peninsula, District of Franklin. *Geological Survey of Canada Paper* **83-26**, 78 p.

Sun, S. S. & McDonough, W. F. (1989). Chemical and isotopic systematics of oceanic basalts: implications for mantle composition and processes. In: Saunders, A. D. & Norry, M. J. (eds.) *Magmatism in the oceanic basins*. London: Geological Society, pp. 313-345.

Takahashi, E. & Scarfe, C. M. (1985). Melting of peridotite to 14 GPa and the genesis of komatiite. *Nature* **315**, 566-568.

Trettin, H. P., Frisch, T. O., Sobczak, L. W., Weber, J. R., Niblett, E. R., Law, L. K., DeLaurier, I. & Witham, K. (1972). The Innuitian Province. In: Price, R. A. & Douglas, R. J. W. (eds.) *Variations in tectonic styles in Canada. Geological Association of Canada, Special Paper* **11**, 83-179.

Walter, M. J. (1998). Melting of garnet peridotite and the origin of komatiite and depleted lithosphere. *Journal of Petrology* **39**, 29-60.

Wedepohl, K. H. & Muramatsu, Y. (1979). The chemical composition of kimberlites compared with the average composition of three basaltic magma types. In: Boyd, F. R. & Meyer, H. O. A. (eds.) *Kimberlites, diatremes and diamonds: their geology and petrology and geochemistry*. Washington: American Geophysical Union, pp. 300-312.

Wyllie, P. J. (1987). Metasomatism and fluid generation in mantle xenoliths. In: Nixon, P. H. (ed.) *Mantle Xenoliths*. Chichester: John Wiley & Sons, pp. 609-621.

Woolley, A. R. & Kempe, D. R. C. (1989). Carbonatites nomenclature, average chemical compositions, and elemental distribution. In: Bell, K. (ed.) *Carbonatites; genesis and evolution*. London: Unwin Hyman Inc., pp. 1-14.

Figure Captions

Figure 3-1. Geological map of Somerset Island (after Steward, 1987) showing kimberlite locations. Legend: light gray, Paleozoic cover rocks; striped, Late Proterozoic cover rocks; dark gray, Precambrian basement; bold lines, normal faults.

Figure 3-2. (a) Primitive mantle-normalized trace element and (b) chondrite-normalized rare earth element patterns for Nikos kimberlites compared to data for kimberlites from South Africa, Zaire, North America and India (Mitchell & Brunfelt, 1975; Paul *et al.*, 1975; Cullers *et al.*, 1982; Wedepohl & Muramatsu, 1979; Muramatsu, 1983; Fieremans *et al.*, 1984; Mitchell, 1986). Primitive mantle and chondrite values after Sun & McDonough (1989).

Figure 3-3. (a) Primitive mantle-normalized trace element and (b) chondrite-normalized rare earth element patterns for Nikos peridotites. Data for Nikos kimberlites are plotted for comparison.

Figure 3-4. (a) Primitive mantle-normalized trace element and (b) chondrite-normalized rare earth element patterns for Nikos pyroxenites. Data for Nikos kimberlites and peridotite field are plotted for comparison.

Figure 3-5. Chondrite-normalized rare earth element patterns for coexisting clinopyroxene and garnet in Nikos peridotites. (a) Clinopyroxene from high temperature peridotites is mildly enriched in LREE but depleted in HREE compared to coexisting garnet. (b) Clinopyroxene-garnet pairs with highly light rare earth element enriched clinopyroxene from low temperature xenoliths.

Figure 3-6. Chondrite-normalized rare earth element patterns for Nikos (a) clinopyroxene and (b) garnet compared to fields based on data from high temperature (high-T) and low temperature (low-T) peridotites from the Kaapvaal craton and high temperature peridotites from the Siberian craton (Shimizu, 1975; Shimizu *et al.*, 1997).

Figure 3-7. Rare earth element mass balance results for (a) high temperature peridotite NK1-7 and (b) low temperature peridotite NK1-4 showing deficiency or surplus (%) of each element calculated using the modal abundances of clinopyroxene and garnet and their respective REE contents compared to the analyzed whole-rock abundance. The rare earth element contents of olivine and orthopyroxene were assumed to be zero.

Figure 3-8. Calculated chondrite-normalized rare earth element patterns (Calc. Whole-rock) for (a) high temperature peridotite NK1-7 and (b) low temperature peridotite NK1-4 using mass balance calculations based on rare earth element contents of constituent garnet and clinopyroxene and their respective modal abundances. Rare earth element patterns for analyzed whole-rock (Whole-rock), garnet and clinopyroxene are plotted for comparison.

Figure 3-9. Calculated chondrite-normalized rare earth element patterns for possible interstitial liquids in equilibrium with constituent mineral phases of the Nikos peridotites (after Bédard, 1994). Nikos kimberlites are plotted for comparison.

Figure 3-10. Calculated chondrite-normalized rare earth element patterns (Calc. WR & Kimb.) for (a) high temperature peridotite NK1-7 and (b) low temperature peridotite NK1-4 before and after the addition of 0.4 wt% (NK1-7) and 1.2 wt% (NK1-4) interstitial kimberlite liquid.

Table 3-1. Major, trace and rare earth element analyses for kimberlites

Sample Rock	NK3-K1 Kimberlite	NK3-K2 Kimberlite	NK3-K3 Kimberlite	NK3-K4 Kimberlite	NK3-K5 Kimberlite
wt%					
SiO_2	19.85	25.05	23.21	22.72	23.62
TiO_2	2.06	2.15	1.62	1.73	1.51
Al_2O_3	2.20	2.81	2.03	1.90	1.64
FeO	7.06	8.13	6.99	7.32	7.26
MnO	0.14	0.16	0.15	0.14	0.15
MgO	19.97	26.12	23.07	23.03	25.59
CaO	21.58	15.34	17.57	18.90	16.61
Na_2O	0.19	0.14	0.06	0.09	0.10
K_2O	1.00	0.66	0.55	0.30	0.59
P_2O_5	0.64	0.64	0.92	0.83	0.85
H_2O	1.43	5.00	5.07	8.55	0.00
CO_2	22.78	12.68	17.10	13.19	20.96
Total	98.90	98.88	98.35	98.71	98.88
$CaCO_3$	38.52	27.38	31.36	30.00	29.65
ppm					
Cr	1000	1200	1220	1200	947
Ni	661	776	815	855	491
Nb	147	165	179	192	136
Ta	10.3	10.5	10.5	10.9	8.9
V	145	145	137	132	99
Zn	70	83	78	83	11
Y	13.0	14.0	16.0	16.0	13.0
Zr	159	155	190	182	154
Hf	3.60	4.10	4.60	4.30	3.50
Cs	1.00	0.80	0.50	0.50	0.40
Ba	2060	1730	2370	2380	1910
Rb	72.0	44.0	30.0	20.0	31.0
Sr	1320	1030	1710	2190	1330
Th	14.4	14.1	18.5	17.5	14.1
U	2.90	3.17	3.52	3.83	2.93
Pb	11.0	14.0	14.0	28.0	35.0
La	133	123	154	143	124
Ce	209	207	273	255	223
Pr	21.7	21.5	28.8	26.2	22.9
Nd	77.3	78.3	103	95.7	82.5
Sm	11.0	11.3	14.3	13.7	11.6
Eu	2.74	2.74	3.43	3.18	2.84
Gd	8.26	8.46	10.6	9.81	8.98
Tb	0.77	0.82	0.97	0.93	0.80
Dy	3.18	3.33	3.92	3.75	3.10
Ho	0.46	0.46	0.54	0.53	0.43
Er	0.90	0.96	1.12	1.03	0.90
Tm	0.09	0.10	0.10	0.10	0.08
Yb	0.42	0.52	0.44	0.48	0.36
Lu	0.07	0.08	0.08	0.07	0.06

Major element compositions were analyzed by X-ray fluorescence analysis at McGill University; analytical procedures have been described by Schmidberger & Francis (1999). Trace and rare earth element compositions were determined using ICP-MS analysis (for analytical procedures, see Table 3-3).

Table 3-2. Major element analyses and calculated mineral modes for bulk xenoliths

Sample	NK1-1	NK1-2	NK1-3	NK1-4	NK1-5	NK1-6	NK1-7	NK1-9	NK1-12	NK1-14	NK1-15	NK1-18	NK1-23	NK2-1	NK2-2
Rock	Perid	Perid	Perid	Perid	Perid	Perid	Perid	Perid	Perid	Perid	Perid	Perid	Perid	Perid	Perid
Texture	coarse	coarse	coarse	coarse	coarse	coarse	porphyr	coarse	coarse	coarse	coarse	coarse	coarse	coarse	porphyr
wt%															
SiO_2	41.25	41.77	40.81	41.60	42.28	40.37	41.24	41.88	40.80	42.02	42.29	42.94	41.01	45.66	42.69
TiO_2	0.07	0.03	0.03	0.06	0.07	0.02	0.03	0.04	0.03	0.03	0.06	0.03	0.10	0.09	0.08
Al_2O_3	1.00	1.31	1.33	2.43	1.95	1.25	1.57	1.59	0.56	1.71	1.09	0.79	2.71	1.31	2.17
FeO	7.49	7.39	7.42	7.09	7.74	7.10	7.06	7.29	7.76	7.27	7.30	6.97	7.81	7.08	7.69
MnO	0.11	0.11	0.11	0.13	0.12	0.10	0.10	0.11	0.11	0.11	0.11	0.10	0.12	0.12	0.12
MgO	43.30	44.44	44.03	40.90	41.49	43.41	43.55	43.48	45.32	42.92	42.69	44.93	40.25	42.09	42.80
CaO	0.58	1.11	0.82	1.20	1.44	0.41	0.72	0.96	0.57	1.13	0.88	0.54	1.79	0.93	2.21
Na_2O	0.02	0.10	0.01	0.01	0.06	0	0	0.03	0.12	0.15	0.01	0.05	0.16	0.40	0.19
K_2O	0.04	0.03	0.04	0.07	0.08	0.03	0.02	0.04	0.16	0.03	0.12	0.03	0.10	0.16	0.11
P_2O_5	0.01	0.02	0.02	0.01	0.01	0.01	0	0.01	0.03	0.02	0.03	0.01	0.02	0.01	0.01
Cr_2O_3	0.46	0.35	0.41	0.75	0.58	0.47	0.48	0.52	0.34	0.44	0.38	0.35	0.41	0.48	0.37
NiO	0.33	0.32	0.33	0.40	0.30	0.33	0.31	0.32	0.37	0.31	0.34	0.35	0.29	0.30	0.32
LOI	5.07	2.71	3.89	4.76	3.50	5.85	4.31	3.59	3.46	3.49	4.09	2.75	4.68	1.32	1.14
Total	99.73	99.69	99.25	99.41	99.62	99.35	99.39	99.86	99.63	99.63	99.39	99.84	99.45	99.95	99.90
mg-no.	0.912	0.915	0.914	0.911	0.905	0.916	0.917	0.914	0.912	0.913	0.913	0.920	0.902	0.914	0.908
Calculated modes in wt%															
Oliv	79	82	83	67	72	81	79	78	89	77	74	78	74	65	78
Opx	15	8	9	22	14	12	13	13	6	12	18	17	8	27	5
Cpx	1	4	2	5	5	1	1	2	4	4	3	1	7	5	10
Garn	5	6	7	6	9	7	8	8	2	7	5	4	11	3	8
Temperatures and pressures															
Temp (°C)	1222	1042	1076	871	1262	1149	1300	1219	1045	1027	1131	1223	964	1216	1316
Press (kb)	52.7	44.7	46.5	33.5	54.6	48.8	55.1	53.4	45.3	42.7	48.0	52.1	39.0	51.5	54.7

Table 3-2. continued

Sample	NK2-3	NK2-5	NK2-10	NK3-4	NK3-11	NK3-13	NK3-15	NK3-16	NK3-20	NK3-24	NK3-25	NK2-7	NK3-14	NK3-1	NK3-17
Rock	Perid	Perid	Perid	Perid	Perid	Perid	Perid	Perid	Perid	Perid	Perid	HMg-Px	HMg-Px	LMg-Px	LMg-Px
Texture	coarse	porphyr	coarse	coarse	coarse	coarse	coarse	coarse	coarse	coarse	coarse	coarse	coarse	coarse	coarse
wt%															
SiO_2	42.46	43.22	41.54	41.02	40.88	39.05	40.83	40.45	43.19	45.04	41.42	48.95	40.72	50.97	50.15
TiO_2	0.09	0.15	0.03	0.11	0.06	0.05	0.07	0.06	0.10	0.03	0.21	0.13	0.23	0.18	0.18
Al_2O_3	2.90	1.06	1.25	3.34	1.10	1.07	1.39	0.93	3.21	2.24	4.28	8.05	11.40	4.71	4.89
FeO	7.21	8.07	7.43	7.15	6.99	6.96	6.47	7.93	7.58	6.19	7.41	4.93	6.85	6.04	6.01
MnO	0.13	0.12	0.11	0.11	0.10	0.09	0.09	0.10	0.13	0.12	0.13	0.18	0.24	0.15	0.15
MgO	41.87	44.14	45.53	37.17	42.70	40.95	40.67	44.79	37.50	39.84	39.46	23.69	27.87	19.44	19.48
CaO	1.98	1.01	1.22	3.64	2.80	2.28	2.82	1.54	3.21	2.19	2.13	9.45	4.68	16.46	16.91
Na_2O	0.15	0.04	0.07	0.21	0.10	0.18	0.04	0.08	0.35	0.08	0.09	0.90	0.36	0.46	0.28
K_2O	0.19	0.05	0.05	0.32	0.05	0.07	0.07	0.04	0.14	0.05	0.52	0.11	1.13	0.11	0.09
P_2O_5	0.02	0.01	0.04	0.02	0.02	0.02	0.02	0.01	0.02	0.01	0.04	0.01	0.11	0.02	0.01
Cr_2O_3	0.71	0.46	0.36	0.43	0.54	0.59	0.38	0.30	0.46	0.66	0.75	1.16	1.50	0.54	0.50
NiO	0.31	0.33	0.32	0.28	0.31	0.30	0.34	0.32	0.28	0.24	0.25	0.38	0.22	0.09	0.09
LOI	1.77	1.01	1.84	5.57	3.88	8.11	6.32	3.01	3.30	3.10	2.81	1.90	4.07	0.52	0.58
Total	99.79	99.67	99.79	99.37	99.53	99.72	99.51	99.56	99.47	99.79	99.50	99.84	99.38	99.69	99.32
mg-no.	0.912	0.907	0.916	0.903	0.916	0.913	0.918	0.910	0.898	0.920	0.905	0.895	0.879	0.852	0.852
Calculated modes in wt%															
Oliv	73	77	86	68	82	83	75	89	62	57	70	4	9	0	0
Opx	7	16	4	2	1	1	6	1	11	26	5	41	44	24	22
Cpx	8	3	5	17	13	12	12	7	15	7	8	39	22	67	68
Garn	12	5	6	13	5	5	6	4	12	11	17	15	25	9	10
Temperatures and pressures															
Temp (°C)	887	1371	1014	1371	1247	830	1343	1280	815	770	1256	737	933	759	720
Press (kb)	34.6	57.9	42.1	59.6	53.1	30.9	58.5	53.5	29.8	24.7	54.0	25.3	36.8	25.1	22.2

LOI, loss on ignition. Total Fe is given as FeO and mg-number = Mg/(Mg+Fe). Perid, peridotite; HMg-Px, High-Mg pyroxenite; LMg-Px, Low-Mg pyroxenite; porphyry, porphyroclastic. Modes were determined using whole-rock compositions and a high-pressure peridotite norm calculation procedure (Schmidberger and Francis, 1999). Temperature and pressure calculations have been discussed by Schmidberger & Francis (1999). Analytical procedures as in Table 3-1.

Table 3-3. Trace and rare earth element analyses for bulk xenoliths

Sample Rock Texture	NK1-1 Perid coarse	NK1-2 Perid coarse	NK1-3 Perid coarse	NK1-4 Perid coarse	NK1-5 Perid coarse	NK1-6 Perid coarse	NK1-7 Perid porphyr	NK1-9 Perid coarse	NK1-12 Perid coarse	NK1-14 Perid coarse	NK1-15 Perid coarse	NK1-18 Perid coarse	NK1-23 Perid coarse	NK2-1 Perid coarse	NK2-2 Perid porphyr
ppm															
Nb	1.70	1.70	2.22	1.67	1.76	1.20	0.60	1.20	3.10	2.03	6.36	1.15	8.42	1.30	0.89
Ta	0.08	0.07	0.09	0.06	0.11	0.06	0.04	0.08	0.17	0.07	0.31	0.06	0.11	0.10	0.07
V	23.0	30.5		44.7		25.0		35.5	18.0	36.3				32.0	56.7
Zn	42.0	38.9		37.1		37.0		42.8	49.0	41.3				38.0	43.8
Y	1.10	0.88	1.84	1.30	1.80	1.60	0.92	1.18	1.00	1.23	0.83	0.31	3.45	0.70	1.57
Zr	6.50	2.86	6.79	3.53	8.81	7.00	3.31	6.31	8.90	3.02	9.91	2.52	8.08	4.30	4.77
Hf	0.100	0.045	0.104	0.079	0.207	0	0.077	0.145	0.200	0.064	0.214	0.051	0.206	0.100	0.135
Cs	0	0.14	0.14	0.21	0.19	0	0.09	0.15	0.10	0.17	0.58	0.14	0.39	0.20	0.19
Ba	31.0	18.9	22.2	45.6	27.9	18.0	10.5	14.8	126	27.4	89.6	13.1	105	23.0	28.6
Rb	1.10	1.15	1.72	3.03	4.29	0.80	1.03	1.53	3.20	1.43	7.25	1.85	4.72	10.0	6.47
Sr	25.7	33.8	56.3	43.3	46.5	17.1	15.2	17.8	56.5	43.7	66.7	41.7	86.5	31.3	33.5
Th	0.340	0.165	0.199	0.209	0.177	0.240	0.061	0.131	0.370	0.200	0.644	0.095	0.939	0.180	0.135
U	0.090	0.031	0.098	0.059	0.078	0	0.012	0.027	0.060	0.055	0.093	0.067	0.129	0	0.063
Pb	0	0.116	0.014	0.174	0.017	0	0.001	0.206	0	0.076	0.028	0.007	0.023	0	0.037
La	1.36	1.92	1.88	1.99	1.44	0.690	0.500	0.972	2.62	2.31	5.01	0.872	8.38	0.510	0.815
Ce	2.81	4.16	3.56	3.46	2.57	1.82	0.875	1.97	5.22	4.99	9.22	1.50	12.26	1.42	1.81
Pr	0.311	0.495	0.438	0.383	0.305	0.230	0.109	0.232	0.584	0.510	1.073	0.166	1.19	0.162	0.245
Nd	1.15	1.87	1.73	1.45	1.15	0.970	0.448	0.922	2.21	2.03	3.85	0.608	3.68	0.630	1.08
Sm	0.210	0.285	0.368	0.226	0.264	0.220	0.143	0.249	0.400	0.258	0.590	0.120	0.562	0.140	0.292
Eu	0.072	0.079	0.119	0.066	0.093	0.073	0.047	0.086	0.110	0.076	0.150	0.039	0.170	0.046	0.091
Gd	0.230	0.218	0.381	0.199	0.349	0.250	0.158	0.221	0.280	0.223	0.444	0.120	0.576	0.160	0.234
Tb	0.040	0.029	0.058	0.032	0.058	0.050	0.023	0.035	0.040	0.035	0.053	0.015	0.094	0.030	0.039
Dy	0.220	0.169	0.306	0.208	0.337	0.280	0.134	0.234	0.210	0.173	0.186	0.059	0.517	0.150	0.278
Ho	0.040	0.035	0.060	0.048	0.062	0.060	0.031	0.046	0.040	0.043	0.028	0.008	0.112	0.030	0.064
Er	0.100	0.098	0.156	0.132	0.147	0.160	0.094	0.106	0.100	0.117	0.076	0.022	0.319	0.070	0.172
Tm	0.013	0.014	0.024	0.020	0.021	0.025	0.018	0.016	0.014	0.022	0.008	0.003	0.051	0.008	0.028
Yb	0.080	0.099	0.154	0.142	0.141	0.160	0.124	0.104	0.070	0.128	0.055	0.021	0.331	0.050	0.181
Lu	0.013	0.016	0.026	0.025	0.025	0.026	0.021	0.017	0.013	0.026	0.008	0.004	0.055	0.008	0.029

Table 3-3. continued

Sample	NK2-3	NK2-5	NK2-10	NK3-4	NK3-11	NK3-13	NK3-15	NK3-16	NK3-20	NK3-24	NK3-25	NK2-7	NK3-14	NK3-1	NK3-17
Rock	Perid	Perid	Perid	Perid	Perid	Perid	Perid	Perid	Perid	Perid	Perid	HMg-Px	HMg-Px	LMg-Px	LMg-Px
Texture	coarse	porphyr	coarse	coarse	coarse	coarse	coarse	coarse	coarse	coarse	coarse	coarse	coarse	coarse	coarse
ppm															
Nb	3.71	1.30	3.51	2.45	1.57	5.81	1.50	1.19	2.46	2.11	4.22	6.50	16.1	1.46	1.40
Ta	0.09	0.07	0.11	0.15	0.10	0.22	0.09	0.08	0.04	0.08	0.24	0.05	1.09	0.09	0.03
V	54.7	34.0			49.6	38.5	34.0	28.9	80.0		68.3	156	117		221
Zn	41.3	35.0			41.3	47.0	38.1	46.8	44.8		43.2	18.0	26.5		18.0
Y	2.52	1.10	1.96	3.50	0.74	0.79	0.48	1.03	3.04	1.14	3.13	8.30	16.1	7.14	7.10
Zr	6.56	4.80	6.85	9.76	4.84	2.62	5.56	3.72	5.57	2.03	11.3	9.40	39.5	10.2	4.80
Hf	0.182	0.100	0.115	0.237	0.139	0.055	0.131	0.092	0.182	0.048	0.265	0.300	0.685	0.345	0.200
Cs	0.21	0.10	0.13	0.38	0.13	0.16	0.10	0.08	0.21	0.18	0.36	0.30	0.81	0.18	0
Ba	93.9	14.0	82.0	50.6	16.9	63.7	23.3	42.5	82.5	51.2	83.9	148	451	50.0	71.0
Rb	7.52	1.90	2.99	23.2	2.91	2.90	3.66	1.77	7.33	3.66	28.7	4.10	30.2	5.06	3.60
Sr	77.7	14.9	92.6	245	202	129	344	40.9	55.9	128	37.5	284	162	90.3	38.8
Th	0.598	0.200	0.495	0.217	0.165	0.529	0.221	0.131	0.265	0.238	0.267	1.45	0.860	0.226	0.350
U	0.193	0	0.187	0.502	0.642	0.386	0.779	0.196	0.125	0.416	0.347	0.800	0.897	0.050	0.150
Pb	0.219	0	0.060	0.028	0.359	0.447	1.29	0.213	0.553	0.027	0.332	0	1.52	0.033	0
La	5.35	0.840	5.21	3.26	1.44	3.23	2.09	1.26	3.19	2.05	3.30	19.30	8.68	2.59	2.20
Ce	7.94	2.09	8.58	5.37	2.51	5.75	3.40	2.22	4.08	3.48	4.74	27.30	16.65	5.89	4.17
Pr	0.757	0.244	0.992	0.601	0.272	0.638	0.330	0.254	0.380	0.362	0.471	1.89	2.05	0.832	0.471
Nd	2.58	0.970	3.48	2.21	1.09	2.35	1.19	0.970	1.52	1.16	1.76	5.13	7.86	3.40	2.13
Sm	0.402	0.210	0.559	0.421	0.276	0.298	0.215	0.208	0.299	0.170	0.327	0.910	1.62	0.768	0.680
Eu	0.128	0.070	0.158	0.154	0.084	0.084	0.093	0.064	0.112	0.052	0.104	0.280	0.654	0.241	0.223
Gd	0.323	0.240	0.496	0.487	0.213	0.240	0.196	0.175	0.420	0.166	0.322	1.07	1.87	0.949	0.970
Tb	0.057	0.040	0.072	0.080	0.028	0.030	0.025	0.028	0.059	0.026	0.063	0.210	0.335	0.173	0.190
Dy	0.341	0.210	0.338	0.489	0.166	0.159	0.125	0.190	0.423	0.152	0.507	1.28	2.52	1.08	1.18
Ho	0.087	0.040	0.063	0.113	0.028	0.030	0.021	0.043	0.099	0.037	0.113	0.300	0.541	0.244	0.270
Er	0.255	0.100	0.170	0.335	0.067	0.081	0.051	0.114	0.330	0.119	0.328	0.900	1.48	0.705	0.770
Tm	0.036	0.014	0.024	0.055	0.009	0.010	0.007	0.017	0.043	0.020	0.051	0.147	0.264	0.102	0.127
Yb	0.302	0.070	0.152	0.366	0.062	0.076	0.050	0.106	0.342	0.140	0.319	0.940	1.53	0.659	0.760
Lu	0.040	0.011	0.025	0.060	0.014	0.013	0.015	0.016	0.050	0.026	0.063	0.139	0.298	0.099	0.109

Rock types as in Table 3-2. Trace and rare earth element compositions were determined using ICP-MS analysis. Reproducibility is 1 to 3% (1SD); detection limits are 2 to 20 ppt for most elements, except Zr (40 ppt), and Sr and Ba (both 150 ppt). All blank levels are lower than the detection limit. For data acquisition parameters and data reduction procedures see Lahaye & Arndt (1996).

Figure 3-11. Clinopyroxene-garnet partition coefficients in Nikos peridotites. Fields for high temperature experimental data (to 1400 °C) after Hauri *et al.* (1994), Halliday *et al.* (1995) and references therein and data for natural systems (800 to 1100 °C) after Griffin & Brueckner (1985) and Harte & Kirkley (1997).

Figure 3-12. Temperature dependence of clinopyroxene-garnet Ce partitioning ($Ce_{Cpx/Garn}$) in the Nikos peridotites.

Figure 3-13. Depth distribution of (a) La and (b) Sr abundances in clinopyroxenes and (c) Zr and (d) Sr abundances (ppm) in garnets of low and high temperature peridotites.

Table 3-4. Major, trace and rare earth element analyses of clinopyroxenes

Sample	NK1-3	NK1-4	NK1-5	NK1-7	NK1-14	NK2-1	NK2-2	NK2-3	NK2-5	NK3-4	NK3-1
Rock	Perid	Perid	Perid	Perid	Perid	Perid	Perid	Perid	Perid	Perid	LMg-Px
wt%											
SiO_2	54.19	53.58	54.72	54.11	53.86	53.87	53.81	53.32	54.35	55.32	53.99
TiO_2	0.13	0.12	0.17	0.08	0.12	0.10	0.20	0.20	0.48	0.15	0.08
Al_2O_3	2.98	2.87	2.52	2.36	2.67	2.31	2.82	2.73	2.33	2.89	1.73
FeO	2.31	1.60	2.65	2.34	2.19	2.44	2.89	2.00	3.05	2.76	3.12
MnO	0.09	0.08	0.10	0.08	0.07	0.08	0.08	0.06	0.11	0.09	0.06
MgO	15.84	16.13	17.52	18.07	16.06	17.45	18.23	15.98	18.54	17.85	16.82
CaO	19.14	20.56	18.87	18.68	19.59	19.31	18.29	21.13	18.18	17.71	23.61
Na_2O	2.46	2.06	1.93	1.61	2.27	1.74	1.76	1.94	1.55	1.86	0.63
Cr_2O_3	2.27	1.95	1.96	1.77	2.19	2.19	1.15	1.85	1.75	1.01	0.45
NiO	0.04	0.03	0.05	0.06	0.04	0.05	0.06	0.04	0.06	0.05	0.08
Total	99.45	98.98	100.48	99.18	99.06	99.55	99.29	99.24	100.40	99.69	100.57
mg-no.	0.924	0.947	0.922	0.932	0.929	0.927	0.918	0.934	0.916	0.920	0.906
ppm											
La	6.21	7.72	0.739	0.828	8.55	0.442	0.806	26.8	1.88	0.474	1.72
Ce	30.5	19.9	3.40	3.78	37.0	1.75	3.81	50.8	7.97	3.34	6.33
Nd	24.7	8.07	3.26	3.96	18.7	2.00	4.77	11.7	6.42	4.22	4.20
Sm	5.60	0.937	1.05	0.877	2.50	0.667	1.11	1.50	1.44	1.13	0.861
Eu	1.50	0.263	0.277	0.269	0.553	0.214	0.306	0.440	0.424	0.317	0.269
Dy	1.07	0.251	0.273	0.238	0.354	0.408	0.425	0.654	0.626	0.614	0.470
Er	0.295	0.122	0.074	0.168	0.152	0.155	0.216	0.283	0.239	0.220	0.165
Yb	0.236	0.092	0.104	0.096	0.122	0.123	0.180	0.229	0.225	0.152	0.141
Ti	778	625	1041	469	925	664	1206	1214	2910	867	522
V	410	449	314	296	451	257	318	454	257	309	298
Cr	16115	14832	15204	13858	18368	15601	8875	14959	14081	7968	3603
Sr	406	112	75.0	86.9	217	45.8	106	318	142	92.7	61.3
Y	3.36	0.66	1.28	0.82	1.63	1.19	1.90	2.03	2.21	1.88	0.91
Zr	84.1	9.6	25.3	9.2	24.4	18.6	12.7	24.0	16.9	14.4	6.3

Perid, peridotite; LMg-Px, Low-Mg pyroxenite. Major element compositions were analyzed by electron microprobe analysis at McGill University; analytical procedures as described by Schmidberger & Francis (1999). Trace element (Ti, V, Cr, Sr, Y, Zr) and REE compositions were determined using ion microprobe analysis at Woods Hole Oceanographic Institution. Analytical procedures as given in Shimizu *et al.* (1997).

Table 3-5. Major, trace and rare earth element analyses of garnets

Sample Rock Color	NK1-3 Perid purple	NK1-4 Perid purple	NK1-5 Perid red	NK1-7 Perid purple	NK1-14 Perid purple	NK2-1 Perid purple	NK2-2 Perid red	NK2-3 Perid purple	NK2-5 Perid purple	NK3-4 Perid red	NK3-1 LMg-Px light red
wt%											
SiO_2	41.44	41.28	42.04	41.46	42.13	41.17	42.08	41.34	41.20	42.22	40.67
TiO_2	0.08	0.09	0.24	0.14	0.08	0.23	0.29	0.08	0.87	0.25	0.05
Al_2O_3	21.19	20.54	20.09	20.29	20.86	19.35	21.57	21.44	18.13	22.30	22.00
FeO	7.46	7.93	7.07	6.24	7.33	7.08	6.87	7.85	6.84	7.16	14.89
MnO	0.39	0.44	0.35	0.30	0.41	0.36	0.31	0.48	0.32	0.32	0.60
MgO	20.43	19.38	20.19	20.67	19.98	19.63	21.16	19.53	19.44	21.15	14.63
CaO	5.12	5.68	5.26	5.22	4.87	5.67	4.50	5.28	6.61	4.01	5.88
Na_2O	0.03	0.02	0.03	0.02	0.03	0.02	0.03	0.03	0.05	0.03	0.01
Cr_2O_3	4.13	4.41	4.80	4.76	4.04	5.78	2.55	3.21	6.77	2.00	1.32
NiO	0.00	0.00	0.01	0.02	0.00	0.01	0.01	0.01	0.01	0.01	0.00
Total	100.29	99.77	100.07	99.10	99.73	99.29	99.37	99.25	100.23	99.48	100.04
mg-no.	0.830	0.813	0.836	0.855	0.829	0.832	0.846	0.816	0.835	0.840	0.637
ppm											
La	0.029	0.025	0.018	0.029	0.044	0.016	0.019	0.032	0.052	0.026	0.004
Ce	0.411	0.147	0.148	0.281	0.680	0.097	0.118	0.275	0.679	0.094	0.023
Nd	2.04	0.474	0.638	1.23	1.24	0.839	0.712	0.495	2.34	0.437	0.342
Sm	1.86	0.586	0.800	0.952	0.908	1.05	0.596	0.421	1.43	0.529	0.403
Eu	0.946	0.213	0.424	0.454	0.349	0.645	0.276	0.239	0.591	0.254	0.281
Dy	3.93	2.19	2.31	1.55	2.12	3.90	2.11	2.38	2.07	2.02	4.57
Er	1.87	1.90	0.952	1.08	1.30	1.39	1.63	1.74	1.12	1.45	3.93
Yb	2.66	2.26	1.24	1.49	1.92	1.75	1.90	2.18	1.34	1.94	4.70
Ti	482	548	1328	951	534	1375	1572	597	4128	1364	1044
V	244	311	351	420	235	382	319	256	363	283	256
Cr	28944	35205	37866	48375	30546	47871	17832	31880	56478	13397	9323
Sr	0.73	0.17	0.51	0.48	0.31	0.57	0.35	0.27	1.10	0.43	0.14
Y	23.4	15.4	15.9	11.4	12.0	20.0	17.3	19.3	11.9	15.9	25.6
Zr	56.7	9.0	77.0	48.9	14.0	98.4	35.6	14.9	66.6	33.4	12.5

Rock types and analytical procedures as in Table 3-4.

Table 3-6. Calculated rare earth element contents for bulk xenoliths

Sample Rock	NK1-3 Perid	NK1-4 Perid	NK1-5 Perid	NK1-7 Perid	NK1-14 Perid	NK2-1 Perid	NK2-2 Perid	NK2-3 Perid	NK2-5 Perid	NK3-4 Perid	NK3-1 LMg-Px
Mass balance calculations based on clinopyroxene and garnet											
ppm											
La	0.122	0.061	0.384	0.035	0.008	0.025	0.078	2.00	0.336	0.085	1.29
Ce	0.616	0.279	0.995	0.165	0.049	0.098	0.372	3.81	1.49	0.586	4.76
Nd	0.614	0.308	0.430	0.204	0.127	0.135	0.511	0.929	0.817	0.781	3.21
Sm	0.232	0.111	0.084	0.119	0.083	0.068	0.154	0.162	0.164	0.260	0.717
Eu	0.092	0.040	0.027	0.051	0.039	0.031	0.051	0.062	0.047	0.086	0.251
Dy	0.283	0.115	0.151	0.222	0.127	0.141	0.211	0.335	0.170	0.358	1.15
Er	0.131	0.059	0.127	0.090	0.089	0.051	0.152	0.231	0.102	0.219	0.806
Yb	0.182	0.069	0.148	0.117	0.121	0.060	0.170	0.279	0.147	0.269	0.920
Mass balance calculations based on clinopyroxene, garnet and kimberlite liquid											
wt% kimberlite	1.30	1.20	1.10	0.40	1.30	0.50	0.70	2.00	0.80	2.00	0.50
ppm											
La	1.88	2.00	1.52	0.550	2.09	0.701	1.03	4.67	1.14	2.79	1.96
Ce	3.64	3.78	2.73	0.983	4.51	1.26	2.00	8.41	2.14	5.24	5.90
Nd	1.74	1.47	1.16	0.476	1.94	0.571	1.12	2.66	1.00	2.51	3.63
Sm	0.39	0.231	0.254	0.133	0.323	0.130	0.239	0.407	0.209	0.502	0.775
Eu	0.129	0.062	0.083	0.051	0.086	0.046	0.072	0.120	0.064	0.144	0.264
Dy	0.324	0.191	0.258	0.141	0.213	0.157	0.233	0.398	0.142	0.420	1.16
Er	0.142	0.137	0.100	0.093	0.114	0.055	0.158	0.246	0.066	0.234	0.807
Yb	0.185	0.152	0.121	0.123	0.151	0.062	0.172	0.283	0.072	0.273	0.918
Mass balance calculations based on clinopyroxene, garnet and apatite											
wt% apatite	0.10	0.05	0.10	0.10	0.01	0.05	0.05	0.15	0.10	0.15	0.05
ppm											
La	1.87	0.936	2.13	1.78	0.446	0.900	0.953	4.63	2.09	2.71	2.17
Ce	3.42	1.68	3.80	2.96	0.749	1.50	1.77	8.01	4.29	4.79	6.16
Nd	1.90	0.950	1.71	1.49	0.449	0.777	1.15	2.86	2.10	2.71	3.85
Sm	0.426	0.208	0.278	0.313	0.132	0.165	0.251	0.453	0.358	0.551	0.814
Eu	0.130	0.059	0.065	0.089	0.048	0.050	0.070	0.119	0.085	0.144	0.270
Dy	0.323	0.135	0.192	0.263	0.138	0.161	0.231	0.396	0.211	0.419	1.17
Er	0.140	0.064	0.137	0.100	0.092	0.056	0.157	0.246	0.112	0.234	0.811
Yb	0.186	0.071	0.152	0.121	0.122	0.062	0.173	0.286	0.151	0.276	0.922

Rock types as in Table 3-4. Quantitative mass balance calculations are based on REE contents and modal abundances of respective minerals. Kimberlite liquid and modal apatite proportions (wt%) for whole-rocks calculations based on clinopyroxene, garnet and apatite were constrained iteratively to obtain the best match between calculated REE patterns and those determined analytically. Apatite composition from Kramers *et al.* (1983).

Table 3-7. Rare earth element contents for calculated interstitial liquid

Sample Rock	NK1-3 Perid	NK1-4 Perid	NK1-5 Perid	NK1-7 Perid	NK1-14 Perid	NK2-1 Perid	NK2-2 Perid	NK2-3 Perid	NK2-5 Perid	NK3-4 Perid	NK3-1 LMg-Px
Interstitial liquid in equilibrium with olivine, orthopyroxene, clinopyroxene and garnet											
wt% liquid	1.20	1.00	0.90	0.25	1.50	0.25	0.40	2.50	0.60	1.50	0.10
ppm											
La	141	178	142	183	145	135	131	200	124	171	142
Ce	249	289	235	278	299	318	238	282	287	251	218
Nd	98.5	98.3	81.2	89.5	105	93.9	89.5	78.8	106	76.1	64.3
Sm	15.2	10.4	11.7	13.6	9.83	11.8	12.8	8.98	15.1	8.93	7.08
Eu	4.82	2.66	3.46	3.37	2.52	3.33	3.34	2.52	4.31	2.82	1.92
Dy	3.28	2.18	2.73	1.42	1.59	2.84	2.27	1.88	3.15	2.37	2.55
Er	0.704	0.591	0.488	0.379	0.462	0.591	0.595	0.607	0.632	0.715	0.815
Yb	0.380	0.392	0.280	0.288	0.306	0.27	0.387	0.439	0.269	0.492	0.536

Rock types as in Table 3-4. Liquid compositions were determined using mass balance calculations based on whole-rock trace element analyses combined with mineral modes (Bédard, 1994). The modal amounts of interstitial melt (wt%) were constrained by iteration to obtain the best match between calculated liquid composition and kimberlite analysis. $C_i^{liq} = C_i^{rock} / (f^{liq} + (f^{Oliv} D_i^{Oliv}) + (f^{Opx} D_i^{Opx}) + (f^{Cpx} D_i^{Cpx}) + (f^{Garn} D_i^{Garn}))$ was used to calculate the concentration of an element i in the trapped liquid (C_i^{liq}), where C_i^{rock} is the concentration of element i in the whole-rock, f the modal proportion as mass fraction of 1, and D_i the mineral/liquid partition coefficient of element i for the constituent mineral phases (Oliv, olivine; Opx, orthopyroxene; Cpx, clinopyroxene; Garn, garnet). Mineral-liquid partition coefficients after Fujimaki *et al.* (1984).

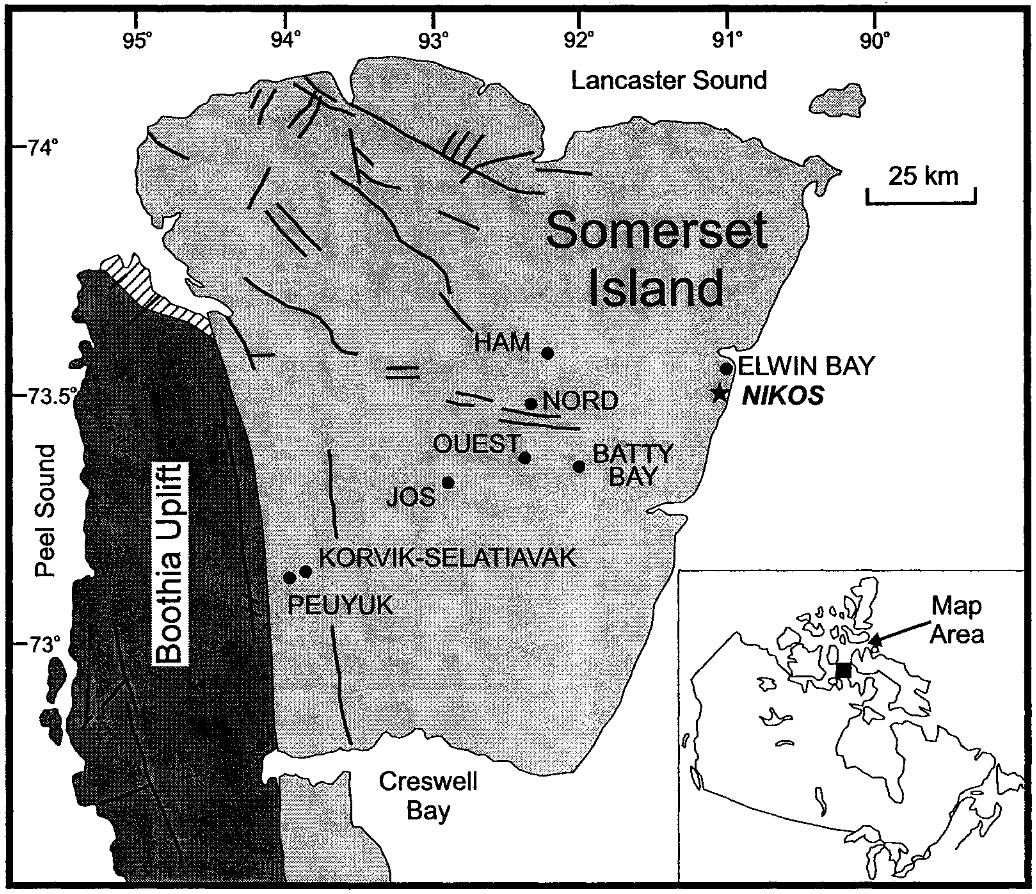
95°
94°
93°
92°
91°
90°
Lancaster Sound
-74°
25 km
Somerset Island
HAM
ELWIN BAY
NIKOS
-73.5°
NORD
OUEST
BATTY BAY
JOS
Peel Sound
Boothia Uplift
KORVIK-SELATIAVAK
PEUYUK
-73°
Map Area
Creswell Bay

Figure 3-1

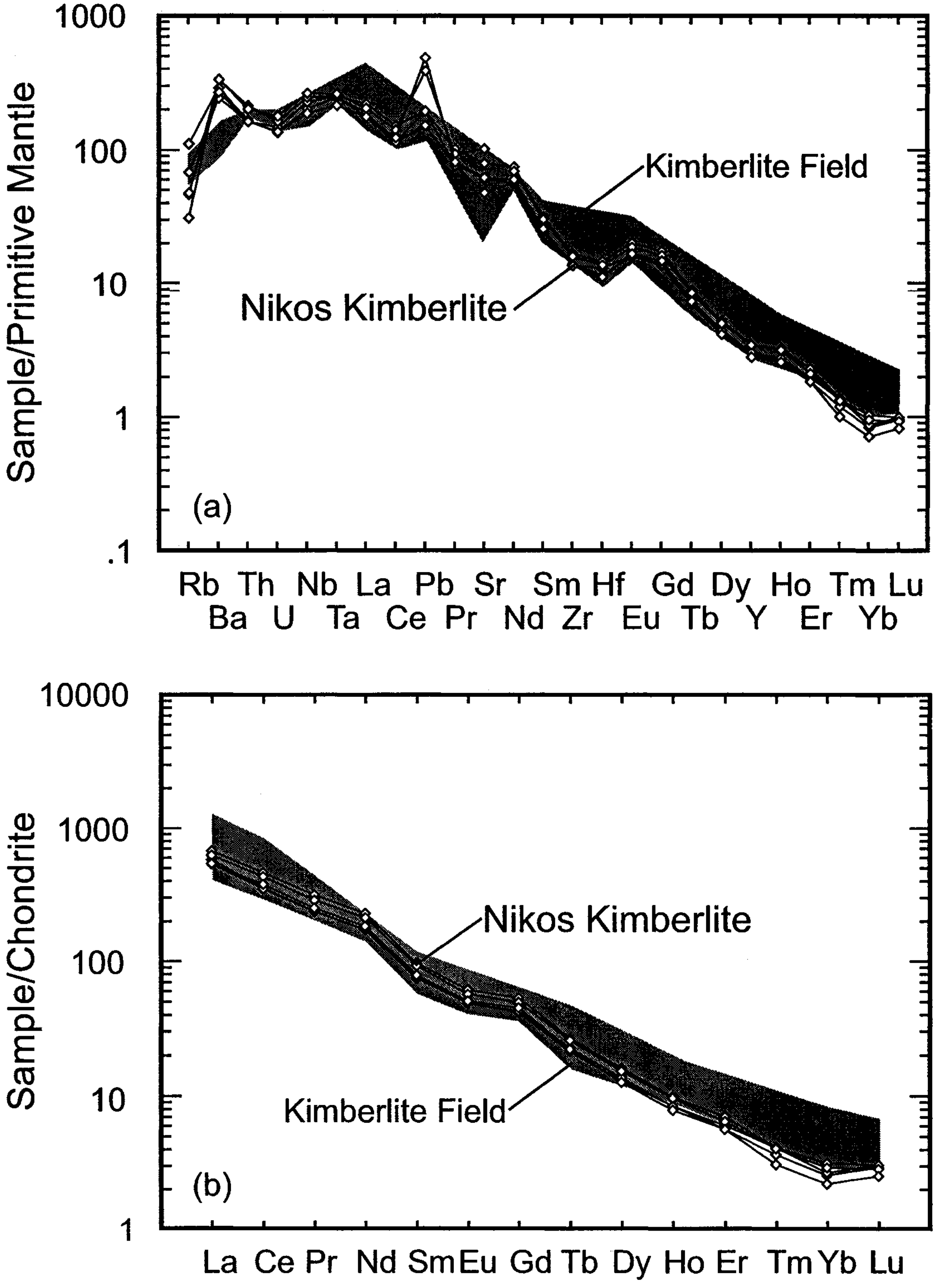
1000
100
10
1
.1
Sample/Primitive Mantle
Kimberlite Field
Nikos Kimberlite
(a)
Rb Th Nb La Pb Sr Sm Hf Gd Dy Ho Tm Lu
Ba U Ta Ce Pr Nd Zr Eu Tb Y Er Yb
10000
1000
100
10
1
Sample/Chondrite
Nikos Kimberlite
Kimberlite Field
(b)
La Ce Pr Nd Sm Eu Gd Tb Dy Ho Er Tm Yb Lu

Figure 3-2

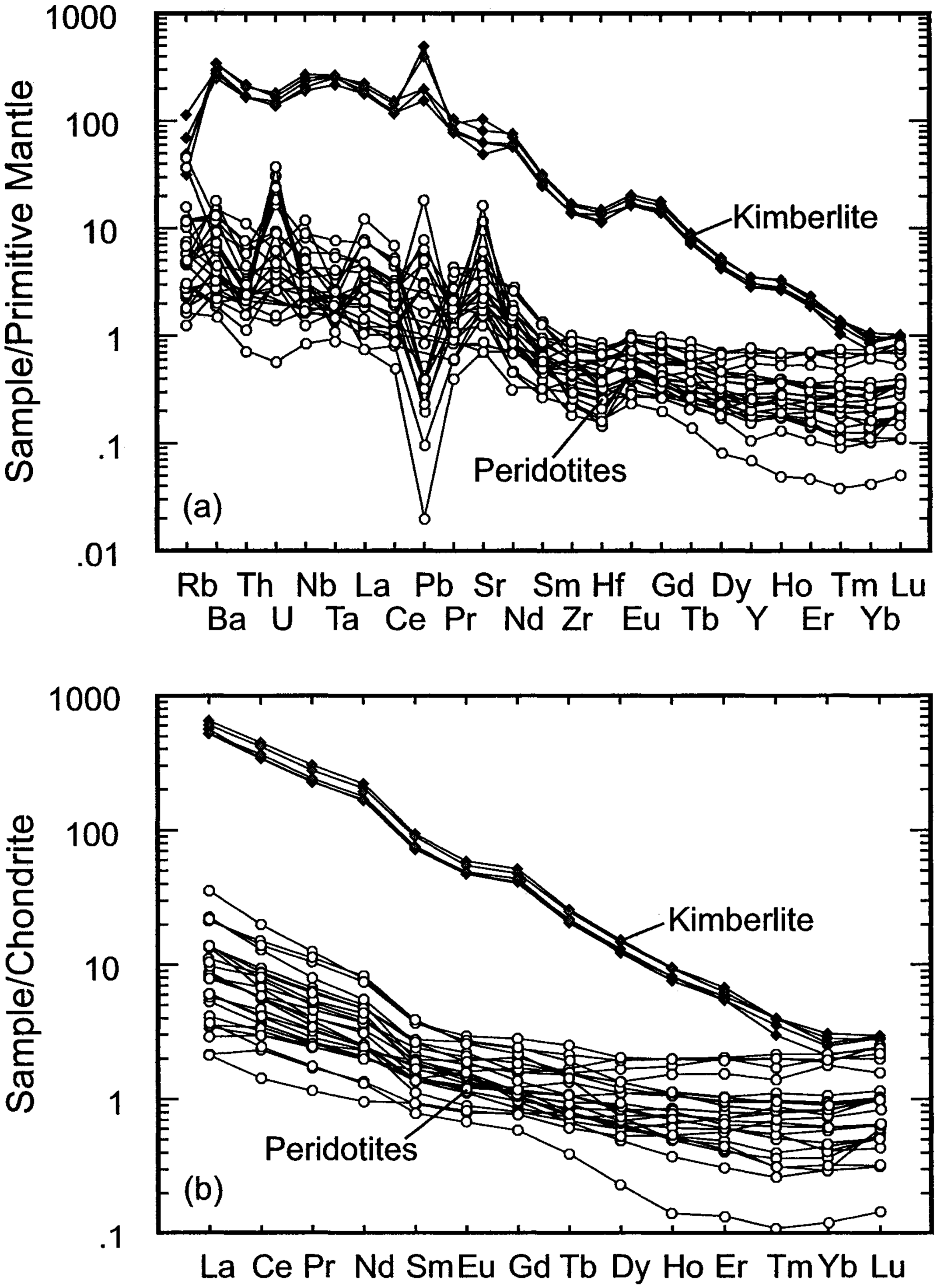
Sample/Primitive Mantle
1000
100
10
1
.1
.01
(a)
Kimberlite
Peridotites
Rb Th Nb La Pb Sr Sm Hf Gd Dy Ho Tm Lu
Ba U Ta Ce Pr Nd Zr Eu Tb Y Er Yb
Sample/Chondrite
1000
100
10
1
.1
(b)
Kimberlite
Peridotites
La Ce Pr Nd Sm Eu Gd Tb Dy Ho Er Tm Yb Lu

Figure 3-3

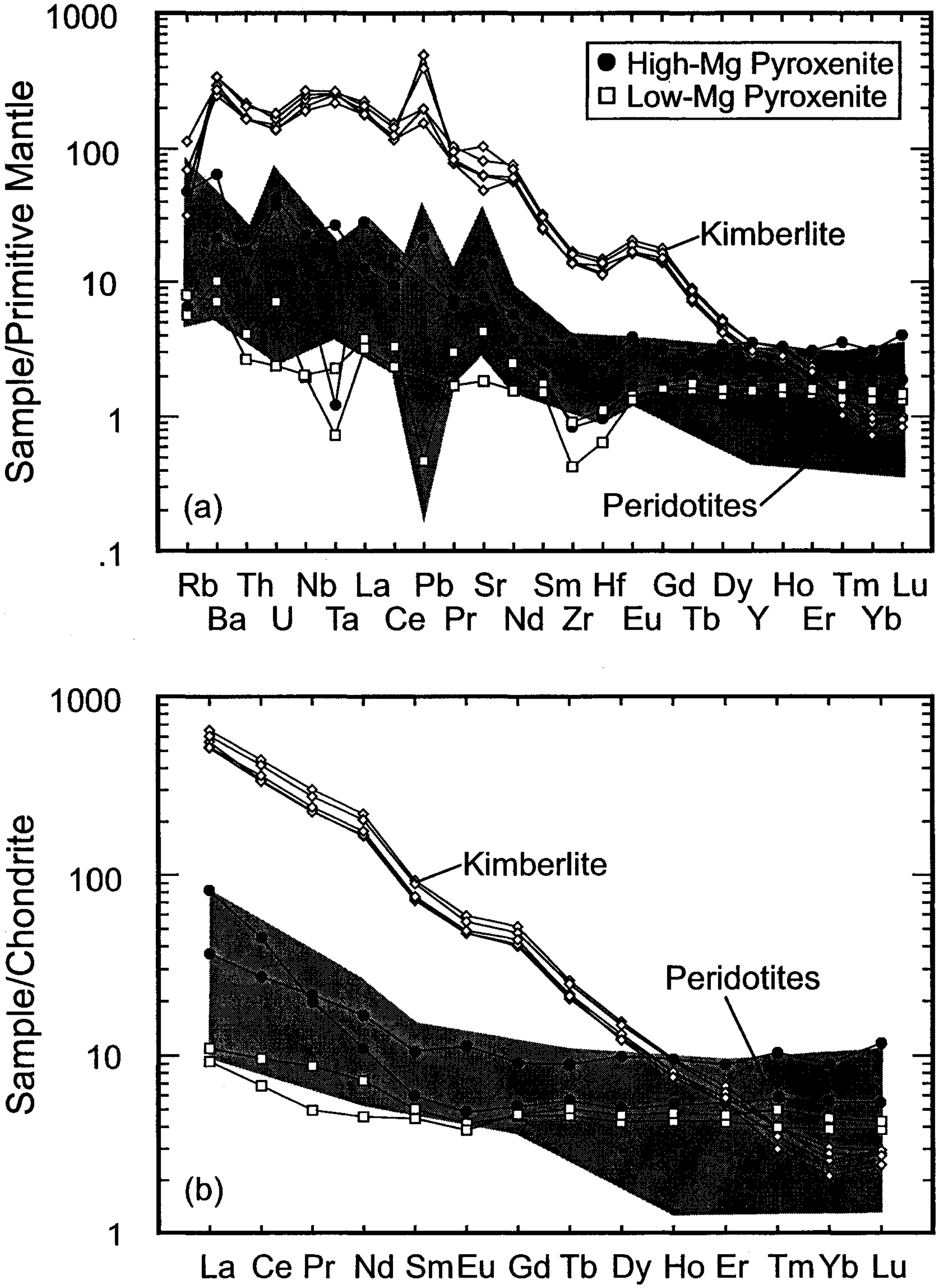
1000
100
10
1
.1
Sample/Primitive Mantle
● High-Mg Pyroxenite
□ Low-Mg Pyroxenite
Kimberlite
Peridotites
(a)
Rb Th Nb La Pb Sr Sm Hf Gd Dy Ho Tm Lu
Ba U Ta Ce Pr Nd Zr Eu Tb Y Er Yb
1000
100
10
1
Sample/Chondrite
Kimberlite
Peridotites
(b)
La Ce Pr Nd Sm Eu Gd Tb Dy Ho Er Tm Yb Lu

Figure 3-4

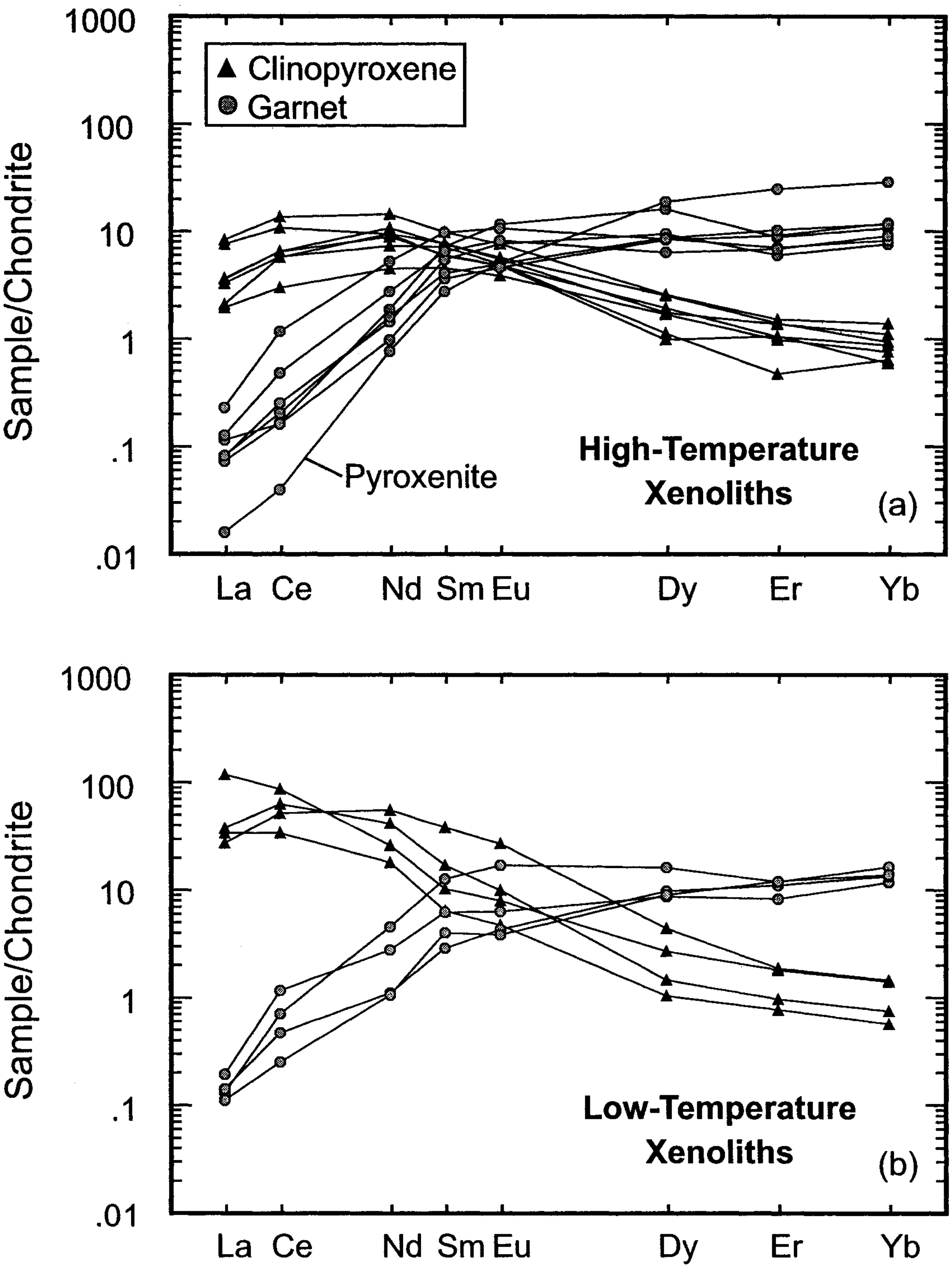
1000
100
10
1
.1
.01
Sample/Chondrite
▲ Clinopyroxene
● Garnet
Pyroxenite
High-Temperature Xenoliths
(a)
La Ce Nd Sm Eu Dy Er Yb
1000
100
10
1
.1
.01
Sample/Chondrite
Low-Temperature Xenoliths
(b)
La Ce Nd Sm Eu Dy Er Yb

Figure 3-5

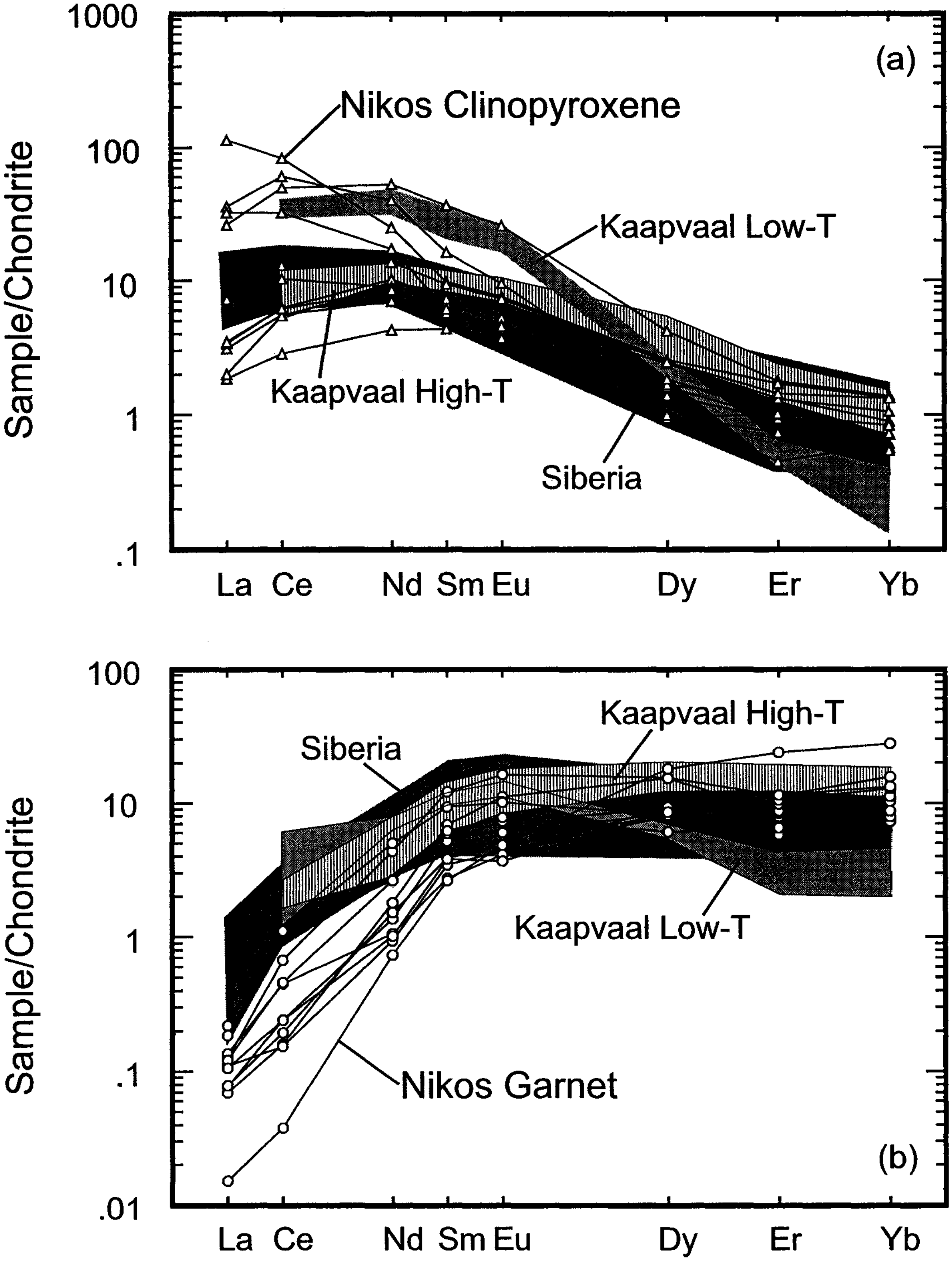

1000
100
10
1
.1
Sample/Chondrite
(a)
Nikos Clinopyroxene
Kaapvaal Low-T
Kaapvaal High-T
Siberia
La
Ce
Nd
Sm
Eu
Dy
Er
Yb
100
10
1
.1
.01
Sample/Chondrite
Kaapvaal High-T
Siberia
Kaapvaal Low-T
Nikos Garnet
(b)
La
Ce
Nd
Sm
Eu
Dy
Er
Yb

Figure 3-6

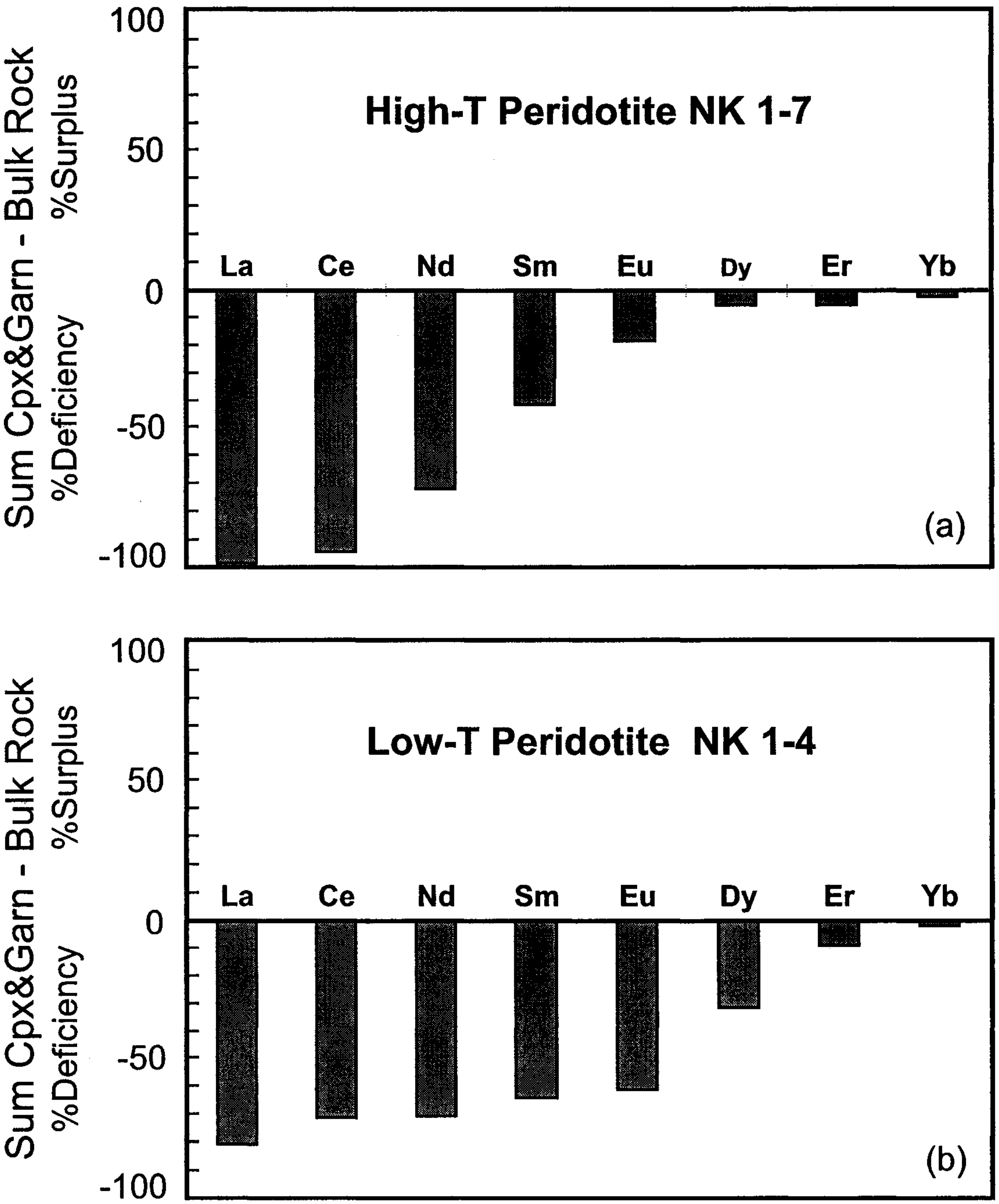
High-T Peridotite NK 1-7
Sum Cpx&Garn - Bulk Rock
%Surplus
%Deficiency
100
50
0
-50
-100
La
Ce
Nd
Sm
Eu
Dy
Er
Yb
(a)
Low-T Peridotite NK 1-4
Sum Cpx&Garn - Bulk Rock
%Surplus
%Deficiency
100
50
0
-50
-100
La
Ce
Nd
Sm
Eu
Dy
Er
Yb
(b)

Figure 3-7

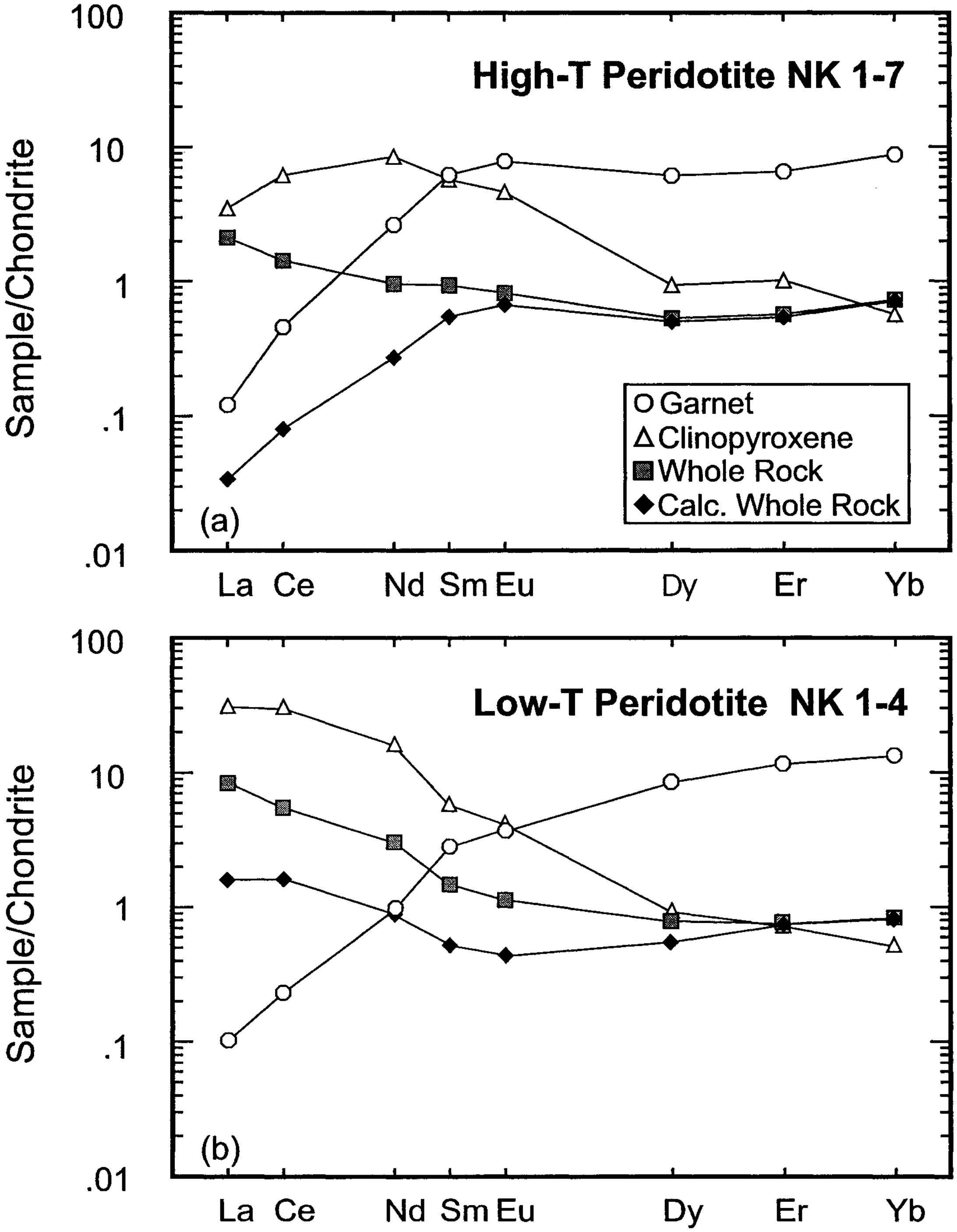
High-T Peridotite NK 1-7
Low-T Peridotite NK 1-4
Sample/Chondrite
100
10
1
.1
.01
La
Ce
Nd
Sm
Eu
Dy
Er
Yb
○ Garnet
△ Clinopyroxene
■ Whole Rock
◆ Calc. Whole Rock
(a)
(b)

Figure 3-8

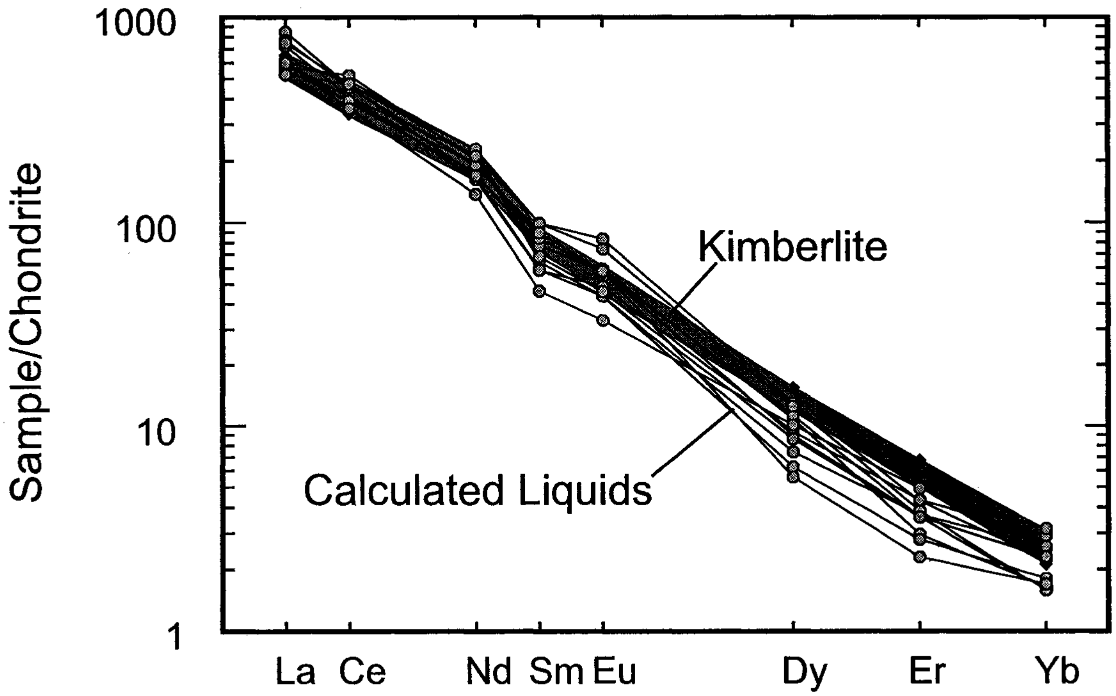
1000
100
10
1
Sample/Chondrite
Kimberlite
Calculated Liquids
La
Ce
Nd
Sm
Eu
Dy
Er
Yb

Figure 3-9

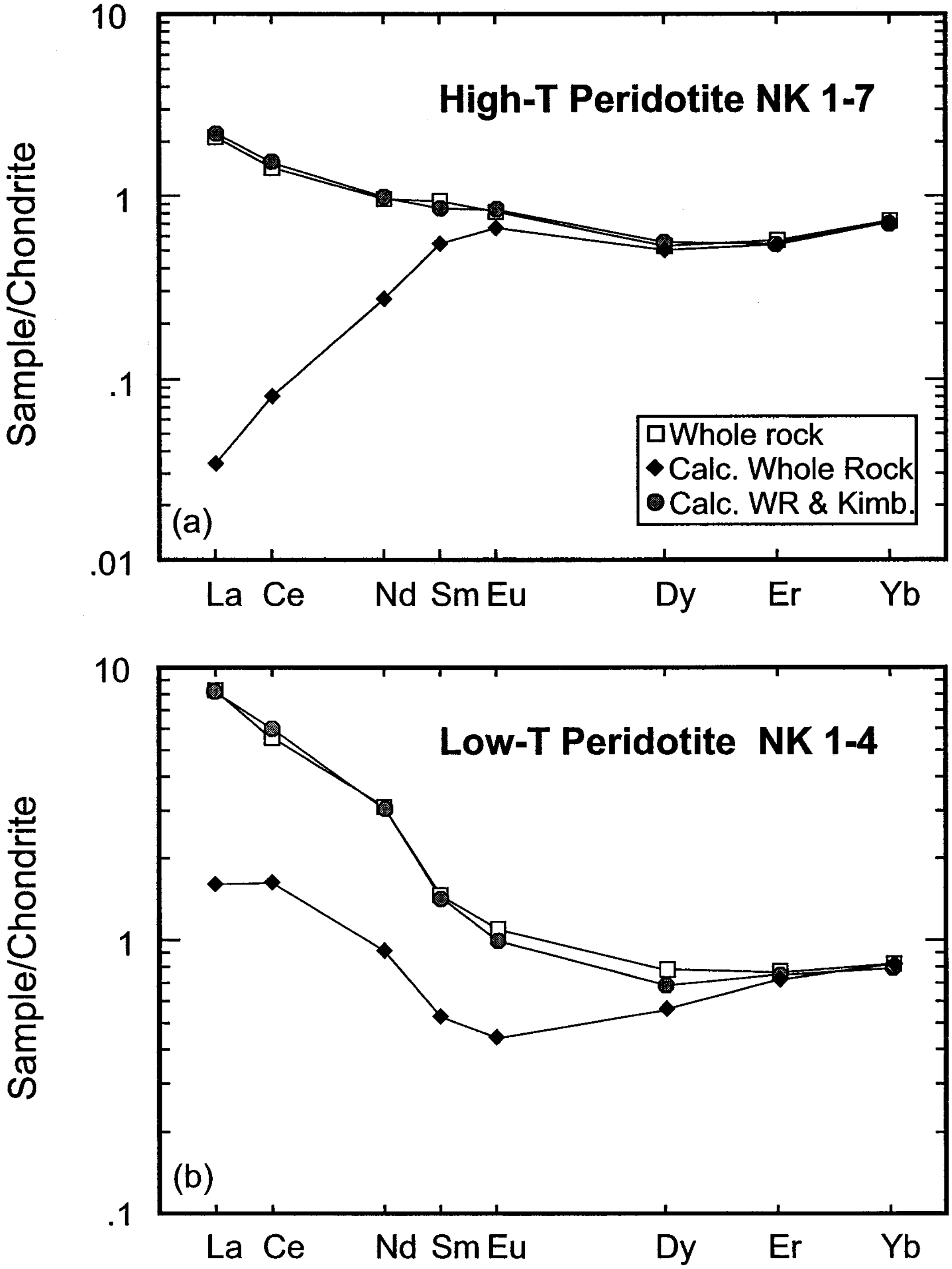

10
1
.1
.01
Sample/Chondrite
High-T Peridotite NK 1-7
□ Whole rock
◆ Calc. Whole Rock
● Calc. WR & Kimb.
(a)
La
Ce
Nd
Sm
Eu
Dy
Er
Yb
10
1
.1
Sample/Chondrite
Low-T Peridotite NK 1-4
(b)
La
Ce
Nd
Sm
Eu
Dy
Er
Yb

Figure 3-10

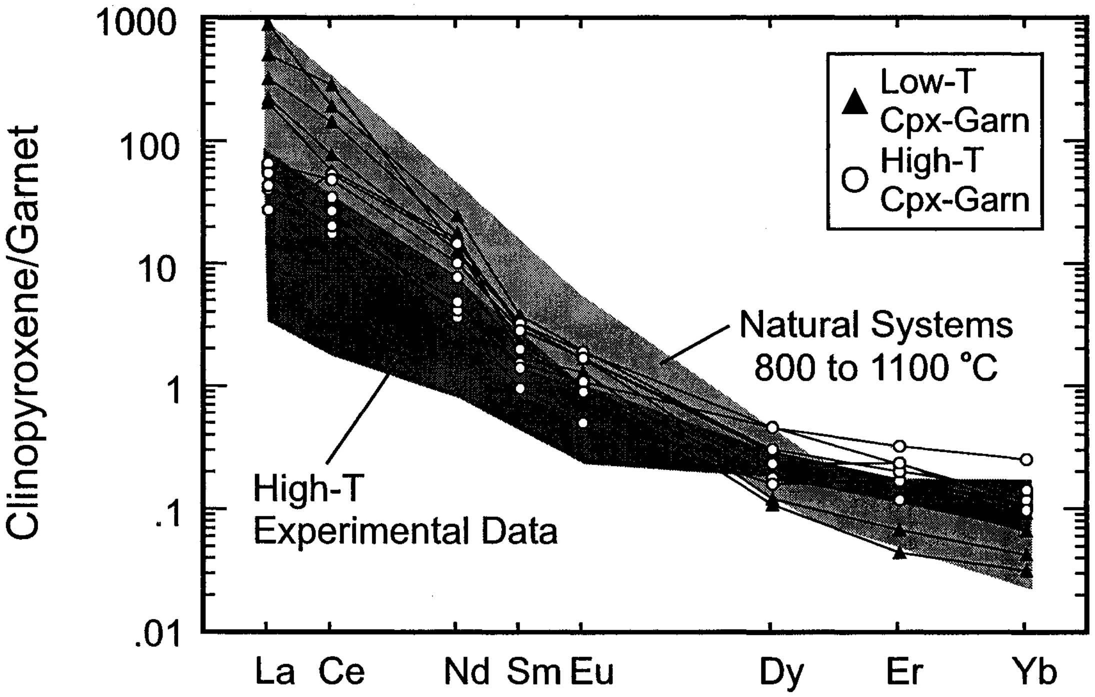

1000
100
10
1
.1
.01
Clinopyroxene/Garnet
La
Ce
Nd
Sm
Eu
Dy
Er
Yb
▲ Low-T Cpx-Garn
○ High-T Cpx-Garn
Natural Systems 800 to 1100 °C
High-T Experimental Data

Figure 3-11

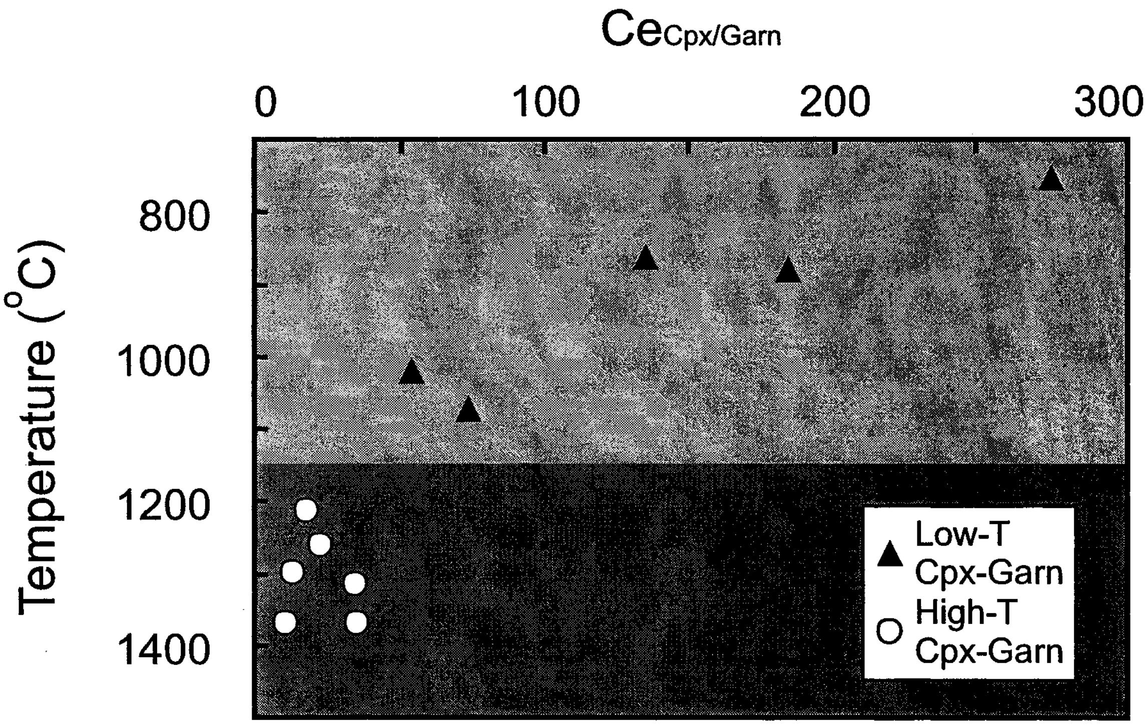

Ce Cpx/Garn
0
100
200
300
800
1000
1200
1400
Temperature (°C)
▲ Low-T Cpx-Garn
○ High-T Cpx-Garn

Figure 3-12

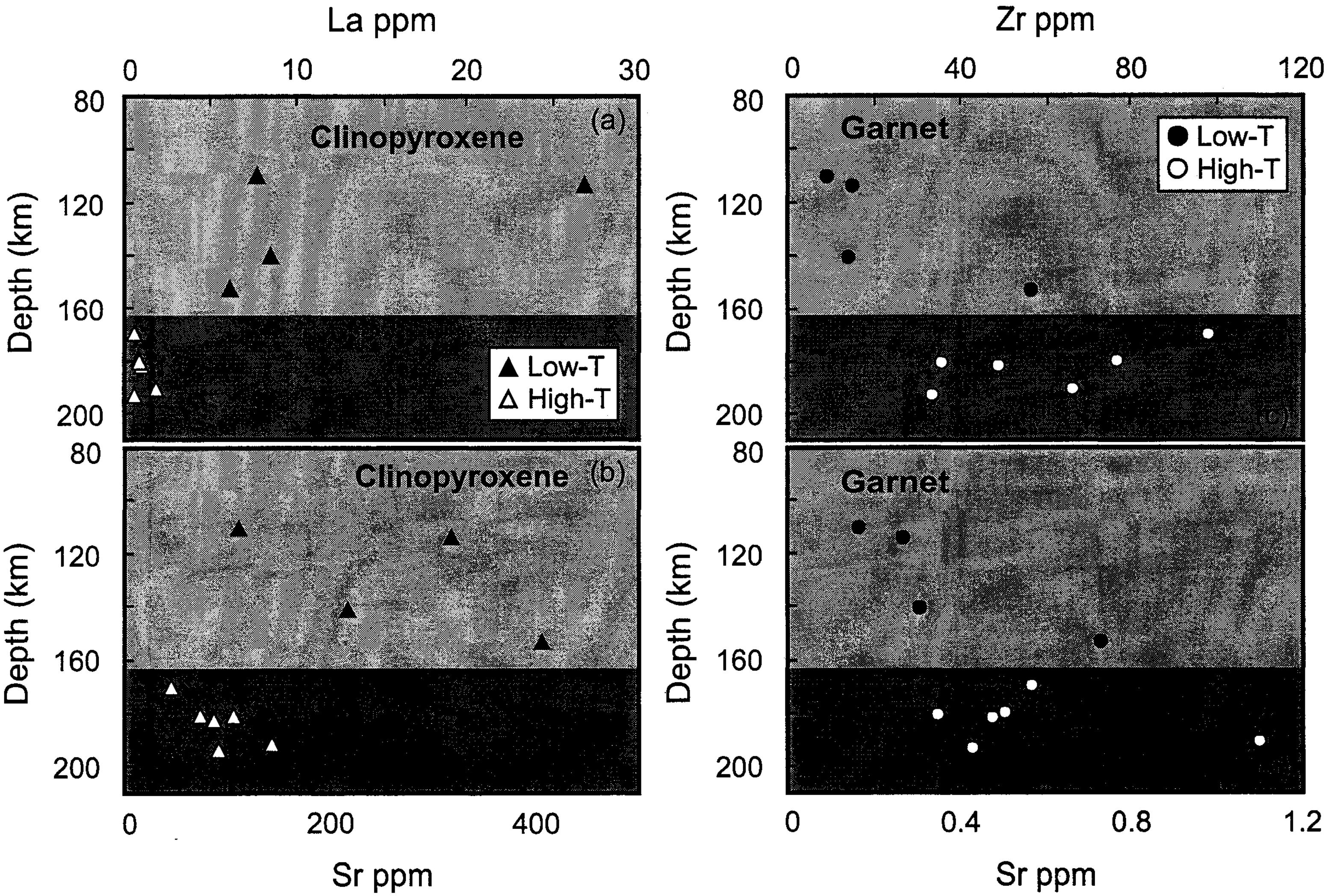
La ppm
0
10
20
30
Zr ppm
0
40
80
120
Depth (km)
80
120
160
200
Clinopyroxene
(a)
▲ Low-T
△ High-T
Garnet
● Low-T
○ High-T
(c)
Clinopyroxene
(b)
Garnet
Sr ppm
0
200
400
0
0.4
0.8
1.2

Figure 3-13

CHAPTER 4

Sr-Nd-Pb isotope systematics of mantle xenoliths from Somerset Island kimberlites: evidence for lithosphere stratification beneath Arctic Canada

Abstract

Sr, Nd and Pb isotopic compositions were determined for a suite of Archean garnet peridotite and garnet pyroxenite xenoliths and their host Nikos kimberlite (100 Ma) from Somerset Island, in order to constrain the isotopic character of the mantle root beneath the northern Canadian craton. The Nikos peridotites are enriched in highly incompatible trace elements (La/Sm_N=4-6), and show $^{143}Nd/^{144}Nd_{(t)}$ (0.51249-0.51276) and a large range in $^{87}Sr/^{86}Sr_{(t)}$ (0.7047-0.7085) and Pb ($^{206}Pb/^{204}Pb_{(t)}$=17.18-19.03) isotope ratios that are distinct from those estimated for "depleted mantle" compositions at the time of kimberlite emplacement. The Nd isotopic compositions of the peridotites overlap those of the Nikos kimberlite, suggesting that the xenoliths were contaminated with kimberlite or a kimberlite-related accessory phase (i.e. apatite). The highly variable Sr and Pb isotopic compositions of the peridotites, however, indicate that kimberlite contribution was restricted to very small amounts (~1 wt% or less). The high-temperature peridotites (>1100°C) that sample the deep Somerset lithosphere trend towards more radiogenic $^{87}Sr/^{86}Sr_{(t)}$ (0.7085) and unradiogenic $^{206}Pb/^{204}Pb_{(t)}$ (17.18) isotopic ratios than those of the low-temperature peridotites (<1100°C). This is in agreement with Sr isotopic compositions of clinopyroxene from the low-temperature peridotites ($^{87}Sr/^{86}Sr_{(t)}$=0.7038-0.7046) that are significantly less radiogenic than those of clinopyroxene from the high-temperature peridotites ($^{87}Sr/^{86}Sr_{(t)}$=0.7052-0.7091). The depth correlation of Sr isotopes for clinopyroxene, and Sr and Pb isotopic compositions for the Nikos whole-rocks indicate that the deep Somerset lithosphere (>160 km) is isotopically distinct from the shallow lithospheric mantle. The isotopic stratification with depth suggests that the lower lithosphere is probably younger and may have been added to the existing Archean shallow

mantle in a Phanerozoic magmatic event. The radiogenic Sr isotope ratios of the high-temperature peridotites and their clinopyroxenes suggest that the underplated deep lithosphere contained recycled (altered oceanic crust and sedimentary component?) material introduced during earlier subduction.

1. INTRODUCTION

Archean cratons are underlain by cold refractory mantle roots characterized by a depletion in fusible major elements compared to fertile mantle (e.g. Nixon, 1987; Herzberg, 1993; McDonough, 1990; Boyd et al., 1997). In contrast to their refractory major element chemistry, however, the peridotites that sample these mantle roots are frequently trace element enriched suggesting that the lithosphere may constitute a significant reservoir for incompatible elements (Erlank et al., 1987; Menzies et al., 1987). Mantle xenoliths that are brought to the surface by kimberlites and alkali basalts are a unique window into the subcontinental mantle, and provide essential insights into the isotopic character and evolution of the lithosphere to depths of greater than 200 km. Previous studies have shown that these peridotite xenoliths have a large range in Sr, Nd and Pb isotopic compositions and trend towards "enriched" time-integrated isotopic signatures relative to bulk Earth (e.g. Menzies and Murthy, 1980; Hawkesworth et al., 1990a; Pearson et al., 1995a). This is inconsistent with their origin as residues of partial melting, which should create refractory mantle roots with an isotopic signature similar to that of "depleted mantle" (Zindler and Hart, 1986). Such isotopic heterogeneities have been widely interpreted to indicate that the subcontinental lithosphere has been infiltrated by small volume melts or fluids with highly variable isotopic compositions over time. These melts or fluids were enriched in large ion lithophile elements (LILE) and light rare earth elements (LREE) and originated from deeper levels of the lithosphere or from the underlying asthenosphere (Erlank et al., 1987; Menzies et al., 1987). Thus the isotopic systematics of samples representing the subcratonic mantle are sensitive indicators of the metasomatic history they have experienced, and provide evidence for the existence of isotopically distinct domains in the lithosphere and a means to constrain their spatial distribution.

In this article, we present Sr, Nd and Pb isotopic compositions for a suite of garnet peridotites and garnet pyroxenites and their host Nikos kimberlite from Somerset Island in the Canadian Arctic (Schmidberger and Francis, 1999; Fig. 1). The results for whole-rocks and constituent mineral phases (i.e. clinopyroxene, garnet) provide insights into the isotopic signature of the deep Archean mantle root beneath the northern Canadian craton. The data set indicates a change in isotopic composition with depth in the lithospheric mantle and provides constraints on the role of the host kimberlite as a possible contaminant during sample transport.

2. SAMPLES

2.1. Kimberlite

The recently discovered Nikos kimberlites were emplaced into late Archean crystalline basement overlain by Paleozoic sediments at the northern margin of the Canadian craton (Frisch and Hunt, 1993; Pell, 1993; Fig. 1). U-Pb dating of perovskite indicates Cretaceous emplacement ages between 90 to 105 Ma for the Somerset Island kimberlites (Heaman, 1989; Smith et al., 1989). A Rb-Sr whole-rock isochron for the Nikos kimberlites (n=4) from this study yields an emplacement age of 97±17 Ma (MSWD=1.1), which is in good agreement with the U-Pb ages.

The southernmost of the three individual Nikos pipes (NK3) has been interpreted to represent kimberlite magma (Schmidberger & Francis, 1999), because of the non-clastic microcrystalline nature of its groundmass. The kimberlite contains olivine, phlogopite, garnet and spinel in a very fine-grained carbonate-rich matrix of calcite, serpentine, perovskite and apatite. The very high $CaCO_3$ contents (27-39 wt%; Schmidberger and Francis, 1999) of the kimberlite whole-rock analyses indicate liquid compositions intermediate between kimberlite and carbonatite (Woolley & Kempe, 1989; Ringwood et al., 1992). The kimberlites show a strong enrichment in highly incompatible trace elements, such as LILE and LREE compared to primitive mantle compositions and chondrites (McDonough and Sun, 1995; Schmidberger and Francis, 2001).

2.2. Mantle xenoliths

The Nikos xenolith suite consists of large (>10 cm), well-preserved garnet peridotites with minor occurrences of garnet pyroxenites (Schmidberger and Francis, 1999). The majority of the peridotites contain large crystals of olivine, orthopyroxene, clinopyroxene and garnet, and exhibit coarse textures, although a few peridotites with porphyroclastic textures are observed. Small amounts (~1% or less) of phlogopite are present, whereas amphibole is absent. The term peridotite is used for the mantle xenoliths in this study since the small differences in modal clinopyroxene content do not justify dividing the suite according to the IUGS (International Union of Geological Sciences) classification into harzburgites (clinopyroxene <5 wt%) or lherzolites (clinopyroxene >5 wt%). A detailed description of xenolith mineralogy and major, trace and rare earth element (REE) chemistry can be found in Schmidberger and Francis (1999) and Schmidberger and Francis (2001). The estimated temperature and pressure conditions of last equilibration (800-1400°C, 25-60 kb) indicate that the Nikos peridotites were sampled at depths between 80 to 190 km by their host kimberlite (Schmidberger and Francis, 1999).

The high magnesium numbers (mg-number=Mg/(Mg+Fe)=0.90-0.93) and olivine-rich mineralogy (avg. 80 wt%) of the peridotites reflect their refractory nature and suggest that these xenoliths are melt-depleted residues (Schmidberger and Francis, 1999; Schmidberger and Francis, 2001). In contrast to their depleted major element chemistry, however, the peridotites are enriched in LILE compared to abundances estimated for primitive mantle and LREE (La/Sm_N=4-6) relative to chondrites, while the heavy rare earth element (HREE) contents are approximately chondritic (Schmidberger and Francis, 2001).

Minor pyroxenite xenoliths consisting of clinopyroxene, orthopyroxene and garnet show a range in mg-numbers (Schmidberger and Francis, 1999). Two high-Mg pyroxenites contain olivine and abundant garnet (avg. 20 wt%), and have mg-numbers (0.88-0.90) that are similar to those of the peridotites. Two low-Mg pyroxenites (mg-number=0.85) have lower modal abundances of garnet (avg. 10 wt%) and higher clinopyroxene contents (avg. 70 wt%) than the high-Mg pyroxenites (avg. 30 wt%). Both the high-Mg and low-Mg pyroxenites are enriched in incompatible trace elements, such as LILE and LREE relative to values for primitive mantle and chondrites (Schmidberger and Francis, 2001). The low-Mg pyroxenites, however, are less enriched in incompatible trace elements than the high-Mg pyroxenites.

2.3. Clinopyroxene and garnet

The emerald green clinopyroxenes in the Somerset peridotites are chromian diopside and the garnets are chromian pyrope (Schmidberger and Francis, 1999). The major element compositions of both clinopyroxene and garnet are homogeneous on the scale of a thin section.

Mass balance calculations using REE contents of clinopyroxene and garnet and their respective modal abundances indicate that calculated LREE abundances for all Nikos xenoliths are significantly lower (e.g. La: 70-99%, Nd and Sm: ~50%) than those of the analyzed whole-rocks, while having similar HREE contents (Schmidberger and Francis, 2001). These results suggest the presence of a kimberlite-related LREE-rich interstitial component (i.e. ~1% kimberlite liquid) and/or accessory mineral phase (i.e. trace amounts of apatite, although as yet undetected in thin sections) to account for the excess trace element abundances (Schmidberger and Francis, 2001).

The mineral trace element compositions indicate that the peridotites can be divided according to temperature and thus depth of origin into low-temperature (<1100°C; 80-150 km) and high-temperature xenoliths (>1100°C; 160-190 km). The clinopyroxenes from the low-temperature peridotites have LREE (e.g. La=6-25 ppm) and Sr (100-400 ppm) abundances that are significantly higher than those of clinopyroxene from the high-temperature peridotites (La=0.4-2 ppm; Sr=50-140 ppm; Schmidberger and Francis, 2001). In addition, the calculated LREE patterns for the majority of the shallow low-temperature peridotites are flat, whereas the deep-seated high-temperature peridotites are characterized by LREE-depleted calculated bulk rock patterns relative to chondrites (Schmidberger and Francis, 2001). These findings suggest that the shallow Somerset lithosphere is geochemically distinct from the underlying lower lithospheric mantle and that the mantle root beneath the northern Canadian craton is characterized by a depth zonation in incompatible trace elements (Schmidberger and Francis, 2001).

3. ANALYTICAL METHODS

All exterior surfaces were first removed from the xenoliths. Samples were then crushed and rock chips were ground in an aluminum mill. Crushed whole-rock kimberlite samples were carefully hand-picked under the binocular microscope prior to grinding to eliminate contamination from peridotite xenocrysts and country rock fragments. Garnet and clinopyroxene separates were hand-picked under the binocular microscope and inclusion free crystals were washed in an ultrasonic bath with acetone, ultrapure water, and then 2.5 N HCl.

For Nd and Sr isotope analyses, the sample powders were spiked with a mixed ^{150}Nd-^{149}Sm isotope tracer and dissolved in a mixture of HF-HNO_3-$HClO_4$. Whole-rock samples and the garnet separates were dissolved at 170°C in Teflon bombs and clinopyroxene separates at 140°C in Savillex® vials for at least 10 days. Sr and REE were separated using conventional chromatographic techniques. Typical procedural blanks are Sr<70 pg, and Nd and Sm<40 pg. Sr aliquots were loaded using a TaF solution on single W filaments, and Nd and Sm were loaded with HCl using a triple Re filament technique. Nd and Sr isotope measurements were obtained by thermal ionization mass spectrometry (TIMS) at GEOTOP, Université du Québec à Montréal (UQAM) using a Sector 54 mass spectrometer operated in the static multicollection mode. For Pb isotope analysis, the sample powders were dissolved in a mixture of HF-HNO_3. Pb was separated using anion-exchange chromatography (after Manhès et al., 1980), U and Th determinations followed the technique of Edwards et al. (1986) and both were conducted at GEOTOP-UQAM. Pb, U and Th concentrations were determined by isotope dilution using ^{206}Pb, ^{233}U-^{236}U and ^{229}Th spikes. Procedural blanks for Pb, U and Th were 10-15, 2-6 and 80-100 pg, respectively and are considered negligible. Pb aliquots were loaded on a single Re filament using a silica gel-H_3PO_4 acid mixture and Pb isotope measurements were obtained using a single Faraday cage detector or Daly analogue detector in peak switching mode. Pb, U and Th concentrations were determined using a Micromass IsoProbe multi-collector inductively coupled mass spectrometer (MC-ICP-MS) coupled to an ARIDUS® microconcentric nebuliser.

4. RESULTS

4.1. Kimberlite

Initial Nd and Sr isotope data for the Nikos kimberlites were calculated for an emplacement age of 100 Ma. $^{143}Nd/^{144}Nd_{(t)}$ ratios are tightly constrained between 0.51254 to 0.51259 (corresponding to initial ε_{Nd} values of +0.6 to +1.5), and are similar to or slightly depleted than the composition of CHUR (chondrite uniform reservoir; Table 1; Fig. 2). The $^{87}Sr/^{86}Sr_{(t)}$ ratios (0.7052) are identical, and are slightly "enriched" compared to the value for bulk Earth. Previous studies on South African kimberlites have divided kimberlites into two groups ("Group I" and "Group II") based on their distinct mineralogy and isotopic signatures, indicating derivation from isotopically distinct mantle domains (Dawson, 1967; Smith, 1983). More recently, South African "Group II" kimberlites were recognized to have similar mineralogy and chemical compositions to those of olivine lamproites and are termed orangeites by Mitchell (1995). Initial Nd and Sr isotopic compositions for the Nikos kimberlites plot close to the field encompassing data for "Group I" kimberlites from North America, South Africa and Siberia, which are undifferentiated to slightly depleted relative to values for CHUR and bulk Earth, respectively (Smith, 1983; Heaman, 1989; Pearson et al., 1995b; Fig. 2). Isotope data for

South African "Group II" and Australian "kimberlites", in contrast, have much lower Nd and higher Sr isotopic ratios than the Nikos kimberlites and all "Group I" kimberlites (McCulloch et al., 1983; Smith, 1983; Fig. 2).

The Pb isotopic compositions of the Nikos kimberlites show a positive correlation in Pb-Pb isotope diagrams at the time of emplacement (Table 2; Fig. 3). The Pb isotope array yields a $^{207}Pb/^{206}Pb$ age of ~2.7 Ga, but is not likely to have any geochronological significance. In an initial $^{206}Pb/^{204}Pb$ versus $^{208}Pb/^{204}Pb$ diagram, the Nikos kimberlite Pb isotope ratios plot between data for "Group I" and "Group II" kimberlites from South Africa (Kramers, 1977; Fraser et al., 1985; Fig. 3). However, South African "Group II" kimberlites exhibit lower $^{206}Pb/^{204}Pb_{(t)}$ at similar $^{207}Pb/^{204}Pb_{(t)}$ isotopic ratios than those of the Nikos and South African "Group I" kimberlites (Kramers, 1977; Smith, 1983; Fraser et al., 1985; Fig. 3).

4.2. Mantle xenoliths

The whole-rock Nd and Sr isotopic compositions for the Nikos xenoliths were corrected for the 100 Ma in-situ decay since the emplacement of their host kimberlite (Table 1). $^{143}Nd/^{144}Nd_{(t)}$ ratios of the peridotites range between 0.51249 to 0.51276 ($\varepsilon_{Nd(t)}$ values of -0.3 to +5.0) and are similar to or depleted relative to the value for CHUR (Fig. 4). The Nd isotopic compositions of the low-temperature peridotites extend to slightly more radiogenic values ($^{143}Nd/^{144}Nd_{(t)}$=0.51257-0.51276) than those in the high-temperature peridotites ($^{143}Nd/^{144}Nd_{(t)}$=0.51249-0.51262). Depleted mantle Nd model ages (T_{DM}) for the peridotites range from 500 to 1250 Ma (except NK1-7: 2600 Ma; Table 1). $^{87}Sr/^{86}Sr_{(t)}$ isotopic ratios in the peridotites show a significant variation (0.7047-0.7085) and are "enriched" relative to bulk Earth (Fig. 4). The shallow low-temperature peridotites have Sr isotopic compositions that are significantly less radiogenic ($^{87}Sr/^{86}Sr_{(t)}$=0.7047-0.7066) than those in the high-temperature peridotites ($^{87}Sr/^{86}Sr_{(t)}$=0.7064-0.7085; Fig. 4). The unradiogenic Sr and radiogenic Nd isotope ratios for one peridotite (NK2-4) suggest that it represents a sample of low-temperature lithosphere, although temperature and pressure estimates were not determined. One low-Mg pyroxenite (NK3-1) yields a very unradiogenic $^{143}Nd/^{144}Nd_{(t)}$ (0.51197) isotopic ratio relative to those of the other pyroxenites and the peridotites (Fig. 4).

The $^{143}Nd/^{144}Nd_{(t)}$ isotopic compositions of the low and high-temperature peridotites are similar to those of the Nikos kimberlite, while having significantly more variable $^{87}Sr/^{86}Sr_{(t)}$ ratios (Fig. 4). The Nd and Sr isotopic signatures of all Nikos peridotites overlap the field of kimberlite-hosted garnet peridotites (including whole-rock and clinopyroxene data) from the South African craton (Menzies & Murthy, 1980; Kramers et al., 1983; Richardson et al., 1985; Jones, 1987; Walker et al., 1989; Hawkesworth et al., 1990a; Macdougall & Haggerty, 1999; Fig. 4). While the low-temperature South African xenoliths encompass the entire garnet peridotite field, many of the high-temperature South African xenoliths appear to be slightly depleted relative to CHUR and bulk Earth. In contrast, Sr isotopic ratios for the Nikos peridotites exhibit the opposite relationship, with the most radiogenic values observed for the high-temperature xenoliths. In comparison, the Nd and Sr isotopic compositions for post-Archean spinel peridotites plot within the depleted quadrant relative to CHUR and bulk Earth, respectively, and are distinct from those for most kimberlite-hosted cratonic mantle xenoliths (Hawkesworth et al., 1990b and references therein).

The high-temperature peridotites have μ ($^{238}U/^{204}Pb$) values that are significantly higher (avg. μ=37) than those of both the low-temperature peridotites (avg. μ=25) and the host Nikos kimberlite (avg. μ=12; Table 2). The μ values for both high and low-temperature peridotites, however, are higher than those estimated for melt-depleted residues (μ~10; Zindler and Hart, 1986; Fig. 5), suggesting the preferential addition of U after lithosphere formation. The Nikos Pb isotopic ratios plot below the Stacey and Kramers (1975) lead isotope evolution curve (μ=9.7) and dominantly to the right of the geochron (Fig. 5). The high-temperature peridotites exhibit $^{206}Pb/^{204}Pb_{(t)}$ (17.181-18.299) isotopic compositions that are less radiogenic than those of the low-temperature peridotites ($^{206}Pb/^{204}Pb_{(t)}$=17.820-19.033), whereas their $^{207}Pb/^{204}Pb_{(t)}$ and $^{208}Pb/^{204}Pb_{(t)}$ ratios are indistinguishable (Table 2; Fig. 5). The Pb isotopic signatures for the Nikos peridotites partly overlap those for the Nikos kimberlites at the time of emplacement (Fig. 5), and both the low and high-temperature Nikos peridotites have Pb isotopic compositions that are within the range of previously reported data for garnet peridotites (including whole-rock and clinopyroxene data) in South African kimberlites (Kramers, 1977; Kramers et al., 1983; Richardson et al., 1985; Walker et al., 1989; Hawkesworth et al., 1990a; Fig. 5).

The Pb isotopic ratios of the one high-Mg pyroxenite are similar to those of the peridotites. One low-Mg pyroxenite (NK3-1) is characterized by very unradiogenic Pb isotopic compositions ($^{206}Pb/^{204}Pb_{(t)}$=16.91), while the other (NK3-17) has highly radiogenic Pb isotopic ratios ($^{206}Pb/^{204}Pb_{(t)}$=19.61; Fig. 5).

4.3. Clinopyroxene and garnet

The Nd isotopic ratios of clinopyroxene in the Nikos peridotites are depleted relative to the value for CHUR (Table 1; Fig. 6). Although the Nd isotopic compositions mostly overlap, two clinopyroxenes from the low-temperature peridotites ($^{143}Nd/^{144}Nd_{(t)}$=0.51268-0.51269) exhibit more radiogenic values than those of clinopyroxenes from the high-temperature xenoliths ($^{143}Nd/^{144}Nd_{(t)}$=0.51254-0.51261). Depleted mantle Nd model ages (T_{DM}) yield 500-800 Ma and 900-1400 Ma for clinopyroxenes from low and high-temperature peridotites, respectively. Rb and Sr abundances for Nikos clinopyroxene separates from two peridotites and one pyroxenite were determined using isotope dilution analysis (Table 1). As the calculated $^{87}Rb/^{86}Sr$ ratios are extremely low (high-temperature peridotite: 0.00020; low-temperature peridotite: 0.00018), the correction of the measured Sr isotopic ratios for in-situ decay (100 Ma) is negligible (Table 1). The $^{87}Sr/^{86}Sr_{(t)}$ ratios for the remaining clinopyroxene separates were calculated using $^{87}Rb/^{86}Sr$ ratios of 0.00020 and 0.00018 for high and low-temperature peridotites, respectively. The Sr isotopic ratios for clinopyroxenes in the low-temperature peridotites ($^{87}Sr/^{86}Sr_{(t)}$=0.7038-0.7046) are similar or less radiogenic than the value for bulk Earth (Fig. 6), and they are significantly less radiogenic than their corresponding whole-rock compositions (Table 1). Their Nd and Sr isotopic ratios plot within the array of data for clinopyroxenes in kimberlite-hosted peridotites from South Africa (Menzies & Murthy, 1980; Kramers et al., 1983; Jones, 1987). In contrast, the clinopyroxenes from the high-temperature Nikos peridotites exhibit a large range in Sr isotope compositions ($^{87}Sr/^{86}Sr_{(t)}$=0.7052-0.7091; Fig. 6), which are significantly more radiogenic than those of the clinopyroxenes from the low-temperature peridotites.

The garnets from the low-temperature peridotites have Nd isotopic ratios ($^{143}Nd/^{144}Nd_{(t)}$=0.51255-0.51271) that extend to slightly more radiogenic compositions than those of garnets from the high-temperature peridotites ($^{143}Nd/^{144}Nd_{(t)}$=0.51242-0.51259; Table 1; Fig. 6) at the time of kimberlite emplacement. $^{87}Rb/^{86}Sr$ ratios for a high (0.39) and a low-temperature peridotite garnet (0.29) were determined by isotope dilution analysis and used to calculate Sr isotopic ratios at 100 Ma ago for the remaining garnets from low and high-temperature peridotites, respectively. The Sr isotopic compositions of garnets in the high-temperature peridotites ($^{87}Sr/^{86}Sr_{(t)}$=0.7067-0.7095) partly overlap those of garnets in the low-temperature peridotites ($^{87}Sr/^{86}Sr_{(t)}$=0.7061-0.7073; Table 1; Fig. 6), but extend to significantly more radiogenic values.

5. DISCUSSION

5.1. Mantle isotopic composition

The Nikos peridotites that sample the Archean mantle root beneath the northern Canadian craton have a refractory mineralogy with high mg-numbers and depletions in fusible major elements indicating that they represent melt-depleted residues (Schmidberger and Francis, 1999). Residual mantle having experienced melt extraction should be characterized by low Nd/Sm, Rb/Sr and U/Pb ratios, as these trace elements are fractionated during partial melting processes (Menzies, 1990). Such trace element signatures will consequently generate time-integrated high $^{143}Nd/^{144}Nd$, low $^{87}Sr/^{86}Sr$, low $^{206}Pb/^{204}Pb$ and low $^{207}Pb/^{204}Pb$ isotopic ratios distinct from the composition of bulk Earth, but similar to those of "depleted mantle" (Zindler and Hart, 1986; Menzies, 1990; Pearson et al., 1995a). In agreement with this reasoning, many spinel peridotites that sample the lithosphere beneath oceanic or post-Archean crustal terranes have Nd and Sr isotopic compositions that plot in the depleted quadrant of the Nd-Sr correlation diagram compared to CHUR and bulk Earth, respectively (Fig. 4), as would be expected for residual mantle (Hawkesworth et al., 1990b and references therein).

In contrast to their depleted major element chemistry, the Nikos peridotites are enriched in highly incompatible trace elements such as the LILE and LREE, resulting in Nd/Sm, Rb/Sr and U/Pb ratios that are higher than those expected for melt-depleted residues (Menzies, 1990; Schmidberger and Francis, 2001; Tables 1, 2). The Nikos peridotites have Nd isotopic compositions that are similar to that of CHUR, but show a significant range in Pb and Sr isotopic compositions and extend to very radiogenic $^{87}Sr/^{86}Sr_{(t)}$ at the time of kimberlite emplacement (Figs. 4, 5). Furthermore, the isotopic compositions of the peridotites do not correlate with indices of partial melting, such as mg-numbers or modal mineralogy, which is inconsistent with an origin as single-stage melt-depleted residues. These characteristics suggest that the Somerset mantle root was infiltrated by metasomatic melts or fluids that enriched the lithospheric mantle in incompatible trace elements and overprinted its isotopic composition. Kimberlite-hosted garnet peridotites that sample the Archean mantle root beneath the South African Kaapvaal craton also exhibit highly variable and "enriched" isotope signatures, a feature which appears to characterize the lithospheric mantle beneath many Archean continents (Figs. 4, 5; Hawkesworth et al., 1990b and references therein).

Mass balance calculations based on modal abundances of clinopyroxene and garnet, and their respective REE abundances indicate discrepancies between calculated and analyzed LREE contents for the Nikos bulk rocks (Schmidberger and Francis, 2001). The LREE deficiencies (~50% for Nd and Sm) suggest the presence of small amounts of a kimberlite-related LREE-rich interstitial component (i.e. kimberlite liquid, ~1 wt%) and/or accessory mineral phase (i.e. apatite, ~0.1 wt%) to account for the excess LREE abundances in the Nikos peridotites (Bedini and Bodinier, 1999; Schmidberger and Francis, 2001). The Nd isotopic compositions of both the low and high-temperature Nikos peridotites overlap those of the host kimberlite at 100 Ma (Fig. 4), and it would appear that the peridotites were contaminated by the Nikos kimberlite. Binary mixing calculations show that a "depleted mantle" endmember ($^{143}Nd/^{144}Nd>0.5132$; Nd=0.8 ppm; Zindler and Hart, 1986) would require the addition of 5 to 10 wt% kimberlite liquid in order to account for the Nd isotopic signatures observed in the Nikos bulk rocks. This extent of contamination with kimberlite liquid, however, would result in bulk rock Nd abundances (5 to 10 ppm) that are significantly higher than those observed in the Nikos peridotites (avg. 1.5 ppm).

The presence of a Nd-bearing phase in addition to clinopyroxene and garnet is also required to explain the observation that a few whole-rock Nd isotopic compositions are less radiogenic than those of their constituent clinopyroxene and garnet. Isotopic mass balance calculations show that minor amounts of interstitial kimberlite liquid (0.5-0.9 wt%) could explain this discrepancy. One peridotite (NK3-4), however, exhibits a whole-rock Nd isotopic composition that is in fact lower than those of the kimberlite, which suggests the presence of a grain boundary component (or accessory mineral) other than kimberlite liquid. Although the Nd isotope data and Nd contents suggest addition of small amounts of kimberlite liquid (~1 wt% or less) or a kimberlite-related accessory mineral (apatite ~0.1 wt% or less), binary mixing calculations indicate that the Nikos peridotites were characterized by Nd isotopic compositions that were less radiogenic than those of a typical "depleted mantle" at the time of kimberlite magmatism.

The large range in Pb isotope ratios and the trend towards extremely radiogenic Sr compositions of the high-temperature peridotites, however, cannot be explained by kimberlite ($^{87}Sr/^{86}Sr_{(t)}$=0.7052) contamination of a precursor "depleted mantle" ($^{87}Sr/^{86}Sr$<0.703), as the kimberlite does not have an appropriate isotopic composition to account for the Sr isotope range of the peridotites. The presence of substantial amounts (>5 wt%) of interstitial kimberlite would, in fact, eradicate the Sr and Pb isotope differences observed between the low and high-temperature peridotites. Although Sr and Pb isotopic compositions of the high-temperature peridotites correlate with their respective Sr and Pb bulk rock abundances, which could be indicative of binary mixing of isotopically distinct components, their isotope data do not trend towards the composition of the Nikos kimberlite. This suggests that addition of host kimberlite was restricted to very small amounts (~1 wt% or less; Fig. 7), which is consistent with previous estimates. Given any amount of kimberlite contamination, the Sr isotopic compositions of the peridotites will be affected to a lesser degree than their Nd isotope ratios since the abundance ratio (peridotite/kimberlite) of Sr is 3 times larger than for Nd.

5.1.1. Age constraints

Clinopyroxene, garnet and corresponding whole-rock of one low (NK1-3) and two high-temperature (NK1-5; NK2-2) Nikos peridotites define internal Sm-Nd isochron ages of 91±9 Ma, 94±5 Ma and 102±8 Ma respectively, essentially identical to the emplacement age of the Somerset kimberlites (Heaman, 1989; Smith et al., 1989). These young "dates" appear to represent cooling ages and suggest that the lithospheric temperatures (up to 1400°C) exceeded the closure temperatures of peridotite minerals and/or that Nd isotopes equilibrated (i.e. "resetting") during the thermal event associated with kimberlite magmatism. Thus, Sm-Nd isochrons using constituent peridotite minerals do not appear to provide information on the timing of stabilization of the lithospheric mantle, but "date" the kimberlite magmatism. These findings are consistent with internal mineral isochrons obtained for South African peridotites, which have been interpreted to date kimberlite emplacement rather than mantle root formation (Pearson et al., 1995a).

Nd model ages may provide time constraints on separation from a depleted mantle (T_{DM}) reservoir, on the condition that bulk rock Sm-Nd systematics remain undisturbed subsequent to the formation event (DePaolo and Wasserburg, 1976). The T_{DM} (500-950 and 700-1250 Ma for low and high-temperature peridotites, respectively) for most Nikos peridotites are much younger than the Archean Re depletion ages for other Somerset Island peridotites (Irvine et al., 1999). These could reflect recent perturbation of the bulk rock Sm/Nd ratios as a result of kimberlite contamination. It has been shown that the Nd isotopic composition of clinopyroxene, which unlike that of the bulk xenolith is not biased by the presence of interstitial phases, provides a reasonable approximation for the whole-rock Nd isotope evolution (Pearson, 1999). T_{DM} age calculations yield 500-800 Ma (avg. 700 Ma) and 900-1400 Ma (avg. 1150 Ma) for clinopyroxenes from low and high-temperature peridotites, respectively, which are also significantly younger than the stabilization age of the lithosphere.

5.2. Pyroxenites

Two low-Mg pyroxenites, possibly representing veins of pyroxene-rich cumulates in the Somerset lithosphere (Schmidberger and Francis, 2001), have isotopic compositions that extend from very unradiogenic (NK3-1) to highly radiogenic (NK3-17) Pb and Nd isotopic ratios, which are distinct from those of the high-Mg pyroxenites and the peridotites (Figs. 4, 5). Thus, although major element compositions and modal mineralogy of the low-Mg pyroxenites are indistinguishable (Schmidberger and Francis, 2001), their isotopic compositions suggest that there is no genetic link between these pyroxenites. The Pb and Nd isotope signatures for one of these low-Mg pyroxenites (NK3-1) indicate that parts of the Somerset lithosphere are characterized by very low U/Pb, Th/Pb and Sm/Nd ratios (possibly ancient feature >1Ga), in order to preserve such unradiogenic Pb and Nd isotopic compositions. In contrast, the high-Mg pyroxenites have Pb and Nd isotopic compositions that are similar to those of the peridotites. These pyroxenites have been interpreted to constitute a pyroxene-rich component in the lithospheric mantle produced by small scale segregation of peridotite compositions into olivine and pyroxene-rich layers (Schmidberger and Francis, 2001).

5.3. Isotopic mantle stratification

The large range in Sr and Pb isotopic ratios observed in the Nikos peridotites and the trend towards significantly higher $^{87}Sr/^{86}Sr_{(t)}$ and lower $^{206}Pb/^{204}Pb_{(t)}$ isotopic ratios for the high-temperature peridotites (Figs. 4, 5) indicate that the deep Somerset lithosphere (>160 km) is isotopically distinct from the shallow lithospheric mantle. These findings imply that the mantle root beneath the northern Canadian craton is characterized by a depth stratification in isotopic composition that predates kimberlite magmatism at 100 Ma ago. This is in good agreement with the vertical zonation suggested by incompatible trace element compositions of the Nikos peridotites, and the decrease in trace elements contents with depth in the Somerset lithosphere (Schmidberger and Francis, 2001).

The Nikos whole-rock compositions are characterized by significantly more radiogenic Sr values than those of their constituent clinopyroxenes, a feature which is most evident for the low-temperature xenoliths. This is inconsistent with isotopic mass balance calculations using solely clinopyroxene and garnet as Sr-bearing minerals, which predict that the whole-rock Sr isotopic composition should plot close to that of clinopyroxene, as it controls the bulk Sr budget. The radiogenic Sr isotope ratios of the Nikos whole-rocks, therefore, require the presence of an accessory phase (in addition to the kimberlite contaminant), most likely phlogopite, characterized by a radiogenic Sr isotopic composition ($^{87}Sr/^{86}Sr>0.75$; Kramers et al., 1983). Small amounts of phlogopite are present in the Nikos peridotites, thus contributing to their bulk rock Sr isotope budgets, and most probably responsible for the radiogenic $^{87}Sr/^{86}Sr_{(t)}$ of the xenoliths.

5.3.1. Clinopyroxene Sr isotope depth zonation

The determination of the Sr isotope compositions in inclusion-free clinopyroxene permits an unbiased isotopic characterization of the mantle lithosphere, unaffected by the presence of interstitial or accessory phases. Furthermore, the Nikos clinopyroxenes are characterized by extremely low Rb/Sr ratios ($^{87}Rb/^{86}Sr<0.0002$), thus their present-day Sr isotope ratios are almost identical to those at the time of kimberlite emplacement as the correction for 100 Ma in-situ decay is negligible.

The clinopyroxenes from the low-temperature Nikos xenoliths have Sr isotopic compositions that are less radiogenic than or similar to the composition of bulk Earth (Zindler and Hart, 1986), and distinct from those of the Nikos kimberlite (Fig. 6). In contrast, the clinopyroxenes from the high-temperature peridotites have Sr isotopic ratios that are significantly more radiogenic than those of the Nikos kimberlite (Fig. 6). The distinct Sr isotope compositions of clinopyroxenes in the low and high-temperature peridotites exhibit a correlation with pressures and thus depths of last equilibration (Fig. 8), in agreement with the whole-rock data (Table 1; Figs. 4, 5) indicating that the shallow Somerset mantle is isotopically distinct from the deep lithosphere. The vertical stratification could have resulted from infiltration of the lower lithosphere with metasomatic melts or fluids originating from deeper levels of the upper mantle. This model, however, cannot be reconciled with the significantly lower Sr (and LREE) abundances of clinopyroxene from the deep-seated peridotites relative to those from the shallow peridotites (Schmidberger and Francis, 2001), as contamination with metasomatic melts or fluids should also increase their incompatible trace element abundances. The significantly more radiogenic Sr isotopic ratios and low incompatible trace element abundances of clinopyroxene in the high-temperature peridotites indicate that the shallow and deep Somerset lithosphere do not share a common petrogenetic history. It is thus possible that the deep lithospheric mantle is younger and was added to the existing shallow lithosphere by downward growth of the mantle root during a later magmatic event (e.g. Pearson, 1999). Mantle stratification and post-Archean lithosphere growth have previously been proposed for the South African Kaapvaal craton (e.g. Menzies, 1990; Pearson et al., 1995a) and recently garnet xenocryst compositions have been interpreted to indicate that the deep lithosphere beneath the Canadian Slave craton represents underplated mantle (Griffin et al., 1999). The respective correlations of Sr and Pb isotopes with Sr and Pb abundances in the deep-seated Nikos peridotites (Fig. 7) suggest that the mantle, which underplated the shallow Somerset lithosphere, contained recycled material (altered oceanic crust and sedimentary component?; e.g. Hauri et al., 1993) characterized by radiogenic Sr and unradiogenic Pb isotopic compositions that was mixed into the mantle during earlier subduction. Recycling of oceanic lithosphere may have been related to an early Paleozoic subduction regime reported for the Canadian Arctic (Trettin et al., 1991), which would suggest that the deep Somerset lithosphere was added in the Phanerozoic.

The enrichment in highly incompatible trace elements observed for the low-temperature Nikos peridotites and constituent clinopyroxenes, and Sr, Nd and Pb isotopic signatures that are distinct from those for "depleted mantle" indicate that the Archean shallow lithosphere was affected by the infiltration of metasomatic melts or fluids. Although the timing of this metasomatism is difficult to constrain, it would appear to have occurred prior to the addition of the deep high-temperature portion of the lithosphere since the latter is less enriched in incompatible trace elements. Depleted mantle Nd model ages (T_{DM}) for clinopyroxene from the low-temperature peridotites (~700 Ma) probably indicate the maximum age for the metasomatism that affected the shallow lithosphere, which could thus have occurred as early as the late Proterozoic. A Proterozoic orogeny is recognized in the Canadian Arctic at ~700 Ma (Trettin et al., 1991), and it is possible that metasomatism of the shallow lithosphere beneath Somerset Island occurred during this event.

6. CONCLUSIONS

The Archean Nikos peridotites are characterized by a refractory olivine-rich mineralogy and major element chemistry. Nd isotopic compositions are similar or slightly depleted relative to CHUR, whereas a significant range in Sr and Pb isotope compositions is recorded, which do not correlate with the degree of major element depletion in the bulk rocks. These geochemical signatures are inconsistent with formation of the Somerset mantle root by single-stage melt extraction in the Archean, as this process would generate a residual lithosphere with isotopic characteristics similar to that of "depleted mantle". The Nd isotopic ratios of the peridotites overlap those of the Nikos kimberlite, suggesting that the xenoliths were contaminated with kimberlite or a kimberlite-related accessory phase (i.e. apatite). The large range in Sr and Pb isotopic ratios observed in the xenoliths, however, indicate that addition of host kimberlite was restricted to very small amounts (~1 wt% or less).

The high-temperature (>1100°C) Nikos peridotites that sample the deep lithospheric mantle are characterized by more radiogenic $^{87}Sr/^{86}Sr_{(t)}$ and less radiogenic $^{206}Pb/^{204}Pb_{(t)}$ isotopic signatures than those of the shallow low-temperature peridotites (<1100°C). These whole-rock data are consistent with significantly less radiogenic Sr isotopic compositions for clinopyroxenes from the low-temperature peridotites than those for clinopyroxenes from the high-temperature peridotites. The depth correlation of Sr isotopes in clinopyroxene, and Sr and Pb isotopic compositions in the Nikos whole-rocks indicate that the deep (>160 km) and shallow Somerset lithosphere do not share the same formational history. The deep-seated high-temperature peridotites may have been added to the existing shallow lithosphere in a Phanerozoic magmatic event, and this mantle could have contained recycled (altered oceanic crust and sedimentary component?) material as a result of earlier subduction.

Acknowledgements

We thank Fabien Rasselet for assistance in the field and hand-picking separates of magmatic kimberlite for isotope analysis. Clément Gariépy is thanked for earlier revisions of the manuscript. The research was funded by an NSERC operating grant to D. Francis and S. Schmidberger is grateful for financial support in the form of a NSERC doctoral scholarship.

REFERENCES

Bedini R. M. and Bodinier J.-L. (1999) Distribution of incompatible trace elements between the constituents of spinel peridotite xenoliths: ICP-MS data from the East African Rift. *Geochim. Cosmochim. Acta* **63**, 3883-3900.

Boyd F. R., Pokhilenko N. P., Pearson D. G., Mertzman S. A., Sobolev N. V. and Finger L. W. (1997) Composition of the Siberian cratonic mantle: evidence from Udachnaya peridotite xenoliths. *Contrib. Mineral. Petrol.* **128**, 228-246.

Dawson J. B. (1967) A review of the geology of kimberlite. In *Ultramafic and related rocks* (ed. P. J. Wyllie). Wiley, New York. pp. 241-251.

DePaolo D. J. and Wasserburg G. J. (1976) Inferences about magma sources and mantle structure from variations of ^{143}Nd/^{144}Nd. *Geophys. Res. Lett.* **3**, 743-746.

Edwards R. L., Chen J. H. and Wasserburg G. J. (1986): ^{238}U-^{234}U-^{230}Th-^{232}Th systematics and the precise measurement of time over the past 500,000 years. *Earth Planet. Sci. Lett.* **81**, 175-192.

Erlank A. J., Waters F. G., Hawkesworth C. J., Haggerty S. E., Allsopp H. L., Rickard R. S. and Menzies M. A. (1987) Evidence for mantle metasomatism in peridotite nodules from the Kimberley pipes, South Africa. In *Mantle metasomatism* (eds. M. A. Menzies and C. J. Hawkesworth). Academic Press, London. pp. 221-311.

Fraser K. J., Hawkesworth C. J., Erlank A. J., Mitchell R. H. and Scott-Smith B.H. (1985) Sr, Nd and Pb isotope and minor element geochemistry of lamproites and kimberlites. *Earth Planet. Sci. Lett.* **76**, 57-70.

Frisch T. and Hunt P. A. (1993) Reconnaissance U-Pb geochronology of the crystalline core of the Boothia Uplift, District of Franklin, Northwest Territories. In *Radiogenic age and isotope studies: Report 7.* Geological Survey of Canada, Paper **93-2**. pp. 3-22.

Griffin W. L., Doyle B. J., Ryan C. G., Pearson N. J., O'Reilly S. Y., Davies R., Kivi K., van Achterbergh E. and Natapov L. M. (1999) Layered mantle lithosphere in the Lac de Gras area, Slave craton: composition, structure and origin. *J. Petrol.* **40**, 705-727.

Hauri E. H., Shimizu N., Dieu J. J. and Hart S. R. (1993) Evidence for hotspot-related carbonatite metasomatism in the oceanic upper mantle. *Nature* **365**, 221-227.

Hawkesworth C. J., Erlank A. J., Kempton P. D. and Waters F. G. (1990a) Mantle metasomatism: isotope and trace-element trends in xenoliths from Kimberley, South Africa. *Chem. Geol.* **85**, 19-34.

Hawkesworth C. J., Kempton P. D., Rogers N. W., Ellam R. M. and van Calsteren P. W. (1990b) Continental mantle lithosphere, and shallow level enrichment processes in the Earth's mantle. *Earth Planet. Sci. Lett.* **96**, 256-268.

Heaman L. H. (1989) The nature of the subcontinental mantle from Sr-Nd-Pb isotopic studies on kimberlite perovskite. *Earth Planet. Sci. Lett.* **92**, 323-334.

Herzberg C. T. (1993) Lithosphere peridotites of the Kaapvaal craton. *Earth Planet. Sci. Lett.* **120**, 13-29.

Irvine G. J., Kopylova M. G., Carlson R. W., Pearson D. G., Shirey S. B. and Kjarsgaard B. A. (1999) Age of the lithospheric mantle beneath and around the Slave craton: a Rhenium-Osmium isotopic study of peridotite xenoliths from the Jericho and Somerset Island kimberlites. *Ninth Annual V. M. Goldschmidt Conference*. LPI Contribution No. 971, 134-135.

Jones R. A. (1987) Strontium and neodymium isotopic and rare earth element evidence for the genesis of megacrysts in kimberlites of southern Africa. In *Mantle Xenoliths* (ed. P. H. Nixon). John Wiley & Sons, Chichester. pp. 711-724.

Kramers J. D. (1977) Lead and strontium isotopes in Cretaceous kimberlites and mantle-derived xenoliths from southern Africa. *Earth Planet. Sci. Lett.* **34**, 419-431.

Kramers J. D., Roddick J. C. M. and Dawson J. B. (1983) Trace element and isotope studies on veined, metasomatic and "MARID" xenoliths from Bultfontein, South Africa. *Earth Planet. Sci. Lett.* **65**, 90-106.

Manhès G., Allègre C. J., Dupré B. and Hamelin B. (1980) Lead isotope study of basic-ultrabasic layered complexes: speculations about the age of the earth and primitive mantle characteristics. *Earth Planet. Sci. Lett.* **47**, 370-382.

Macdougall J. D. and Haggerty S. E. (1999) Ultradeep xenoliths from African kimberlites: Sr and Nd isotopic compositions suggest complex history. *Earth Planet. Sci. Lett.* **170**, 73-82.

McCulloch M. T., Jaques A. L., Nelson D. R. and Lewis J. D. (1983) Nd and Sr isotopes in kimberlites and lamproites from Western Australia: an enriched mantle origin. *Nature* **302**, 400-403.

McDonough W. F. (1990) Constraints on the composition of the continental lithospheric mantle. *Earth Planet. Sci. Lett.* **101**, 1-18.

McDonough W. F. and Sun S. S. (1995) The composition of the earth. *Chem. Geol.* **120**, 223-253.

Menzies M. A. (1990) Archean, Proterozoic, and Phanerozoic lithospheres. In *Continental mantle* (ed. M. A. Menzies). Oxford Univ. Press, Oxford. pp. 67-86.

Menzies M. A. and Murthy R. (1980) Enriched mantle: Nd and Sr isotopes in diopsides from kimberlite nodules. *Nature* **283**, 634-636.

Menzies M. A., Rogers N., Tindle A. and Hawkesworth C. J. (1987) Metasomatic and enrichment processes in lithospheric peridotites, an effect of asthenosphere-lithosphere interaction. In *Mantle metasomatism* (eds. M. A. Menzies and C. J. Hawkesworth). Academic Press, London. pp. 313-361.

Mitchell R. H. (1995) *Kimberlites, orangeites, and related rocks*. Plenum Press, New York.

Nixon P. H. (1987) Kimberlitic xenoliths and their cratonic setting. In *Mantle Xenoliths* (ed. P. H. Nixon). John Wiley & Sons, Chichester. pp. 215-239.

Pearson D. G. (1999) The age of continental roots. *Lithos* **48**, 171-194.

Pearson D. G., Carlson R. W., Shirey S. B., Boyd F. R. and Nixon P. H. (1995a) Stabilisation of Archean lithospheric mantle: a Re-Os isotope study of peridotite xenoliths from the Kaapvaal craton. *Earth Planet. Sci. Lett.* **134**, 341-357.

Pearson D. G., Shirey S. B., Carlson R. W., Boyd F. R., Pokhilenko N. P. and Shimizu N. (1995b) Re-Os, Sm-Nd, and Rb-Sr isotope evidence for thick Archean lithospheric mantle beneath the Siberian craton modified by multistage metasomatism. *Geochim. Cosmochim. Acta* **59**, 959-977.

Pell J. (1993) New kimberlite discoveries on Somerset Island. In *Exploration Overview 1993*, p. 47. NWT Geology Division, Department of Indian and Northern Affairs, Yellowknife (NWT).

Richardson S. H., Erlank A. J. and Hart S. R. (1985) Kimberlite-borne garnet peridotite xenoliths from old enriched subcontinental mantle. *Earth Planet. Sci. Lett.* **75**, 116-128.

Ringwood A. E., Kesson S. E., Hibberson W. and Ware N. (1992) Origin of kimberlites and related magmas. *Earth Planet. Sci. Lett.* **113**, 521-538.

Schmidberger S. S. and Francis D. (1999) Nature of the mantle roots beneath the North American craton: mantle xenolith evidence from Somerset Island kimberlites. *Lithos* **48**, 195-216.

Schmidberger S. S. and Francis D. (2001) Constraints on the trace element composition of the Archean mantle root beneath Somerset Island, Arctic Canada. *J. Petrol.* **42**, 1095-1117.

Smith C. B. (1983) Pb, Sr and Nd isotopic evidence for sources of southern African Cretaceous kimberlites. *Nature* **304**, 51-54.

Smith C. B., Allsopp H. L., Garvie O. G., Kramers J. D., Jackson P. F. S. and Clement C. R. (1989) Note on the U-Pb perovskite method for dating kimberlites: examples from the Wesselton and DeBeers mines, South Africa, and Somerset Island, Canada. *Chem. Geol. (Isot. Sect.)* **79**, 137-145.

Stacey J. S. and Kramers J. D. (1975) Approximation of terrestrial lead isotope evolution by a two-stage model. *Earth Planet. Sci. Lett.* **26**, 207-223.

Steward W. D. (1987) Late Proterozoic to Early Tertiary stratigraphy of Somerset Island and northern Boothia Peninsula, District of Franklin. *Geological Survey of Canada Paper* **83-26**. pp. 78.

Trettin H. P. (1991) Geology of Canada: Summary and remaining problems. In *Geology of the Innuitian orogen and Arctic platform of Canada and Greenland* (ed. H. P. Trettin). Geological Survey of Canada. pp. 547-553.

Walker R. J., Carlson R. W., Shirey S. B. and Boyd F. R. (1989) Os, Sr, Nd, and Pb isotope systematics of southern African peridotite xenoliths: Implications for the chemical evolution of subcontinental mantle. *Geochim. Cosmochim. Acta* **53**, 1583-1595.

Woolley A. R. and Kempe D. R. C. (1989) Carbonatites nomenclature, average chemical compositions, and elemental distribution. In *Carbonatites; genesis and evolution* (ed. K. Bell). Unwin Hyman Inc, London. pp. 1-14.

Zindler A. and Hart S. R. (1986) Chemical Geodynamics. *Ann. Rev. Earth Planet. Sci.* **14**, 493-571.

FIGURE CAPTIONS

Figure 4-1: Geological map of Somerset Island (after Steward, 1987) showing kimberlite locations. The mantle xenoliths from this study were collected from the Nikos kimberlite pipes (black diamond). Legend: light gray, Paleozoic cover rocks; striped, Late Proterozoic cover rocks; dark gray, Precambrian basement; bold lines, normal faults.

Figure 4-2: Initial Nd and Sr isotopic compositions for Nikos kimberlites. The Nd and Sr isotopic ratios for kimberlites from North America, Siberia, South Africa and Australia ("Group I" and "Group II" kimberlites; for further explanation see text) are shown for comparison (data from McCulloch et al., 1983; Smith, 1983; Heaman, 1989; Pearson et al., 1995b). Values for bulk Earth and CHUR (chondrite uniform reservoir) are those for 100 Ma ago, assuming present day ratios of $^{87}Sr/^{86}Sr_{(bulk\ Earth)}=0.7045$ and $^{87}Rb/^{86}Sr_{(bulk\ Earth)}=0.083$ ($\lambda=1.42 \times 10^{-11}$ y^{-1}) and $^{143}Nd/^{144}Nd_{(CHUR)}=0.512638$ and $^{147}Sm/^{144}Nd_{(CHUR)}=0.1967$ ($\lambda=6.54 \times 10^{-12}\ y^{-1}$).

Figure 4-3: Initial Pb isotopic compositions for Nikos kimberlites. The Pb isotopic ratios for South African "Group I" and "Group II" kimberlites are shown for comparison (data from Kramers, 1977; Smith, 1983; Fraser et al., 1985).

Figure 4-4: Nd and Sr isotopic compositions for Nikos xenoliths at 100 Ma ago. The Nd and Sr isotopic ratios for the Nikos kimberlites, and the fields for garnet peridotites (including whole-rock and clinopyroxene data) from South African kimberlites and spinel peridotites world-wide are shown for comparison (data from Menzies and Murthy, 1980; Kramers et al., 1983; Richardson et al., 1985;

Jones, 1987; Walker et al., 1989; Hawkesworth et al., 1990a,b; Macdougall and Haggerty, 1999 and references therein).

Figure 4-5: Pb isotopic compositions for Nikos xenoliths at 100 Ma ago. The Pb isotopic ratios for the Nikos kimberlites and the field for kimberlite-hosted garnet peridotites (including whole-rock and clinopyroxene data) from South Africa are shown for comparison (data from Kramers, 1977; Kramers et al., 1983; Richardson et al., 1985; Walker et al., 1989; Hawkesworth et al., 1990a). S/K: Stacey and Kramers (1975) lead isotope evolution curve (time intervals in Ga).

Figure 4-6: Nd and Sr isotopic compositions for Nikos clinopyroxenes and garnets at 100 Ma ago. The Nd and Sr isotopic ratios for the Nikos kimberlites and the field for clinopyroxenes from kimberlite-hosted peridotites from South Africa are shown for comparison (data from Menzies & Murthy, 1980; Kramers et al., 1983; Jones, 1987).

Figure 4-7: Sr and Pb isotopic compositions versus 1/Sr and 1/Pb for low and high-temperature Nikos peridotites at 100 Ma ago. Data for the Nikos kimberlites at 100 Ma are shown for comparison.

Figure 4-8: Sr isotopic compositions for Nikos clinopyroxenes plotted versus pressure of last equilibration. For sample NK2-4 pressure of last equilibration was not determined and it is plotted in the lower portion of the shallow lithosphere.

Table 4-1. Rb, Sr, Sm, and Nd abundances and Sr and Nd isotope compositions for Nikos kimberlites and xenoliths.

Sample	Temp °C	Press kb	Rb ppm	Sr ppm	^{87}Rb/^{86}Sr	^{87}Sr/^{86}Sr measured	^{87}Sr/^{86}Sr (t)	Sm ppm	Nd ppm	^{147}Sm/^{144}Nd	^{143}Nd/^{144}Nd measured	^{143}Nd/^{144}Nd (t)	T_{DM} Ma	ε_{Nd} (t)
Kimberlites														
NK3-K1			72	1320	0.16	0.705403 ±14	0.7052	10.1	74.6	0.0819	0.512617 ±11	0.512563		1.1
NK3-K2			44	1030	0.12	0.705334 ±14	0.7052	10.7	78.3	0.0828	0.512593 ±07	0.512539		0.6
NK3-K3			30	1710	0.05	0.705248 ±14	0.7052	14.7	110	0.0808	0.512640 ±07	0.512587		1.5
NK3-K4			20	2190	0.03	0.705243 ±16	0.7052	12.7	94.5	0.0814	0.512634 ±12	0.512580		1.4
duplicate						0.705245 ±13								
NK3-K5			31	1330	0.07	0.705272 ±13	0.7052	11.6	82.5	0.0850	0.512631 ±05	0.512575		1.3
Low-Temperature Peridotites														
NK3-20	815	29.8	7.3	55.9	0.38	0.705677 ±10	0.7051	0.37	1.58	0.1411	0.512763 ±11	0.512671	812	3.2
NK1-4	871	33.5	3.0	43.3	0.20	0.706917 ±14	0.7066	0.24	1.49	0.0984	0.512676 ±14	0.512611	628	2.0
NK1-4 Cpx			0.01[a]	115[a]	0	0.703776 ±11	0.7038	1.38	9.50	0.0875	0.512620 ±05	0.512562	641	1.0
NK1-4 Gt			0.02[a]	0.17	0.29	0.707539 ±14	0.7071	0.43	0.49	0.5256	0.513049 ±09	0.512705		3.8
NK2-3	887	34.6	7.5	77.7	0.28	0.706093 ±14	0.7057	0.38	2.63	0.0879	0.512701 ±12	0.512643	545	2.6
NK2-3 Cpx				318		0.704584 ±14	0.7046	2.09	14.6	0.0864	0.512732 ±10	0.512676	501	3.3
NK2-3 Gt				0.27		0.706887 ±16	0.7065	0.70	1.99	0.2135	0.512829 ±08	0.512690		3.5
Nk1-23	964	39.0	4.7	86.5	0.16	0.705329 ±11	0.7051	0.51	3.64	0.0853	0.512755 ±10	0.512699	470	3.7
NK2-10	1014	42.1	3.0	92.6	0.09	0.705637 ±13	0.7055	0.47	2.93	0.0964	0.512648 ±05	0.512585	653	1.5
NK1-14	1027	42.7	1.4	43.7	0.10	0.705792 ±14	0.7057	0.31	1.97	0.0944	0.512657 ±13	0.512595	631	1.7
Nk1-14 Cpx				217		0.703814 ±14	0.7038	3.19	23.9	0.0806	0.512621 ±08	0.512568	607	1.1
Nk1-14 Gt				0.31		0.706495 ±11	0.7061	1.08	2.08	0.3137	0.512807 ±09	0.512602		1.8
NK1-2	1042	44.7	1.2	33.8	0.10	0.705534 ±14	0.7054	0.27	1.75	0.0938	0.512655 ±16	0.512594	630	1.6
NK1-12	1054	45.3	3.2	56.5	0.16	0.706203 ±14	0.7060	0.40	2.21	0.1094	0.512670 ±19	0.512599	702	1.8
NK1-3	1076	46.5	1.7	56.3	0.09	0.706668 ±14	0.7065	0.33	1.53	0.1324	0.512655 ±14	0.512568	928	1.2
NK1-3 Cpx				406		0.704149 ±14	0.7041	5.60	28.0	0.1207	0.512646 ±08	0.512567	827	1.1
NK1-3 Gt				0.73		0.706472 ±14	0.7061	1.99	2.82	0.4272	0.512829 ±07	0.512550		0.8
NK2-4[b]			1.9	14.9	0.37	0.705188 ±16	0.7047	0.21	0.97	0.1280	0.512847 ±08	0.512763	541	5.0
NK2-4 Cpx				133[a]		0.703879 ±13	0.7039	1.54	6.88	0.1357	0.512775 ±09	0.512686	733	3.5
NK 2-4 Gt						0.707703 ±13	0.7073	1.62	2.45	0.3999	0.512886 ±11	0.512624		2.2
High-Temperature Peridotites														
NK1-6	1149	48.4	0.8	17.1	0.14	0.706544 ±13	0.7064	0.22	0.97	0.1371	0.512674 ±29	0.512584	947	1.5
NK2-1	1216	51.5	10	31.3	0.93	0.709277 ±13	0.7080	0.14	0.66	0.1299	0.512624 ±17	0.512539	958	0.6
duplicate						0.709286 ±10					0.512607 ±23			
NK2-1 Cpx				45.8		0.709132 ±17	0.7091	0.79	2.97	0.1604	0.512664 ±12	0.512559	1386	1.0
NK2-1 Gt			0.08[a]	0.57	0.39	0.710015 ±14	0.7095	1.16	1.13	0.6205	0.512966 ±17	0.512560		1.0
NK1-9	1219	53.4	1.5	17.8	0.25	0.706912 ±13	0.7066	0.23	0.88	0.1548	0.512661 ±21	0.512560	1264	1.0

Table 4-1. (Continued)

Sample	Temp °C	Press kb	Rb ppm	Sr ppm	$^{87}Rb/^{86}Sr$	$^{87}Sr/^{86}Sr$ measured	$^{87}Sr/^{86}Sr$ (t)	Sm ppm	Nd ppm	$^{147}Sm/^{144}Nd$	$^{143}Nd/^{144}Nd$ measured	$^{143}Nd/^{144}Nd$ (t)	T_{CHUR} Ma	ε_{Nd} (t)
NK1-1	1222	52.7	1.1	25.7	0.12	0.707152 ±10	0.7070							
NK3-11	1247	53.1	2.9	202	0.04	0.708065 ±24	0.7080	0.25	1.05	0.1405	0.512655 ±15	0.512563	1032	1.0
NK3-25	1256	54.0	29	37.5	2.21	0.709693 ±17	0.7066	0.33	1.76	0.1120	0.512628 ±31	0.512554	783	0.9
NK1-5	1262	54.6	4.3	46.5	0.27	0.706955 ±13	0.7066	0.26	1.09	0.1451	0.512694 ±16	0.512600	1013	1.8
Nk1-5 Cpx				75.0		0.706674 ±14	0.7067	1.36	5.88	0.1395	0.512700 ±10	0.512609	924	2.0
Nk1-5 Gt				0.51		0.707442 ±14	0.7069	1.13	1.07	0.6334	0.512999 ±09	0.512584		1.5
NK3-16	1280	53.5	1.8	40.9	0.13	0.707234 ±13	0.7071	0.17	0.88	0.1177	0.512662 ±10	0.512585	775	1.5
NK1-7	1300	55.1	1.0	15.2	0.20	0.706660 ±14	0.7064	0.14	0.44	0.1904	0.512749 ±38	0.512624	2610	2.3
Nk1-7 Cpx				86.9		0.706066 ±17	0.7061							
Nk1-7 Gt				0.48		0.707249 ±14	0.7067	1.33	1.45	0.5551	0.512886 ±10	0.512523		0.3
NK2-2	1316	54.7	6.5	33.5	0.56	0.708523 ±14	0.7077	0.30	1.24	0.1488	0.512686 ±11	0.512588	1090	1.6
NK2-2 Cpx			0.01[a]	106[a]	0	0.707280 ±13	0.7073	1.38	5.71	0.1456	0.512687 ±10	0.512591	1037	1.6
NK 2-2 Gt				0.35		0.709472 ±14	0.7089	0.73	0.91	0.4850	0.512911 ±10	0.512594		1.7
NK3-15	1343	58.5	3.7	344	0.03	0.708533 ±14	0.7085	0.20	1.16	0.1043	0.512639 ±14	0.512571	713	1.2
NK3-4	1371	58.5	23	245	0.27	0.708867 ±13	0.7085	0.42	2.21	0.1150	0.512569 ±21	0.512494	897	-0.3
Nk 3-4 Cpx				92.7		0.705199 ±14	0.7052	1.07	4.31	0.1501	0.512639 ±10	0.512541	1224	0.6
Nk 3-4 Gt				0.43		0.708717 ±14	0.7082	0.69	0.72	0.5752	0.512797 ±10	0.512421		-1.7
Pyroxenites														
NK2-7 HMg	737	25.3	4.1	284	0.04	0.704128 ±11	0.7041	0.80	4.98	0.0973	0.512554 ±10	0.512490	781	-0.4
NK3-14 HMg	933	36.8	30	162	0.54	0.706629 ±11	0.7059	1.67	8.29	0.1218	0.512720 ±41	0.512640	714	2.6
NK3-17 LMg	720	22.2	3.6	38.8	0.27	0.706108 ±10	0.7057	0.58	1.99	0.1745	0.512980 ±09	0.512866	660	7.0
NK3-1 LMg	759	25.1	5.1	90.3	0.16	0.704840 ±21	0.7046	0.67	3.05	0.1330	0.512058 ±10	0.511971	2055	-10.5
Nk 3-1 Cpx			0.01[a]	89.4[a]	0	0.704268 ±13	0.7043	1.06	4.77	0.1342	0.511879 ±15	0.511791	2426	-14.0
Nk 3-1 Gt			0.02[a]	0.14	0.35	0.706110 ±16	0.7056	0.48	0.77	0.3806	0.512956 ±21	0.512707		3.9

Minerals and rock types: *Cpx* = clinopyroxene; *Gt* = garnet; *HMg* = high-Mg pyroxenite; *LMg* = low-Mg pyroxenite. (t): Sr and Nd isotope ratios corrected for 100 Ma in-situ decay. $^{87}Sr/^{86}Sr$ are normalized to $^{86}Sr/^{88}Sr$=0.1194 and $^{143}Nd/^{144}Nd$ to $^{146}Nd/^{144}Nd$=0.7219. NBS 987 Sr standard yielded an average value of $^{87}Sr/^{86}Sr$=0.710253±0.000013 (2σ; n=10). Measurements of Ames Nd standard gave an average value of $^{143}Nd/^{144}Nd$=0.512132±0.000011 (2σ; n=8). Precision for individual Sr and Nd isotope measurements is quoted at the 2σ level. Sm and Nd abundances were determined by isotope dilution analysis with uncertainties <0.5%. Rb and Sr abundances for bulk rocks were measured by ICP-MS analysis (for analytical procedures see Schmidberger and Francis, 2001). [a]Rb and Sr abundances for Cpx and Gt were determined by isotope dilution analysis with uncertainties <1% and these were used to calculate $^{87}Rb/^{86}Sr$ ratios for the remaining mineral separates (for further explanation see text). Sr abundances for other Cpx and Gt separates were measured by ion microprobe analysis. [b]Temperature and pressure estimates not determined.

Table 4-2. Pb, U and Th abundances and Pb isotopic compositions for Nikos kimberlites and xenoliths.

Sample	Pb ppm	U ppm	Th ppm	$^{238}U/^{204}Pb$ μ	$^{206}Pb/^{204}Pb$ measured	$^{207}Pb/^{204}Pb$ measured	$^{208}Pb/^{204}Pb$ measured	$^{206}Pb/^{204}Pb$ (t)	$^{207}Pb/^{204}Pb$ (t)	$^{208}Pb/^{204}Pb$ (t)
Kimberlites										
NK3-K1	11	2.9	14.4	17.0	18.485	15.478	38.584	18.220	15.465	38.151
NK3-K2	14	3.2	14.1	14.6	18.483	15.466	38.699	18.255	15.455	38.367
NK3-K3	14	3.5	18.5	16.2	18.712	15.512	38.903	18.458	15.500	38.466
NK3-K4	28	3.8	17.5	8.8	18.758	15.513	38.906	18.621	15.506	38.700
NK3-K5	35	2.9	14.1	5.4	18.704	15.537	38.899	18.619	15.533	38.766
average	*20*	*3.3*	*15.7*	*12.4*						
Low-Temperature Peridotites										
NK3-20	0.08	0.03	0.08	22.2	18.823	15.587	38.815	18.476	15.570	38.496
NK1-4	0.22	0.08	0.22	22.7	18.675	15.542	38.654	18.320	15.525	38.315
NK2-3	0.27	0.16	0.32	36.7	19.147	15.509	38.953	18.573	15.481	38.568
NK1-23	0.07	0.04	0.07	30.7	18.600	15.451	38.316	18.120	15.428	37.997
NK2-10	0.66	0.17	0.30	16.3	19.287	15.550	38.556	19.033	15.538	38.405
NK1-14	0.14	0.06	0.26	28.3	18.771	15.517	38.771	18.328	15.496	38.166
NK1-2	0.15	0.04	0.15	18.5	18.587	15.494	38.545	18.298	15.480	38.209
NK1-12	0.26	0.06	0.21	15.1	18.798	15.515	38.540	18.563	15.504	38.269
NK1-3	0.17	0.10	0.16	37.5	18.407	15.394	38.128	17.820	15.366	37.818
NK2-4	0.08	0.03	0.07	21.9	18.994	15.503	38.759	18.652	15.487	38.435
average	*0.21*	*0.08*	*0.18*	*25.0*						
High-Temperature Peridotites										
NK2-1	0.09	0.02	0.06	14.8	18.520	15.427	38.386	18.288	15.416	38.157
NK1-9	0.10	0.03	0.08	20.2	18.614	15.496	38.521	18.299	15.481	38.232
NK1-1	0.14	0.08	0.13	37.7	18.571	15.454	38.404	17.981	15.426	38.109
NK3-11	0.58	0.69	0.10	77.6	19.193	15.575	38.645	17.980	15.516	38.586
NK3-25	0.42	0.37	0.16	56.6	18.314	15.436	38.286	17.430	15.394	38.158
NK1-5	0.24	0.08	0.12	20.3	18.426	15.492	38.337	18.109	15.476	38.168
NK3-16	0.29	0.21	0.08	46.3	18.377	15.549	38.531	17.654	15.515	38.442
NK1-7	0.04	0.01	0.05	17.2	18.494	15.509	38.320	18.225	15.496	37.914
NK2-2	0.17	0.08	0.06	28.6	18.682	15.472	38.203	18.236	15.450	38.082
NK3-4	0.33	0.48	0.11	93.4	18.641	15.455	38.288	17.181	15.385	38.181
average	*0.21*	*0.17*	*0.10*	*37.1*						
Pyroxenites										
NK2-7HMg	1.99	0.35	0.49	11.5	18.964	15.509	38.756	18.785	15.500	38.675
NK3-17LMg	0.75	0.13	0.33	11.6	19.788	15.632	38.860	19.607	15.623	38.715
NK3-1LMg	0.39	0.04	0.14	6.6	17.015	15.349	37.285	16.912	15.344	37.169

Rock types: *HMg* high-Mg pyroxenite, *LMg* low-Mg pyroxenite. (t): Pb isotope ratios corrected for 100 Ma in-situ decay. Mass fractionation corrections of 0.09% amu^{-1} and 0.24% amu^{-1} were applied to Pb isotope ratios (based on repeated measurements of NIST SRM 981 Pb standard) using Faraday and Daly analogue detectors, respectively. Average values for the internal precision (2σ) of the $^{206}Pb/^{204}Pb$, $^{207}Pb/^{204}Pb$ and $^{208}Pb/^{204}Pb$ ratios are ±0.016, ±0.014 and ±0.038, respectively). Pb, U and Th abundances for xenoliths were determined by isotope dilution analysis with uncertainties <1%, and for kimberlites by ICP-MS analysis (for analytical procedures see Schmidberger and Francis, 2001).

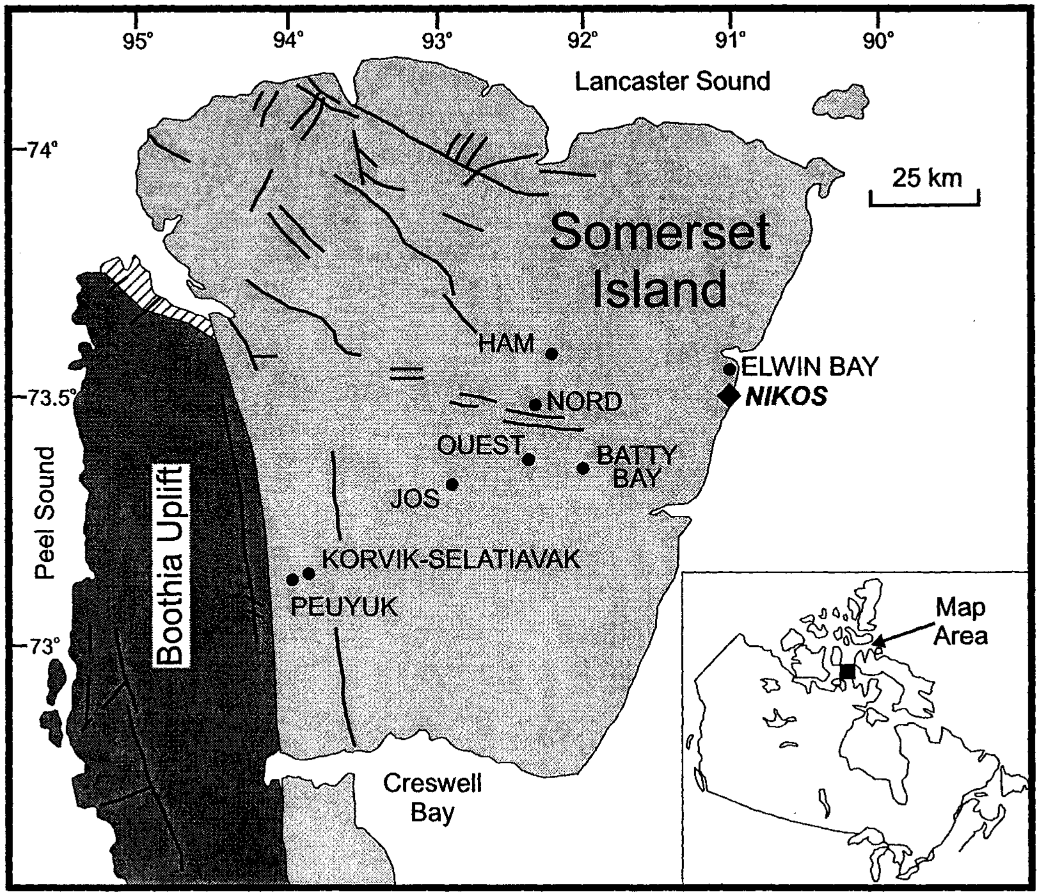
95°
94°
93°
92°
91°
90°
Lancaster Sound
-74°
25 km
Somerset Island
HAM
ELWIN BAY
NIKOS
-73.5°
NORD
QUEST
BATTY BAY
JOS
Peel Sound
Boothia Uplift
KORVIK-SELATIAVAK
PEUYUK
-73°
Map Area
Creswell Bay

Figure 4-1

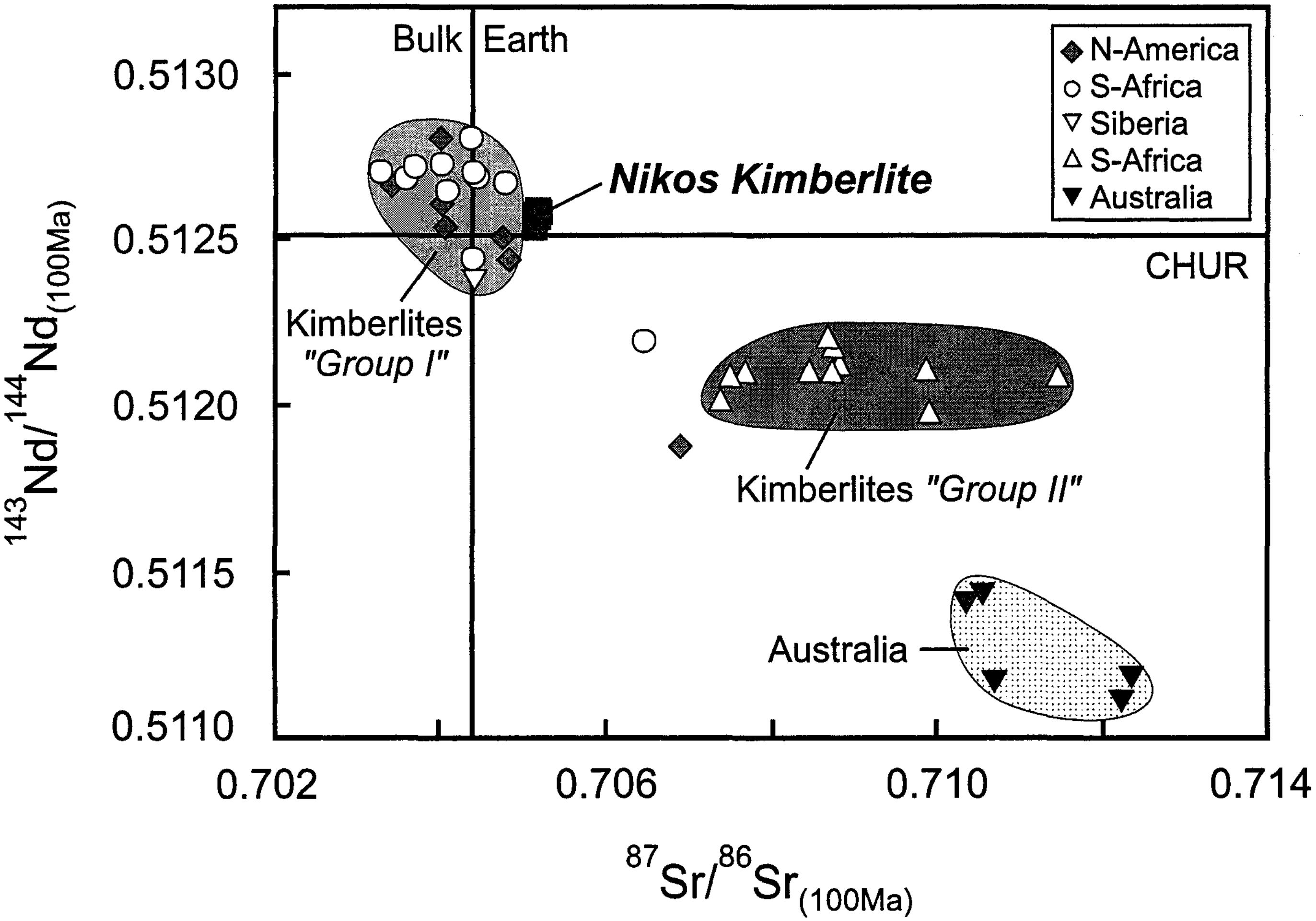

Bulk Earth
N-America
S-Africa
Siberia
S-Africa
Australia
Nikos Kimberlite
CHUR
Kimberlites "Group I"
Kimberlites "Group II"
Australia
0.5130
0.5125
0.5120
0.5115
0.5110
$^{143}Nd/^{144}Nd_{(100Ma)}$
0.702
0.706
0.710
0.714
$^{87}Sr/^{86}Sr_{(100Ma)}$

Figure 4-2

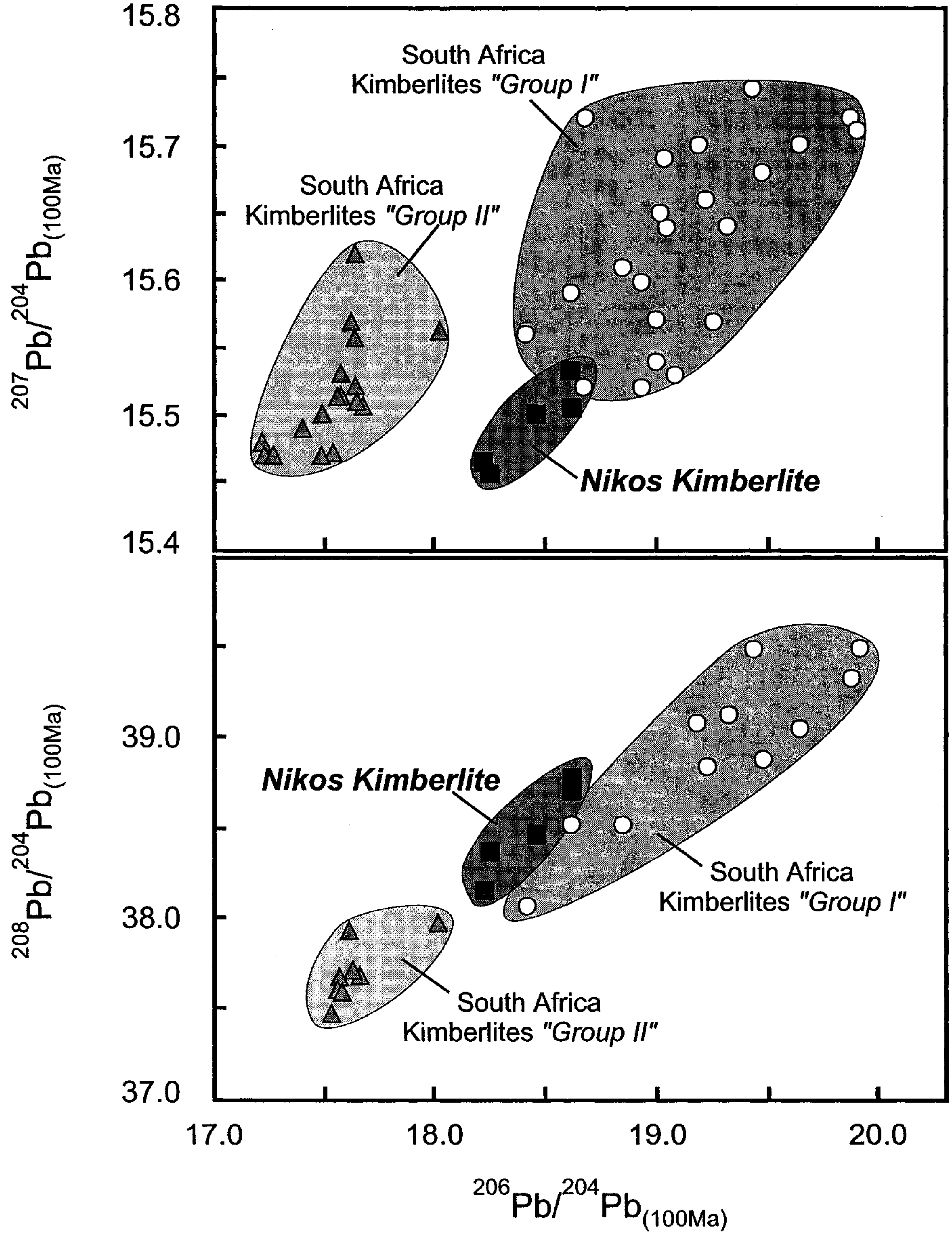
15.8
15.7
15.6
15.5
15.4
$^{207}Pb/^{204}Pb_{(100Ma)}$
South Africa Kimberlites "Group I"
South Africa Kimberlites "Group II"
Nikos Kimberlite
39.0
38.0
37.0
$^{208}Pb/^{204}Pb_{(100Ma)}$
Nikos Kimberlite
South Africa Kimberlites "Group I"
South Africa Kimberlites "Group II"
17.0
18.0
19.0
20.0
$^{206}Pb/^{204}Pb_{(100Ma)}$

Figure 4-3

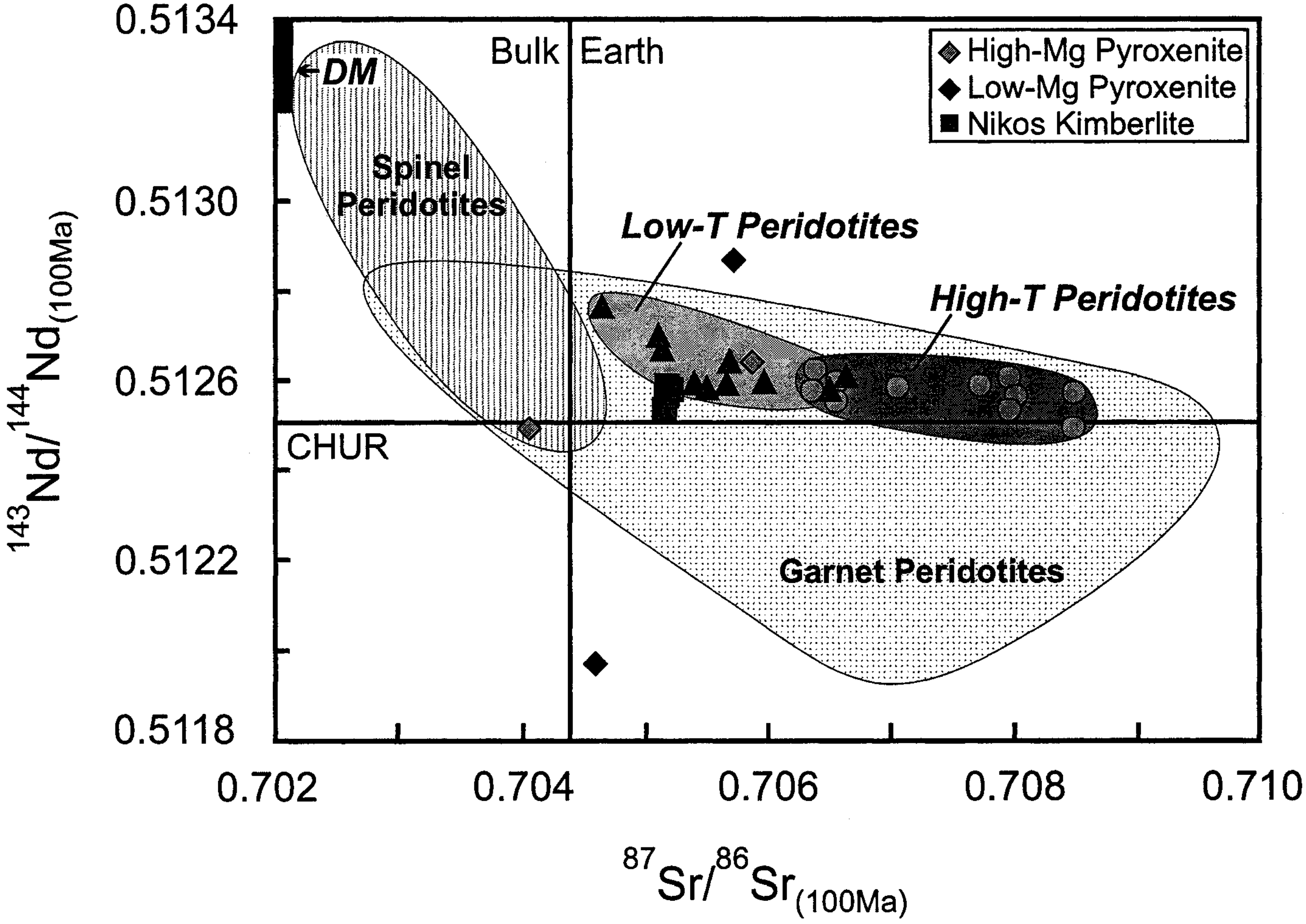

0.5134
0.5130
0.5126
0.5122
0.5118
$^{143}Nd/^{144}Nd_{(100Ma)}$
0.702
0.704
0.706
0.708
0.710
$^{87}Sr/^{86}Sr_{(100Ma)}$
Bulk Earth
CHUR
DM
Spinel Peridotites
Low-T Peridotites
High-T Peridotites
Garnet Peridotites
High-Mg Pyroxenite
Low-Mg Pyroxenite
Nikos Kimberlite

Figure 4-4

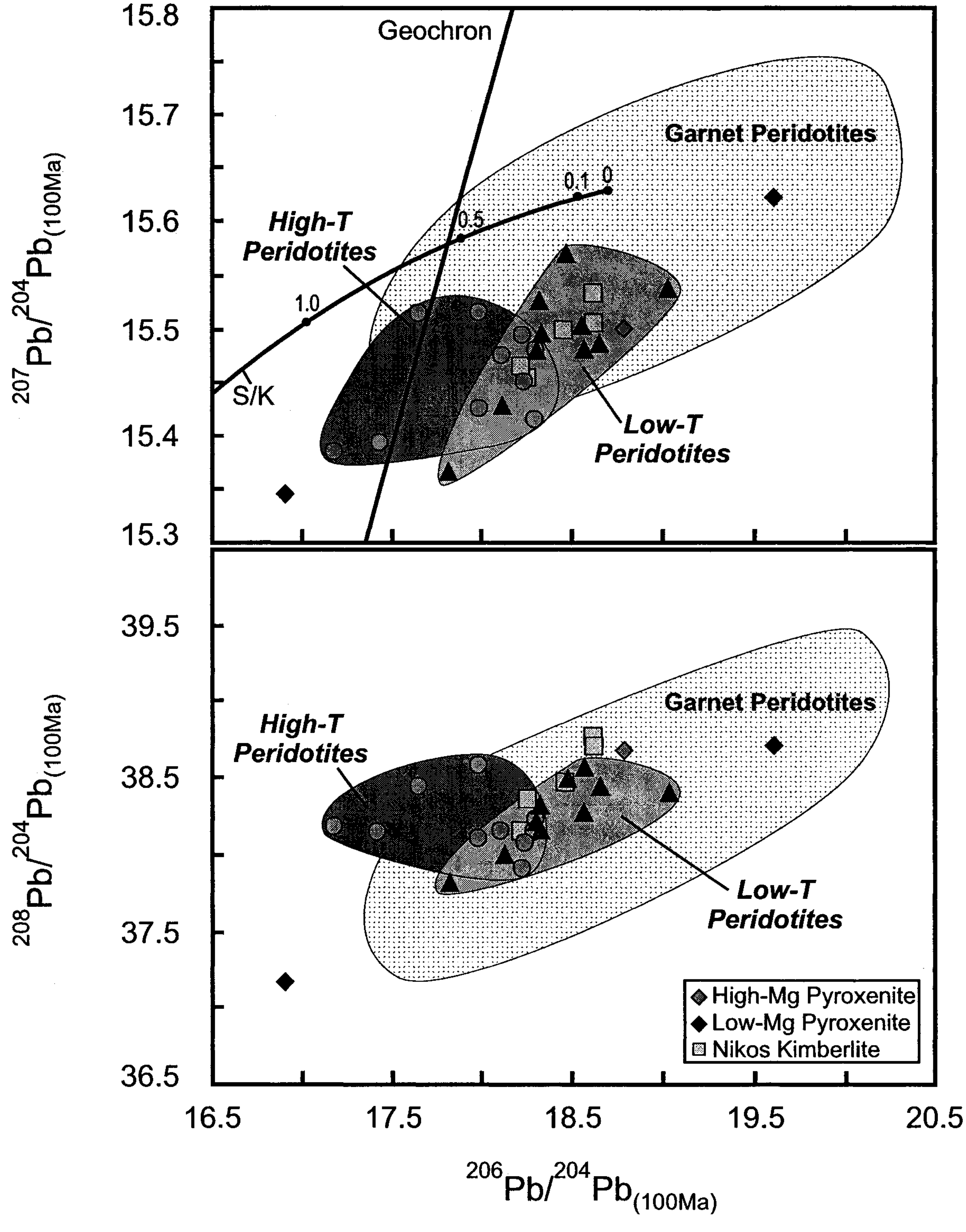
15.8
15.7
15.6
15.5
15.4
15.3
Geochron
Garnet Peridotites
0.1
0
0.5
1.0
S/K
High-T Peridotites
Low-T Peridotites
$^{207}Pb/^{204}Pb_{(100Ma)}$
39.5
38.5
37.5
36.5
Garnet Peridotites
High-T Peridotites
Low-T Peridotites
◆ High-Mg Pyroxenite
◆ Low-Mg Pyroxenite
▨ Nikos Kimberlite
$^{208}Pb/^{204}Pb_{(100Ma)}$
16.5
17.5
18.5
19.5
20.5
$^{206}Pb/^{204}Pb_{(100Ma)}$

Figure 4-5

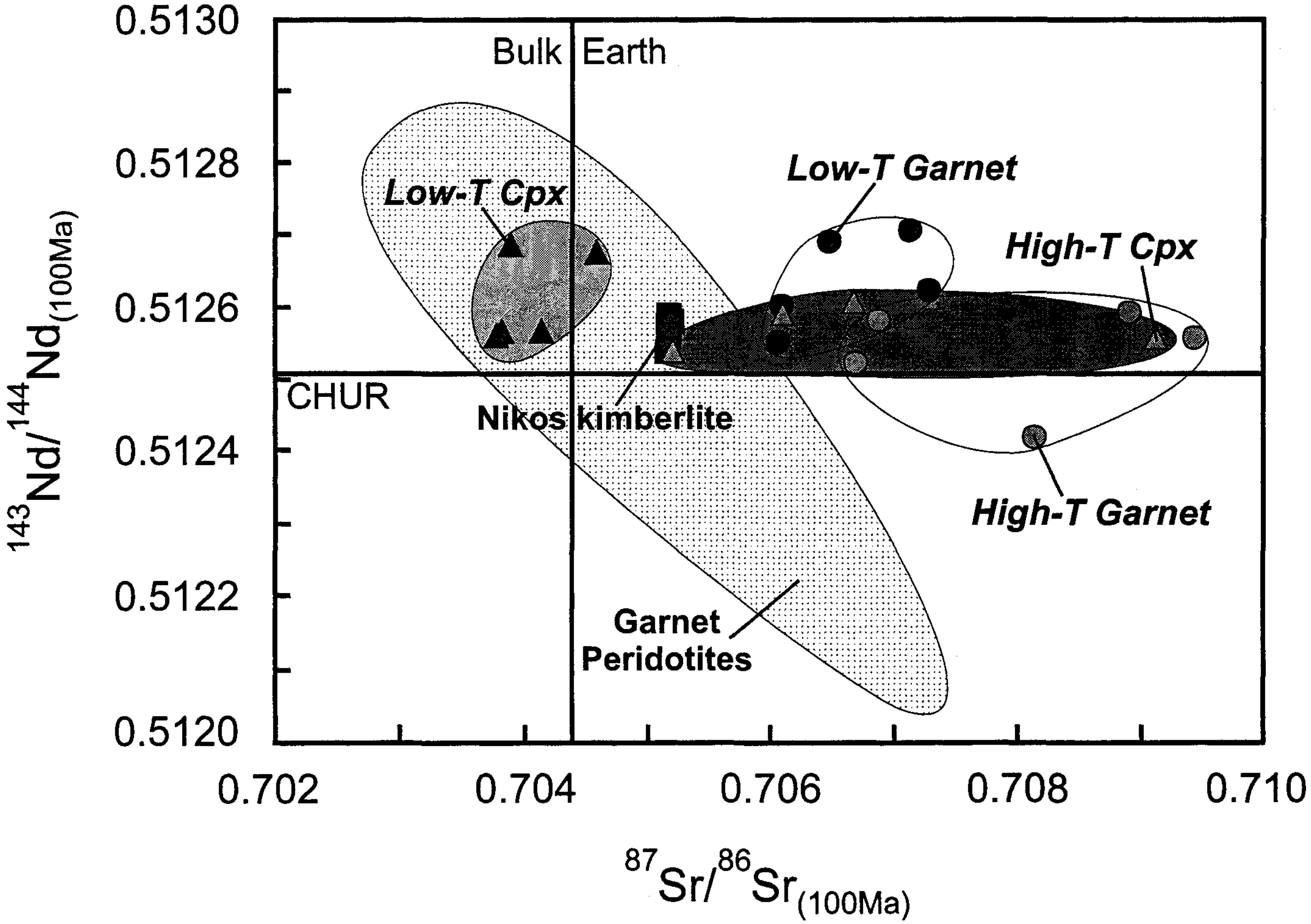
0.5130
0.5128
0.5126
0.5124
0.5122
0.5120
^{143}Nd/^{144}Nd$_{(100Ma)}$
0.702
0.704
0.706
0.708
0.710
^{87}Sr/^{86}Sr$_{(100Ma)}$
Bulk Earth
CHUR
Low-T Cpx
Low-T Garnet
High-T Cpx
High-T Garnet
Nikos kimberlite
Garnet Peridotites

Figure 4-6

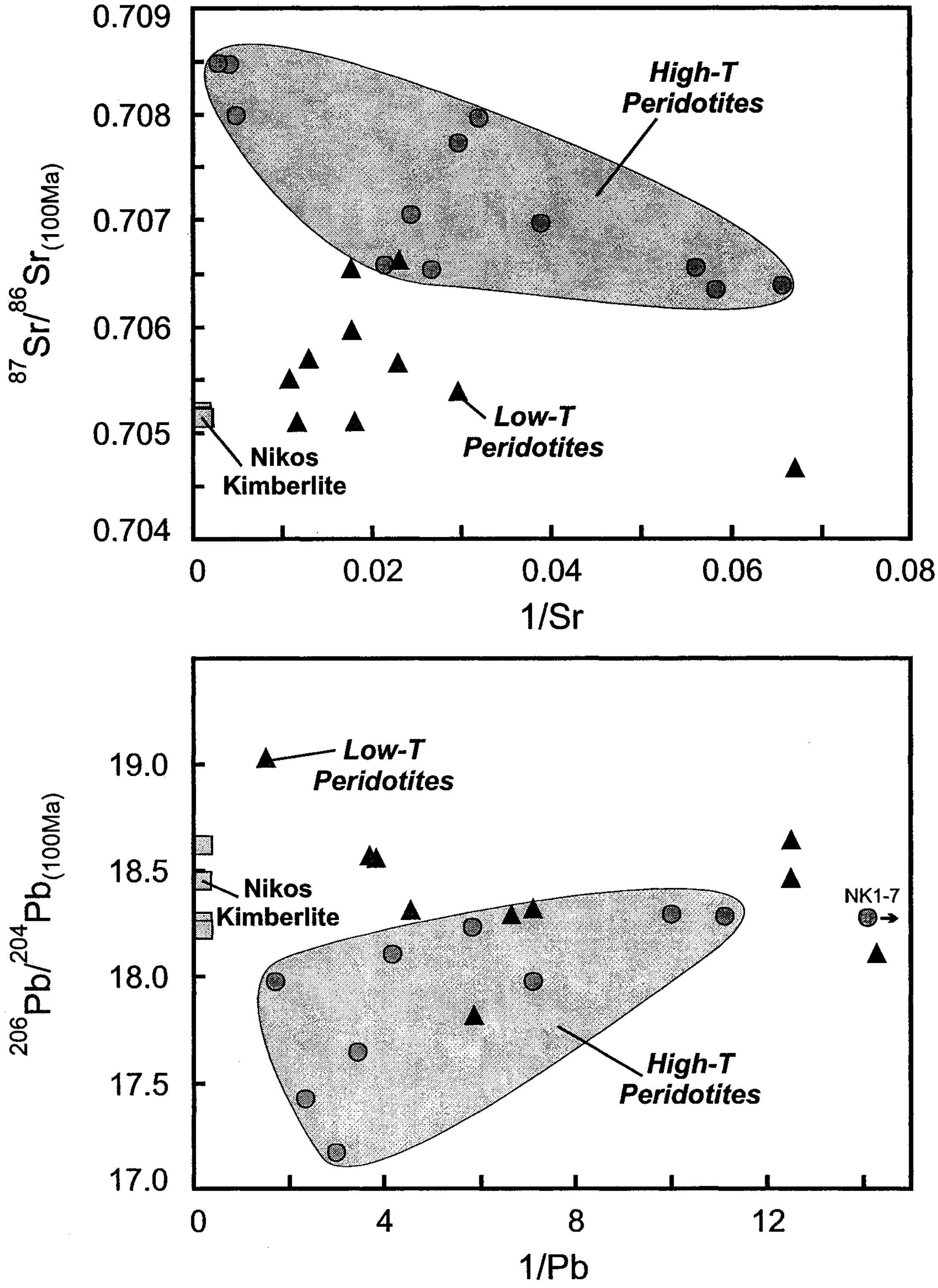

0.709
0.708
0.707
0.706
0.705
0.704
$^{87}Sr/^{86}Sr_{(100Ma)}$
High-T Peridotites
Low-T Peridotites
Nikos Kimberlite
0
0.02
0.04
0.06
0.08
1/Sr
19.0
18.5
18.0
17.5
17.0
$^{206}Pb/^{204}Pb_{(100Ma)}$
Low-T Peridotites
Nikos Kimberlite
NK1-7
High-T Peridotites
0
4
8
12
1/Pb

Figure 4-7

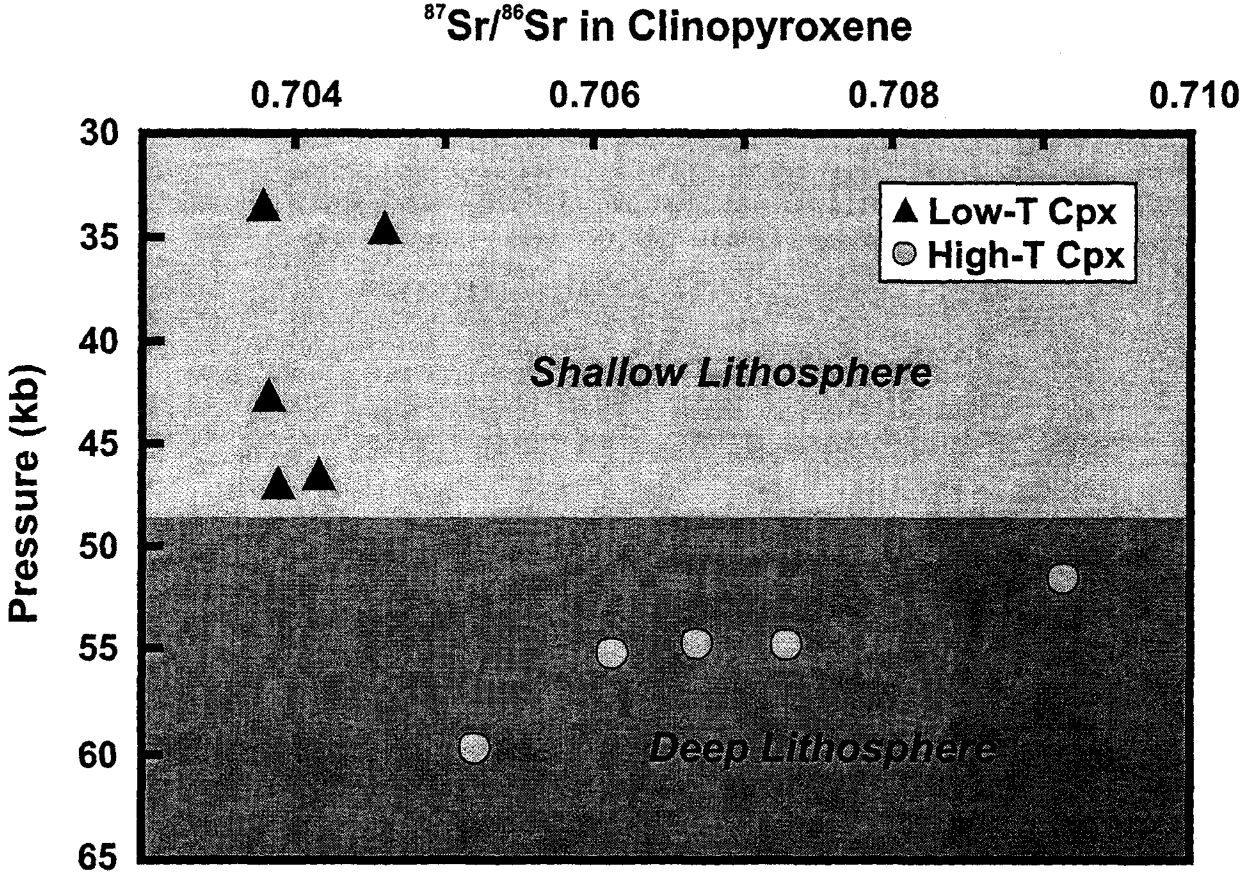
$^{87}Sr/^{86}Sr$ in Clinopyroxene
0.704
0.706
0.708
0.710
Pressure (kb)
30
35
40
45
50
55
60
65
▲ Low-T Cpx
● High-T Cpx
Shallow Lithosphere
Deep Lithosphere

Figure 4-8

CHAPTER 5

Probing Archean lithosphere using the Lu-Hf isotope systematics of peridotite xenoliths from Somerset Island kimberlites, Canada

Abstract

A knowledge of the Hf isotopic composition of the subcontinental lithosphere beneath Archean cratons is essential to constrain the Hf isotope budget of the Earth's mantle. Hf isotopic measurements were obtained by MC-ICP-MS for a suite of refractory peridotite xenoliths and constituent garnets from the Nikos kimberlite (100 Ma) on Somerset Island in order to constrain the isotopic composition and age of the lithosphere beneath the northern Canadian craton. The low-temperature Nikos peridotites (<1100°C), which represent the shallow Somerset lithosphere, are characterized by both higher $^{176}Lu/^{177}Hf$ ratios (0.03-0.05) and Hf isotopic values ($^{176}Hf/^{177}Hf_{(0.1Ga)}$=0.28296-0.28419) than the deep-seated high-temperature peridotites (>1100°C; 0.004-0.03, 0.28265-0.28333, respectively). These differences in Hf isotope signatures suggest that shallow and deep subcontinental lithosphere beneath Somerset Island represent isotopically distinct domains and do not share a common petrogenetic history.

The Lu-Hf isotope systematics of the shallow low-temperature peridotites define a positively sloped line that plot along a 2.8 Ga reference isochron. A number of these peridotites are characterized by highly radiogenic Hf isotopic compositions suggestive of long-term radiogenic ingrowth (billions of years). These findings are consistent with an interpretation that the shallow Somerset lithosphere (to depths of ~150 km) stabilized in the Archean. The majority of the high-temperature peridotites plot closer to the composition of the host kimberlite. Although the observed isotopic variation may be attributed in part to kimberlite-related Hf addition, it is possible that these deep-seated xenoliths represent younger mantle.

The superchondritic $^{176}Lu/^{177}Hf$ ratios observed for a number of the shallow low-temperature peridotites indicate strong fractionation of Lu and Hf, suggesting mantle root formation in the garnet stability field (depths >80 km). The Hf isotope compositions for the Somerset low-temperature peridotites indicate that part of the mantle root beneath the North American craton is characterized by a more radiogenic Hf isotope signature than that estimated for a typical “depleted” mantle.

Keywords: Archean lithosphere, Canadian craton, kimberlite, Lu-Hf system, peridotite, mantle xenoliths

1. Introduction

The mantle roots underlying the Archean cratons extend to depths of at least 200 km [1,2], and are depleted in basaltic constituents relative to fertile mantle [e.g.; 3-5]. The lower density and higher viscosity of these refractory peridotite roots relative to the surrounding asthenosphere contribute to their stability and long-term isolation from the convecting mantle [6,7]. The isotopic diversity recorded by both continental peridotites and basalts compared to oceanic volcanics, along with their unusually "enriched" Sr and Nd isotope signatures relative to bulk Earth ([8-10] and references therein) were the first indications of the antiquity of the subcratonic lithosphere [11,12]. These enriched isotope signatures are predominantly the result of repeated episodes of metasomatic activity, which have occurred since lithosphere stabilization (i.e. over billions of years; [13,14]). Consequently, determining the age of Archean cratonic mantle roots has proven difficult. Re-Os isotope systematics appear to be less susceptible to metasomatic alteration, and have provided valuable age constraints for the subcontinental lithosphere [12]. Re depletion ages range from the mid to late Archean (3.5 to 2.7 Ga) for the mantle roots beneath South Africa, Siberia and North America [15-18]. In contrast to the abundant Nd, Pb, Sr and Os isotope data, the Hf isotope composition of subcontinental lithospheric mantle has yet to be investigated. This region constitutes an important reservoir in the Hf budget of the Earth's mantle, and establishing its Hf isotopic composition is important in order to better understand its origin, geochemical evolution, and its role in the stabilization of the Archean cratons.

The Lu-Hf isotopic system is characterized by the long-lived radioactive parent isotope ^{176}Lu that decays to ^{176}Hf by beta emission with a half-life of 37 Ga [19,20], allowing the dating of ancient samples [21]. Lu (a heavy rare earth element, HREE) and Hf (a high field strength element, HFSE) are both refractory silicate-hosted (e.g.; [22]) elements, but exhibit significant differences in their geochemical behavior (e.g.; different mineral/melt partition coefficients; [23,24]) in the presence of mineral phases such as garnet and zircon. This can result in the strong fractionation of parent and daughter elements during magmatic and metamorphic processes, indicating the important potential of the Lu-Hf isotopic system in geochronology and as a geological tracer [e.g.; 25-28].

In this paper we report Hf isotopic compositions and $^{176}Lu/^{177}Hf$ ratios obtained using the MC-ICP-MS (multicollector inductively coupled plasma mass spectrometry) method for a suite of refractory peridotites and their constituent garnets from the Cretaceous (100 Ma) Nikos kimberlite on Somerset Island in the Canadian Arctic (Fig. 1; [29]). To our knowledge, these are the first Lu-Hf isotope data obtained for kimberlite-hosted mantle xenoliths to-date. The main objective of this study is to constrain the Hf isotopic composition of the lithospheric mantle beneath the northern Canadian craton in order to contribute to a better understanding of the Hf isotope composition and evolution of the Earth's mantle. The data permit an evaluation of the effectiveness of the Lu-Hf geochronometer in providing meaningful age constraints on the stabilization of the mantle root. The results also provide information on elemental fractionation during partial melting at the time of lithosphere formation, and on the Hf isotopic composition of the Archean mantle.

2. Samples

2.1. Kimberlite

The Nikos kimberlite is part of the Somerset Island kimberlite field [30] that was emplaced ~100 Ma ago (U-Pb ages on perovskite; [31,32]) into Archean crystalline basement (Nd model ages up to 3.0 Ga; [33]) at the northern margin of the Canadian craton (Fig. 1). The Nikos host kimberlite occurs as three closely associated individual pipes (each ~50 m diameter and 30-40 m apart) that contain abundant mantle xenoliths. Unlike many other Somerset Island kimberlites, the southern Nikos pipe (NK3) exhibits a non-brecciated, magmatic texture [29]. Four kimberlite samples were collected from this magmatic pipe for analysis, two of which (NK3-K1, NK3-K2) exhibit abundant mantle xenoliths relative to the remaining samples (NK3-K3, NK3-K4). The kimberlite contains olivine, phlogopite, garnet and spinel in a fine-grained matrix of calcite, serpentine, perovskite and apatite. Calcites occur as tabular euhedral crystals that are deflected around large olivine phenocrysts indicating their primary magmatic nature [29]. Two samples (NK3-K1, NK3-K2) are observed to contain garnet fragments in thin section, which probably represent xenocrysts. The Nikos kimberlite is characterized by very high whole-rock $CaCO_3$ contents (27-39 wt%), and a strong enrichment in incompatible trace elements such as LILE (large ion lithophile elements) and LREE (light rare earth elements) relative to chondrites and primitive mantle compositions [34,35].

2.2. Mantle xenoliths

The Nikos mantle xenoliths are large, well-preserved garnet peridotite nodules containing olivine, orthopyroxene, clinopyroxene, garnet and minor phlogopite (~1 wt% or less; [29]). One spinel peridotite (NK2-9) consists of olivine, orthopyroxene, clinopyroxene and chromian spinel. The majority of the xenoliths exhibit coarse textures, and only minor occurrences of porphyroclastic textures are observed (e.g.; NK1-7). The peridotites are characterized by refractory major element chemistry and have high magnesium-numbers (mg-number=Mg/(Mg+Fe)=0.90-0.93) suggesting that they are melt-depleted residues. Despite their depleted major element compositions, the Nikos peridotites are enriched in highly incompatible trace elements (e.g.; LILE, LREE), while having approximately chondritic HREE contents. Mass balance calculations indicate that constituent peridotite minerals control HREE budgets, but cannot account for the high LREE abundances observed in the whole-rocks, suggesting the presence of small amounts of a kimberlite-related LREE-rich interstitial component (i.e. ~1% kimberlite liquid) and/or accessory mineral (i.e. trace amounts of apatite; [35]).

The Nikos peridotites and constituent minerals have Sr and Pb isotopic signatures and incompatible trace element compositions (e.g.; La/Sm_N) that correlate with temperature and pressure (and thus depth) estimates of last equilibration, suggesting that the samples can be divided into low-temperature (800-1100°C; 25-50 kb; 80-150 km) and high-temperature peridotites (1100-1400°C; 50-60 kb; 160-190 km; [35,36]). The low-temperature peridotites and clinopyroxenes are characterized by less radiogenic $^{87}Sr/^{86}Sr_{(0.1Ga)}$ (0.7038-0.7066) and higher $^{206}Pb/^{204}Pb_{(0.1Ga)}$ (17.82-19.03) signatures at the time of kimberlite emplacement than those of the high-temperature peridotites ($^{87}Sr/^{86}Sr_{(0.1Ga)}$=0.7052-0.7095; $^{206}Pb/^{204}Pb_{(0.1Ga)}$=17.18-18.30). In addition, the low-temperature xenoliths show a stronger enrichment in incompatible trace elements (avg. La/Sm_N=6) relative to those in the high-temperature xenoliths (avg. La/Sm_N=3). These results indicate that the shallow low-temperature and the deep high-temperature lithosphere represent chemically distinct mantle reservoirs that do not share a common petrogenetic history [36]. In comparison, Nd isotopic compositions of low and high-temperature peridotites ($^{143}Nd/^{144}Nd_{(0.1Ga)}$=0.51255-0.51276; 0.51242-0.51262; respectively), which are slightly depleted compared to CHUR (chondrite uniform reservoir), overlap, and they are similar to those of the Nikos kimberlite ($^{143}Nd/^{144}Nd_{(0.1Ga)}$=0.51254-0.51259). More detailed discussions on mineralogy, and geochemical and isotopic composition of the peridotites and their host kimberlite can be found in [29,35,36].

2.3. Garnets

The Nikos garnets are chromian pyropes and their major element chemistry indicates that the crystals are compositionally homogeneous on a thin section scale [29]. The garnets in the low-temperature peridotites are characterized by low mg-numbers (0.81-0.84), low TiO_2 (0.08-0.09 wt%) and Zr (10-50 ppm) contents, and high FeO (7.2-7.9 wt%) and MnO (0.4-0.5 wt%) abundances compared to those in the high-temperature peridotites (mg-numbers=0.83-0.86; TiO_2=0.1-0.3 wt%; Zr=35-100 ppm; FeO=6.2-7.2 wt%; MnO=0.3-0.4 wt%; [35]). Sr isotopic compositions for garnets in the high-temperature peridotites ($^{87}Sr/^{86}Sr_{(0.1Ga)}$=0.7067-0.7095) extend to more radiogenic values than those for garnets in the low-temperature peridotites ($^{87}Sr/^{86}Sr_{(0.1Ga)}$=0.7061-0.7073) at the time of kimberlite emplacement [36].

3. Analytical methods

All exterior surfaces were first removed from the peridotites. The xenoliths were then crushed and rock chips were ground in an aluminum mill. Garnet separates were hand-picked under a binocular microscope and inclusion free grains were washed in an ultrasonic bath with acetone, ultra pure water and 2.5 N HCl, and then ground to small fragments in an agate mill. Crushed kimberlite whole rocks were carefully handpicked under a binocular microscope prior to grinding in an attempt to eliminate contamination from peridotite xenocrysts and country rock fragments.

For Lu-Hf isotope analysis, the sample powders (~0.8-1 g for whole rocks and ~0.2-0.25 g for garnets) were spiked with separate ^{180}Hf (98.3% enriched) and ^{176}Lu (70.9% enriched) tracers prior to dissolution. The ^{180}Hf contribution from the Hf isotope tracer represented ~3% of the total ^{180}Hf in the mixtures in order to minimize the correction of the measured ^{176}Hf/^{177}Hf ratio for spike addition [21]. Whole rock samples and garnet separates were dissolved in a mixture of $HF-HNO_3-HClO_4$ in Teflon bombs at 170°C for at least 10 days in order to ensure complete digestion and sample-spike homogenization. Prior to analysis, Hf was isolated from the REE in a fluoride precipitation step and then purified using a two-stage elution procedure (anion and cation exchange; [21]). Lu was separated as part of the REE fraction on a cation exchange column [21], then isolated from the LREE fraction using HDEHP columns. Total procedural blanks for Hf and Lu were less than 20 pg, a factor of at least 1000 for Hf and 800 for Lu lower than the total amount of Hf and Lu processed in the least abundant samples, thus rendering the blank correction negligible.

Hf and Lu isotope measurements were obtained using a Micromass IsoProbe multicollector inductively coupled plasma mass spectrometer (MC-ICP-MS) at GEOTOP, Université du Québec à Montréal. The Hf isotopic data were acquired in static, multicollection mode using 8 Faraday collectors with cup efficiencies set at unity. The mass configuration array included monitoring of isobaric interferences using isotopes

^{182}W (for ^{180}W), ^{175}Lu (for ^{176}Lu) and ^{173}Yb (for ^{176}Yb), identical to that outlined in [37]. ^{181}Ta was not monitored for potential interferences of ^{180}Ta on ^{180}Hf because of the extremely low abundances of Ta (<<0.1 ppm) in the peridotite samples [35], combined with the very low natural abundance (~0.012%) of ^{180}Ta. At the start of each analytical session, a 50 ppb solution of the JMC 475 Hf standard was aspirated into the ICP source using an ARIDUS® microconcentric nebulizer at an uptake rate of ~50 μL/minute and analyzed for approximately 10 minutes. This corresponds to ~25 ng of total Hf consumed per analysis, roughly the same magnitude as that processed for the samples used in this study. The uptake rate of the ARIDUS® instrument was kept constant and verified on a regular basis; sweep gas settings were optimized to yield maximum ion signal intensity and minimize oxide levels. The level of Hf-oxide was typically at ≤0.1% of the ion signal for the metal. The intensity of the ion signal was typically 2.0×10^{-11} A of ^{180}Hf corresponding to an absolute sensitivity of ~120 volts/ppm. Data acquisition consisted of a 50 seconds "on-peak-zero" baseline measurement (i.e. gas and 2% HNO_3 blank) with the same 2% HNO_3 solution used to dilute the samples. Subsequent to sample introduction, two half-mass unit baseline measurements were obtained within the mass range 172.5 to 182.5, bracketing the mass range used for data acquisition. The JMC 475 standard and samples were analyzed for one block of 50 scans with a 10 seconds integration time per cycle. The measured Hf isotopic ratios were normalized to $^{179}Hf/^{177}Hf=0.7325$ and corrected for mass bias using the exponential law [38]. Removal of "spike addition" was achieved using an iterative calculation [21]. Repeated measurements (n=22) of the JMC 475 standard (in 2% HNO_3) during the course of this study (April 2000 to May 2001) yielded the following results: $^{176}Hf/^{177}Hf=0.282158 \pm 23$,

^{178}Hf/^{177}Hf=1.46727±13 and ^{180}Hf/^{177}Hf=1.88669±21 (2σ standard deviation errors). Solutions made from high purity Lu and Yb metals from the Ames laboratory (20 and 10 ppb, respectively) and W (100 ppb) were analyzed prior to the measurement of samples in order to determine their mass bias and thus accurately correct for isobaric interferences, if present. However, intensities of ^{175}Lu, ^{173}Yb and ^{182}W were at or below the limit of detection for the majority of the samples. For spiked ^{176}Lu isotope dilution analyses, Yb is not separated from Lu in the chemical procedure. Thus careful evaluation of their respective mass biases are warranted in order to correct for the isobaric interference of ^{176}Yb on ^{176}Lu. Prior to sample analysis, the mass bias for Lu and Yb were determined by measuring the ^{176}Lu/^{175}Lu and ^{176}Yb/^{173}Yb for solutions of Ames Lu (20 ppb) and Yb (10 ppb) metals, and then compared to the recommended values of 0.02656 and 0.78761 [21], respectively. Evaluation of this correction was determined using a series (n=8) of Yb-doped and ^{176}Lu spiked gravimetrically prepared Ames Lu solutions. The quantity of Lu used in these solutions matched those for the peridotites; however, their Yb/Lu values were double those of the samples so as to purposely exaggerate the correction. The results indicate that the calculated Lu concentrations reproduce to better than 0.2% (2σ level). Moreover, the reproducibility for calculation of the isotopic compositions and concentrations of Hf were evaluated by a triplicate analysis (on three separate dissolutions of the same powder) of a fine-grained calc-alkaline basalt, which yielded ^{176}Hf/^{177}Hf values of 0.282633±11, 0.282638±8, 0.282636±8 and Hf concentrations of 3.47, 3.46, 3.48 ppm, respectively. The latter are identical to a Hf concentration of 3.42 ±0.17 ppm obtained by conventional ICP-MS analysis [39], despite the fact that the abundance of Ta

(0.4 ppm; [39]) in the basalt is more than four times the concentration of Ta measured in the Nikos peridotites.

4. Results

4.1. Kimberlite

The two kimberlite samples containing the least amounts of peridotite xenoliths (NK3-K3, NK3-K4) are characterized by low $^{176}Lu/^{177}Hf$ ratios (0.003) and have chondritic to slightly superchondritic [40] initial $^{176}Hf/^{177}Hf_{(0.1Ga)}$ (0.282711 and 0.282852), corresponding to initial $\varepsilon_{Hf(0.1Ga)}$ values of 0 and +5.0 (Table 1; Fig. 2a). Two kimberlite samples (NK3-K1, NK3-K2) that contained abundant mantle xenoliths also have low $^{176}Lu/^{177}Hf$ ratios (0.004), but higher initial $^{176}Hf/^{177}Hf_{(0.1Ga)}$ (0.283191 and 0.283307; initial $\varepsilon_{Hf(0.1Ga)}$=+17 and +21.1). Kimberlites from South Africa have been divided into two groups ("Group I" and "Group II") based on their distinct mineralogy and Sr-Nd-Pb isotopic signatures (e.g.; [41,42]). Recent studies have shown that both South African "Group I" and "Group II" kimberlites are characterized by low $^{176}Lu/^{177}Hf$ ratios similar to those of the Nikos kimberlite (Fig. 2a; [43]). The initial $\varepsilon_{Hf(0.1Ga)}$ values for two Nikos kimberlite samples plot within the field of initial $\varepsilon_{Hf(T)}$ values for South African "Group I" kimberlites, while those samples that containd abundant peridotite plot towards higher values. South African "Group II" kimberlites, in comparison, are characterized by negative initial $\varepsilon_{Hf(T)}$ values (Fig. 2a).

4.2. Mantle xenoliths

The low-temperature peridotites exhibit a significant range in $^{176}Lu/^{177}Hf$ ratios (0.027-0.048) and have radiogenic Hf isotopic compositions ($^{176}Hf/^{177}Hf_{(0.1Ga)}$=0.282963-0.284190; $\varepsilon_{Hf(0.1Ga)}$=+9.0 to +52.3) at the time of kimberlite emplacement (Table 1; Fig.

2b). In comparison, the high-temperature peridotites are characterized by lower ^{176}Lu/^{177}Hf ratios (0.004-0.016) and, in general, less radiogenic Hf isotopic compositions (^{176}Hf/^{177}Hf$_{(0.1Ga)}$=0.282654-0.283212; $\varepsilon_{Hf(0.1Ga)}$=-2.0 to +17.8; Fig. 2b). The Hf isotopic compositions of all Nikos peridotites (except one sample, NK3-25) are depleted relative a chondritic reservoir [40]. One high-temperature xenolith (NK1-7), which in contrast to most other samples is characterized by a porphyroclastic texture, has a ^{176}Lu/^{177}Hf and ^{176}Hf/^{177}Hf$_{(0.1Ga)}$ ratio (0.035 and 0.283312, respectively; $\varepsilon_{Hf(0.1Ga)}$=+21.3; avg. of duplicate analyses; Fig. 2b) similar to those of the low-temperature peridotites.

In a ^{176}Lu/^{177}Hf versus ^{176}Hf/^{177}Hf diagram, the data for the low-temperature xenoliths show a positively sloped correlation. The regression line for the Lu-Hf data indicates that this array corresponds to an errorchron age of 2.8±0.8 Ga (n=6; MSWD=24) with an initial ^{176}Hf/^{177}Hf ratio of 0.28164±57 (ε_{Hf}=+23; Fig. 3). One low-temperature sample (NK1-2) is not included in the data regression as the presence of carbonate-rich veins suggest kimberlite contamination. Since the low-temperature peridotites were sampled over a large depth interval (80-150 km) and the errorchron age is associated with a large error, a 2.8 Ga reference isochron with a corresponding initial Hf isotopic ratio is plotted for comparison rather than the errorchron (Fig. 3). The majority of the high-temperature peridotites exhibit lower ^{176}Lu/^{177}Hf ratios and trend towards the composition of the Nikos kimberlite (Table 1; Fig. 2b). No data plot to the right of the reference isochron.

Duplicate analyses were obtained on separate dissolutions of the rock powders (not on sample splits after initial dissolution). The ^{176}Lu/^{177}Hf ratios vary by 5-8% and Hf isotope ratios by 4-8 ε_{Hf} units for the low-temperature peridotites (NK1-4, NK1-14, NK1-

2; Table 1). Although these variations are relatively large, in each case the parent-daughter ratio correlates with isotopic composition. The variations in the Lu/Hf ratios and Hf isotopic compositions are thus attributed to sample heterogeneity of the whole rock powders, resulting from the coarse-grained nature of the peridotites, in particular, the presence of large crystals of garnet (up to 5mm), and their (Archean) age. Duplicate analyses of Hf isotopic composition for two other low-temperature peridotites (NK1-23, NK1-3) are within error. For two high-temperature peridotites (NK1-19, NK1-7) parent-daughter ratios do not correlate with isotopic ratios, which is probably the result of kimberlite contamination (see later discussion). For samples with duplicate ^{176}Lu/^{177}Hf and Hf isotope ratios, these are plotted as average values in the figures.

4.3. Garnets

The garnets of the low-temperature xenoliths exhibit a large range in ^{176}Lu/^{177}Hf ratios (0.093-0.243) and their ^{176}Hf/^{177}Hf$_{(0.1Ga)}$ compositions (0.283096-0.286947; $\varepsilon_{Hf(0.1Ga)}$=+13.7 to +150) extend to extremely radiogenic values at the time of kimberlite emplacement (Table 2). In comparison, the garnets from the high-temperature peridotites have lower ^{176}Lu/^{177}Hf ratios (0.015-0.057) and less radiogenic ^{176}Hf/^{177}Hf$_{(0.1Ga)}$ compositions (0.282749-0.283407; $\varepsilon_{Hf(0.1Ga)}$=+1.4 to +24.7; Table 2). The garnets from the low-temperature peridotites are characterized by slightly higher Lu (avg. 0.30 ppm), but significantly lower Hf abundances (avg. 0.31 ppm) than garnets from the high-temperature peridotites (avg. Lu=0.25 ppm; Hf=0.95 ppm; Table 2). Tie lines for individual garnet-whole-rock pairs in the low-temperature peridotites are all positively sloped and correspond to internal isochrons "ages" ranging from 900 to 250 Ma (Table 2; Fig. 4). In contrast, the garnet-whole rock tie lines for most high-temperature peridotites (except porphyroclastic xenolith NK1-7; 330 Ma) define negative (or flat) trends (Fig. 4). Duplicate analyses of garnet separate NK1-7 yield a difference of ~0.9% for the $^{176}Lu/^{177}Hf$ value and identical $^{176}Hf/^{177}Hf$ compositions (Table 2), supporting our interpretation that sample heterogeneity is responsible for the variation exhibited by the replicate analyses of the whole rock powders.

5. Discussion

5.1. Kimberlite mantle source

Two Nikos kimberlite samples (NK3-K3, NK3-K4) are characterized by chondritic or slightly superchondritic initial Hf isotope compositions ($\varepsilon_{Hf(0.1Ga)}$=0 and +5.0), and these plot within the field of Lu-Hf isotope data for South African kimberlites (Fig. 2a; [43]). In comparison, initial $\varepsilon_{Hf(0.1Ga)}$ values (+17 and +21.1; NK3-K1, NK3-K2) for two kimberlite samples that contain abundant mantle xenoliths are much higher. The significant variation in Hf isotope ratios could be inherited from a (non-homogenous) kimberlite mantle source, or indicate the presence of xenocrysts (e.g.; garnet) in the kimberlite derived by fragmentation of peridotite xenoliths. It appears likely that xenocrystic garnet (as observed in thin sections) is responsible for the high $\varepsilon_{Hf(0.1Ga)}$ values of two kimberlite samples (NK3-K1, NK3-K2), since it has high $^{176}Lu/^{177}Hf$ and thus high time-integrated Hf isotopic ratios. This interpretation is supported by $\varepsilon_{Nd(0.1Ga)}$ values (+1.1 and +0.6, respectively; [36]) that correlate negatively with $\varepsilon_{Hf(0.1Ga)}$ values in these two samples, the opposite of what is observed for most terrestrial rocks [44].

The kimberlite samples that are characterized by low $\varepsilon_{Hf(0.1Ga)}$ values (NK3-K3, NK3-K4) are interpreted to represent the Hf isotopic composition of the Nikos kimberlite at the time of emplacement, and these are plotted in the figures. Since kimberlites represent low degree partial melts (1% or less; [45]), the small difference in their $\varepsilon_{Hf(0.1Ga)}$ values (0 and +5.0) may be attributed to the inhomogeneous composition of the mantle source. In a Hf-Nd diagram, the two Nikos kimberlite samples exhibit a positive correlation of these isotope ratios with chondritic to slightly superchondritic compositions, and plot within the terrestrial Hf-Nd array (Fig. 5).

5.2. Shallow versus deep lithosphere

The refractory major element compositions of the Nikos peridotites that sample the Somerset lithosphere indicate that these xenoliths are melt-depleted residues [29]. The Lu abundances of both the low and high-temperature peridotites show a good positive correlation with their bulk rock Al_2O_3 contents, which constitute a measure for the degree of major element depletion in residual peridotites (Fig. 6). These findings suggest that the Lu levels observed in these xenoliths were controlled by variable degrees of partial melting during lithosphere formation.

The low-temperature Nikos peridotites were sampled over a very large depth interval of about 70 km by their host kimberlite. These xenoliths are characterized by Lu-Hf isotopic compositions that plot close to a line corresponding to a reference isochron age of 2.8 Ga (Fig. 3). This reference isochron age is almost identical to Re depletion ages (2.7 Ga) that were recently reported for other Somerset Island peridotites [18]. A number of the low-temperature peridotites exhibit very radiogenic Hf isotopic compositions at the time of kimberlite magmatism ($^{176}Hf/^{177}Hf_{(0.1Ga)}$=0.2835-0.2841, $\varepsilon_{Hf(0.1Ga)}$=+30 to +50; Table 1; Figs. 2b, 5) compared to estimates for a typical “depleted” mantle (~0.2832, +18, respectively; [40, 46]. Long-term (billions of years) radiogenic ingrowth is required to produce the highly depleted Hf isotopic signatures. These results provide evidence for an ancient (Archean) depletion event that resulted in the stabilization of the mantle root beneath the northern Canadian craton to depths of about 150 km. The initial Hf isotopic value (^{176}Hf/^{177}Hf=0.28164±57) associated with this reference isochron corresponds to an ε_{Hf} value of +23 that within error could be as low as +3. These results suggest that the low-temperature Nikos peridotites were derived from a mantle having melt-depleted characteristics at the time of lithosphere stabilization rather than from a primitive mantle reservoir [40, 46]. A number of the low-temperature Nikos xenoliths are characterized by slightly subchondritic ^{176}Lu/^{177}Hf ratios (<0.033), while having superchondritic Hf isotopic compositions (^{176}Hf/^{177}Hf>0.282772; [40]), suggesting recent perturbation of their ^{176}Lu/^{177}Hf ratios. Since Lu levels correlate with other indices of melt depletion and thus appear to have been controlled by partial melting (Fig. 6), these xenoliths may have experienced minor Hf addition rather than Lu loss. The Nikos kimberlite is characterized by low ^{176}Lu/^{177}Hf ratios and high Hf abundances, and it appears likely that these xenoliths may have been affected by interaction with the host magma during sample transport. The addition of very small amounts of a kimberlite component (~0.5% bulk kimberlite or significantly less of a kimberlite-related Hf-bearing accessory mineral) as indicated by mass balance calculations, would produce slightly subchondritic ^{176}Lu/^{177}Hf ratios. In contrast to the low-temperature xenoliths, the majority of the high-temperature peridotites plot closer to the composition of the kimberlite (Fig. 2b, 3). This feature could be interpreted as the result of more extensive contamination with host kimberlite since these xenoliths resided closer to the area of kimberlite formation, and/or that these peridotites are younger and represent mantle of distinct origin.

The highly variable Hf isotopic compositions of the Nikos peridotites are predominantly superchondritic at the time of kimberlite magmatism (Fig. 5). A number of the peridotites extend to significantly higher Hf values compared to "depleted" mantle and plot above the terrestrial Hf-Nd array [44]. In comparison, the Nd isotopic compositions of the peridotites ($\varepsilon_{Nd(0.1Ga)}$=+1 to +4; [36]), which are distinctly lower than estimates for "depleted" mantle ($\varepsilon_{Nd(0.1Ga)}$ ~+10; Fig. 5; [8]), show little variation, and overlap those of the Nikos kimberlite ($\varepsilon_{Nd(0.1Ga)}$=+1 to +2; Fig. 5). The Nd isotope results have been interpreted to indicate that the xenoliths were contaminated with small amounts of host magma during sample transport [36]. In contrast to tightly constrained Nd isotopic signatures, the low-temperature peridotites are characterized by significantly less radiogenic Sr (Fig. 7) and higher Pb (not shown) isotopic compositions ($^{87}Sr/^{86}Sr_{(0.1Ga)}$=0.7051-0.7066; $^{206}Pb/^{204}Pb_{(0.1Ga)}$=17.82-19.03) than the high-temperature peridotites ($^{87}Sr/^{86}Sr_{(0.1Ga)}$=0.7064-0.7080; $^{206}Pb/^{204}Pb_{(0.1Ga)}$=17.18-18.30). In addition, the Sr isotope ratios of the Nikos peridotites, with the exception of one sample (NK1-23), differ from those of the host kimberlite (Fig. 7; [36]). The distinct Sr and Pb isotope compositions of low and high-temperature peridotites restrict the amount of interstitial kimberlite component to less than 1 wt% [36] as kimberlite contribution in excess of this amount would eradicate the observed isotopic differences. The Hf isotopic compositions of the Nikos peridotites are highly variable and the majority extend to significantly more radiogenic compositions than the host kimberlite (Figs. 2b, 5). As the average Hf abundance ratio (kimberlite/peridotite) of 20:1 is similar to that for Sr, but 3 times lower than for Nd (60:1), Hf is significantly less susceptible to kimberlite contamination than Nd. Since kimberlite addition was restricted to very small amounts, it is likely that the Hf isotopic differences observed for the Nikos peridotites existed prior to the kimberlite event (Figs. 2b, 5).

While all the Nikos xenoliths are refractory residues that were generated by extensive melt extraction, the low-temperature peridotites exhibit $\varepsilon_{Hf(0.1Ga)}$ values (+9 to +50) that are significantly higher and more variable than those of the high-temperature peridotites (-2 to +20). The distinct Hf isotopic compositions for low and high-temperature peridotites are in agreement with the previously reported differences in Sr and Pb isotope compositions [36] indicating that shallow and deep Somerset lithosphere do not share a common petrogenetic history. The depth stratification could have resulted from infiltration of the lower lithosphere with metasomatic melts or fluids. This model cannot be reconciled, however, with the significantly less enriched incompatible trace element signatures of the deep-seated peridotites (avg. La/Sm_N=3) relative to those of the shallow xenoliths (avg. La/Sm_N=6; [35]). Alternatively, the deep lithosphere could be younger and was added to the Archean subcratonic mantle by downward growth of the shallow lithosphere, an interpretation consistent with the isotopic and trace element record [35,36]. Mantle stratification and post-Archean lithosphere growth have previously been proposed for other cratonic areas such as the Kaapvaal craton beneath South Africa (e.g.; [10,16]) and appear to be a common feature for the lithospheric mantle root beneath the continents.

5.3. Garnet Hf isotope systematics

The garnets from the low-temperature peridotites are characterized by low Hf abundances (avg. 0.31 ppm) and their highly variable $^{176}Hf/^{177}Hf_{(0.1Ga)}$ compositions (0.28310-0.28695) extend to significantly more radiogenic values than those for garnets from the high-temperature peridotites (avg. Hf=0.95 ppm; $^{176}Hf/^{177}Hf_{(0.1Ga)}$=0.28275-0.28341; Table 2; Fig. 4). These signatures correlate with chemical characteristics such as TiO_2 contents that are lower for garnets from the shallow peridotites (0.08-0.09 wt%) relative to those for garnets from the deep-seated peridotites (0.1-0.3 wt%; [35]). The results indicate significant isotopic and chemical differences for garnets from low and high-temperature Nikos peridotites, and are consistent with the finding based on the whole rock Hf, Sr and Pb isotopic compositions that shallow and deep Somerset lithosphere represent mantle of distinct origin.

Internal Lu-Hf isochrons using garnet-whole rock pairs (Fig. 4) for the low-temperature peridotites yield "ages" ranging from 900 to 500 Ma, and 300 to 250 Ma for two samples that could have experienced minor kimberlite addition as suggested by the presence of carbonate-rich veins (NK1-2) and a slightly subchondritic $^{176}Lu/^{177}Hf$ ratio (NK1-3). The "dates" defined by the Lu-Hf whole rock-garnet isochrons decrease with increasing temperature (and thus depth), and the oldest "age" is obtained for the shallowest garnet-whole rock pair (870°C, 110 km; Fig. 8). No garnet-whole rock pair at any depth, however, defines an internal isochron corresponding to an Archean age. These findings indicate that lithospheric temperatures (870°C and higher) exceeded the closure temperatures for Hf (and Lu) diffusion in the garnet-whole rock system. The depth correlation of the Lu-Hf "ages" suggests that the extent of Hf isotope re-equilibration in the garnet-whole rock system varied as a function of temperature. In comparison, internal Sm-Nd isochrons for these same garnet-whole rock pairs yield "ages" of 200 to 90 Ma, and the youngest "date" essentially coincides with the age of kimberlite formation [36]. The Lu-Hf "date" for individual garnet-whole rock pairs is always older than that obtained using Sm-Nd systematics. Although Nd isotope systematics appear to be more susceptible to kimberlite contamination, these findings are also consistent with recent results based on high-grade metamorphic rocks suggesting that in garnet-whole rock systems the closure temperature of Lu-Hf is greater than or equal to that of Sm-Nd [28].

Tie lines joining garnet and corresponding whole rock for the low-temperature peridotites have positive slopes (Fig. 4), a feature consistent with Hf isotope re-equilibration in the garnet-whole rock system. In contrast, the tie lines joining garnet-whole rock pairs for the high-temperature samples (except porphyroclastic peridotite NK1-7) have negative (or flat) slopes, which could reflect recent Hf infiltration (Fig. 4). The fact that the whole rock Hf isotope compositions of the high-temperature xenoliths plot close to that of the Nikos kimberlite is consistent with an interpretation that these peridotites experienced Hf addition during sample transport.

5.4. Evolution of Archean lithosphere

The Hf isotopic composition of lithospheric mantle underlying Archean cratons has yet to be clearly established because of former difficulties with the analytical method prior to the development of MC-ICP-MS. Recent investigations have focused on Hf and Nd isotopic determinations for 3.8 Ga old supracrustal rocks from the Isua province of Greenland in order to characterize the isotopic composition of the early terrestrial mantle [46,47]. These samples exhibit a significant range in both initial Hf and Nd isotope ratios, which are dominantly more radiogenic than those of chondrites, suggestive of derivation from "depleted" mantle. The Lu/Hf and Sm/Nd ratios observed in these early Archean rocks, however, are distinct from those inferred for a "depleted" mantle reservoir [46-48], which as for most terrestrial rocks has been characterized by the covariant evolution of Hf and Nd isotopes [25,49,50]. This relationship has been interpreted to reflect the similar fractionation of Lu and Hf, and Sm and Nd during melt extraction from garnet-free residual peridotite assemblages [25,49,51]. In contrast, melting of mantle peridotite in the presence of garnet (i.e. depths >80 km) results in a significant fractionation of Lu/Hf and Sm/Nd ratios as garnet preferentially incorporates Lu relative to Hf, to a greater extent than Sm relative to Nd [24,46]. The data obtained from the 3.8 Ga old Isua samples suggest that elemental fractionation during partial melting in the early Archean mantle was much stronger than in the post-Archean "depleted" mantle reservoir and most likely occurred in the presence of garnet [46-48].

A number of the low-temperature Nikos peridotites, which represent the shallow lithosphere beneath the Canadian craton, are characterized by Hf isotopic signatures that are significantly higher compared to that estimated for "depleted" mantle [40,46]. These xenoliths exhibit superchondritic $^{176}Lu/^{177}Hf$ ratios (Figs. 2b, 3), indicative of strong fractionation of the Lu/Hf ratios during generation of the melt-depleted peridotites. The results can be interpreted as evidence that garnet was present as a residual phase during partial melting and that the Somerset lithosphere stabilized at a minimum depth of 80 km. Over billions of years, these fractionated $^{176}Lu/^{177}Hf$ ratios resulted in the very radiogenic $^{176}Hf/^{177}Hf$ compositions recorded by the low-temperature Nikos peridotites at the time of kimberlite emplacement.

6. Conclusions

The Hf isotopic compositions of the Nikos peridotites indicate significant differences exist between the low (shallow; <1100°C) and high-temperature (deep-seated; >1100°C) xenoliths. Although contamination with a kimberlite-related component may have been superimposed on the Hf isotope compositions of a number of xenoliths, it is likely that shallow and deep Somerset lithosphere do not share a common petrogenetic history. The Lu-Hf systematics of the low-temperature Nikos peridotites suggest that the Somerset lithosphere stabilized in the Archean to depths of at least 150 km.

A number of the low-temperature peridotites exhibit superchondritic ^{176}Lu/^{177}Hf ratios that suggest mantle root formation in the presence of residual garnet (depths >80 km). These fractionated ^{176}Lu/^{177}Hf ratios resulted in the radiogenic ^{176}Hf/^{177}Hf signatures observed at the time of kimberlite magmatism. These first Hf isotopic ratios for the subcontinental mantle indicate that at least part of the lithosphere beneath the North American craton is characterized by more radiogenic Hf isotope signatures than estimates for "depleted" mantle.

Acknowledgments

We thank Fabien Rasselet for assistance in the field and for handpicking separates of magmatic kimberlite for isotope analysis. S. Schmidberger and A. Simonetti are indebted to J. Blichert-Toft for introducing them to the secrets of Lu-Hf chemistry. The MC-ICP-MS facility is supported by a MFA grant from NSERC and the research was funded by a NSERC operating grant to D. Francis. S. Schmidberger is grateful for financial support in the form of a NSERC doctoral scholarship. The manuscript was greatly improved by comments from the reviewers, J. Blichert-Toft, J. Vervoort, and G. Nowell, and from discussions with the editor, Alex Halliday.

References

[1] T.H. Jordan, Structure and formation of the continental tectosphere, J. Petrol., Special Lithosphere Issue (1988) 11-37.

[2] S.P. Grand, Mantle shear structure beneath the Americas and surrounding oceans, J. Geophys. Res. 99 (1994) 11591-11621.

[3] F.R. Boyd, S.A. Mertzman, Composition and structure of the Kaapvaal lithosphere, southern Africa, in: B.O. Mysen (Ed.), Magmatic processes: physiochemical principles, Geological Society, Special Publications 1 (1987) pp. 13-24.

[4] P.H. Nixon, Kimberlitic xenoliths and their cratonic setting, in: P.H. Nixon (Ed.), Mantle xenoliths, John Wiley, Chichester, 1987, pp. 215-239.

[5] W.F. McDonough, Constraints on the composition of the continental lithospheric mantle, Earth Planet. Sci. Lett. 101 (1990) 1-18.

[6] T.H. Jordan, Mineralogies, densities and seismic velocities of garnet lherzolites and their geophysical implications, in: F.R. Boyd, H.O.A. Meyer (Eds.), The mantle sample: Inclusions in kimberlites and other volcanics, American Geophysical Union, Washington, 1979, pp. 1-13.

[7] H.N. Pollack, Cratonization and thermal evolution of the mantle, Earth Planet. Sci. Lett. 80 (1986) 175-182.

[8] A. Zindler, S. Hart, Chemical geodynamics, Ann. Rev. Earth Planet. Sci. 14 (1986) 493-571.

[9] A.J. Erlank, F.G. Waters, C.J. Hawkesworth, S.E. Haggerty, H.L. Allsopp, R.S. Rickard, M.A. Menzies, Evidence for mantle metasomatism in peridotite nodules from the Kimberley pipes, South Africa, in: M.A. Menzies, C.J. Hawkesworth (Eds.), Mantle metasomatism, Academic Press, London, 1987, pp. 221-311.

[10] M.A. Menzies, Archean, Proterozoic, and Phanerozoic lithospheres, in: M.A. Menzies (Ed.), Continental mantle, Oxford Univ. Press, Oxford, 1990, pp. 67-86.

[11] C. Brooks, D.E. James, S.R. Hart, Ancient lithosphere: its role in young continental volcanism, Science 139 (1976) 1086-1094.

[12] D.G. Pearson, The age of continental roots, Lithos 48 (1999) 171-194.

[13] G.M. Yaxley, A.J. Crawford, D.H. Green, Evidence for carbonatite metasomatism in spinel peridotite xenoliths from western Victoria, Earth Planet. Sci. Lett. 107 (1991) 305-317.

[14] R.L. Rudnick, W.F. McDonough, B.W. Chappell, Carbonatite metasomatism in the northern Tanzanian mantle, Earth Planet. Sci. Lett. 114 (1993) 463-475.

[15] R.W. Carlson, A.J. Irving, Depletion and enrichment history of subcontinental lithospheric mantle: Os, Sr, Nd and Pb evidence for xenoliths from the Wyoming Craton, Earth Planet. Sci. Lett. 126 (1994) 457-472.

[16] D.G. Pearson, R.W. Carlson, S.B. Shirey, F.R. Boyd, P.H. Nixon, Stabilisation of Archean lithospheric mantle: a Re-Os isotope study of peridotite xenoliths from the Kaapvaal craton, Earth Planet. Sci. Lett. 134 (1995a) 341-357.

[17] D.G. Pearson, S.B. Shirey, R.W. Carlson, F.R. Boyd, N.P. Pokhilenko, N. Shimizu, Re-Os, Sm-Nd, and Rb-Sr isotope evidence for thick Archean lithospheric mantle beneath the Siberian craton modified by multistage metasomatism, Geochim. Cosmochim. Acta 59 (1995b) 959-977.

[18] G.J. Irvine, M.G. Kopylova, R.W. Carlson, D.G. Pearson, S.B. Shirey, B.A. Kjarsgaard, Age of the lithospheric mantle beneath and around the Slave craton: a Rhenium-Osmium isotopic study of peridotite xenoliths from the Jericho and Somerset Island kimberlites, Ninth Annual V. M. Goldschmidt Conference, LPI Contribution No. 971 (1999) 134-135.

[19] J. Dalmasso, G. Barci-Funel, G.J. Ardisson, Reinvestigation of the decay of the long-lived odd-odd ^{176}Lu nucleus, Appl. Radiat. Isot. 43 (1992) 69-76.

[20] Y. Nir-El, N. Lavi, Measurement of half-life of ^{176}Lu, Appl. Radiat. Isot. 49 (1998) 1653-1655.

[21] J. Blichert-Toft, C. Chauvel, F. Albarède, Separation of Hf and Lu for high-precision isotope analysis of rock samples by magnetic sector-multiple collector ICP-MS, Contrib. Mineral. Petrol. 127 (1997) 248-260.

[22] R.M. Bedini, J.-L. Bodinier, Distribution of incompatible trace elements between the constituents of spinel peridotite xenoliths: ICP-MS data from the East African Rift, Geochim. Cosmochim. Acta 63 (1999) 3883-3900.

[23] S.R. Hart, T. Dunn, Experimental clinopyroxene-melt partitioning of 24 trace elements, Contrib. Mineral. Petrol. 113 (1993) 1-8.

[24] H. Fujimaki, M. Tatsumoto, K.I. Aoki, Partition coefficients of Hf, Zr, and REE between phenocrysts and groundmasses, J. Geophys. Res. 89 (1984) B662-B672.

[25] P.J. Patchett, M. Tatsumoto, Hafnium isotope variations in oceanic basalts, Geophys. Res. Lett. 7 (1980) 1077-1080.

[26] P.J. Patchett, M. Tatsumoto, Lu-Hf total-rock isochron for the eucrite meteorites, Nature 288 (1980) 571-574.

[27] S. Duchêne, J. Blichert-Toft, B. Luais, P. Télouk, J.-M. Lardeaux, F. Albarède, The Lu-Hf dating of garnets and the ages of the Alpine high-pressure metamorphism, Nature 387 (1997) 586-589.

[28] E.E. Scherer, K.L. Cameron, J. Blichert-Toft, Lu-Hf garnet geochronology: Closure temperature relative to the Sm-Nd system and the effects of trace mineral inclusions, Geochim. Cosmochim. Acta 64 (2000) 3413-3432.

[29] S.S. Schmidberger, D. Francis, Nature of the mantle roots beneath the North American craton: mantle xenolith evidence from Somerset Island kimberlites, Lithos 48 (1999) 195-216.

[30] J. Pell, New kimberlite discoveries on Somerset Island, in: Exploration Overview 1993, Yellowknife: NWT Geology Division, Department of Indian and Northern Affairs (1993) pp. 47.

[31] L.H. Heaman, The nature of the subcontinental mantle from Sr-Nd-Pb isotopic studies on kimberlite perovskite, Earth Planet. Sci. Lett. 92 (1989) 323-334.

[32] C.B. Smith, H.L. Allsopp, O.G.Garvie, J.D.Kramers, P.F.S. Jackson, C.R. Clement, Note on the U-Pb perovskite method for dating kimberlites: examples from the Wesselton and DeBeers mines, South Africa, and Somerset Island, Canada, Chem. Geol. (Isot. Geos.) 79 (1989) 137-145.

[33] T. Frisch, P.A. Hunt, Reconnaissance U-Pb geochronology of the crystalline core of the Boothia Uplift, District of Franklin, Northwest Territories, in: Radiogenic age and isotope studies: Report 7, Geological Survey of Canada, Paper 93-2 (1993) pp. 3-22.

[34] W.F. McDonough, S.S. Sun, The composition of the earth, Chem. Geol. 120 (1995) 223-253.

[35] S.S. Schmidberger, D. Francis, Constraints on the trace element composition of the Archean mantle root beneath Somerset Island, Arctic Canada, J. Petrol. 42 (2001) 1095-1117.

[36] S.S. Schmidberger, A. Simonetti, D. Francis, Sr-Nd-Pb isotope systematics of mantle xenoliths from Somerset Island kimberlites: Evidence for lithosphere stratification beneath Arctic Canada, Geochim. Cosmochim. Acta 65 (2001).

[37] N. Machado, A. Simonetti, U-Pb dating and the Hf isotope composition of zircon by laser-ablation-MC-ICP-MS, in: Laser-ablation-ICPMS in the Earth Sciences, Mineralogical Association of Canada, Short Course 29 (2001) pp. 121-146.

[38] W.A. Russell, D.A. Papanastassiou, T.A. Tombrello, Ca isotope fractionation on the Earth and other solar system materials, Geochim. Cosmochim. Acta 42 (1978) 1075-1090.

[39] S.S. Schmidberger, E. Hegner, Geochemistry and isotope systematics of calc-alkaline volcanic rocks from the Saar-Nahe basin (SW Germany) - implications for Late-Variscan orogenic development, Contrib. Mineral. Petrol. 135 (1999) 373-385.

[40] J. Blichert-Toft, F. Albarède, The Lu-Hf isotope geochemistry of chondrites and the evolution of the mantle-crust system, Earth Planet. Sci. Lett. 148 (1997) 243-258.

[41] J.B. Dawson, A review of the geology of kimberlite, in: P.J. Wyllie (Ed.), Ultramafic and related rocks, Wiley, New York, 1967, pp. 241-251.

[42] C.B Smith, Pb, Sr and Nd isotopic evidence for sources of southern African Cretaceous kimberlites, Nature 304 (1983) 51-54.

[43] G.M. Nowell, D.G. Pearson, P.D. Kempton, S.R. Noble, C.B. Smith, Origins of kimberlites: a Hf isotope perspective, in: Proceedings of the Seventh Int. Kimb. Conf., 1999, pp. 616-624.

[44] J.D. Vervoort, P.J. Patchett, F. Albarède, J. Blichert-Toft, R. Rudnick, H. Downes, Hf-Nd isotopic evolution of the lower crust, Earth Planet. Sci. Lett. 181 (2000) 115-129.

[45] J.A. Dalton, D.C. Presnall, The continuum of primary carbonatitic-kimberlitic melt compositions in equilibrium with lherzolite: data from the system CaO-MgO-Al_2O_3-SiO_2-CO_2 at 6 GPa, J. Petrol. 39 (1998) 1953-1964.

[46] J.D. Vervoort, J. Blichert-Toft, Evolution of the depleted mantle: Hf isotope evidence from juvenile rocks through time, Geochim. Cosmochim. Acta 63 (1999) 533-556.

[47] J. Blichert-Toft, F. Albarède, M. Rosing, R. Frei, D. Bridgwater, The Nd and Hf isotopic evolution of the mantle through the Archean. Results from the Isua supracrustals, West Greenland, and from the Birimian terranes of West Africa, Geochim. Cosmochim. Acta 63 (1999) 3901-3914.

[48] F. Albarède, J. Blichert-Toft, J.D. Vervoort, J.D. Gleason, M. Rosing, Hf-Nd isotope evidence for a transient dynamic regime in the early terrestrial mantle, Nature 404 (2000) 488-490.

[49] P.J. Patchett, Hafnium isotope results from mid-ocean ridges and Kerguelen, Lithos 16 (1983) 47-51.

[50] J.D. Vervoort, P.J. Patchett, J. Blichert-Toft, F. Albarède, Relationships between Lu-Hf and Sm-Nd isotopic systems in the global sedimentary system, Earth Planet. Sci. Lett. 168 (1999) 79-99.

[51] C.M. Johnson, B.L. Beard, Evidence from hafnium isotopes for ancient sub-oceanic mantle beneath the Rio Grande rift, Nature 362 (1993) 441-444.

[52] W.D. Steward, Late Proterozoic to Early Tertiary stratigraphy of Somerset Island and northern Boothia Peninsula, District of Franklin, Geological Survey of Canada, Paper 83-26 (1987) pp. 78.

Figure captions

Figure 5-1: Geological map of Somerset Island (after [52]) showing kimberlite locations. The mantle xenoliths from this study were collected from the Nikos kimberlite (black diamond). Legend: light gray, Paleozoic cover rocks; striped, Late Proterozoic cover rocks; dark gray, Precambrian basement; bold lines, normal faults.

Figure 5-2: (a) $^{176}Lu/^{177}Hf$ versus initial $\varepsilon_{Hf(T)}$ (100 Ma ago) for the Nikos kimberlite. Also shown are two samples that most likely experienced contamination by xenocrystic garnet (for further explanation see text). Data for South African "Group I" (90-110 Ma) and "Group II" (120-150 Ma) kimberlites are shown for comparison [43]. (b) $^{176}Lu/^{177}Hf$ versus $\varepsilon_{Hf(0.1Ga)}$ for Nikos peridotites at the time of kimberlite emplacement. For samples with duplicate analyses, the average composition is plotted.

Figure 5-3: $^{176}Lu/^{177}Hf$ versus $^{176}Hf/^{177}Hf$ diagram for Nikos peridotites. 2.8 Ga (billion years) Lu-Hf reference isochron is plotted, which corresponds to the regression line for data (and corresponding initial $^{176}Hf/^{177}Hf$) for the low-temperature peridotites (solid diamonds). See text for further details.

Figure 5-4: $^{176}Lu/^{177}Hf$ versus $^{176}Hf/^{177}Hf$ diagram for Nikos garnets and peridotites. Tie lines connect garnet with corresponding whole rock composition. Also shown are the "dates" (in million years) obtained for individual internal Lu-Hf isochrons using garnet-whole-rock pairs.

Figure 5-5: Hf-Nd variation diagram for Nikos peridotites at the time of kimberlite emplacement (Nd data from [36]). The Hf-Nd array for terrestrial samples

[44] and the composition of "depleted" mantle are plotted for comparison [8,40,46].

Figure 5-6: Lu (ppm) versus Al_2O_3 contents (wt%) for Nikos peridotites (Al_2O_3 data from [35]).

Figure 5-7: $\varepsilon_{Hf(0.1Ga)}$ versus $^{87}Sr/^{86}Sr_{(0.1Ga)}$ for Nikos peridotites (Sr data from [36]).

Figure 5-8: Lu-Hf and Sm-Nd internal isochron "dates" versus temperature (and depth) of last equilibration for low-temperature garnet-whole rock pairs (Sm-Nd data from [36]).

Table 5-1. Lu-Hf isotope data for Nikos peridotites and kimberlite.

Sample	Temp. °C	Press. kb	Lu ppm	Hf ppm	^{176}Lu/^{177}Hf	^{176}Hf/^{177}Hf measured	^{176}Hf/^{177}Hf$_{(0.1Ga)}$	ε_{Hf}	$\varepsilon_{Hf(0.1Ga)}$
Low-temperature peridotites									
NK1-4	871	33.5	0.0227	0.0768	0.0422	0.283900 ±20	0.283821	39.9	39.3
NK1-4 Dup.			0.0289	0.0923	0.0446	0.284072 ±20	0.283988	46.0	45.2
NK2-3	887	34.6	0.0371	0.1389	0.0381	0.283566 ±23	0.283495	28.1	27.8
NK1-23	964	39.0	0.0349	0.1722	0.0289	0.283344 ±30	0.283290	20.2	20.5
NK1-23 Dup.				0.1905		0.283342 ±28		20.2	
NK1-14	1027	42.7	0.0198	0.0589	0.0480	0.284280 ±28	0.284190	53.3	52.3
NK1-14 Dup.			0.0209	0.0658	0.0452	0.284152 ±26	0.284068	48.8	48.0
NK1-2	1042	44.7	0.0160	0.0720	0.0316	0.283662 ±33	0.283603	31.5	31.6
NK1-2 Dup.			0.0167	0.0694	0.0343	0.283885 ±19	0.283820	39.3	39.3
NK1-3	1076	46.5	0.0182	0.0966	0.0269	0.283014 ±14	0.282963	8.5	9.0
NK1-3 Dup.				0.0905		0.282989 ±14		7.7	
NK2-9[a]	808		0.0028	0.0142	0.0284	0.283180 ±58	0.283127	14.4	14.7
High-temperature peridotites									
NK1-6	1149	48.8	0.0080	0.0718	0.0159	0.283164 ±16	0.283134	13.9	15.0
NK2-1	1216	51.5	0.0074	0.1080	0.0097	0.282884 ±30	0.282866	4.0	5.5
NK1-9	1219	53.4	0.0173	0.1624	0.0152	0.282834 ±07	0.282805	2.2	3.4
NK1-19	1228	51.9	0.0064	0.0588	0.0155	0.283012 ±13	0.282983	8.5	9.7
NK1-19 Dup.			0.0058	0.0589	0.0141	0.283139 ±15	0.283113	13.0	14.3
NK3-25	1256	54.0	0.0281	0.3038	0.0132	0.282679 ±51	0.282654	-3.3	-2.0
NK1-5	1262	54.6	0.0177	0.2091	0.0121	0.282805 ±14	0.282782	1.2	2.6
NK1-7[b]	1300	55.1	0.0164	0.0669	0.0349	0.283364 ±15	0.283298	20.9	20.8
NK1-7 Dup.			0.0187	0.0798	0.0334	0.283389 ±16	0.283326	21.8	21.8
NK2-2	1316	54.7	0.0220	0.1637	0.0191	0.283248 ±24	0.283212	16.8	17.8
NK1-10	1405	63.7	0.0043	0.1682	0.0037	0.282874 ±20	0.282867	3.6	5.6
Kimberlite									
NK3-K1			0.0751	2.973	0.0036	0.283197 ±25	0.283191	15.0	17.0
NK3-K2			0.0730	2.648	0.0039	0.283314 ±39	0.283307	19.2	21.1
NK3-K3			0.0899	3.751	0.0034	0.282858 ±13	0.282852	3.1	5.0
NK3-K4			0.0574	2.821	0.0029	0.282716 ±37	0.282711	-2.0	0

[a] spinel peridotite; [b] porphyroclastic texture. $\varepsilon_{Hf(0.1Ga)}$ values calculated for 100 Ma in-situ decay using present day ratios of ^{176}Hf/^{177}Hf$_{(CHUR)}$=0.282772 and ^{176}Lu/^{177}Hf$_{(CHUR)}$=0.0332 [40] and λ=1.876x10^{-11} yr^{-1} [19,20]. Precision for individual Hf isotope measurements is quoted at the 2σ level. Lu and Hf concentrations were determined by isotope dilution analysis; uncertainties for ^{176}Lu/^{177}Hf are ~2%.

Table 5-2. Lu-Hf isotope data for Nikos garnets.

Sample	Temp. °C	Press. kb	Lu ppm	Hf ppm	^{176}Lu/^{177}Hf	^{176}Hf/^{177}Hf measured	^{176}Hf/^{177}Hf$_{(0.1Ga)}$	ε_{Hf}	$\varepsilon_{Hf(0.1Ga)}$	Date Ma
Low-temperature garnets										
NK1-4 Gt	871	33.5	0.2742	0.1609	0.2430	0.287403 ±59	0.286947	164	150	905
NK2-3 Gt	887	34.6	0.2812	0.2262	0.1774	0.285589 ±15	0.285256	99.6	90.1	769
NK2-10 Gt	1014	42.1	0.2636	0.4060	0.0926	0.283270 ±37	0.283096	17.6	13.7	499
NK1-14 Gt	1027	42.7	0.2741	0.2238	0.1747	0.285419 ±13	0.285091	93.6	84.2	
NK1-2 Gt	1042	44.7	0.3667	0.3479	0.1503	0.284465 ±18	0.284183	59.9	52.1	313
NK1-3 Gt	1076	46.5	0.3255	0.4952	0.0937	0.283309 ±11	0.283133	19.0	15.0	235
High-temperature garnets										
NK2-1 Gt	1216	51.5	0.1670	1.549	0.0154	0.282778 ±08	0.282749	0.2	1.4	
NK1-9 Gt	1219	53.4	0.2516	1.064	0.0337	0.282831 ±09	0.282768	2.1	2.1	
NK1-5 Gt	1262	54.6	0.2148	1.229	0.0249	0.282873 ±07	0.282826	3.6	4.1	
NK3-16 Gt	1280	53.5	0.3539	1.024	0.0493	0.282993 ±15	0.282900	7.8	6.7	
NK1-7 Gt	1300	55.1	0.2442	0.6252	0.0557	0.283512 ±13	0.283407	26.2	24.7	326
NK1-7 Gt Dup.			0.2411	0.6117	0.0562	0.283509 ±71	0.283403	26.1	24.5	
NK2-2 Gt	1316	54.7	0.2666	0.8145	0.0467	0.283165 ±74	0.283078	13.9	13.0	
NK3-4 Gt	1371	58.5	0.2702	0.6780	0.0568	0.283508 ±22	0.283401	26.0	24.5	

Analytical procedures as in Table 5-1. Date refers to internal isochron “age” using garnet-whole rock pairs.

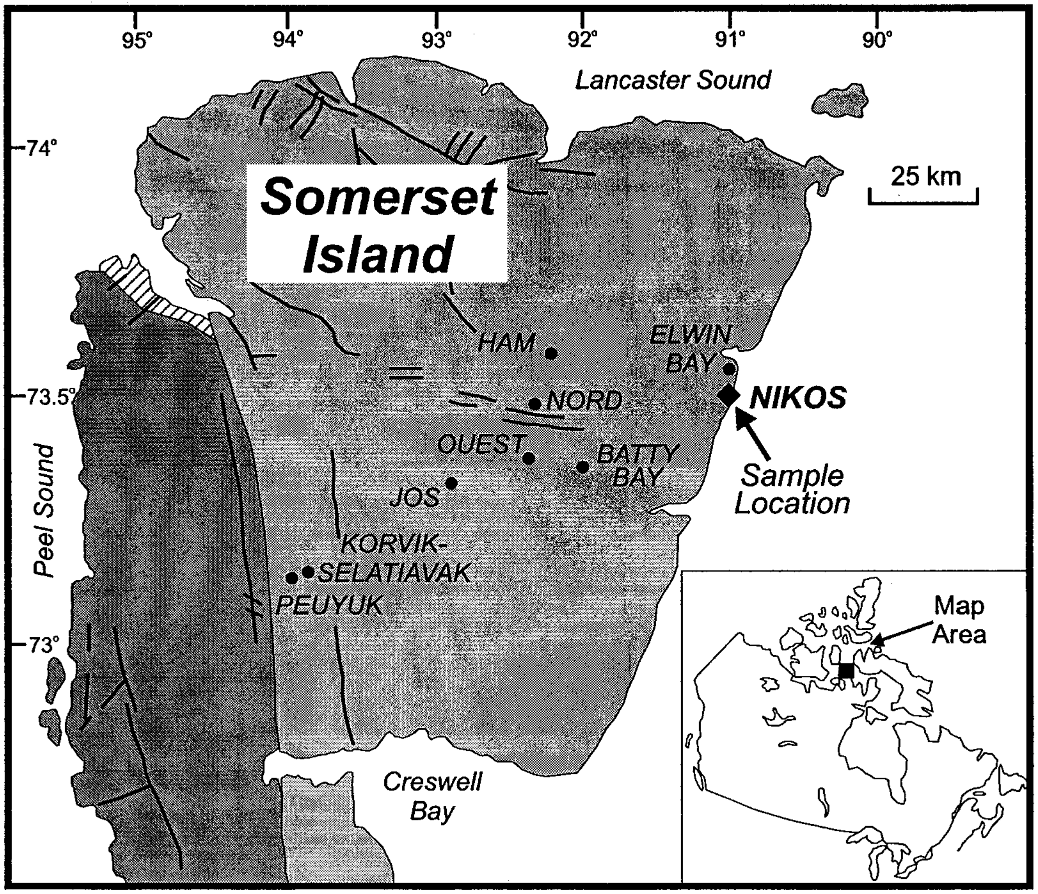
95°
94°
93°
92°
91°
90°
Lancaster Sound
-74°
25 km
Somerset Island
HAM
ELWIN BAY
-73.5°
NORD
NIKOS
OUEST
BATTY BAY
JOS
Sample Location
Peel Sound
KORVIK-SELATIAVAK
PEUYUK
-73°
Map Area
Creswell Bay

Figure 5-1

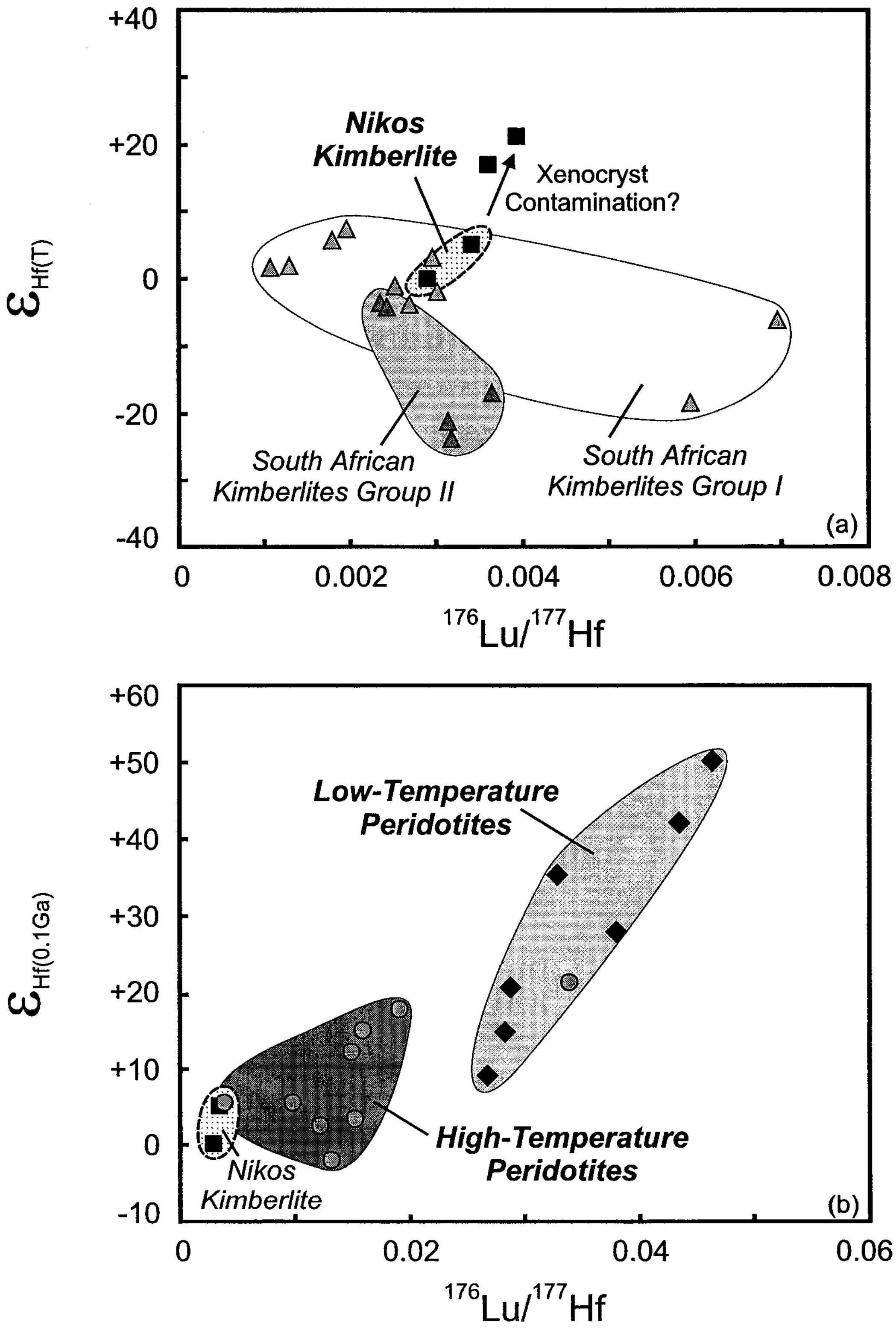
+40
+20
0
-20
-40
$\varepsilon_{Hf(T)}$
Nikos Kimberlite
Xenocryst Contamination?
South African Kimberlites Group II
South African Kimberlites Group I
(a)
0
0.002
0.004
0.006
0.008
$^{176}Lu/^{177}Hf$
+60
+50
+40
+30
+20
+10
0
-10
$\varepsilon_{Hf(0.1Ga)}$
Low-Temperature Peridotites
High-Temperature Peridotites
Nikos Kimberlite
(b)
0
0.02
0.04
0.06
$^{176}Lu/^{177}Hf$

Figure 5-2

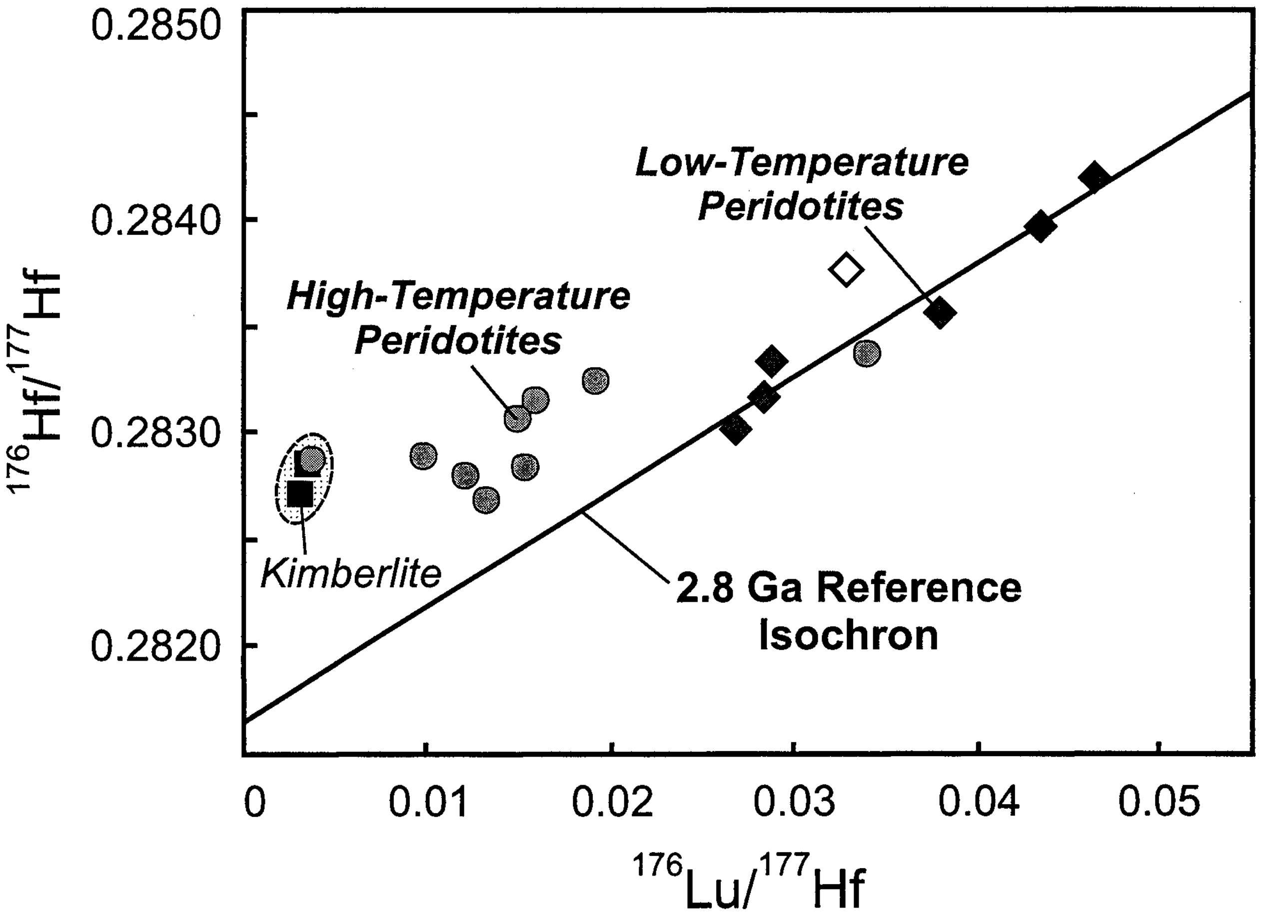
0.2850
0.2840
0.2830
0.2820
^{176}Hf/^{177}Hf
0
0.01
0.02
0.03
0.04
0.05
^{176}Lu/^{177}Hf
Low-Temperature Peridotites
High-Temperature Peridotites
Kimberlite
2.8 Ga Reference Isochron

Figure 5-3

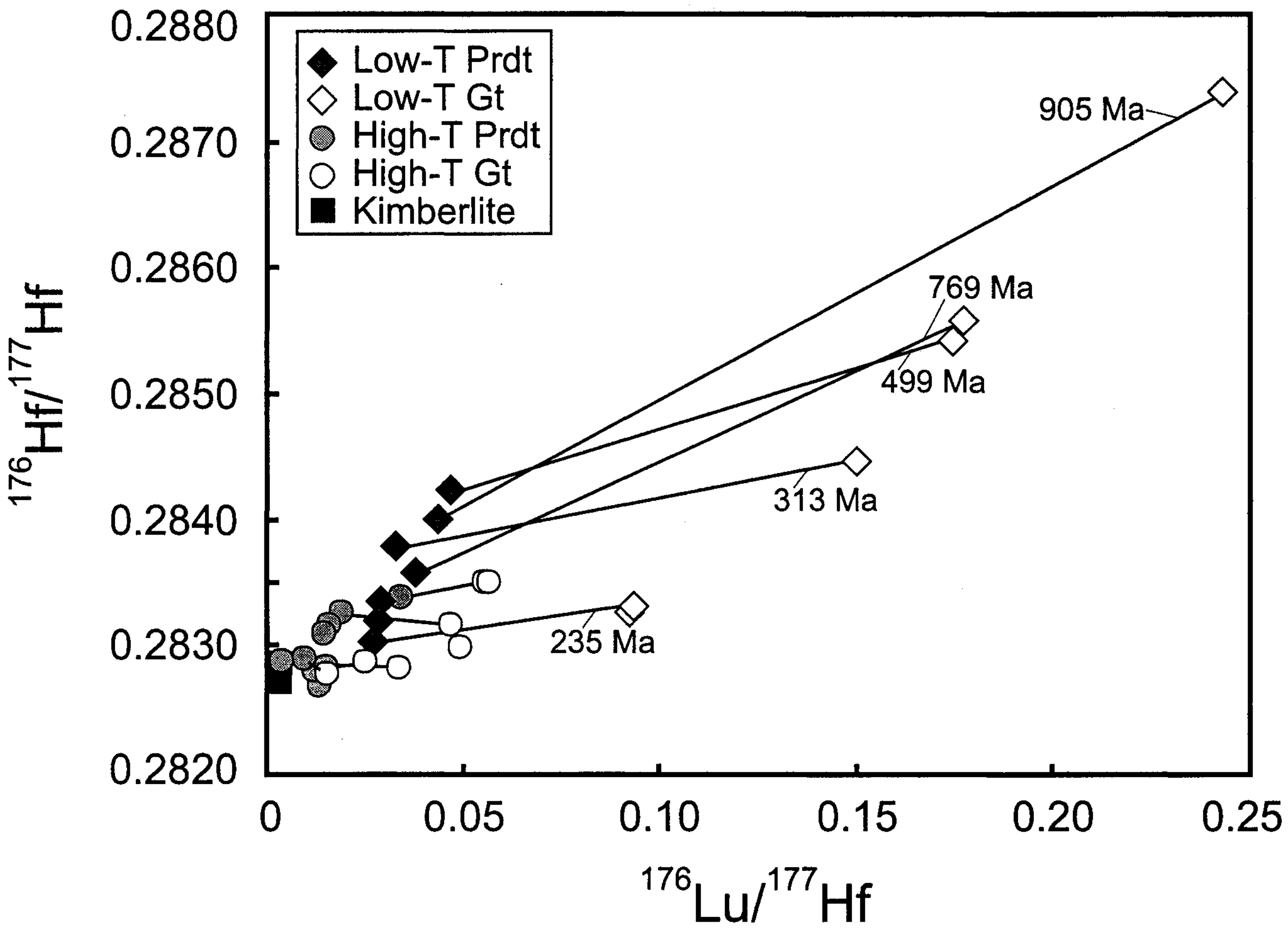

0.2880
0.2870
0.2860
0.2850
0.2840
0.2830
0.2820
$^{176}Hf/^{177}Hf$
0
0.05
0.10
0.15
0.20
0.25
$^{176}Lu/^{177}Hf$
◆ Low-T Prdt
◇ Low-T Gt
● High-T Prdt
○ High-T Gt
■ Kimberlite
905 Ma
769 Ma
499 Ma
313 Ma
235 Ma

Figure 5-4

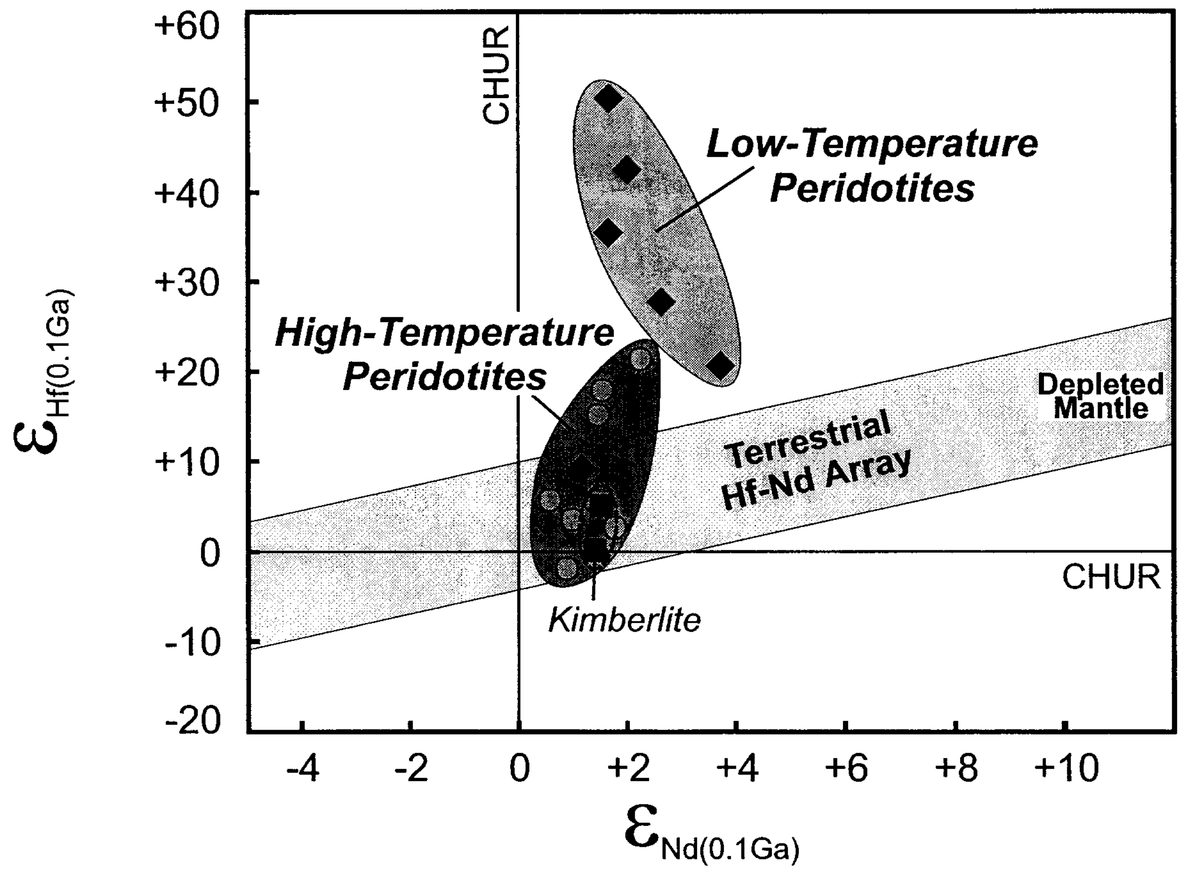

+60
+50
+40
+30
+20
+10
0
-10
-20
$\varepsilon_{Hf(0.1Ga)}$
CHUR
Low-Temperature Peridotites
High-Temperature Peridotites
Depleted Mantle
Terrestrial Hf-Nd Array
CHUR
Kimberlite
-4
-2
0
+2
+4
+6
+8
+10
$\varepsilon_{Nd(0.1Ga)}$

Figure 5-5

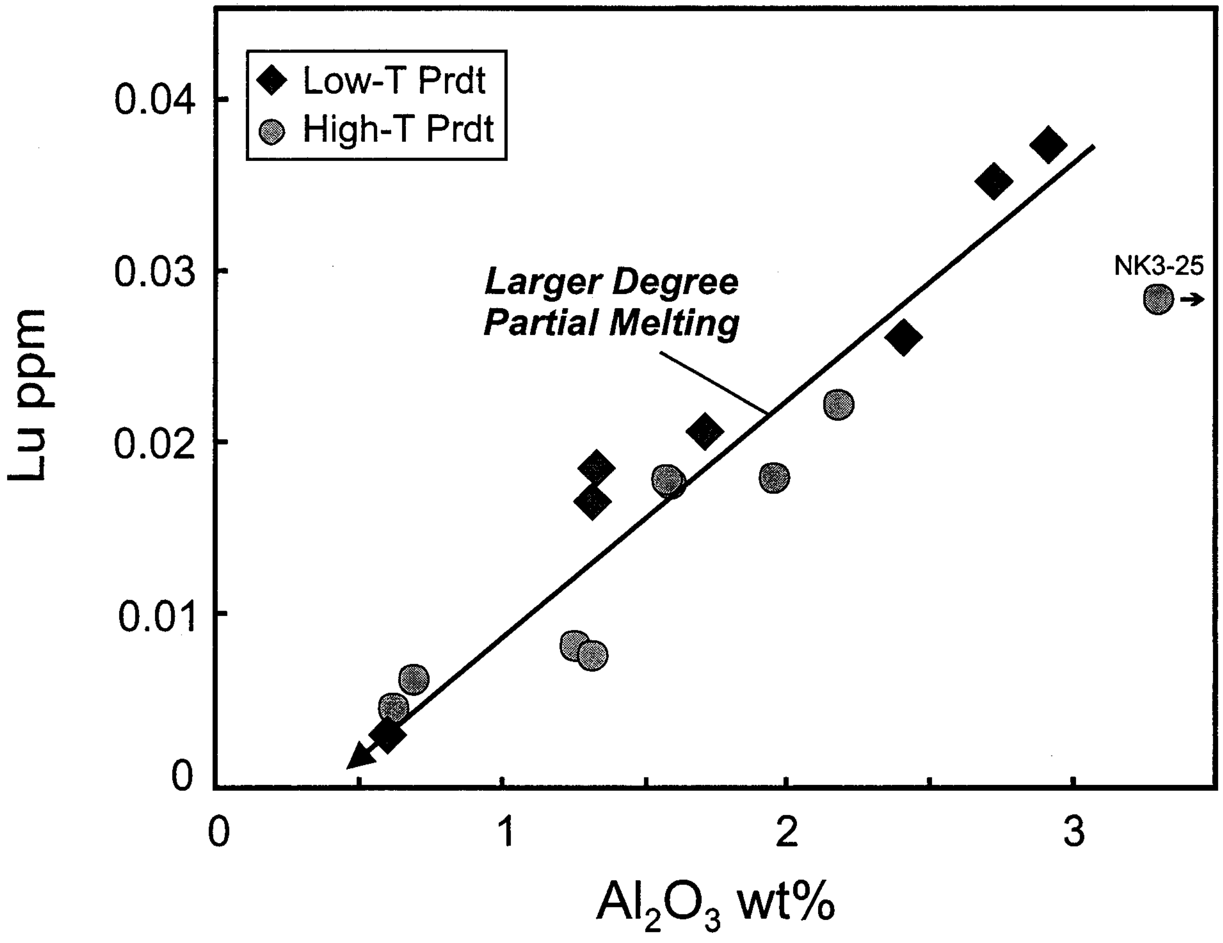
◆ Low-T Prdt
● High-T Prdt
Lu ppm
0.04
0.03
0.02
0.01
0
0
1
2
3
Al_2O_3 wt%
Larger Degree Partial Melting
NK3-25

Figure 5-6

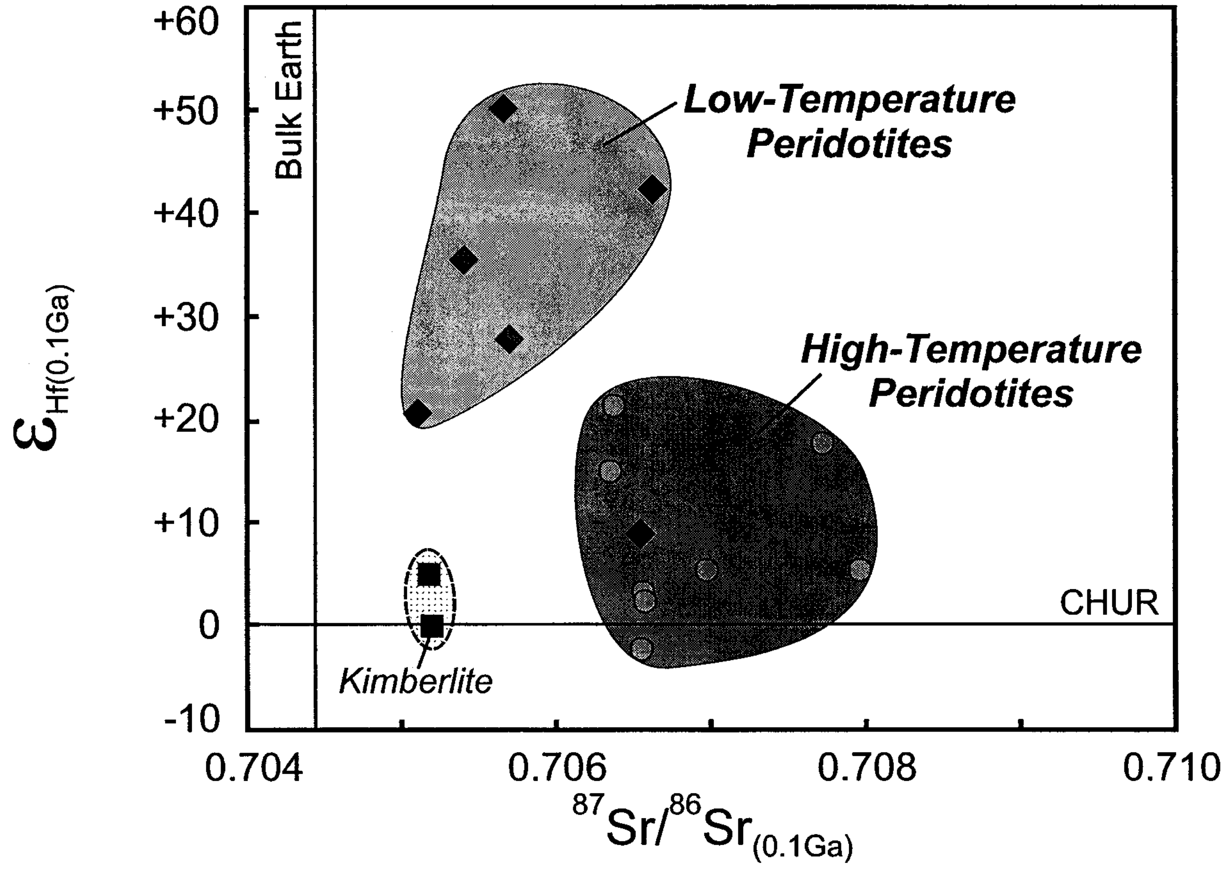

+60
+50
+40
+30
+20
+10
0
-10
$\varepsilon_{Hf(0.1Ga)}$
Bulk Earth
Low-Temperature Peridotites
High-Temperature Peridotites
CHUR
Kimberlite
0.704
0.706
0.708
0.710
$^{87}Sr/^{86}Sr_{(0.1Ga)}$

Figure 5-7

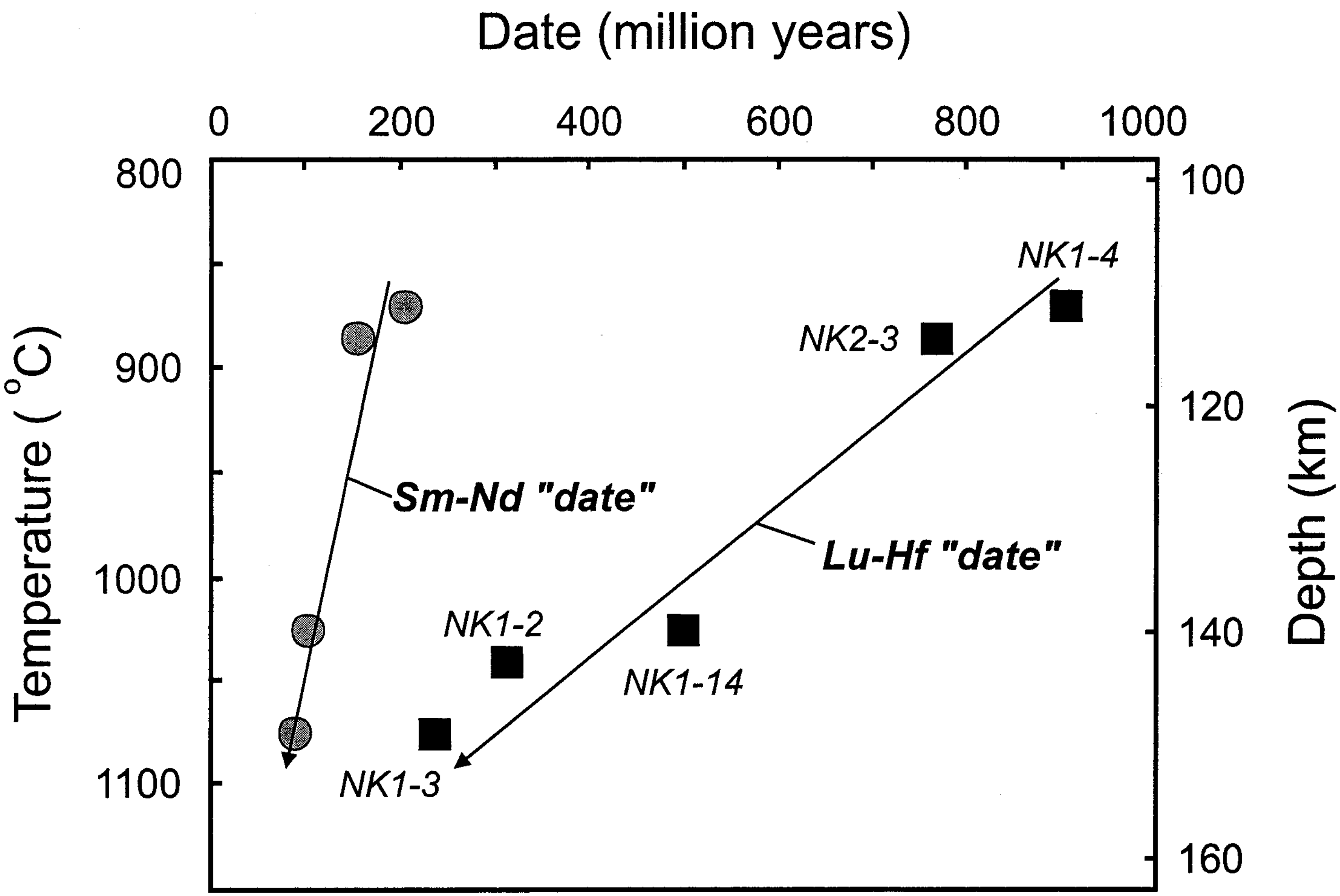
Date (million years)
0
200
400
600
800
1000
Temperature (°C)
800
900
1000
1100
Depth (km)
100
120
140
160
Sm-Nd "date"
Lu-Hf "date"
NK1-4
NK2-3
NK1-2
NK1-14
NK1-3

Figure 5-8

CHAPTER 6

GENERAL CONCLUSIONS

The subcratonic lithosphere beneath Somerset Island sampled by the Nikos kimberlite consists of refractory peridotites with minor occurrences of pyroxenites. The olivine-rich (avg. 80 wt.%) mineralogy and depleted major element compositions (e.g. Fe, Al, Ca) of the Nikos peridotites indicate formation and stabilization of the mantle root beneath the northern Canadian craton as the result of extensive melt extraction. The high abundances of large ion lithophile elements (LILE) and light rare earth elements (LREE) observed for the xenoliths provide evidence that these melt-depleted residues experienced metasomatism during residence in the mantle and/or sample transport. Nd isotopic compositions of the peridotites overlap those of the Nikos kimberlites and appear to reflect sample contamination with small amounts of kimberlite magma. These results indicate that metasomatic processes play an important role in modifying the chemical composition of the subcratonic lithospheric mantle.

The shallow low-temperature (<1100°C) and the deep-seated high-temperature (>1100°C) Nikos peridotites and their constituent clinopyroxene and garnet are characterized by distinct Sr, Pb and Hf isotopic compositions, which is in agreement with their differences in the abundances of trace and rare earth elements (REE). This provides evidence for a chemical and isotopic depth stratification of the Somerset lithosphere indicating that the shallow and deep subcontinental mantle do not share a common petrogenetic history. These results suggest a multi-stage evolution for the mantle root beneath the northern Canadian craton and the involvement of distinct magmatic processes.

The Lu-Hf isotope systematics for the shallow low-temperature peridotites plot along a 2.8 Ga reference isochron. A number of these xenoliths are characterized by highly radiogenic Hf isotopic compositions suggestive of billions of years of radiogenic ingrowth. These findings are consistent with an interpretation that the shallow Somerset lithosphere stabilized in the Archean to depth of ~150 km. The data indicate that part of the Canadian mantle root is characterized by a more radiogenic Hf isotope signature than that estimated for a typical "depleted" mantle. The majority of the high-temperature peridotites are probably younger and they could have been added to the shallow lithosphere by downward growth of the Archean mantle root. To date, the results presented in this thesis are the first Lu-Hf isotope data that have been reported for the subcontinental lithosphere. Comparing the Lu-Hf isotope results obtained for the Canadian mantle to those for other cratonic roots such as beneath South Africa, Siberia and North America would enable to obtain a better understanding of the origin and geochemical evolution of subcontinental lithosphere, which is an important reservoir in the Hf isotope budget of the Earth's mantle.

Dating peridotite sulfides using the Re-Os isotope technique, which appears to be little susceptible to metasomatic effects, can provide constraints on the stabilization age of the lithosphere. Investigating the Re-Os systematics of the Nikos peridotites and their accessory sulfides would offer the advantage of an integrated Hf, Os, Sr, Nd and Pb isotope study on a single peridotite xenolith suite. A combined Lu-Hf and Re-Os isotope investigation would for the first time enable a comparison of data obtained using silicate-hosted (Lu-Hf) and sulfide-hosted (Re-Os) elements, and help constrain the stabilization history of the Canadian mantle root.

APPENDIX A

^{180}Hf isotope tracer calibration

Isotope dilution analysis is used for accurate concentration determinations of an element by mass spectrometry (Moore et al., 1973; Faure, 1986). In this technique an isotope tracer ("spike") solution that is artificially enriched in one isotope of a particular element and of a precisely known concentration is added to a sample, the latter having a natural isotopic composition but unknown concentration of the element. The isotopic composition of the mixture can then be used to calculate the concentration of the element in question for the sample. The accuracy of the isotope dilution method depends on the accurate calibration of the isotope tracer solution, i.e. its isotopic composition and concentration have to be determined precisely and verified separately.

In order to obtain high-precision Hf concentration determinations, this study involved the calibration of a ^{180}Hf tracer (~98.2%) using the Micromass IsoProbe multicollector inductively coupled plasma mass spectrometer (MC-ICP-MS). The isotopic composition of the ^{180}Hf isotope tracer was determined by repeated measurements of a ~100 ppb spike solution in static, multicollection mode (Table A-1). As there are no certified values for the isotope ratios in the ^{180}Hf tracer, which may be used as a monitor for instrument-induced mass bias, a 50 ppb solution of the Hf standard JMC 475 was measured repeatedly prior to the spike analysis. The measured Hf isotopic ratios of the ^{180}Hf tracer were corrected using the mass discrimination coefficient based on the standard analyses and using the exponential law (Russell et al., 1978), which is expressed as follows:

$$R_{true} = R_{measured}(M_2/M_1)^f$$

where R is the ratio of the ion beams at masses M_2 and M_1 and f is the mass discrimination coefficient. The isotopic composition indicates a ^{180}Hf enrichment of 98.26% for the isotope tracer (Table A-1).

The ^{180}Hf tracer was diluted to an approximate concentration of 30 ppb from the stock solution (4000 ppm), and this was verified by isotope dilution against a solution of the JMC 475 Hf standard (~100 ppb). The concentration of the Hf standard was determined gravimetrically using a buoyancy correction calculation (Table A-1). A number of standard-Hf tracer mixtures with different ^{180}Hf proportions (mole fractions 0.95:0.05 to 0.05:0.95; n=6; Table A-1) were prepared and analyzed for their isotopic compositions by MC-ICP-MS. The Hf concentration of the ^{180}Hf tracer solution added to each mixture of Hf tracer (S) and standard (N) can be determined as follows (after Faure, 1986):

$$C_S = (C_N * W_S / W_N * wt_N/wt_S) / ((Ab180_S - R*Ab177_S)/(R*Ab177_N - Ab180_N))$$

where C_S and C_N are the Hf concentrations, W the atomic weights, wt the weights of the element, Ab the isotopic abundances of spike and standard, respectively. R is the fractionation corrected ^{180}Hf/^{177}Hf ratio of the mixture. The calculated concentrations of the ^{180}Hf tracer added to the individual mixtures yield an average value for ^{180}Hf of 30.436±0.070 ppb and total Hf content of 30.974±0.072 ppb (1SD; Table A-1). The total number of moles/g of ^{180}Hf in these mixtures when plotted versus their corresponding isotopic compositions fall on a mixing line (R^2 = 0.999) between the two endmembers compositions ^{180}Hf tracer and Hf standard JMC 475 (Table A-1; Fig. A-1).

References

Faure G. (1986) *Principles of isotope geology*. John Wiley & Sons, New York. pp. 589.

Moore L. J., Moody J. R., Barnes I. L., Gramich J. W., Murphy T. J., Paulsen P. J. and Shields W. R. (1973) Trace determination of rubidium and strontium in silicate glass standard reference materials. *Anal. Chem.* **45**, 2384-2387.

Russell W. A., Papanastassiou D. A. and Tombrello T. A. (1978) Ca isotope fractionation on the Earth and other solar system materials. *Geochim. Cosmochim. Acta* **42**, 1075-1090.

Table A-1. Hf isotope tracer calibration - parameters and calculations

^{180}Hf tracer and standard isotopic compositions

	^{174}Hf/^{177}Hf	^{176}Hf/^{177}Hf		^{178}Hf/^{177}Hf	^{179}Hf/^{177}Hf	^{180}Hf/^{177}Hf	# anal
Standard JMC 475	0.00867	0.282153		1.46731	0.7325	1.88677	12
^{180}Hf tracer	0.00859	0.241646		2.67303	2.85041	383.417	5

Abundance	^{174}Hf	^{176}Hf	^{177}Hf	^{178}Hf	^{179}Hf	^{180}Hf	atomic mass
Standard JMC 475	0.0016	0.0525	0.1860	0.2729	0.1362	0.3509	178.485
^{180}Hf tracer	0.00002	0.0006	0.0026	0.0069	0.0073	0.9826	179.915

Mixture standard-^{180}Hf tracer isotopic compositions

	mole fraction ^{180}Hf	^{176}Hf/^{177}Hf	^{178}Hf/^{177}Hf	^{179}Hf/^{177}Hf	^{180}Hf/^{177}Hf
Mixture1	0.95:0.05	0.282129	1.46747	0.732944	1.98409
Mixture1 Dup	0.95:0.05	0.282134	1.46749	0.733032	1.98421
Mixture2	0.60:0.40	0.282009	1.47132	0.739595	3.16882
Mixture2 Dup	0.60:0.40	0.281993	1.47138	0.739687	3.16892
Mixture3	0.40:0.60	0.281839	1.47609	0.748093	4.68133
Mixture3 Dup	0.40:0.60	0.281845	1.47610	0.748091	4.68147
Mixture4	0.20:0.80	0.281381	1.49054	0.773212	9.23102
Mixture4 Dup	0.20:0.80	0.281302	1.49051	0.773374	9.23189
Mixture5	0.10:0.90	0.280358	1.51845	0.822726	18.0688
Mixture5 Dup	0.10:0.90	0.280170	1.51803	0.822235	18.0654
Mixture6	0.05:0.95	0.278548	1.57078	0.914750	34.6600
Mixture6 Dup	0.05:0.95	0.278432	1.57020	0.914205	34.6429

Table A-1. Continued.

Isotope dilution calculation after Faure (1986)

Standard JMC 475 used for ^{180}Hf tracer calibration
Concentration calculation with buoyancy correction

	Weight (g)	Hf (ng)	Volume (ml)	Concentration (ppb)	(moles/g)
Standard stock solution	0.1711	101086		590801	
HNO_3 added	1000.92				
Standard dilution	1001.09		992.07		
Displaced air	1.2004				
Standard dilution buoyancy corrected	1002.29			100.855	1.98×10^{-10}

Mixture Standard-^{180}Hf tracer	^{180}Hf/^{177}Hf Average	Weight Standard (g)	^{180}Hf tracer (g)	Standard Hf total (ng)	^{180}Hf (ng)	^{180}Hf tracer Hf total (ng)	^{180}Hf (ng)	Hf total (ppb)	^{180}Hf (ppb)	Mixture ^{180}Hf (moles/g)
Mixture1	1.98415	5.05257	0.30733	509.575	178.795	9.515	9.350	30.961	30.424	1.95×10^{-10}
Mixture2	3.16887	1.95142	1.57410	196.810	69.055	48.537	47.694	30.835	30.299	1.84×10^{-10}
Mixture3	4.68140	1.00579	1.76298	101.439	35.592	54.747	53.797	31.054	30.515	1.79×10^{-10}
Mixture4	9.23145	1.00457	4.69620	101.316	35.549	145.456	142.931	30.973	30.435	1.74×10^{-10}
Mixture5	18.0671	0.50233	5.28655	50.662	17.776	164.109	161.260	31.043	30.504	1.72×10^{-10}
Mixture6	34.6514	0.24959	5.58345	25.172	8.832	172.968	169.965	30.979	30.441	1.70×10^{-10}
Average ^{180}Hf tracer								30.974	30.436	1.69×10^{-10}
Std deviation (1SD)								0.072	0.070	
Std error (%)								0.094	0.094	

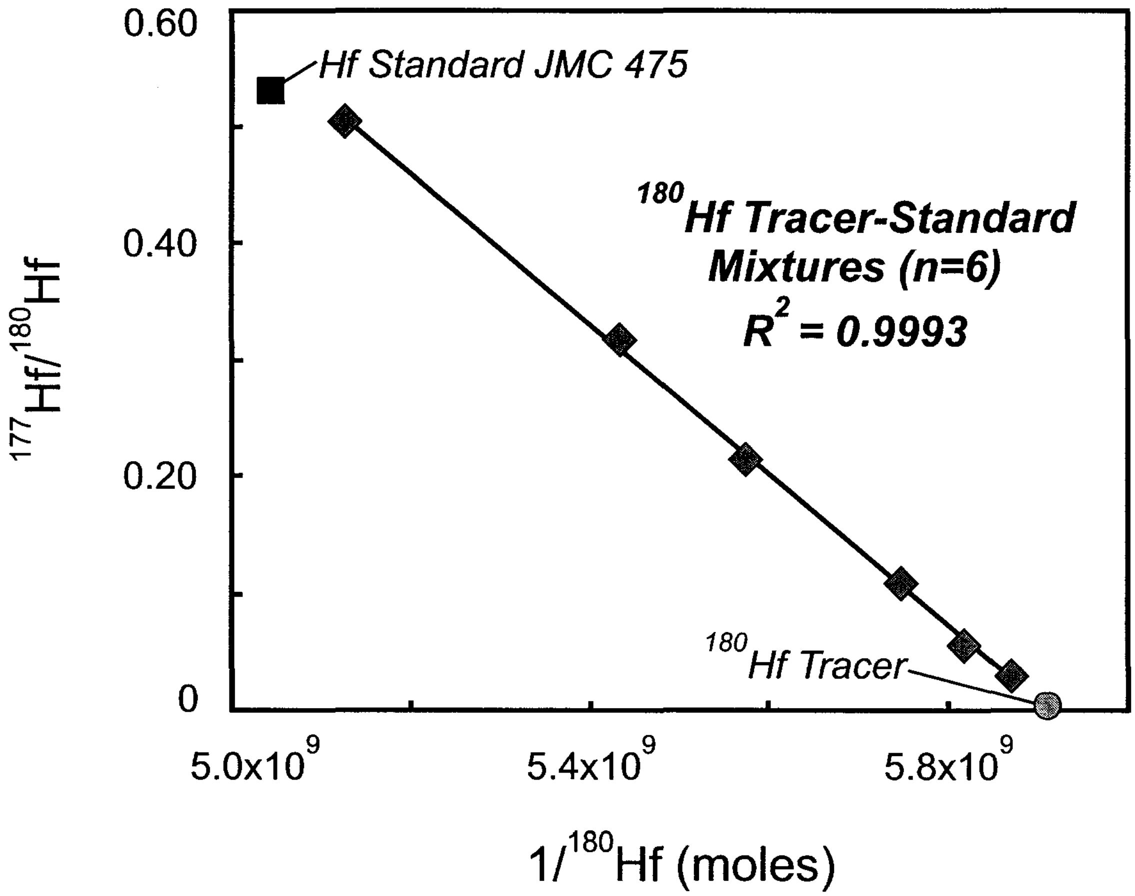
0.60
0.40
0.20
0
^{177}Hf/^{180}Hf
5.0x10^9
5.4x10^9
5.8x10^9
1/^{180}Hf (moles)
Hf Standard JMC 475
^{180}Hf Tracer-Standard Mixtures (n=6)
R^2 = 0.9993
^{180}Hf Tracer

Figure A-1

APPENDIX B

Table B-1. Major element analyses and calculated mineral modes for Nikos peridotites.

Sample	NK1-1	NK1-2	NK1-3	NK1-4	NK1-5	NK1-6	NK1-7	NK1-8	NK1-9	NK1-10	NK1-11	NK1-12	NK1-13	NK1-14
Rock	Prdt	Prdt	Prdt	Prdt	Prdt	Prdt	Prdt	Prdt	Prdt	Prdt	Prdt	Prdt	Prdt	Prdt
Texture	coarse	coarse	coarse	coarse	coarse	coarse	porphcl	coarse	coarse	coarse	coarse	coarse	coarse	coarse
SiO_2	41.25	41.77	40.81	41.60	42.28	40.37	41.24	43.34	41.88	41.09	42.60	40.80	42.20	42.02
TiO_2	0.07	0.03	0.03	0.06	0.07	0.02	0.03	0.03	0.04	0.02	0.05	0.03	0	0.03
Al_2O_3	1.00	1.31	1.33	2.43	1.95	1.25	1.57	1.01	1.59	0.62	0.49	0.56	0.20	1.71
FeO	7.49	7.39	7.42	7.09	7.74	7.10	7.06	6.89	7.29	6.93	7.21	7.76	6.90	7.27
MnO	0.11	0.11	0.11	0.13	0.12	0.10	0.10	0.10	0.11	0.10	0.10	0.11	0.10	0.11
MgO	43.30	44.44	44.03	40.90	41.49	43.41	43.55	44.37	43.48	44.81	45.17	45.32	44.60	42.92
CaO	0.58	1.11	0.82	1.20	1.44	0.41	0.72	0.49	0.96	0.20	0.40	0.57	0.30	1.13
Na_2O	0.02	0.10	0.01	0.01	0.06	0	0	0.08	0.03	0.08	0	0.12	0	0.15
K_2O	0.04	0.03	0.04	0.07	0.08	0.03	0.02	0.04	0.04	0.03	0.08	0.16	0.10	0.03
P_2O_5	0.01	0.02	0.02	0.01	0.01	0.01	0	0.01	0.01	0.01	0.02	0.03	0	0.02
Cr_2O_3	0.46	0.35	0.41	0.75	0.58	0.47	0.48	0.43	0.52	0.44	0.35	0.34	0.30	0.44
NiO	0.33	0.32	0.33	0.40	0.30	0.33	0.31	0.34	0.32	0.35	0.35	0.37	0.40	0.31
LOI	5.07	2.71	3.89	4.76	3.50	5.85	4.31	2.43	3.59	4.68	2.52	3.46	4.70	3.49
Total	99.73	99.69	99.25	99.41	99.62	99.35	99.37	99.56	99.87	99.36	99.33	99.63	99.80	99.63
mg-no.	0.912	0.915	0.914	0.911	0.905	0.916	0.917	0.920	0.914	0.920	0.918	0.912	0.921	0.913
Calculated modes in wt%														
Olivine	79	82	83	67	72	81	79	75	78	83	80	89	75	77
Opx	15	8	9	22	14	12	13	20	13	13	17	6	22	12
Cpx	1	4	2	5	5	1	1	1	2	1	1	4	2	4
Garnet	5	6	7	6	9	7	8	5	8	3	3	2		7
Spinel													1	
Temperatures and pressures														
Temp (ºC)	1222	1042	1076	871	1262	1149	1300	1409	1219	1405	1301	1054	n.a.	1027
Press (kb)	52.7	44.7	46.5	33.5	54.6	48.4	55.1	63.6	53.4	63.7	57.1	45.3	n.a.	42.7

Prdt: peridotite; H-Prxn: High-Mg pyroxenite; L-Prxn: Low-Mg pyroxenite; Opx: orthopyroxene; Cpx: clinopyroxene; porphcl: porphyroclastic. Major elements in wt%. Total Fe is given as FeO and mg-no.=Mg/(Mg+Fe). LOI: loss on ignition. For analytical techniques see Chapter 2. Mode calculation procedures and temperature and pressure calculations are discussed in Chapter 2.

Table B-1. Continued.

Sample	NK1-15	NK1-16	NK1-17	NK1-18	NK1-19	NK1-20	NK1-21	NK1-22	NK1-23	NK2-1	NK2-2	NK2-3	NK2-5	NK2-6
Rock	Prdt	Prdt	Prdt	Prdt	Prdt	Prdt	Prdt	Prdt	Prdt	Prdt	Prdt	Prdt	Prdt	Prdt
Texture	coarse	coarse	coarse	coarse	coarse	coarse	coarse	coarse	coarse	coarse	porphcl	coarse	porphcl	porphcl
SiO_2	42.29	41.17	41.22	42.94	43.60	42.34	41.44	39.97	41.01	45.66	42.69	42.46	43.22	41.50
TiO_2	0.06	0.03	0.01	0.03	0.06	0.06	0.02	0.02	0.10	0.09	0.08	0.09	0.15	0.10
Al_2O_3	1.09	0.93	0.81	0.79	0.69	0.70	0.81	0.93	2.71	1.31	2.17	2.90	1.06	0.30
FeO	7.30	7.27	7.05	6.97	7.17	7.02	6.98	7.24	7.81	7.08	7.69	7.21	8.07	7.70
MnO	0.11	0.10	0.11	0.10	0.11	0.10	0.10	0.10	0.12	0.12	0.12	0.13	0.12	0.10
MgO	42.69	43.95	45.40	44.93	42.78	42.94	44.78	43.01	40.25	42.09	42.80	41.87	44.14	48.20
CaO	0.88	0.67	0.49	0.54	0.70	0.82	0.27	0.91	1.79	0.93	2.21	1.98	1.01	0.30
Na_2O	0.01	0	0.08	0.05	0.08	0.08	0	0.02	0.16	0.40	0.19	0.15	0.04	0.10
K_2O	0.12	0.03	0.03	0.03	0.05	0.06	0.03	0.02	0.10	0.16	0.11	0.19	0.05	0.10
P_2O_5	0.03	0.01	0.03	0.01	0.01	0.02	0.01	0.01	0.02	0.01	0.01	0.02	0.01	0
Cr_2O_3	0.38	0.48	0.47	0.35	0.33	0.30	0.51	0.47	0.41	0.48	0.37	0.71	0.46	0.30
NiO	0.34	0.33	0.31	0.35	0.32	0.30	0.35	0.35	0.29	0.30	0.32	0.31	0.33	0.40
LOI	4.09	4.58	3.88	2.75	3.65	5.00	4.55	6.46	4.68	1.32	1.14	1.77	1.01	0.90
Total	99.39	99.52	99.89	99.84	99.55	99.73	99.82	99.50	99.46	99.94	99.89	99.80	99.67	99.80
mg-no.	0.913	0.915	0.920	0.920	0.914	0.916	0.920	0.914	0.902	0.914	0.908	0.912	0.907	0.918
Calculated modes in wt%														
Olivine	74	81	85	78	70	75	81	83	74	65	77	73	77	90
Opx	18	12	9	17	25	19	14	9	8	27	5	7	16	7
Cpx	3	1	1	1	2	3	0	3	7	5	10	8	3	2
Garnet	5	5	4	4	3	3	5	5	11	3	8	12	5	
Spinel														1
Temperatures and pressures														
Temp (ºC)	1131	n.a.	989	1223	1228	n.a.	n.a.	1265	964	1216	1316	887	1371	n.a.
Press (kb)	48.0	n.a.	40.6	52.1	51.9	n.a.	n.a.	53.5	39.0	51.5	54.7	34.6	57.9	n.a.

Table B-1. Continued.

Sample	NK2-8	NK2-9	NK2-10	NK3-2	NK3-3	NK3-4	NK3-5	NK3-6	NK3-7	NK3-10	NK3-11	NK3-12	NK3-13	NK3-15
Rock	Prdt	Prdt	Prdt	Prdt	Prdt	Prdt	Prdt	Prdt	Prdt	Prdt	Prdt	Prdt	Prdt	Prdt
Texture	coarse	coarse	coarse	fluidal	coarse	coarse	coarse	coarse	coarse	coarse	coarse	coarse	coarse	coarse
SiO_2	43.90	42.00	41.54	41.43	43.20	41.02	42.08	42.09	38.07	39.60	40.88	39.60	39.05	40.83
TiO_2	0	0	0.03	0.04	0	0.11	0.02	0.04	0.12	0.10	0.06	0.10	0.05	0.07
Al_2O_3	1.30	0.60	1.25	1.28	0.60	3.34	0.44	0.99	2.16	1.20	1.10	0.30	1.07	1.39
FeO	7.10	7.30	7.43	6.79	6.90	7.15	6.71	6.51	6.76	7.00	6.99	6.70	6.96	6.47
MnO	0.10	0.10	0.11	0.10	0.10	0.11	0.10	0.09	0.10	0.10	0.10	0.10	0.09	0.09
MgO	43.10	47.10	45.53	40.93	45.60	37.17	43.99	42.72	39.63	42.10	42.70	44.40	40.95	40.67
CaO	0.60	0.20	1.22	1.72	0.40	3.64	0.76	1.00	4.55	1.30	2.80	0.80	2.28	2.82
Na_2O	0	0.10	0.07	0	0.10	0.21	0.03	0.04	0.03	0	0.10	0	0.18	0.04
K_2O	0	0	0.05	0.08	0.10	0.32	0.07	0.08	0.28	0.20	0.05	0	0.07	0.07
P_2O_5	0	0	0.04	0.02	0	0.02	0.01	0.02	0.02	0	0.02	0	0.02	0.02
Cr_2O_3	0.50	0.50	0.36	0.43	0.50	0.43	0.34	0.31	0.45	0.50	0.54	0.30	0.59	0.38
NiO	0.30	0.40	0.32	0.31	0.30	0.28	0.34	0.30	0.31	0.30	0.31	0.30	0.30	0.34
LOI	3.00	1.60	1.84	6.54	2.20	5.57	4.88	5.55	6.75	7.40	3.88	6.70	8.11	6.32
Total	99.80	99.80	99.79	99.64	99.90	99.37	99.77	99.73	99.22	99.80	99.54	99.20	99.71	99.50
mg-no.	0.916	0.920	0.916	0.915	0.922	0.903	0.921	0.921	0.913	0.914	0.916	0.922	0.913	0.918
Calculated modes in wt%														
Olivine	65	84	86	72	75	68	78	74	74	78	82	85	84	75
Opx	31	14	4	15	22	2	17	18	0	14	0	10	0	6
Cpx	3	1	5	6	2	17	3	3	19	7	13	4	12	12
Garnet			6	7		13	2	5	8		5		5	6
Spinel	2	1			1					2		1		
Temperatures and pressures														
Temp (ºC)	n.a.	n.a.	1014	1023	n.a.	1371	1194	1253	1213	n.a.	1247	n.a.	830	1343
Press (kb)	n.a.	n.a.	42.1	34.3	n.a.	59.6	52.4	53.4	51.0	n.a.	53.1	n.a.	30.9	58.5

Table B-1. Continued.

Sample	NK3-16	NK3-18	NK3-20	NK3-22	NK3-24	NK3-25	NK2-7	NK3-14	NK3-1	NK3-8	NK3-17
Rock	Prdt	Prdt	Prdt	Prdt	Prdt	Prdt	H-Prxn	H-Prxn	L-Prxn	L-Prxn	L-Prxn
Texture	coarse	coarse	coarse	porphcl	coarse	coarse	coarse	coarse	coarse	coarse	coarse
SiO_2	40.45	40.60	43.19	42.10	45.04	41.42	48.95	40.72	50.97	50.35	50.15
TiO_2	0.06	0.10	0.10	0	0.03	0.21	0.13	0.23	0.18	3.76	0.18
Al_2O_3	0.93	0.40	3.21	3.30	2.24	4.28	8.05	11.40	4.71	0.81	4.89
FeO	7.93	7.30	7.58	7.60	6.19	7.41	4.93	6.85	6.04	10.26	6.01
MnO	0.10	0.10	0.13	0.20	0.12	0.13	0.18	0.24	0.15	0.15	0.15
MgO	44.79	45.40	37.50	42.00	39.84	39.46	23.69	27.87	19.44	30.84	19.48
CaO	1.54	0.70	3.21	1.80	2.19	2.13	9.45	4.68	16.46	1.76	16.91
Na_2O	0.08	0	0.35	0	0.08	0.09	0.90	0.36	0.46	0.24	0.28
K_2O	0.04	0.20	0.14	0.10	0.05	0.52	0.11	1.13	0.11	0.15	0.09
P_2O_5	0.01	0	0.02	0	0.01	0.04	0.01	0.11	0.02	0.02	0.01
Cr_2O_3	0.30	0.40	0.46	0.70	0.66	0.75	1.16	1.50	0.54	0.02	0.50
NiO	0.32	0.30	0.28	0.30	0.24	0.25	0.38	0.22	0.09	0.03	0.09
LOI	3.01	4.50	3.30	1.70	3.10	2.81	1.90	4.07	0.52	1.24	0.58
Total	99.56	99.90	99.47	99.60	99.79	99.51	99.84	99.37	99.70	99.63	99.32
mg-no.	0.910	0.918	0.898	0.908	0.920	0.905	0.895	0.879	0.852	0.843	0.852
Calculated modes in wt%											
Olivine	89	84	62	68	57	70	4	9	0	n.a.	0
Opx	0	11	11	20	26	5	41	44	24	n.a.	22
Cpx	7	3	15	9	7	8	39	22	67	n.a.	68
Garnet	4		12		11	17	15	25	9	n.a.	10
Spinel		1		3						n.a.	
Temperatures and pressures											
Temp (ºC)	1280	n.a.	815	n.a.	770	1256	737	933	759	n.a.	720
Press (kb)	53.5	n.a.	29.8	n.a.	24.7	54.0	25.3	36.8	25.1	n.a.	22.2

Table B-2. Major element analyses of olivine.

Sample	NK1-1	NK1-2	NK1-3	NK1-4	NK1-5	NK1-6	NK1-7	NK1-8	NK1-9	NK1-10	NK1-11	NK1-12	NK1-13	NK1-14
Rock	Prdt	Prdt	Prdt	Prdt	Prdt	Prdt	Prdt	Prdt	Prdt	Prdt	Prdt	Prdt	Prdt	Prdt
# anal.	15	9	8	5	8	16	15	18	17	15	14	14	14	9
SiO_2	40.81	41.02	41.03	40.95	41.28	40.81	41.01	40.97	40.62	40.73	41.21	40.70	40.80	41.01
FeO	7.84	7.48	7.37	7.53	8.05	7.15	7.35	7.28	7.95	7.20	7.36	7.76	6.61	7.39
MnO	0.11	0.10	0.10	0.11	0.10	0.10	0.10	0.10	0.11	0.10	0.10	0.11	0.09	0.09
MgO	50.71	50.20	50.43	50.26	50.62	51.30	50.67	50.48	50.57	51.02	51.02	50.53	51.31	50.34
CaO	0.04	0.01	0.01	0.00	0.05	0.02	0.05	0.04	0.03	0.03	0.04	0.01	0.03	0.02
Cr_2O_3	0.03	0.01	0.01	0.01	0.03	0.02	0.04	0.04	0.03	0.03	0.03	0.01	0.04	0.01
NiO	0.38	0.35	0.35	0.39	0.37	0.38	0.37	0.41	0.38	0.40	0.39	0.39	0.41	0.36
Total	99.92	99.16	99.30	99.24	100.50	99.76	99.59	99.32	99.69	99.53	100.16	99.51	99.28	99.22
mg-no.	0.920	0.923	0.924	0.922	0.918	0.927	0.925	0.925	0.919	0.927	0.925	0.921	0.933	0.924
Cation proportions														
Si	0.993	1.003	1.002	1.001	0.999	0.992	0.999	1.000	0.992	0.993	0.998	0.994	0.994	1.002
Fe	0.159	0.153	0.150	0.154	0.163	0.145	0.150	0.149	0.162	0.147	0.149	0.159	0.135	0.151
Mn	0.002	0.002	0.002	0.002	0.002	0.002	0.002	0.002	0.002	0.002	0.002	0.002	0.002	0.002
Mg	1.841	1.831	1.836	1.832	1.827	1.859	1.840	1.838	1.841	1.855	1.842	1.841	1.864	1.834
Ca	0.001	0.000	0.000	0.000	0.001	0.000	0.001	0.001	0.001	0.001	0.001	0.000	0.001	0.001
Cr	0.001	0.000	0.000	0.000	0.001	0.000	0.001	0.001	0.001	0.001	0.001	0.000	0.001	0.000
Ni	0.007	0.007	0.007	0.008	0.007	0.007	0.007	0.008	0.007	0.008	0.008	0.008	0.008	0.007
Sum	3.005	2.996	2.997	2.998	3.000	3.007	3.000	2.998	3.007	3.006	3.000	3.005	3.005	2.997

Prdt: peridotite; H-Prxn: High-Mg pyroxenite; [a]porphyroclastic olivine; [b]olivine inclusion in garnet. Major elements in wt%. Total Fe is given as FeO and mg-no.=Mg/(Mg+Fe). For analytical techniques see Chapter 2.

Table B-2. Continued.

Sample	NK1-15	NK1-16	NK1-17	NK1-18	Nk1-19	NK1-20	NK1-22	NK1-23	NK2-1	NK2-2	NK2-3	NK2-5	NK2-5[a]	NK2-6
Rock	Prdt	Prdt	Prdt	Prdt	Prdt	Prdt	Prdt	Prdt	Prdt	Prdt	Prdt	Prdt	Prdt	Prdt
# anal.	10	14	17	9	15	10	15	16	14	15	10	11	7	11
SiO_2	40.94	41.01	40.94	41.26	41.10	41.35	41.24	40.78	41.27	40.41	41.43	41.13	40.98	41.15
FeO	7.37	7.36	7.09	7.21	7.88	7.21	7.34	8.53	7.84	8.14	7.07	8.31	8.22	7.39
MnO	0.10	0.10	0.10	0.10	0.11	0.10	0.10	0.09	0.11	0.10	0.10	0.12	0.11	0.10
MgO	50.52	50.84	51.04	50.88	50.34	50.98	50.97	50.47	50.57	50.46	51.04	50.06	50.01	50.60
CaO	0.03	0.05	0.02	0.03	0.05	0.02	0.05	0.01	0.05	0.06	0.01	0.07	0.07	0.05
Cr_2O_3	0.02	0.05	0.01	0.04	0.06	0.04	0.05	0.00	0.03	0.03	0.00	0.05	0.07	0.04
NiO	0.41	0.36	0.36	0.43	0.42	0.43	0.35	0.37	0.38	0.36	0.40	0.38	0.37	0.35
Total	99.39	99.78	99.55	99.96	99.95	100.13	100.10	100.25	100.27	99.56	100.05	100.13	99.83	99.68
mg-no.	0.924	0.925	0.928	0.926	0.919	0.927	0.925	0.913	0.920	0.917	0.928	0.915	0.916	0.924
Cation proportions														
Si	0.999	0.997	0.996	1.000	1.000	1.001	0.999	0.992	1.000	0.989	1.002	1.000	0.999	1.001
Fe	0.150	0.150	0.144	0.146	0.160	0.146	0.149	0.174	0.159	0.167	0.143	0.169	0.168	0.150
Mn	0.002	0.002	0.002	0.002	0.002	0.002	0.002	0.002	0.002	0.002	0.002	0.002	0.002	0.002
Mg	1.839	1.843	1.852	1.840	1.826	1.840	1.841	1.832	1.827	1.842	1.841	1.815	1.818	1.835
Ca	0.001	0.001	0.000	0.001	0.001	0.001	0.001	0.000	0.001	0.001	0.000	0.002	0.002	0.001
Cr	0.000	0.001	0.000	0.001	0.001	0.001	0.001	0.000	0.001	0.001	0.000	0.001	0.001	0.001
Ni	0.008	0.007	0.007	0.008	0.008	0.008	0.007	0.007	0.007	0.007	0.008	0.007	0.007	0.007
Sum	3.000	3.001	3.003	2.998	2.998	2.998	2.999	3.007	2.998	3.009	2.997	2.997	2.997	2.997

Table B-2. Continued.

Sample	NK2-6[a]	NK2-8	NK2-9	NK2-10	NK2-10[b]	NK3-3	NK3-4	NK3-5	NK3-6	NK3-7	NK3-10	NK3-11	NK3-12	NK3-13
Rock	Prdt	Prdt	Prdt	Prdt	Prdt	Prdt	Prdt	Prdt	Prdt	Prdt	Prdt	Prdt	Prdt	Prdt
# anal.	12	13	12	12	4	10	15	14	22	14	14	13	10	12
SiO_2	41.14	40.73	41.22	40.78	41.06	41.56	40.68	41.37	41.09	40.68	41.30	41.11	40.95	41.24
FeO	7.37	7.37	7.21	7.43	8.21	7.08	8.45	7.38	7.46	7.67	6.88	7.66	7.15	7.81
MnO	0.11	0.10	0.11	0.10	0.13	0.09	0.11	0.11	0.10	0.11	0.10	0.11	0.11	0.11
MgO	50.54	50.73	51.23	50.83	50.28	51.23	50.52	50.94	50.67	50.36	51.66	50.44	51.49	50.93
CaO	0.05	0.00	0.01	0.01	0.04	0.01	0.05	0.04	0.06	0.04	0.01	0.04	0.04	0.01
Cr_2O_3	0.04	0.00	0.00	0.01	0.03	0.00	0.02	0.03	0.03	0.02	0.00	0.04	0.04	0.00
NiO	0.35	0.42	0.37	0.36	0.36	0.38	0.29	0.42	0.40	0.37	0.35	0.37	0.37	0.35
Total	99.59	99.35	100.15	99.53	100.11	100.36	100.10	100.28	99.81	99.25	100.31	99.77	100.14	100.46
mg-no.	0.924	0.925	0.927	0.924	0.916	0.928	0.914	0.925	0.924	0.921	0.930	0.922	0.928	0.921
Cation proportions														
Si	1.001	0.995	0.998	0.995	0.998	1.002	0.991	1.000	0.999	0.996	0.996	1.000	0.992	0.998
Fe	0.150	0.151	0.146	0.152	0.167	0.143	0.172	0.149	0.152	0.157	0.139	0.156	0.145	0.158
Mn	0.002	0.002	0.002	0.002	0.003	0.002	0.002	0.002	0.002	0.002	0.002	0.002	0.002	0.002
Mg	1.834	1.848	1.849	1.849	1.823	1.843	1.835	1.837	1.837	1.839	1.859	1.830	1.859	1.837
Ca	0.001	0.000	0.000	0.000	0.001	0.000	0.001	0.001	0.001	0.001	0.000	0.001	0.001	0.000
Cr	0.001	0.000	0.000	0.000	0.001	0.000	0.000	0.001	0.001	0.000	0.000	0.001	0.001	0.000
Ni	0.007	0.008	0.007	0.007	0.007	0.007	0.006	0.008	0.008	0.007	0.007	0.007	0.007	0.007
Sum	2.997	3.004	3.002	3.005	3.000	2.997	3.008	2.998	3.000	3.003	3.003	2.998	3.007	3.002

Table B-2. Continued.

Sample	NK3-15	NK3-16	NK3-18	NK3-20	NK3-22	NK3-23	NK3-24	NK3-25	NK3-14	NK3-19
Rock	Prdt	Prdt	Prdt	Prdt	Prdt	Prdt	Prdt	Prdt	H-Prxn	H-Prxn
# anal.	14	18	15	15	12	16	10	10	8	17
SiO_2	40.38	41.13	41.19	40.81	40.63	40.82	40.45	41.29	40.75	41.48
FeO	7.16	8.26	7.56	8.23	7.68	7.83	7.13	8.47	8.01	7.62
MnO	0.10	0.10	0.11	0.10	0.10	0.10	0.09	0.11	0.12	0.12
MgO	51.08	50.26	51.26	50.42	50.83	50.87	51.33	50.48	50.12	51.15
CaO	0.04	0.05	0.04	0.02	0.01	0.04	0.01	0.05	0.01	0.02
Cr_2O_3	0.02	0.03	0.03	0.01	0.00	0.03	0.00	0.02	0.00	0.01
NiO	0.43	0.35	0.36	0.33	0.39	0.39	0.40	0.36	0.35	0.32
Total	99.21	100.18	100.55	99.91	99.64	100.07	99.41	100.79	99.36	100.71
mg-no.	0.927	0.916	0.924	0.916	0.922	0.921	0.928	0.914	0.918	0.923
Cation proportions										
Si	0.988	0.999	0.995	0.995	0.992	0.992	0.988	0.998	0.998	0.999
Fe	0.147	0.168	0.153	0.168	0.157	0.159	0.146	0.171	0.164	0.153
Mn	0.002	0.002	0.002	0.002	0.002	0.002	0.002	0.002	0.002	0.002
Mg	1.864	1.821	1.846	1.833	1.850	1.844	1.869	1.820	1.830	1.838
Ca	0.001	0.001	0.001	0.001	0.000	0.001	0.000	0.001	0.000	0.001
Cr	0.000	0.001	0.001	0.000	0.000	0.001	0.000	0.000	0.000	0.000
Ni	0.008	0.007	0.007	0.006	0.008	0.008	0.008	0.007	0.007	0.006
Sum	3.010	2.999	3.004	3.004	3.008	3.006	3.012	3.000	3.001	3.000

Table B-3. Major element analyses of orthopyroxene.

Sample	NK1-1	NK1-2	NK1-3	NK1-4	NK1-5	NK1-6	NK1-7	NK1-8	NK1-9	NK1-10	NK1-11	NK1-12	NK1-13	NK1-14
Rock	Prdt	Prdt	Prdt	Prdt	Prdt	Prdt	Prdt	Prdt	Prdt	Prdt	Prdt	Prdt	Prdt	Prdt
# anal.	10	5	7	11	10	5	12	20	8	16	13	22	17	11
SiO_2	57.25	57.11	57.18	56.76	56.69	56.49	57.44	57.82	57.76	57.83	57.25	58.01	57.19	58.06
TiO_2	0.14	0.04	0.05	0.05	0.09	0.04	0.04	0.03	0.08	0.02	0.05	0.05	0.07	0.04
Al_2O_3	1.18	0.95	0.97	0.98	1.22	1.17	1.36	1.21	1.11	1.19	1.20	1.00	0.69	1.02
FeO	5.09	4.72	4.65	4.70	5.00	4.54	4.42	4.39	5.18	4.37	4.61	4.74	4.29	4.58
MnO	0.12	0.12	0.13	0.13	0.13	0.11	0.11	0.10	0.12	0.11	0.12	0.13	0.11	0.11
MgO	34.98	35.80	35.89	36.08	35.00	35.89	34.99	35.23	35.11	35.43	35.57	35.45	35.81	35.64
CaO	0.63	0.34	0.30	0.26	0.71	0.39	0.93	0.67	0.57	0.58	0.63	0.33	0.49	0.36
Na_2O	0.12	0.09	0.08	0.06	0.14	0.14	0.18	0.14	0.13	0.11	0.13	0.15	0.10	0.08
Cr_2O_3	0.61	0.38	0.34	0.31	0.49	0.48	0.54	0.58	0.49	0.59	0.59	0.35	0.45	0.36
NiO	0.10	0.08	0.08	0.08	0.10	0.10	0.10	0.11	0.10	0.12	0.12	0.10	0.11	0.09
Total	100.23	99.62	99.68	99.39	99.57	99.34	100.10	100.30	100.65	100.34	100.26	100.30	99.31	100.34
mg-no.	0.925	0.931	0.932	0.932	0.926	0.934	0.934	0.935	0.924	0.935	0.932	0.930	0.937	0.933
Cation proportions														
Si	1.964	1.965	1.966	1.958	1.958	1.951	1.967	1.974	1.971	1.973	1.959	1.980	1.972	1.979
Ti	0.004	0.001	0.001	0.001	0.002	0.001	0.001	0.001	0.002	0.001	0.001	0.001	0.002	0.001
Al	0.048	0.038	0.039	0.040	0.049	0.047	0.055	0.049	0.045	0.048	0.049	0.040	0.028	0.041
Fe	0.146	0.136	0.134	0.136	0.144	0.131	0.127	0.125	0.148	0.125	0.132	0.135	0.124	0.130
Mn	0.004	0.003	0.004	0.004	0.004	0.003	0.003	0.003	0.003	0.003	0.003	0.004	0.003	0.003
Mg	1.789	1.837	1.839	1.856	1.803	1.849	1.787	1.793	1.787	1.802	1.816	1.804	1.841	1.812
Ca	0.023	0.013	0.011	0.009	0.026	0.014	0.034	0.024	0.021	0.021	0.023	0.012	0.018	0.013
Na	0.008	0.006	0.005	0.004	0.009	0.010	0.012	0.009	0.008	0.007	0.009	0.010	0.007	0.006
Cr	0.016	0.010	0.009	0.009	0.013	0.013	0.015	0.016	0.013	0.016	0.016	0.010	0.012	0.010
Ni	0.003	0.002	0.002	0.002	0.003	0.003	0.003	0.003	0.003	0.003	0.003	0.003	0.003	0.002
Sum	4.004	4.012	4.011	4.018	4.012	4.022	4.002	3.998	4.002	3.998	4.011	3.999	4.009	3.997

Prdt: peridotite; H-Prxn: High-Mg pyroxenite; L-Prxn: Low-Mg pyroxenite; [a]porphyroclastic orthopyroxene. Major elements in wt%. Total Fe is given as FeO and mg-no.=Mg/(Mg+Fe). For analytical techniques see Chapter 2.

Table B-3. Continued.

Sample	NK1-15	NK1-16	NK1-17	NK1-18	NK1-19	NK1-20	NK1-22	NK1-23	NK2-1	NK2-2	NK2-3	NK2-5	NK2-5[a]	NK2-6
Rock	Prdt	Prdt	Prdt	Prdt	Prdt	Prdt	Prdt	Prdt	Prdt	Prdt	Prdt	Prdt	Prdt	Prdt
# anal.	7	8	8	12	17	30	15	23	16	6	8	9	5	11
SiO_2	56.52	56.66	57.14	56.72	56.93	57.08	57.18	57.66	56.77	56.70	56.66	56.77	56.97	57.33
TiO_2	0.01	0.02	0.01	0.03	0.10	0.02	0.03	0.06	0.06	0.10	0.08	0.27	0.28	0.16
Al_2O_3	1.11	1.35	1.00	1.22	1.27	1.24	1.32	1.00	1.24	1.48	0.96	1.48	1.52	1.19
FeO	4.73	4.61	4.56	4.59	4.98	4.58	4.61	5.34	4.82	5.10	4.58	5.19	5.19	4.62
MnO	0.10	0.09	0.11	0.10	0.10	0.11	0.11	0.11	0.12	0.11	0.11	0.12	0.13	0.12
MgO	35.62	35.44	36.11	35.47	35.14	35.45	35.25	35.45	34.97	35.18	35.97	34.38	34.44	35.23
CaO	0.52	0.84	0.35	0.68	0.89	0.58	0.85	0.20	0.73	0.87	0.23	1.09	1.09	0.73
Na_2O	0.10	0.15	0.09	0.15	0.15	0.11	0.15	0.04	0.14	0.17	0.04	0.18	0.19	0.15
Cr_2O_3	0.49	0.68	0.36	0.59	0.60	0.60	0.68	0.23	0.55	0.33	0.27	0.64	0.66	0.61
NiO	0.11	0.10	0.08	0.11	0.12	0.11	0.10	0.07	0.11	0.11	0.09	0.11	0.11	0.10
Total	99.31	99.95	99.81	99.66	100.28	99.88	100.28	100.18	99.49	100.15	98.99	100.24	100.57	100.23
mg-no.	0.931	0.932	0.934	0.932	0.926	0.932	0.932	0.922	0.928	0.925	0.933	0.922	0.922	0.931
Cation proportions														
Si	1.955	1.949	1.962	1.954	1.954	1.960	1.958	1.975	1.960	1.949	1.961	1.952	1.952	1.963
Ti	0.000	0.001	0.000	0.001	0.003	0.001	0.001	0.002	0.002	0.003	0.002	0.007	0.007	0.004
Al	0.045	0.055	0.040	0.050	0.051	0.050	0.053	0.041	0.051	0.060	0.039	0.060	0.061	0.048
Fe	0.137	0.133	0.131	0.132	0.143	0.132	0.132	0.153	0.139	0.147	0.133	0.149	0.149	0.132
Mn	0.003	0.003	0.003	0.003	0.003	0.003	0.003	0.003	0.003	0.003	0.003	0.004	0.004	0.003
Mg	1.837	1.817	1.849	1.822	1.798	1.815	1.800	1.810	1.800	1.803	1.856	1.763	1.760	1.798
Ca	0.019	0.031	0.013	0.025	0.033	0.021	0.031	0.007	0.027	0.032	0.009	0.040	0.040	0.027
Na	0.007	0.010	0.006	0.010	0.010	0.007	0.010	0.002	0.009	0.011	0.002	0.012	0.012	0.010
Cr	0.013	0.019	0.010	0.016	0.016	0.016	0.018	0.006	0.015	0.009	0.007	0.017	0.018	0.017
Ni	0.003	0.003	0.002	0.003	0.003	0.003	0.003	0.002	0.003	0.003	0.002	0.003	0.003	0.003
Sum	4.019	4.019	4.016	4.017	4.014	4.009	4.010	4.001	4.009	4.020	4.015	4.008	4.007	4.005

Table B-3. Continued.

Sample	NK2-6[a]	NK2-8	NK2-9	NK2-10	NK3-2	NK3-3	NK3-4	NK3-5	NK3-6	NK3-7	NK3-10	NK3-11	NK3-12	NK3-13
Rock	Prdt	Prdt	Prdt	Prdt	Prdt	Prdt	Prdt	Prdt	Prdt	Prdt	Prdt	Prdt	Prdt	Prdt
# anal.	9	13	12	8	8	14	15	11	4	5	16	3	22	12
SiO_2	57.18	56.32	56.75	56.78	52.85	57.41	57.09	57.54	57.18	56.82	57.07	57.47	57.04	57.21
TiO_2	0.15	0.00	0.00	0.05	0.05	0.00	0.07	0.02	0.02	0.10	0.03	0.09	0.08	0.04
Al_2O_3	1.19	1.92	1.94	1.01	1.88	1.68	1.34	1.07	1.27	1.27	2.09	1.26	0.85	0.98
FeO	4.60	5.25	4.87	4.79	22.04	4.58	5.39	4.60	4.66	4.89	4.43	4.75	4.40	4.99
MnO	0.12	0.14	0.13	0.10	0.16	0.13	0.12	0.12	0.11	0.10	0.13	0.11	0.12	0.13
MgO	35.25	35.20	35.14	35.98	22.90	35.16	34.90	35.75	35.44	35.56	35.54	35.28	35.70	35.62
CaO	0.73	0.18	0.54	0.35	0.35	0.56	0.76	0.65	0.81	0.70	0.20	0.77	0.61	0.24
Na_2O	0.15	0.01	0.01	0.10	0.03	0.01	0.14	0.08	0.12	0.13	0.02	0.16	0.12	0.04
Cr_2O_3	0.63	0.27	0.50	0.33	0.03	0.45	0.27	0.53	0.46	0.38	0.25	0.61	0.54	0.25
NiO	0.10	0.07	0.08	0.10	0.02	0.07	0.11	0.11	0.11	0.10	0.07	0.11	0.10	0.07
Total	100.10	99.36	99.95	99.59	100.30	100.04	100.17	100.46	100.17	100.05	99.81	100.62	99.56	99.55
mg-no.	0.932	0.923	0.928	0.931	0.649	0.932	0.920	0.933	0.931	0.928	0.935	0.930	0.935	0.927
Cation proportions														
Si	1.961	1.946	1.948	1.957	1.954	1.964	1.961	1.964	1.959	1.952	1.954	1.961	1.964	1.970
Ti	0.004	0.000	0.000	0.001	0.001	0.000	0.002	0.000	0.001	0.003	0.001	0.002	0.002	0.001
Al	0.048	0.078	0.079	0.041	0.082	0.068	0.054	0.043	0.051	0.051	0.084	0.051	0.035	0.040
Fe	0.132	0.152	0.140	0.138	0.681	0.131	0.155	0.131	0.133	0.140	0.127	0.136	0.127	0.144
Mn	0.004	0.004	0.004	0.003	0.005	0.004	0.003	0.003	0.003	0.003	0.004	0.003	0.004	0.004
Mg	1.802	1.814	1.799	1.849	1.263	1.794	1.788	1.820	1.811	1.821	1.814	1.796	1.833	1.829
Ca	0.027	0.006	0.020	0.013	0.014	0.020	0.028	0.024	0.030	0.026	0.007	0.028	0.022	0.009
Na	0.010	0.001	0.000	0.006	0.002	0.001	0.010	0.005	0.008	0.009	0.001	0.011	0.008	0.002
Cr	0.017	0.007	0.013	0.009	0.001	0.012	0.007	0.014	0.013	0.010	0.007	0.017	0.015	0.007
Ni	0.003	0.002	0.002	0.003	0.001	0.002	0.003	0.003	0.003	0.003	0.002	0.003	0.003	0.002
Sum	4.007	4.011	4.006	4.020	4.004	3.996	4.011	4.009	4.012	4.019	4.000	4.007	4.012	4.007

Table B-3. Continued.

Sample	NK3-15	NK3-16	NK3-18	NK3-20	NK3-22	NK3-23	NK3-24	NK3-25	NK2-7	NK3-14	NK3-19	NK3-1	NK3-8	NK3-17
Rock	Prdt	Prdt	Prdt	Prdt	Prdt	Prdt	Prdt	Prdt	H-Prxn	H-Prxn	H-Prxn	L-Prxn	L-Prxn	L-Prxn
# anal.	19	13	9	10	15	8	11	7	7	4	18	8	12	5
SiO_2	57.73	56.56	56.70	57.07	57.58	56.81	57.82	56.79	57.02	57.59	57.33	56.16	57.00	55.64
TiO_2	0.07	0.16	0.11	0.06	0.03	0.03	0.02	0.09	0.06	0.07	0.04	0.03	0.24	0.02
Al_2O_3	1.29	1.40	0.85	0.99	1.45	1.14	1.22	1.24	0.95	1.03	0.94	1.11	0.76	1.17
FeO	4.36	5.12	4.80	5.73	4.87	4.76	4.55	5.34	4.97	4.98	4.92	9.68	7.94	9.66
MnO	0.10	0.12	0.12	0.11	0.12	0.10	0.11	0.12	0.11	0.11	0.13	0.14	0.14	0.12
MgO	35.23	34.61	35.19	35.31	35.34	35.21	35.97	34.78	35.70	35.74	35.57	32.66	33.43	32.55
CaO	0.74	0.79	0.64	0.21	0.37	0.66	0.21	0.68	0.22	0.28	0.34	0.20	0.84	0.22
Na_2O	0.13	0.17	0.12	0.02	0.03	0.11	0.02	0.13	0.03	0.11	0.10	0.01	0.11	0.00
Cr_2O_3	0.45	0.48	0.52	0.22	0.36	0.48	0.27	0.35	0.18	0.34	0.36	0.18	0.01	0.17
NiO	0.12	0.10	0.10	0.07	0.07	0.11	0.08	0.10	0.08	0.08	0.09	0.15	0.02	0.15
Total	100.22	99.51	99.15	99.79	100.22	99.41	100.26	99.62	99.33	100.33	99.82	100.32	100.48	99.71
mg-no.	0.935	0.923	0.929	0.917	0.928	0.930	0.934	0.921	0.928	0.928	0.928	0.857	0.882	0.857
Cation proportions														
Si	1.972	1.956	1.965	1.967	1.968	1.962	1.971	1.962	1.968	1.968	1.970	1.961	1.973	1.956
Ti	0.002	0.004	0.003	0.002	0.001	0.001	0.001	0.002	0.002	0.002	0.001	0.001	0.006	0.001
Al	0.052	0.057	0.035	0.040	0.058	0.047	0.049	0.050	0.039	0.041	0.038	0.046	0.031	0.048
Fe	0.125	0.148	0.139	0.165	0.139	0.137	0.130	0.154	0.144	0.142	0.141	0.283	0.230	0.284
Mn	0.003	0.003	0.004	0.003	0.003	0.003	0.003	0.004	0.003	0.003	0.004	0.004	0.004	0.004
Mg	1.794	1.785	1.818	1.815	1.801	1.813	1.829	1.792	1.837	1.822	1.823	1.701	1.725	1.706
Ca	0.027	0.029	0.024	0.008	0.014	0.024	0.008	0.025	0.008	0.010	0.013	0.008	0.031	0.008
Na	0.009	0.012	0.008	0.001	0.002	0.007	0.001	0.009	0.002	0.007	0.007	0.000	0.008	0.000
Cr	0.012	0.013	0.014	0.006	0.010	0.013	0.007	0.010	0.005	0.009	0.010	0.005	0.000	0.005
Ni	0.003	0.003	0.003	0.002	0.002	0.003	0.002	0.003	0.002	0.002	0.003	0.004	0.000	0.004
Sum	3.998	4.010	4.012	4.009	3.998	4.011	4.001	4.010	4.009	4.008	4.008	4.012	4.009	4.017

Table B-4. Major element analyses of clinopyroxene.

Sample	NK1-1	NK1-2	NK1-3	NK1-4	NK1-5	NK1-6	NK1-7	NK1-8	NK1-9	NK1-10	NK1-11	NK1-12	NK1-13	NK1-14
Rock	Prdt	Prdt	Prdt	Prdt	Prdt	Prdt	Prdt	Prdt	Prdt	Prdt	Prdt	Prdt	Prdt	Prdt
# anal.	7	9	5	10	15	5	9	5	14	11	6	13	9	8
SiO_2	53.73	53.89	54.19	54.21	54.72	54.07	54.11	55.45	54.36	54.62	54.48	55.22	53.76	53.86
TiO_2	0.29	0.13	0.13	0.10	0.17	0.13	0.08	0.42	0.15	0.87	0.69	0.16	0.45	0.12
Al_2O_3	2.28	2.74	2.98	2.93	2.52	3.70	2.36	1.07	2.64	1.46	0.94	3.76	0.64	2.67
FeO	2.45	2.25	2.31	1.61	2.65	2.35	2.34	2.73	2.45	3.17	2.93	2.57	2.41	2.19
MnO	0.07	0.08	0.09	0.06	0.10	0.07	0.08	0.09	0.09	0.12	0.13	0.08	0.09	0.07
MgO	17.12	16.07	15.84	15.94	17.52	14.91	18.07	19.73	16.58	19.19	19.03	14.97	19.44	16.06
CaO	18.91	19.67	19.14	20.54	18.87	17.20	18.68	18.51	18.82	18.28	19.71	17.39	20.46	19.59
Na_2O	1.92	2.20	2.46	2.19	1.93	3.36	1.61	0.85	2.07	1.14	1.06	3.48	0.68	2.27
Cr_2O_3	2.47	2.22	2.27	1.96	1.96	3.26	1.77	0.85	2.21	1.36	1.42	2.64	0.99	2.19
NiO	0.06	0.04	0.04	0.04	0.05	0.04	0.06	0.04	0.05	0.03	0.03	0.04	0.04	0.04
Total	99.29	99.30	99.45	99.59	100.48	99.10	99.18	99.75	99.41	100.26	100.40	100.30	98.98	99.06
mg-no.	0.926	0.927	0.924	0.946	0.922	0.919	0.932	0.928	0.923	0.915	0.921	0.912	0.935	0.929
Cation proportions														
Si	1.958	1.964	1.970	1.966	1.965	1.969	1.965	1.993	1.973	1.964	1.964	1.984	1.964	1.967
Ti	0.008	0.004	0.004	0.003	0.005	0.004	0.002	0.011	0.004	0.023	0.019	0.004	0.012	0.003
Al	0.098	0.118	0.128	0.125	0.107	0.159	0.101	0.046	0.113	0.062	0.040	0.159	0.028	0.115
Fe	0.075	0.069	0.070	0.049	0.080	0.072	0.071	0.082	0.074	0.095	0.088	0.077	0.074	0.067
Mn	0.002	0.003	0.003	0.002	0.003	0.002	0.003	0.003	0.003	0.004	0.004	0.002	0.003	0.002
Mg	0.930	0.873	0.859	0.862	0.939	0.810	0.978	1.057	0.897	1.029	1.023	0.802	1.059	0.874
Ca	0.738	0.768	0.745	0.798	0.726	0.671	0.727	0.713	0.732	0.705	0.761	0.670	0.801	0.766
Na	0.136	0.156	0.173	0.154	0.134	0.237	0.113	0.060	0.145	0.080	0.074	0.243	0.048	0.161
Cr	0.071	0.064	0.065	0.056	0.056	0.094	0.051	0.024	0.063	0.039	0.041	0.075	0.029	0.063
Ni	0.002	0.001	0.001	0.001	0.001	0.001	0.002	0.001	0.002	0.001	0.001	0.001	0.001	0.001
Sum	4.017	4.019	4.017	4.017	4.015	4.019	4.013	3.990	4.007	4.002	4.014	4.016	4.019	4.020

Prdt: peridotite; H-Prxn: High-Mg pyroxenite; L-Prxn: Low-Mg pyroxenite. Major elements in wt%. Total Fe is given as FeO and mg-no.=Mg/(Mg+Fe). For analytical techniques see Chapter 2.

Table B-4. Continued.

Sample	NK1-15	NK1-17	NK1-18	NK1-19	NK1-22	NK1-23	NK2-1	NK2-2	NK2-3	NK2-5	NK2-8	NK2-9	NK2-10	NK3-2
Rock	Prdt	Prdt	Prdt	Prdt	Prdt	Prdt	Prdt	Prdt	Prdt	Prdt	Prdt	Prdt	Prdt	Prdt
# anal.	10	9	5	3	11	21	16	7	8	10	9	6	5	6
SiO_2	53.84	54.28	53.93	52.82	54.35	54.57	53.87	54.21	53.92	54.35	53.49	54.09	53.99	52.68
TiO_2	0.05	0.02	0.07	0.86	0.05	0.26	0.10	0.21	0.18	0.48	0.01	0.00	0.14	0.39
Al_2O_3	2.21	2.38	2.31	1.02	2.09	3.32	2.31	2.89	2.65	2.33	1.81	1.32	2.91	3.86
FeO	2.21	2.17	2.31	3.15	2.41	2.24	2.44	2.80	1.99	3.05	1.20	1.33	2.34	8.29
MnO	0.07	0.06	0.07	0.10	0.09	0.06	0.08	0.09	0.06	0.11	0.06	0.05	0.06	0.06
MgO	16.99	16.31	17.28	18.39	18.02	15.54	17.45	18.07	16.15	18.54	17.25	18.29	15.82	13.15
CaO	19.68	20.13	19.09	20.25	19.25	20.09	19.31	18.35	20.92	18.18	24.10	23.57	19.45	20.65
Na_2O	1.84	2.12	1.81	0.89	1.56	2.31	1.74	1.78	1.90	1.55	0.60	0.26	2.43	1.61
Cr_2O_3	2.15	2.00	2.33	0.97	2.17	1.60	2.19	1.14	1.78	1.75	0.62	0.57	2.10	0.08
NiO	0.05	0.04	0.06	0.06	0.06	0.03	0.05	0.06	0.03	0.06	0.03	0.03	0.04	0.02
Total	99.07	99.52	99.26	98.51	100.05	100.00	99.55	99.60	99.59	100.40	99.17	99.53	99.29	100.79
mg-no.	0.932	0.931	0.930	0.912	0.930	0.925	0.927	0.920	0.935	0.916	0.962	0.961	0.923	0.739
Cation proportions														
Si	1.965	1.973	1.963	1.948	1.962	1.971	1.957	1.959	1.961	1.953	1.955	1.965	1.967	1.937
Ti	0.001	0.001	0.002	0.024	0.001	0.007	0.003	0.006	0.005	0.013	0.000	0.000	0.004	0.011
Al	0.095	0.102	0.099	0.044	0.089	0.141	0.099	0.123	0.114	0.099	0.078	0.057	0.125	0.167
Fe	0.067	0.066	0.070	0.097	0.073	0.068	0.074	0.085	0.061	0.092	0.037	0.041	0.071	0.255
Mn	0.002	0.002	0.002	0.003	0.003	0.002	0.003	0.003	0.002	0.003	0.002	0.002	0.002	0.002
Mg	0.925	0.884	0.938	1.012	0.970	0.837	0.945	0.973	0.876	0.994	0.940	0.991	0.860	0.721
Ca	0.770	0.784	0.745	0.800	0.744	0.777	0.752	0.711	0.815	0.700	0.944	0.917	0.759	0.814
Na	0.130	0.149	0.127	0.064	0.109	0.161	0.122	0.125	0.134	0.108	0.043	0.018	0.171	0.115
Cr	0.062	0.057	0.067	0.028	0.062	0.046	0.063	0.033	0.051	0.050	0.018	0.016	0.061	0.002
Ni	0.001	0.001	0.002	0.002	0.002	0.001	0.002	0.002	0.001	0.002	0.001	0.001	0.001	0.001
Sum	4.019	4.020	4.015	4.023	4.015	4.010	4.019	4.019	4.019	4.013	4.018	4.007	4.021	4.024

Table B-4. Continued.

Sample	NK3-3	NK3-4	NK3-5	NK3-6	NK3-7	NK3-11	NK3-12	NK3-13	NK3-15	NK3-16	NK3-18	NK3-20	NK3-22	NK3-23
Rock	Prdt	Prdt	Prdt	Prdt	Prdt	Prdt	Prdt	Prdt	Prdt	Prdt	Prdt	Prdt	Prdt	Prdt
# anal.	3	10	5	13	9	15	6	9	9	9	6	8	15	11
SiO_2	55.10	55.32	54.51	54.72	53.62	54.53	54.13	54.20	54.83	53.75	53.71	54.08	53.92	53.81
TiO_2	0.00	0.15	0.24	0.04	0.21	0.19	0.71	0.08	0.83	0.29	0.22	0.20	0.09	0.06
Al_2O_3	1.26	2.89	1.62	2.02	2.67	2.38	0.73	2.23	1.30	2.80	1.75	2.67	2.59	2.03
FeO	1.38	2.76	2.43	2.40	2.59	2.46	2.78	2.12	2.95	2.83	2.27	2.28	1.41	2.34
MnO	0.07	0.09	0.10	0.09	0.09	0.09	0.09	0.07	0.12	0.08	0.09	0.06	0.06	0.09
MgO	18.08	17.85	18.15	18.33	17.38	17.35	19.93	16.48	19.03	17.58	17.25	16.15	16.48	17.82
CaO	23.69	17.71	20.66	19.92	19.21	19.01	19.81	21.69	19.28	18.50	19.36	21.74	22.07	20.08
Na_2O	0.46	1.86	1.13	1.25	1.77	1.88	0.81	1.61	1.01	1.91	1.79	1.65	1.46	1.44
Cr_2O_3	0.75	1.01	1.59	1.42	1.49	2.35	0.98	1.51	0.68	1.85	2.82	1.46	1.31	1.79
NiO	0.04	0.05	0.07	0.06	0.05	0.05	0.03	0.03	0.03	0.05	0.05	0.04	0.03	0.06
Total	100.83	99.69	100.49	100.24	99.08	100.30	100.00	100.03	100.06	99.64	99.31	100.32	99.43	99.51
mg-no.	0.959	0.920	0.931	0.932	0.923	0.926	0.928	0.933	0.920	0.917	0.931	0.927	0.954	0.931
Cation proportions														
Si	1.975	1.988	1.963	1.968	1.955	1.964	1.957	1.965	1.974	1.949	1.960	1.956	1.961	1.957
Ti	0.000	0.004	0.006	0.001	0.006	0.005	0.019	0.002	0.022	0.008	0.006	0.005	0.002	0.002
Al	0.053	0.122	0.069	0.085	0.115	0.101	0.031	0.095	0.055	0.120	0.075	0.114	0.111	0.087
Fe	0.041	0.083	0.073	0.072	0.079	0.074	0.084	0.064	0.089	0.086	0.069	0.069	0.043	0.071
Mn	0.002	0.003	0.003	0.003	0.003	0.003	0.003	0.002	0.004	0.002	0.003	0.002	0.002	0.003
Mg	0.966	0.956	0.975	0.983	0.945	0.932	1.074	0.891	1.022	0.950	0.938	0.871	0.893	0.966
Ca	0.910	0.682	0.797	0.768	0.751	0.733	0.768	0.843	0.744	0.719	0.757	0.843	0.860	0.782
Na	0.032	0.130	0.079	0.087	0.125	0.131	0.057	0.113	0.070	0.134	0.127	0.116	0.103	0.101
Cr	0.021	0.029	0.045	0.041	0.043	0.067	0.028	0.043	0.019	0.053	0.081	0.042	0.038	0.052
Ni	0.001	0.001	0.002	0.002	0.002	0.002	0.001	0.001	0.001	0.001	0.002	0.001	0.001	0.002
Sum	4.003	3.997	4.012	4.010	4.022	4.012	4.022	4.020	4.001	4.023	4.018	4.018	4.014	4.022

Table B-4. Continued.

Sample	NK3-24	NK3-25	NK2-7	NK3-14	NK3-19	NK3-1	NK3-8	NK3-17
Rock	Prdt	Prdt	H-Prxn	H-Prxn	H-Prxn	L-Prxn	L-Prxn	L-Prxn
# anal.	5	5	4	9	8	8	11	4
SiO_2	54.13	53.85	53.65	54.56	54.68	53.99	54.66	53.02
TiO_2	0.05	0.16	0.16	0.17	0.09	0.08	0.53	0.09
Al_2O_3	1.77	2.61	2.70	4.04	2.80	1.73	1.32	1.80
FeO	1.71	2.75	1.95	3.03	2.45	3.12	4.66	3.04
MnO	0.06	0.09	0.05	0.12	0.08	0.06	0.12	0.05
MgO	16.75	17.65	16.02	14.26	16.07	16.82	18.20	16.60
CaO	22.68	19.00	21.86	18.38	19.45	23.61	19.96	23.59
Na_2O	1.05	1.71	1.58	3.38	2.49	0.63	1.07	0.50
Cr_2O_3	0.95	1.44	1.15	2.02	1.84	0.45	0.04	0.37
NiO	0.03	0.05	0.05	0.03	0.04	0.08	0.02	0.09
Total	99.17	99.32	99.17	100.00	100.00	100.57	100.58	99.16
mg-no.	0.946	0.920	0.936	0.894	0.921	0.906	0.874	0.907
Cation proportions								
Si	1.976	1.958	1.960	1.974	1.976	1.958	1.974	1.952
Ti	0.001	0.004	0.004	0.005	0.003	0.002	0.014	0.003
Al	0.076	0.112	0.116	0.172	0.119	0.074	0.056	0.078
Fe	0.052	0.084	0.060	0.092	0.074	0.095	0.141	0.094
Mn	0.002	0.003	0.002	0.004	0.002	0.002	0.004	0.002
Mg	0.912	0.957	0.873	0.769	0.866	0.909	0.980	0.911
Ca	0.887	0.740	0.856	0.713	0.753	0.918	0.772	0.931
Na	0.074	0.120	0.112	0.237	0.175	0.045	0.075	0.036
Cr	0.027	0.041	0.033	0.058	0.053	0.013	0.001	0.011
Ni	0.001	0.002	0.001	0.001	0.001	0.002	0.001	0.003
Sum	4.008	4.020	4.016	4.025	4.022	4.018	4.019	4.019

Table B-5. Major element analyses of garnet.

Sample	NK1-1	NK1-2	NK1-3	NK 1-4	NK1-5	NK1-6	NK1-7	NK1-9	NK1-10	NK1-11	NK1-12	NK1-14	NK1-15	NK1-16
Rock	Prdt	Prdt	Prdt	Prdt	Prdt	Prdt	Prdt	Prdt	Prdt	Prdt	Prdt	Prdt	Prdt	Prdt
# anal.	8	5	6	40	13	7	6	12	7	8	16	9	10	9
SiO_2	40.72	41.91	41.44	41.28	42.04	41.51	41.46	41.14	42.08	41.20	42.27	42.13	41.06	40.87
TiO_2	0.33	0.09	0.08	0.09	0.24	0.08	0.14	0.19	0.11	0.19	0.08	0.08	0.02	0.14
Al_2O_3	18.87	20.04	21.19	20.54	20.09	20.58	20.29	20.19	19.31	18.83	21.02	20.86	19.29	17.80
FeO	7.09	7.15	7.46	7.93	7.07	6.86	6.24	7.17	6.35	6.60	7.71	7.33	6.74	6.29
MnO	0.41	0.45	0.39	0.44	0.35	0.38	0.30	0.38	0.33	0.34	0.46	0.41	0.36	0.31
MgO	19.58	20.48	20.43	19.38	20.19	20.66	20.67	19.97	20.58	20.46	20.30	19.98	19.57	19.62
CaO	5.75	5.05	5.12	5.68	5.26	4.62	5.22	5.28	4.81	5.10	4.29	4.87	6.12	6.47
Na_2O	0.04	0.02	0.03	0.02	0.03	0.03	0.02	0.03	0.01	0.03	0.04	0.03	0.02	0.03
Cr_2O_3	6.54	3.99	4.13	4.41	4.80	4.42	4.76	4.97	6.09	6.26	3.77	4.04	6.16	7.65
NiO	0.01	0.00	0.00	0.00	0.01	0.01	0.02	0.01	0.01	0.01	0.00	0.00	0.01	0.00
Total	99.33	99.17	100.27	99.77	100.07	99.15	99.10	99.32	99.69	99.03	99.95	99.73	99.35	99.17
mg-no.	0.831	0.836	0.830	0.813	0.836	0.843	0.855	0.832	0.852	0.847	0.824	0.829	0.838	0.848
Cation proportions														
Si	2.966	3.022	2.961	2.980	3.009	2.989	2.987	2.975	3.021	2.992	3.018	3.017	2.981	2.986
Ti	0.018	0.005	0.004	0.005	0.013	0.004	0.008	0.010	0.006	0.011	0.004	0.004	0.001	0.008
Al	1.620	1.703	1.785	1.747	1.695	1.747	1.723	1.721	1.634	1.612	1.769	1.761	1.651	1.533
Fe	0.432	0.431	0.446	0.478	0.423	0.413	0.376	0.433	0.381	0.401	0.460	0.439	0.409	0.384
Mn	0.025	0.028	0.024	0.027	0.021	0.023	0.018	0.023	0.020	0.021	0.028	0.025	0.022	0.019
Mg	2.126	2.201	2.177	2.086	2.155	2.218	2.220	2.153	2.203	2.215	2.162	2.133	2.119	2.137
Ca	0.449	0.390	0.392	0.439	0.403	0.357	0.403	0.409	0.370	0.397	0.328	0.373	0.476	0.507
Na	0.005	0.001	0.004	0.003	0.004	0.004	0.003	0.004	0.002	0.004	0.006	0.004	0.003	0.004
Cr	0.378	0.227	0.233	0.251	0.272	0.252	0.271	0.284	0.346	0.360	0.213	0.229	0.353	0.442
Ni	0.000	0.000	0.000	0.000	0.001	0.001	0.001	0.000	0.001	0.001	0.000	0.000	0.000	0.000
Sum	8.019	8.008	8.027	8.017	7.997	8.008	8.009	8.014	7.984	8.013	7.989	7.986	8.016	8.020

Prdt: peridotite; H-Prxn: High-Mg pyroxenite; L-Prxn: Low-Mg pyroxenite; [a]garnet in clinopyroxene. Major elements in wt%. Total Fe is given as FeO and mg-no.=Mg/(Mg+Fe). For analytical techniques see Chapter 2.

Table B-5. Continued.

Sample	NK1-17	NK1-18	NK1-20	NK1-22	NK1-23	NK2-1	NK2-2	NK2-3	NK2-5	NK2-10	NK3-2	NK3-4	NK3-5	NK3-6
Rock	Prdt	Prdt	Prdt	Prdt	Prdt	Prdt	Prdt	Prdt	Prdt	Prdt	Prdt	Prdt	Prdt	Prdt
# anal.	8	6	5	12	14	9	5	8	12	6	11	12	6	15
SiO_2	41.38	41.13	41.24	41.25	41.47	41.17	42.08	41.34	41.20	41.42	38.08	42.22	41.10	41.92
TiO_2	0.02	0.13	0.10	0.14	0.09	0.23	0.29	0.08	0.87	0.09	0.05	0.25	0.08	0.10
Al_2O_3	20.78	18.93	19.27	18.05	22.46	19.35	21.57	21.44	18.13	21.27	21.47	22.30	18.24	20.10
FeO	7.01	6.46	6.51	6.34	9.26	7.08	6.87	7.85	6.84	7.57	24.45	7.16	6.59	6.46
MnO	0.42	0.31	0.32	0.32	0.49	0.36	0.31	0.48	0.32	0.41	0.44	0.32	0.36	0.30
MgO	19.88	20.38	20.95	19.66	19.07	19.63	21.16	19.53	19.44	20.01	9.06	21.15	18.92	20.29
CaO	5.45	5.90	5.11	6.28	4.84	5.67	4.50	5.28	6.61	5.07	5.61	4.01	7.09	5.76
Na_2O	0.04	0.01	0.02	0.02	0.02	0.02	0.03	0.03	0.05	0.03	0.05	0.03	0.02	0.01
Cr_2O_3	4.12	6.83	6.52	7.65	2.27	5.78	2.55	3.21	6.77	3.74	0.07	2.00	7.69	5.15
NiO	0.01	0.01	0.01	0.01	0.00	0.01	0.01	0.01	0.01	0.02	0.00	0.01	0.00	0.01
Total	99.10	100.07	100.05	99.72	99.97	99.29	99.37	99.25	100.23	99.62	99.30	99.48	100.10	100.10
mg-no.	0.835	0.849	0.851	0.847	0.786	0.832	0.846	0.816	0.835	0.825	0.398	0.840	0.837	0.849
Cation proportions														
Si	2.988	2.966	2.965	2.994	2.975	2.988	3.003	2.983	2.980	2.976	2.954	3.002	2.982	2.999
Ti	0.001	0.007	0.006	0.008	0.005	0.012	0.015	0.004	0.047	0.005	0.003	0.013	0.004	0.005
Al	1.769	1.609	1.633	1.544	1.899	1.655	1.814	1.823	1.545	1.801	1.963	1.869	1.561	1.695
Fe	0.423	0.389	0.392	0.385	0.555	0.430	0.410	0.474	0.414	0.455	1.586	0.426	0.400	0.386
Mn	0.026	0.019	0.020	0.020	0.030	0.022	0.019	0.029	0.020	0.025	0.029	0.020	0.022	0.018
Mg	2.140	2.191	2.246	2.127	2.040	2.124	2.251	2.101	2.096	2.144	1.048	2.243	2.048	2.164
Ca	0.422	0.456	0.394	0.489	0.372	0.441	0.344	0.408	0.512	0.391	0.467	0.306	0.551	0.442
Na	0.005	0.002	0.002	0.002	0.002	0.003	0.004	0.002	0.007	0.001	0.007	0.004	0.003	0.002
Cr	0.235	0.389	0.371	0.439	0.129	0.332	0.144	0.183	0.387	0.213	0.005	0.113	0.441	0.292
Ni	0.000	0.001	0.000	0.000	0.000	0.001	0.001	0.001	0.001	0.001	0.000	0.001	0.000	0.000
Sum	8.010	8.028	8.027	8.008	8.007	8.008	8.004	8.010	8.009	8.011	8.062	7.996	8.013	8.003

Table B-5. Continued.

Sample	NK3-7	NK3-11	NK3-13	NK3-15	NK3-16	NK3-20	NK3-24	NK3-25	NK2-7	NK3-14	NK3-19	NK3-1	NK3-1[a]	NK3-17
Rock	Prdt	Prdt	Prdt	Prdt	Prdt	Prdt	Prdt	Prdt	H-Prxn	H-Prxn	H-Prxn	L-Prxn	L-Prxn	L-Prxn
# anal.	6	11	5	12	16	14	7	20	6	26	5	27	10	3
SiO_2	41.48	41.43	41.04	42.22	41.43	42.01	41.53	41.84	41.67	42.18	41.43	40.67	40.79	40.53
TiO_2	0.27	0.30	0.04	0.10	0.39	0.07	0.02	0.32	0.04	0.10	0.07	0.05	0.01	0.09
Al_2O_3	21.58	18.73	21.58	20.36	19.84	22.56	23.02	20.76	23.35	22.42	21.09	22.00	22.04	22.49
FeO	6.99	6.88	8.52	6.28	7.00	9.38	8.07	7.23	8.11	8.10	7.43	14.89	14.64	14.88
MnO	0.34	0.36	0.54	0.29	0.30	0.46	0.49	0.33	0.48	0.43	0.43	0.60	0.55	0.56
MgO	20.71	19.76	18.85	20.63	20.28	19.03	20.01	20.11	20.11	20.46	20.41	14.63	15.80	14.97
CaO	4.96	5.93	5.43	5.04	5.40	4.80	4.93	5.02	4.65	4.22	5.32	5.88	5.79	6.07
Na_2O	0.03	0.03	0.01	0.01	0.04	0.01	0.01	0.03	0.01	0.04	0.02	0.01	0.01	0.01
Cr_2O_3	3.32	6.62	3.45	4.67	4.90	1.92	1.48	3.71	1.49	2.42	4.12	1.32	1.08	1.27
NiO	0.01	0.01	0.00	0.00	0.01	0.01	0.02	0.01	0.00	0.00	0.01	0.00	0.01	0.00
Total	99.70	100.05	99.45	99.61	99.57	100.26	99.55	99.36	99.91	100.36	100.33	100.04	100.72	100.87
mg-no.	0.841	0.837	0.798	0.854	0.838	0.783	0.815	0.832	0.815	0.818	0.830	0.637	0.658	0.642
Cation proportions														
Si	2.966	2.991	2.969	3.019	2.986	2.999	2.969	3.007	2.965	2.991	2.962	2.995	2.978	2.961
Ti	0.014	0.016	0.002	0.005	0.021	0.004	0.001	0.017	0.002	0.005	0.004	0.003	0.001	0.005
Al	1.818	1.594	1.840	1.716	1.685	1.898	1.940	1.759	1.958	1.874	1.777	1.909	1.896	1.937
Fe	0.418	0.415	0.516	0.376	0.422	0.560	0.483	0.434	0.483	0.480	0.444	0.917	0.894	0.909
Mn	0.021	0.022	0.033	0.018	0.018	0.028	0.030	0.020	0.029	0.026	0.026	0.037	0.034	0.035
Mg	2.208	2.128	2.033	2.200	2.179	2.026	2.133	2.154	2.134	2.163	2.175	1.606	1.720	1.632
Ca	0.380	0.459	0.421	0.386	0.417	0.367	0.377	0.387	0.355	0.321	0.407	0.464	0.453	0.475
Na	0.002	0.004	0.002	0.002	0.006	0.002	0.001	0.004	0.002	0.006	0.003	0.001	0.002	0.002
Cr	0.188	0.378	0.197	0.264	0.279	0.108	0.084	0.211	0.084	0.136	0.233	0.077	0.062	0.073
Ni	0.001	0.000	0.000	0.000	0.000	0.000	0.001	0.001	0.000	0.000	0.001	0.000	0.001	0.000
Sum	8.016	8.008	8.012	7.986	8.013	7.993	8.018	7.993	8.012	8.001	8.031	8.009	8.040	8.030

National Library
of Canada

Acquisitions and
Bibliographic Services

395 Wellington Street
Ottawa ON K1A 0N4
Canada

Bibliothèque nationale
du Canada

Acquisitions et
services bibliographiques

395, rue Wellington
Ottawa ON K1A 0N4
Canada

Your file Votre référence

Our file Notre référence

The author has granted a non-exclusive licence allowing the National Library of Canada to reproduce, loan, distribute or sell copies of this thesis in microform, paper or electronic formats.

The author retains ownership of the copyright in this thesis. Neither the thesis nor substantial extracts from it may be printed or otherwise reproduced without the author's permission.

L'auteur a accordé une licence non exclusive permettant à la Bibliothèque nationale du Canada de reproduire, prêter, distribuer ou vendre des copies de cette thèse sous la forme de microfiche/film, de reproduction sur papier ou sur format électronique.

L'auteur conserve la propriété du droit d'auteur qui protège cette thèse. Ni la thèse ni des extraits substantiels de celle-ci ne doivent être imprimés ou autrement reproduits sans son autorisation.

0-612-78765-6

Canada

Abstract

Hf, Sr, Nd and Pb isotopes, and major, trace and rare earth elements (REE) were determined for a suite of peridotite and pyroxenite xenoliths, constituent garnet and clinopyroxene and the host Nikos kimberlite (100 Ma) from Somerset Island, in order to constrain the chemical and isotopic composition of the lithosphere beneath the northern Canadian craton. The refractory Nikos peridotites are characterized by high olivine forsterite contents (avg. Fo=92.3) and depletions in incompatible major elements (Fe, Al, Ca), but are enriched in incompatible trace elements, such as large ion lithophile elements (LILE) and light rare earth elements (LREE), while having approximately chondritic heavy rare earth element (HREE) contents. Mass balance calculations using REE contents of clinopyroxene and garnet indicate that calculated LREE abundances for the Nikos xenoliths are significantly lower (e.g. Nd ~50%) than those of the analyzed whole-rocks. These results suggest the presence of small amounts of a kimberlite-related LREE-rich interstitial component (i.e. ~1% kimberlite liquid and/or ~0.01% apatite) to account for the excess LREE abundances, with little effect on the HREE budgets of the xenoliths.

The $^{143}Nd/^{144}Nd_{(0.1Ga)}$ (0.51249-0.51276) isotopic compositions of the Nikos peridotites are little variable and overlap those of the Nikos kimberlite at the time of sample transport. The low-temperature peridotites (<1100°C) that sample the shallow lithosphere are characterized by more radiogenic $^{176}Hf/^{177}Hf_{(0.1Ga)}$ (0.28296-0.28419) and Pb ($^{206}Pb/^{204}Pb_{(0.1Ga)}$=17.82-19.03), but lower $^{87}Sr/^{86}Sr_{(0.1Ga)}$ (0.7047-0.7066) isotopic ratios than those of the high-temperature peridotites (>1100°C; 0.28265-0.28333; 17.18-18.30; 0.7064-0.7085, respectively). Incompatible trace element compositions of the xenoliths confirm this depth stratification indicating that shallow and deep (>160 km) Somerset lithosphere are characterized by distinct chemical and isotopic characteristics.

The Lu-Hf isotope compositions of the low-temperature peridotites plot along a 2.8 Ga reference isochron, which is consistent with an interpretation that the shallow Somerset lithosphere stabilized in the Archean to depth of ~150 km. The deep lithospheric mantle, which is probably younger, does not share the same petrogenetic history and may contain recycled material (altered oceanic crust and sedimentary component?). The Hf isotope compositions for the shallow low-temperature peridotites

indicate that part of the lithosphere beneath the Canadian craton is characterized by more radiogenic Hf isotope signatures than estimates for “depleted” mantle.

Résumé

Les compositions isotopiques en Hf, Sr, Nd et Pb et les teneurs en éléments majeurs et traces (incluant les éléments des terres rares, REE) ont été analysées pour des xénolites de péridotite et de pyroxénite, des grenats et des clinopyroxènes provenant de la kimberlite Nikos sur l'Île Somerset (Arctique canadien). Le but était de mieux cerner la composition chimique et isotopique du manteau lithosphérique sous-continental dans la partie nord du craton canadien. Les péridotites sont de nature réfractaire et caractérisées par des olivines ayant de forts contenus en forstérite (moyenne=92.3) et un appauvrissement en éléments majeurs incompatibles (Fe, Al, Ca); cependant elles sont enrichies en éléments traces incompatibles (LILE) et en terres rares légères (LREE), tout en ayant des teneurs en terres rares lourdes (HREE) approximativement chondritiques. Des calculs de bilan de masse utilisant les abondances des REE dans le clinopyroxène et le grenat livrent des teneurs en LREE pour les xénolites (roches totales) qui sont significativement plus faibles (e.g. Nd ~50%) que les concentrations mesurées. Ces résultats suggèrent la présence d'une composante intersticielle riche en LREE reliée à la kimberlite (~1% de liquide kimberlitique et/ou ~0.01% d'apatite) pour expliquer l'excès en LREE, ce qui n'influencera pas les budgets des HREE.

Les rapports isotopiques de ^{143}Nd/^{144}Nd$_{(0.1Ga)}$ (0.51249-0.51276) des péridotites sont peu variables et identiques à ceux de la kimberlite au moment de la mise en place. Les péridotites de basse température (<1100°C), qui échantillonnent la partie supérieure de la lithosphère sous-continentale, sont caractérisées par des rapports ^{176}Hf/^{177}Hf$_{(0.1Ga)}$ (0.28296-0.28419) et Pb (^{206}Pb/^{204}Pb$_{(0.1Ga)}$=17.82-19.03) plus radiogéniques, mais des rapports ^{87}Sr/^{86}Sr$_{(0.1Ga)}$ (0.7047-0.7066) plus faibles, quand on les compare à ceux des péridotites de haute température (>1100°C; 0.28265-0.28333; 17.18-18.30; 0.7064-0.7085). La stratification en profondeur du manteau lithosphérique sous-continental de l'Île Somerset est également confirmée par les teneurs très distinctes des éléments traces incompatibles dans les xénolites de basse température versus ceux de haute température.

Les rapports isotopiques de Lu-Hf des péridotites de basse température tracent une isochrone de référence de 2.8 milliards d'années, suggérant que le manteau lithosphérique supérieur sous l'Île Somerset s'est stabilisé durant l'Archéen. La partie plus profonde de

ce manteau, qui est probablement plus jeune, n'est pas cogénétique du précédent et pourrait contenir du matériel recyclé (croûte océanique altérée et composante sédimentaire subductée?). Les rapports isotopiques de Hf des péridotites de basse température indiquent qu' une partie de la lithosphère sous-continentale du craton canadien est plus radiogénique que la compositions isotopique de Hf du manteau appauvri.

ACKNOWLEDGEMENTS

I am grateful for financial support in the form of a NSERC doctoral scholarship and NSERC research funds for isotope, major and trace element analyses made available from Dr. Don Francis' operating grant.

I am extremely appreciative of my supervisor's, Dr. Don Francis, constant advice and support, discussions on mantle xenoliths and kimberlites and editorial skills.

I thank Dr. Tariq Ahmedali and Glenna Keating for performing the whole rock X-ray fluorescence analyses and George Panagiotidis for producing thin sections for microprobe analysis. I would like to thank Glenn Poirier for assistance in obtaining the electron microprobe results. Fabien Rasselet is thanked for assistance in the field, handpicking separates of magmatic kimberlite for major and trace element and isotope analysis, and performing the CO_2 analyses with the assistance of Constance Guignard. I am grateful to Dr. Nobu Shimizu from Woods Hole Oceanographic Institution and Dr. Tony Simonetti for their help with ion microprobe analyses. I would also like to thank Dr. Janne Blichert-Toft for introducing me to the secrets of Lu-Hf chemistry.

I am especially appreciative for countless discussions and the help and support provided by my husband Tony. Most of all, I am grateful of Tony and Patrick for their encouragement, friendship and love.

Table of Contents

Extended Abstract ii
Résumé iv
Acknowledgements vi
Table of Contents vii
List of Tables ix
List of Figures x
List of Appendices xii
Preface xiii
Contributions of Authors xv

CHAPTER 1 1

Introduction 2
References 5

CHAPTER 2: Nature of the Mantle Roots Beneath the North American Craton: Mantle Xenolith Evidence From Somerset Island Kimberlites 8

Abstract 9
1. Introduction 11
2. Geology 12
3. Kimberlite Host 13
4. Mantle Xenoliths 14
5. Analytical Data 15
6. Discussion 20
7. Conclusions 26
Acknowledgements 26
References 28
Figure Captions 32
Tables 34
Figures 41

CHAPTER 3: Constraints on the Trace Element Composition of the Archean Mantle Root Beneath Somerset Island, Arctic Canada 53

Abstract 54
Introduction 55
Samples and Procedures 56
Analytical Data 59
Discussion 63
Conclusions 73
Acknowledgements 75
References 76
Figure Captions 82
Tables 85

Figures 94

CHAPTER 4: Sr-Nd-Pb Isotope Systematics of Mantle Xenoliths From Somerset Island Kimberlites: Evidence for Lithosphere Stratification Beneath Arctic Canada 107

Abstract 108
1. Introduction 110
2. Samples 111
3. Analytical Methods 115
4. Results 116
5. Discussion 121
6. Conclusions 129
Acknowledgements 130
References 132
Figure Captions 136
Tables 138
Figures 141

CHAPTER 5: Probing Archean Lithosphere Using the Lu-Hf Isotope Systematics of Peridotite Xenoliths Form Somerset Island Kimberlites, Canada 149

Abstract 150
1. Introduction 152
2. Samples 154
3. Analytical Methods 156
4. Results 160
5. Discussion 163
6. Conclusions 170
Acknowledgements 171
References 172
Figure Captions 177
Tables 179
Figures 181

CHAPTER 6: GENERAL CONCLUSIONS 189

APPENDIX A 192

APPENDIX B 199

List of Tables

Table

2-1 Major and trace element analyses of kimberlites 34
2-2 Representative analyses of bulk xenoliths 35
2-3 Representative analyses of olivines 36
2-4 Representative analyses of orthopyroxenes 37
2-5 Representative analyses of clinopyroxenes 38
2-6 Representative analyses of garnets 36
2-7 Temperature and pressure estimates 40
3-1 Major, trace and rare earth element analyses for kimberlites 85
3-2 Major element analyses and calculated mineral modes for bulk xenoliths 86
3-3 Trace and rare earth element analyses for bulk xenoliths 88
3-4 Major, trace and rare earth element analyses of clinopyroxenes 90
3-5 Major, trace and rare earth element analyses of garnets 91
3-6 Calculated rare earth element contents for bulk xenoliths 92
3-7 Rare earth element contents for calculated interstitial liquid 93
4-1 Rb, Sr, Sm and Nd abundances and Sr and Nd isotope compositions for Nikos kimberlites and xenoliths 138
4-2 Pb, U and Th abundances and Pb isotopic compositions for Nikos kimberlites and xenoliths 140
5-1 Lu-Hf isotope data for Nikos peridotites and kimberlite 179
5-2 Lu-Hf isotope data for Nikos garnets 180

List of Figures

Figure	Description	
2-1	Geological map of Somerset Island	41
2-2	Photomicrographs of xenoliths from the Nikos kimberlite showing a) coarse texture in peridotite, b) porphyroclastic texture in peridotite and c) coarse texture in pyroxenite	42
2-3	Histogram of whole rock magnesium numbers of peridotites, and high-Mg and low-Mg pyroxenites	45
2-4	Variations of major elements a) Al_2O_3, b) CaO, c) NiO with MgO (wt.%) of Nikos peridotites	46
2-5	Histogram of Al_2O_3 content (wt.%) of Nikos peridotites	47
2-6	Modal mineral proportions of Nikos xenoliths	48
2-7	Pressures and temperatures of last equilibration of the Nikos xenoliths ...	49
2-8	Modal olivine content (wt.%) versus $Mg^{\#}$ in olivine of the Nikos peridotites	50
2-9	Variation of FeO and SiO_2 (wt.%) of the Nikos peridotites	51
2-10	NiO (wt.%) in olivine versus modal orthopyroxene content (wt.%) of the Nikos peridotites	52
3-1	Geological map of Somerset Island	94
3-2	(a) Primitive mantle-normalized trace element and (b) chondrite-normalized rare earth element patterns for Nikos kimberlites	95
3-3	(a) Primitive mantle-normalized trace element and (b) chondrite-normalized rare earth element patterns for Nikos peridotites	96
3-4	(a) Primitive mantle-normalized trace element and (b) chondrite-normalized rare earth element patterns for Nikos pyroxenites	97
3-5	Chondrite-normalized rare earth element patterns for coexisting clinopyroxene and garnet in (a) high temperature and (b) low temperature Nikos peridotites	98
3-6	Chondrite-normalized rare earth element patterns for Nikos (a) clinopyroxene and (b) garnet compared to high and low temperature peridotites from the Kaapvaal and Siberian cratons	99
3-7	Rare earth element mass balance results for (a) high temperature peridotite NK1-7 and (b) low temperature peridotite NK1-4	100
3-8	Calculated chondrite-normalized rare earth element patterns for (a) high temperature peridotite NK1-7 and (b) low temperature peridotite NK1-4	101

3-9 Calculated chondrite-normalized rare earth element patterns for possible interstitial liquids in equilibrium with constituent mineral phases of the Nikos peridotites 102

3-10 Calculated chondrite-normalized rare earth element patterns for (a) high temperature peridotite NK1-7 and (b) low temperature peridotite NK1-4 before and after the addition of interstitial kimberlite liquid 103

3-11 Clinopyroxene-garnet partition coefficients in Nikos peridotites 104

3-12 Temperature dependence of clinopyroxene-garnet Ce partitioning in the Nikos peridotites 105

3-13 Depth distribution of (a) La and (b) Sr abundances in clinopyroxenes and (c) Zr and (d) Sr abundances (ppm) in garnets of low and high temperature peridotites 106

4-1 Geological map of Somerset Island 141

4-2 Initial Nd and Sr isotopic compositions for Nikos kimberlites 142

4-3 Initial Pb isotopic compositions for Nikos kimberlites 143

4-4 Nd and Sr isotopic compositions for Nikos xenoliths 100 Ma ago 144

4-5 Pb isotopic compositions for Nikos xenoliths 100 Ma ago 145

4-6 Nd and Sr isotopic compositions for Nikos clinopyroxenes and garnets 100 Ma ago 146

4-7 Sr and Pb isotopic compositions versus 1/Sr and 1/Pb for low and high-temperature Nikos peridotites 100 Ma ago 147

4-8 Sr isotopic compositions for Nikos clinopyroxenes plotted versus depth of last equilibration 148

5-1 Geological map of Somerset Island 181

5-2 ^{176}Lu/^{177}Hf versus (a) initial $\varepsilon_{Hf(T)}$ for Nikos kimberlites and (b) $\varepsilon_{Hf(0.1Ga)}$ for Nikos peridotites at the time of kimberlite emplacement 182

5-3 ^{176}Lu/^{177}Hf versus ^{176}Hf/^{177}Hf diagram for Nikos peridotites 183

5-4 ^{176}Lu/^{177}Hf versus ^{176}Hf/^{177}Hf diagram for Nikos garnets 184

5-5 Hf-Nd variation diagram for Nikos peridotites 100 Ma ago................. 185

5-6 Lu (ppm) versus Al_2O_3 contents (wt%) for Nikos peridotites 186

5-7 $\varepsilon_{Hf(0.1Ga)}$ versus ^{87}Sr/^{86}Sr$_{(0.1Ga)}$ for Nikos peridotites 187

5-8 Lu-Hf and Sm-Nd internal isochron “dates” versus temperature of last equilibration for low-temperature garnet-whole rock pairs 188

List of Appendices

A ^{180}Hf isotope tracer calibration 192
B Whole-rock and mineral compositions of Nikos peridotites 199

Preface

This thesis consists of four papers, three of which are already published or in press and the last of which has been submitted to Earth and Planetary Science Letters. Each chapter is self-contained with an abstract, introduction, analytical techniques, presentation of results, discussion and conclusions. References, tables and figures are placed at the end of each chapter and are in the format of the journal.

The extended abstract provides an integrated summary of the major and trace element and Hf, Sr, Nd and Pb isotope results for the Nikos peridotites and pyroxenites, constituent minerals and the host kimberlite. Chapter 1 presents an introduction, which states the rationale and objectives of the research and contains a comprehensive review of the literature. The major element chemistry of the xenoliths, mineral phases and kimberlites, modal mineralogy, and geothermobarometric calculations (i.e. temperature and pressure estimates) are presented in Chapter 2. The trace and rare earth element (REE) compositions of the Nikos xenoliths and constituent clinopyroxene and garnet are documented in Chapter 3, with a discussion of their implications for the incompatible element budgets of the Somerset lithosphere. The Sr, Nd and Pb isotope data for the Nikos xenoliths, minerals and host kimberlite are reported in Chapter 4 and shown to indicate an isotopic stratification with depth in the underlying Somerset lithosphere. The Lu-Hf isotope systematics of the peridotites and constituent garnets are discussed in Chapter 5 along with their constraints on the age of stabilization of the Somerset lithosphere, and the petrogenetic history of shallow and deep subcontinental mantle. To date, these results are the first Lu-Hf isotope data ever reported for a kimberlite-hosted mantle xenolith suite. Chapter 6 ends the thesis with a more general discussion of the implications of the results.

The following is an excerpt from the "Guidelines Concerning Thesis Preparation" as required by the Faculty of Graduate Studies and Research at McGill University:

»Candidates have the option of including, as part of the thesis, the text of one or more papers submitted, or to be submitted, for publication, or the clearly-duplicated text of one or more published papers. These must be bound together as an integral part of the thesis and connecting texts that provide logical bridges between the different papers are mandatory.

The thesis must conform to all other requirements of the "Guidelines Concerning Thesis Preparation" and should be in a literary form that is more than a mere collection of manuscripts published or to be published. The thesis must include: A table of contents, a general abstract in English and French, an introduction which clearly states the rational and objectives of the research, a comprehensive review of the literature, and a general conclusion and summary.

Additional material must be provided when appropriate (e.g., in appendices) and in sufficient detail to allow a clear and precise judgement to be made of the importance and originality of the research reported in the thesis.

In the case of manuscripts co-authored by the candidate and others, the candidate is required to make an explicit statement in the thesis as to who contributed to such work and to what extent. The supervisor must attest to the accuracy of this statement at the doctoral oral defense. Since the task of the examiners is made more difficult in these cases, it is in the candidate's interest to clearly specify the responsibilities of all the authors of the co-authored papers.«

Contributions of Authors

During 1997 to 2001, I obtained the Hf, Sr, Nd and Pb whole rock and Hf, Sr and Nd mineral isotope data, which included sample preparation and analysis by thermal ionization (TIMS) and multicollector inductively coupled plasma mass spectrometry (MC-ICP-MS) using the Micromass IsoProbe at GEOTOP-UQAM-McGill. For Lu-Hf isotope analysis, the chemical procedure for the separation of Lu and Hf was set up by myself in collaboration with Tony Simonetti. This involved the calibration of a ^{180}Hf tracer in order to obtain high-precision Hf concentration determinations (see Appendix A). For my thesis work, I acquired the ability to conduct electron microprobe analysis and obtained the major element compositions of constituent peridotite minerals (i.e. olivine, orthopyroxene, clinopyroxene, garnet) for all xenolith samples (n=55) at McGill University. I have also carried out ion microprobe analyses with the assistance of Dr. Nobu Shimizu at Woods Hole Oceanographic Institution, an analytical technique capable of measuring the trace element and REE abundances in clinopyroxene and garnet. The major element X-ray fluorescence analyses were obtained by Dr. Tariq Ahmedali and Glenna Keating at McGill University and the trace element ICP-MS analyses at the CRPG (Nancy), France and Université de Montréal. The thesis author, Stefanie Schmidberger, is responsible for the preparation and writing of the four scientific manuscripts and acknowledges the critical reviews of the co-authors Don Francis, Tony Simonetti and Clément Gariépy. Interpretations of the analytical data are the result of numerous discussions with, and input from the various co-authors.

The current status of the papers contained in this thesis is as follows:

Chapter 2: PUBLISHED. Schmidberger S. S. and Francis D. (1999) Nature of the mantle roots beneath the North American craton: Mantle xenolith evidence from Somerset Island kimberlites. *Lithos* **48**, 195-216.

Chapter 3: PUBLISHED. Schmidberger S. S. and Francis D. (2001) Constraints on the trace element composition of the Archean mantle root beneath Somerset Island, Arctic Canada. *J. Petrol.* **42**, 1095-1117.

Chapter 4: PUBLISHED. Schmidberger S. S., Simonetti A. and Francis D. (2001) Sr-Nd-Pb isotope systematics of mantle xenoliths from Somerset Island kimberlites: Evidence for lithosphere stratification beneath Arctic Canada. *Geochim. Cosmochim. Acta.* **65**, 4243-4255.

Chapter 5: Schmidberger S. S., Simonetti A., Francis D. and Gariépy C. Probing Archean lithosphere using the Lu-Hf isotope systematics of peridotite xenoliths from Somerset Island kimberlites, Canada. SUBMITTED TO: *Earth Planet. Sci. Lett.*

CHAPTER 1

Introduction

Archean cratons are underlain by cold, refractory mantle roots (e.g.; Nixon et al., 1981; Boyd and Mertzman, 1987) that extend to depths greater than 200 km (Jordan, 1988; Grand, 1994). The low density of the subcratonic mantle, which is thought to be the residue of extensive partial melting (e.g.; Boyd, 1989; Herzberg, 1993, Walter, 1998), can explain its long-term stability and isolation from the convecting asthenosphere (Jordan, 1978; Pollack, 1986; Shapiro et al., 1999). Peridotite xenoliths that are sampled by kimberlites and alkali basalts are a unique window into the subcratonic mantle and provide invaluable insights into its chemical composition (e.g.; Menzies, 1990). Many of these peridotites are strongly depleted in incompatible major elements such as Fe, Al and Ca and have higher mg-numbers (mg-number=Mg/[Mg+Fe] >0.92) than peridotites that sample oceanic or post-Archean lithospheric mantle (e.g.; Nixon, 1987; Boyd, 1989; Herzberg, 1993) and fertile mantle compositions such as pyrolite or primitive mantle (mg-numbers=0.88-0.92; Ringwood, 1975; McDonough, 1990). Experimental results at high pressure show that extensive melting of peridotite produces picritic to komatiitic melts and a residue characterized by highly refractory major element compositions (e.g.; Takahashi and Scarfe, 1985; Baker and Stolper, 1994). Investigations of mantle xenolith suites from the South African Kaapvaal and the Siberian cratons, which dominate the available dataset, have indicated that the subcratonic lithosphere could be characterized by low olivine/orthopyroxene (avg. orthopyroxene >20 wt.%) and low Mg/Si (1.1-1.5) ratios compared to that beneath oceanic terranes (e.g.; Boyd et al., 1997; Griffin et al., 1999). The most extreme orthopyroxene-rich mineralogies, however, cannot be explained by single-stage melt extraction from fertile mantle and require that either post-formational processes modified the composition of the lithosphere (e.g.; Kelemen et al. 1992; Boyd et al., 1997), or that parts of the mantle are significantly more silica-rich compared to primitive mantle models (Herzberg, 1993). Samples of the lithospheric mantle under other Archean cratons (e.g.; Canadian craton) are still rare, and the chemical composition and evolution of the deep cratonic mantle roots have yet to be clearly established.

Determining the age of the subcontinental lithosphere is important in order to constrain its stabilization history and evolution, and its role in the formation of the Archean cratons. The isotopic diversity found in continental basalts, and to a lesser extent in cratonic peridotite xenoliths (Zindler and Hart, 1986 and references therein), first suggested the antiquity and long-term stability of the deep subcontinental mantle roots (Brooks et al., 1976; Pearson, 1999). These peridotite xenoliths are frequently enriched in incompatible trace elements such as large ion lithophile elements (LILE) and light rare earth elements (LREE) relative to compositions for primitive mantle and chondrites (McDonough and Sun, 1995) suggesting that the subcontinental lithosphere has been infiltrated by small volume metasomatic melts or fluids over time (Erlank et al., 1987; Menzies et al., 1987; McDonough, 1990; Shimizu, 1999). Dating these peridotites using the conventional isotope techniques such as Rb-Sr or Sm-Nd is thus difficult, since they are highly susceptible to metasomatic alteration of the whole-rock trace element abundances and isotopic compositions (Pearson, 1999). Re-Os systematics appear to be less affected by metasomatism and have provided valuable age constraints for the subcratonic mantle (Pearson, 1999). Re depletion ages range from 3.5 to 2.7 Ga for the lithosphere beneath South Africa, Siberia and North America (Carlson and Irving, 1994;

Pearson et al., 1995a,b; Irvine et al., 1999), and indicate that these cratonic mantle roots stabilized in the Archean.

The Lu-Hf isotopic system is characterized by both refractory and relatively immobile elements that are hosted by silicate minerals (Bedini and Bodinier, 1999). The distinct chemical properties (i.e. different mineral-melt partition coefficient, e.g.; Hart and Dunn, 1993; Fujimaki et al., 1984) of the parent (Lu) and daughter (Hf) elements in the presence of mineral phases such as garnet and zircon result in their fractionation during igneous processes, indicating an important potential for the Lu-Hf system in geochronology and tracing geological processes (e.g.; Duchêne et al., 1997; Blichert-Toft and Albarède, 1997; Blichert-Toft et al., 1997; Vervoort and Blichert-Toft, 1999; Scherer et al., 2000).

This thesis focuses on the investigation of the Hf, Sr, Nd and Pb isotope systematics and major, trace and rare earth element (REE) compositions of a suite of peridotite and pyroxenite xenoliths from the Cretaceous (100 Ma) Nikos kimberlite on Somerset Island in the Canadian Arctic (NWT; Heaman, 1989; Smith et al., 1989; Pell, 1993). The modal mineralogy and major element compositions of the xenoliths provide constraints on the chemical nature of the lithosphere beneath the Canadian craton and enable a comparison with data for South African, Siberian and other Canadian xenolith suites. Incompatible trace element abundances of peridotite minerals (i.e. clinopyroxene and garnet) and whole-rock compositions are used to model the trace element budgets of the Somerset lithosphere. The Hf, Sr, Nd and Pb isotopic compositions of the Nikos xenoliths and kimberlite provide insight into the isotopic stratification of the subcratonic lithosphere with depth and enable to evaluate petrogenetic models for the shallow and deep subcratonic mantle. The Lu-Hf isotope systematics of the Nikos peridotites provide information on the age of stabilization of the Somerset lithosphere.

References

Baker M. B. and Stolper E. M. (1994) Determining the composition of high-pressure mantle melts using diamond aggregates. *Geochim. Cosmochim. Acta* **58**, 2811-2827.

Bedini R. M. and Bodinier J.-L. (1999) Distribution of incompatible trace elements between the constituents of spinel peridotite xenoliths: ICP-MS data from the East African Rift. *Geochim. Cosmochim. Acta* **63**, 3883-3900.

Blichert-Toft J. and Albarède F. (1997) The Lu-Hf isotope geochemistry of chondrites and the evolution of the mantle-crust system. *Earth Planet. Sci. Lett.* **148**, 243-258.

Blichert-Toft J., Chauvel C. and Albarède F. (1997) Separation of Hf and Lu for high-precision isotope analysis of rock samples by magnetic sector-multiple collector ICP-MS. *Contrib. Mineral. Petrol.* **127**, 248-260.

Brooks C., James D. E. and Hart S. R. (1976) Ancient lithosphere: its role in young continental volcanism. *Science* **139**, 1086-1094.

Boyd F. R. (1989) Compositional distinction between oceanic and cratonic lithosphere. *Earth Planet. Sci. Lett.* **96**, 15-26.

Boyd F. R. and Mertzman S. A. (1987) Composition and structure of the Kaapvaal lithosphere, southern Africa. In *Magmatic processes: physiochemical principles* (ed. B. O. Mysen). Geochem. Soc. Spec. Publ. pp. 13-24.

Boyd F. R., Pokhilenko N. P., Pearson D. G., Mertzman S. A., Sobolev N. V. and Finger L. W. (1997) Composition of the Siberian cratonic mantle: evidence from Udachnaya peridotite xenoliths. *Contrib. Mineral. Petrol.* **128**, 228-246.

Carlson R. W. and Irving A. J. (1994) Depletion and enrichment history of subcontinental lithospheric mantle: Os, Sr, Nd and Pb evidence for xenoliths from the Wyoming Craton. *Earth Planet. Sci. Lett.* **126**, 457-472.

J. Dalmasso, G. Barci-Funel, G.J. Ardisson, Reinvestigation of the decay of the long-lived odd-odd ^{176}Lu nucleus, Appl. Radiat. Isot. 43 (1992) 69-76

Duchêne S., Blichert-Toft J., Luais B., Télouk P., Lardeaux J.-M. and Albarède F. (1997) The Lu-Hf dating of garnets and the ages of the Alpine high-pressure metamorphism. *Nature* **387**, 586-589.

Erlank A. J., Waters F. G., Hawkesworth C. J., Haggerty S. E., Allsopp H. L., Rickard R. S. and Menzies M. A. (1987) Evidence for mantle metasomatism in peridotite nodules from the Kimberley pipes, South Africa. In *Mantle metasomatism* (eds. M. A. Menzies and C. J. Hawkesworth). Academic Press, London. pp. 221-311.

Fujimaki H., Tatsumoto M. and Aoki K. I. (1984) Partition coefficients of Hf, Zr, and REE between phenocrysts and groundmasses. *J. Geophys. Res.* **89**, B662-B672.

Grand S. P. (1994) Mantle shear structure beneath the Americas and surrounding oceans. *J. Geophys. Res.* **99**, 11.591-11.621.

Griffin W. L., O'Reilly S. Y. and Ryan C. G. (1999) The composition and origin of subcontinental lithospheric mantle. In *Mantle petrology: field observations and high pressure experimentation* (eds. Y. Fei, C. M. Bertka and B. O. Mysen). Geochem. Soc. Spec. Publ. 6. pp. 13-45.

Hart S. R. and Dunn T. (1993) Experimental clinopyroxene-melt partitioning of 24 trace elements. *Contrib. Mineral. Petrol.* **113**, 1-8.

Heaman L. H. (1989) The nature of the subcontinental mantle from Sr-Nd-Pb isotopic studies on kimberlite perovskite. *Earth Planet. Sci. Lett.* **92**, 323-334.

Herzberg C. T. (1993) Lithosphere peridotites of the Kaapvaal craton. *Earth Planet. Sci. Lett.* **120**, 13-29.

Irvine G. J., Kopylova M. G., Carlson R. W., Pearson D. G., Shirey S. B. and Kjarsgaard B. A. (1999) Age of the lithospheric mantle beneath and around the Slave craton: a Rhenium-Osmium isotopic study of peridotite xenoliths from the Jericho and Somerset Island kimberlites. *Ninth Annual V. M. Goldschmidt Conference*. LPI Contribution No. 971, 134-135.

Jordan T. H. (1978) Composition and development of the continental tectosphere. *Nature* **274**, 544-548.

Jordan T. H. (1988) Structure and formation of the continental tectosphere. *J. Petrol.*, Spec. Lithosphere Issue, 11-37.

Kelemen P. B., Dick H. J. B. and Quick J. E. (1992) Formation of harzburgite by pervasive melt/rock reaction in the upper mantle. *Nature* **358**, 635-641.

McDonough W. F. (1990) Constraints on the composition of the continental lithospheric mantle. *Earth Planet. Sci. Lett.* **101**, 1-18.

McDonough W. F. and Sun S. S. (1995) The composition of the earth. *Chem. Geol.* **120**, 223-253

Menzies M. A. (1990) Archean, Proterozoic, and Phanerozoic lithospheres. In *Continental mantle* (ed. M. A. Menzies). Oxford Univ. Press, Oxford. pp. 67-86.

Menzies M. A., Rogers N., Tindle A. and Hawkesworth C. J. (1987) Metasomatic and enrichment processes in lithospheric peridotites, an effect of asthenosphere-lithosphere interaction. In *Mantle metasomatism* (eds. M. A. Menzies and C. J. Hawkesworth). Academic Press, London. pp. 313-361.

Nixon P. H. (1987) Kimberlitic xenoliths and their cratonic setting. In *Mantle Xenoliths* (ed. P. H. Nixon). John Wiley & Sons, Chichester. pp. 215-239.

Nixon P. H., Rogers N. W., Gibso, I. L. and Grey A. (1981) Depleted and fertile mantle xenoliths from southern African kimberlites. *Annu. Rev. Earth Planet. Sci.* **9**, 285-309.

Pearson D. G. (1999) The age of continental roots. *Lithos* **48**, 171-194.

Pearson D. G., Carlson R. W., Shirey S. B., Boyd F. R. and Nixon P. H. (1995a) Stabilisation of Archean lithospheric mantle: a Re-Os isotope study of peridotite xenoliths from the Kaapvaal craton. *Earth Planet. Sci. Lett.* **134**, 341-357.

Pearson D. G., Shirey S. B., Carlson R. W., Boyd F. R., Pokhilenko N. P. and Shimizu N. (1995b) Re-Os, Sm-Nd, and Rb-Sr isotope evidence for thick Archean lithospheric mantle beneath the Siberian craton modified by multistage metasomatism. *Geochim. Cosmochim. Acta* **59**, 959-977.

Pell J. (1993) New kimberlite discoveries on Somerset Island. In *Exploration Overview 1993*. NWT Geology Division, Department of Indian and Northern Affairs, Yellowknife. pp. 47.

Pollack H. N. (1986) Cratonization and thermal evolution of the mantle. *Earth Planet. Sci. Lett.* **80**, 175-182.

Ringwood A. E. (1975) *Composition and petrology of the Earth's mantle*. McGraw-Hill, New York, pp.618.

Scherer E. E., Cameron K. L. and Blichert-Toft J. (2000) Lu-Hf garnet geochronology: Closure temperature relative to the Sm-Nd system and the effects of trace mineral inclusions. *Geochim. Cosmochim. Acta* **64**, 3413-3432.

Shapiro S. S., Hager B. H. and Jordan T. H. (1999) Stability and dynamics of the continental tectosphere. *Lithos* **48**, 115-133.

Shimizu N. (1999) Young geochemical features in cratonic peridotites from Southern Africa and Siberia. In *Mantle petrology: field observations and high pressure experimentation* (eds. Y. Fei, C. M. Bertka and B. O. Mysen). Geochem. Soc. Spec. Publ. 6. pp. 47-55.

Smith C. B., Allsopp H. L., Garvie O. G., Kramers J. D., Jackson P. F. S. and Clement C. R. (1989) Note on the U-Pb perovskite method for dating kimberlites: examples from the Wesselton and DeBeers mines, South Africa, and Somerset Island, Canada. *Chem. Geol. (Isot. Sect.)* **79**, 137-145.

Takahashi E. and Scarfe C. M. (1985) Melting of peridotite to 14 GPa and the genesis of komatiite. *Nature* **315**, 566-568.

Vervoort J. D. and Blichert-Toft J. (1999) Evolution of the depleted mantle: Hf isotope evidence from juvenile rocks through time. *Geochim. Cosmochim. Acta* **63**, 533-556.

Walter M. J. (1998) Melting of garnet peridotite and the origin of komatiite and depleted lithosphere. *J. Petrol.* **39**, 29-60.

Zindler A. and Hart S. R. (1986) Chemical Geodynamics. *Ann. Rev. Earth Planet. Sci.* **14**, 493-571.

CHAPTER 2

Nature of the mantle roots beneath the North American craton: mantle xenolith evidence from Somerset Island kimberlites

Abstract

The recently discovered Nikos kimberlite on Somerset Island, in the Canadian Arctic, hosts an unusually well preserved suite of mantle xenoliths dominated by garnet-peridotite (lherzolite, harzburgite, dunite) showing coarse and porphyroclastic textures, with minor garnet-pyroxenite. The whole rock and mineral data for fifty-four Nikos xenoliths indicate a highly refractory underlying mantle with high olivine forsterite contents (ave. Fo = 92.3) and moderate to high olivine abundances (ave. 80 wt.%). These characteristics are similar to those reported for peridotites from the Archean Kaapvaal and Siberian cratons (ave. olivine Fo = 92.5), but are clearly distinct from the trend defined by oceanic peridotites and mantle xenoliths in alkaline basalts and kimberlites from post-Archean continental terranes (ave. olivine Fo = 91.0). The Nikos xenoliths yield pressures and temperatures of last equilibration between 20 to 55 kb and 650 to 1300 °C, and a number of the peridotite nodules appear to have equilibrated in the diamond stability field. The pressure and temperature data define a conductive paleogeotherm corresponding to a surface heat flow of 44 mW/m^2. Paleogeotherms based on xenolith data from the central Slave province of the Canadian craton require a lower surface heat flow (~40 mW/m^2) indicating a cooler geothermal regime than that beneath the Canadian Arctic. A large number of kimberlite-hosted peridotites from the Kaapvaal craton in South Africa and parts of the Siberian craton are characterized by high orthopyroxene contents (ave. Kaapvaal 32 wt.%, Siberia 20 wt.%). The calculated modal mineral assemblages for the Nikos peridotites show moderate to low contents of orthopyroxene (ave. 12 wt.%), indicating that the orthopyroxene-rich mineralogy characteristic of the

Kaapvaal and Siberian cratons is not a feature of the cratonic upper mantle beneath Somerset Island.

Keywords: Canadian craton, kimberlite, mantle roots, mantle xenolith, peridotite, Somerset Island

1. Introduction

Global seismic tomography has shown that cold mantle roots with high seismic velocities underlie most Archean cratons to depths of at least 350 to 400 km (Jordan, 1988; Grand, 1994). Kimberlite-hosted mantle xenoliths are the only direct samples of these mantle roots beneath Archean cratonic areas and thus provide constraints on their composition and structure. Studies of such xenoliths in kimberlites from South Africa have shown the highly refractory nature of the mantle roots beneath the Archean Kaapvaal craton, with high olivine forsterite contents (Mg/(Mg+Fe) greater than 0.91; e.g. Cox et al, 1973; Nixon et al., 1981; Boyd, 1987). A large number of these mantle nodules are characterized by high modal orthopyroxene (up to 45 wt.%; Boyd and Canil, 1997) and low Mg/Si ratios (Boyd et al., 1997). The occurrence of orthopyroxene-rich mineral assemblages has also been reported for the Siberian craton (ave. Opx = 20 wt.%; Boyd et al., 1997). These compositional characteristics indicate that the deep-seated mantle roots of Archean cratons are chemically distinct from the upper mantle beneath oceanic and post-Archean crustal terranes (Boyd, 1989; Boyd et al., 1997; Shi et al., 1998). Whether the orthopyroxene-rich character reported for the mantle roots beneath the Kaapvaal and Siberian cratons is characteristic of cratonic mantle roots in general, however, has yet to be established.

In this paper, we present geochemical data for a suite of mantle xenoliths from the Nikos kimberlite on Somerset Island in the Canadian Arctic. Mineral chemistry and modal mineral analysis provide constraints on the nature of the mantle roots beneath the Canadian craton and enable a comparison with the compositional characteristics reported for the Archean Kaapvaal and Siberian cratons.

2. Geology

Somerset Island is part of the Innuitian tectonic province on the northern margin of the North American continent (Trettin et al, 1972). The local stratigraphy comprises middle Proterozoic to early Paleozoic sedimentary sequences that overlie the crystalline Precambrian basement of the Boothia Uplift (Steward, 1987). The Precambrian basement represents a northward salient of the Canadian shield that was deformed and faulted in the late Proterozoic to early Paleozoic, possibly related to compression associated with the Caledonian Orogeny in northern Europe and Greenland (Okulitch and Trettin, 1991). Granulite facies gneisses from the crystalline basement of the Boothia Uplift yield zircon dates between 2.5 and 2.2 Ga for their protoliths, while Sm-Nd model ages of 3.0 to 2.2 Ga suggest the presence of reworked Archean crustal material in these gneisses (Frisch and Hunt, 1993).

Other kimberlite occurrences on Somerset Island and their mantle xenoliths have been previously described (e.g. Mitchell, 1977; Jago and Mitchell, 1987; Fig. 1). The kimberlite pipes were emplaced during the Cretaceous along a major fault system related to the development of the Boothia Uplift (Mitchell, 1975). U-Pb dates on perovskite indicate kimberlite formation ages between 88 and 105 Ma (Heaman, 1989; Smith et al., 1989). Kimberlite emplacement coincides with major compressive deformation in the southeastern Arctic Islands induced by rifting that preceded sea-floor spreading in the Labrador Sea and Baffin Bay and the associated rotation of Greenland away from the North American continent that began in the early Cretaceous (Okulitch and Trettin, 1991). The timing of kimberlite emplacement on Somerset Island coincides with a world wide period of kimberlite activity in the Cretaceous (Nixon, 1987).

3. Kimberlite host

Previous field work and petrographic studies have shown that the majority of the Somerset kimberlites are brecciated diatremes or hypabyssal root zones (Mitchell and Meyer, 1980), consisting of fragments of kimberlite host, country rock, and mantle-derived xenocrysts. Establishing the compositions of the liquids for such kimberlites is problematic because of the difficulty of accounting for the country rocks and xenocrysts present in the kimberlite breccia. Magmatic kimberlite, containing less than 15 vol% of clasts larger than 4 mm, is rare on Somerset Island (Mitchell and Meyer, 1980; Mitchell, 1986).

The recently discovered Nikos kimberlite (Pell, 1993) outcrops along a steep cliff on the eastern coast of Somerset Island (73°28'N and 90°58'W; Fig. 1) and consists of three individual pipes that were sampled during the summer of 1996. Petrographic observations of the kimberlite samples indicate that one of these pipes (NK3) is characterized by a non-brecciated, magmatic texture. The magmatic kimberlite exhibits a porphyritic microcrystalline texture containing phenocrysts of olivine, phlogopite, and spinel in a very fine-grained carbonate-rich matrix. Two generations of olivine can be identified, rounded olivine phenocrysts (>1 mm) that most probably crystallized prior to the intrusion of the kimberlite and small euhedral to subhedral olivines (<1 mm). Garnet megacrysts (up to 5 mm) may represent xenocrysts derived by fragmentation of garnet peridotite xenoliths or be a liquidus phase at high pressure in the kimberlite magma (Mitchell, 1978; Mitchell and Meyer, 1980). The microcrystalline groundmass consists of calcite, serpentine, perovskite, and apatite. Calcite occurs as aggregates of tabular euhedral crystals or as sub-parallel laths, which are deflected around large olivine crystals, indicating their primary magmatic nature. Serpentine occurs as spherical microcrystalline segregations and as an alteration product of olivine marginally replacing these phenocrysts.

The whole rock analyses of kimberlite NK3 (n = 5) indicate an extremely carbonate rich composition, with $CaCO_3$ contents between 27 to 39 wt.% (ave. 31 wt.%), low SiO_2 abundances (20-25 wt.%), and a strong enrichment in incompatible trace element contents (Ba = 2200-3000 ppm; Sr = 1100-2200 ppm; Table 1). The high carbonate contents of the kimberlitic liquid indicate compositions intermediate between kimberlite (ave. $CaCO_3$ = 14 wt.%; Mitchell, 1986; Ringwood et al., 1992) and carbonatite ($CaCO_3$ = 50-80 wt.%; Woolley and Kempe, 1989), in keeping with recent experimental studies that have shown that a continuous spectrum of melt compositions from carbonatite to kimberlite can be produced by increasing degree of melting at pressures on the order of 60 kb (Dalton and Presnall, 1997).

4. Mantle xenoliths

The Nikos kimberlite hosts an unusually well preserved suite of large (10-20 cm) mantle-derived xenoliths, fifty-four of which were collected and analyzed in this study. The Nikos xenolith suite is dominated by garnet-peridotites (about 90%) comprising lherzolites, harzburgites, and lesser dunites. Also present are small numbers of pyroxene-rich nodules that are classified as garnet-pyroxenite rather than eclogite (Dawson, 1980; Hatton and Gurney, 1987) because of their low modal garnet (10-15 wt.%) and Al_2O_3 contents (5-10 wt.%), and the low jadeite component in clinopyroxene (Na_2O <1.6 wt.%).

The majority of the peridotite nodules have textures ranging from coarse equant to coarse tabular (Fig. 2a), based on the textural classification for mantle-derived rocks of Harte (1977). Large subhedral crystals of well preserved and relatively strain-free olivine (up to 10 mm) and orthopyroxene (ave. 2-5 mm) dominate the mineral assemblage. Clinopyroxene occurs as emerald green anhedral crystals with smooth grain boundaries (1-3 mm). Purple red garnet occurs as large porphyroclasts (ave. 5 mm) and is variably surrounded by kelyphitic rims of phlogopite and small spinel crystals. A small number of peridotite xenoliths exhibit porphyroclastic textures (<10%; Fig. 2b), characterized by large porphyroclasts (up to 10 mm) of strained olivine with undulose extinction surrounded by strain-free olivine neoblasts (0.1-0.5 mm) with tabular to polygonal equant habits. In these rocks, orthopyroxene occurs as porphyroclasts (2-5 mm) with irregular habit, and clinopyroxene and garnet are optically similar to those found in the coarse peridotites. The pyroxenite nodules show coarse equant textures (Fig. 2c) with large subhedral crystals (2-5 mm) of clinopyroxene and orthopyroxene, and smaller crystals (1 mm) of pale red garnet with a polygonal habit.

5. Analytical data

5.1. Whole rock chemistry

Whole rock analyses indicate that the Nikos peridotites are strongly depleted in fusible elements such as Fe, Ti, Ca, Al, and Na compared to estimated primitive mantle compositions (McDonough, 1990; Table 2). The whole rock magnesium numbers ($Mg^{\#}$ = Mg/(Mg+Fe); Fig. 3) for the lherzolites (ave. $Mg^{\#}$ = 0.91), harzburgites (ave. $Mg^{\#}$ = 0.92), and dunites (ave. $Mg^{\#}$ = 0.92) indicate a shift toward higher values for the harzburgites and dunites consistent with their larger degree of depletion. The Nikos nodules are significantly more refractory than oceanic peridotites and mantle xenoliths derived from beneath post-Archean continental crust ($Mg^{\#}$ = 0.89-0.91; Boyd, 1989). There is a good negative correlation between Al and Ca, and Mg (Fig. 4a, b), and a rough positive correlation between Ni and Mg (Fig. 4c). Compared to spinel-lherzolites from the

Canadian Cordillera (Shi et al., 1998), the late Phanerozoic orogenic belt that borders the western margin of the Canadian shield, the Nikos peridotites contain much lower Al_2O_3 contents (Fig. 5) and higher $Mg^{\#}$'s (Fig. 8). This indicates that the mantle roots beneath the Canadian shield are significantly more refractory than the lithopheric mantle beneath the Phanerozoic Cordillera. Spinel-harzburgites occurring in some of the Cordilleran xenolith suites from the southwestern Yukon and northern British Columbia, however, exhibit Al_2O_3 contents indistinguishable from those for the Nikos xenoliths (Fig. 5). These refractory harzburgites are associated with a seismically-detected hot mantle anomaly (Shi et al., 1998).

The pyroxenites, on the other hand, show a large variation in $Mg^{\#}$'s. The pyroxenites having high $Mg^{\#}$'s between 0.88 to 0.92 (high-Mg pyroxenites) overlap those of the peridotites. The $Mg^{\#}$'s for the other group of pyroxenites, however, are significantly lower ($Mg^{\#} = 0.84$-0.85; low-Mg pyroxenites), indicating that they are more Fe-rich than the coexisting peridotite xenoliths (Fig. 3).

5.2. Mineral chemistry

5.2.1. Olivine

Olivine in the peridotites is magnesium-rich and ranges in $Mg^{\#}$ from 0.91 to 0.93 (ave. 0.921) in the lherzolites and 0.92 to 0.93 (ave. 0.925) in the harzburgites, indicating higher values for the more refractory nodules (Table 3 for representative analyses). Individual olivine crystals do not exhibit chemical zoning and are homogeneous on thin section scale. There is no compositional difference between the olivines of the coarse and porphyroclastic peridotites. The Somerset olivine $Mg^{\#}$'s (ave. 0.923) are similar to those for peridotites from the Kaapvaal and Siberian cratons (ave. 0.925), but somewhat higher than the values reported for the Jericho (ave. 0.913; Kopylova et al., 1999) and the Torrie xenoliths (ave. 0.920; MacKenzie and Canil, 1999) from the Slave province of the Canadian craton. This suggests that parts of the mantle root beneath the center of the Slave Province are slightly less refractory than the mantle underlying the cratonic margin beneath Somerset Island. The NiO contents of the olivine (ave. 0.38 wt.%) in both the lherzolites and harzburgites are, however, similar to those reported for the Slave craton (Jericho xenoliths ave. 0.39 wt.%, Kopylova et al., 1999; Torrie xenoliths ave. 0.36 wt.%, MacKenzie and Canil, 1999).

5.2.2. Orthopyroxene

The $Mg^{\#}$'s of orthopyroxene in the peridotites range between 0.92 and 0.94 (ave. 0.930; Table 4), and are slightly higher than those of coexisting olivine suggesting equilibrated mineral parageneses (Gurney et al, 1979). The coarse and the porphyroclastic peridotites can not be distinguished in terms of their orthopyroxene $Mg^{\#}$'s. Orthopyroxenes in the pyroxenites exhibit a larger variation in $Mg^{\#}$'s, with an average value of 0.90 for high-Mg pyroxenites and 0.85 for low-Mg pyroxenites. Low Al_2O_3 abundances in both the peridotite and pyroxenite orthopyroxenes, ranging between 0.69 to 1.42 wt.%, reflect the presence of coexisting garnet.

5.2.3. Clinopyroxene

The clinopyroxenes are chromium-rich diopsides (Table 5) and exhibit $Mg^{\#}$'s in the peridotites (ave. 0.929) that are similar to those of the coexisting orthopyroxene (Table 4). The $Mg^{\#}$'s of high-Mg pyroxenite clinopyroxene (0.92-0.94) overlap those of the clinopyroxene in the peridotites, whereas $Mg^{\#}$'s of low-Mg pyroxenites (0.91) are considerably lower. The clinopyroxene Cr_2O_3 contents in the peridotites and the high-Mg pyroxenites range between 0.9 and 3.3 wt.% while the clinopyroxene of the low-Mg pyroxenites exhibits lower Cr_2O_3 abundances (0.4 wt.%). The chromium-diopsides of the

Nikos peridotites have slightly higher Cr_2O_3 contents than those reported for the Jericho (0.6-2.2 wt.%; Kopylova et al., 1999) and the Torrie xenoliths (0.3-1.5 wt.%; MacKenzie and Canil, 1999) in the Slave province.

5.2.4. Garnet

The garnet in the peridotites and the high-Mg pyroxenites is a chromium-pyrope with high magnesium contents and $Mg^{\#}$'s ranging between 0.79 and 0.86 (Table 6). $Mg^{\#}$'s of garnet in the low-Mg pyroxenites are significantly lower (0.64). The garnets exhibit no chemical zoning and are homogeneous on the scale of a thin section. The pyrope-rich garnet of the Nikos xenoliths has high Cr_2O_3 contents ranging between 1.5 and 7.7 wt.%, with the highest values observed in the harzburgites (4.0-7.7 wt.%). CaO abundances in garnet are low and indistinguishable in peridotites and pyroxenites (4.5-6.4 wt.%). The garnets in the peridotites and high-Mg pyroxenites would be classified as Group 9 garnets in the statistical classification of garnets of Dawson and Stephens (1975), in agreement with previous results for garnets in peridotite xenoliths from other Somerset Island kimberlites (Kjarsgaard and Peterson, 1992). The garnets in the low-Mg pyroxenites would be classified as Group 3 garnets because of their higher FeO and lower MgO contents.

5.3. Mineral modes

The modal mineral proportions of all Nikos xenoliths were calculated using a high-pressure peridotite norm calculation that determines the modal proportions of olivine, orthopyroxene, clinopyroxene, and garnet or spinel based on the whole rock compositions (Table 2). As a cross calibration, the normative mineralogy of twenty samples was calculated by reconstructing the bulk xenoliths from their mineral analyses using a least-squares technique. Both methods yield similar results, with modal mineral proportions differing by 3.0±1.8 wt.% (1 SD) for olivine, 3.0±2.5 wt.% (1 SD) for orthopyroxene, 1.3±0.6 wt.% (1 SD) for clinopyroxene, and 3.3±1.4 wt.% (1 SD) for garnet for all samples. The peridotite nodules range from garnet-lherzolites and garnet-harzburgites to garnet-dunites (ave. of all peridotites: olivine, 80 wt.%; orthopyroxene, 12 wt.%; chrome-diopside, 5 wt.%; pyrope-rich garnet, 3 wt.%). The majority of lherzolites fall rather close to the harzburgite field with only slightly more than 5 wt.% clinopyroxene (Fig. 6). These lherzolites exhibit major element compositions that are continuous with those of the harzburgites (Fig. 4a-c) and their division in two different rock types is somewhat artificial. The pyroxenites exhibit mineral assemblages consisting of clinopyroxene and orthopyroxene (ave. >80 wt.%), and garnet (ave. 12 wt.%). The high-Mg pyroxenites contain 5-10 wt.% olivine, while the low-Mg pyroxenites contain no olivine. Traces of spinel and minor amounts of phlogopite (less than 1 vol%) can be observed in individual xenolith samples.

5.4. Temperature and pressure

Temperatures and pressures of last equilibration were calculated for the Somerset xenoliths using geothermometers and barometers based on the compositions of coexisting pyroxenes and the solubility of Al_2O_3 in orthopyroxene in the presence of garnet. Temperatures were determined using the thermometers of Finnerty and Boyd (1987) and Brey and Köhler (1990). That of Finnerty and Boyd (1987) uses an empirical data fit to the miscibility gap between coexisting orthopyroxene and clinopyroxene and has been cross calibrated with the diamond/graphite transition (Kennedy and Kennedy, 1976) and the phlogopite stability field at upper mantle conditions. The thermometer of Brey and Köhler (1990) is based on a thermodynamic model for the solubility of orthopyroxene in clinopyroxene and was calibrated in reversed experiments between 900 to 1400 °C and 10 to 60 kb using natural fertile lherzolite compositions. These more recent experiments avoid Fe loss problems by using olivine crystals as sample containers.

MacGregor (1974) showed that the solubility of Al_2O_3 in orthopyroxene in the presence of garnet decreases with increasing pressure. Perkins and Newton (1980) used the same empirical method, but different thermodynamic parameters. The pressures calculated for the Nikos xenoliths using their calibration, however, were significantly lower than those obtained with the barometer of MacGregor (1974). The aluminum in enstatite (Al-in-en) barometer of MacGregor (1974) was evaluated by Finnerty and Boyd (1987) and found to yield results that are the most consistent with the diamond/graphite transition.

The pressures and temperatures for the Nikos xenoliths (Table 7) are shown in Figure 7. The method of Finnerty and Boyd (1987) combined with the Al-in-en barometer of MacGregor (1974) yields temperatures and pressures (Table 7) that are on average about 100 °C and 5 kb lower than the thermometer of Brey and Köhler (1990). The calculated pressures and temperatures, however, define similar trends in P-T space for both thermometers. In the following discussion, only the results using the thermometer of Brey and Köhler (1990) will be used.

6. Discussion

6.1. Paleogeothermal regime

The Nikos xenoliths record a wide range of equilibration conditions in the upper mantle, indicating that they were derived over a depth range between 55 and 170 km (Fig. 7). Although the pressure and temperature estimates for the harzburgites and lherzolites overlap, the harzburgites tend to plot at the higher end of the P-T array. This suggests that the upper part of the mantle sampled by the Nikos kimberlites tends to be more fertile than the lower portion of the mantle. A number of the peridotite samples plot to the right of the diamond/graphite transition (Kennedy and Kennedy, 1976) and appear to have equilibrated within the diamond stability field. The pyroxenites yield the lowest pressures and temperatures, indicating that they may be derived from shallower depths.

The calculated pressure and temperature data were fitted to a conductive geotherm using the approach of Pollack and Chapman (1977) assuming a lower crustal heat production of 0.25 $\mu W/m^3$ for the Canadian shield and a heat production of 10^{-2} $\mu W/m^3$ for the underlying mantle. The paleogeotherm for the Nikos xenoliths corresponds to a surface heat flow of 44 mW/m^2 at the time of last equilibration in the mantle (Fig. 7). These results are similar to recently reported pressure and temperature results for other xenoliths from the Nikos kimberlite (Zhao et al., 1997; Fig. 7) and those reported for the Batty Bay kimberlite, located 35 km to the southwest on Somerset Island (Kjarsgaard and Peterson, 1992). Boyd and Canil (1997) report a conductive geotherm of 40 mW/m^2 for a peridotite suite from the Grizzly kimberlite pipe in the Slave province, consistent with pressure and temperature conditions obtained for peridotites from the Jurassic Jericho kimberlite in the Slave province (Fig. 7; Kopylova et al., 1999). These results suggest that the geothermal gradient is cooler beneath the center of the Slave craton than towards its margin beneath Somerset Island, or that the thermal conditions have changed from the Jurassic to the Cretaceous. The latter possibility is supported by the higher present day heat flow measurements at Yellowknife in the Slave province (51 mW/m^2; Lewis and

Wang, 1992) and at Resolute Bay in the Canadian Arctic (52 mW/m^2; Lachenbruch, 1957).

Above ~1100 °C the pressure and temperature estimates for the Nikos peridotites deviate from the 44 mW/m^2 geotherm and are shifted towards slightly higher temperatures. This inflection is not correlated with any textural change in the xenoliths, as coarse peridotites are present at both the low and high temperature ends of the array. The inflection in the P-T array suggests the existence of a thermal boundary and may possibly represent the transition from lithospheric to asthenospheric mantle. This inflection would indicate a minimum thickness for the lithosphere of ~140 km beneath Somerset Island. The lithosphere boundary beneath the center of the Slave province has been estimated to be at depths between 195 and 200 km on the basis of both seismic studies (Bostock, 1997) and xenolith evidence (Boyd and Canil, 1997). The 140 km depth of the inflection in the Nikos P-T array may suggest that the transition from the base of the lithosphere shallows from the center of the Slave craton to its margin beneath Somerset Island. This interpretation is consistent with results for the Kaapvaal craton, where the lithosphere-asthenosphere transition has been reported to shallow away from the cratonic center (200 km) to its margins (~140 km; Boyd, 1987).

Porphyroclastic peridotites from the Kaapvaal craton in South Africa have been interpreted to represent asthenospheric mantle, whereas coarse peridotites are interpreted to represent lithospheric mantle (Boyd, 1987). Although a similar relationship apparently exists in the Jericho pipe of the Slave province (Kopylova et al., 1999), porphyroclastic xenoliths are rare in the Nikos pipe and do not give consistently higher P-T results. The lack of a correlation between texture and equilibration conditions observed for the Nikos peridotites is consistent with findings for the xenoliths from the Batty Bay kimberlite (Kjarsgaard and Peterson, 1992).

6.2. Nature of the Canadian mantle roots

Peridotite represents the dominant rock type (>90%) of the Nikos xenolith suite, indicating a peridotitic composition for Canadian mantle roots similar to that reported for the Kaapvaal and Siberian cratons (Nixon, 1987; Boyd et al, 1997). The chemical compositions of the Nikos peridotites are depleted in fusible elements compared to primitive mantle compositions (McDonough, 1990) and fertile spinel-lherzolites from beneath the Canadian Cordillera (Shi et al., 1998). The high olivine forsterite contents (ave. Fo = 92.3) and moderate to high modal abundances of olivine (ave. 80 wt.%) indicate the highly refractory nature of the Nikos peridotites and suggest that they represent the residues of large degree partial melting. The spectrum from lherzolite to harzburgite can be modeled using fractional melting equations based on Yb contents of the xenoliths. The results indicate an average of ~30% melt extraction from the most fertile lherzolite to refractory harzburgite.

The chemical signatures of the Nikos peridotites are similar to the compositions reported for the Archean Kaapvaal and Siberian cratons (ave. olivine Fo = 92.5; Boyd et al., 1997) and clearly distinct from the trend defined by peridotites from oceanic domains (ave. olivine Fo = 91.0; Boyd, 1989) and spinel-peridotites from the Canadian Cordillera (Shi et al., 1998) that represent the mantle beneath Phanerozoic accreted terranes along the western margin of the Canadian shield (Fig. 8). Spinel-harzburgites associated with a mantle thermal anomaly beneath the southwestern Yukon (Shi et al., 1998), however, have intermediate compositions with higher modal olivine and olivine forsterite contents compared to the more fertile spinel-lherzolites, and trend towards the more depleted compositions of the Nikos peridotites. These spinel-harzburgites were interpreted to represent the residue of ~20-25 % partial melting of lherzolite mantle (Francis, 1987; Shi et al., 1998).

Many peridotite xenoliths from the Kaapvaal craton are anomalously enriched in orthopyroxene, with average modal orthopyroxene contents of 32 wt.% (Boyd et al., 1997). Minor occurrences of such orthopyroxene-rich mineral assemblages have been reported from the Siberian craton (Boyd et al., 1997), however, these peridotites have an average orthopyroxene content of only 20 wt.% and are thus less enriched in orthopyroxene than the Kaapvaal xenoliths. This orthopyroxene-rich nature can not be attributed solely to the extraction of basaltic components from primitive mantle by extensive partial melting (Herzberg, 1993). Such processes would induce depletion in both clinopyroxene and orthopyroxene content, and a shift of the residual mineral assemblage to higher olivine, but lower orthopyroxene abundances. A recent experimental study on depleted cratonic harzburgite by Kinzler and Grove (1998), however, has shown that the majority of the orthopyroxene enriched mineral assemblages from the Kaapvaal and Siberian cratons can be produced by polybaric, near fractional melting of primitive mantle at >2 GPa. The most extreme orthopyroxene enriched peridotites, however, cannot be explained by such processes and these require that either parts of the mantle are significantly enriched in silica compared to primitive mantle models (Herzberg, 1993) or that post melt-extraction processes have modified the composition of the Kaapvaal mantle roots (e.g. Boyd et al., 1997: Kelemen et al., 1997). Igneous separation of orthopyroxene-rich cumulate layers or metamorphic segregation of the residual mantle into orthopyroxene-rich and olivine-rich layers have been proposed by Boyd et al. (1997) as possible explanations for the orthopyroxene-rich nature of cratonic mantle roots. Such processes would induce a negative correlation between Si and Fe, opposite to the trend observed in melting experiments on fertile garnet-peridotite (Hirose and Kushiro, 1993; Baker and Stolper, 1994). In the Nikos xenolith suite, however, a negative correlation between Si and Fe (Fig. 9) that has been reported for Siberian and Kaapvaal peridotites (Boyd et al., 1997) is not observed. Kelemen et al. (1997) interpreted a positive correlation between NiO in olivine and modal orthopyroxene contents in some cratonic mantle xenolith suites to be indicative of metasomatic infiltration of residual mantle by Fe-poor silicic melts, possibly originating from subducted oceanic lithosphere. This would induce the formation of orthopyroxene at the expense of olivine, resulting in increased NiO in the residual olivine associated with high orthopyroxene abundances. This trend between modal orthopyroxene and olivine NiO contents is not well developed in the Nikos peridotites (Fig. 10).

Compared to xenolith suites from the Kaapvaal and Siberian cratons, the Nikos peridotites are characterized by lower orthopyroxene abundances (ave. 12 wt.%). The chemical and modal signatures of the Nikos peridotites are similar to those recently reported for the Grizzly kimberlite peridotites in the Slave province (Boyd and Canil, 1997), which also have high magnesium numbers (ave. $Mg^{\#} = 0.927$), but mineral assemblages characterized by relatively low orthopyroxene (ave. ~11 wt.%; MacKenzie and Canil, 1999). The trend towards higher olivine and lower orthopyroxene abundances exhibited by the Nikos peridotites suggests an origin by large degree partial melting of primitive mantle compositions. This interpretation is supported by continuous trends in major element variations, in particular the negative correlation of MgO and Al_2O_3 (Fig. 4a), suggesting that the Nikos peridotites are related by partial melting. It is also consistent with an overall positive correlation between modal olivine abundance and olivine forsterite content (Fig. 8).

7. Conclusions

The Nikos peridotites define a hotter paleogeotherm than that reported for the mantle beneath the central Slave province. An inflection in the pressure and temperature array may indicate that the transition from lithospheric to asthenospheric mantle is shallower under Somerset Island (140 km) than under the center of the Slave craton (200 km).

The high forsterite contents associated with moderate to high olivine abundances of the Nikos peridotites are characteristic of peridotite xenolith suites derived from subcontinental mantle beneath Archean cratons. These characteristics clearly indicate that they are distinctly more refractory than oceanic peridotites and post-Archean mantle xenolith suites. The modal abundances of the Nikos xenoliths suggest that they formed by extensive degrees of partial melting of primitive mantle. However, the high orthopyroxene abundances that characterize the Kaapvaal craton and parts of the Siberian craton are not characteristic of the Nikos peridotite suite. More studies of mantle xenolith suites from other Archean cratons are needed to determine whether the orthopyroxene-rich mantle roots beneath the Kaapvaal craton are an exception, or a general feature of cratonic mantle roots.

Acknowledgements

We would like to thank Tariq Ahmedali for performing the bulk rock X-ray fluorescence analyses and Glenn Poirier for his help in obtaining the electron microprobe results. We also thank Fabien Rasselet for assistance in the field, hand picking separates of magmatic kimberlite for major and trace element analysis, and performing the CO_2

analyses with the assistance of Constance Guignard. Tony Simonetti is thanked for discussions and earlier revisions of the manuscript.

References

Baker, M.B. and Stolper, E.M., 1994. Determining the composition of high-pressure mantle melts using diamond aggregates. Geochim. Cosmochim. Acta, 58: 2811-2827.

Bostock, M.G., 1997. Anisotropic upper-mantle stratigraphy and architecture of the Slave craton. Nature, 390: 392-395.

Boyd, F.R., 1987. High- and low-temperature garnet peridotite xenoliths and their possible relation to the lithosphere-asthenosphere boundary beneath southern Africa. In: P. H. Nixon (Editor), Mantle Xenoliths. John Wiley & Sons, Chichester, pp. 403-412.

Boyd, F.R., 1989. Compositional distinction between oceanic and cratonic lithosphere. Earth Planet. Sci. Lett., 96: 15-26.

Boyd, F.R. and Canil, D., 1997. Peridotite xenoliths from the Slave craton, Northwest Territories. In: Seventh annual V.M. Goldschmidt Conference, Houston, 34-35.

Boyd, F.R. and Mertzman, S.A., 1987. Composition and structure of the Kaapvaal lithosphere, southern Africa. In: B. O. Mysen (Editor), Magmatic processes: physiochemical principles. Geochem. Soc. Spec. Publ., pp. 13-24.

Boyd, F.R., Pokhilenko, N.P., Pearson, D.G., Mertzman, S.A., Sobolev, N.V. and Finger, L.W., 1997. Composition of the Siberian cratonic mantle: evidence from Udachnaya peridotite xenoliths. Contrib. Mineral. Petrol., 128: 228-246.

Brey, G.P. and Köhler, T., 1990. Geothermobarometry in four-phase lherzolites II. New thermobarometers, and practical assessment of existing thermobarometers. J. Petrol., 31: 1353-1378.

Carswell, D.A., Clarke, D.B. and Mitchell, R.H., 1979. The petrology and geochemistry of ultramafic nodules from Pipe 200, northern Lesotho. In: F. R. Boyd and H. O. A. Meyer (Editors), Proceedings of the Second International Kimberlite Conference. AGU, Washington, pp. 127-144.

Cox, K.G., Gurney, J.J. and Harte, B., 1973. Xenoliths from the Matsoku pipe. In: P. H. Nixon (Editor), Lesotho Kimberlites. Lesotho National Development Corporation, Maseru, Lesotho, pp. 76-100.

Cox, K.G., Smith, M.R. and Beswetherick, S., 1987. Textural studies of garnet lherzolites: evidence of exsolution origin from high-temperature harzburgites. In: P. H. Nixon (Editor), Mantle Xenoliths. John Wiley & Sons, Chichester, pp. 537-550.

Dalton, J.A. and Presnall, D.C., 1997. Phase relations in the system $CaO-MgO-Al_2O_3-SiO_2-CO_2$ from 3.0 to 7.0 GPa: carbonatites, kimberlites and carbonatite-kimberlite relations. In: GAC/MAC annual meeting, Ottawa, A-34.

Danchin, F.R., 1979. Mineral and bulk chemistry of garnet lherzolite and garnet harzburgite from the Premier mine, South Africa. In: F. R. Boyd and H. O. A. Meyer (Editors), Proceedings of the Second International Kimberlite Conference. AGU, Washington, pp. 104-126.

Dawson, J.B., 1980. Kimberlites and their xenoliths. Springer-Verlag, Berlin, 252 pp.

Dawson, J.B. and Stephens, W.E., 1975. Statistical classification of garnets from kimberlite and associated xenoliths. J. Geol., 83: 589-607.

Finnerty, A.A. and Boyd, F.R., 1987. Thermobarometry for garnet peridotites: basis for the determination of thermal and compositional structure of the upper mantle. In: P. H. Nixon (Editor), Mantle Xenoliths. John Wiley & Sons, Chichester, pp. 381-402.

Francis, D., 1987. Mantle-melt interaction recorded in spinel lherzolite xenoliths from the Alligator Lake volcanic complex, Yukon, Canada. J. Petrol., 28: 569-597.

Frisch, T. and Hunt, P.A., 1993. Reconnaissance U-Pb geochronology of the crystalline core of the Boothia Uplift, District of Franklin, Northwest Territories. In: Radiogenic age and isotope studies: Report 7. Geological Survey of Canada, Paper, pp. 3-22.

Grand, S.P., 1994. Mantle shear structure beneath the Americas and surrounding oceans. J. Geophys. Res., 99: 11.591-11.621.

Gurney, J.J., Harris, J.W. and Rickard, R.S., 1979. Silicate and oxide inclusions in diamonds from the Finsch kimberlite pipe. In: F. R. Boyd and H. O. A. Meyer (Editors), Kimberlites, diatremes and diamonds: their geology and petrology and geochemistry. AGU, Washington, pp. 1-15.

Harte, B., 1977. Rock nomenclature with particular relation to deformation and recrystallization textures in olivine-bearing xenoliths. J. Geol., 85: 279-288.

Hatton, C.J. and Gurney, J.J., 1987. Roberts Victor eclogites and their relation to the mantle. In: P. H. Nixon (Editor), Mantle Xenoliths. John Wiley & Sons, Chichester, pp. 453-463.

Heaman, L.H., 1989. The nature of the subcontinental mantle from Sr-Nd-Pb isotopic studies on kimberlite perovskite. Earth Planet. Sci. Lett., 92: 323-334.

Herzberg, C.T., 1993. Lithosphere peridotites of the Kaapvaal craton. Earth Planet. Sci. Lett., 120: 13-29.

Hirose, K. and Kushiro, I., 1993. Partial melting of dry peridotites at high pressures: Determination of compositions of melts segregated from peridotite using aggregates of diamond. Earth Planet. Sci. Lett., 114: 477-489.

Jago, B.C. and Mitchell, R.H., 1987. Ultrabasic xenoliths from the Ham kimberlite, Somerset Island, Northwest Territories. Canadian Mineral., 25: 515-525.

Jordan, T.H., 1988. Structure and formation of the continental tectosphere. J. Petrol., Spec. Lithosphere Issue: 11-37.

Kelemen, P.B., Bernstein, S. and Hart, S.R., 1997. SiO_2 addition to cratonic mantle via melt/rock reaction above subduction zones. In: Workshop on Continental Roots, Harvard University and MIT.

Kennedy, C.S. and Kennedy, G.C., 1976. The equilibrium boundary between graphite and diamond. J. Geophys. Res., 81: 2467-2470.

Kinzler, R.J. and Grove, T.L., 1998. Origin of depleted cratonic harzburgite by deep fractional melt extraction and shallow olivine cumulate infusion. Proceedings of the Seventh International Kimberlite Conference: in press.

Kjarsgaard, B.A. and Peterson, T.D., 1992. Kimberlite-derived ultramafic xenoliths from the diamond stability field: a new Cretaceous geotherm for Somerset Island, Northwest Territories. In: Current Research, 1992-B. Geological Survey of Canada, pp. 1-6.

Kopylova, M.G., Russell, J.K. and Cookenboo, H., 1999. Petrology of peridotite and pyroxenite xenoliths from the Jericho kimberlite: implications for the thermal state of the mantle beneath the Slave craton, Northern Canada. J. Petrol. 40, 79-104.

Lachenbruch, A.H., 1957. Thermal effects of the ocean on permafrost. Geol. Soc. Am. Bull. 68: 1515-1529.

Lewis, T.J. and Wang, K., 1992. Influence of terrain on bedrock temperatures. Palaeogeography, Palaeoclimatology, Palaeoecology, 98: 87-100.

MacGregor, I.D., 1974. The system $MgO-Al_2O_3-SiO_2$: solubility of Al_2O_3 in enstatite for spinel and garnet peridotite compositions. American Mineralog., 59: 110-119.

MacKenzie, J.M. and Canil, D., 1999. Composition and thermal evolution of cratonic mantle beneath the central Archean Slave Province, NWT, Canada. Contrib. Mineral. Petrol. 134, 313-324.

McDonough, W.F., 1990. Constraints on the composition of the continental lithospheric mantle. Earth Planet. Sci. Lett., 101: 1-18.

Mitchell, R.H., 1975. Geology, magnetic expression, and structural control of the central Somerset Island kimberlites. Can. J. Earth Sci., 12: 757-764.

Mitchell, R.H., 1977. Ultramafic xenoliths from the Elwin Bay kimberlite: the first Canadian paleogeotherm. Can. J. Earth Sci., 14: 1202-1210.

Mitchell, R.H., 1978. Mineralogy of the Elwin Bay kimberlite, Somerset Island, N.W.T., Canada. American Mineralog., 63: 47-57.

Mitchell, R.H., 1986. Kimberlites: Mineralogy, Geochemistry, and Petrology. Plenum Press, New York, 442 pp.

Mitchell, R.H. and Meyer, H.O.A., 1980. Mineralogy of micaceous kimberlite from the Jos dyke, Somerset Island. Canadian Mineralog., 18: 241-250.

Nixon, P.H., 1987. Kimberlitic xenoliths and their cratonic setting. In: P. H. Nixon (Editor), Mantle Xenoliths. John Wiley & Sons, Chichester, pp. 215-239.

Nixon, P.H. and Boyd, F.R., 1973. Petrogenesis of the granular and sheared ultrabasic nodule suite in kimberlites. In: P. H. Nixon (Editor), Lesotho Kimberlites. Lesotho National Development Corporation, Maseru, Lesotho, pp. 48-56.

Nixon, P.H., Rogers, N.W., Gibson, I.L. and Grey, A., 1981. Depleted and fertile mantle xenoliths from southern African kimberlites. Annu. Rev. Earth Planet. Sci., 9: 285-309.

Okulitch, A.V. and Trettin, H.P., 1991. Late Cretaceous - Early Tertiary deformation, Artic Islands. In: H. P. Trettin (Editor), Geology of the Innuitian Orogen and Artic Platform of Canada and Greenland. Geological Survey of Canada, pp. 469-489.

Pell, J., 1993. New kimberlite discoveries on Somerset Island. In: Exploration Overview 1993, NWT Geology Division, Department of Indian and Northern Affairs, Yellowknife, 47 pp.

Perkins, D. and Newton, R.C., 1980. The compositions of coexisting pyroxenes and garnet in the system CaO-MgO-Al_2O_3-SiO_2 at 900^o -1100^o C and high pressures. Contrib. Mineral. Petrol., 75: 291-300.

Pollack, H.N. and Chapman, D.S., 1977. On the regional variation of heat flow, geotherms and lithospheric thickness. Tectonophysics, 38: 279-296.

Ringwood, A.E., Kesson, S.E., Hibberson, W. and Ware, N., 1992. Origin of kimberlites and related magmas. Earth Planet. Sci. Lett., 113: 521-538.

Shi, L., Francis, D., Ludden, J., Frederiksen, A. and Bostock, M., 1998. Xenolith evidence of lithospheric melting above anomalously hot upper mantle under the northern Canadian Cordillera. Contrib. Mineral. Petrol., 131: 39-53.

Smith, C.B., Allsopp, H.L., Garvie, O.G., Kramers, J.D., Jackson, P.F.S. and Clement, C.R., 1989. Note on the U-Pb perovskite method for dating kimberlites: examples from the Wesselton and DeBeers mines, South Africa, and Somerset Island, Canada. Chem. Geol. (Isotope Geos.), 79: 137-145.

Steward, W.D., 1987. Late Proterozoic to Early Tertiary stratigraphy of Somerset Island and northern Boothia Peninsula, District of Franklin. Geological Survey of Canada Paper, 83-26: 78 pp.

Trettin, H.P., Frisch, T.O., Sobczak, L.W., Weber, J.R., Niblett, E.R., Law, L.K., DeLaurier, I. and Witham, K., 1972. The Innuitian Province. In: R. A. Price and R. J. W. Douglas (Editors), Variations in tectonic styles in Canada. Geological Association of Canada, Special Paper, pp. 83-179.

Woolley, A.R. and Kempe, D.R.C., 1989. Carbonatites nomenclature, average chemical compositions, and elemental distribution. In: K. Bell (Editor), Carbonatites; genesis and evolution. Unwin Hyman Inc., London, pp. 1-14.

Zhao, D., Essene, E.J., Zhang, Y., Hall, C.M. and Wang, L., 1997. Newly discovered kimberlites and mantle xenoliths from Somerset Island and Brodeur Peninsula, Canada: Pressure, temperature, oxygen fugacity, volatile content and age. In: NWT Geology Division, Department of Indian and Northern Affairs, Yellowknife, pp. 1-105.

Figure Captions

Figure 2-1. Geological map of Somerset Island (after Steward, 1987) showing kimberlite locations. Legend: light gray, Paleozoic cover rocks; striped, Late Proterozoic cover rocks; dark gray, Precambrian basement; bold lines, normal faults.

Figure 2-2. Photomicrographs of xenoliths from the Nikos kimberlite showing a) coarse texture in peridotite, b) porphyroclastic texture in peridotite and c) coarse texture in pyroxenite. Upper photographs with plane polars, lower photographs with crossed polars.

Figure 2-3. Histogram of whole rock magnesium numbers ($Mg^{\#} = Mg/(Mg+Fe)$) of peridotites, and high-Mg and low-Mg pyroxenites.

Figure 2-4. Variations of major elements a) Al_2O_3, b) CaO, c) NiO with MgO (wt.%) of Nikos peridotites. Primitive mantle composition after McDonough (1990).

Figure 2-5. Histogram of Al_2O_3 content (wt.%) of Nikos peridotites compared to data for the bi-modal northern Cordilleran spinel-harzburgite and spinel-lherzolite suite and the uni-modal southern Cordilleran spinel-lherzolite suite (Shi et al., 1998). Primitive mantle composition after McDonough (1990).

Figure 2-6. Modal mineral proportions of Nikos xenoliths compared to data for kimberlite-hosted mantle xenoliths from the Kaapvaal craton in South Africa (Cox et al., 1973; Nixon and Boyd, 1973; Carswell et al., 1979; Danchin, 1979; Boyd and Mertzman, 1987; Cox et al., 1987). Primitive mantle composition after McDonough (1990).

Figure 2-7. Pressures and temperatures of last equilibration of the Nikos xenoliths using the thermometer of Brey and Köhler (1990) combined with the Al-in-en barometer of MacGregor (1974). Diamond/graphite transition after Kennedy and

Kennedy (1976). Model conductive geotherms representing a surface heat flow of 40 mW/m^2 and 44 mW/m^2 after Pollack and Chapman (1977). Data for peridotites from the Jericho kimberlite (Kopylova et al., 1999) in the Canadian Slave province and other xenolith data from the Nikos kimberlite on Somerset Island (Zhao et al., 1997) are shown for comparison.

Figure 2-8. Modal olivine content (wt.%) versus Mg$^\#$ in olivine of the Nikos peridotites. Field for the Kaapvaal and Siberian cratons (Boyd, 1989; Boyd et al., 1997) and data for the Canadian Cordillera (Shi et al., 1998; lherzolites, open circles; harzburgites, open triangles) are shown for comparison. Trend defined by oceanic peridotites after Boyd (1989).

Figure 2-9. Variation of FeO and SiO_2 (wt.%) of the Nikos peridotites indicating no correlation of these elements in the xenoliths.

Figure 2-10. NiO (wt.%) in olivine versus modal orthopyroxene content (wt.%) of the Nikos peridotites.

Table 2-1

Major and trace element analyses of kimberlites

The major and trace elements were analyzed by X-ray fluorescence analysis at McGill University with a Philips PW 2400 spectrometer. The major elements and Ba, V, Co, Cr, and Ni were analyzed on fused discs using a α-coefficient technique with an analytical precision of less than 0.06 wt.% (1 SD). Total Fe is given as FeO. Other trace elements were analyzed on pressed pellets using a Rh Kb Compton scatter matrix correction with an analytical precision of 5%.

Sample	NK3-K1	NK3-K2	NK3-K3	NK3-K4	NK3-K5
Rock	Kimberlite	Kimberlite	Kimberlite	Kimberlite	Kimberlite
Major elements in wt.%					
SiO_2	19.85	25.05	23.21	22.72	23.62
TiO_2	2.06	2.15	1.62	1.73	1.51
Al_2O_3	2.20	2.81	2.03	1.90	1.64
FeO	7.06	8.13	6.99	7.32	7.26
MnO	0.14	0.16	0.15	0.14	0.15
MgO	19.97	26.12	23.07	23.03	25.59
CaO	21.58	15.34	17.57	18.90	16.61
Na_2O	0.19	0.14	0.06	0.09	0.10
K_2O	1.00	0.66	0.55	0.30	0.59
P_2O_5	0.64	0.64	0.92	0.83	0.85
H_2O	1.43	5.00	5.07	8.55	0
CO_2	22.78	12.68	17.10	13.19	20.96
Total	98.90	98.88	98.35	98.71	98.88
$CaCO_3$	38.52	27.38	31.36	30.00	29.65
Trace elements in ppm					
Ba	2694	2231	2972	3007	2445
Rb	72	46	30	22	38
Sr	1299	1072	1647	2233	1418
Th	18.2	17.4	22.3	23.1	18.7
U	0	1.4	0	0	0
Zr	139	162	163	146	147
Nb	166	169	198	190	179
Y	9.3	11.3	11.8	9.5	10.4
Cr	1366	1586	1721	1526	1362
Ni	672	817	861	855	917
Co	52	64	59	64	65
V	153	151	136	140	126
Sc	28	16	15	19	23

Table 2-2
Representative analyses of bulk xenoliths
LOI: loss on ignition. Total Fe is given as FeO and Mg$^{\#}$=Mg/(Mg+Fe). Lherz: lherzolite, Harz: harzburgite, Pyrox: pyroxenite, porphyr: porphyroclastic. Modes were calculated using the whole rock compositions and a high-pressure peridotite norm recipe. Analytical procedure as in Table 2-1.

Sample	NK1-5	NK2-3	NK2-10	NK3-20	NK3-25	NK1-2	NK1-3	NK1-6	NK1-7	NK1-17	NK1-18	NK2-7	NK3-1	NK3-17
Rock	Lherz	Lherz	Lherz	Lherz	Lherz	Harz	Harz	Harz	Harz	Harz	Harz	Pyrox	Pyrox	Pyrox
Texture	coarse	coarse	coarse	coarse	coarse	coarse	coarse	coarse	porphyr	coarse	coarse	coarse	coarse	coarse
Major elements in wt.%.														
SiO_2	42.28	42.46	41.54	43.19	41.42	41.77	40.81	40.37	41.24	41.22	42.94	48.95	50.97	50.15
TiO_2	0.07	0.09	0.03	0.10	0.21	0.03	0.03	0.02	0.03	0.01	0.03	0.13	0.18	0.18
Al_2O_3	1.95	2.90	1.25	3.21	4.28	1.31	1.33	1.25	1.57	0.81	0.79	8.05	4.71	4.89
FeO	7.74	7.21	7.43	7.58	7.41	7.39	7.42	7.10	7.06	7.05	6.97	4.93	6.04	6.01
MnO	0.12	0.13	0.11	0.13	0.13	0.11	0.11	0.10	0.10	0.11	0.10	0.18	0.15	0.15
MgO	41.49	41.87	45.53	37.50	39.46	44.44	44.03	43.41	43.55	45.40	44.93	23.69	19.44	19.48
CaO	1.44	1.98	1.22	3.21	2.13	1.11	0.82	0.41	0.72	0.49	0.54	9.45	16.46	16.91
Na_2O	0.06	0.15	0.07	0.35	0.09	0.10	0.01	0.00	0.00	0.08	0.05	0.90	0.46	0.28
K_2O	0.08	0.19	0.05	0.14	0.52	0.03	0.04	0.03	0.02	0.03	0.03	0.11	0.11	0.09
P_2O_5	0.01	0.02	0.04	0.02	0.04	0.02	0.02	0.01	0.01	0.03	0.01	0.01	0.02	0.01
Cr_2O_3	0.85	1.04	0.53	0.67	1.09	0.52	0.60	0.68	0.70	0.68	0.51	1.69	0.79	0.73
NiO	0.30	0.31	0.32	0.28	0.25	0.32	0.33	0.33	0.31	0.31	0.35	0.38	0.09	0.09
LOI	3.50	1.77	1.84	3.30	2.81	2.71	3.89	5.85	4.31	3.88	2.75	1.90	0.52	0.58
Total	99.89	100.13	99.97	99.68	99.85	99.85	99.42	99.57	99.62	100.10	100.00	100.37	99.94	99.55
Mg$^{\#}$	0.905	0.912	0.916	0.898	0.905	0.915	0.914	0.916	0.917	0.920	0.920	0.895	0.852	0.852
Calculated modes in wt.%.														
Oliv	71.0	69.0	87.8	56.9	60.9	83.5	84.1	82.5	79.2	87.9	80.6	4.4	0	0
Opx	18.1	15.8	4.2	22.5	19.5	8.8	9.1	12.3	13.8	7.7	15.1	41.0	23.6	22.2
Cpx	6.1	8.6	5.1	14.2	9.8	4.7	3.4	1.7	2.9	2.3	2.3	39.2	67.0	67.6
Garn	4.8	6.6	3.0	6.4	9.9	3.0	3.5	3.5	4.1	2.2	2.0	15.4	9.4	10.3

Table 2-3

Representative analyses of olivines

The mineral compositions (wt.%) were determined using a JEOL 8900L electron microprobe at McGill University. The mineral phases were analyzed by wavelength dispersive spectroscopy with an acceleration voltage of 20 kV, beam current of 20 nA, and a beam diameter of 5 μm. On-peak counting times were 20 s, and the background counting times 10 s.

Sample Rock	NK1-5 Lherz	NK2-3 Lherz	NK2-10 Lherz	NK3-20 Lherz	NK3-25 Lherz	NK1-2 Harz	NK1-3 Harz	NK1-6 Harz	NK1-7 Harz	NK1-17 Harz	NK1-18 Harz
SiO_2	40.75	41.43	40.78	41.26	41.29	41.02	41.03	40.81	41.01	40.94	41.26
FeO	8.15	7.07	7.43	8.59	8.47	7.48	7.37	7.15	7.35	7.09	7.21
MnO	0.12	0.10	0.10	0.09	0.11	0.10	0.10	0.10	0.10	0.10	0.10
MgO	49.43	51.04	50.83	50.27	50.48	50.20	50.43	51.30	50.67	51.04	50.88
CaO	0.04	0.01	0.01	0.01	0.05	0.01	0.01	0.02	0.05	0.02	0.03
Cr_2O_3	0.04	0.00	0.01	0.00	0.02	0.01	0.01	0.02	0.04	0.01	0.04
NiO	0.35	0.40	0.36	0.38	0.36	0.35	0.35	0.38	0.37	0.36	0.43
Total	98.94	100.08	99.56	100.63	100.83	99.19	99.33	99.79	99.62	99.58	99.99
$Mg^{\#}$	0.915	0.928	0.924	0.912	0.914	0.923	0.924	0.927	0.925	0.928	0.926
Formulae based on three cations											
Si	1.004	1.003	0.993	1.000	0.998	1.004	1.002	0.989	1.004	0.995	1.001
Fe	0.168	0.143	0.151	0.174	0.171	0.153	0.151	0.145	0.150	0.144	0.146
Mn	0.003	0.002	0.002	0.002	0.002	0.002	0.002	0.002	0.002	0.002	0.002
Mg	1.815	1.843	1.845	1.816	1.819	1.832	1.837	1.854	1.835	1.850	1.840
Ca	0.001	0.000	0.000	0.000	0.001	0.000	0.000	0.000	0.001	0.000	0.001
Cr	0.001	0.000	0.000	0.000	0.000	0.000	0.000	0.000	0.001	0.000	0.001
Ni	0.007	0.008	0.007	0.007	0.007	0.007	0.007	0.007	0.007	0.007	0.008
O	4.001	4.003	3.992	4.000	3.997	4.004	4.002	3.989	3.999	3.995	4.001

Table 2-4
Representative analyses of orthopyroxenes (analytical procedure as in Table 2-3)

Sample Rock	NK1-5 Lherz	NK2-3 Lherz	NK2-10 Lherz	NK3-20 Lherz	NK3-25 Lherz	NK1-2 Harz	NK1-3 Harz	NK1-6 Harz	NK1-7 Harz	NK1-17 Harz	NK1-18 Harz	NK2-7 Pyrox	NK3-1 Pyrox	NK3-17 Pyrox
SiO_2	56.69	56.66	56.78	57.04	56.79	57.11	57.18	56.35	56.50	56.56	56.34	57.02	56.16	55.64
TiO_2	0.09	0.08	0.06	0.00	0.09	0.04	0.05	0.04	0.06	0.01	0.03	0.06	0.03	0.02
Al_2O_3	1.22	0.96	1.04	1.01	1.24	0.95	0.97	1.14	1.35	0.90	1.20	0.95	1.11	1.17
FeO	5.00	4.58	5.01	4.95	5.34	4.72	4.65	4.53	4.57	4.46	4.48	4.97	9.68	9.66
MnO	0.13	0.11	0.11	0.12	0.12	0.12	0.13	0.11	0.11	0.12	0.11	0.11	0.14	0.12
MgO	35.00	35.97	35.27	35.35	34.78	35.80	35.89	35.82	35.62	36.18	35.18	35.70	32.66	32.55
CaO	0.71	0.23	0.34	0.53	0.68	0.34	0.30	0.38	0.83	0.34	0.72	0.22	0.20	0.22
Na_2O	0.14	0.04	0.09	0.01	0.13	0.09	0.08	0.15	0.15	0.09	0.13	0.03	0.01	0.00
Cr_2O_3	0.49	0.27	0.35	0.29	0.35	0.38	0.34	0.47	0.56	0.33	0.61	0.18	0.18	0.17
NiO	0.10	0.09	0.11	0.07	0.10	0.08	0.08	0.10	0.09	0.07	0.12	0.08	0.15	0.15
Total	99.59	99.00	99.18	99.37	99.64	99.63	99.69	99.09	99.84	99.06	98.95	99.34	100.34	99.72
$Mg^{\#}$	0.926	0.933	0.926	0.927	0.921	0.931	0.932	0.934	0.933	0.935	0.933	0.928	0.857	0.857
Formulae based on four cations														
Si	1.952	1.953	1.961	1.962	1.956	1.959	1.960	1.940	1.934	1.946	1.948	1.963	1.955	1.948
Ti	0.002	0.002	0.002	0.002	0.002	0.001	0.001	0.001	0.002	0.000	0.001	0.002	0.001	0.001
Al	0.049	0.039	0.043	0.040	0.050	0.038	0.039	0.046	0.054	0.037	0.049	0.039	0.045	0.048
Fe	0.144	0.132	0.145	0.165	0.154	0.135	0.133	0.130	0.131	0.128	0.130	0.143	0.282	0.283
Mn	0.004	0.003	0.003	0.003	0.004	0.003	0.004	0.003	0.003	0.003	0.003	0.003	0.004	0.004
Mg	1.797	1.849	1.816	1.810	1.787	1.831	1.834	1.839	1.818	1.856	1.814	1.832	1.695	1.699
Ca	0.026	0.008	0.013	0.008	0.025	0.012	0.011	0.014	0.030	0.012	0.027	0.008	0.008	0.008
Na	0.009	0.002	0.006	0.001	0.009	0.006	0.005	0.010	0.010	0.006	0.009	0.002	0.000	0.000
Cr	0.013	0.007	0.010	0.006	0.010	0.010	0.009	0.013	0.015	0.009	0.017	0.005	0.005	0.005
Ni	0.003	0.002	0.003	0.002	0.003	0.002	0.002	0.003	0.002	0.002	0.003	0.002	0.004	0.004
O	5.979	5.977	5.984	5.989	5.983	5.980	5.981	5.966	5.965	5.965	5.976	5.984	5.979	5.975

Table 2-5
Representative analyses of clinopyroxenes (analytical procedure as in Table 2-3)

Sample Rock	NK1-5 Lherz	NK2-3 Lherz	NK2-10 Lherz	NK3-20 Lherz	NK3-25 Lherz	NK1-2 Harz	NK1-3 Harz	NK1-6 Harz	NK1-7 Harz	NK1-17 Harz	NK1-18 Harz	NK2-7 Pyrox	NK3-1 Pyrox	NK3-17 Pyrox
SiO_2	53.68	53.45	53.44	54.08	54.14	53.89	54.19	54.07	54.11	54.11	53.65	53.65	53.99	53.02
TiO_2	0.16	0.21	0.17	0.20	0.17	0.13	0.13	0.13	0.08	0.04	0.07	0.16	0.08	0.09
Al_2O_3	2.48	2.89	3.08	2.67	2.61	2.74	2.98	3.70	2.36	2.26	2.25	2.70	1.73	1.80
FeO	2.64	1.96	2.34	2.28	2.70	2.25	2.31	2.35	2.34	2.08	2.32	1.95	3.12	3.04
MnO	0.10	0.05	0.09	0.06	0.10	0.08	0.09	0.07	0.08	0.07	0.07	0.05	0.06	0.05
MgO	17.46	15.80	15.58	16.15	17.74	16.07	15.84	14.91	18.07	16.39	17.46	16.02	16.82	16.60
CaO	18.79	20.91	19.23	21.74	19.12	19.67	19.14	17.20	18.68	20.51	19.06	21.86	23.61	23.59
Na_2O	1.79	2.06	2.40	1.65	1.66	2.20	2.46	3.36	1.61	1.85	1.78	1.58	0.63	0.50
Cr_2O_3	1.99	1.96	2.30	1.46	1.52	2.22	2.27	3.26	1.77	1.87	2.34	1.15	0.45	0.37
NiO	0.05	0.04	0.04	0.04	0.06	0.04	0.04	0.04	0.06	0.04	0.08	0.05	0.08	0.09
Total	99.17	99.34	98.68	100.33	99.86	99.32	99.46	99.11	99.22	99.26	99.13	99.19	100.59	99.17
$Mg^{\#}$	0.922	0.935	0.922	0.927	0.921	0.927	0.924	0.919	0.932	0.934	0.931	0.936	0.906	0.907
Formulae based on four cations														
Si	1.947	1.936	1.951	1.947	1.949	1.954	1.961	1.960	1.958	1.965	1.947	1.952	1.949	1.943
Ti	0.004	0.005	0.005	0.005	0.005	0.004	0.004	0.004	0.002	0.001	0.002	0.004	0.002	0.003
Al	0.106	0.117	0.132	0.113	0.111	0.117	0.127	0.158	0.101	0.097	0.096	0.116	0.074	0.078
Fe	0.080	0.061	0.071	0.069	0.081	0.068	0.070	0.071	0.071	0.063	0.070	0.059	0.094	0.093
Mn	0.003	0.002	0.003	0.002	0.003	0.003	0.003	0.002	0.003	0.002	0.002	0.002	0.002	0.002
Mg	0.944	0.865	0.848	0.867	0.952	0.869	0.855	0.806	0.975	0.887	0.945	0.869	0.905	0.907
Ca	0.730	0.822	0.752	0.839	0.737	0.764	0.742	0.668	0.724	0.798	0.741	0.852	0.913	0.926
Na	0.126	0.137	0.170	0.115	0.116	0.155	0.172	0.236	0.113	0.131	0.125	0.111	0.044	0.036
Cr	0.057	0.053	0.066	0.042	0.043	0.064	0.065	0.094	0.051	0.054	0.067	0.033	0.013	0.011
Ni	0.001	0.001	0.001	0.001	0.002	0.001	0.001	0.001	0.002	0.001	0.002	0.001	0.002	0.003
O	5.967	5.961	5.970	5.971	5.969	5.970	5.973	5.970	5.976	5.973	5.965	5.973	5.971	5.970

Table 2-6
Representative analyses of garnets (analytical procedure as in Table 2-3)

Sample	NK1-5	NK2-3	NK2-10	NK3-20	NK3-25	NK1-2	NK1-3	NK1-6	NK1-7	NK1-17	NK1-18	NK2-7	NK3-1	NK3-17
Rock	Lherz	Lherz	Lherz	Lherz	Lherz	Harz	Harz	Harz	Harz	Harz	Harz	Pyrox	Pyrox	Pyrox
SiO_2	41.35	41.34	41.42	42.01	41.84	41.91	41.65	41.51	41.46	41.38	41.05	41.67	40.67	40.53
TiO_2	0.25	0.08	0.09	0.07	0.32	0.09	0.09	0.08	0.14	0.02	0.13	0.04	0.05	0.09
Al_2O_3	18.92	21.44	21.27	22.56	20.76	20.04	19.70	20.58	20.29	20.78	18.51	23.35	22.00	22.49
FeO	6.89	7.85	7.57	9.38	7.23	7.15	7.27	6.86	6.24	7.01	6.36	8.11	14.89	14.88
MnO	0.38	0.48	0.41	0.46	0.33	0.45	0.48	0.38	0.30	0.42	0.32	0.48	0.60	0.56
MgO	20.52	19.53	20.01	19.03	20.11	20.48	20.23	20.66	20.67	19.88	19.79	20.11	14.63	14.97
CaO	5.11	5.28	5.07	4.80	5.02	5.05	5.22	4.62	5.22	5.45	5.94	4.65	5.88	6.07
Na_2O	0.03	0.03	0.03	0.01	0.03	0.02	0.02	0.03	0.02	0.04	0.02	0.01	0.01	0.01
Cr_2O_3	4.78	3.21	3.74	1.92	3.71	3.99	4.29	4.42	4.76	4.12	6.77	1.49	1.32	1.27
NiO	0.01	0.01	0.02	0.01	0.01	0.00	0.00	0.01	0.02	0.01	0.02	0.00	0.00	0.00
Total	98.22	99.27	99.63	100.27	99.38	99.18	98.97	99.16	99.12	99.14	98.92	99.93	100.05	100.89
$Mg^{\#}$	0.842	0.816	0.825	0.783	0.832	0.836	0.832	0.843	0.855	0.835	0.847	0.815	0.637	0.642
Formulae based on eight cations														
Si	3.012	2.978	2.971	3.001	3.009	3.017	3.011	2.985	2.983	2.983	2.990	2.960	2.991	2.950
Ti	0.014	0.004	0.005	0.004	0.017	0.005	0.005	0.004	0.008	0.001	0.007	0.002	0.003	0.005
Al	1.624	1.821	1.798	1.900	1.760	1.701	1.679	1.745	1.720	1.766	1.589	1.955	1.907	1.929
Fe	0.419	0.473	0.454	0.561	0.435	0.431	0.440	0.413	0.375	0.423	0.387	0.482	0.916	0.906
Mn	0.023	0.029	0.025	0.028	0.020	0.028	0.030	0.023	0.018	0.026	0.020	0.029	0.037	0.034
Mg	2.228	2.098	2.140	2.027	2.156	2.198	2.181	2.216	2.217	2.137	2.149	2.131	1.604	1.625
Ca	0.399	0.408	0.390	0.367	0.387	0.389	0.404	0.356	0.402	0.421	0.464	0.354	0.463	0.474
Na	0.005	0.004	0.004	0.002	0.004	0.003	0.003	0.004	0.003	0.005	0.003	0.002	0.001	0.001
Cr	0.275	0.183	0.212	0.108	0.211	0.227	0.245	0.251	0.271	0.235	0.390	0.083	0.077	0.073
Ni	0.000	0.001	0.001	0.000	0.001	0.000	0.000	0.001	0.001	0.000	0.001	0.000	0.000	0.000
O	11.972	11.981	11.979	12.007	12.008	11.983	11.976	11.985	11.982	11.976	11.984	11.978	11.983	11.955

Table 2-7
Temperature and pressure estimates

Sample	Rock	Texture	Two-Pyrox Brey &Köhler (1990)	Al-in-Opx MacGregor (1974)	Two-Pyrox Finnerty & Boyd (1987)	Al-in-Opx MacGregor (1974)
			Temp (°C)	P (kb)	Temp (°C)	P (kb)
NK1-5	Lherz	coarse	1261	54.5	1125	46.3
NK1-14	Lherz	coarse	1026	42.5	933	36.7
NK1-23	Lherz	coarse	632	18.3	670	20.7
NK2-3	Lherz	coarse	761	26.6	710	23.4
NK2-10	Lherz	coarse	1001	40.8	901	34.5
NK3-4	Lherz	coarse	1237	51.7	1124	44.9
NK3-15	Lherz	coarse	1218	51.1	1103	44.2
NK3-20	Lherz	coarse	819	31.0	638	19.5
NK3-22	Lherz	porphyr	762	22.6	651	16.1
NK3-24	Lherz	coarse	738	23.1	646	17.5
NK3-25	Lherz	coarse	1260	53.9	1121	45.5
NK1-1	Harz	coarse	1186	49.2	1080	44.0
NK1-2	Harz	coarse	1045	44.7	935	37.7
NK1-3	Harz	coarse	1070	46.1	962	39.3
NK1-4	Harz	coarse	878	33.9	832	31.1
NK1-6	Harz	coarse	1144	48.8	1029	41.8
NK1-7	Harz	porphyr	1293	54.8	1162	46.9
NK1-9	Harz	coarse	1132	48.0	1058	43.5
NK1-12	Harz	coarse	1054	45.3	980	40.6
NK1-13	Harz	coarse	1267	63.8	1147	55.9
NK1-15	Harz	coarse	1132	48.4	1022	41.6
NK1-17	Harz	coarse	1007	43.2	926	38.1
NK1-18	Harz	coarse	1215	52.0	1103	45.2
NK3-18	Harz	coarse	1197	56.1	1067	47.7
NK2-7	Pyrox	coarse	713	23.8	606	17.0
NK3-19	Pyrox	coarse	1033	44.3	949	38.9
NK3-1	Pyrox	coarse	739	23.2	-	-
NK3-17	Pyrox	coarse	657	18.4	-	-

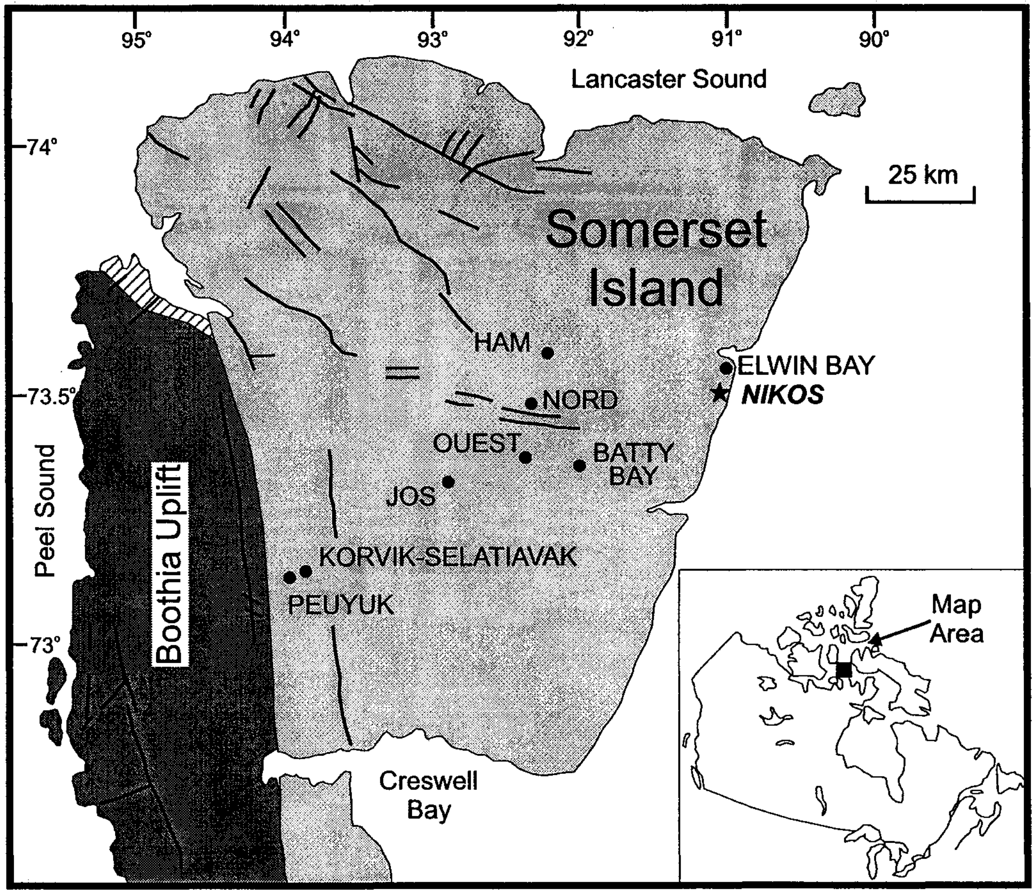

95°
94°
93°
92°
91°
90°
Lancaster Sound
-74°
25 km
Somerset Island
HAM
ELWIN BAY
NIKOS
-73.5°
NORD
OUEST
BATTY BAY
JOS
Peel Sound
Boothia Uplift
KORVIK-SELATIAVAK
PEUYUK
-73°
Map Area
Creswell Bay

Figure 2-1

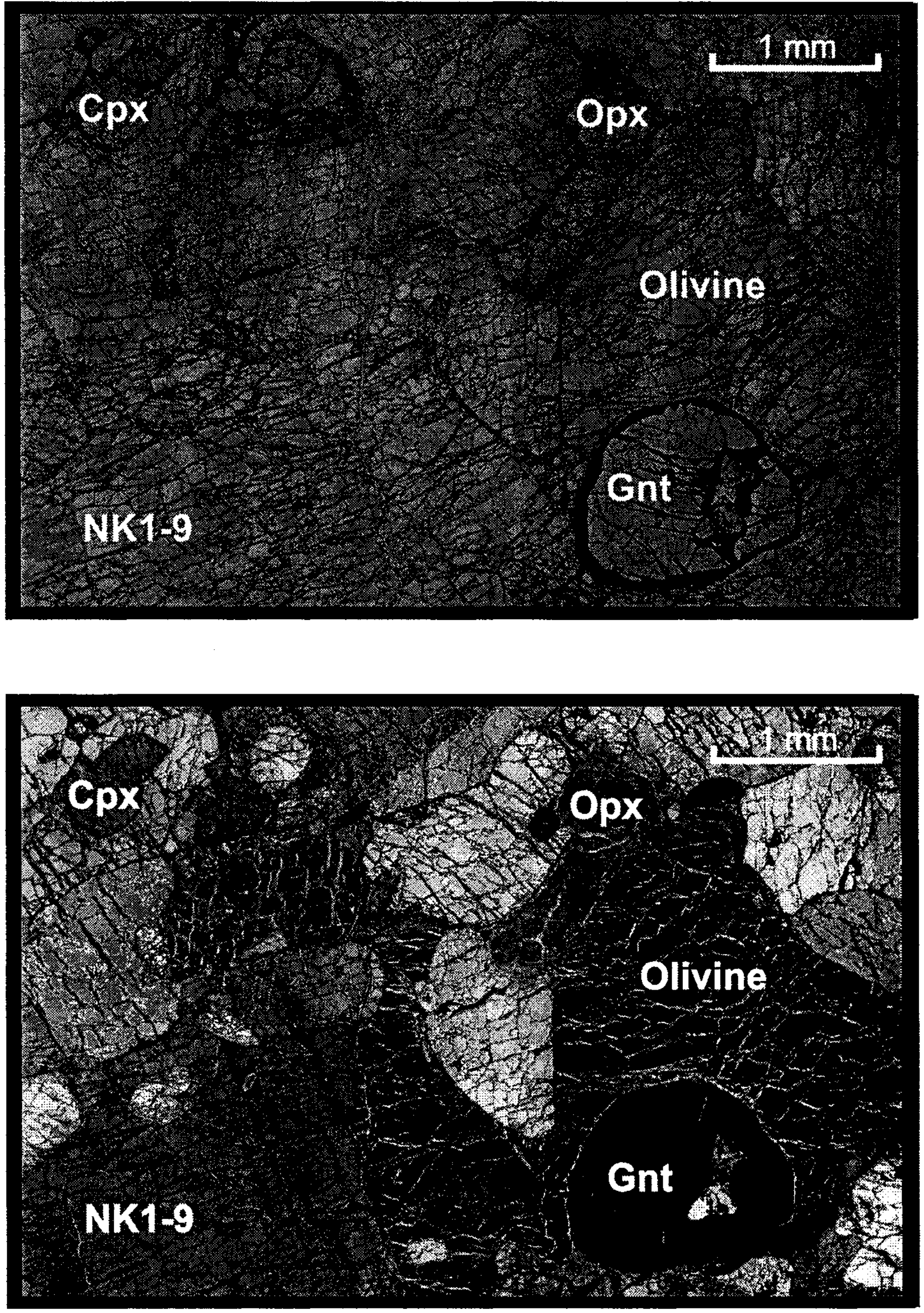

Figure 2-2a

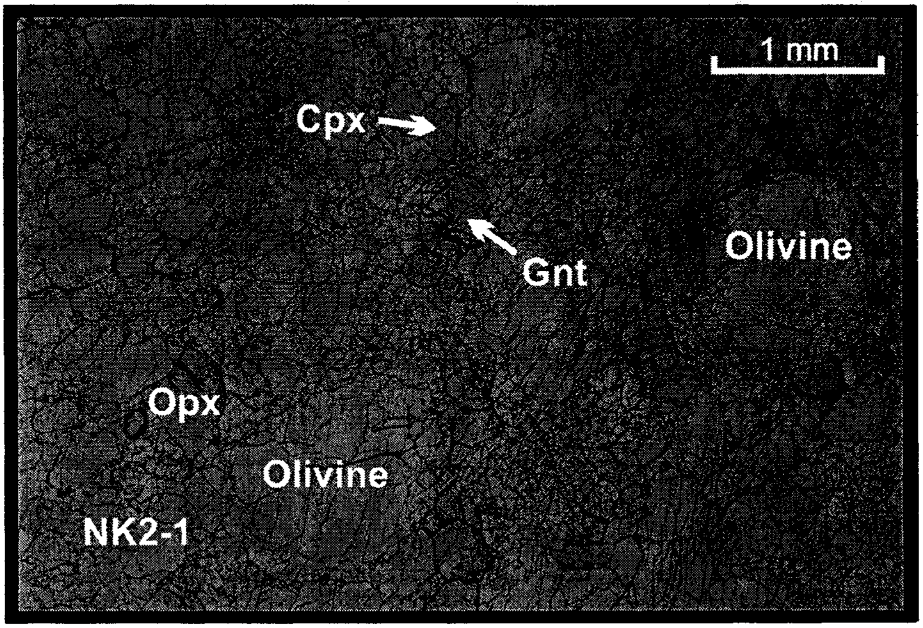
1 mm
Cpx
Gnt
Olivine
Opx
Olivine
NK2-1

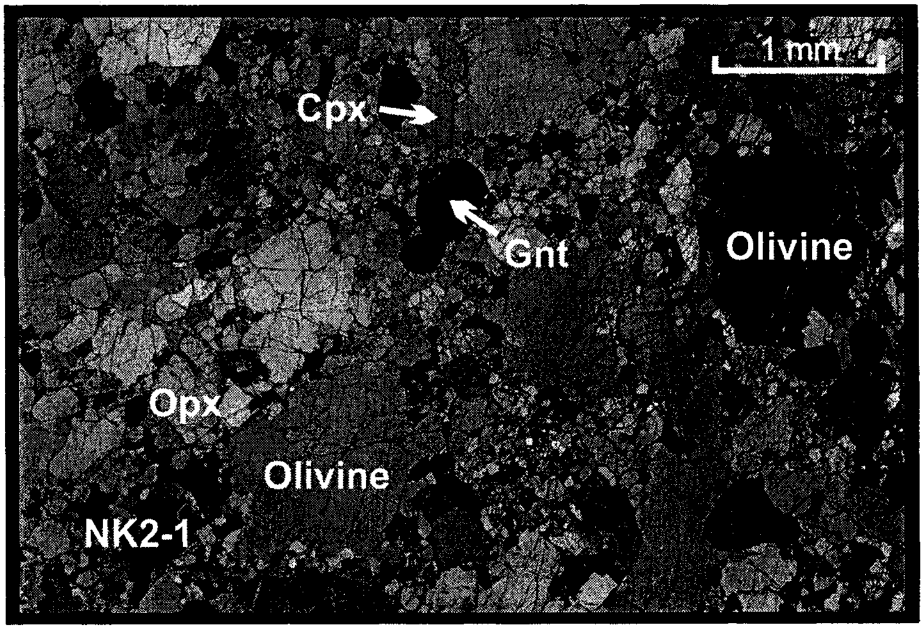
1 mm
Cpx
Gnt
Olivine
Opx
Olivine
NK2-1

Figure 2-2b

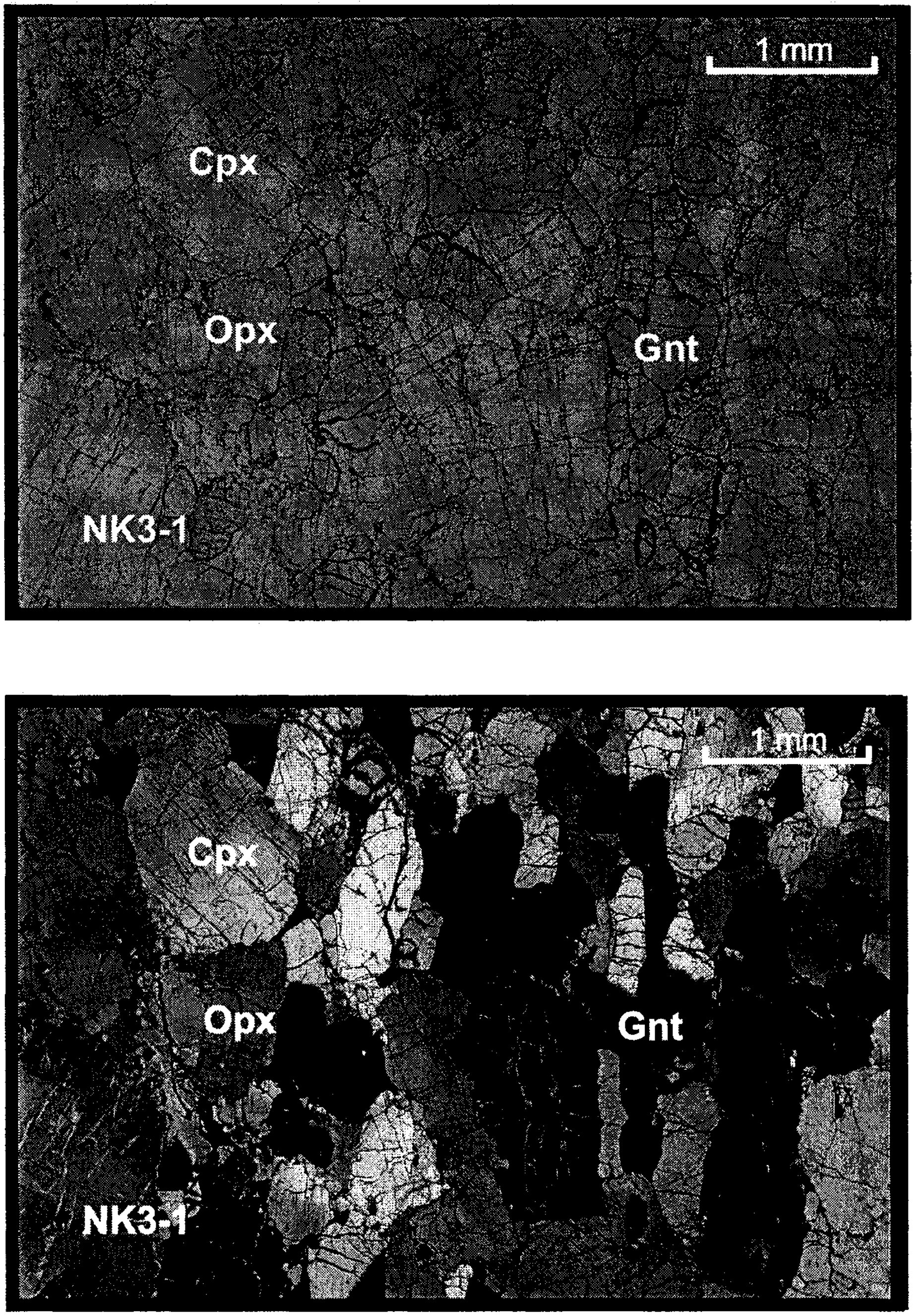

Figure 2-2c

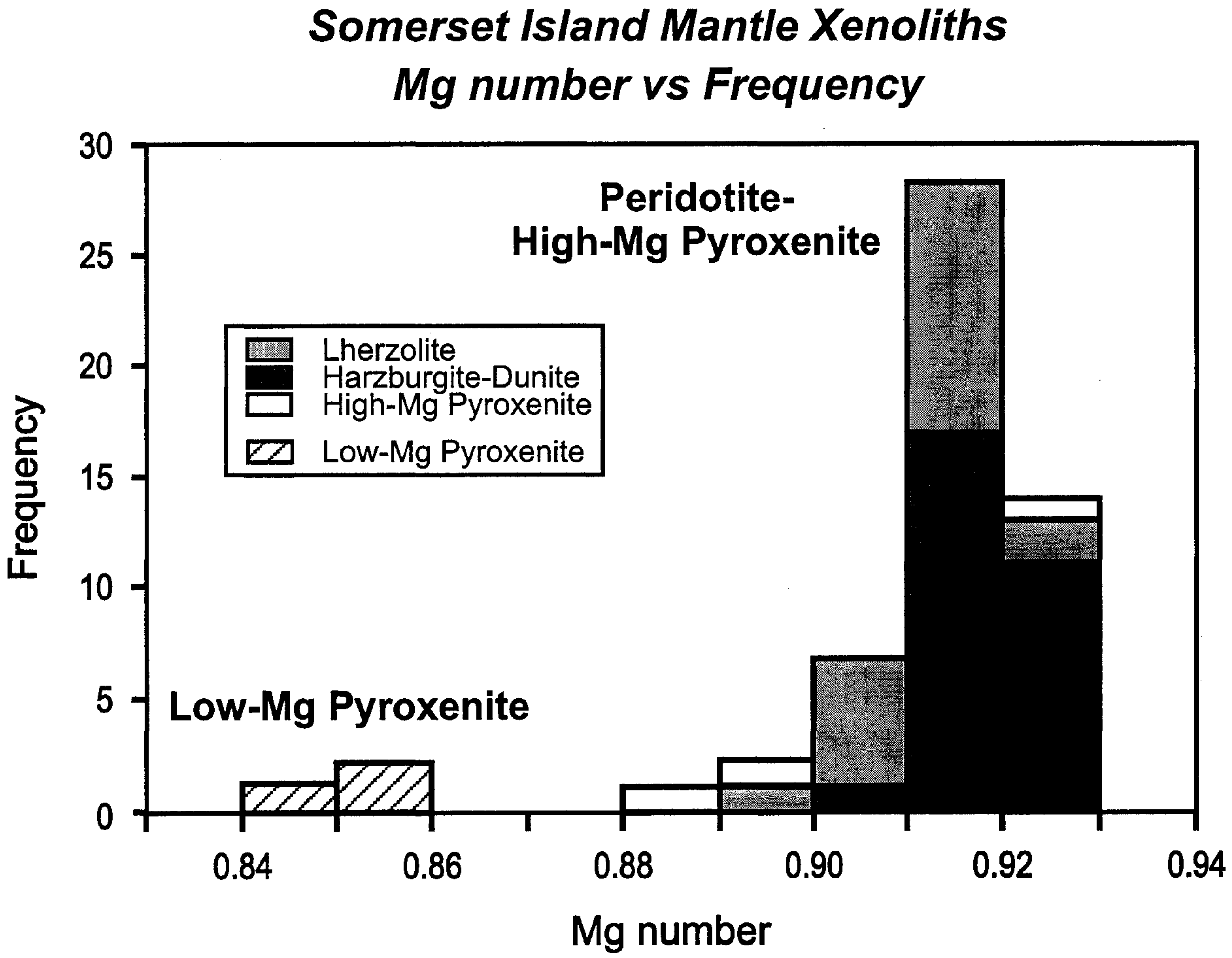
Somerset Island Mantle Xenoliths
Mg number vs Frequency
Peridotite-
High-Mg Pyroxenite
Lherzolite
Harzburgite-Dunite
High-Mg Pyroxenite
Low-Mg Pyroxenite
Low-Mg Pyroxenite
Frequency
0
5
10
15
20
25
30
0.84
0.86
0.88
0.90
0.92
0.94
Mg number

Figure 2-3

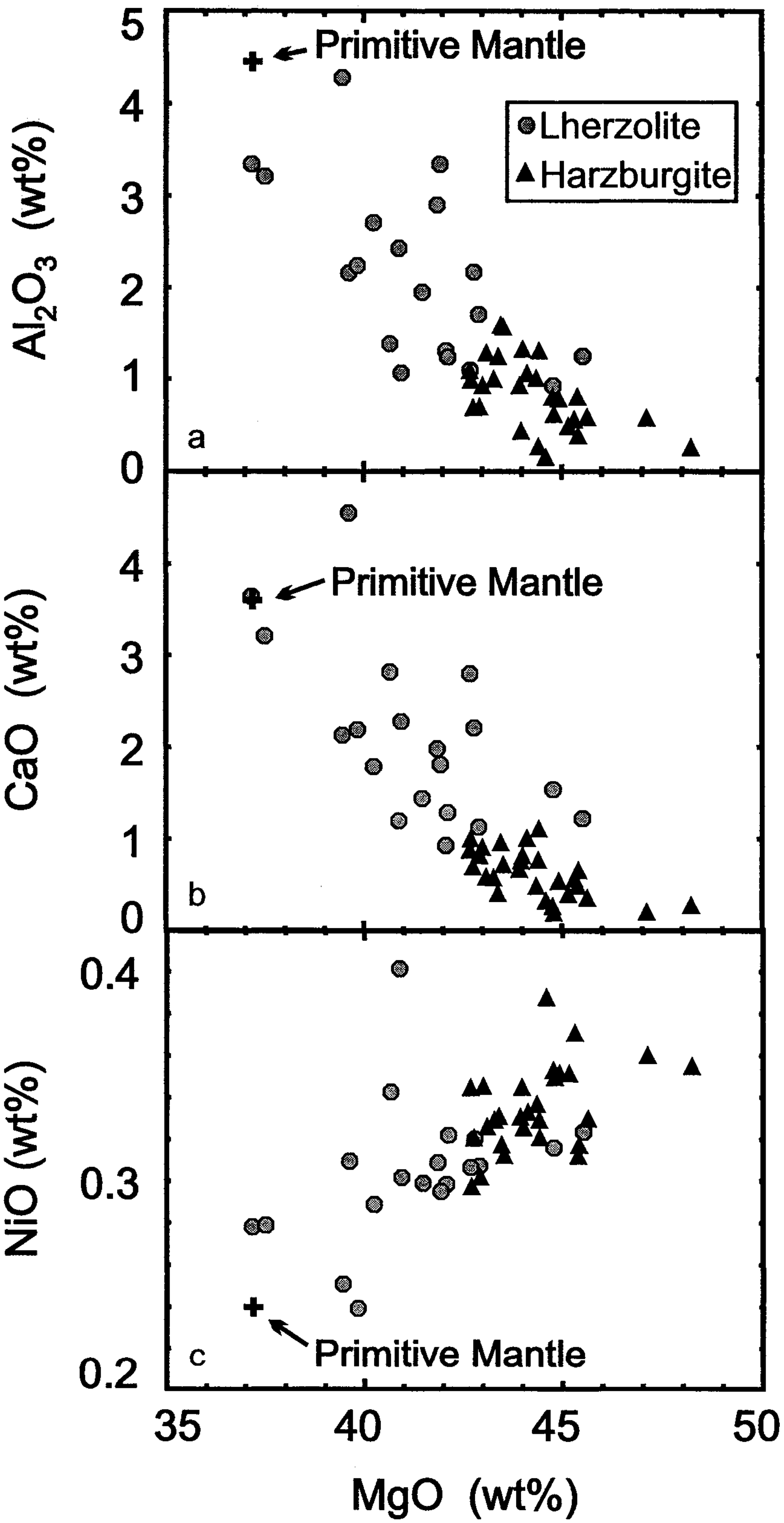
Primitive Mantle
Lherzolite
Harzburgite
Al_2O_3 (wt%)
a
5
4
3
2
1
0
Primitive Mantle
CaO (wt%)
b
4
3
2
1
0
Primitive Mantle
NiO (wt%)
c
0.4
0.3
0.2
35
40
45
50
MgO (wt%)

Figure 2-4

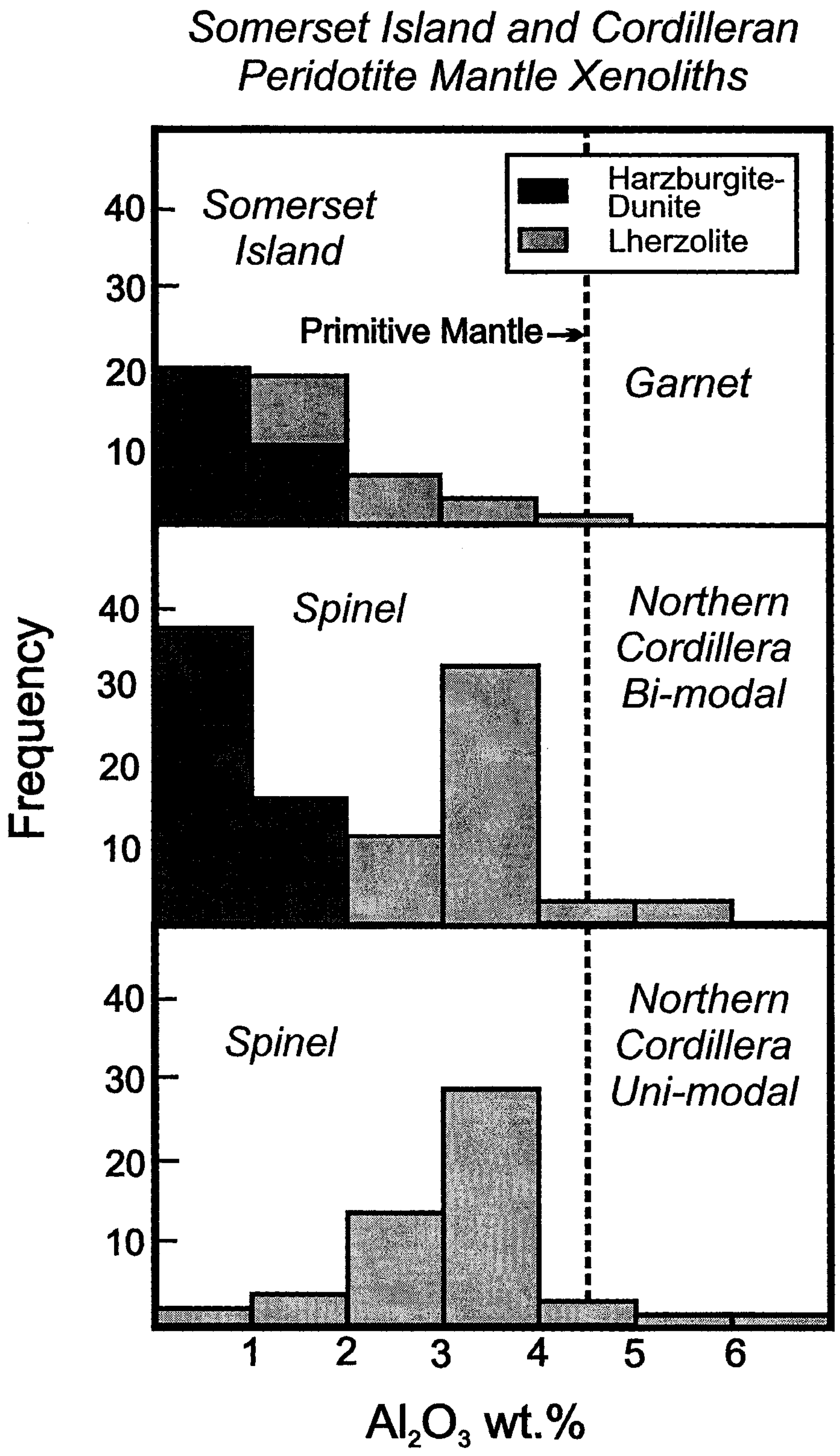
Somerset Island and Cordilleran Peridotite Mantle Xenoliths
Harzburgite-Dunite
Lherzolite
Somerset Island
Primitive Mantle
Garnet
Spinel
Northern Cordillera Bi-modal
Spinel
Northern Cordillera Uni-modal
Frequency
40
30
20
10
1
2
3
4
5
6
Al_2O_3 wt.%

Figure 2-5

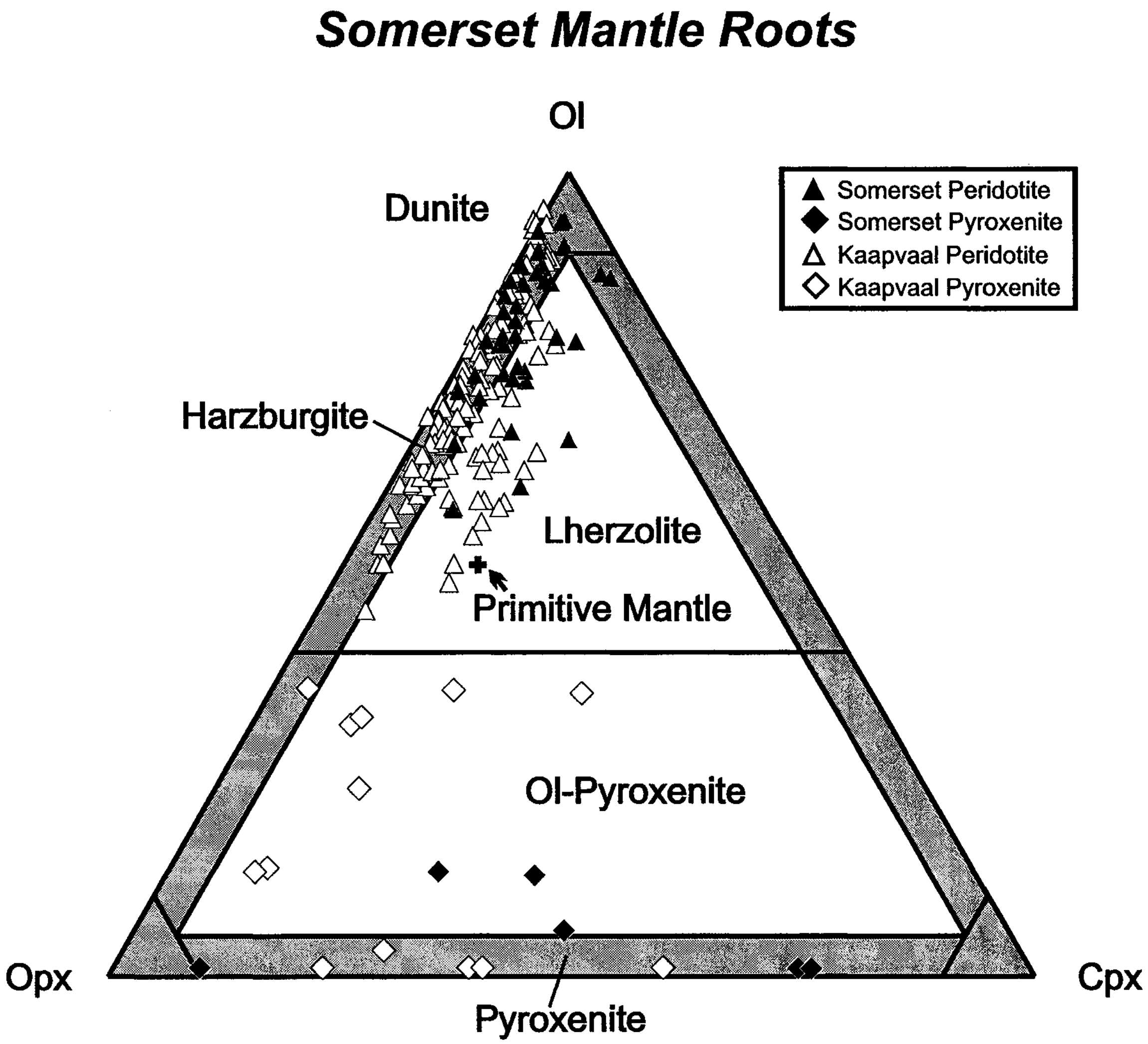
Somerset Mantle Roots
Ol
Dunite
Harzburgite
Lherzolite
Primitive Mantle
Ol-Pyroxenite
Pyroxenite
Opx
Cpx
▲ Somerset Peridotite
◆ Somerset Pyroxenite
△ Kaapvaal Peridotite
◇ Kaapvaal Pyroxenite

Figure 2-6

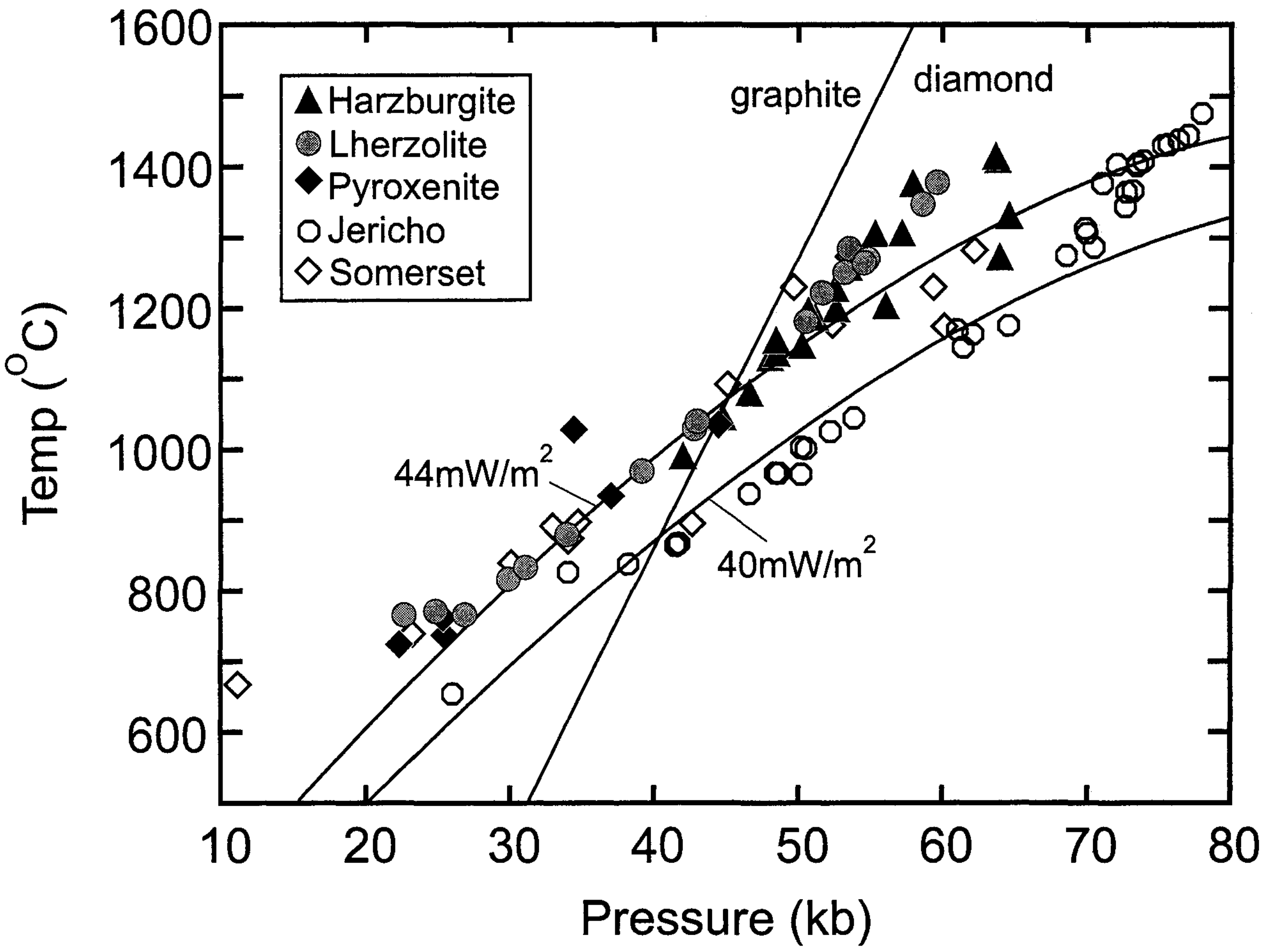

1600
1400
1200
1000
800
600
Temp (^{o}C)
10
20
30
40
50
60
70
80
Pressure (kb)
▲ Harzburgite
● Lherzolite
◆ Pyroxenite
○ Jericho
◇ Somerset
graphite
diamond
44mW/m^{2}
40mW/m^{2}

Figure 2-7

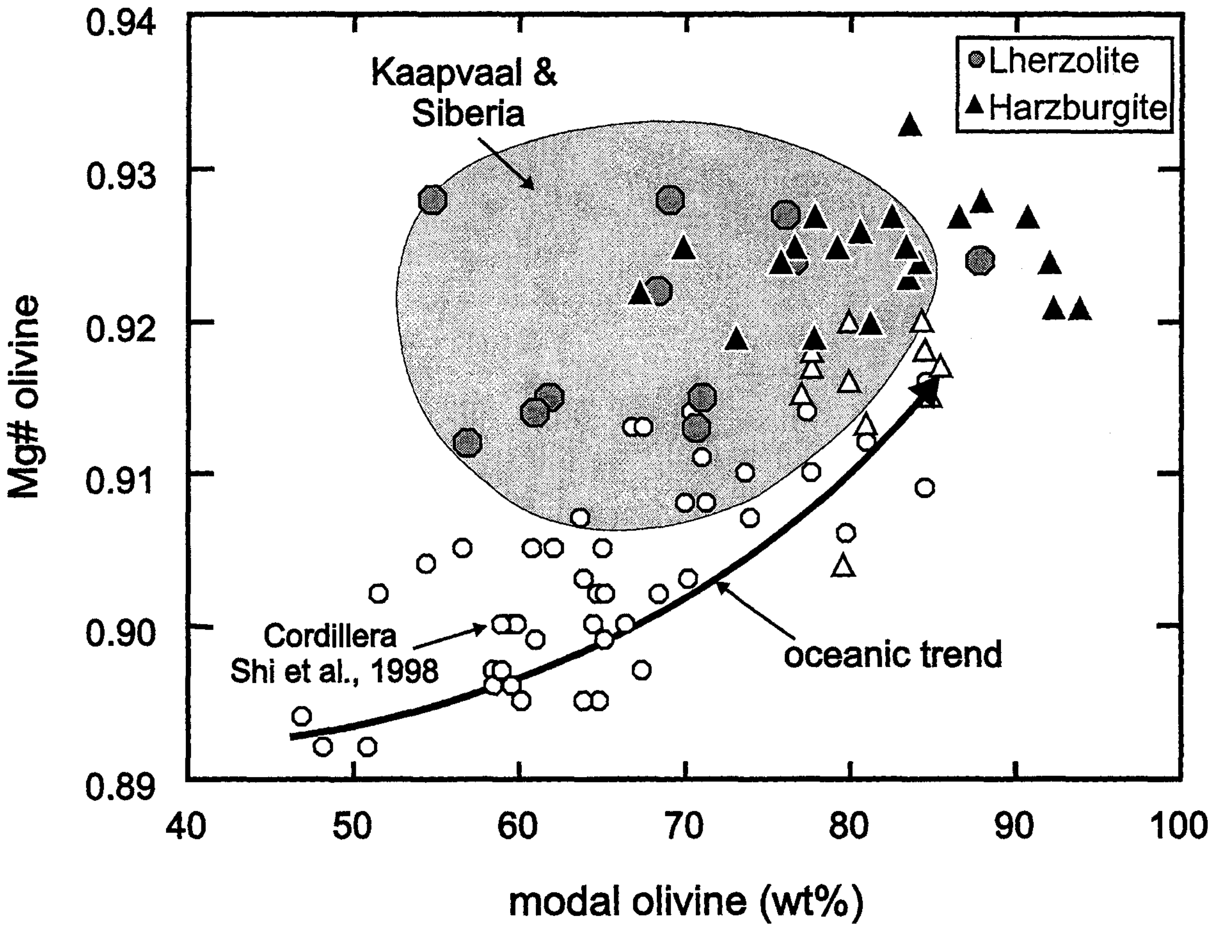

0.94
0.93
0.92
0.91
0.90
0.89
40
50
60
70
80
90
100
Mg# olivine
modal olivine (wt%)
Lherzolite
Harzburgite
Kaapvaal & Siberia
Cordillera Shi et al., 1998
oceanic trend

Figure 2-8

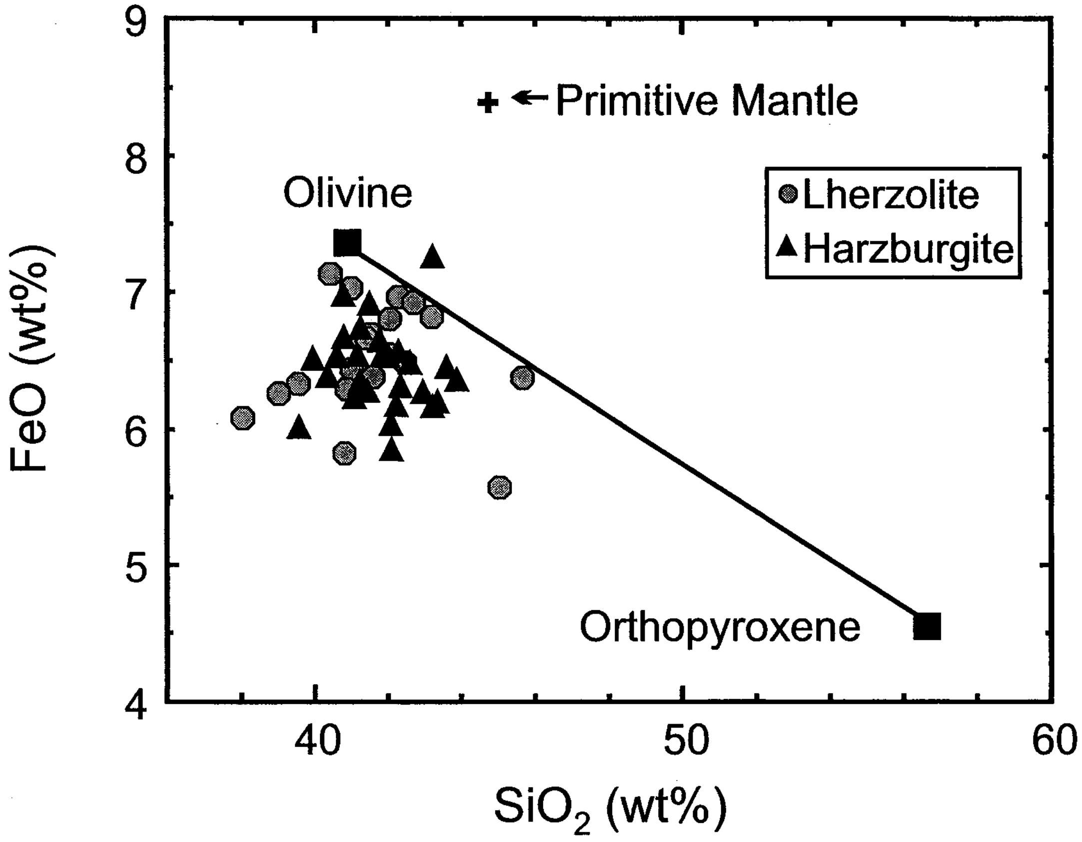
9
8
7
6
5
4
40
50
60
FeO (wt%)
SiO_2 (wt%)
✚ ← Primitive Mantle
Olivine
Orthopyroxene
● Lherzolite
▲ Harzburgite

Figure 2-9

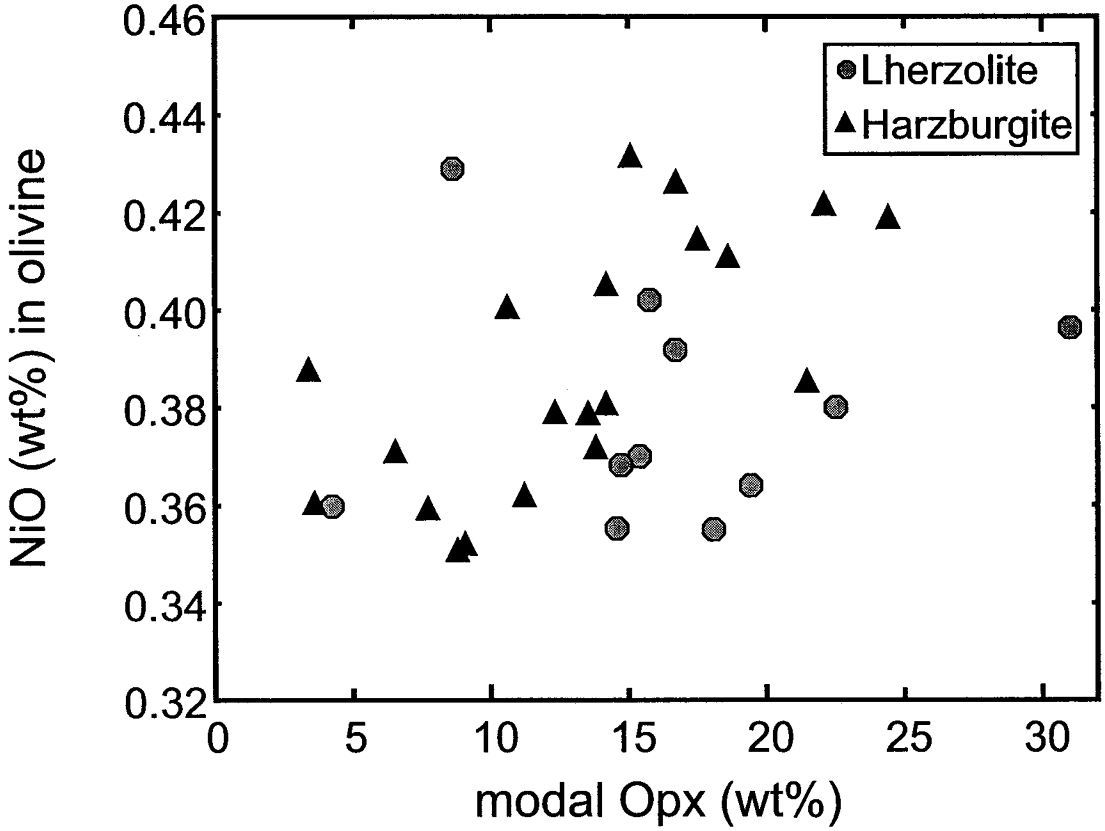

0.46
0.44
0.42
0.40
0.38
0.36
0.34
0.32
NiO (wt%) in olivine
0
5
10
15
20
25
30
modal Opx (wt%)
● Lherzolite
▲ Harzburgite

Figure 2-10

CHAPTER 3

Constraints on the trace element composition of the Archean mantle root beneath Somerset Island, Arctic Canada

ABSTRACT

Peridotites that sample Archean mantle roots are frequently incompatible trace element enriched despite their refractory major element compositions. To constrain the trace element budget of the lithosphere beneath the Canadian craton, trace element and rare earth element (REE) abundances were determined for a suite of garnet-peridotites and garnet-pyroxenites from the Nikos kimberlite pipe on Somerset Island, Canadian Arctic, their constituent garnet and clinopyroxene, and the host kimberlite. These refractory mantle xenoliths are depleted in fusible major elements, but enriched in incompatible trace elements, such as large ion lithophile elements (LILE), Th, U and light rare earth elements (LREE). Mass balance calculations based on modal abundances of clinopyroxene and garnet and their respective REE contents yield discrepancies between calculated and analyzed REE contents for the Nikos bulk rocks that amount to LREE deficiencies of 70 to 99%, suggesting the presence of small amounts of interstitial kimberlite liquid (0.4 to 2 wt%) to account for the excess LREE abundances. These results indicate that the peridotites had in fact depleted or flat LREE patterns before contamination by their host kimberlite. LREE and Sr enrichment in clinopyroxene and low Zr and Sr abundances in garnet in low temperature peridotites (800 to 1100 °C) compared to high temperature peridotites (1200 to 1400 °C) suggest that the shallow lithosphere is geochemically distinct from the deep lithosphere beneath the northern margin of the Canadian craton. The Somerset mantle root appears to be characterized by a depth zonation that may date from the time of its stabilization in the Archean.

Key words: Canada; mantle; metasomatism; peridotite; trace elements

INTRODUCTION

The mantle underlying many Archean cratons has anomalously high seismic velocities to depths of 350 to 400 km (Jordan, 1988; Grand, 1994), indicating the presence of cold refractory roots, depleted in the fusible major elements compared to fertile mantle (Boyd & Mertzman, 1987; McDonough, 1990). These deep residual peridotite roots probably contribute to the stability of Archean continental lithosphere because of their lower density and higher viscosity compared to that of the surrounding asthenospheric mantle (Boyd & McCallister, 1976; Jordan, 1979; Pollack, 1986). Mantle xenoliths that are hosted by kimberlites and alkaline basalts are our only window into the subcontinental lithosphere. They provide essential evidence on the chemical composition and evolution of the upper mantle to depths of greater than 200 km. Studies of these mantle xenoliths enable us to characterize the abundance and distribution of major, minor and trace elements in peridotites and between their constituent minerals. Most subcratonic peridotite samples have undergone a complex history of melt extraction that has changed their chemical composition and resulted in depletion of the residual mantle in fusible major elements such as Fe, Al and Ca (e.g. Nixon, 1987; Herzberg, 1993; Boyd *et al.*, 1997). In contrast to their depletion in incompatible major elements, however, many peridotite xenoliths have unexpectedly high abundances of incompatible trace elements, such as large ion lithophile elements (LILE) and light rare earth elements (LREE; Erlank *et al.*, 1987; Menzies *et al.*, 1987). Although these findings have been widely interpreted to indicate that the lithospheric mantle has been affected by interaction with incompatible element enriched percolating melts or fluids over time (Hawkesworth *et al.*, 1983; Menzies & Hawkesworth, 1987), it is important to establish the chemical nature of these metasomatic agents and whether metasomatism is an ancient feature or associated with the kimberlite magmatic event itself.

Previous studies on Somerset Island peridotites have shown that Re-Os isotope systematics for these xenoliths yield Re depletion ages of up to 2.7 Ga (Irvine *et al.*, 1999), indicating the existence of Archean lithospheric mantle underneath the northern margin of the Canadian craton. In this study, we present trace element and rare earth element (REE) data for a suite of garnet-peridotites and garnet-pyroxenites, constituent garnet and clinopyroxene, and the host kimberlite from the Nikos kimberlite pipes on Somerset Island, in the southern Canadian Arctic (Fig. 1). The geochemical data provide information on mantle depletion and constraints on incompatible trace element enrichment during metasomatism following melt extraction. REE distribution patterns for constituent garnet and clinopyroxene give insights into trace element partitioning and are used to constrain the change in chemical composition of the refractory mantle root with depth. Models of trapped liquid compositions along grain boundaries indicate that the Nikos kimberlite probably acted as the metasomatic agent during sample entrainment.

SAMPLES AND PROCEDURES

Kimberlite

The recently discovered Cretaceous (100 Ma) Nikos kimberlite (Heaman, 1989; Smith *et al.*, 1989; Pell, 1993; Fig. 1) consists of three individual pipes that are described in more detail in Schmidberger & Francis (1999). The Nikos kimberlites were emplaced into late Archean crystalline basement overlain by Paleozoic cover rocks of the northern margin of the Canadian craton (Steward, 1987; Frisch & Hunt, 1993). Although it has been argued that Somerset Island is part of the Proterozoic Innuitian tectonic province (Trettin *et al.*, 1972), late Archean Re depletion ages for other Somerset Island peridotite xenoliths (Irvine *et al.*, 1999) indicate the presence of an Archean mantle root beneath the southern Canadian Arctic.

The southernmost Nikos kimberlite pipe (NK3) is characterized by a non-brecciated, magmatic texture, and appears to represent kimberlite liquid (Schmidberger & Francis, 1999). The magmatic kimberlite exhibits a porphyritic microcrystalline texture, consisting of phenocrysts of olivine, phlogopite and spinel in a very fine-grained carbonate-rich matrix of calcite, serpentine, perovskite and apatite. Calcite occurs as aggregates of tabular sub-parallel crystals showing flow texture around larger olivine phenocrysts, which has been interpreted to be a primary magmatic feature (Schmidberger & Francis, 1999). Crushed whole-rock kimberlite samples were carefully handpicked under the binocular microscope prior to grinding to eliminate contamination from xenocrysts and country rock fragments.

Mantle xenoliths

The mantle xenolith suite for this study consists of large (10 to 30 cm), well-preserved garnet-peridotites and lesser garnet-pyroxenites, thirty of which were analyzed for their major and trace element and REE contents in this study (Tables 2 and 3). The majority of the Nikos peridotites show coarse textures, typical of mantle xenoliths, with large crystals of olivine, orthopyroxene, clinopyroxene and garnet, although a few xenoliths with porphyroclastic textures are observed. Small differences in modal clinopyroxene contents do not justify dividing the suite according to the IUGS classification into harzburgitic (clinopyroxene <5 wt%) and lherzolitic (clinopyroxene >5 wt%) rock types, and the more general term peridotite is preferred for the xenoliths in the present study. A detailed description of mineralogy and petrology of the mantle xenoliths can be found in Schmidberger & Francis (1999). Whole-rock analyses of the peridotite xenoliths are strongly depleted in fusible major elements such as Fe, Al and Ca when compared to primitive mantle compositions (McDonough, 1990; Schmidberger & Francis, 1999; Table 2). High magnesium numbers (mg-number=Mg/(Mg+Fe)) between 0.90 to 0.93 and their refractory olivine-rich mineralogy confirm the depleted nature of these peridotites (Table 2). The Somerset whole-rock characteristics are similar to those for kimberlite-hosted peridotites from the Canadian Slave province (Kopylova *et al.*, 1999; MacKenzie & Canil, 1999), and a detailed comparison of both xenolith suites can be found in Schmidberger & Francis (1999). Temperature and pressure estimates of last equilibration for the Nikos xenoliths (800 to 1400 °C and 25 to 60 kb) suggest that the peridotites were entrained from depths between 80 to 190 km (Schmidberger & Francis, 1999; Table 2).

The pyroxenites contain large crystals of clinopyroxene and orthopyroxene, and smaller crystals of garnet. These pyroxene-rich rocks have a range of mg-numbers (Schmidberger & Francis, 1999; Table 2). The high-Mg pyroxenites contain olivine and abundant garnet (15 to 25 wt%) and have mg-numbers (0.88 to 0.90; NK2-7, NK3-14) that overlap those of the peridotites. The low-Mg pyroxenites (mg-number: 0.85; NK3-1, NK3-17), on the other hand, are less garnet-rich (9 to 10 wt%) and have higher modal amounts of clinopyroxene (67 to 68 wt%) compared to the high-Mg pyroxenites (22 to 39 wt%).

Clinopyroxene and garnet

The emerald green clinopyroxene of the Somerset peridotites is a chromian diopside (Schmidberger & Francis, 1999), while the garnets are chromian pyrope, the majority of which are purple in color (Table 5). A small number of samples contain blood red garnets (NK1-5, NK2-2, NK3-4). These garnets tend to have higher MgO, SiO_2 and Al_2O_3, but lower CaO, Cr_2O_3 and MnO contents, compared to the purple garnets (Table 5). The high temperature estimates of 1200 to 1400 °C (Schmidberger & Francis, 1999) for samples with red garnet possibly suggest that these xenoliths were derived from deep lithospheric mantle, whereas the temperatures calculated for xenoliths with purple garnet are much more variable (800 to 1400 °C). Major element analyses of garnet and clinopyroxene indicate that these minerals are not chemically zoned and are compositionally homogeneous on the scale of a thin section. Inclusion-free crystals of clinopyroxene and garnet were handpicked under the binocular microscope from ten peridotites and one low-Mg pyroxenite sample, and were analyzed for their REE and trace element (Ti, V, Cr, Sr, Y, Zr) contents with a Cameca IMS 3f ion microprobe at Woods Hole Oceanographic Institution. The major elements of these separates were determined using electron microprobe analysis at McGill University, as described in Schmidberger & Francis (1999).

ANALYTICAL DATA

Kimberlite

The kimberlite whole-rock analyses are extremely high in $CaCO_3$ (27 to 39 wt%; Table 1), indicating liquid compositions intermediate between kimberlite and carbonatite (Woolley & Kempe, 1989; Ringwood *et al.*, 1992). Primitive-mantle normalized trace element patterns for the Nikos kimberlites (Table 1; Fig. 2a) show a strong enrichment in LILE (e.g. Ba, Sr) and Nb, Th, U and Pb, typical of small-degree partial melts such as kimberlites (Mitchell, 1986; Dalton & Presnall, 1998). The REE patterns for the Nikos kimberlites exhibit steep slopes with $(La/Sm)_N$ of 7 and relative depletion in heavy rare earth elements (HREE; Fig. 2b). Although LREE characteristics are similar to those for kimberlites from South Africa, Zaire, North America and India (Mitchell & Brunfelt, 1975; Paul *et al.*, 1975; Cullers *et al.*, 1982; Wedepohl & Muramatsu, 1979; Muramatsu, 1983; Fieremans *et al.*, 1984; Mitchell, 1986; Fig. 2b), HREE levels are distinctly lower in the Nikos kimberlites, particularly from Er to Lu. With the exception of Ba and Pb, which are strongly enriched, the levels of most other trace elements in the Nikos kimberlites overlap the fields for kimberlites from South Africa, Zaire, North America and India (Fig. 2b).

Mantle xenoliths

Incompatible trace element patterns for the bulk peridotites are subparallel and indicate that LILE (e.g. Ba, Sr), Nb, Th and U concentrations are enriched when compared to primitive mantle abundances (Sun & McDonough, 1989; McDonough & Sun, 1995; Table 3; Fig. 3a). Their trace element patterns are, however, clearly distinct from those of the Nikos kimberlites, which have much higher LILE, Nb, Th, U and Pb contents (Fig. 3a). Chondrite-normalized HREE patterns for the peridotites are flat, whereas the LREE are fractionated with $(La/Sm)_N$ of 4 to 6, resulting in concave-upward LREE patterns. The kimberlites, on the other hand, have much steeper slopes for LREE and, in particular, HREE compared to the peridotites (Fig. 3b).

The pyroxenites also contain high concentrations of incompatible trace elements such as LILE, Nb, Th and U, compared to values for primitive mantle (Table 3; Fig. 4a). The high-Mg pyroxenites (NK2-7, NK3-14), however, are considerably more enriched in incompatible trace elements than the low-Mg pyroxenites (NK3-1, NK3-17), and have trace element patterns that overlap those for peridotites showing the highest abundances of these elements (Fig. 4a). Incompatible trace element patterns for the low-Mg pyroxenites, on the other hand, are similar to those for peridotites with the lowest trace elements levels. Furthermore, the high-Mg pyroxenites have strongly fractionated LREE patterns ($(\mathrm{La/Sm})_N$ = 4 to 14), whereas low-Mg pyroxenites exhibit much less LREE fractionation ($(\mathrm{La/Sm})_N$ = 2). The HREE abundances for both the high and low-Mg pyroxenites tend to be higher than those for the peridotites (Fig. 4b), probably reflecting their higher modal abundance of garnet (av. 15 wt%) compared to that of the peridotites (av. 7 wt%; Table 2).

Clinopyroxene and garnet

The clinopyroxenes show convex-upward chondrite-normalized REE patterns with enriched LREE compared to chondrites (1 to 100 times) and relatively depleted HREE, with approximately chondritic abundances (Table 4; Fig 5a, b). The clinopyroxenes from peridotites yielding high temperatures of equilibration (1200 to 1400 °C) are only moderately enriched in LREE abundances (1 to 10 times chondrite; Fig. 5a). In comparison, clinopyroxenes from low temperature peridotites (800 to 1100 °C; NK1-3, NK1-4, NK1-14, NK2-3) exhibit significantly greater LREE enrichment (up to 100 times chondrite; Fig. 5b) and high Sr contents (>100 ppm; Table 4). In contrast, HREE patterns for both high temperature and low temperature peridotites are indistinguishable.

The clinopyroxenes in high temperature Nikos peridotite xenoliths have LREE contents that overlap those of clinopyroxenes in high temperature peridotites (>1100 °C) from the Kaapvaal craton in South Africa, although the HREE concentrations of the Kaapvaal clinopyroxenes tend to be higher (Shimizu, 1975; Boyd, 1987; Fig. 6a). Unlike many of the high temperature Kaapvaal xenoliths (Boyd, 1987), the high temperature Somerset peridotites are not characterized by strong deformation textures. In comparison, clinopyroxenes from high temperature Siberian peridotites (Shimizu *et al.*, 1997) have LREE contents that are intermediate between those of the low and high temperature Nikos clinopyroxenes, and overlapping HREE contents (Fig. 6a).

The low temperature Nikos peridotites have clinopyroxenes with LREE contents that overlap those of clinopyroxenes from low temperature Kaapvaal peridotites (<1100 °C), although the latter have considerably lower HREE contents (Fig. 6a). Clinopyroxenes from low temperature Siberian peridotites appear to exhibit highly variable REE patterns.

The REE patterns for garnets are HREE enriched and LREE depleted compared to those of coexisting clinopyroxene, crossing the latter between Sm and Eu (Table 5; Fig 5a, b). Garnet REE patterns for low temperature xenoliths are indistinguishable from those for high temperature peridotites. Strong depletion in LREE compared to HREE is consistent with garnet/liquid REE partition coefficients (Hauri *et al.*, 1994; Halliday *et al.*, 1995 and references therein) and has been interpreted to represent equilibrium REE distribution between garnet and a coexisting liquid (Shimizu, 1999). Sinusoidal patterns, characterized by an enrichment in the middle rare earth elements (MREE) compared to LREE and HREE (that have been interpreted to reflect recent, non-equilibrated melt-mineral reactions in other xenolith suites; Hoal *et al.*, 1994; Shimizu, 1999), are not observed in the Nikos garnets. The LREE contents of garnet in the low-Mg pyroxenite NK3-1 (Fig. 5a) are extremely low, indicating the highly depleted nature of this sample.

The REE patterns for the Nikos garnets are subparallel to those for garnets from high temperature Kaapvaal peridotites, although the latter contain higher overall REE abundances (Shimizu, 1975; Fig. 6b). Garnets from low temperature Kaapvaal peridotites have sinusoidal, non-equilibrated REE patterns with higher LREE and considerably lower HREE contents than those in the Nikos garnets (Fig. 6b). The LREE concentrations in the Nikos garnets are lower than those of garnets from Siberian high temperature peridotites, but their HREE contents overlap (Shimizu *et al.*, 1997; Fig. 6b).

DISCUSSION

Mantle composition

Late Archean Re depletion ages for other Somerset Island peridotites (up to 2.7 Ga; Irvine *et al.*, 1999) indicate that the northern margin of the Canadian craton is underlain by an Archean lithospheric mantle root, which may be only slightly younger than the Archean subcontinental lithosphere beneath the central Slave province, whose kimberlite xenoliths yield Re depletion ages of up to 3 Ga (Irvine *et al.*, 1999). In comparison, peridotite xenoliths in kimberlites on the Kaapvaal and Siberian cratons yield Re depletion ages (3.3 to 3.5 Ga; Pearson *et al.*, 1995a; Pearson *et al.*, 1995b), indicating that their mantle roots stabilized by the mid Archean.

Pressure and temperature estimates for the Nikos peridotites suggest the existence of a lithospheric mantle root to a depth of at least 190 km beneath Somerset Island, significantly deeper than the lithospheric mantle beneath Proterozoic mobile belts surrounding the Archean cratons (<160 km; Finnerty & Boyd, 1987; Nixon, 1987). High mg-numbers and depletion in fusible major elements, typical of Archean mantle xenolith suites (e.g. Boyd, 1987; Boyd *et al.*, 1997), indicate the refractory nature of the Nikos peridotites, that have been interpreted to represent the residues of large degree partial melting in the mantle (~30% melt extraction; Schmidberger & Francis, 1999). These results are supported by experimental studies (Walter, 1998) on the melting of pyrolitic mantle at high pressures and temperatures, which indicate that the most refractory Nikos peridotites would require a minimum of 30% melt extraction from a primitive mantle source.

Melt extraction should also result in the depletion in incompatible trace elements of the residual mineral assemblages (Harte, 1983; Carlson & Irving, 1994). Trace element patterns for the Nikos peridotites, however, are enriched in LILE, Th, U and LREE compared to those estimated for primitive mantle compositions (McDonough & Sun, 1995). These signatures suggest that interaction with melts or fluids during metasomatism has resulted in incompatible trace element enrichment of the mantle beneath Somerset Island. Metasomatism and partial melt extraction may have been related to a single magmatic event (e.g. Shi *et al.*, 1998) or incompatible trace element enrichment could reflect the infiltration of a metasomatic agent into lithospheric mantle that had previously been depleted in fusible major elements, as proposed for the mantle beneath the Kaapvaal craton in South Africa (e.g. Menzies & Hawkesworth, 1987; Hoal *et al.*, 1994; Pearson *et al.*, 1995a).

Depleted subcontinental lithosphere

It is important to establish the chemical composition of cratonic mantle roots because their refractory nature preserves a record of the large degree of partial melting involved in their formation during stabilization of the continents (Boyd & McCallister, 1976; Jordan, 1979; Walter, 1998). High pressure melting experiments show that the incipient melting of a carbonate-bearing garnet-peridotite produces alkalic liquids such as carbonatites and kimberlites and then picritic to komatiitic melts at larger degrees of partial melting, leaving a refractory residue that is highly depleted in fusible major elements such as Fe, Al and Ca (e.g. Takahashi & Scarfe, 1985; Baker & Stolper, 1994; Dalton & Presnall, 1998). Experimental data suggest that melting at pressures between 4.5 to 6 GPa (depths of up to 200 km), and temperatures between about 1500 to 1700 °C, produces harzburgitic residues because of the preferential melting of clinopyroxene (Canil, 1992; Walter, 1998). Loss of clinopyroxene, the main LREE carrier in peridotites, to the liquid phase depletes the residue in these elements, whereas the stability of garnet in the restite favors the retention of HREE in the residual mineral assemblage (Frey, 1969; Nagasawa et al., 1969; Hauri *et al.*, 1994). Progressive melting should result in chondrite-normalized bulk-rock REE patterns characterized by smooth LREE depleted profiles (Navon & Stolper, 1987). The Somerset peridotites are, however, characterized by enrichment in LILE and LREE compared to the HREE, despite their refractory major element signatures, as are peridotite xenolith suites from cratonic areas in South Africa and Siberia (Erlank *et al.*, 1987; Menzies *et al.*, 1987). These presumed metasomatic effects make it difficult to establish the chemical composition of the mantle roots prior to their interaction with metasomatic agents.

Previous studies have shown that bulk REE contents in peridotites are controlled by clinopyroxene and garnet, whereas orthopyroxene and olivine contribute little to REE budgets (e.g. Shimizu, 1975; Eggins *et al.*, 1998). The whole-rock REE compositions can, therefore, be modeled by quantitative mass balance calculations using the modal abundances of clinopyroxene and garnet and their respective REE contents. These mass balance calculations indicate that, in contrast to the analyzed whole-rock compositions, the calculated whole-rocks have much lower LREE abundances, while having similar

HREE contents (Table 6; Fig. 7). In particular, La and Ce are deficient in the calculated peridotite compositions by 99 to 90% for the high temperature peridotites (e.g. NK1-7; Fig. 7a) and 80 to 70% for the low temperature peridotites (e.g. NK1-4; Fig. 7b). Nd, Sm and Eu deficiencies in the calculated whole-rocks of both low temperature and high temperature peridotites range from 70 to 40%, but decrease for Dy, Er and Yb to less than 20% (Fig. 7). The calculated whole-rock REE patterns for the low temperature peridotites are approximately chondritic (e.g. NK1-4; Fig. 8b) or only slightly enriched (NK2-3). In contrast, the calculated LREE of high temperature peridotites are depleted compared to chondrites (e.g. NK1-7; Fig. 8a) and the calculated whole-rock patterns correspond to those expected for refractory mantle, with a residual mineral assemblage of olivine + orthopyroxene + garnet ± clinopyroxene, that has been depleted by a large degree of partial melting (~30 to 40 %; Navon & Stolper, 1987; Walter, 1998).

The large discrepancy for the LREE between the calculated and analyzed whole-rock compositions that was obtained for all xenoliths suggests that an interstitial phase(s) is present, either a trapped melt, or an accessory mineral phase, that contributes significantly to the LREE budget of the peridotites.

Interstitial kimberlite liquid

To account for the excess LREE contents of the whole-rock analyses, we modeled the possible presence of interstitial melt along grain boundaries of the peridotites. The calculations are based on bulk-rock trace element analyses and mineral modes, determined using a high-pressure norm calculation described in Schmidberger & Francis (1999), and a trapped melt in equilibrium with them (Bédard, 1994). The distribution of REE between minerals and trapped liquid in these calculations is determined using mineral-melt partition coefficients for the constituent peridotite phases (olivine, orthopyroxene, clinopyroxene, garnet) and a kimberlitic melt (Fujimaki *et al.*, 1984). The mass balance calculations indicate that the discrepancies can be explained by the presence of 0.1 to 2.5 wt% trapped liquid with a composition overlapping that of the Nikos kimberlite (Table 7; Fig. 9). The similarity of the trapped liquid trace element composition to that of the kimberlite suggests the presence of interstitial kimberlitic melt or a kimberlite-derived phase(s) to account for the excess LREE in the analyzed whole-rocks. The addition of 0.4 to 2 wt% kimberlite liquid to the calculated whole-rock compositions yields REE patterns that are remarkably similar to those of the analyzed bulk rocks (Table 6; Fig. 10).

Accessory minerals

The mineral apatite is known to be a major carrier for LREE with elemental abundances up to several thousand ppm (e.g. Ce: 2600 to 3000 ppm; Kramers *et al.*, 1983; Irving & Frey, 1984; O'Reilly *et al.*, 1991) and accessory apatite has been described in peridotite xenoliths (Dawson, 1980; Kramers *et al.*, 1983; O'Reilly *et al.*, 1991). Even if present in only trace amounts, apatite can play a major role in the LREE budget of mantle rocks (O'Reilly *et al.*, 1991).

We modeled the presence of apatite as a possible accessory mineral phase in the Nikos peridotites using an apatite REE composition determined by isotope dilution analysis (Kramers *et al.*, 1983) from a metasomatized South African xenolith suite. Similar REE abundances have been reported for apatite from metasomatized Australian spinel-lherzolites using proton microprobe analysis (O'Reilly *et al.*, 1991). The inclusion of small modal amounts of apatite (0.01 to 0.15 wt%) in the mass balance calculations also yields whole-rock REE patterns that are similar to the bulk-rock analyses (Table 6). Minor amounts of apatite could, therefore, also account for the LREE surplus in the Nikos whole-rock analyses. Although apatite is as yet undetected in thin sections, the presence of 0.1 wt% apatite along grain boundaries would be hard to observe optically. The presence of apatite in the Nikos peridotites could have resulted from interaction of the xenoliths with their host kimberlite, precipitating intergranular apatite during xenolith transport at 100 Ma. Whole-rock phosphorus abundances (Table 2), however, while consistent with mass balance calculations assuming the presence of a trapped interstitial kimberlite liquid in the Somerset bulk rocks (Tables 1 and 6), are 2 to 5 times lower for most xenoliths than those required by the apatite contents necessary to match the trace elements (Table 6).

Mineral phases such as phlogopite were also considered as possible LREE carriers, however, mass balance calculations indicate that more than 25 wt% mica would be required to account for the excess LREE contents. Although traces of phlogopite (maximum 1 wt%) are observed in some Nikos peridotite xenoliths, its modal abundance is completely insufficient to explain the discrepancy between calculated and analyzed whole-rock peridotite compositions.

The results of these mass balance calculations indicate that the shallow low temperature peridotites had in fact flat LREE patterns, whereas those of the deeper-seated high temperature peridotites were LREE depleted compared to chondrites before contamination by their host kimberlite.

Pyroxenites

The dominant rock type (over 90%) of the Nikos xenolith suite is peridotitic in composition, representing the Archean cratonic mantle root beneath Somerset Island, whereas pyroxenite appears to represent only a minor constituent (less than 10%; Schmidberger & Francis, 1999). The major element chemistry and mineralogy of the Nikos pyroxenites indicate that the division into high-Mg pyroxenites and low-Mg pyroxenites (Schmidberger & Francis, 1999) correlates with distinct incompatible traces element patterns. In contrast to their higher mg-numbers and a more refractory whole-rock composition, the high-Mg pyroxenites are more enriched in incompatible trace elements such as LILE and LREE than the low-Mg pyroxenites.

The major and trace element differences between high-Mg and low-Mg pyroxenites suggest that there is no direct genetic link between these two types of pyroxenites, an interpretation that is supported by their distinct Nd-Sr-Pb isotope systematics (Schmidberger & Francis, 1998). The low-Mg pyroxenites have REE profiles showing less fractionation between LREE and HREE compared to those of the peridotites and the high-Mg pyroxenites. The coarse textures, low mg-numbers and relatively depleted trace element signatures compared to the remaining samples suggest that they are cumulates, possibly representing veins in a peridotitic lithospheric mantle.

The similarity of the high-Mg pyroxenites to the peridotites in terms of their mg-numbers and high abundances of LILE and LREE is supported by their overlapping Nd-Sr-Pb isotope systematics (Schmidberger & Francis, 1998). These pyroxenites may constitute a pyroxene-rich component in the lithospheric mantle produced by small scale segregation of peridotite compositions into olivine and pyroxene-rich layers by metamorphic differentiation (Boyd et al., 1997).

Trace element partitioning

The significance of the distribution of incompatible elements between mineral pairs can be evaluated by comparing their trace element abundance ratios to experimentally determined trace element partition coefficients and to those reported in other natural systems (Iving & Frey, 1978; Irving & Frey, 1984, Harte & Kirkley, 1997; Shimizu *et al.*, 1997). The clinopyroxene/garnet REE partition coefficients for the Nikos xenoliths decrease from La to Yb, which is consistent with mineral-melt distribution coefficients for garnet that increase from the LREE to the HREE as those for clinopyroxene decrease (e.g. Halliday *et al.*, 1995 and references therein; Fig. 11). REE partitioning for clinopyroxene-garnet pairs from the high temperature peridotites (e.g. $La_{Cpx/Garn}$: 20 to 40) is consistent with experimental data for high temperature systems up to 1400 °C ($La_{Cpx/Garn}$: 20 to 80; Hauri *et al.*, 1994; Halliday *et al.*, 1995 and references therein; Fig. 11). These findings suggest that the distribution of REE between clinopyroxene and garnet equilibrated at high temperatures in these xenoliths. In contrast, clinopyroxene-garnet pairs from the low temperature peridotites and the low-Mg pyroxenite sample yield clinopyroxene/garnet partition coefficients that are significantly higher than those for the high temperature peridotites ($La_{Cpx/Garn}$: 200 to 840; Fig. 11). These partition coefficients overlap those observed in natural systems at temperatures between 800 to 1100 °C ($La_{Cpx/Garn}$: 60 to >1000; Griffin & Brueckner, 1985; Harte & Kirkley, 1997), suggesting that REE equilibration in the shallow lithosphere occurred at lower temperatures. These results confirm findings that clinopyroxene/garnet partition coefficients for the REE (e.g. $Ce_{Cpx/Garn}$; Fig. 12) vary significantly with temperature (Griffin & Brueckner, 1985).

Mantle stratification

Pressure estimates for the low temperature peridotites indicate entrainment from depths between 80 to 150 km in the lithospheric mantle. The clinopyroxenes in low temperature peridotites have REE patterns (Fig. 5b) that show strong enrichment in the LREE with abundances of up to 100 times chondrite (e.g. La: 6 to 27 ppm). These clinopyroxenes are also characterized by high Sr abundances (100 to 400 ppm; Fig. 13a, b). In contrast, the clinopyroxenes in the high temperature peridotites from depths estimated to be between 160 to 190 km have significantly lower LREE and Sr abundances than clinopyroxenes in the shallower low temperature peridotites (e.g. La up to 10 times chondrite; Figs. 5a and 13a, b).

Incompatible trace element abundances in the Nikos garnets range considerably and also correlate with temperature and pressure estimates for their xenoliths. Garnets in the low temperature peridotites are characterized by low Zr and Sr contents (9 to 60 ppm and 0.2 to 0.7 ppm, respectively), whereas garnets in the high temperature peridotites have Zr and Sr abundances (35 to 100 ppm and 0.4 to 1.1 ppm, respectively) that are significantly higher (Fig. 13c, d). Although this variation of Zr and Sr in garnet with depth could be interpreted as reflecting temperature dependent partitioning of these elements between clinopyroxene and garnet, Zr and Sr contents in the calculated whole-rocks using modal abundances of clinopyroxene and garnet and their respective Zr and Sr abundances also correlate with depth of derivation. The garnet in a peridotite from 150 km depth (NK1-3) has Zr and Sr contents overlapping those of garnets from the high temperature peridotites, but its coexisting clinopyroxene has trace element abundances and clinopyroxene/garnet partition coefficients similar to those of the low temperature peridotites (Fig. 13). The intermediate depth estimate (150 km) for this sample is consistent with it representing a transition between an upper and lower lithospheric mantle.

The correlation between incompatible trace element characteristics in clinopyroxene and garnet and estimated depth of entrainment for the Nikos peridotites is supported by calculated REE whole-rock patterns for the low temperature peridotites that are distinct from those of the high temperature peridotites, suggesting the existence of a vertically zoned lithospheric mantle root beneath Somerset Island. The strong LREE and Sr enrichment observed for clinopyroxenes in the low temperature peridotites compared to those in the high temperature peridotites suggests that the shallow lithospheric mantle beneath the Canadian craton is a significant reservoir for incompatible trace elements. The shallow lithospheric mantle could have been metasomatized by incompatible element-rich fluids or LREE enriched melts that intersected their solidus boundaries during passage through the lithosphere, originating from deeper levels of the subcontinental mantle (Wyllie, 1987). This, however, is difficult to reconcile with relatively low incompatible trace element abundances observed in the clinopyroxenes of underlying high temperature peridotites that appear to have been less affected by metasomatic melts of fluids ascending from depths. It, therefore, appears likely, that the subcontinental mantle root underneath Somerset Island is characterized by a vertical zonation in trace element distribution and that the shallow lithosphere is geochemically distinct from the deep lithosphere beneath the northern Canadian craton. The existence of this vertical layering may date from the time of its stabilization in the Archean.

Trace element systematics for clinopyroxene and garnet from Kaapvaal and Siberian peridotite xenoliths suggest that the continental lithosphere beneath these cratons is also chemically layered (e.g. Shimizu, 1975; Shimizu *et al.*, 1997). The shallow subcontinental lithospheric mantle is characterized by mineral compositions enriched in incompatible trace elements, whereas the deep lithospheric mantle has relatively low mineral incompatible trace element abundances (Shimizu, 1975; Shimizu *et al.*, 1997; Fig. 6). It is not likely that these trace element enriched signatures reflect interaction between mineral phases and the host kimberlite during sample transport, as this process should have equally affected both the low and high temperature peridotites. The trace element enriched clinopyroxene compositions of the shallow lithosphere beneath Somerset Island are similar to those observed for the Kaapvaal and the Siberian cratons, which may suggest that the upper portions of lithospheric mantle are generally enriched in incompatible trace elements compared to the deeper lithosphere.

CONCLUSIONS

Despite their high mg-numbers and refractory major element compositions, the Nikos peridotites exhibit whole-rock incompatible trace element patterns that are enriched in LILE, Th, U and LREE compared to primitive mantle compositions. The calculated whole-rock REE patterns of both the high and low temperature xenoliths have much lower LREE contents compared to the LREE enriched analyzed whole-rock compositions, while having similar HREE contents. The REE deficiency amounts to 99 to 70% for La and Ce, but 20% or less for the HREE, indicating the presence of an interstitial phase containing the excess LREE abundances observed in the analyzed peridotites. Models of an interstitial melt in equilibrium with constituent peridotite minerals yield REE patterns that are comparable to those of the Nikos kimberlites. Mass balance calculations indicate that small amounts of kimberlitic liquid (0.4 to 2 wt%) may account for excess REE contents that are observed in the Nikos peridotites. Trace amounts of apatite (0.01 to 0.15 wt%), crystallized from the host kimberlite, might also solve mass balance problems for the incompatible REE abundances. Whole-rock phosphorus contents, however, appear to be lower than those required by the apatite mass balance calculations. Most significantly, however, the calculated whole-rock compositions indicate that the shallow low temperature peridotites were characterized by flat LREE patterns, whereas the deeper-seated high temperature peridotites had depleted LREE patterns prior to contamination by their host kimberlite.

REE partitioning between garnet and clinopyroxene for high temperature xenoliths that sample the deep lithospheric mantle is consistent with high temperature experimental data indicating that these clinopyroxene-garnet pairs equilibrated at high temperatures and pressures in the lower lithosphere. REE clinopyroxene/garnet partition coefficients for the low temperature xenoliths are larger than those for the high temperature xenoliths and overlap data for mantle-derived rocks from natural systems at lower temperatures (800 to 1100 °C). These findings suggest that REE partitioning between constituent clinopyroxene and garnet in the subcontinental lithosphere is a function of temperature and thus depth.

The strong enrichment in REE and Sr in clinopyroxenes and low Zr and Sr contents in garnets observed for the low temperature peridotites compared to abundances of these elements in the high temperature peridotites suggest that the shallow subcontinental lithosphere beneath the northern Canadian craton is geochemically distinct from the underlying lower lithospheric mantle. The Somerset mantle root appears to be characterized by a depth zonation in incompatible elements that may date from the time of its stabilization in the late Archean.

ACKNOWLEDGEMENTS

We thank Tariq Ahmedali and Glenna Keating for performing the whole-rock X-ray fluorescence analyses and Glenn Poirier for assistance in obtaining the electron microprobe results. We are grateful to Nobu Shimizu from Woods Hole Oceanographic Institution and Tony Simonetti for their help with ion microprobe analyses. We also thank Fabien Rasselet for assistance in the field, hand picking separates of magmatic kimberlite for major and trace element analysis, and performing the CO_2 analyses with the assistance of Constance Guignard. We appreciate the comments of Roberta Rudnick, Bill Griffin and Graham Pearson that have significantly improved the manuscript.

REFERENCES

Baker, M. B. & Stolper, E. M. (1994). Determining the composition of high-pressure mantle melts using diamond aggregates. *Geochimica Cosmochimica Acta* **58**, 2811-2827.

Bédard, J. H. (1994). A procedure for calculating the equilibrium distribution of trace elements among the minerals of cumulate rocks, and the concentration of trace elements in the coexisting liquids. *Chemical Geology* **118**, 143-153.

Boyd, F. R. (1987). High- and low-temperature garnet peridotite xenoliths and their possible relation to the lithosphere-asthenosphere boundary beneath southern Africa. In: Nixon, P. H. (ed.) *Mantle Xenoliths*. Chichester: John Wiley & Sons, pp. 403-412.

Boyd, F. R. & McCallister, R. H. (1976). Densities of fertile and sterile garnet peridotites. *Geophysical Research Letters* **3**, 509-512.

Boyd, F. R. & Mertzman, S. A. (1987). Composition and structure of the Kaapvaal lithosphere, southern Africa. In: Mysen, B. O. (ed.) *Magmatic processes: physiochemical principles*: Geochemical Society Special Publications **1**, pp. 13-24.

Boyd, F. R., Pokhilenko, N. P., Pearson, D. G., Mertzman, S. A., Sobolev, N. V. & Finger, L. W. (1997). Composition of the Siberian cratonic mantle: evidence from Udachnaya peridotite xenoliths. *Contributions to Mineralogy and Petrology* **128**, 228-246.

Canil, D. (1992). Orthopyroxene stability along the peridotite solidus and the origin of cratonic lithosphere beneath southern Africa. *Earth and Planetary Science Letters* **111**, 83-95.

Carlson, R. W. & Irving, A. J. (1994). Depletion and enrichment history of subcontinental lithospheric mantle: an Os, Sr, Nd and Pb isotopic study of ultramafic xenoliths from the northwestern Wyoming Craton. *Earth and Planetary Science Letters* **126**, 457-472.

Cullers, L. R., Mullenax, J., Dimarco, M. J. & Nordeng, S. (1982). The trace element content and petrogenesis of kimberlites in Riley County, Kansas U.S.A. *American Mineralogist* **67**, 223-233.

Dalton, J. A. & Presnall, D. C. (1998). The continuum of primary carbonatitic-kimberlitic melt compositions in equilibrium with lherzolite: data from the system CaO-MgO-Al_2O_3-SiO_2-CO_2 at 6 GPa. *Journal of Petrology* **39**, 1953-1964.

Dawson, J. B. (1980). *Kimberlites and their xenoliths*. Berlin: Springer-Verlag.

Eggins, S. M., Rudnick, R. L. & McDonough, W. F. (1998). The composition of peridotites and their minerals: a laser-ablation ICP-MS study. *Earth and Planetary Science Letters* **154**, 53-71.

Erlank, A. J., Waters, F. G., Hawkesworth, C. J., Haggerty, S. E., Allsopp, H. L., Rickard, R. S. & Menzies, M. A. (1987). Evidence for mantle metasomatism in peridotite nodules from the Kimberley pipes, South Africa. In: Menzies, M. A. & Hawkesworth, C. J. (eds.) *Mantle metasomatism*. London: Academic Press, pp. 221-311.

Fieremans, M., Hertogen, J. & Demaiffe, D. (1984). Petrography, geochemistry and strontium isotopic composition of the Mbuji-Mayi and Kundelungu kimberlites. In: Kornprobst, J. (ed.) *Kimberlites I: Kimberlites and related rocks*. New York: Elsevier, pp. 107-120.

Finnerty, A. A. & Boyd, F. R. (1987). Thermobarometry for garnet peridotites: basis for the determination of thermal and compositional structure of the upper mantle. In: Nixon, P. H. (ed.) *Mantle Xenoliths*. Chichester: John Wiley & Sons, pp. 381-402.

Frey, F. A. (1969). Rare earth element abundances in a high-temperature peridotite intrusion. *Geochimica Cosmochimica Acta* **33**, 1429-1447.

Frisch, T. & Hunt, P. A. (1993). Reconnaissance U-Pb geochronology of the crystalline core of the Boothia Uplift, District of Franklin, Northwest Territories. In: *Radiogenic age and isotope studies: Report 7*. Geological Survey of Canada, Paper 93-2, pp. 3-22.

Fujimaki, H., Tatsumoto, M. & Aoki, K. (1984). Partition coefficients of Hf, Zr and REE between phenocrysts and groundmasses. Proceedings of the fourteenth lunar and planetary science conference, Part 2. *Journal of Geophysical Research* **89**, Suppl. B662-B672.

Grand, S. P. (1994). Mantle shear structure beneath the Americas and surrounding oceans. *Journal of Geophysical Research* **99**, 11.591-11.621.

Griffin, W. L. & Brueckner, H. K. (1985). REE, Rb-Sr and Sm-Nd studies of Norwegian eclogites. *Chemical Geology (Isotope Geoscience Section)* **52**, 249-271.

Halliday, A. N., Lee, D.-C., Tommasini, S., Davies, G. R., Paslick, C. R., Fitton, J. G. & James, D. E. (1995). Incompatible trace elements in OIB and MORB and source enrichment in the sub-oceanic mantle. *Earth and Planetary Science Letters* **133**, 379-395.

Harte, B. (1983). Mantle peridotites and processes - the kimberlite sample. In: Hawkesworth, C. J. & Norry, M. J. (eds.) *Continental basalts and mantle xenoliths*. Cheshire: Shiva Publishing Limited, pp. 46-91.

Harte, B & Kirkley, M. B. (1997) Partitioning of trace elements between clinopyroxene and garnet: data from mantle eclogites. *Chemical Geology* **136**, 1-24.

Hauri, E. H., Wagner, T. P. & Grove, T. L. (1994). Experimental and natural partitioning of Th, U, Pb and other trace elements between garnet, clinopyroxene and basaltic melts. *Chemical Geology* **117**, 149-166.

Hawkesworth, C. J., Erlank, A. J., Marsh, J. S., Menzies, M. A. & van Calsteren, P. W. (1983). Evolution of the continental lithosphere: evidence from volcanics and xenoliths in southern Africa. In: Hawkesworth, C. J. & Norry, M. J. (eds.) *Continental basalts and mantle xenoliths*. Cheshire: Shiva Publishing Limited, pp. 111-138.

Heaman, L. H. (1989). The nature of the subcontinental mantle from Sr-Nd-Pb isotopic studies on kimberlite perovskite. *Earth and Planetary Science Letters* **92**, 323-334.

Herzberg, C. T. (1993). Lithosphere peridotites of the Kaapvaal craton. *Earth and Planetary Science Letters* **120**, 13-29.

Hoal, K. E. O., Hoal, B. G., Erlank, A. J. & Shimizu, N. (1994). Metasomatism of the mantle lithosphere recorded by rare earth elements in garnets. *Earth and Planetary Science Letters* **126**, 303-313.

Irvine, G. J., Kopylova, M. G., Carlson, R. W., Pearson, D. G., Shirey, S. B. & Kjarsgaard, B. A. (1999). Age of the lithospheric mantle beneath and around the Slave craton: a rhenium-osmium isotopic study of peridotite xenoliths from the Jericho and Somerset Island kimberlites. Houston, Lunar and Planetary Institute, Contribution no. 971, *Ninth Annual V. M. Goldschmidt Conference*, 134-135.

Irving, A. J. & Frey, F. A. (1978). The distribution of trace elements between garnet megacrysts and volcanic liquids of kimberlitic to rhyolitic composition. *Geochimica Cosmochimica Acta* **42**, 771-787.

Irving, A. J. & Frey, F. A. (1984). Trace element abundances in megacrysts and their host basalts: constraints on partition coefficients and megacryst genesis. *Geochimica Cosmochimica Acta* **48**, 1201-1221.

Jordan, T. H. (1979). Mineralogies, densities and seismic velocities of garnet lherzolites and their geophysical implications. In: Boyd, F. R. & Meyer, H. O. A. (eds.) *The mantle sample: Inclusions in kimberlites and other volcanics*. Washington: American Geophysical Union, pp. 1-13.

Jordan, T. H. (1988). Structure and formation of the continental tectosphere. *Journal of Petrology,* Special Lithosphere Issue, 11-37.

Kopylova, M. G., Russell, J. K. & Cookenboo, H. (1999). Petrology of peridotite and pyroxenite xenoliths from the Jericho kimberlite: implications for the thermal state of the mantle beneath the Slave craton, Northern Canada. *Journal of Petrology* **40**, 79-104.

Kramers, J. D., Roddick, J. C. M. & Dawson, J. B. (1983). Trace element and isotope studies on veined, metasomatic and "MARID" xenoliths from Bultfontein, South Africa. *Earth and Planetary Science Letters* **65**, 90-106.

Lahaye, Y. & Arndt, N. (1996). Alteration of a komatiite flow from Alexo, Ontario, Canada. *Journal of Petrology* **37**, 1261-1284.

MacKenzie, J. M. & Canil, D. (1999). Composition and thermal evolution of cratonic mantle beneath the central Archean Slave Province, NWT, Canada. *Contributions to Mineralogy and Petrology* **134**, 313-324.

McDonough, W. F. (1990). Constraints on the composition of the continental lithospheric mantle. *Earth and Planetary Science Letters* **101**, 1-18.

McDonough, W. F. & Sun, S. S. (1995). The composition of the earth. *Chemical Geology* **120**, 223-253.

Menzies, M. A. & Hawkesworth, C. J. (1987). Upper mantle processes and composition. In: Nixon, P. H. (ed.) *Mantle Xenoliths*. Chichester: John Wiley & Sons, pp. 725-738.

Menzies, M. A., Rogers, N., Tindle, A. & Hawkesworth, C. J. (1987). Metasomatic and enrichment processes in lithospheric peridotites, an effect of asthenosphere-lithosphere interaction. In: Menzies, M. A. & Hawkesworth, C. J. (eds.) *Mantle metasomatism.* London: Academic Press, pp. 313-361.

Mitchell, R. H. (1986). *Kimberlites: Mineralogy, Geochemistry, and Petrology.* New York: Plenum Press.

Mitchell, R. H. & Brunfelt, A. O. (1975). Rare earth element geochemistry of kimberlites. *Physics and Chemistry of the Earth* **9**, 671-686.

Muramatsu, Y. (1983). Geochemical investigations of kimberlites from the Kimberley area, South Africa. *Geochemical Journal* **17**, 71-86.

Nagasawa, H., Wakita, H., Higuchi, H. & Onuma, N. (1969). Rare earths in peridotite nodules: an explanation of the genetic relationships between basalt and peridotite nodules. *Earth and Planetary Science Letters* **5**, 377-381.

Navon, O. & Stolper, E. (1987). Geochemical consequences of melt percolation: the upper mantle as a chromatographic column. *Journal of Geology* **95**, 285-307.

Nixon, P. H. (1987). Kimberlitic xenoliths and their cratonic setting. In: Nixon, P. H. (ed.) *Mantle Xenoliths.* Chichester: John Wiley & Sons, pp. 215-239.

O'Reilly, S. Y., Griffin, W. L. & Ryan, C. G. (1991). Residence of trace elements in metasomatized spinel lherzolite xenoliths: a proton-microprobe study. *Contributions to Mineralogy and Petrology* **109**, 98-113.

Paul, D. K., Potts, P. J., Gibson, G. L. & Harris, P. G. (1975). Rare earth element abundance in Indian kimberlites. *Earth and Planetary Science Letters* **15**, 151-158.

Pearson, D. G., Carlson, R. W., Shirey, S. B., Boyd, F. R. & Nixon, P. H. (1995a). Stabilisation of Archean lithospheric mantle: a Re-Os isotope study of peridotite xenoliths from the Kaapvaal craton. *Earth and Planetary Science Letters* **134**, 341-357.

Pearson, D. G., Shirey, S. B., Carlson, R. W., Boyd, F. R., Pokhilenko, N. P. & Shimizu, N. (1995b). Re-Os, Sm-Nd, and Rb-Sr isotope evidence for thick Archean lithospheric mantle beneath the Siberian craton modified by multistage metasomatism. *Geochimica Cosmochimica Acta* **59**, 959-977.

Pell, J. (1993). New kimberlite discoveries on Somerset Island. *Exploration Overview 1993.* Yellowknife: NWT Geology Division, Department of Indian and Northern Affairs, pp. 47.

Pollack, H. N. (1986). Cratonization and thermal evolution of the mantle. *Earth and Planetary Science Letters* **80**, 175-182.

Ringwood, A. E., Kesson, S. E., Hibberson, W. & Ware, N. (1992). Origin of kimberlites and related magmas. *Earth and Planetary Science Letters* **113**, 521-538.

Schmidberger, S.S. & Francis, D. (1998). Pb, Nd, Sr, and Hf isotope data for Somerset Island mantle xenoliths – Evidence for Archean deep mantle roots beneath Northern Canada. *Annual meeting GAC/MAC*, A-167.

Schmidberger, S. S. & Francis, D. (1999). Nature of the mantle roots beneath the North American craton: mantle xenolith evidence from Somerset Island kimberlites. *Lithos* **48**, 195-216.

Shi, L., Francis, D., Ludden, J., Frederiksen, A. & Bostock, M. (1998). Xenolith evidence of lithospheric melting above anomalously hot upper mantle under the nortern Canadian Cordillera. *Contributions to Mineralogy and Petrology* **131**, 39-53.

Shimizu, N. (1975). Rare earth elements in garnets and clinopyroxenes from garnet lherzolite nodules in kimberlites. *Earth and Planetary Science Letters* **25**, 26-32.

Shimizu, N. (1999). Young geochemical features in cratonic peridotites from Southern Africa and Siberia. In: Fei, Y., Bertka, C. M. & Mysen, B. O. (eds.) *Mantle petrology: field observations and high pressure experimentation: a tribute to Francis R. (Joe) Boyd*: The Geochemical Society, pp. 47-55.

Shimizu, N., Pokhilenko, N. P., Boyd, F. R. & Pearson, D. G. (1997). Geochemical characteristics of mantle xenoliths from the Udachnaya kimberlite pipe. *Russian Geology and Geophysics* **38**, 205-217.

Smith, C. B., Allsopp, H. L., Garvie, O. G., Kramers, J. D., Jackson, P. F. S. & Clement, C. R. (1989). Note on the U-Pb perovskite method for dating kimberlites: examples from the Wesselton and DeBeers mines, South Africa, and Somerset Island, Canada. *Chemical Geology (Isotope Geos.)* **79**, 137-145.

Steward, W. D. (1987). Late Proterozoic to Early Tertiary stratigraphy of Somerset Island and northern Boothia Peninsula, District of Franklin. *Geological Survey of Canada Paper* **83-26**, 78 p.

Sun, S. S. & McDonough, W. F. (1989). Chemical and isotopic systematics of oceanic basalts: implications for mantle composition and processes. In: Saunders, A. D. & Norry, M. J. (eds.) *Magmatism in the oceanic basins*. London: Geological Society, pp. 313-345.

Takahashi, E. & Scarfe, C. M. (1985). Melting of peridotite to 14 GPa and the genesis of komatiite. *Nature* **315**, 566-568.

Trettin, H. P., Frisch, T. O., Sobczak, L. W., Weber, J. R., Niblett, E. R., Law, L. K., DeLaurier, I. & Witham, K. (1972). The Innuitian Province. In: Price, R. A. & Douglas, R. J. W. (eds.) *Variations in tectonic styles in Canada. Geological Association of Canada, Special Paper* **11**, 83-179.

Walter, M. J. (1998). Melting of garnet peridotite and the origin of komatiite and depleted lithosphere. *Journal of Petrology* **39**, 29-60.

Wedepohl, K. H. & Muramatsu, Y. (1979). The chemical composition of kimberlites compared with the average composition of three basaltic magma types. In: Boyd, F. R. & Meyer, H. O. A. (eds.) *Kimberlites, diatremes and diamonds: their geology and petrology and geochemistry*. Washington: American Geophysical Union, pp. 300-312.

Wyllie, P. J. (1987). Metasomatism and fluid generation in mantle xenoliths. In: Nixon, P. H. (ed.) *Mantle Xenoliths*. Chichester: John Wiley & Sons, pp. 609-621.

Woolley, A. R. & Kempe, D. R. C. (1989). Carbonatites nomenclature, average chemical compositions, and elemental distribution. In: Bell, K. (ed.) *Carbonatites; genesis and evolution*. London: Unwin Hyman Inc., pp. 1-14.

Figure Captions

Figure 3-1. Geological map of Somerset Island (after Steward, 1987) showing kimberlite locations. Legend: light gray, Paleozoic cover rocks; striped, Late Proterozoic cover rocks; dark gray, Precambrian basement; bold lines, normal faults.

Figure 3-2. (a) Primitive mantle-normalized trace element and (b) chondrite-normalized rare earth element patterns for Nikos kimberlites compared to data for kimberlites from South Africa, Zaire, North America and India (Mitchell & Brunfelt, 1975; Paul *et al.*, 1975; Cullers *et al.*, 1982; Wedepohl & Muramatsu, 1979; Muramatsu, 1983; Fieremans *et al.*, 1984; Mitchell, 1986). Primitive mantle and chondrite values after Sun & McDonough (1989).

Figure 3-3. (a) Primitive mantle-normalized trace element and (b) chondrite-normalized rare earth element patterns for Nikos peridotites. Data for Nikos kimberlites are plotted for comparison.

Figure 3-4. (a) Primitive mantle-normalized trace element and (b) chondrite-normalized rare earth element patterns for Nikos pyroxenites. Data for Nikos kimberlites and peridotite field are plotted for comparison.

Figure 3-5. Chondrite-normalized rare earth element patterns for coexisting clinopyroxene and garnet in Nikos peridotites. (a) Clinopyroxene from high temperature peridotites is mildly enriched in LREE but depleted in HREE compared to coexisting garnet. (b) Clinopyroxene-garnet pairs with highly light rare earth element enriched clinopyroxene from low temperature xenoliths.

Figure 3-6. Chondrite-normalized rare earth element patterns for Nikos (a) clinopyroxene and (b) garnet compared to fields based on data from high temperature (high-T) and low temperature (low-T) peridotites from the Kaapvaal craton and high temperature peridotites from the Siberian craton (Shimizu, 1975; Shimizu *et al.*, 1997).

Figure 3-7. Rare earth element mass balance results for (a) high temperature peridotite NK1-7 and (b) low temperature peridotite NK1-4 showing deficiency or surplus (%) of each element calculated using the modal abundances of clinopyroxene and garnet and their respective REE contents compared to the analyzed whole-rock abundance. The rare earth element contents of olivine and orthopyroxene were assumed to be zero.

Figure 3-8. Calculated chondrite-normalized rare earth element patterns (Calc. Whole-rock) for (a) high temperature peridotite NK1-7 and (b) low temperature peridotite NK1-4 using mass balance calculations based on rare earth element contents of constituent garnet and clinopyroxene and their respective modal abundances. Rare earth element patterns for analyzed whole-rock (Whole-rock), garnet and clinopyroxene are plotted for comparison.

Figure 3-9. Calculated chondrite-normalized rare earth element patterns for possible interstitial liquids in equilibrium with constituent mineral phases of the Nikos peridotites (after Bédard, 1994). Nikos kimberlites are plotted for comparison.

Figure 3-10. Calculated chondrite-normalized rare earth element patterns (Calc. WR & Kimb.) for (a) high temperature peridotite NK1-7 and (b) low temperature peridotite NK1-4 before and after the addition of 0.4 wt% (NK1-7) and 1.2 wt% (NK1-4) interstitial kimberlite liquid.

Table 3-1. Major, trace and rare earth element analyses for kimberlites

Sample	NK3-K1	NK3-K2	NK3-K3	NK3-K4	NK3-K5
Rock	Kimberlite	Kimberlite	Kimberlite	Kimberlite	Kimberlite
wt%					
SiO_2	19.85	25.05	23.21	22.72	23.62
TiO_2	2.06	2.15	1.62	1.73	1.51
Al_2O_3	2.20	2.81	2.03	1.90	1.64
FeO	7.06	8.13	6.99	7.32	7.26
MnO	0.14	0.16	0.15	0.14	0.15
MgO	19.97	26.12	23.07	23.03	25.59
CaO	21.58	15.34	17.57	18.90	16.61
Na_2O	0.19	0.14	0.06	0.09	0.10
K_2O	1.00	0.66	0.55	0.30	0.59
P_2O_5	0.64	0.64	0.92	0.83	0.85
H_2O	1.43	5.00	5.07	8.55	0.00
CO_2	22.78	12.68	17.10	13.19	20.96
Total	98.90	98.88	98.35	98.71	98.88
$CaCO_3$	38.52	27.38	31.36	30.00	29.65
ppm					
Cr	1000	1200	1220	1200	947
Ni	661	776	815	855	491
Nb	147	165	179	192	136
Ta	10.3	10.5	10.5	10.9	8.9
V	145	145	137	132	99
Zn	70	83	78	83	11
Y	13.0	14.0	16.0	16.0	13.0
Zr	159	155	190	182	154
Hf	3.60	4.10	4.60	4.30	3.50
Cs	1.00	0.80	0.50	0.50	0.40
Ba	2060	1730	2370	2380	1910
Rb	72.0	44.0	30.0	20.0	31.0
Sr	1320	1030	1710	2190	1330
Th	14.4	14.1	18.5	17.5	14.1
U	2.90	3.17	3.52	3.83	2.93
Pb	11.0	14.0	14.0	28.0	35.0
La	133	123	154	143	124
Ce	209	207	273	255	223
Pr	21.7	21.5	28.8	26.2	22.9
Nd	77.3	78.3	103	95.7	82.5
Sm	11.0	11.3	14.3	13.7	11.6
Eu	2.74	2.74	3.43	3.18	2.84
Gd	8.26	8.46	10.6	9.81	8.98
Tb	0.77	0.82	0.97	0.93	0.80
Dy	3.18	3.33	3.92	3.75	3.10
Ho	0.46	0.46	0.54	0.53	0.43
Er	0.90	0.96	1.12	1.03	0.90
Tm	0.09	0.10	0.10	0.10	0.08
Yb	0.42	0.52	0.44	0.48	0.36
Lu	0.07	0.08	0.08	0.07	0.06

Major element compositions were analyzed by X-ray fluorescence analysis at McGill University; analytical procedures have been described by Schmidberger & Francis (1999). Trace and rare earth element compositions were determined using ICP-MS analysis (for analytical procedures, see Table 3-3).

Table 3-2. Major element analyses and calculated mineral modes for bulk xenoliths

Sample	NK1-1	NK1-2	NK1-3	NK1-4	NK1-5	NK1-6	NK1-7	NK1-9	NK1-12	NK1-14	NK1-15	NK1-18	NK1-23	NK2-1	NK2-2
Rock	Perid	Perid	Perid	Perid	Perid	Perid	Perid	Perid	Perid	Perid	Perid	Perid	Perid	Perid	Perid
Texture	coarse	coarse	coarse	coarse	coarse	coarse	porphyr	coarse	coarse	coarse	coarse	coarse	coarse	coarse	porphyr
wt%															
SiO_2	41.25	41.77	40.81	41.60	42.28	40.37	41.24	41.88	40.80	42.02	42.29	42.94	41.01	45.66	42.69
TiO_2	0.07	0.03	0.03	0.06	0.07	0.02	0.03	0.04	0.03	0.03	0.06	0.03	0.10	0.09	0.08
Al_2O_3	1.00	1.31	1.33	2.43	1.95	1.25	1.57	1.59	0.56	1.71	1.09	0.79	2.71	1.31	2.17
FeO	7.49	7.39	7.42	7.09	7.74	7.10	7.06	7.29	7.76	7.27	7.30	6.97	7.81	7.08	7.69
MnO	0.11	0.11	0.11	0.13	0.12	0.10	0.10	0.11	0.11	0.11	0.11	0.10	0.12	0.12	0.12
MgO	43.30	44.44	44.03	40.90	41.49	43.41	43.55	43.48	45.32	42.92	42.69	44.93	40.25	42.09	42.80
CaO	0.58	1.11	0.82	1.20	1.44	0.41	0.72	0.96	0.57	1.13	0.88	0.54	1.79	0.93	2.21
Na_2O	0.02	0.10	0.01	0.01	0.06	0	0	0.03	0.12	0.15	0.01	0.05	0.16	0.40	0.19
K_2O	0.04	0.03	0.04	0.07	0.08	0.03	0.02	0.04	0.16	0.03	0.12	0.03	0.10	0.16	0.11
P_2O_5	0.01	0.02	0.02	0.01	0.01	0.01	0	0.01	0.03	0.02	0.03	0.01	0.02	0.01	0.01
Cr_2O_3	0.46	0.35	0.41	0.75	0.58	0.47	0.48	0.52	0.34	0.44	0.38	0.35	0.41	0.48	0.37
NiO	0.33	0.32	0.33	0.40	0.30	0.33	0.31	0.32	0.37	0.31	0.34	0.35	0.29	0.30	0.32
LOI	5.07	2.71	3.89	4.76	3.50	5.85	4.31	3.59	3.46	3.49	4.09	2.75	4.68	1.32	1.14
Total	99.73	99.69	99.25	99.41	99.62	99.35	99.39	99.86	99.63	99.63	99.39	99.84	99.45	99.95	99.90
mg-no.	0.912	0.915	0.914	0.911	0.905	0.916	0.917	0.914	0.912	0.913	0.913	0.920	0.902	0.914	0.908
Calculated modes in wt%															
Oliv	79	82	83	67	72	81	79	78	89	77	74	78	74	65	78
Opx	15	8	9	22	14	12	13	13	6	12	18	17	8	27	5
Cpx	1	4	2	5	5	1	1	2	4	4	3	1	7	5	10
Garn	5	6	7	6	9	7	8	8	2	7	5	4	11	3	8
Temperatures and pressures															
Temp (°C)	1222	1042	1076	871	1262	1149	1300	1219	1045	1027	1131	1223	964	1216	1316
Press (kb)	52.7	44.7	46.5	33.5	54.6	48.8	55.1	53.4	45.3	42.7	48.0	52.1	39.0	51.5	54.7

Table 3-2. continued

Sample	NK2-3	NK2-5	NK2-10	NK3-4	NK3-11	NK3-13	NK3-15	NK3-16	NK3-20	NK3-24	NK3-25	NK2-7	NK3-14	NK3-1	NK3-17
Rock	Perid	Perid	Perid	Perid	Perid	Perid	Perid	Perid	Perid	Perid	Perid	HMg-Px	HMg-Px	LMg-Px	LMg-Px
Texture	coarse	porphyr	coarse	coarse	coarse	coarse	coarse	coarse	coarse	coarse	coarse	coarse	coarse	coarse	coarse
wt%															
SiO_2	42.46	43.22	41.54	41.02	40.88	39.05	40.83	40.45	43.19	45.04	41.42	48.95	40.72	50.97	50.15
TiO_2	0.09	0.15	0.03	0.11	0.06	0.05	0.07	0.06	0.10	0.03	0.21	0.13	0.23	0.18	0.18
Al_2O_3	2.90	1.06	1.25	3.34	1.10	1.07	1.39	0.93	3.21	2.24	4.28	8.05	11.40	4.71	4.89
FeO	7.21	8.07	7.43	7.15	6.99	6.96	6.47	7.93	7.58	6.19	7.41	4.93	6.85	6.04	6.01
MnO	0.13	0.12	0.11	0.11	0.10	0.09	0.09	0.10	0.13	0.12	0.13	0.18	0.24	0.15	0.15
MgO	41.87	44.14	45.53	37.17	42.70	40.95	40.67	44.79	37.50	39.84	39.46	23.69	27.87	19.44	19.48
CaO	1.98	1.01	1.22	3.64	2.80	2.28	2.82	1.54	3.21	2.19	2.13	9.45	4.68	16.46	16.91
Na_2O	0.15	0.04	0.07	0.21	0.10	0.18	0.04	0.08	0.35	0.08	0.09	0.90	0.36	0.46	0.28
K_2O	0.19	0.05	0.05	0.32	0.05	0.07	0.07	0.04	0.14	0.05	0.52	0.11	1.13	0.11	0.09
P_2O_5	0.02	0.01	0.04	0.02	0.02	0.02	0.02	0.01	0.02	0.01	0.04	0.01	0.11	0.02	0.01
Cr_2O_3	0.71	0.46	0.36	0.43	0.54	0.59	0.38	0.30	0.46	0.66	0.75	1.16	1.50	0.54	0.50
NiO	0.31	0.33	0.32	0.28	0.31	0.30	0.34	0.32	0.28	0.24	0.25	0.38	0.22	0.09	0.09
LOI	1.77	1.01	1.84	5.57	3.88	8.11	6.32	3.01	3.30	3.10	2.81	1.90	4.07	0.52	0.58
Total	99.79	99.67	99.79	99.37	99.53	99.72	99.51	99.56	99.47	99.79	99.50	99.84	99.38	99.69	99.32
mg-no.	0.912	0.907	0.916	0.903	0.916	0.913	0.918	0.910	0.898	0.920	0.905	0.895	0.879	0.852	0.852
Calculated modes in wt%															
Oliv	73	77	86	68	82	83	75	89	62	57	70	4	9	0	0
Opx	7	16	4	2	1	1	6	1	11	26	5	41	44	24	22
Cpx	8	3	5	17	13	12	12	7	15	7	8	39	22	67	68
Garn	12	5	6	13	5	5	6	4	12	11	17	15	25	9	10
Temperatures and pressures															
Temp (°C)	887	1371	1014	1371	1247	830	1343	1280	815	770	1256	737	933	759	720
Press (kb)	34.6	57.9	42.1	59.6	53.1	30.9	58.5	53.5	29.8	24.7	54.0	25.3	36.8	25.1	22.2

LOI, loss on ignition. Total Fe is given as FeO and mg-number = Mg/(Mg+Fe). Perid, peridotite; HMg-Px, High-Mg pyroxenite; LMg-Px, Low-Mg pyroxenite; porphyry, porphyroclastic. Modes were determined using whole-rock compositions and a high-pressure peridotite norm calculation procedure (Schmidberger and Francis, 1999). Temperature and pressure calculations have been discussed by Schmidberger & Francis (1999). Analytical procedures as in Table 3-1.

Table 3-3. Trace and rare earth element analyses for bulk xenoliths

Sample Rock Texture	NK1-1 Perid coarse	NK1-2 Perid coarse	NK1-3 Perid coarse	NK1-4 Perid coarse	NK1-5 Perid coarse	NK1-6 Perid coarse	NK1-7 Perid porphyr	NK1-9 Perid coarse	NK1-12 Perid coarse	NK1-14 Perid coarse	NK1-15 Perid coarse	NK1-18 Perid coarse	NK1-23 Perid coarse	NK2-1 Perid coarse	NK2-2 Perid porphyr
ppm															
Nb	1.70	1.70	2.22	1.67	1.76	1.20	0.60	1.20	3.10	2.03	6.36	1.15	8.42	1.30	0.89
Ta	0.08	0.07	0.09	0.06	0.11	0.06	0.04	0.08	0.17	0.07	0.31	0.06	0.11	0.10	0.07
V	23.0	30.5		44.7		25.0		35.5	18.0	36.3				32.0	56.7
Zn	42.0	38.9		37.1		37.0		42.8	49.0	41.3				38.0	43.8
Y	1.10	0.88	1.84	1.30	1.80	1.60	0.92	1.18	1.00	1.23	0.83	0.31	3.45	0.70	1.57
Zr	6.50	2.86	6.79	3.53	8.81	7.00	3.31	6.31	8.90	3.02	9.91	2.52	8.08	4.30	4.77
Hf	0.100	0.045	0.104	0.079	0.207	0	0.077	0.145	0.200	0.064	0.214	0.051	0.206	0.100	0.135
Cs	0	0.14	0.14	0.21	0.19	0	0.09	0.15	0.10	0.17	0.58	0.14	0.39	0.20	0.19
Ba	31.0	18.9	22.2	45.6	27.9	18.0	10.5	14.8	126	27.4	89.6	13.1	105	23.0	28.6
Rb	1.10	1.15	1.72	3.03	4.29	0.80	1.03	1.53	3.20	1.43	7.25	1.85	4.72	10.0	6.47
Sr	25.7	33.8	56.3	43.3	46.5	17.1	15.2	17.8	56.5	43.7	66.7	41.7	86.5	31.3	33.5
Th	0.340	0.165	0.199	0.209	0.177	0.240	0.061	0.131	0.370	0.200	0.644	0.095	0.939	0.180	0.135
U	0.090	0.031	0.098	0.059	0.078	0	0.012	0.027	0.060	0.055	0.093	0.067	0.129	0	0.063
Pb	0	0.116	0.014	0.174	0.017	0	0.001	0.206	0	0.076	0.028	0.007	0.023	0	0.037
La	1.36	1.92	1.88	1.99	1.44	0.690	0.500	0.972	2.62	2.31	5.01	0.872	8.38	0.510	0.815
Ce	2.81	4.16	3.56	3.46	2.57	1.82	0.875	1.97	5.22	4.99	9.22	1.50	12.26	1.42	1.81
Pr	0.311	0.495	0.438	0.383	0.305	0.230	0.109	0.232	0.584	0.510	1.073	0.166	1.19	0.162	0.245
Nd	1.15	1.87	1.73	1.45	1.15	0.970	0.448	0.922	2.21	2.03	3.85	0.608	3.68	0.630	1.08
Sm	0.210	0.285	0.368	0.226	0.264	0.220	0.143	0.249	0.400	0.258	0.590	0.120	0.562	0.140	0.292
Eu	0.072	0.079	0.119	0.066	0.093	0.073	0.047	0.086	0.110	0.076	0.150	0.039	0.170	0.046	0.091
Gd	0.230	0.218	0.381	0.199	0.349	0.250	0.158	0.221	0.280	0.223	0.444	0.120	0.576	0.160	0.234
Tb	0.040	0.029	0.058	0.032	0.058	0.050	0.023	0.035	0.040	0.035	0.053	0.015	0.094	0.030	0.039
Dy	0.220	0.169	0.306	0.208	0.337	0.280	0.134	0.234	0.210	0.173	0.186	0.059	0.517	0.150	0.278
Ho	0.040	0.035	0.060	0.048	0.062	0.060	0.031	0.046	0.040	0.043	0.028	0.008	0.112	0.030	0.064
Er	0.100	0.098	0.156	0.132	0.147	0.160	0.094	0.106	0.100	0.117	0.076	0.022	0.319	0.070	0.172
Tm	0.013	0.014	0.024	0.020	0.021	0.025	0.018	0.016	0.014	0.022	0.008	0.003	0.051	0.008	0.028
Yb	0.080	0.099	0.154	0.142	0.141	0.160	0.124	0.104	0.070	0.128	0.055	0.021	0.331	0.050	0.181
Lu	0.013	0.016	0.026	0.025	0.025	0.026	0.021	0.017	0.013	0.026	0.008	0.004	0.055	0.008	0.029

Table 3-3. continued

Sample	NK2-3	NK2-5	NK2-10	NK3-4	NK3-11	NK3-13	NK3-15	NK3-16	NK3-20	NK3-24	NK3-25	NK2-7	NK3-14	NK3-1	NK3-17
Rock	Perid	Perid	Perid	Perid	Perid	Perid	Perid	Perid	Perid	Perid	Perid	HMg-Px	HMg-Px	LMg-Px	LMg-Px
Texture	coarse	porphyr	coarse	coarse	coarse	coarse	coarse	coarse	coarse	coarse	coarse	coarse	coarse	coarse	coarse
ppm															
Nb	3.71	1.30	3.51	2.45	1.57	5.81	1.50	1.19	2.46	2.11	4.22	6.50	16.1	1.46	1.40
Ta	0.09	0.07	0.11	0.15	0.10	0.22	0.09	0.08	0.04	0.08	0.24	0.05	1.09	0.09	0.03
V	54.7	34.0			49.6	38.5	34.0	28.9	80.0		68.3	156	117		221
Zn	41.3	35.0			41.3	47.0	38.1	46.8	44.8		43.2	18.0	26.5		18.0
Y	2.52	1.10	1.96	3.50	0.74	0.79	0.48	1.03	3.04	1.14	3.13	8.30	16.1	7.14	7.10
Zr	6.56	4.80	6.85	9.76	4.84	2.62	5.56	3.72	5.57	2.03	11.3	9.40	39.5	10.2	4.80
Hf	0.182	0.100	0.115	0.237	0.139	0.055	0.131	0.092	0.182	0.048	0.265	0.300	0.685	0.345	0.200
Cs	0.21	0.10	0.13	0.38	0.13	0.16	0.10	0.08	0.21	0.18	0.36	0.30	0.81	0.18	0
Ba	93.9	14.0	82.0	50.6	16.9	63.7	23.3	42.5	82.5	51.2	83.9	148	451	50.0	71.0
Rb	7.52	1.90	2.99	23.2	2.91	2.90	3.66	1.77	7.33	3.66	28.7	4.10	30.2	5.06	3.60
Sr	77.7	14.9	92.6	245	202	129	344	40.9	55.9	128	37.5	284	162	90.3	38.8
Th	0.598	0.200	0.495	0.217	0.165	0.529	0.221	0.131	0.265	0.238	0.267	1.45	0.860	0.226	0.350
U	0.193	0	0.187	0.502	0.642	0.386	0.779	0.196	0.125	0.416	0.347	0.800	0.897	0.050	0.150
Pb	0.219	0	0.060	0.028	0.359	0.447	1.29	0.213	0.553	0.027	0.332	0	1.52	0.033	0
La	5.35	0.840	5.21	3.26	1.44	3.23	2.09	1.26	3.19	2.05	3.30	19.30	8.68	2.59	2.20
Ce	7.94	2.09	8.58	5.37	2.51	5.75	3.40	2.22	4.08	3.48	4.74	27.30	16.65	5.89	4.17
Pr	0.757	0.244	0.992	0.601	0.272	0.638	0.330	0.254	0.380	0.362	0.471	1.89	2.05	0.832	0.471
Nd	2.58	0.970	3.48	2.21	1.09	2.35	1.19	0.970	1.52	1.16	1.76	5.13	7.86	3.40	2.13
Sm	0.402	0.210	0.559	0.421	0.276	0.298	0.215	0.208	0.299	0.170	0.327	0.910	1.62	0.768	0.680
Eu	0.128	0.070	0.158	0.154	0.084	0.084	0.093	0.064	0.112	0.052	0.104	0.280	0.654	0.241	0.223
Gd	0.323	0.240	0.496	0.487	0.213	0.240	0.196	0.175	0.420	0.166	0.322	1.07	1.87	0.949	0.970
Tb	0.057	0.040	0.072	0.080	0.028	0.030	0.025	0.028	0.059	0.026	0.063	0.210	0.335	0.173	0.190
Dy	0.341	0.210	0.338	0.489	0.166	0.159	0.125	0.190	0.423	0.152	0.507	1.28	2.52	1.08	1.18
Ho	0.087	0.040	0.063	0.113	0.028	0.030	0.021	0.043	0.099	0.037	0.113	0.300	0.541	0.244	0.270
Er	0.255	0.100	0.170	0.335	0.067	0.081	0.051	0.114	0.330	0.119	0.328	0.900	1.48	0.705	0.770
Tm	0.036	0.014	0.024	0.055	0.009	0.010	0.007	0.017	0.043	0.020	0.051	0.147	0.264	0.102	0.127
Yb	0.302	0.070	0.152	0.366	0.062	0.076	0.050	0.106	0.342	0.140	0.319	0.940	1.53	0.659	0.760
Lu	0.040	0.011	0.025	0.060	0.014	0.013	0.015	0.016	0.050	0.026	0.063	0.139	0.298	0.099	0.109

Rock types as in Table 3-2. Trace and rare earth element compositions were determined using ICP-MS analysis. Reproducibility is 1 to 3% (1SD); detection limits are 2 to 20 ppt for most elements, except Zr (40 ppt), and Sr and Ba (both 150 ppt). All blank levels are lower than the detection limit. For data acquisition parameters and data reduction procedures see Lahaye & Arndt (1996).

Figure 3-11. Clinopyroxene-garnet partition coefficients in Nikos peridotites. Fields for high temperature experimental data (to 1400 °C) after Hauri *et al.* (1994), Halliday *et al.* (1995) and references therein and data for natural systems (800 to 1100 °C) after Griffin & Brueckner (1985) and Harte & Kirkley (1997).

Figure 3-12. Temperature dependence of clinopyroxene-garnet Ce partitioning ($Ce_{Cpx/Garn}$) in the Nikos peridotites.

Figure 3-13. Depth distribution of (a) La and (b) Sr abundances in clinopyroxenes and (c) Zr and (d) Sr abundances (ppm) in garnets of low and high temperature peridotites.

Table 3-4. Major, trace and rare earth element analyses of clinopyroxenes

Sample Rock	NK1-3 Perid	NK1-4 Perid	NK1-5 Perid	NK1-7 Perid	NK1-14 Perid	NK2-1 Perid	NK2-2 Perid	NK2-3 Perid	NK2-5 Perid	NK3-4 Perid	NK3-1 LMg-Px
wt%											
SiO_2	54.19	53.58	54.72	54.11	53.86	53.87	53.81	53.32	54.35	55.32	53.99
TiO_2	0.13	0.12	0.17	0.08	0.12	0.10	0.20	0.20	0.48	0.15	0.08
Al_2O_3	2.98	2.87	2.52	2.36	2.67	2.31	2.82	2.73	2.33	2.89	1.73
FeO	2.31	1.60	2.65	2.34	2.19	2.44	2.89	2.00	3.05	2.76	3.12
MnO	0.09	0.08	0.10	0.08	0.07	0.08	0.08	0.06	0.11	0.09	0.06
MgO	15.84	16.13	17.52	18.07	16.06	17.45	18.23	15.98	18.54	17.85	16.82
CaO	19.14	20.56	18.87	18.68	19.59	19.31	18.29	21.13	18.18	17.71	23.61
Na_2O	2.46	2.06	1.93	1.61	2.27	1.74	1.76	1.94	1.55	1.86	0.63
Cr_2O_3	2.27	1.95	1.96	1.77	2.19	2.19	1.15	1.85	1.75	1.01	0.45
NiO	0.04	0.03	0.05	0.06	0.04	0.05	0.06	0.04	0.06	0.05	0.08
Total	99.45	98.98	100.48	99.18	99.06	99.55	99.29	99.24	100.40	99.69	100.57
mg-no.	0.924	0.947	0.922	0.932	0.929	0.927	0.918	0.934	0.916	0.920	0.906
ppm											
La	6.21	7.72	0.739	0.828	8.55	0.442	0.806	26.8	1.88	0.474	1.72
Ce	30.5	19.9	3.40	3.78	37.0	1.75	3.81	50.8	7.97	3.34	6.33
Nd	24.7	8.07	3.26	3.96	18.7	2.00	4.77	11.7	6.42	4.22	4.20
Sm	5.60	0.937	1.05	0.877	2.50	0.667	1.11	1.50	1.44	1.13	0.861
Eu	1.50	0.263	0.277	0.269	0.553	0.214	0.306	0.440	0.424	0.317	0.269
Dy	1.07	0.251	0.273	0.238	0.354	0.408	0.425	0.654	0.626	0.614	0.470
Er	0.295	0.122	0.074	0.168	0.152	0.155	0.216	0.283	0.239	0.220	0.165
Yb	0.236	0.092	0.104	0.096	0.122	0.123	0.180	0.229	0.225	0.152	0.141
Ti	778	625	1041	469	925	664	1206	1214	2910	867	522
V	410	449	314	296	451	257	318	454	257	309	298
Cr	16115	14832	15204	13858	18368	15601	8875	14959	14081	7968	3603
Sr	406	112	75.0	86.9	217	45.8	106	318	142	92.7	61.3
Y	3.36	0.66	1.28	0.82	1.63	1.19	1.90	2.03	2.21	1.88	0.91
Zr	84.1	9.6	25.3	9.2	24.4	18.6	12.7	24.0	16.9	14.4	6.3

Perid, peridotite; LMg-Px, Low-Mg pyroxenite. Major element compositions were analyzed by electron microprobe analysis at McGill University; analytical procedures as described by Schmidberger & Francis (1999). Trace element (Ti, V, Cr, Sr, Y, Zr) and REE compositions were determined using ion microprobe analysis at Woods Hole Oceanographic Institution. Analytical procedures as given in Shimizu *et al.* (1997).

Table 3-5. Major, trace and rare earth element analyses of garnets

Sample Rock Color	NK1-3 Perid purple	NK1-4 Perid purple	NK1-5 Perid red	NK1-7 Perid purple	NK1-14 Perid purple	NK2-1 Perid purple	NK2-2 Perid red	NK2-3 Perid purple	NK2-5 Perid purple	NK3-4 Perid red	NK3-1 LMg-Px light red
wt%											
SiO_2	41.44	41.28	42.04	41.46	42.13	41.17	42.08	41.34	41.20	42.22	40.67
TiO_2	0.08	0.09	0.24	0.14	0.08	0.23	0.29	0.08	0.87	0.25	0.05
Al_2O_3	21.19	20.54	20.09	20.29	20.86	19.35	21.57	21.44	18.13	22.30	22.00
FeO	7.46	7.93	7.07	6.24	7.33	7.08	6.87	7.85	6.84	7.16	14.89
MnO	0.39	0.44	0.35	0.30	0.41	0.36	0.31	0.48	0.32	0.32	0.60
MgO	20.43	19.38	20.19	20.67	19.98	19.63	21.16	19.53	19.44	21.15	14.63
CaO	5.12	5.68	5.26	5.22	4.87	5.67	4.50	5.28	6.61	4.01	5.88
Na_2O	0.03	0.02	0.03	0.02	0.03	0.02	0.03	0.03	0.05	0.03	0.01
Cr_2O_3	4.13	4.41	4.80	4.76	4.04	5.78	2.55	3.21	6.77	2.00	1.32
NiO	0.00	0.00	0.01	0.02	0.00	0.01	0.01	0.01	0.01	0.01	0.00
Total	100.29	99.77	100.07	99.10	99.73	99.29	99.37	99.25	100.23	99.48	100.04
mg-no.	0.830	0.813	0.836	0.855	0.829	0.832	0.846	0.816	0.835	0.840	0.637
ppm											
La	0.029	0.025	0.018	0.029	0.044	0.016	0.019	0.032	0.052	0.026	0.004
Ce	0.411	0.147	0.148	0.281	0.680	0.097	0.118	0.275	0.679	0.094	0.023
Nd	2.04	0.474	0.638	1.23	1.24	0.839	0.712	0.495	2.34	0.437	0.342
Sm	1.86	0.586	0.800	0.952	0.908	1.05	0.596	0.421	1.43	0.529	0.403
Eu	0.946	0.213	0.424	0.454	0.349	0.645	0.276	0.239	0.591	0.254	0.281
Dy	3.93	2.19	2.31	1.55	2.12	3.90	2.11	2.38	2.07	2.02	4.57
Er	1.87	1.90	0.952	1.08	1.30	1.39	1.63	1.74	1.12	1.45	3.93
Yb	2.66	2.26	1.24	1.49	1.92	1.75	1.90	2.18	1.34	1.94	4.70
Ti	482	548	1328	951	534	1375	1572	597	4128	1364	1044
V	244	311	351	420	235	382	319	256	363	283	256
Cr	28944	35205	37866	48375	30546	47871	17832	31880	56478	13397	9323
Sr	0.73	0.17	0.51	0.48	0.31	0.57	0.35	0.27	1.10	0.43	0.14
Y	23.4	15.4	15.9	11.4	12.0	20.0	17.3	19.3	11.9	15.9	25.6
Zr	56.7	9.0	77.0	48.9	14.0	98.4	35.6	14.9	66.6	33.4	12.5

Rock types and analytical procedures as in Table 3-4.

Table 3-6. Calculated rare earth element contents for bulk xenoliths

Sample Rock	NK1-3 Perid	NK1-4 Perid	NK1-5 Perid	NK1-7 Perid	NK1-14 Perid	NK2-1 Perid	NK2-2 Perid	NK2-3 Perid	NK2-5 Perid	NK3-4 Perid	NK3-1 LMg-Px
Mass balance calculations based on clinopyroxene and garnet											
ppm											
La	0.122	0.061	0.384	0.035	0.008	0.025	0.078	2.00	0.336	0.085	1.29
Ce	0.616	0.279	0.995	0.165	0.049	0.098	0.372	3.81	1.49	0.586	4.76
Nd	0.614	0.308	0.430	0.204	0.127	0.135	0.511	0.929	0.817	0.781	3.21
Sm	0.232	0.111	0.084	0.119	0.083	0.068	0.154	0.162	0.164	0.260	0.717
Eu	0.092	0.040	0.027	0.051	0.039	0.031	0.051	0.062	0.047	0.086	0.251
Dy	0.283	0.115	0.151	0.222	0.127	0.141	0.211	0.335	0.170	0.358	1.15
Er	0.131	0.059	0.127	0.090	0.089	0.051	0.152	0.231	0.102	0.219	0.806
Yb	0.182	0.069	0.148	0.117	0.121	0.060	0.170	0.279	0.147	0.269	0.920
Mass balance calculations based on clinopyroxene, garnet and kimberlite liquid											
wt% kimberlite	1.30	1.20	1.10	0.40	1.30	0.50	0.70	2.00	0.80	2.00	0.50
ppm											
La	1.88	2.00	1.52	0.550	2.09	0.701	1.03	4.67	1.14	2.79	1.96
Ce	3.64	3.78	2.73	0.983	4.51	1.26	2.00	8.41	2.14	5.24	5.90
Nd	1.74	1.47	1.16	0.476	1.94	0.571	1.12	2.66	1.00	2.51	3.63
Sm	0.39	0.231	0.254	0.133	0.323	0.130	0.239	0.407	0.209	0.502	0.775
Eu	0.129	0.062	0.083	0.051	0.086	0.046	0.072	0.120	0.064	0.144	0.264
Dy	0.324	0.191	0.258	0.141	0.213	0.157	0.233	0.398	0.142	0.420	1.16
Er	0.142	0.137	0.100	0.093	0.114	0.055	0.158	0.246	0.066	0.234	0.807
Yb	0.185	0.152	0.121	0.123	0.151	0.062	0.172	0.283	0.072	0.273	0.918
Mass balance calculations based on clinopyroxene, garnet and apatite											
wt% apatite	0.10	0.05	0.10	0.10	0.01	0.05	0.05	0.15	0.10	0.15	0.05
ppm											
La	1.87	0.936	2.13	1.78	0.446	0.900	0.953	4.63	2.09	2.71	2.17
Ce	3.42	1.68	3.80	2.96	0.749	1.50	1.77	8.01	4.29	4.79	6.16
Nd	1.90	0.950	1.71	1.49	0.449	0.777	1.15	2.86	2.10	2.71	3.85
Sm	0.426	0.208	0.278	0.313	0.132	0.165	0.251	0.453	0.358	0.551	0.814
Eu	0.130	0.059	0.065	0.089	0.048	0.050	0.070	0.119	0.085	0.144	0.270
Dy	0.323	0.135	0.192	0.263	0.138	0.161	0.231	0.396	0.211	0.419	1.17
Er	0.140	0.064	0.137	0.100	0.092	0.056	0.157	0.246	0.112	0.234	0.811
Yb	0.186	0.071	0.152	0.121	0.122	0.062	0.173	0.286	0.151	0.276	0.922

Rock types as in Table 3-4. Quantitative mass balance calculations are based on REE contents and modal abundances of respective minerals. Kimberlite liquid and modal apatite proportions (wt%) for whole-rocks calculations based on clinopyroxene, garnet and apatite were constrained iteratively to obtain the best match between calculated REE patterns and those determined analytically. Apatite composition from Kramers *et al.* (1983).

Table 3-7. Rare earth element contents for calculated interstitial liquid

Sample Rock	NK1-3 Perid	NK1-4 Perid	NK1-5 Perid	NK1-7 Perid	NK1-14 Perid	NK2-1 Perid	NK2-2 Perid	NK2-3 Perid	NK2-5 Perid	NK3-4 Perid	NK3-1 LMg-Px
Interstitial liquid in equilibrium with olivine, orthopyroxene, clinopyroxene and garnet											
wt% liquid	1.20	1.00	0.90	0.25	1.50	0.25	0.40	2.50	0.60	1.50	0.10
ppm											
La	141	178	142	183	145	135	131	200	124	171	142
Ce	249	289	235	278	299	318	238	282	287	251	218
Nd	98.5	98.3	81.2	89.5	105	93.9	89.5	78.8	106	76.1	64.3
Sm	15.2	10.4	11.7	13.6	9.83	11.8	12.8	8.98	15.1	8.93	7.08
Eu	4.82	2.66	3.46	3.37	2.52	3.33	3.34	2.52	4.31	2.82	1.92
Dy	3.28	2.18	2.73	1.42	1.59	2.84	2.27	1.88	3.15	2.37	2.55
Er	0.704	0.591	0.488	0.379	0.462	0.591	0.595	0.607	0.632	0.715	0.815
Yb	0.380	0.392	0.280	0.288	0.306	0.27	0.387	0.439	0.269	0.492	0.536

Rock types as in Table 3-4. Liquid compositions were determined using mass balance calculations based on whole-rock trace element analyses combined with mineral modes (Bédard, 1994). The modal amounts of interstitial melt (wt%) were constrained by iteration to obtain the best match between calculated liquid composition and kimberlite analysis. $C_i^{liq} = C_i^{rock} / (f^{liq} + (f^{Oliv} D_i^{Oliv}) + (f^{Opx} D_i^{Opx}) + (f^{Cpx} D_i^{Cpx}) + (f^{Garn} D_i^{Garn}))$ was used to calculate the concentration of an element i in the trapped liquid (C_i^{liq}), where C_i^{rock} is the concentration of element i in the whole-rock, f the modal proportion as mass fraction of 1, and D_i the mineral/liquid partition coefficient of element i for the constituent mineral phases (Oliv, olivine; Opx, orthopyroxene; Cpx, clinopyroxene; Garn, garnet). Mineral-liquid partition coefficients after Fujimaki *et al.* (1984).

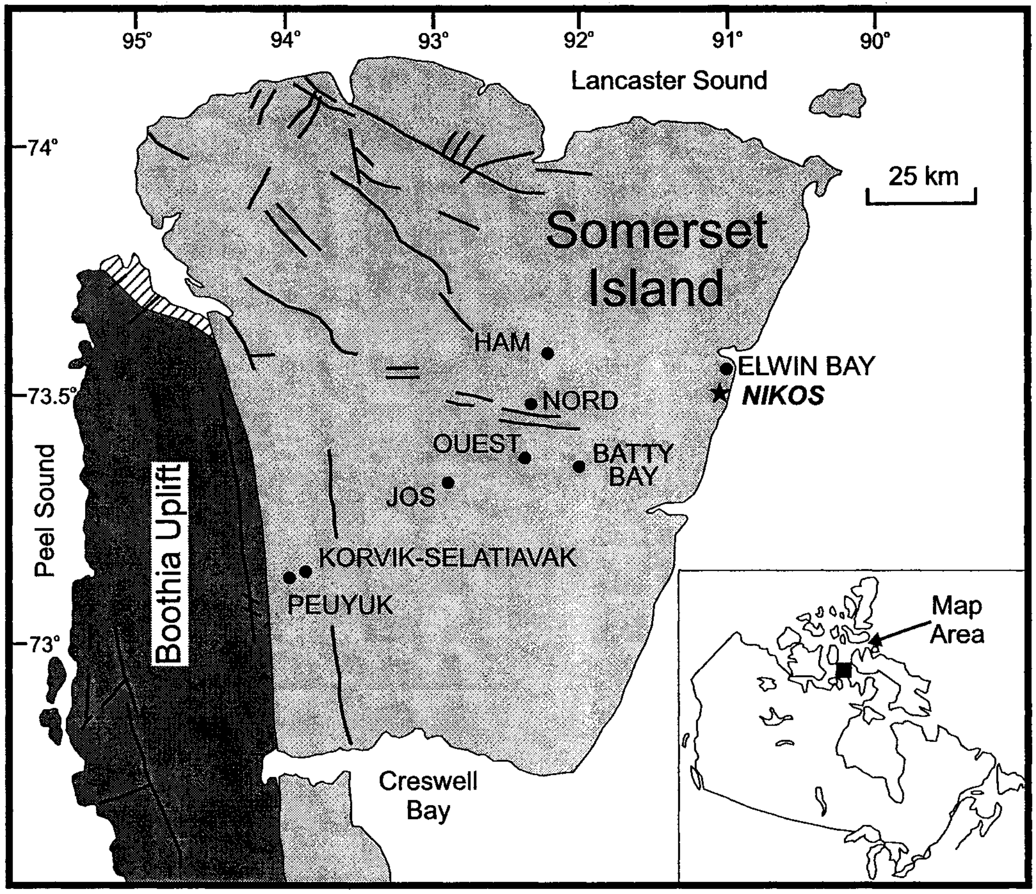

95°
94°
93°
92°
91°
90°
Lancaster Sound
-74°
25 km
Somerset Island
HAM
ELWIN BAY
NIKOS
-73.5°
NORD
OUEST
BATTY BAY
JOS
Peel Sound
Boothia Uplift
KORVIK-SELATIAVAK
PEUYUK
-73°
Map Area
Creswell Bay

Figure 3-1

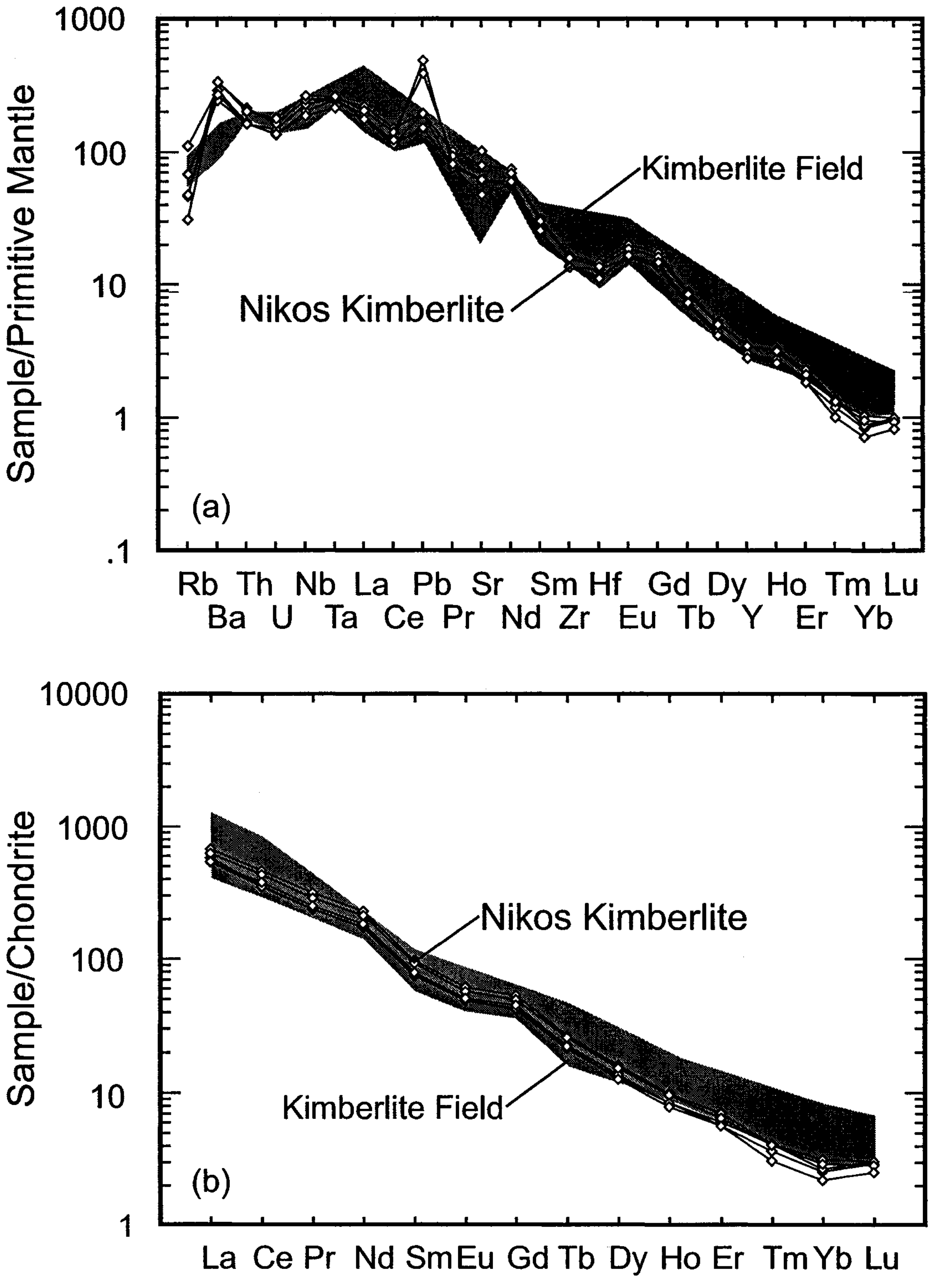
Sample/Primitive Mantle
1000
100
10
1
.1
Kimberlite Field
Nikos Kimberlite
(a)
Rb Th Nb La Pb Sr Sm Hf Gd Dy Ho Tm Lu
Ba U Ta Ce Pr Nd Zr Eu Tb Y Er Yb
Sample/Chondrite
10000
1000
100
10
1
Nikos Kimberlite
Kimberlite Field
(b)
La Ce Pr Nd Sm Eu Gd Tb Dy Ho Er Tm Yb Lu

Figure 3-2

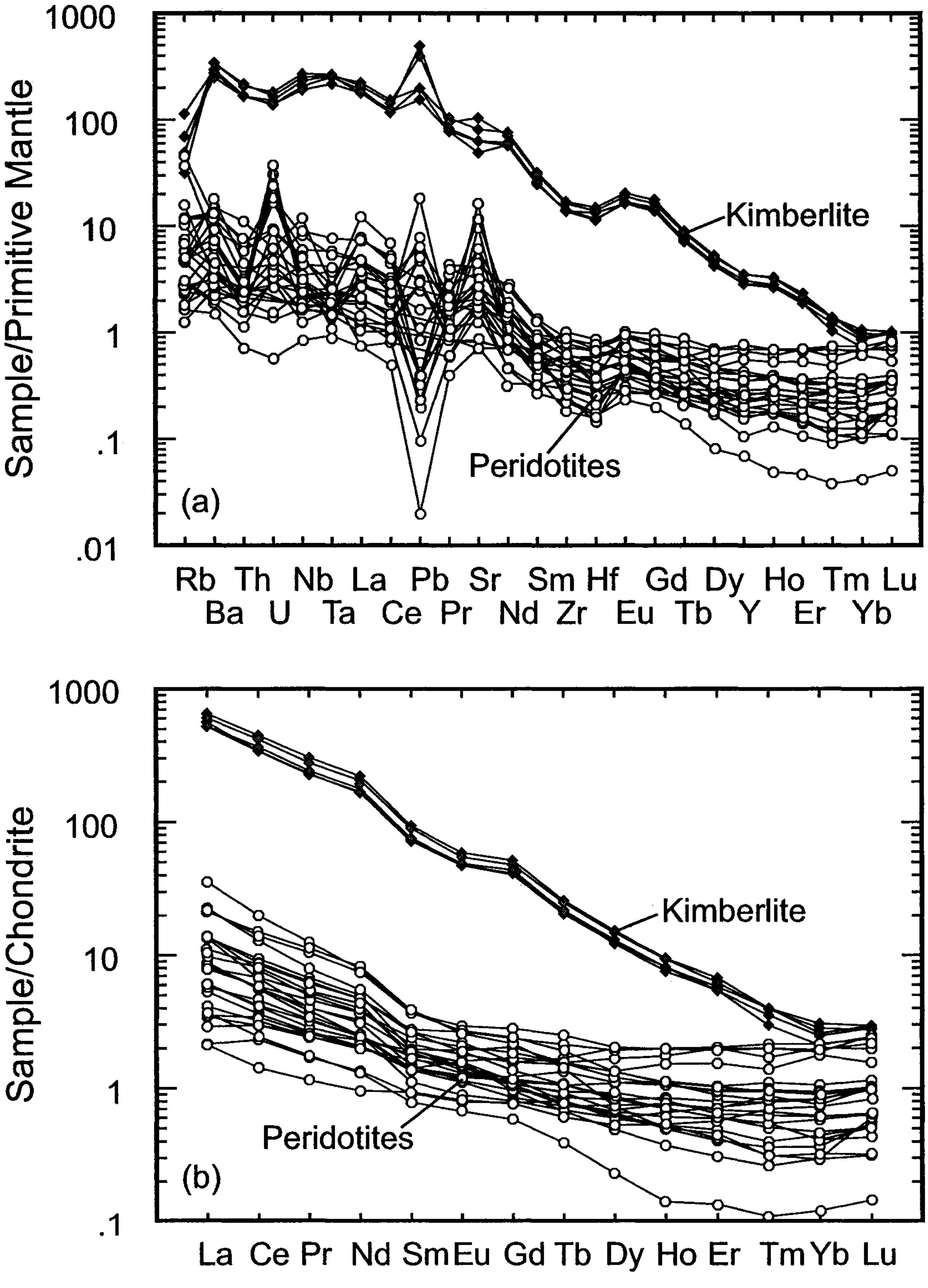

Sample/Primitive Mantle
1000
100
10
1
.1
.01
Kimberlite
Peridotites
(a)
Rb Th Nb La Pb Sr Sm Hf Gd Dy Ho Tm Lu
Ba U Ta Ce Pr Nd Zr Eu Tb Y Er Yb
Sample/Chondrite
1000
100
10
1
.1
Kimberlite
Peridotites
(b)
La Ce Pr Nd Sm Eu Gd Tb Dy Ho Er Tm Yb Lu

Figure 3-3

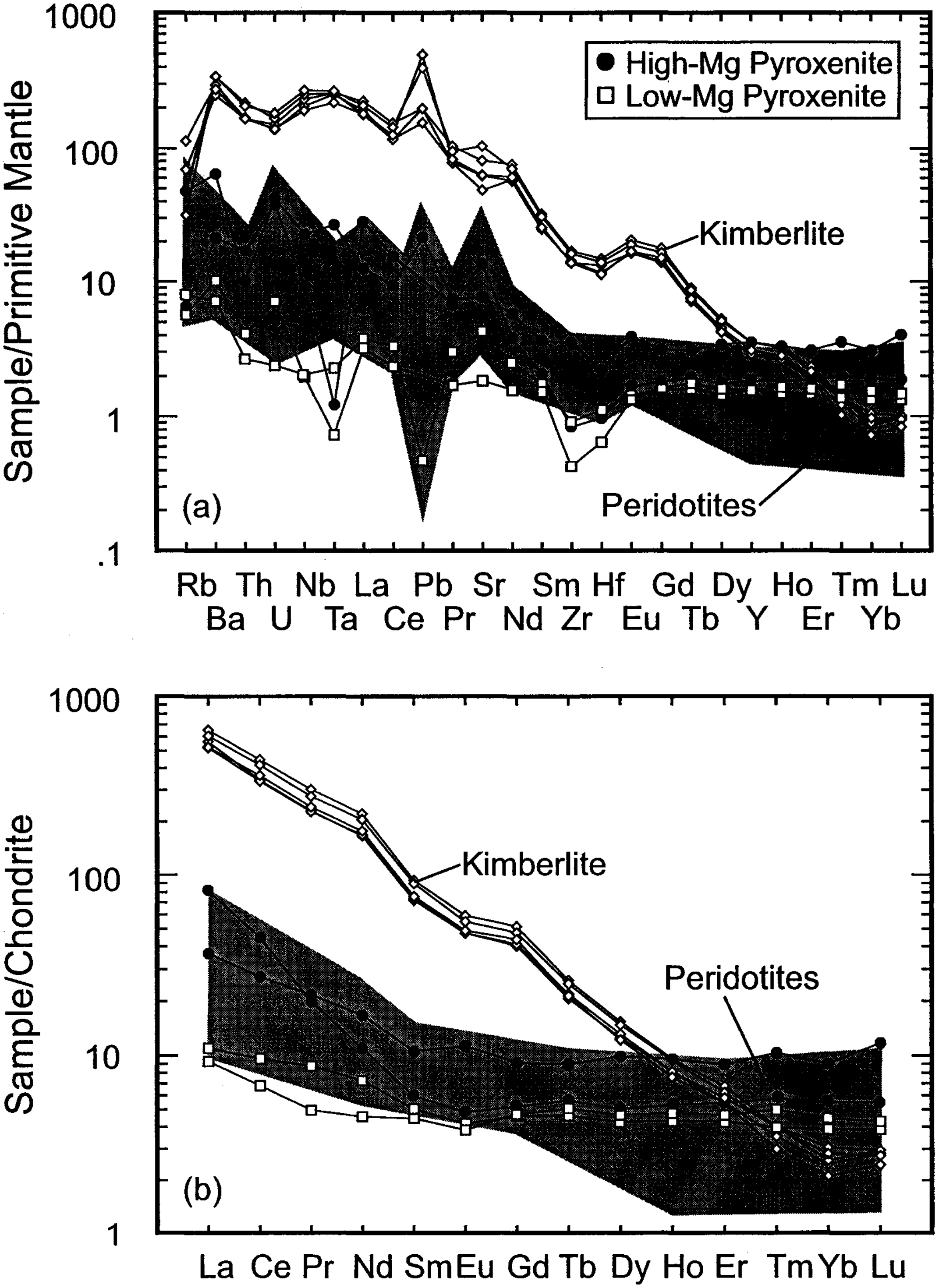
1000
100
10
1
.1
Sample/Primitive Mantle
High-Mg Pyroxenite
Low-Mg Pyroxenite
Kimberlite
Peridotites
(a)
Rb Th Nb La Pb Sr Sm Hf Gd Dy Ho Tm Lu
Ba U Ta Ce Pr Nd Zr Eu Tb Y Er Yb
1000
100
10
1
Sample/Chondrite
Kimberlite
Peridotites
(b)
La Ce Pr Nd Sm Eu Gd Tb Dy Ho Er Tm Yb Lu

Figure 3-4

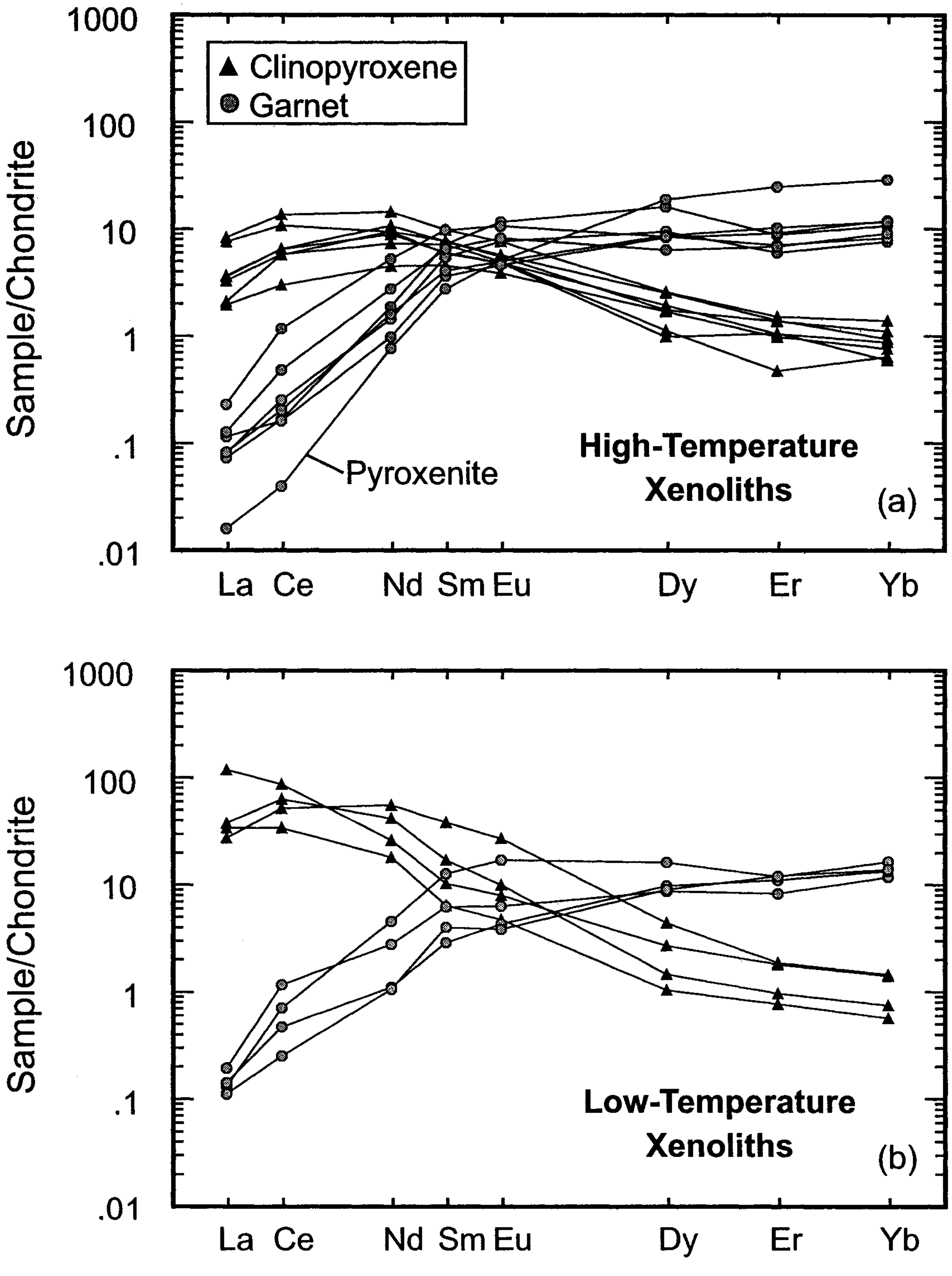1000
100
10
1
.1
.01
Sample/Chondrite
▲ Clinopyroxene
● Garnet
Pyroxenite
High-Temperature Xenoliths
(a)
La
Ce
Nd
Sm
Eu
Dy
Er
Yb
1000
100
10
1
.1
.01
Sample/Chondrite
Low-Temperature Xenoliths
(b)
La
Ce
Nd
Sm
Eu
Dy
Er
Yb

Figure 3-5

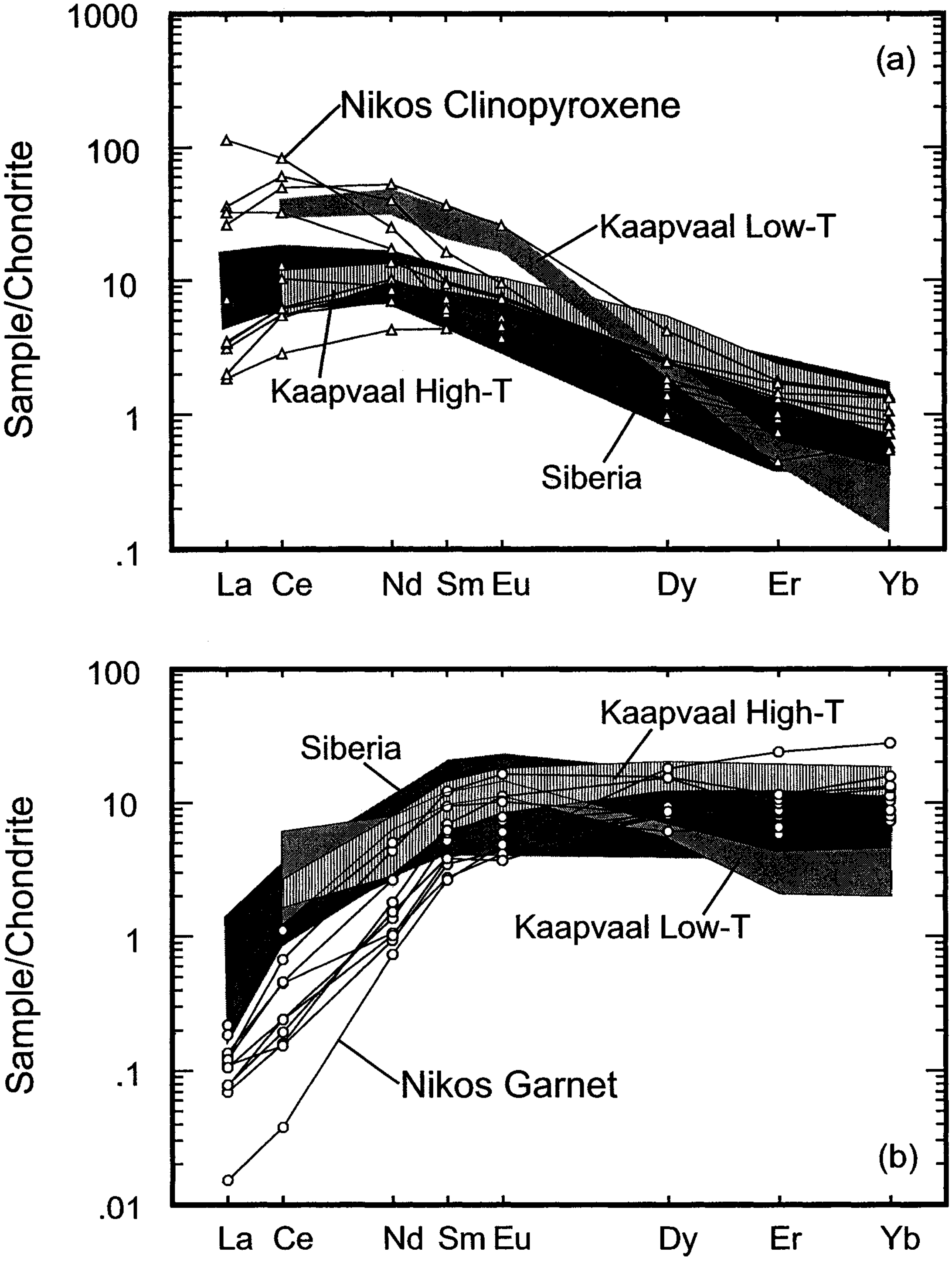

1000
100
10
1
.1
Sample/Chondrite
(a)
Nikos Clinopyroxene
Kaapvaal Low-T
Kaapvaal High-T
Siberia
La Ce Nd Sm Eu Dy Er Yb
100
10
1
.1
.01
Sample/Chondrite
Kaapvaal High-T
Siberia
Kaapvaal Low-T
Nikos Garnet
(b)
La Ce Nd Sm Eu Dy Er Yb

Figure 3-6

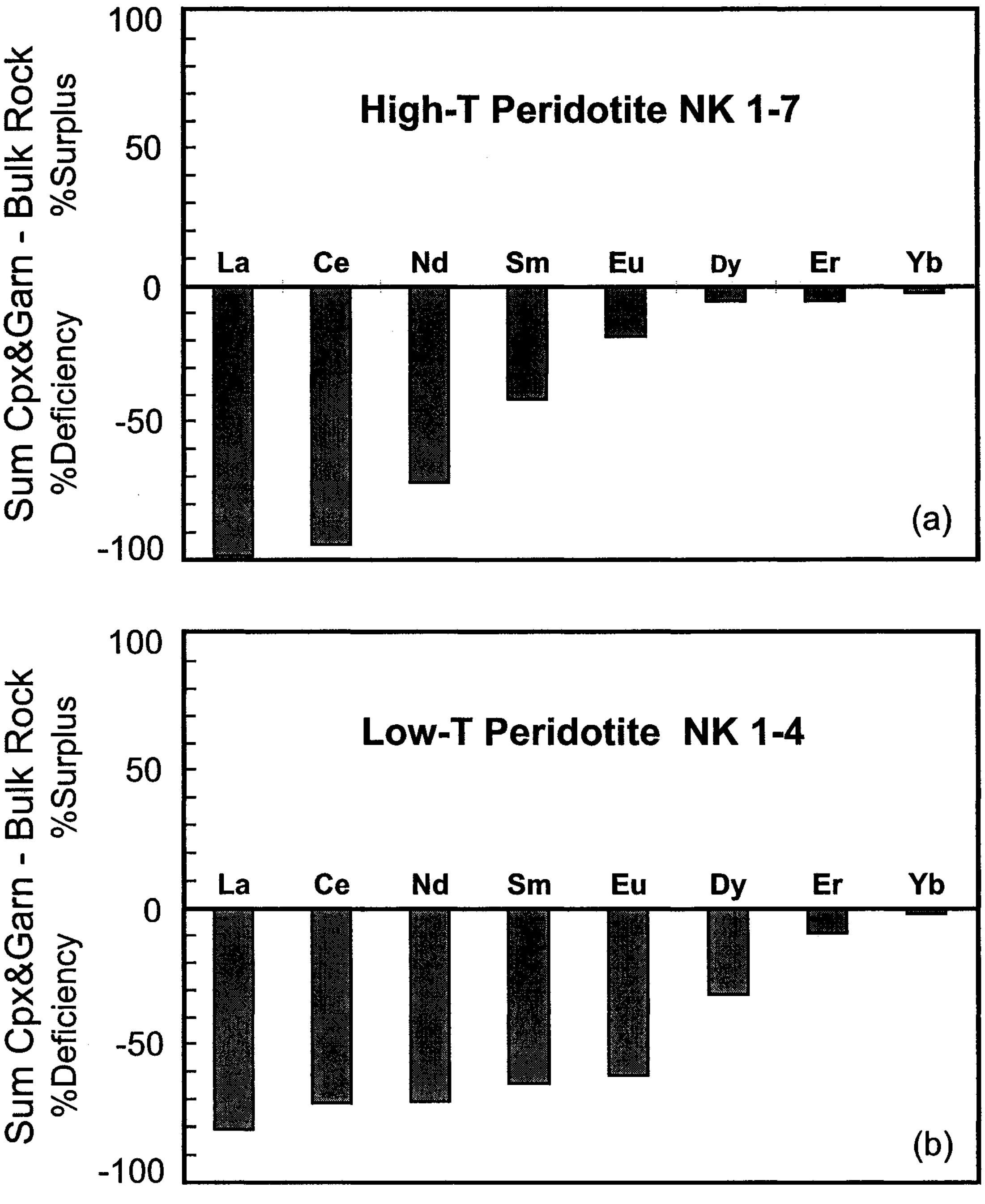
Sum Cpx&Garn - Bulk Rock
%Surplus
%Deficiency
100
50
0
-50
-100
High-T Peridotite NK 1-7
La
Ce
Nd
Sm
Eu
Dy
Er
Yb
(a)
Sum Cpx&Garn - Bulk Rock
%Surplus
%Deficiency
100
50
0
-50
-100
Low-T Peridotite NK 1-4
La
Ce
Nd
Sm
Eu
Dy
Er
Yb
(b)

Figure 3-7

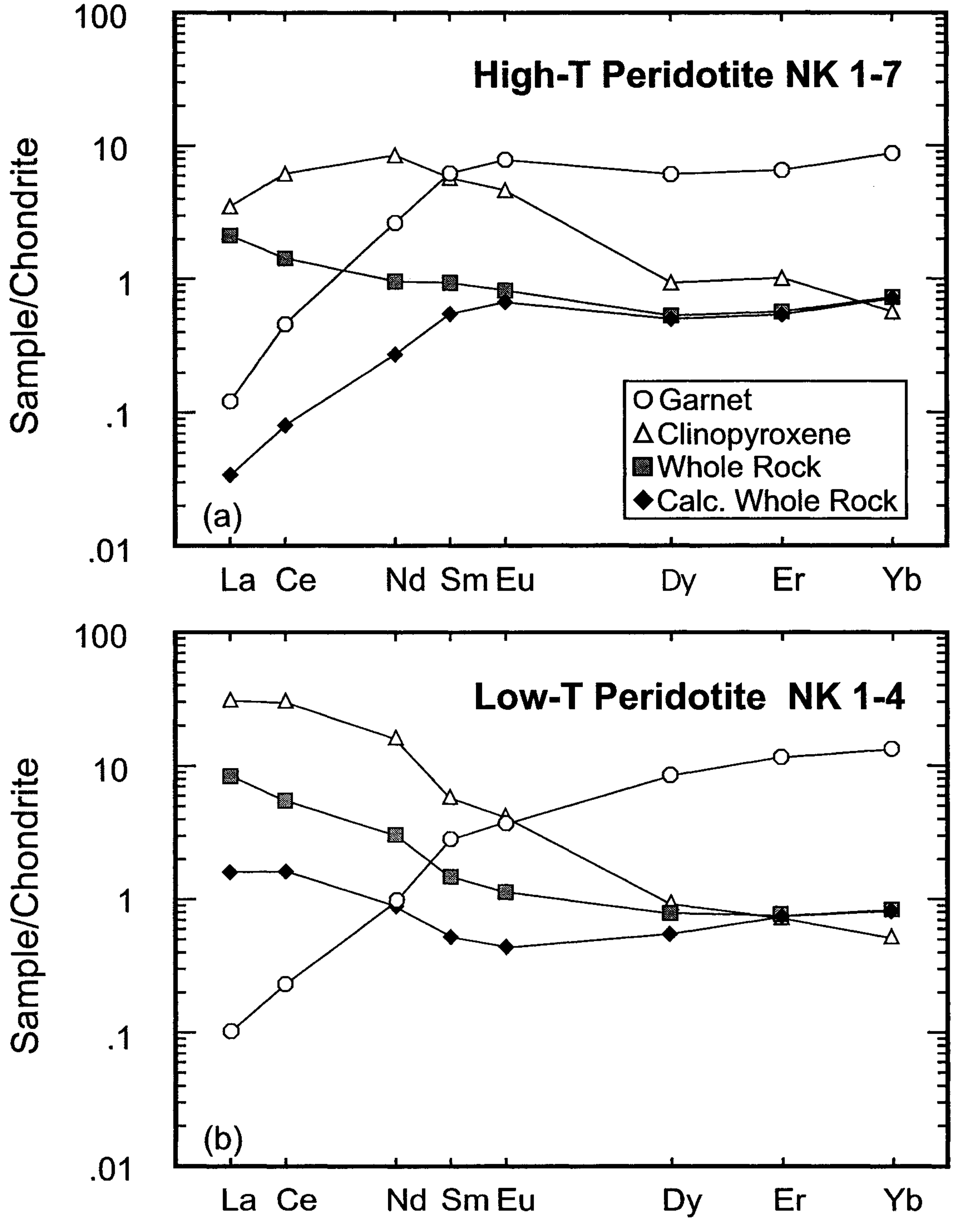
High-T Peridotite NK 1-7
Sample/Chondrite
100
10
1
.1
.01
(a)
O Garnet
Δ Clinopyroxene
■ Whole Rock
◆ Calc. Whole Rock
La
Ce
Nd
Sm
Eu
Dy
Er
Yb
Low-T Peridotite NK 1-4
Sample/Chondrite
100
10
1
.1
.01
(b)
La
Ce
Nd
Sm
Eu
Dy
Er
Yb

Figure 3-8

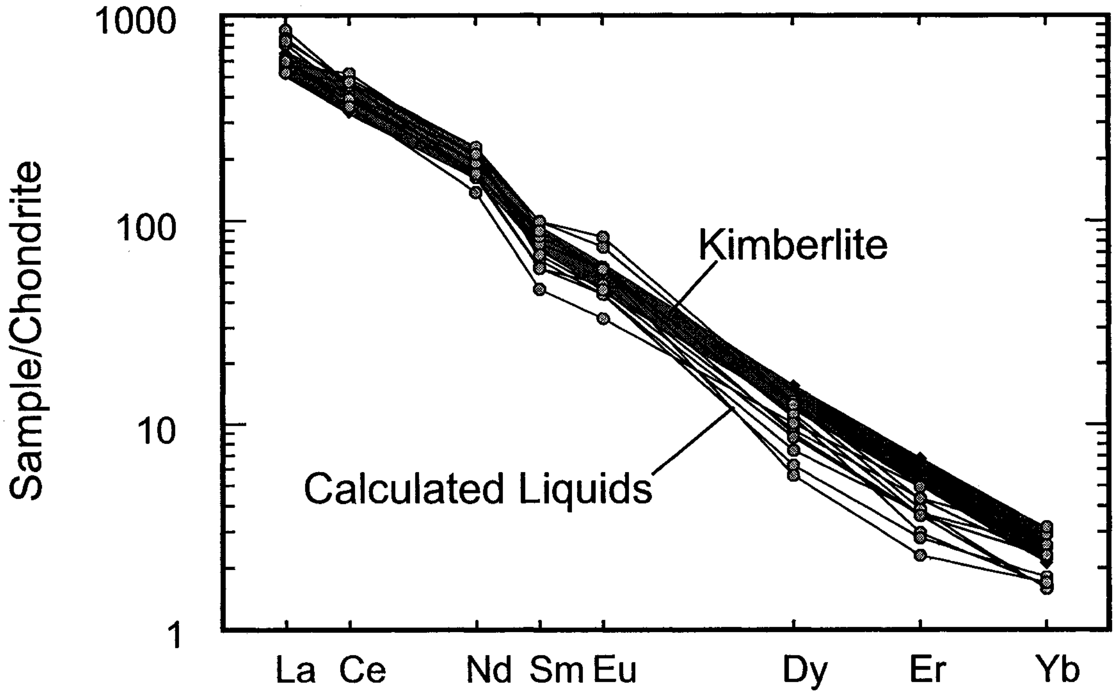
Sample/Chondrite
1000
100
10
1
Kimberlite
Calculated Liquids
La
Ce
Nd
Sm
Eu
Dy
Er
Yb

Figure 3-9

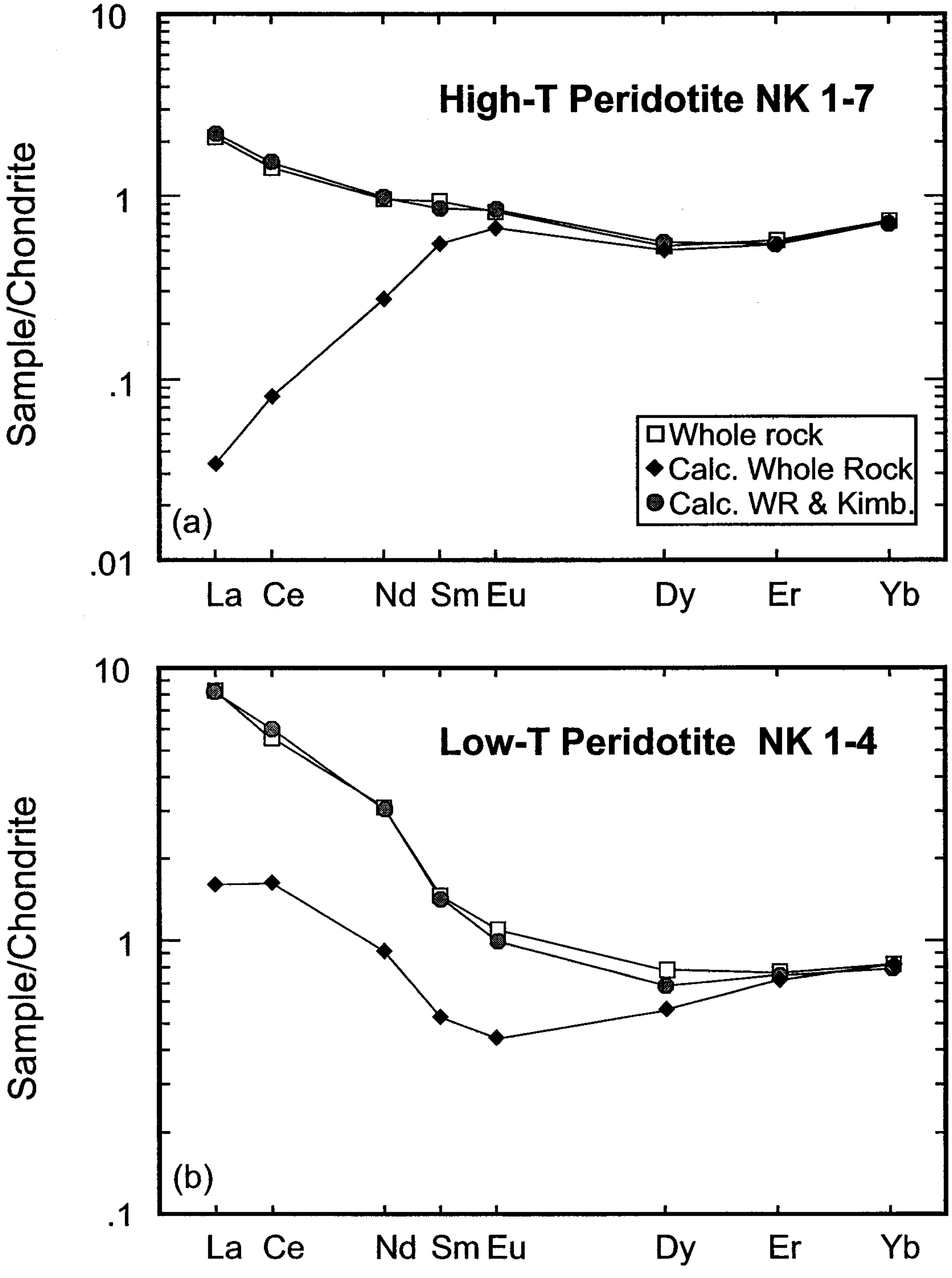
High-T Peridotite NK 1-7
Sample/Chondrite
10
1
.1
.01
☐ Whole rock
◆ Calc. Whole Rock
● Calc. WR & Kimb.
(a)
La
Ce
Nd
Sm
Eu
Dy
Er
Yb
Low-T Peridotite NK 1-4
Sample/Chondrite
10
1
.1
(b)
La
Ce
Nd
Sm
Eu
Dy
Er
Yb

Figure 3-10

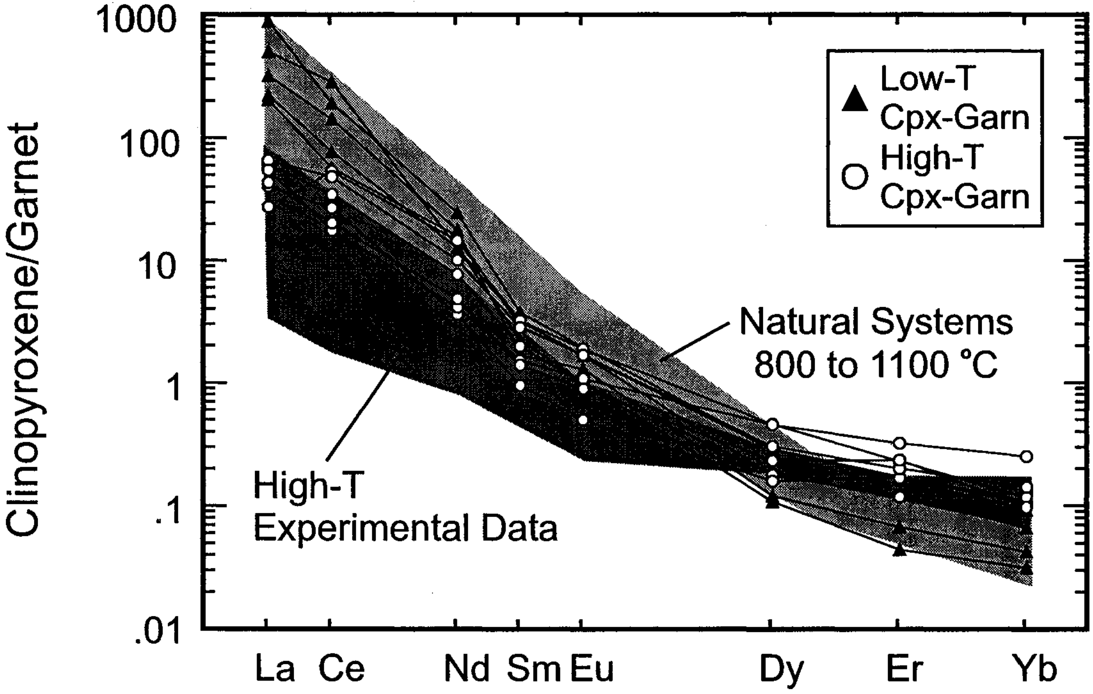

Clinopyroxene/Garnet
1000
100
10
1
.1
.01
La
Ce
Nd
Sm
Eu
Dy
Er
Yb
▲ Low-T Cpx-Garn
○ High-T Cpx-Garn
Natural Systems 800 to 1100 °C
High-T Experimental Data

Figure 3-11

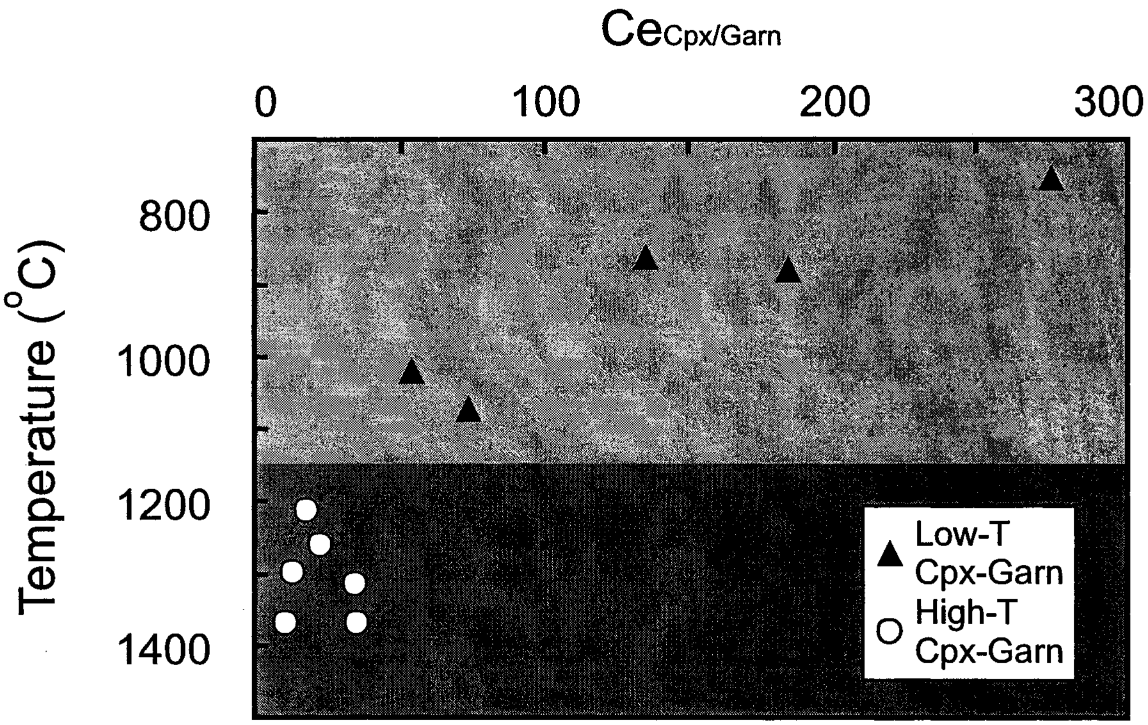

Ce Cpx/Garn
0
100
200
300
Temperature (°C)
800
1000
1200
1400
Low-T Cpx-Garn
High-T Cpx-Garn

Figure 3-12

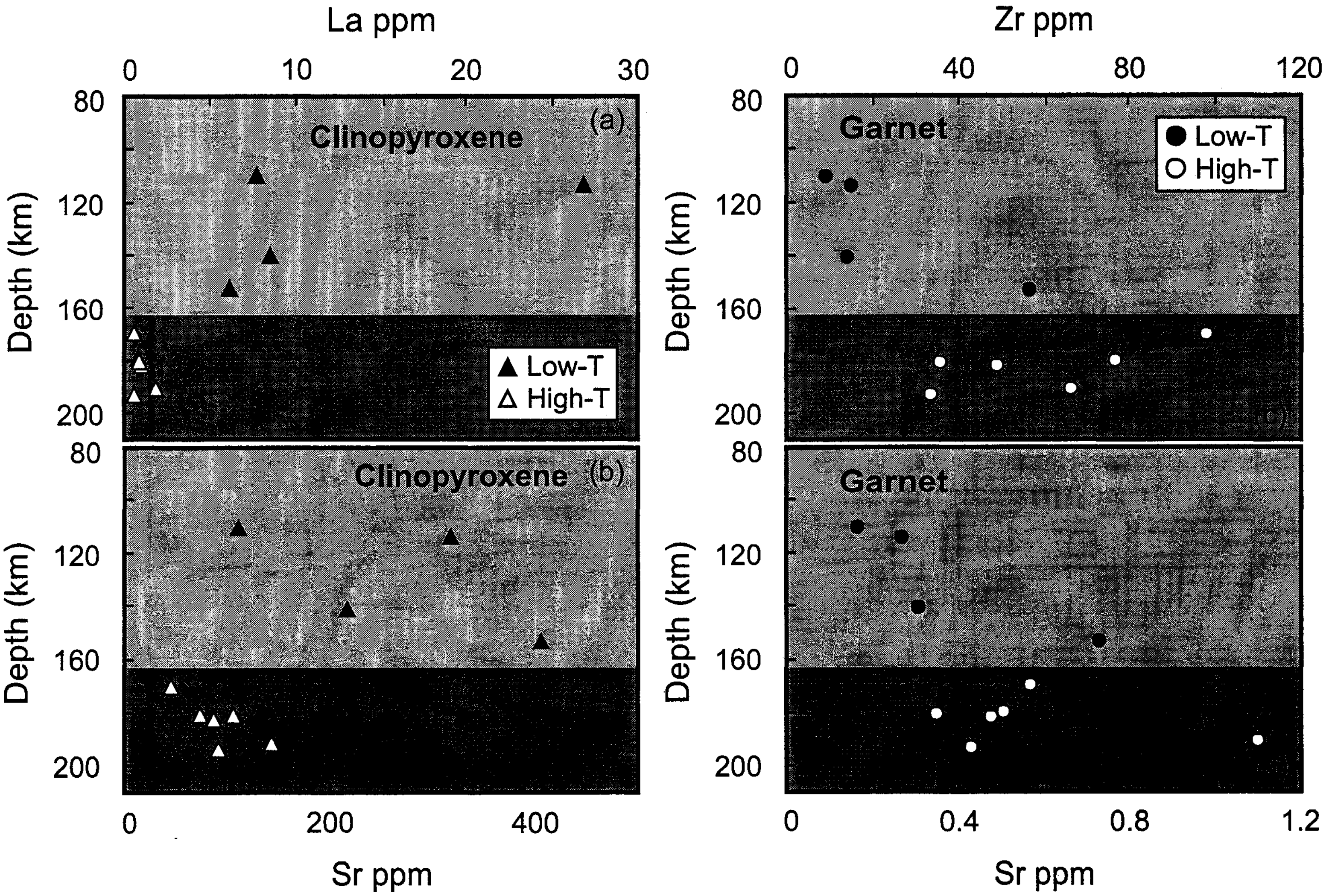

La ppm
0
10
20
30
Zr ppm
0
40
80
120
80
120
160
200
Depth (km)
Clinopyroxene
(a)
Garnet
Low-T
High-T
Clinopyroxene
(b)
Garnet
(c)
0
200
400
Sr ppm
0
0.4
0.8
1.2
Sr ppm

Figure 3-13

CHAPTER 4

Sr-Nd-Pb isotope systematics of mantle xenoliths from Somerset Island kimberlites: evidence for lithosphere stratification beneath Arctic Canada

Abstract

Sr, Nd and Pb isotopic compositions were determined for a suite of Archean garnet peridotite and garnet pyroxenite xenoliths and their host Nikos kimberlite (100 Ma) from Somerset Island, in order to constrain the isotopic character of the mantle root beneath the northern Canadian craton. The Nikos peridotites are enriched in highly incompatible trace elements (La/Sm_N=4-6), and show $^{143}Nd/^{144}Nd_{(t)}$ (0.51249-0.51276) and a large range in $^{87}Sr/^{86}Sr_{(t)}$ (0.7047-0.7085) and Pb ($^{206}Pb/^{204}Pb_{(t)}$=17.18-19.03) isotope ratios that are distinct from those estimated for "depleted mantle" compositions at the time of kimberlite emplacement. The Nd isotopic compositions of the peridotites overlap those of the Nikos kimberlite, suggesting that the xenoliths were contaminated with kimberlite or a kimberlite-related accessory phase (i.e. apatite). The highly variable Sr and Pb isotopic compositions of the peridotites, however, indicate that kimberlite contribution was restricted to very small amounts (~1 wt% or less). The high-temperature peridotites (>1100°C) that sample the deep Somerset lithosphere trend towards more radiogenic $^{87}Sr/^{86}Sr_{(t)}$ (0.7085) and unradiogenic $^{206}Pb/^{204}Pb_{(t)}$ (17.18) isotopic ratios than those of the low-temperature peridotites (<1100°C). This is in agreement with Sr isotopic compositions of clinopyroxene from the low-temperature peridotites ($^{87}Sr/^{86}Sr_{(t)}$=0.7038-0.7046) that are significantly less radiogenic than those of clinopyroxene from the high-temperature peridotites ($^{87}Sr/^{86}Sr_{(t)}$=0.7052-0.7091). The depth correlation of Sr isotopes for clinopyroxene, and Sr and Pb isotopic compositions for the Nikos whole-rocks indicate that the deep Somerset lithosphere (>160 km) is isotopically distinct from the shallow lithospheric mantle. The isotopic stratification with depth suggests that the lower lithosphere is probably younger and may have been added to the existing Archean shallow

mantle in a Phanerozoic magmatic event. The radiogenic Sr isotope ratios of the high-temperature peridotites and their clinopyroxenes suggest that the underplated deep lithosphere contained recycled (altered oceanic crust and sedimentary component?) material introduced during earlier subduction.

1. INTRODUCTION

Archean cratons are underlain by cold refractory mantle roots characterized by a depletion in fusible major elements compared to fertile mantle (e.g. Nixon, 1987; Herzberg, 1993; McDonough, 1990; Boyd et al., 1997). In contrast to their refractory major element chemistry, however, the peridotites that sample these mantle roots are frequently trace element enriched suggesting that the lithosphere may constitute a significant reservoir for incompatible elements (Erlank et al., 1987; Menzies et al., 1987). Mantle xenoliths that are brought to the surface by kimberlites and alkali basalts are a unique window into the subcontinental mantle, and provide essential insights into the isotopic character and evolution of the lithosphere to depths of greater than 200 km. Previous studies have shown that these peridotite xenoliths have a large range in Sr, Nd and Pb isotopic compositions and trend towards “enriched” time-integrated isotopic signatures relative to bulk Earth (e.g. Menzies and Murthy, 1980; Hawkesworth et al., 1990a; Pearson et al., 1995a). This is inconsistent with their origin as residues of partial melting, which should create refractory mantle roots with an isotopic signature similar to that of “depleted mantle” (Zindler and Hart, 1986). Such isotopic heterogeneities have been widely interpreted to indicate that the subcontinental lithosphere has been infiltrated by small volume melts or fluids with highly variable isotopic compositions over time. These melts or fluids were enriched in large ion lithophile elements (LILE) and light rare earth elements (LREE) and originated from deeper levels of the lithosphere or from the underlying asthenosphere (Erlank et al., 1987; Menzies et al., 1987). Thus the isotopic systematics of samples representing the subcratonic mantle are sensitive indicators of the metasomatic history they have experienced, and provide evidence for the existence of isotopically distinct domains in the lithosphere and a means to constrain their spatial distribution.

In this article, we present Sr, Nd and Pb isotopic compositions for a suite of garnet peridotites and garnet pyroxenites and their host Nikos kimberlite from Somerset Island in the Canadian Arctic (Schmidberger and Francis, 1999; Fig. 1). The results for whole-rocks and constituent mineral phases (i.e. clinopyroxene, garnet) provide insights into the isotopic signature of the deep Archean mantle root beneath the northern Canadian craton. The data set indicates a change in isotopic composition with depth in the lithospheric mantle and provides constraints on the role of the host kimberlite as a possible contaminant during sample transport.

2. SAMPLES

2.1. Kimberlite

The recently discovered Nikos kimberlites were emplaced into late Archean crystalline basement overlain by Paleozoic sediments at the northern margin of the Canadian craton (Frisch and Hunt, 1993; Pell, 1993; Fig. 1). U-Pb dating of perovskite indicates Cretaceous emplacement ages between 90 to 105 Ma for the Somerset Island kimberlites (Heaman, 1989; Smith et al., 1989). A Rb-Sr whole-rock isochron for the Nikos kimberlites (n=4) from this study yields an emplacement age of 97±17 Ma (MSWD=1.1), which is in good agreement with the U-Pb ages.

The southernmost of the three individual Nikos pipes (NK3) has been interpreted to represent kimberlite magma (Schmidberger & Francis, 1999), because of the non-clastic microcrystalline nature of its groundmass. The kimberlite contains olivine, phlogopite, garnet and spinel in a very fine-grained carbonate-rich matrix of calcite, serpentine, perovskite and apatite. The very high $CaCO_3$ contents (27-39 wt%; Schmidberger and Francis, 1999) of the kimberlite whole-rock analyses indicate liquid compositions intermediate between kimberlite and carbonatite (Woolley & Kempe, 1989; Ringwood et al., 1992). The kimberlites show a strong enrichment in highly incompatible trace elements, such as LILE and LREE compared to primitive mantle compositions and chondrites (McDonough and Sun, 1995; Schmidberger and Francis, 2001).

2.2. Mantle xenoliths

The Nikos xenolith suite consists of large (>10 cm), well-preserved garnet peridotites with minor occurrences of garnet pyroxenites (Schmidberger and Francis, 1999). The majority of the peridotites contain large crystals of olivine, orthopyroxene, clinopyroxene and garnet, and exhibit coarse textures, although a few peridotites with porphyroclastic textures are observed. Small amounts (~1% or less) of phlogopite are present, whereas amphibole is absent. The term peridotite is used for the mantle xenoliths in this study since the small differences in modal clinopyroxene content do not justify dividing the suite according to the IUGS (International Union of Geological Sciences) classification into harzburgites (clinopyroxene <5 wt%) or lherzolites (clinopyroxene >5 wt%). A detailed description of xenolith mineralogy and major, trace and rare earth element (REE) chemistry can be found in Schmidberger and Francis (1999) and Schmidberger and Francis (2001). The estimated temperature and pressure conditions of last equilibration (800-1400°C, 25-60 kb) indicate that the Nikos peridotites were sampled at depths between 80 to 190 km by their host kimberlite (Schmidberger and Francis, 1999).

The high magnesium numbers (mg-number=Mg/(Mg+Fe)=0.90-0.93) and olivine-rich mineralogy (avg. 80 wt%) of the peridotites reflect their refractory nature and suggest that these xenoliths are melt-depleted residues (Schmidberger and Francis, 1999; Schmidberger and Francis, 2001). In contrast to their depleted major element chemistry, however, the peridotites are enriched in LILE compared to abundances estimated for primitive mantle and LREE (La/Sm_N=4-6) relative to chondrites, while the heavy rare earth element (HREE) contents are approximately chondritic (Schmidberger and Francis, 2001).

Minor pyroxenite xenoliths consisting of clinopyroxene, orthopyroxene and garnet show a range in mg-numbers (Schmidberger and Francis, 1999). Two high-Mg pyroxenites contain olivine and abundant garnet (avg. 20 wt%), and have mg-numbers (0.88-0.90) that are similar to those of the peridotites. Two low-Mg pyroxenites (mg-number=0.85) have lower modal abundances of garnet (avg. 10 wt%) and higher clinopyroxene contents (avg. 70 wt%) than the high-Mg pyroxenites (avg. 30 wt%). Both the high-Mg and low-Mg pyroxenites are enriched in incompatible trace elements, such as LILE and LREE relative to values for primitive mantle and chondrites (Schmidberger and Francis, 2001). The low-Mg pyroxenites, however, are less enriched in incompatible trace elements than the high-Mg pyroxenites.

2.3. Clinopyroxene and garnet

The emerald green clinopyroxenes in the Somerset peridotites are chromian diopside and the garnets are chromian pyrope (Schmidberger and Francis, 1999). The major element compositions of both clinopyroxene and garnet are homogeneous on the scale of a thin section.

Mass balance calculations using REE contents of clinopyroxene and garnet and their respective modal abundances indicate that calculated LREE abundances for all Nikos xenoliths are significantly lower (e.g. La: 70-99%, Nd and Sm: ~50%) than those of the analyzed whole-rocks, while having similar HREE contents (Schmidberger and Francis, 2001). These results suggest the presence of a kimberlite-related LREE-rich interstitial component (i.e. ~1% kimberlite liquid) and/or accessory mineral phase (i.e. trace amounts of apatite, although as yet undetected in thin sections) to account for the excess trace element abundances (Schmidberger and Francis, 2001).

The mineral trace element compositions indicate that the peridotites can be divided according to temperature and thus depth of origin into low-temperature (<1100°C; 80-150 km) and high-temperature xenoliths (>1100°C; 160-190 km). The clinopyroxenes from the low-temperature peridotites have LREE (e.g. La=6-25 ppm) and Sr (100-400 ppm) abundances that are significantly higher than those of clinopyroxene from the high-temperature peridotites (La=0.4-2 ppm; Sr=50-140 ppm; Schmidberger and Francis, 2001). In addition, the calculated LREE patterns for the majority of the shallow low-temperature peridotites are flat, whereas the deep-seated high-temperature peridotites are characterized by LREE-depleted calculated bulk rock patterns relative to chondrites (Schmidberger and Francis, 2001). These findings suggest that the shallow Somerset lithosphere is geochemically distinct from the underlying lower lithospheric mantle and that the mantle root beneath the northern Canadian craton is characterized by a depth zonation in incompatible trace elements (Schmidberger and Francis, 2001).

3. ANALYTICAL METHODS

All exterior surfaces were first removed from the xenoliths. Samples were then crushed and rock chips were ground in an aluminum mill. Crushed whole-rock kimberlite samples were carefully hand-picked under the binocular microscope prior to grinding to eliminate contamination from peridotite xenocrysts and country rock fragments. Garnet and clinopyroxene separates were hand-picked under the binocular microscope and inclusion free crystals were washed in an ultrasonic bath with acetone, ultrapure water, and then 2.5 N HCl.

For Nd and Sr isotope analyses, the sample powders were spiked with a mixed ^{150}Nd-^{149}Sm isotope tracer and dissolved in a mixture of HF-HNO_3-$HClO_4$. Whole-rock samples and the garnet separates were dissolved at 170°C in Teflon bombs and clinopyroxene separates at 140°C in Savillex® vials for at least 10 days. Sr and REE were separated using conventional chromatographic techniques. Typical procedural blanks are Sr<70 pg, and Nd and Sm<40 pg. Sr aliquots were loaded using a TaF solution on single W filaments, and Nd and Sm were loaded with HCl using a triple Re filament technique. Nd and Sr isotope measurements were obtained by thermal ionization mass spectrometry (TIMS) at GEOTOP, Université du Québec à Montréal (UQAM) using a Sector 54 mass spectrometer operated in the static multicollection mode. For Pb isotope analysis, the sample powders were dissolved in a mixture of HF-HNO_3. Pb was separated using anion-exchange chromatography (after Manhès et al., 1980), U and Th determinations followed the technique of Edwards et al. (1986) and both were conducted at GEOTOP-UQAM. Pb, U and Th concentrations were determined by isotope dilution using ^{206}Pb, ^{233}U-^{236}U and ^{229}Th spikes. Procedural blanks for Pb, U and Th were 10-15, 2-6 and 80-100 pg, respectively and are considered negligible. Pb aliquots were loaded on a single Re filament using a silica gel-H_3PO_4 acid mixture and Pb isotope measurements were obtained using a single Faraday cage detector or Daly analogue detector in peak switching mode. Pb, U and Th concentrations were determined using a Micromass IsoProbe multi-collector inductively coupled mass spectrometer (MC-ICP-MS) coupled to an ARIDUS® microconcentric nebuliser.

4. RESULTS

4.1. Kimberlite

Initial Nd and Sr isotope data for the Nikos kimberlites were calculated for an emplacement age of 100 Ma. $^{143}Nd/^{144}Nd_{(t)}$ ratios are tightly constrained between 0.51254 to 0.51259 (corresponding to initial ε_{Nd} values of +0.6 to +1.5), and are similar to or slightly depleted than the composition of CHUR (chondrite uniform reservoir; Table 1; Fig. 2). The $^{87}Sr/^{86}Sr_{(t)}$ ratios (0.7052) are identical, and are slightly "enriched" compared to the value for bulk Earth. Previous studies on South African kimberlites have divided kimberlites into two groups ("Group I" and "Group II") based on their distinct mineralogy and isotopic signatures, indicating derivation from isotopically distinct mantle domains (Dawson, 1967; Smith, 1983). More recently, South African "Group II" kimberlites were recognized to have similar mineralogy and chemical compositions to those of olivine lamproites and are termed orangeites by Mitchell (1995). Initial Nd and Sr isotopic compositions for the Nikos kimberlites plot close to the field encompassing data for "Group I" kimberlites from North America, South Africa and Siberia, which are undifferentiated to slightly depleted relative to values for CHUR and bulk Earth, respectively (Smith, 1983; Heaman, 1989; Pearson et al., 1995b; Fig. 2). Isotope data for

South African "Group II" and Australian "kimberlites", in contrast, have much lower Nd and higher Sr isotopic ratios than the Nikos kimberlites and all "Group I" kimberlites (McCulloch et al., 1983; Smith, 1983; Fig. 2).

The Pb isotopic compositions of the Nikos kimberlites show a positive correlation in Pb-Pb isotope diagrams at the time of emplacement (Table 2; Fig. 3). The Pb isotope array yields a $^{207}Pb/^{206}Pb$ age of ~2.7 Ga, but is not likely to have any geochronological significance. In an initial $^{206}Pb/^{204}Pb$ versus $^{208}Pb/^{204}Pb$ diagram, the Nikos kimberlite Pb isotope ratios plot between data for "Group I" and "Group II" kimberlites from South Africa (Kramers, 1977; Fraser et al., 1985; Fig. 3). However, South African "Group II" kimberlites exhibit lower $^{206}Pb/^{204}Pb_{(t)}$ at similar $^{207}Pb/^{204}Pb_{(t)}$ isotopic ratios than those of the Nikos and South African "Group I" kimberlites (Kramers, 1977; Smith, 1983; Fraser et al., 1985; Fig. 3).

4.2. Mantle xenoliths

The whole-rock Nd and Sr isotopic compositions for the Nikos xenoliths were corrected for the 100 Ma in-situ decay since the emplacement of their host kimberlite (Table 1). $^{143}Nd/^{144}Nd_{(t)}$ ratios of the peridotites range between 0.51249 to 0.51276 ($\varepsilon_{Nd(t)}$ values of -0.3 to +5.0) and are similar to or depleted relative to the value for CHUR (Fig. 4). The Nd isotopic compositions of the low-temperature peridotites extend to slightly more radiogenic values ($^{143}Nd/^{144}Nd_{(t)}$=0.51257-0.51276) than those in the high-temperature peridotites ($^{143}Nd/^{144}Nd_{(t)}$=0.51249-0.51262). Depleted mantle Nd model ages (T_{DM}) for the peridotites range from 500 to 1250 Ma (except NK1-7: 2600 Ma; Table 1). $^{87}Sr/^{86}Sr_{(t)}$ isotopic ratios in the peridotites show a significant variation (0.7047-0.7085) and are "enriched" relative to bulk Earth (Fig. 4). The shallow low-temperature peridotites have Sr isotopic compositions that are significantly less radiogenic ($^{87}Sr/^{86}Sr_{(t)}$=0.7047-0.7066) than those in the high-temperature peridotites ($^{87}Sr/^{86}Sr_{(t)}$=0.7064-0.7085; Fig. 4). The unradiogenic Sr and radiogenic Nd isotope ratios for one peridotite (NK2-4) suggest that it represents a sample of low-temperature lithosphere, although temperature and pressure estimates were not determined. One low-Mg pyroxenite (NK3-1) yields a very unradiogenic $^{143}Nd/^{144}Nd_{(t)}$ (0.51197) isotopic ratio relative to those of the other pyroxenites and the peridotites (Fig. 4).

The $^{143}Nd/^{144}Nd_{(t)}$ isotopic compositions of the low and high-temperature peridotites are similar to those of the Nikos kimberlite, while having significantly more variable $^{87}Sr/^{86}Sr_{(t)}$ ratios (Fig. 4). The Nd and Sr isotopic signatures of all Nikos peridotites overlap the field of kimberlite-hosted garnet peridotites (including whole-rock and clinopyroxene data) from the South African craton (Menzies & Murthy, 1980; Kramers et al., 1983; Richardson et al., 1985; Jones, 1987; Walker et al., 1989; Hawkesworth et al., 1990a; Macdougall & Haggerty, 1999; Fig. 4). While the low-temperature South African xenoliths encompass the entire garnet peridotite field, many of the high-temperature South African xenoliths appear to be slightly depleted relative to CHUR and bulk Earth. In contrast, Sr isotopic ratios for the Nikos peridotites exhibit the opposite relationship, with the most radiogenic values observed for the high-temperature xenoliths. In comparison, the Nd and Sr isotopic compositions for post-Archean spinel peridotites plot within the depleted quadrant relative to CHUR and bulk Earth, respectively, and are distinct from those for most kimberlite-hosted cratonic mantle xenoliths (Hawkesworth et al., 1990b and references therein).

The high-temperature peridotites have μ ($^{238}U/^{204}Pb$) values that are significantly higher (avg. μ=37) than those of both the low-temperature peridotites (avg. μ=25) and the host Nikos kimberlite (avg. μ=12; Table 2). The μ values for both high and low-temperature peridotites, however, are higher than those estimated for melt-depleted residues (μ~10; Zindler and Hart, 1986; Fig. 5), suggesting the preferential addition of U after lithosphere formation. The Nikos Pb isotopic ratios plot below the Stacey and Kramers (1975) lead isotope evolution curve (μ=9.7) and dominantly to the right of the geochron (Fig. 5). The high-temperature peridotites exhibit $^{206}Pb/^{204}Pb_{(t)}$ (17.181-18.299) isotopic compositions that are less radiogenic than those of the low-temperature peridotites ($^{206}Pb/^{204}Pb_{(t)}$=17.820-19.033), whereas their $^{207}Pb/^{204}Pb_{(t)}$ and $^{208}Pb/^{204}Pb_{(t)}$ ratios are indistinguishable (Table 2; Fig. 5). The Pb isotopic signatures for the Nikos peridotites partly overlap those for the Nikos kimberlites at the time of emplacement (Fig. 5), and both the low and high-temperature Nikos peridotites have Pb isotopic compositions that are within the range of previously reported data for garnet peridotites (including whole-rock and clinopyroxene data) in South African kimberlites (Kramers, 1977; Kramers et al., 1983; Richardson et al., 1985; Walker et al., 1989; Hawkesworth et al., 1990a; Fig. 5).

The Pb isotopic ratios of the one high-Mg pyroxenite are similar to those of the peridotites. One low-Mg pyroxenite (NK3-1) is characterized by very unradiogenic Pb isotopic compositions ($^{206}Pb/^{204}Pb_{(t)}$=16.91), while the other (NK3-17) has highly radiogenic Pb isotopic ratios ($^{206}Pb/^{204}Pb_{(t)}$=19.61; Fig. 5).

4.3. Clinopyroxene and garnet

The Nd isotopic ratios of clinopyroxene in the Nikos peridotites are depleted relative to the value for CHUR (Table 1; Fig. 6). Although the Nd isotopic compositions mostly overlap, two clinopyroxenes from the low-temperature peridotites ($^{143}Nd/^{144}Nd_{(t)}$=0.51268-0.51269) exhibit more radiogenic values than those of clinopyroxenes from the high-temperature xenoliths ($^{143}Nd/^{144}Nd_{(t)}$=0.51254-0.51261). Depleted mantle Nd model ages (T_{DM}) yield 500-800 Ma and 900-1400 Ma for clinopyroxenes from low and high-temperature peridotites, respectively. Rb and Sr abundances for Nikos clinopyroxene separates from two peridotites and one pyroxenite were determined using isotope dilution analysis (Table 1). As the calculated $^{87}Rb/^{86}Sr$ ratios are extremely low (high-temperature peridotite: 0.00020; low-temperature peridotite: 0.00018), the correction of the measured Sr isotopic ratios for in-situ decay (100 Ma) is negligible (Table 1). The $^{87}Sr/^{86}Sr_{(t)}$ ratios for the remaining clinopyroxene separates were calculated using $^{87}Rb/^{86}Sr$ ratios of 0.00020 and 0.00018 for high and low-temperature peridotites, respectively. The Sr isotopic ratios for clinopyroxenes in the low-temperature peridotites ($^{87}Sr/^{86}Sr_{(t)}$=0.7038-0.7046) are similar or less radiogenic than the value for bulk Earth (Fig. 6), and they are significantly less radiogenic than their corresponding whole-rock compositions (Table 1). Their Nd and Sr isotopic ratios plot within the array of data for clinopyroxenes in kimberlite-hosted peridotites from South Africa (Menzies & Murthy, 1980; Kramers et al., 1983; Jones, 1987). In contrast, the clinopyroxenes from the high-temperature Nikos peridotites exhibit a large range in Sr isotope compositions ($^{87}Sr/^{86}Sr_{(t)}$=0.7052-0.7091; Fig. 6), which are significantly more radiogenic than those of the clinopyroxenes from the low-temperature peridotites.

The garnets from the low-temperature peridotites have Nd isotopic ratios ($^{143}Nd/^{144}Nd_{(t)}$=0.51255-0.51271) that extend to slightly more radiogenic compositions than those of garnets from the high-temperature peridotites ($^{143}Nd/^{144}Nd_{(t)}$=0.51242-0.51259; Table 1; Fig. 6) at the time of kimberlite emplacement. $^{87}Rb/^{86}Sr$ ratios for a high (0.39) and a low-temperature peridotite garnet (0.29) were determined by isotope dilution analysis and used to calculate Sr isotopic ratios at 100 Ma ago for the remaining garnets from low and high-temperature peridotites, respectively. The Sr isotopic compositions of garnets in the high-temperature peridotites ($^{87}Sr/^{86}Sr_{(t)}$=0.7067-0.7095) partly overlap those of garnets in the low-temperature peridotites ($^{87}Sr/^{86}Sr_{(t)}$=0.7061-0.7073; Table 1; Fig. 6), but extend to significantly more radiogenic values.

5. DISCUSSION

5.1. Mantle isotopic composition

The Nikos peridotites that sample the Archean mantle root beneath the northern Canadian craton have a refractory mineralogy with high mg-numbers and depletions in fusible major elements indicating that they represent melt-depleted residues (Schmidberger and Francis, 1999). Residual mantle having experienced melt extraction should be characterized by low Nd/Sm, Rb/Sr and U/Pb ratios, as these trace elements are fractionated during partial melting processes (Menzies, 1990). Such trace element signatures will consequently generate time-integrated high $^{143}Nd/^{144}Nd$, low $^{87}Sr/^{86}Sr$, low $^{206}Pb/^{204}Pb$ and low $^{207}Pb/^{204}Pb$ isotopic ratios distinct from the composition of bulk Earth, but similar to those of "depleted mantle" (Zindler and Hart, 1986; Menzies, 1990; Pearson et al., 1995a). In agreement with this reasoning, many spinel peridotites that sample the lithosphere beneath oceanic or post-Archean crustal terranes have Nd and Sr isotopic compositions that plot in the depleted quadrant of the Nd-Sr correlation diagram compared to CHUR and bulk Earth, respectively (Fig. 4), as would be expected for residual mantle (Hawkesworth et al., 1990b and references therein).

In contrast to their depleted major element chemistry, the Nikos peridotites are enriched in highly incompatible trace elements such as the LILE and LREE, resulting in Nd/Sm, Rb/Sr and U/Pb ratios that are higher than those expected for melt-depleted residues (Menzies, 1990; Schmidberger and Francis, 2001; Tables 1, 2). The Nikos peridotites have Nd isotopic compositions that are similar to that of CHUR, but show a significant range in Pb and Sr isotopic compositions and extend to very radiogenic $^{87}Sr/^{86}Sr_{(t)}$ at the time of kimberlite emplacement (Figs. 4, 5). Furthermore, the isotopic compositions of the peridotites do not correlate with indices of partial melting, such as mg-numbers or modal mineralogy, which is inconsistent with an origin as single-stage melt-depleted residues. These characteristics suggest that the Somerset mantle root was infiltrated by metasomatic melts or fluids that enriched the lithospheric mantle in incompatible trace elements and overprinted its isotopic composition. Kimberlite-hosted garnet peridotites that sample the Archean mantle root beneath the South African Kaapvaal craton also exhibit highly variable and "enriched" isotope signatures, a feature which appears to characterize the lithospheric mantle beneath many Archean continents (Figs. 4, 5; Hawkesworth et al., 1990b and references therein).

Mass balance calculations based on modal abundances of clinopyroxene and garnet, and their respective REE abundances indicate discrepancies between calculated and analyzed LREE contents for the Nikos bulk rocks (Schmidberger and Francis, 2001). The LREE deficiencies (~50% for Nd and Sm) suggest the presence of small amounts of a kimberlite-related LREE-rich interstitial component (i.e. kimberlite liquid, ~1 wt%) and/or accessory mineral phase (i.e. apatite, ~0.1 wt%) to account for the excess LREE abundances in the Nikos peridotites (Bedini and Bodinier, 1999; Schmidberger and Francis, 2001). The Nd isotopic compositions of both the low and high-temperature Nikos peridotites overlap those of the host kimberlite at 100 Ma (Fig. 4), and it would appear that the peridotites were contaminated by the Nikos kimberlite. Binary mixing calculations show that a "depleted mantle" endmember ($^{143}Nd/^{144}Nd>0.5132$; Nd=0.8 ppm; Zindler and Hart, 1986) would require the addition of 5 to 10 wt% kimberlite liquid in order to account for the Nd isotopic signatures observed in the Nikos bulk rocks. This extent of contamination with kimberlite liquid, however, would result in bulk rock Nd abundances (5 to 10 ppm) that are significantly higher than those observed in the Nikos peridotites (avg. 1.5 ppm).

The presence of a Nd-bearing phase in addition to clinopyroxene and garnet is also required to explain the observation that a few whole-rock Nd isotopic compositions are less radiogenic than those of their constituent clinopyroxene and garnet. Isotopic mass balance calculations show that minor amounts of interstitial kimberlite liquid (0.5-0.9 wt%) could explain this discrepancy. One peridotite (NK3-4), however, exhibits a whole-rock Nd isotopic composition that is in fact lower than those of the kimberlite, which suggests the presence of a grain boundary component (or accessory mineral) other than kimberlite liquid. Although the Nd isotope data and Nd contents suggest addition of small amounts of kimberlite liquid (~1 wt% or less) or a kimberlite-related accessory mineral (apatite ~0.1 wt% or less), binary mixing calculations indicate that the Nikos peridotites were characterized by Nd isotopic compositions that were less radiogenic than those of a typical "depleted mantle" at the time of kimberlite magmatism.

The large range in Pb isotope ratios and the trend towards extremely radiogenic Sr compositions of the high-temperature peridotites, however, cannot be explained by kimberlite ($^{87}Sr/^{86}Sr_{(t)}$=0.7052) contamination of a precursor "depleted mantle" ($^{87}Sr/^{86}Sr<0.703$), as the kimberlite does not have an appropriate isotopic composition to account for the Sr isotope range of the peridotites. The presence of substantial amounts (>5 wt%) of interstitial kimberlite would, in fact, eradicate the Sr and Pb isotope differences observed between the low and high-temperature peridotites. Although Sr and Pb isotopic compositions of the high-temperature peridotites correlate with their respective Sr and Pb bulk rock abundances, which could be indicative of binary mixing of isotopically distinct components, their isotope data do not trend towards the composition of the Nikos kimberlite. This suggests that addition of host kimberlite was restricted to very small amounts (~1 wt% or less; Fig. 7), which is consistent with previous estimates. Given any amount of kimberlite contamination, the Sr isotopic compositions of the peridotites will be affected to a lesser degree than their Nd isotope ratios since the abundance ratio (peridotite/kimberlite) of Sr is 3 times larger than for Nd.

5.1.1. Age constraints

Clinopyroxene, garnet and corresponding whole-rock of one low (NK1-3) and two high-temperature (NK1-5; NK2-2) Nikos peridotites define internal Sm-Nd isochron ages of 91±9 Ma, 94±5 Ma and 102±8 Ma respectively, essentially identical to the emplacement age of the Somerset kimberlites (Heaman, 1989; Smith et al., 1989). These young "dates" appear to represent cooling ages and suggest that the lithospheric temperatures (up to 1400°C) exceeded the closure temperatures of peridotite minerals and/or that Nd isotopes equilibrated (i.e. "resetting") during the thermal event associated with kimberlite magmatism. Thus, Sm-Nd isochrons using constituent peridotite minerals do not appear to provide information on the timing of stabilization of the lithospheric mantle, but "date" the kimberlite magmatism. These findings are consistent with internal mineral isochrons obtained for South African peridotites, which have been interpreted to date kimberlite emplacement rather than mantle root formation (Pearson et al., 1995a).

Nd model ages may provide time constraints on separation from a depleted mantle (T_{DM}) reservoir, on the condition that bulk rock Sm-Nd systematics remain undisturbed subsequent to the formation event (DePaolo and Wasserburg, 1976). The T_{DM} (500-950 and 700-1250 Ma for low and high-temperature peridotites, respectively) for most Nikos peridotites are much younger than the Archean Re depletion ages for other Somerset Island peridotites (Irvine et al., 1999). These could reflect recent perturbation of the bulk rock Sm/Nd ratios as a result of kimberlite contamination. It has been shown that the Nd isotopic composition of clinopyroxene, which unlike that of the bulk xenolith is not biased by the presence of interstitial phases, provides a reasonable approximation for the whole-rock Nd isotope evolution (Pearson, 1999). T_{DM} age calculations yield 500-800 Ma (avg. 700 Ma) and 900-1400 Ma (avg. 1150 Ma) for clinopyroxenes from low and high-temperature peridotites, respectively, which are also significantly younger than the stabilization age of the lithosphere.

5.2. Pyroxenites

Two low-Mg pyroxenites, possibly representing veins of pyroxene-rich cumulates in the Somerset lithosphere (Schmidberger and Francis, 2001), have isotopic compositions that extend from very unradiogenic (NK3-1) to highly radiogenic (NK3-17) Pb and Nd isotopic ratios, which are distinct from those of the high-Mg pyroxenites and the peridotites (Figs. 4, 5). Thus, although major element compositions and modal mineralogy of the low-Mg pyroxenites are indistinguishable (Schmidberger and Francis, 2001), their isotopic compositions suggest that there is no genetic link between these pyroxenites. The Pb and Nd isotope signatures for one of these low-Mg pyroxenites (NK3-1) indicate that parts of the Somerset lithosphere are characterized by very low U/Pb, Th/Pb and Sm/Nd ratios (possibly ancient feature >1Ga), in order to preserve such unradiogenic Pb and Nd isotopic compositions. In contrast, the high-Mg pyroxenites have Pb and Nd isotopic compositions that are similar to those of the peridotites. These pyroxenites have been interpreted to constitute a pyroxene-rich component in the lithospheric mantle produced by small scale segregation of peridotite compositions into olivine and pyroxene-rich layers (Schmidberger and Francis, 2001).

5.3. Isotopic mantle stratification

The large range in Sr and Pb isotopic ratios observed in the Nikos peridotites and the trend towards significantly higher $^{87}Sr/^{86}Sr_{(t)}$ and lower $^{206}Pb/^{204}Pb_{(t)}$ isotopic ratios for the high-temperature peridotites (Figs. 4, 5) indicate that the deep Somerset lithosphere (>160 km) is isotopically distinct from the shallow lithospheric mantle. These findings imply that the mantle root beneath the northern Canadian craton is characterized by a depth stratification in isotopic composition that predates kimberlite magmatism at 100 Ma ago. This is in good agreement with the vertical zonation suggested by incompatible trace element compositions of the Nikos peridotites, and the decrease in trace elements contents with depth in the Somerset lithosphere (Schmidberger and Francis, 2001).

The Nikos whole-rock compositions are characterized by significantly more radiogenic Sr values than those of their constituent clinopyroxenes, a feature which is most evident for the low-temperature xenoliths. This is inconsistent with isotopic mass balance calculations using solely clinopyroxene and garnet as Sr-bearing minerals, which predict that the whole-rock Sr isotopic composition should plot close to that of clinopyroxene, as it controls the bulk Sr budget. The radiogenic Sr isotope ratios of the Nikos whole-rocks, therefore, require the presence of an accessory phase (in addition to the kimberlite contaminant), most likely phlogopite, characterized by a radiogenic Sr isotopic composition ($^{87}Sr/^{86}Sr>0.75$; Kramers et al., 1983). Small amounts of phlogopite are present in the Nikos peridotites, thus contributing to their bulk rock Sr isotope budgets, and most probably responsible for the radiogenic $^{87}Sr/^{86}Sr_{(t)}$ of the xenoliths.

5.3.1. Clinopyroxene Sr isotope depth zonation

The determination of the Sr isotope compositions in inclusion-free clinopyroxene permits an unbiased isotopic characterization of the mantle lithosphere, unaffected by the presence of interstitial or accessory phases. Furthermore, the Nikos clinopyroxenes are characterized by extremely low Rb/Sr ratios ($^{87}Rb/^{86}Sr<0.0002$), thus their present-day Sr isotope ratios are almost identical to those at the time of kimberlite emplacement as the correction for 100 Ma in-situ decay is negligible.

The clinopyroxenes from the low-temperature Nikos xenoliths have Sr isotopic compositions that are less radiogenic than or similar to the composition of bulk Earth (Zindler and Hart, 1986), and distinct from those of the Nikos kimberlite (Fig. 6). In contrast, the clinopyroxenes from the high-temperature peridotites have Sr isotopic ratios that are significantly more radiogenic than those of the Nikos kimberlite (Fig. 6). The distinct Sr isotope compositions of clinopyroxenes in the low and high-temperature peridotites exhibit a correlation with pressures and thus depths of last equilibration (Fig. 8), in agreement with the whole-rock data (Table 1; Figs. 4, 5) indicating that the shallow Somerset mantle is isotopically distinct from the deep lithosphere. The vertical stratification could have resulted from infiltration of the lower lithosphere with metasomatic melts or fluids originating from deeper levels of the upper mantle. This model, however, cannot be reconciled with the significantly lower Sr (and LREE) abundances of clinopyroxene from the deep-seated peridotites relative to those from the shallow peridotites (Schmidberger and Francis, 2001), as contamination with metasomatic melts or fluids should also increase their incompatible trace element abundances. The significantly more radiogenic Sr isotopic ratios and low incompatible trace element abundances of clinopyroxene in the high-temperature peridotites indicate that the shallow and deep Somerset lithosphere do not share a common petrogenetic history. It is thus possible that the deep lithospheric mantle is younger and was added to the existing shallow lithosphere by downward growth of the mantle root during a later magmatic event (e.g. Pearson, 1999). Mantle stratification and post-Archean lithosphere growth have previously been proposed for the South African Kaapvaal craton (e.g. Menzies, 1990; Pearson et al., 1995a) and recently garnet xenocryst compositions have been interpreted to indicate that the deep lithosphere beneath the Canadian Slave craton represents underplated mantle (Griffin et al., 1999). The respective correlations of Sr and Pb isotopes with Sr and Pb abundances in the deep-seated Nikos peridotites (Fig. 7) suggest that the mantle, which underplated the shallow Somerset lithosphere, contained recycled material (altered oceanic crust and sedimentary component?; e.g. Hauri et al., 1993) characterized by radiogenic Sr and unradiogenic Pb isotopic compositions that was mixed into the mantle during earlier subduction. Recycling of oceanic lithosphere may have been related to an early Paleozoic subduction regime reported for the Canadian Arctic (Trettin et al., 1991), which would suggest that the deep Somerset lithosphere was added in the Phanerozoic.

The enrichment in highly incompatible trace elements observed for the low-temperature Nikos peridotites and constituent clinopyroxenes, and Sr, Nd and Pb isotopic signatures that are distinct from those for "depleted mantle" indicate that the Archean shallow lithosphere was affected by the infiltration of metasomatic melts or fluids. Although the timing of this metasomatism is difficult to constrain, it would appear to have occurred prior to the addition of the deep high-temperature portion of the lithosphere since the latter is less enriched in incompatible trace elements. Depleted mantle Nd model ages (T_{DM}) for clinopyroxene from the low-temperature peridotites (~700 Ma) probably indicate the maximum age for the metasomatism that affected the shallow lithosphere, which could thus have occurred as early as the late Proterozoic. A Proterozoic orogeny is recognized in the Canadian Arctic at ~700 Ma (Trettin et al., 1991), and it is possible that metasomatism of the shallow lithosphere beneath Somerset Island occurred during this event.

6. CONCLUSIONS

The Archean Nikos peridotites are characterized by a refractory olivine-rich mineralogy and major element chemistry. Nd isotopic compositions are similar or slightly depleted relative to CHUR, whereas a significant range in Sr and Pb isotope compositions is recorded, which do not correlate with the degree of major element depletion in the bulk rocks. These geochemical signatures are inconsistent with formation of the Somerset mantle root by single-stage melt extraction in the Archean, as this process would generate a residual lithosphere with isotopic characteristics similar to that of "depleted mantle". The Nd isotopic ratios of the peridotites overlap those of the Nikos kimberlite, suggesting that the xenoliths were contaminated with kimberlite or a kimberlite-related accessory phase (i.e. apatite). The large range in Sr and Pb isotopic ratios observed in the xenoliths, however, indicate that addition of host kimberlite was restricted to very small amounts (~1 wt% or less).

The high-temperature (>1100°C) Nikos peridotites that sample the deep lithospheric mantle are characterized by more radiogenic $^{87}Sr/^{86}Sr_{(t)}$ and less radiogenic $^{206}Pb/^{204}Pb_{(t)}$ isotopic signatures than those of the shallow low-temperature peridotites (<1100°C). These whole-rock data are consistent with significantly less radiogenic Sr isotopic compositions for clinopyroxenes from the low-temperature peridotites than those for clinopyroxenes from the high-temperature peridotites. The depth correlation of Sr isotopes in clinopyroxene, and Sr and Pb isotopic compositions in the Nikos whole-rocks indicate that the deep (>160 km) and shallow Somerset lithosphere do not share the same formational history. The deep-seated high-temperature peridotites may have been added to the existing shallow lithosphere in a Phanerozoic magmatic event, and this mantle could have contained recycled (altered oceanic crust and sedimentary component?) material as a result of earlier subduction.

Acknowledgements

We thank Fabien Rasselet for assistance in the field and hand-picking separates of magmatic kimberlite for isotope analysis. Clément Gariépy is thanked for earlier revisions of the manuscript. The research was funded by an NSERC operating grant to D. Francis and S. Schmidberger is grateful for financial support in the form of a NSERC doctoral scholarship.

REFERENCES

Bedini R. M. and Bodinier J.-L. (1999) Distribution of incompatible trace elements between the constituents of spinel peridotite xenoliths: ICP-MS data from the East African Rift. *Geochim. Cosmochim. Acta* **63**, 3883-3900.

Boyd F. R., Pokhilenko N. P., Pearson D. G., Mertzman S. A., Sobolev N. V. and Finger L. W. (1997) Composition of the Siberian cratonic mantle: evidence from Udachnaya peridotite xenoliths. *Contrib. Mineral. Petrol.* **128**, 228-246.

Dawson J. B. (1967) A review of the geology of kimberlite. In *Ultramafic and related rocks* (ed. P. J. Wyllie). Wiley, New York. pp. 241-251.

DePaolo D. J. and Wasserburg G. J. (1976) Inferences about magma sources and mantle structure from variations of ^{143}Nd/^{144}Nd. *Geophys. Res. Lett.* **3**, 743-746.

Edwards R. L., Chen J. H. and Wasserburg G. J. (1986): ^{238}U-^{234}U-^{230}Th-^{232}Th systematics and the precise measurement of time over the past 500,000 years. *Earth Planet. Sci. Lett.* **81**, 175-192.

Erlank A. J., Waters F. G., Hawkesworth C. J., Haggerty S. E., Allsopp H. L., Rickard R. S. and Menzies M. A. (1987) Evidence for mantle metasomatism in peridotite nodules from the Kimberley pipes, South Africa. In *Mantle metasomatism* (eds. M. A. Menzies and C. J. Hawkesworth). Academic Press, London. pp. 221-311.

Fraser K. J., Hawkesworth C. J., Erlank A. J., Mitchell R. H. and Scott-Smith B.H. (1985) Sr, Nd and Pb isotope and minor element geochemistry of lamproites and kimberlites. *Earth Planet. Sci. Lett.* **76**, 57-70.

Frisch T. and Hunt P. A. (1993) Reconnaissance U-Pb geochronology of the crystalline core of the Boothia Uplift, District of Franklin, Northwest Territories. In *Radiogenic age and isotope studies: Report 7.* Geological Survey of Canada, Paper **93-2**. pp. 3-22.

Griffin W. L., Doyle B. J., Ryan C. G., Pearson N. J., O'Reilly S. Y., Davies R., Kivi K., van Achterbergh E. and Natapov L. M. (1999) Layered mantle lithosphere in the Lac de Gras area, Slave craton: composition, structure and origin. *J. Petrol.* **40**, 705-727.

Hauri E. H., Shimizu N., Dieu J. J. and Hart S. R. (1993) Evidence for hotspot-related carbonatite metasomatism in the oceanic upper mantle. *Nature* **365**, 221-227.

Hawkesworth C. J., Erlank A. J., Kempton P. D. and Waters F. G. (1990a) Mantle metasomatism: isotope and trace-element trends in xenoliths from Kimberley, South Africa. *Chem. Geol.* **85**, 19-34.

Hawkesworth C. J., Kempton P. D., Rogers N. W., Ellam R. M. and van Calsteren P. W. (1990b) Continental mantle lithosphere, and shallow level enrichment processes in the Earth's mantle. *Earth Planet. Sci. Lett.* **96**, 256-268.

Heaman L. H. (1989) The nature of the subcontinental mantle from Sr-Nd-Pb isotopic studies on kimberlite perovskite. *Earth Planet. Sci. Lett.* **92**, 323-334.

Herzberg C. T. (1993) Lithosphere peridotites of the Kaapvaal craton. *Earth Planet. Sci. Lett.* **120**, 13-29.

Irvine G. J., Kopylova M. G., Carlson R. W., Pearson D. G., Shirey S. B. and Kjarsgaard B. A. (1999) Age of the lithospheric mantle beneath and around the Slave craton: a Rhenium-Osmium isotopic study of peridotite xenoliths from the Jericho and Somerset Island kimberlites. *Ninth Annual V. M. Goldschmidt Conference*. LPI Contribution No. 971, 134-135.

Jones R. A. (1987) Strontium and neodymium isotopic and rare earth element evidence for the genesis of megacrysts in kimberlites of southern Africa. In *Mantle Xenoliths* (ed. P. H. Nixon). John Wiley & Sons, Chichester. pp. 711-724.

Kramers J. D. (1977) Lead and strontium isotopes in Cretaceous kimberlites and mantle-derived xenoliths from southern Africa. *Earth Planet. Sci. Lett.* **34**, 419-431.

Kramers J. D., Roddick J. C. M. and Dawson J. B. (1983) Trace element and isotope studies on veined, metasomatic and "MARID" xenoliths from Bultfontein, South Africa. *Earth Planet. Sci. Lett.* **65**, 90-106.

Manhès G., Allègre C. J., Dupré B. and Hamelin B. (1980) Lead isotope study of basic-ultrabasic layered complexes: speculations about the age of the earth and primitive mantle characteristics. *Earth Planet. Sci. Lett.* **47**, 370-382.

Macdougall J. D. and Haggerty S. E. (1999) Ultradeep xenoliths from African kimberlites: Sr and Nd isotopic compositions suggest complex history. *Earth Planet. Sci. Lett.* **170**, 73-82.

McCulloch M. T., Jaques A. L., Nelson D. R. and Lewis J. D. (1983) Nd and Sr isotopes in kimberlites and lamproites from Western Australia: an enriched mantle origin. *Nature* **302**, 400-403.

McDonough W. F. (1990) Constraints on the composition of the continental lithospheric mantle. *Earth Planet. Sci. Lett.* **101**, 1-18.

McDonough W. F. and Sun S. S. (1995) The composition of the earth. *Chem. Geol.* **120**, 223-253.

Menzies M. A. (1990) Archean, Proterozoic, and Phanerozoic lithospheres. In *Continental mantle* (ed. M. A. Menzies). Oxford Univ. Press, Oxford. pp. 67-86.

Menzies M. A. and Murthy R. (1980) Enriched mantle: Nd and Sr isotopes in diopsides from kimberlite nodules. *Nature* **283**, 634-636.

Menzies M. A., Rogers N., Tindle A. and Hawkesworth C. J. (1987) Metasomatic and enrichment processes in lithospheric peridotites, an effect of asthenosphere-lithosphere interaction. In *Mantle metasomatism* (eds. M. A. Menzies and C. J. Hawkesworth). Academic Press, London. pp. 313-361.

Mitchell R. H. (1995) *Kimberlites, orangeites, and related rocks*. Plenum Press, New York.

Nixon P. H. (1987) Kimberlitic xenoliths and their cratonic setting. In *Mantle Xenoliths* (ed. P. H. Nixon). John Wiley & Sons, Chichester. pp. 215-239.

Pearson D. G. (1999) The age of continental roots. *Lithos* **48**, 171-194.

Pearson D. G., Carlson R. W., Shirey S. B., Boyd F. R. and Nixon P. H. (1995a) Stabilisation of Archean lithospheric mantle: a Re-Os isotope study of peridotite xenoliths from the Kaapvaal craton. *Earth Planet. Sci. Lett.* **134**, 341-357.

Pearson D. G., Shirey S. B., Carlson R. W., Boyd F. R., Pokhilenko N. P. and Shimizu N. (1995b) Re-Os, Sm-Nd, and Rb-Sr isotope evidence for thick Archean lithospheric mantle beneath the Siberian craton modified by multistage metasomatism. *Geochim. Cosmochim. Acta* **59**, 959-977.

Pell J. (1993) New kimberlite discoveries on Somerset Island. In *Exploration Overview 1993*, p. 47. NWT Geology Division, Department of Indian and Northern Affairs, Yellowknife (NWT).

Richardson S. H., Erlank A. J. and Hart S. R. (1985) Kimberlite-borne garnet peridotite xenoliths from old enriched subcontinental mantle. *Earth Planet. Sci. Lett.* **75**, 116-128.

Ringwood A. E., Kesson S. E., Hibberson W. and Ware N. (1992) Origin of kimberlites and related magmas. *Earth Planet. Sci. Lett.* **113**, 521-538.

Schmidberger S. S. and Francis D. (1999) Nature of the mantle roots beneath the North American craton: mantle xenolith evidence from Somerset Island kimberlites. *Lithos* **48**, 195-216.

Schmidberger S. S. and Francis D. (2001) Constraints on the trace element composition of the Archean mantle root beneath Somerset Island, Arctic Canada. *J. Petrol.* **42**, 1095-1117.

Smith C. B. (1983) Pb, Sr and Nd isotopic evidence for sources of southern African Cretaceous kimberlites. *Nature* **304**, 51-54.

Smith C. B., Allsopp H. L., Garvie O. G., Kramers J. D., Jackson P. F. S. and Clement C. R. (1989) Note on the U-Pb perovskite method for dating kimberlites: examples from the Wesselton and DeBeers mines, South Africa, and Somerset Island, Canada. *Chem. Geol. (Isot. Sect.)* **79**, 137-145.

Stacey J. S. and Kramers J. D. (1975) Approximation of terrestrial lead isotope evolution by a two-stage model. *Earth Planet. Sci. Lett.* **26**, 207-223.

Steward W. D. (1987) Late Proterozoic to Early Tertiary stratigraphy of Somerset Island and northern Boothia Peninsula, District of Franklin. *Geological Survey of Canada Paper* **83-26**. pp. 78.

Trettin H. P. (1991) Geology of Canada: Summary and remaining problems. In *Geology of the Innuitian orogen and Arctic platform of Canada and Greenland* (ed. H. P. Trettin). Geological Survey of Canada. pp. 547-553.

Walker R. J., Carlson R. W., Shirey S. B. and Boyd F. R. (1989) Os, Sr, Nd, and Pb isotope systematics of southern African peridotite xenoliths: Implications for the chemical evolution of subcontinental mantle. *Geochim. Cosmochim. Acta* **53**, 1583-1595.

Woolley A. R. and Kempe D. R. C. (1989) Carbonatites nomenclature, average chemical compositions, and elemental distribution. In *Carbonatites; genesis and evolution* (ed. K. Bell). Unwin Hyman Inc, London. pp. 1-14.

Zindler A. and Hart S. R. (1986) Chemical Geodynamics. *Ann. Rev. Earth Planet. Sci.* **14**, 493-571.

FIGURE CAPTIONS

Figure 4-1: Geological map of Somerset Island (after Steward, 1987) showing kimberlite locations. The mantle xenoliths from this study were collected from the Nikos kimberlite pipes (black diamond). Legend: light gray, Paleozoic cover rocks; striped, Late Proterozoic cover rocks; dark gray, Precambrian basement; bold lines, normal faults.

Figure 4-2: Initial Nd and Sr isotopic compositions for Nikos kimberlites. The Nd and Sr isotopic ratios for kimberlites from North America, Siberia, South Africa and Australia ("Group I" and "Group II" kimberlites; for further explanation see text) are shown for comparison (data from McCulloch et al., 1983; Smith, 1983; Heaman, 1989; Pearson et al., 1995b). Values for bulk Earth and CHUR (chondrite uniform reservoir) are those for 100 Ma ago, assuming present day ratios of $^{87}Sr/^{86}Sr_{(bulk\ Earth)}=0.7045$ and $^{87}Rb/^{86}Sr_{(bulk\ Earth)}=0.083$ ($\lambda=1.42 \times 10^{-11}$ y^{-1}) and $^{143}Nd/^{144}Nd_{(CHUR)}=0.512638$ and $^{147}Sm/^{144}Nd_{(CHUR)}=0.1967$ ($\lambda=6.54 \times 10^{-12}$ y^{-1}).

Figure 4-3: Initial Pb isotopic compositions for Nikos kimberlites. The Pb isotopic ratios for South African "Group I" and "Group II" kimberlites are shown for comparison (data from Kramers, 1977; Smith, 1983; Fraser et al., 1985).

Figure 4-4: Nd and Sr isotopic compositions for Nikos xenoliths at 100 Ma ago. The Nd and Sr isotopic ratios for the Nikos kimberlites, and the fields for garnet peridotites (including whole-rock and clinopyroxene data) from South African kimberlites and spinel peridotites world-wide are shown for comparison (data from Menzies and Murthy, 1980; Kramers et al., 1983; Richardson et al., 1985;

Jones, 1987; Walker et al., 1989; Hawkesworth et al., 1990a,b; Macdougall and Haggerty, 1999 and references therein).

Figure 4-5: Pb isotopic compositions for Nikos xenoliths at 100 Ma ago. The Pb isotopic ratios for the Nikos kimberlites and the field for kimberlite-hosted garnet peridotites (including whole-rock and clinopyroxene data) from South Africa are shown for comparison (data from Kramers, 1977; Kramers et al., 1983; Richardson et al., 1985; Walker et al., 1989; Hawkesworth et al., 1990a). S/K: Stacey and Kramers (1975) lead isotope evolution curve (time intervals in Ga).

Figure 4-6: Nd and Sr isotopic compositions for Nikos clinopyroxenes and garnets at 100 Ma ago. The Nd and Sr isotopic ratios for the Nikos kimberlites and the field for clinopyroxenes from kimberlite-hosted peridotites from South Africa are shown for comparison (data from Menzies & Murthy, 1980; Kramers et al., 1983; Jones, 1987).

Figure 4-7: Sr and Pb isotopic compositions versus 1/Sr and 1/Pb for low and high-temperature Nikos peridotites at 100 Ma ago. Data for the Nikos kimberlites at 100 Ma are shown for comparison.

Figure 4-8: Sr isotopic compositions for Nikos clinopyroxenes plotted versus pressure of last equilibration. For sample NK2-4 pressure of last equilibration was not determined and it is plotted in the lower portion of the shallow lithosphere.

Table 4-1. Rb, Sr, Sm, and Nd abundances and Sr and Nd isotope compositions for Nikos kimberlites and xenoliths.

Sample	Temp °C	Press kb	Rb ppm	Sr ppm	^{87}Rb/^{86}Sr	^{87}Sr/^{86}Sr measured	^{87}Sr/^{86}Sr (t)	Sm ppm	Nd ppm	^{147}Sm/^{144}Nd	^{143}Nd/^{144}Nd measured	^{143}Nd/^{144}Nd (t)	T_{DM} Ma	ε_{Nd} (t)
Kimberlites														
NK3-K1			72	1320	0.16	0.705403 ±14	0.7052	10.1	74.6	0.0819	0.512617 ±11	0.512563		1.1
NK3-K2			44	1030	0.12	0.705334 ±14	0.7052	10.7	78.3	0.0828	0.512593 ±07	0.512539		0.6
NK3-K3			30	1710	0.05	0.705248 ±14	0.7052	14.7	110	0.0808	0.512640 ±07	0.512587		1.5
NK3-K4			20	2190	0.03	0.705243 ±16	0.7052	12.7	94.5	0.0814	0.512634 ±12	0.512580		1.4
duplicate						0.705245 ±13								
NK3-K5			31	1330	0.07	0.705272 ±13	0.7052	11.6	82.5	0.0850	0.512631 ±05	0.512575		1.3
Low-Temperature Peridotites														
NK3-20	815	29.8	7.3	55.9	0.38	0.705677 ±10	0.7051	0.37	1.58	0.1411	0.512763 ±11	0.512671	812	3.2
NK1-4	871	33.5	3.0	43.3	0.20	0.706917 ±14	0.7066	0.24	1.49	0.0984	0.512676 ±14	0.512611	628	2.0
NK1-4 Cpx			0.01[a]	115[a]	0	0.703776 ±11	0.7038	1.38	9.50	0.0875	0.512620 ±05	0.512562	641	1.0
NK1-4 Gt			0.02[a]	0.17	0.29	0.707539 ±14	0.7071	0.43	0.49	0.5256	0.513049 ±09	0.512705		3.8
NK2-3	887	34.6	7.5	77.7	0.28	0.706093 ±14	0.7057	0.38	2.63	0.0879	0.512701 ±12	0.512643	545	2.6
NK2-3 Cpx				318		0.704584 ±14	0.7046	2.09	14.6	0.0864	0.512732 ±10	0.512676	501	3.3
NK2-3 Gt				0.27		0.706887 ±16	0.7065	0.70	1.99	0.2135	0.512829 ±08	0.512690		3.5
Nk1-23	964	39.0	4.7	86.5	0.16	0.705329 ±11	0.7051	0.51	3.64	0.0853	0.512755 ±10	0.512699	470	3.7
NK2-10	1014	42.1	3.0	92.6	0.09	0.705637 ±13	0.7055	0.47	2.93	0.0964	0.512648 ±05	0.512585	653	1.5
NK1-14	1027	42.7	1.4	43.7	0.10	0.705792 ±14	0.7057	0.31	1.97	0.0944	0.512657 ±13	0.512595	631	1.7
Nk1-14 Cpx				217		0.703814 ±14	0.7038	3.19	23.9	0.0806	0.512621 ±08	0.512568	607	1.1
Nk1-14 Gt				0.31		0.706495 ±11	0.7061	1.08	2.08	0.3137	0.512807 ±09	0.512602		1.8
NK1-2	1042	44.7	1.2	33.8	0.10	0.705534 ±14	0.7054	0.27	1.75	0.0938	0.512655 ±16	0.512594	630	1.6
NK1-12	1054	45.3	3.2	56.5	0.16	0.706203 ±14	0.7060	0.40	2.21	0.1094	0.512670 ±19	0.512599	702	1.8
NK1-3	1076	46.5	1.7	56.3	0.09	0.706668 ±14	0.7065	0.33	1.53	0.1324	0.512655 ±14	0.512568	928	1.2
NK1-3 Cpx				406		0.704149 ±14	0.7041	5.60	28.0	0.1207	0.512646 ±08	0.512567	827	1.1
NK1-3 Gt				0.73		0.706472 ±14	0.7061	1.99	2.82	0.4272	0.512829 ±07	0.512550		0.8
NK2-4[b]			1.9	14.9	0.37	0.705188 ±16	0.7047	0.21	0.97	0.1280	0.512847 ±08	0.512763	541	5.0
NK2-4 Cpx				133[a]		0.703879 ±13	0.7039	1.54	6.88	0.1357	0.512775 ±09	0.512686	733	3.5
NK 2-4 Gt						0.707703 ±13	0.7073	1.62	2.45	0.3999	0.512886 ±11	0.512624		2.2
High-Temperature Peridotites														
NK1-6	1149	48.4	0.8	17.1	0.14	0.706544 ±13	0.7064	0.22	0.97	0.1371	0.512674 ±29	0.512584	947	1.5
NK2-1	1216	51.5	10	31.3	0.93	0.709277 ±13	0.7080	0.14	0.66	0.1299	0.512624 ±17	0.512539	958	0.6
duplicate						0.709286 ±10					0.512607 ±23			
NK2-1 Cpx				45.8		0.709132 ±17	0.7091	0.79	2.97	0.1604	0.512664 ±12	0.512559	1386	1.0
NK2-1 Gt			0.08[a]	0.57	0.39	0.710015 ±14	0.7095	1.16	1.13	0.6205	0.512966 ±17	0.512560		1.0
NK1-9	1219	53.4	1.5	17.8	0.25	0.706912 ±13	0.7066	0.23	0.88	0.1548	0.512661 ±21	0.512560	1264	1.0

Table 4-1. (Continued)

Sample	Temp °C	Press kb	Rb ppm	Sr ppm	$^{87}Rb/^{86}Sr$	$^{87}Sr/^{86}Sr$ measured	$^{87}Sr/^{86}Sr$ (t)	Sm ppm	Nd ppm	$^{147}Sm/^{144}Nd$	$^{143}Nd/^{144}Nd$ measured	$^{143}Nd/^{144}Nd$ (t)	T_{CHUR} Ma	ε_{Nd} (t)
NK1-1	1222	52.7	1.1	25.7	0.12	0.707152 ±10	0.7070							
NK3-11	1247	53.1	2.9	202	0.04	0.708065 ±24	0.7080	0.25	1.05	0.1405	0.512655 ±15	0.512563	1032	1.0
NK3-25	1256	54.0	29	37.5	2.21	0.709693 ±17	0.7066	0.33	1.76	0.1120	0.512628 ±31	0.512554	783	0.9
NK1-5	1262	54.6	4.3	46.5	0.27	0.706955 ±13	0.7066	0.26	1.09	0.1451	0.512694 ±16	0.512600	1013	1.8
Nk1-5 Cpx				75.0		0.706674 ±14	0.7067	1.36	5.88	0.1395	0.512700 ±10	0.512609	924	2.0
Nk1-5 Gt				0.51		0.707442 ±14	0.7069	1.13	1.07	0.6334	0.512999 ±09	0.512584		1.5
NK3-16	1280	53.5	1.8	40.9	0.13	0.707234 ±13	0.7071	0.17	0.88	0.1177	0.512662 ±10	0.512585	775	1.5
NK1-7	1300	55.1	1.0	15.2	0.20	0.706660 ±14	0.7064	0.14	0.44	0.1904	0.512749 ±38	0.512624	2610	2.3
Nk1-7 Cpx				86.9		0.706066 ±17	0.7061							
Nk1-7 Gt				0.48		0.707249 ±14	0.7067	1.33	1.45	0.5551	0.512886 ±10	0.512523		0.3
NK2-2	1316	54.7	6.5	33.5	0.56	0.708523 ±14	0.7077	0.30	1.24	0.1488	0.512686 ±11	0.512588	1090	1.6
NK2-2 Cpx			0.01[a]	106[a]	0	0.707280 ±13	0.7073	1.38	5.71	0.1456	0.512687 ±10	0.512591	1037	1.6
NK 2-2 Gt				0.35		0.709472 ±14	0.7089	0.73	0.91	0.4850	0.512911 ±10	0.512594		1.7
NK3-15	1343	58.5	3.7	344	0.03	0.708533 ±14	0.7085	0.20	1.16	0.1043	0.512639 ±14	0.512571	713	1.2
NK3-4	1371	58.5	23	245	0.27	0.708867 ±13	0.7085	0.42	2.21	0.1150	0.512569 ±21	0.512494	897	-0.3
Nk 3-4 Cpx				92.7		0.705199 ±14	0.7052	1.07	4.31	0.1501	0.512639 ±10	0.512541	1224	0.6
Nk 3-4 Gt				0.43		0.708717 ±14	0.7082	0.69	0.72	0.5752	0.512797 ±10	0.512421		-1.7
Pyroxenites														
NK2-7 HMg	737	25.3	4.1	284	0.04	0.704128 ±11	0.7041	0.80	4.98	0.0973	0.512554 ±10	0.512490	781	-0.4
NK3-14 HMg	933	36.8	30	162	0.54	0.706629 ±11	0.7059	1.67	8.29	0.1218	0.512720 ±41	0.512640	714	2.6
NK3-17 LMg	720	22.2	3.6	38.8	0.27	0.706108 ±10	0.7057	0.58	1.99	0.1745	0.512980 ±09	0.512866	660	7.0
NK3-1 LMg	759	25.1	5.1	90.3	0.16	0.704840 ±21	0.7046	0.67	3.05	0.1330	0.512058 ±10	0.511971	2055	-10.5
Nk 3-1 Cpx			0.01[a]	89.4[a]	0	0.704268 ±13	0.7043	1.06	4.77	0.1342	0.511879 ±15	0.511791	2426	-14.0
Nk 3-1 Gt			0.02[a]	0.14	0.35	0.706110 ±16	0.7056	0.48	0.77	0.3806	0.512956 ±21	0.512707		3.9

Minerals and rock types: *Cpx* = clinopyroxene; *Gt* = garnet; *HMg* = high-Mg pyroxenite; *LMg* = low-Mg pyroxenite. (t): Sr and Nd isotope ratios corrected for 100 Ma in-situ decay. $^{87}Sr/^{86}Sr$ are normalized to $^{86}Sr/^{88}Sr=0.1194$ and $^{143}Nd/^{144}Nd$ to $^{146}Nd/^{144}Nd=0.7219$. NBS 987 Sr standard yielded an average value of $^{87}Sr/^{86}Sr=0.710253\pm0.000013$ (2σ; n=10). Measurements of Ames Nd standard gave an average value of $^{143}Nd/^{144}Nd=0.512132\pm0.000011$ (2σ; n=8). Precision for individual Sr and Nd isotope measurements is quoted at the 2σ level. Sm and Nd abundances were determined by isotope dilution analysis with uncertainties <0.5%. Rb and Sr abundances for bulk rocks were measured by ICP-MS analysis (for analytical procedures see Schmidberger and Francis, 2001). [a]Rb and Sr abundances for Cpx and Gt were determined by isotope dilution analysis with uncertainties <1% and these were used to calculate $^{87}Rb/^{86}Sr$ ratios for the remaining mineral separates (for further explanation see text). Sr abundances for other Cpx and Gt separates were measured by ion microprobe analysis. [b]Temperature and pressure estimates not determined.

Table 4-2. Pb, U and Th abundances and Pb isotopic compositions for Nikos kimberlites and xenoliths.

Sample	Pb ppm	U ppm	Th ppm	$^{238}U/^{204}Pb$ μ	$^{206}Pb/^{204}Pb$ measured	$^{207}Pb/^{204}Pb$ measured	$^{208}Pb/^{204}Pb$ measured	$^{206}Pb/^{204}Pb$ (t)	$^{207}Pb/^{204}Pb$ (t)	$^{208}Pb/^{204}Pb$ (t)
Kimberlites										
NK3-K1	11	2.9	14.4	17.0	18.485	15.478	38.584	18.220	15.465	38.151
NK3-K2	14	3.2	14.1	14.6	18.483	15.466	38.699	18.255	15.455	38.367
NK3-K3	14	3.5	18.5	16.2	18.712	15.512	38.903	18.458	15.500	38.466
NK3-K4	28	3.8	17.5	8.8	18.758	15.513	38.906	18.621	15.506	38.700
NK3-K5	35	2.9	14.1	5.4	18.704	15.537	38.899	18.619	15.533	38.766
average	*20*	*3.3*	*15.7*	*12.4*						
Low-Temperature Peridotites										
NK3-20	0.08	0.03	0.08	22.2	18.823	15.587	38.815	18.476	15.570	38.496
NK1-4	0.22	0.08	0.22	22.7	18.675	15.542	38.654	18.320	15.525	38.315
NK2-3	0.27	0.16	0.32	36.7	19.147	15.509	38.953	18.573	15.481	38.568
NK1-23	0.07	0.04	0.07	30.7	18.600	15.451	38.316	18.120	15.428	37.997
NK2-10	0.66	0.17	0.30	16.3	19.287	15.550	38.556	19.033	15.538	38.405
NK1-14	0.14	0.06	0.26	28.3	18.771	15.517	38.771	18.328	15.496	38.166
NK1-2	0.15	0.04	0.15	18.5	18.587	15.494	38.545	18.298	15.480	38.209
NK1-12	0.26	0.06	0.21	15.1	18.798	15.515	38.540	18.563	15.504	38.269
NK1-3	0.17	0.10	0.16	37.5	18.407	15.394	38.128	17.820	15.366	37.818
NK2-4	0.08	0.03	0.07	21.9	18.994	15.503	38.759	18.652	15.487	38.435
average	*0.21*	*0.08*	*0.18*	*25.0*						
High-Temperature Peridotites										
NK2-1	0.09	0.02	0.06	14.8	18.520	15.427	38.386	18.288	15.416	38.157
NK1-9	0.10	0.03	0.08	20.2	18.614	15.496	38.521	18.299	15.481	38.232
NK1-1	0.14	0.08	0.13	37.7	18.571	15.454	38.404	17.981	15.426	38.109
NK3-11	0.58	0.69	0.10	77.6	19.193	15.575	38.645	17.980	15.516	38.586
NK3-25	0.42	0.37	0.16	56.6	18.314	15.436	38.286	17.430	15.394	38.158
NK1-5	0.24	0.08	0.12	20.3	18.426	15.492	38.337	18.109	15.476	38.168
NK3-16	0.29	0.21	0.08	46.3	18.377	15.549	38.531	17.654	15.515	38.442
NK1-7	0.04	0.01	0.05	17.2	18.494	15.509	38.320	18.225	15.496	37.914
NK2-2	0.17	0.08	0.06	28.6	18.682	15.472	38.203	18.236	15.450	38.082
NK3-4	0.33	0.48	0.11	93.4	18.641	15.455	38.288	17.181	15.385	38.181
average	*0.21*	*0.17*	*0.10*	*37.1*						
Pyroxenites										
NK2-7HMg	1.99	0.35	0.49	11.5	18.964	15.509	38.756	18.785	15.500	38.675
NK3-17LMg	0.75	0.13	0.33	11.6	19.788	15.632	38.860	19.607	15.623	38.715
NK3-1LMg	0.39	0.04	0.14	6.6	17.015	15.349	37.285	16.912	15.344	37.169

Rock types: *HMg* high-Mg pyroxenite, *LMg* low-Mg pyroxenite. (t): Pb isotope ratios corrected for 100 Ma in-situ decay. Mass fractionation corrections of 0.09% amu^{-1} and 0.24% amu^{-1} were applied to Pb isotope ratios (based on repeated measurements of NIST SRM 981 Pb standard) using Faraday and Daly analogue detectors, respectively. Average values for the internal precision (2σ) of the $^{206}Pb/^{204}Pb$, $^{207}Pb/^{204}Pb$ and $^{208}Pb/^{204}Pb$ ratios are ±0.016, ±0.014 and ±0.038, respectively). Pb, U and Th abundances for xenoliths were determined by isotope dilution analysis with uncertainties <1%, and for kimberlites by ICP-MS analysis (for analytical procedures see Schmidberger and Francis, 2001).

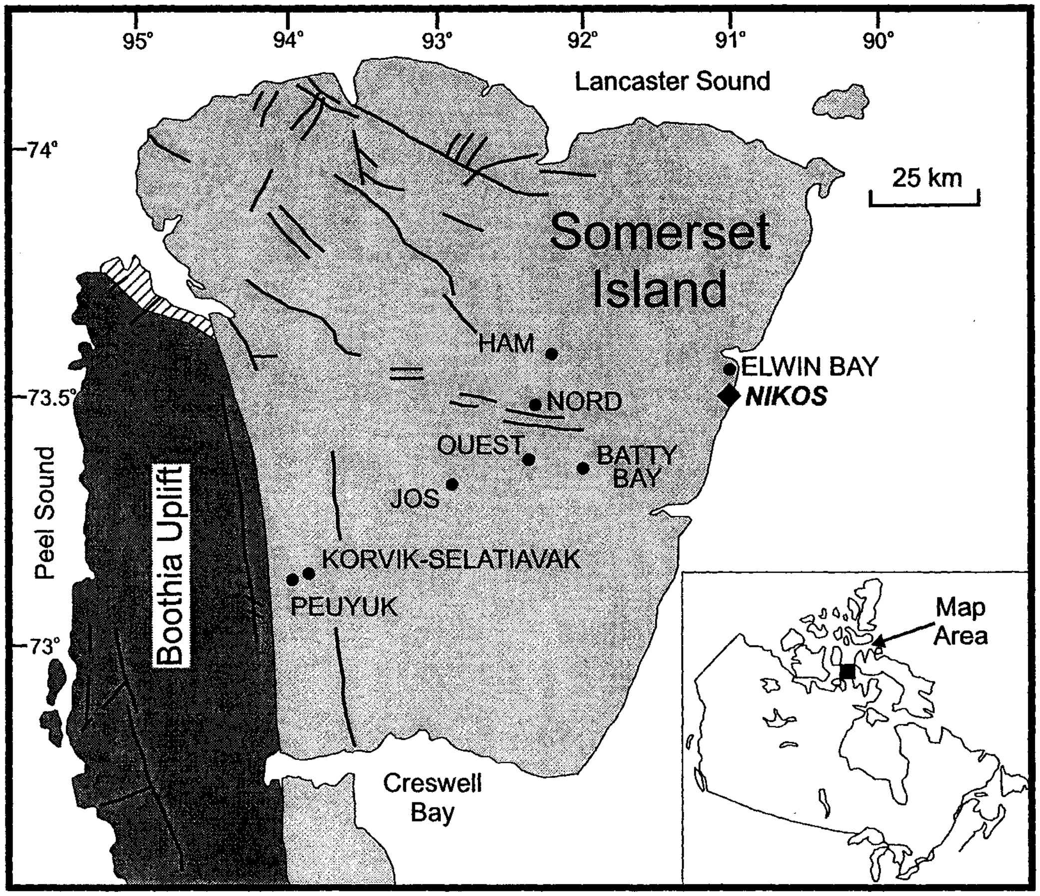
95°
94°
93°
92°
91°
90°
Lancaster Sound
74°
25 km
Somerset Island
HAM
ELWIN BAY
NIKOS
73.5°
NORD
QUEST
BATTY BAY
JOS
Peel Sound
Boothia Uplift
KORVIK-SELATIAVAK
PEUYUK
73°
Map Area
Creswell Bay

Figure 4-1

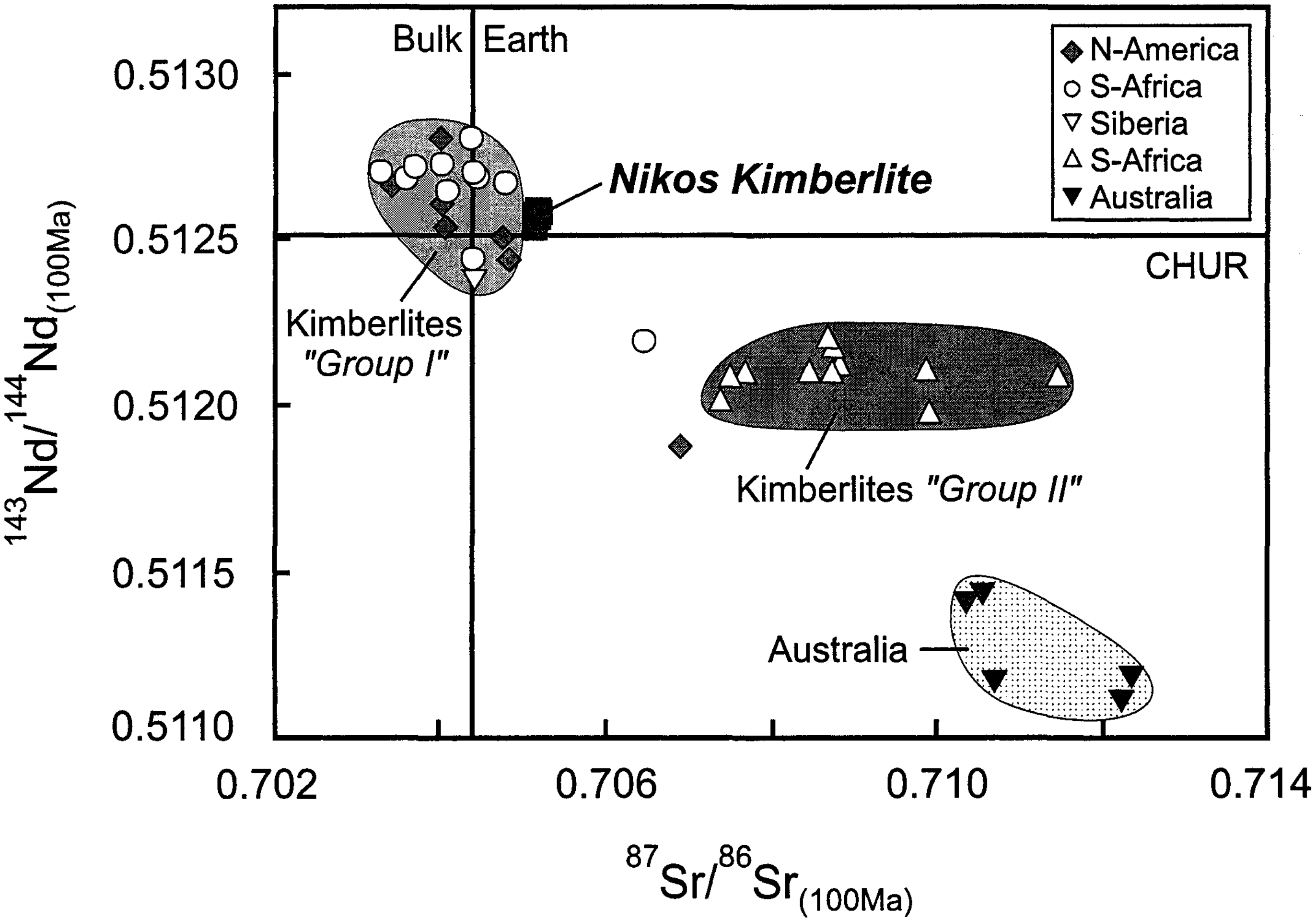
Bulk Earth
CHUR
Nikos Kimberlite
Kimberlites "Group I"
Kimberlites "Group II"
Australia
◆ N-America
○ S-Africa
▽ Siberia
△ S-Africa
▼ Australia
0.5130
0.5125
0.5120
0.5115
0.5110
0.702
0.706
0.710
0.714
^{143}Nd/^{144}Nd$_{(100Ma)}$
^{87}Sr/^{86}Sr$_{(100Ma)}$

Figure 4-2

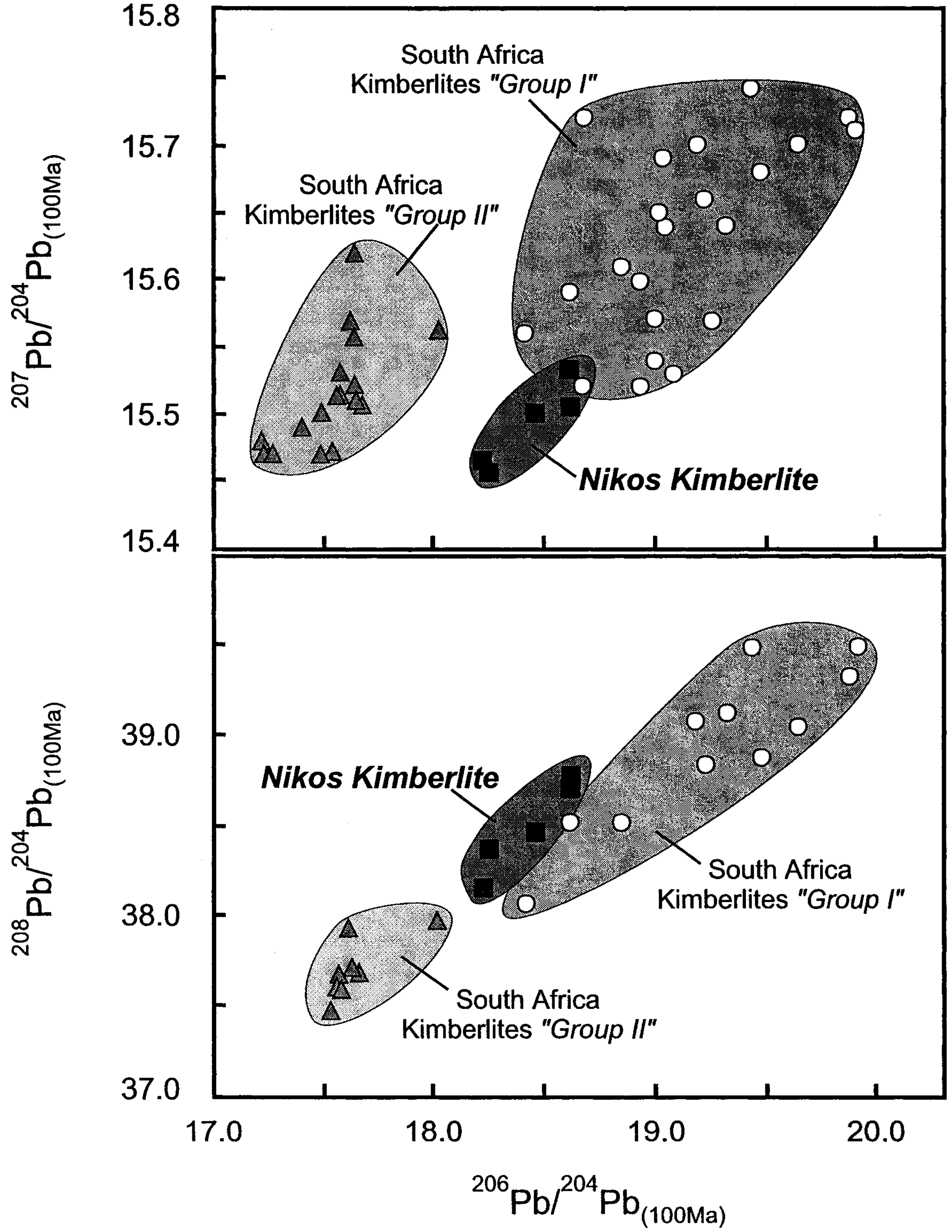
15.8
15.7
15.6
15.5
15.4
$^{207}Pb/^{204}Pb_{(100Ma)}$
South Africa Kimberlites "Group I"
South Africa Kimberlites "Group II"
Nikos Kimberlite
39.0
38.0
37.0
$^{208}Pb/^{204}Pb_{(100Ma)}$
Nikos Kimberlite
South Africa Kimberlites "Group I"
South Africa Kimberlites "Group II"
17.0
18.0
19.0
20.0
$^{206}Pb/^{204}Pb_{(100Ma)}$

Figure 4-3

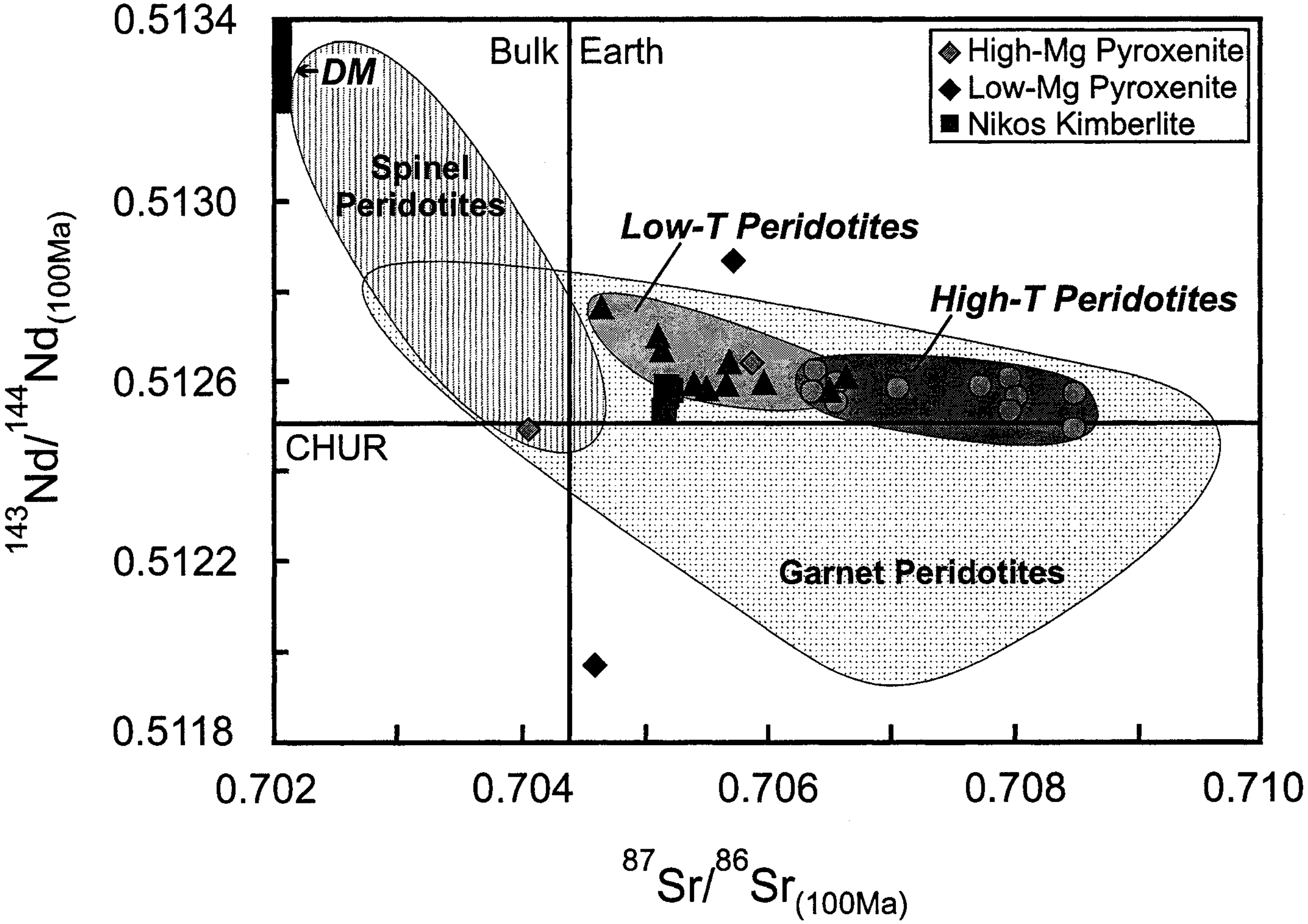
0.5134
0.5130
0.5126
0.5122
0.5118
$^{143}Nd/^{144}Nd_{(100Ma)}$
0.702
0.704
0.706
0.708
0.710
$^{87}Sr/^{86}Sr_{(100Ma)}$
Bulk Earth
CHUR
DM
Spinel Peridotites
Low-T Peridotites
High-T Peridotites
Garnet Peridotites
High-Mg Pyroxenite
Low-Mg Pyroxenite
Nikos Kimberlite

Figure 4-4

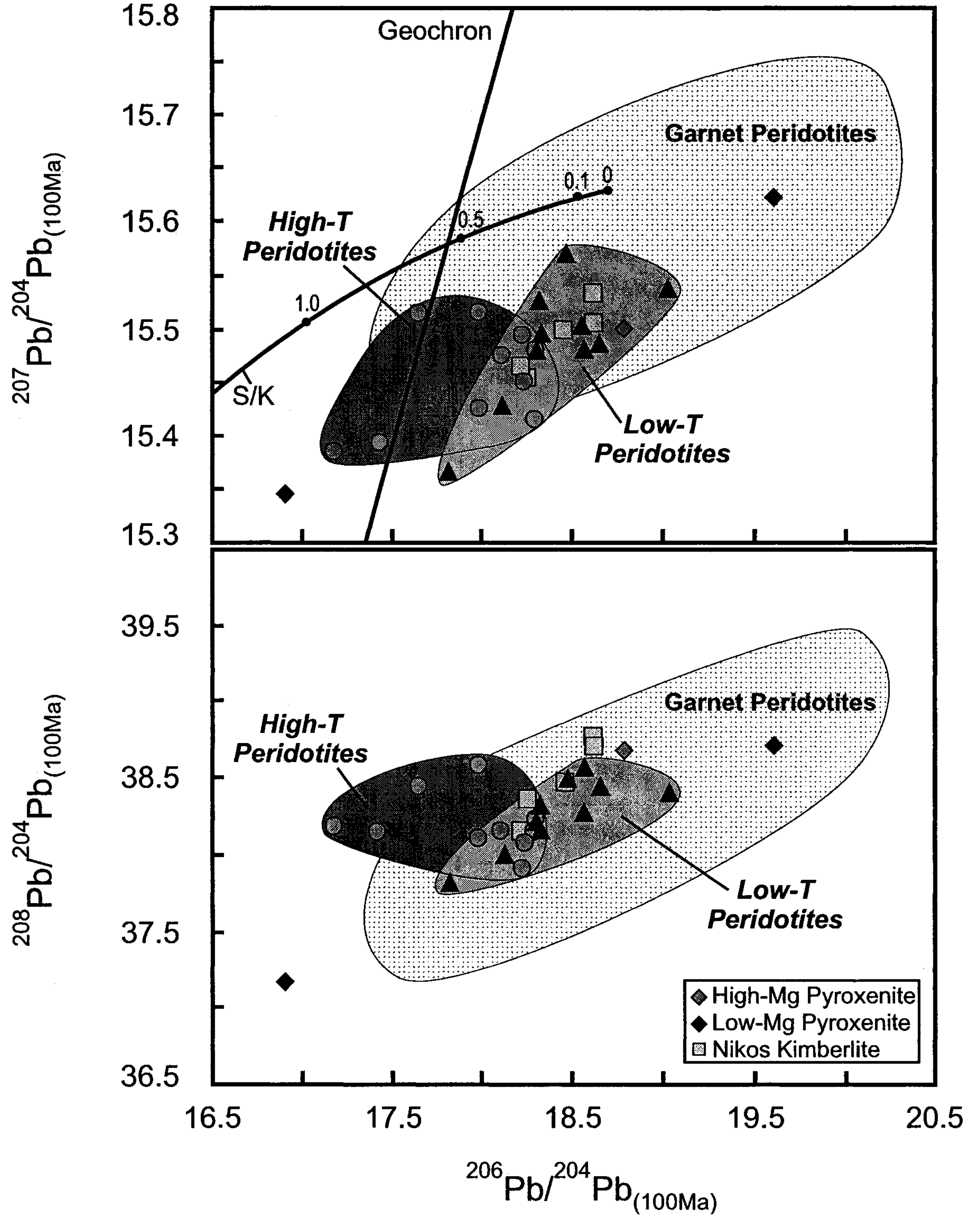

15.8
15.7
15.6
15.5
15.4
15.3
$^{207}Pb/^{204}Pb_{(100Ma)}$
Geochron
Garnet Peridotites
High-T Peridotites
Low-T Peridotites
S/K
1.0
0.5
0.1
0
39.5
38.5
37.5
36.5
$^{208}Pb/^{204}Pb_{(100Ma)}$
Garnet Peridotites
High-T Peridotites
Low-T Peridotites
◆ High-Mg Pyroxenite
◆ Low-Mg Pyroxenite
▨ Nikos Kimberlite
16.5
17.5
18.5
19.5
20.5
$^{206}Pb/^{204}Pb_{(100Ma)}$

Figure 4-5

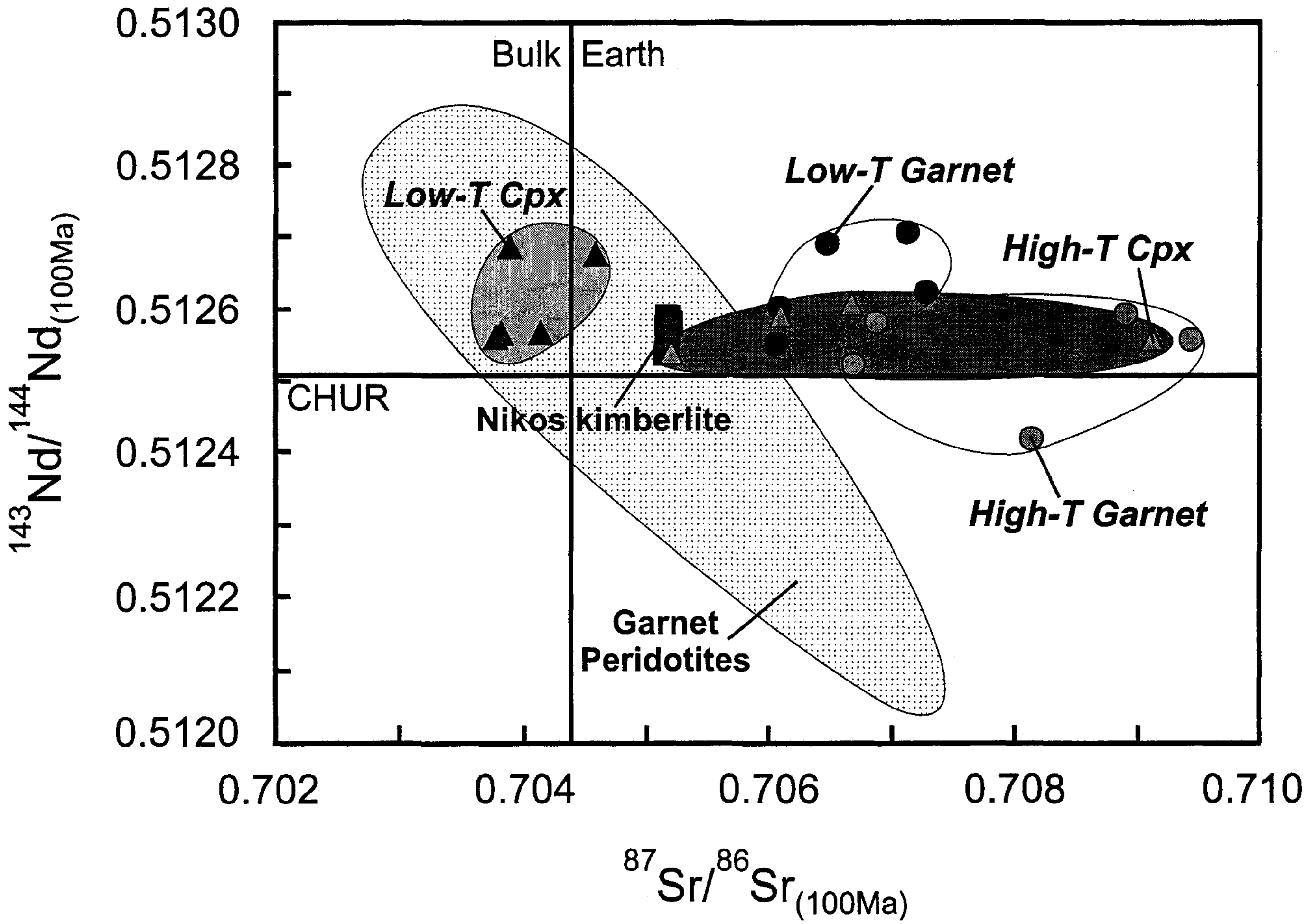

0.5130
0.5128
0.5126
0.5124
0.5122
0.5120
0.702
0.704
0.706
0.708
0.710
$^{143}Nd/^{144}Nd_{(100Ma)}$
$^{87}Sr/^{86}Sr_{(100Ma)}$
Bulk Earth
CHUR
Low-T Cpx
Low-T Garnet
High-T Cpx
High-T Garnet
Nikos kimberlite
Garnet Peridotites

Figure 4-6

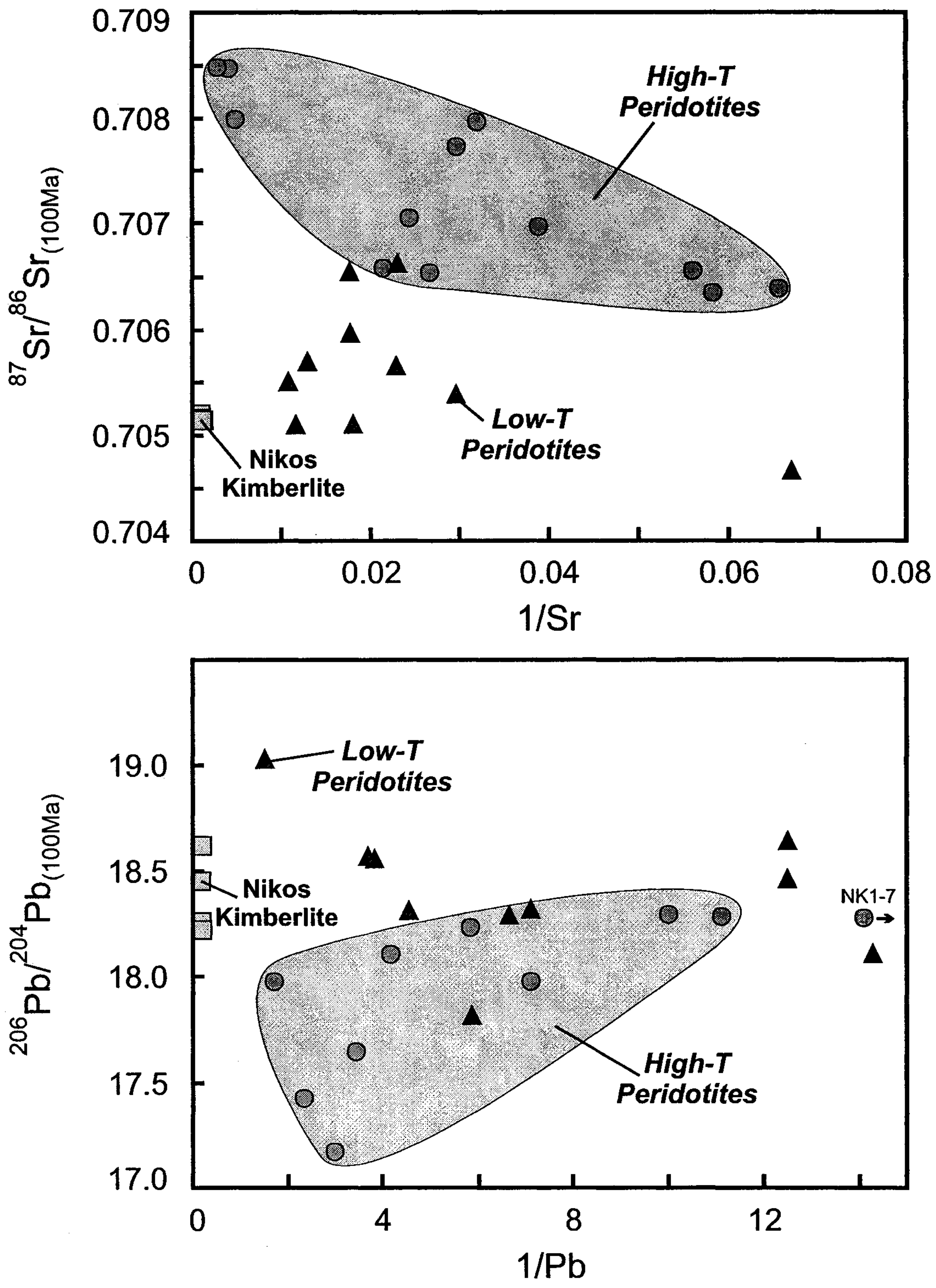
0.709
0.708
0.707
0.706
0.705
0.704
$^{87}Sr/^{86}Sr_{(100Ma)}$
High-T
Peridotites
Low-T
Peridotites
Nikos
Kimberlite
0
0.02
0.04
0.06
0.08
1/Sr
19.0
18.5
18.0
17.5
17.0
$^{206}Pb/^{204}Pb_{(100Ma)}$
Low-T
Peridotites
Nikos
Kimberlite
NK1-7
High-T
Peridotites
0
4
8
12
1/Pb

Figure 4-7

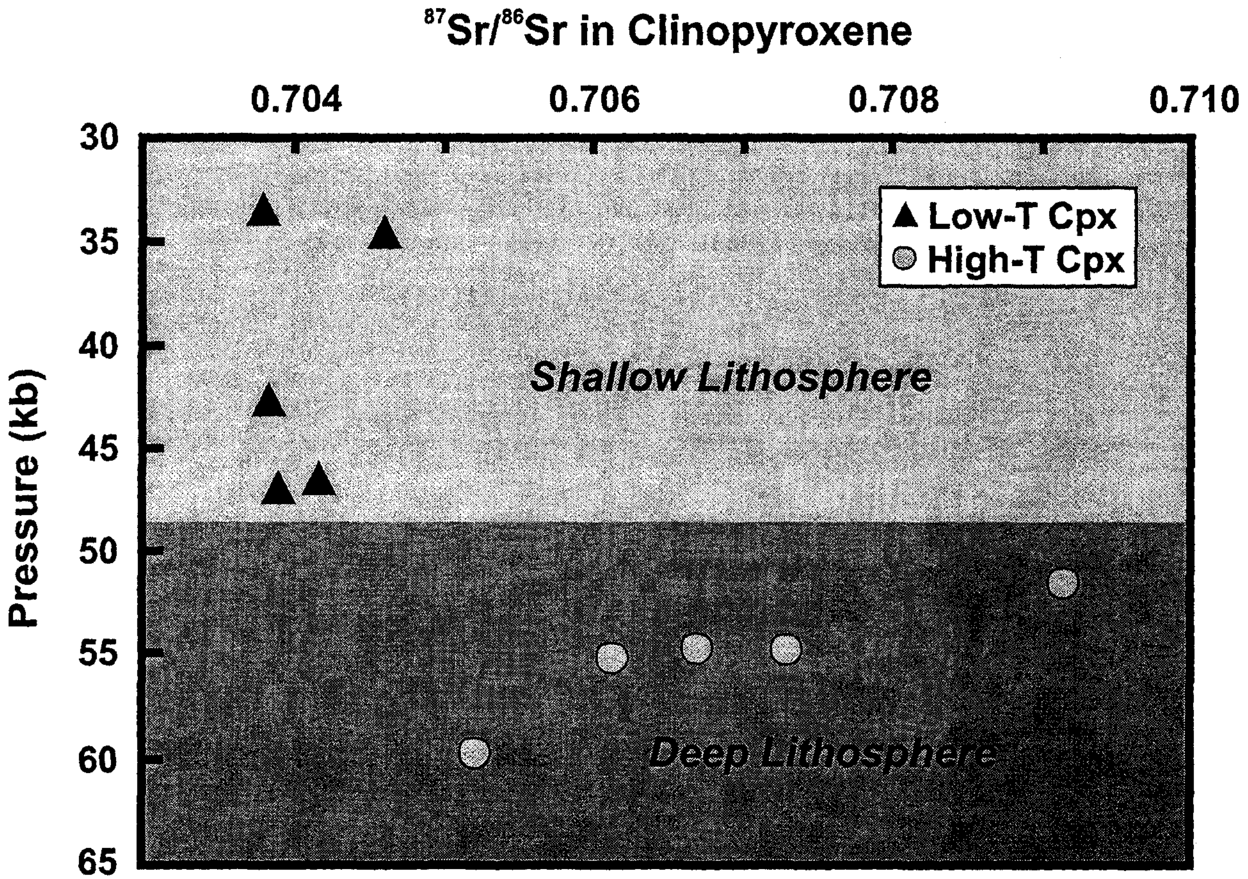
$^{87}Sr/^{86}Sr$ in Clinopyroxene
0.704
0.706
0.708
0.710
Pressure (kb)
30
35
40
45
50
55
60
65
▲ Low-T Cpx
● High-T Cpx
Shallow Lithosphere
Deep Lithosphere

Figure 4-8

CHAPTER 5

Probing Archean lithosphere using the Lu-Hf isotope systematics of peridotite xenoliths from Somerset Island kimberlites, Canada

Abstract

A knowledge of the Hf isotopic composition of the subcontinental lithosphere beneath Archean cratons is essential to constrain the Hf isotope budget of the Earth's mantle. Hf isotopic measurements were obtained by MC-ICP-MS for a suite of refractory peridotite xenoliths and constituent garnets from the Nikos kimberlite (100 Ma) on Somerset Island in order to constrain the isotopic composition and age of the lithosphere beneath the northern Canadian craton. The low-temperature Nikos peridotites (<1100°C), which represent the shallow Somerset lithosphere, are characterized by both higher $^{176}Lu/^{177}Hf$ ratios (0.03-0.05) and Hf isotopic values ($^{176}Hf/^{177}Hf_{(0.1Ga)}$=0.28296-0.28419) than the deep-seated high-temperature peridotites (>1100°C; 0.004-0.03, 0.28265-0.28333, respectively). These differences in Hf isotope signatures suggest that shallow and deep subcontinental lithosphere beneath Somerset Island represent isotopically distinct domains and do not share a common petrogenetic history.

The Lu-Hf isotope systematics of the shallow low-temperature peridotites define a positively sloped line that plot along a 2.8 Ga reference isochron. A number of these peridotites are characterized by highly radiogenic Hf isotopic compositions suggestive of long-term radiogenic ingrowth (billions of years). These findings are consistent with an interpretation that the shallow Somerset lithosphere (to depths of ~150 km) stabilized in the Archean. The majority of the high-temperature peridotites plot closer to the composition of the host kimberlite. Although the observed isotopic variation may be attributed in part to kimberlite-related Hf addition, it is possible that these deep-seated xenoliths represent younger mantle.

The superchondritic $^{176}Lu/^{177}Hf$ ratios observed for a number of the shallow low-temperature peridotites indicate strong fractionation of Lu and Hf, suggesting mantle root formation in the garnet stability field (depths >80 km). The Hf isotope compositions for the Somerset low-temperature peridotites indicate that part of the mantle root beneath the North American craton is characterized by a more radiogenic Hf isotope signature than that estimated for a typical "depleted" mantle.

Keywords: Archean lithosphere, Canadian craton, kimberlite, Lu-Hf system, peridotite, mantle xenoliths

1. Introduction

The mantle roots underlying the Archean cratons extend to depths of at least 200 km [1,2], and are depleted in basaltic constituents relative to fertile mantle [e.g.; 3-5]. The lower density and higher viscosity of these refractory peridotite roots relative to the surrounding asthenosphere contribute to their stability and long-term isolation from the convecting mantle [6,7]. The isotopic diversity recorded by both continental peridotites and basalts compared to oceanic volcanics, along with their unusually "enriched" Sr and Nd isotope signatures relative to bulk Earth ([8-10] and references therein) were the first indications of the antiquity of the subcratonic lithosphere [11,12]. These enriched isotope signatures are predominantly the result of repeated episodes of metasomatic activity, which have occurred since lithosphere stabilization (i.e. over billions of years; [13,14]). Consequently, determining the age of Archean cratonic mantle roots has proven difficult. Re-Os isotope systematics appear to be less susceptible to metasomatic alteration, and have provided valuable age constraints for the subcontinental lithosphere [12]. Re depletion ages range from the mid to late Archean (3.5 to 2.7 Ga) for the mantle roots beneath South Africa, Siberia and North America [15-18]. In contrast to the abundant Nd, Pb, Sr and Os isotope data, the Hf isotope composition of subcontinental lithospheric mantle has yet to be investigated. This region constitutes an important reservoir in the Hf budget of the Earth's mantle, and establishing its Hf isotopic composition is important in order to better understand its origin, geochemical evolution, and its role in the stabilization of the Archean cratons.

The Lu-Hf isotopic system is characterized by the long-lived radioactive parent isotope ^{176}Lu that decays to ^{176}Hf by beta emission with a half-life of 37 Ga [19,20], allowing the dating of ancient samples [21]. Lu (a heavy rare earth element, HREE) and Hf (a high field strength element, HFSE) are both refractory silicate-hosted (e.g.; [22]) elements, but exhibit significant differences in their geochemical behavior (e.g.; different mineral/melt partition coefficients; [23,24]) in the presence of mineral phases such as garnet and zircon. This can result in the strong fractionation of parent and daughter elements during magmatic and metamorphic processes, indicating the important potential of the Lu-Hf isotopic system in geochronology and as a geological tracer [e.g.; 25-28].

In this paper we report Hf isotopic compositions and ^{176}Lu/^{177}Hf ratios obtained using the MC-ICP-MS (multicollector inductively coupled plasma mass spectrometry) method for a suite of refractory peridotites and their constituent garnets from the Cretaceous (100 Ma) Nikos kimberlite on Somerset Island in the Canadian Arctic (Fig. 1; [29]). To our knowledge, these are the first Lu-Hf isotope data obtained for kimberlite-hosted mantle xenoliths to-date. The main objective of this study is to constrain the Hf isotopic composition of the lithospheric mantle beneath the northern Canadian craton in order to contribute to a better understanding of the Hf isotope composition and evolution of the Earth's mantle. The data permit an evaluation of the effectiveness of the Lu-Hf geochronometer in providing meaningful age constraints on the stabilization of the mantle root. The results also provide information on elemental fractionation during partial melting at the time of lithosphere formation, and on the Hf isotopic composition of the Archean mantle.

2. Samples

2.1. Kimberlite

The Nikos kimberlite is part of the Somerset Island kimberlite field [30] that was emplaced ~100 Ma ago (U-Pb ages on perovskite; [31,32]) into Archean crystalline basement (Nd model ages up to 3.0 Ga; [33]) at the northern margin of the Canadian craton (Fig. 1). The Nikos host kimberlite occurs as three closely associated individual pipes (each ~50 m diameter and 30-40 m apart) that contain abundant mantle xenoliths. Unlike many other Somerset Island kimberlites, the southern Nikos pipe (NK3) exhibits a non-brecciated, magmatic texture [29]. Four kimberlite samples were collected from this magmatic pipe for analysis, two of which (NK3-K1, NK3-K2) exhibit abundant mantle xenoliths relative to the remaining samples (NK3-K3, NK3-K4). The kimberlite contains olivine, phlogopite, garnet and spinel in a fine-grained matrix of calcite, serpentine, perovskite and apatite. Calcites occur as tabular euhedral crystals that are deflected around large olivine phenocrysts indicating their primary magmatic nature [29]. Two samples (NK3-K1, NK3-K2) are observed to contain garnet fragments in thin section, which probably represent xenocrysts. The Nikos kimberlite is characterized by very high whole-rock $CaCO_3$ contents (27-39 wt%), and a strong enrichment in incompatible trace elements such as LILE (large ion lithophile elements) and LREE (light rare earth elements) relative to chondrites and primitive mantle compositions [34,35].

2.2. Mantle xenoliths

The Nikos mantle xenoliths are large, well-preserved garnet peridotite nodules containing olivine, orthopyroxene, clinopyroxene, garnet and minor phlogopite (~1 wt% or less; [29]). One spinel peridotite (NK2-9) consists of olivine, orthopyroxene, clinopyroxene and chromian spinel. The majority of the xenoliths exhibit coarse textures, and only minor occurrences of porphyroclastic textures are observed (e.g.; NK1-7). The peridotites are characterized by refractory major element chemistry and have high magnesium-numbers (mg-number=Mg/(Mg+Fe)=0.90-0.93) suggesting that they are melt-depleted residues. Despite their depleted major element compositions, the Nikos peridotites are enriched in highly incompatible trace elements (e.g.; LILE, LREE), while having approximately chondritic HREE contents. Mass balance calculations indicate that constituent peridotite minerals control HREE budgets, but cannot account for the high LREE abundances observed in the whole-rocks, suggesting the presence of small amounts of a kimberlite-related LREE-rich interstitial component (i.e. ~1% kimberlite liquid) and/or accessory mineral (i.e. trace amounts of apatite; [35]).

The Nikos peridotites and constituent minerals have Sr and Pb isotopic signatures and incompatible trace element compositions (e.g.; La/Sm_N) that correlate with temperature and pressure (and thus depth) estimates of last equilibration, suggesting that the samples can be divided into low-temperature (800-1100°C; 25-50 kb; 80-150 km) and high-temperature peridotites (1100-1400°C; 50-60 kb; 160-190 km; [35,36]). The low-temperature peridotites and clinopyroxenes are characterized by less radiogenic $^{87}Sr/^{86}Sr_{(0.1Ga)}$ (0.7038-0.7066) and higher $^{206}Pb/^{204}Pb_{(0.1Ga)}$ (17.82-19.03) signatures at the time of kimberlite emplacement than those of the high-temperature peridotites ($^{87}Sr/^{86}Sr_{(0.1Ga)}$=0.7052-0.7095; $^{206}Pb/^{204}Pb_{(0.1Ga)}$=17.18-18.30). In addition, the low-temperature xenoliths show a stronger enrichment in incompatible trace elements (avg. La/Sm_N=6) relative to those in the high-temperature xenoliths (avg. La/Sm_N=3). These results indicate that the shallow low-temperature and the deep high-temperature lithosphere represent chemically distinct mantle reservoirs that do not share a common petrogenetic history [36]. In comparison, Nd isotopic compositions of low and high-temperature peridotites ($^{143}Nd/^{144}Nd_{(0.1Ga)}$=0.51255-0.51276; 0.51242-0.51262; respectively), which are slightly depleted compared to CHUR (chondrite uniform reservoir), overlap, and they are similar to those of the Nikos kimberlite ($^{143}Nd/^{144}Nd_{(0.1Ga)}$=0.51254-0.51259). More detailed discussions on mineralogy, and geochemical and isotopic composition of the peridotites and their host kimberlite can be found in [29,35,36].

2.3. Garnets

The Nikos garnets are chromian pyropes and their major element chemistry indicates that the crystals are compositionally homogeneous on a thin section scale [29]. The garnets in the low-temperature peridotites are characterized by low mg-numbers (0.81-0.84), low TiO_2 (0.08-0.09 wt%) and Zr (10-50 ppm) contents, and high FeO (7.2-7.9 wt%) and MnO (0.4-0.5 wt%) abundances compared to those in the high-temperature peridotites (mg-numbers=0.83-0.86; TiO_2=0.1-0.3 wt%; Zr=35-100 ppm; FeO=6.2-7.2 wt%; MnO=0.3-0.4 wt%; [35]). Sr isotopic compositions for garnets in the high-temperature peridotites ($^{87}Sr/^{86}Sr_{(0.1Ga)}$=0.7067-0.7095) extend to more radiogenic values than those for garnets in the low-temperature peridotites ($^{87}Sr/^{86}Sr_{(0.1Ga)}$=0.7061-0.7073) at the time of kimberlite emplacement [36].

3. Analytical methods

All exterior surfaces were first removed from the peridotites. The xenoliths were then crushed and rock chips were ground in an aluminum mill. Garnet separates were hand-picked under a binocular microscope and inclusion free grains were washed in an ultrasonic bath with acetone, ultra pure water and 2.5 N HCl, and then ground to small fragments in an agate mill. Crushed kimberlite whole rocks were carefully handpicked under a binocular microscope prior to grinding in an attempt to eliminate contamination from peridotite xenocrysts and country rock fragments.

For Lu-Hf isotope analysis, the sample powders (~0.8-1 g for whole rocks and ~0.2-0.25 g for garnets) were spiked with separate ^{180}Hf (98.3% enriched) and ^{176}Lu (70.9% enriched) tracers prior to dissolution. The ^{180}Hf contribution from the Hf isotope tracer represented ~3% of the total ^{180}Hf in the mixtures in order to minimize the correction of the measured ^{176}Hf/^{177}Hf ratio for spike addition [21]. Whole rock samples and garnet separates were dissolved in a mixture of HF-HNO_3-$HClO_4$ in Teflon bombs at 170°C for at least 10 days in order to ensure complete digestion and sample-spike homogenization. Prior to analysis, Hf was isolated from the REE in a fluoride precipitation step and then purified using a two-stage elution procedure (anion and cation exchange; [21]). Lu was separated as part of the REE fraction on a cation exchange column [21], then isolated from the LREE fraction using HDEHP columns. Total procedural blanks for Hf and Lu were less than 20 pg, a factor of at least 1000 for Hf and 800 for Lu lower than the total amount of Hf and Lu processed in the least abundant samples, thus rendering the blank correction negligible.

Hf and Lu isotope measurements were obtained using a Micromass IsoProbe multicollector inductively coupled plasma mass spectrometer (MC-ICP-MS) at GEOTOP, Université du Québec à Montréal. The Hf isotopic data were acquired in static, multicollection mode using 8 Faraday collectors with cup efficiencies set at unity. The mass configuration array included monitoring of isobaric interferences using isotopes

^{182}W (for ^{180}W), ^{175}Lu (for ^{176}Lu) and ^{173}Yb (for ^{176}Yb), identical to that outlined in [37]. ^{181}Ta was not monitored for potential interferences of ^{180}Ta on ^{180}Hf because of the extremely low abundances of Ta (<<0.1 ppm) in the peridotite samples [35], combined with the very low natural abundance (~0.012%) of ^{180}Ta. At the start of each analytical session, a 50 ppb solution of the JMC 475 Hf standard was aspirated into the ICP source using an ARIDUS® microconcentric nebulizer at an uptake rate of ~50 μL/minute and analyzed for approximately 10 minutes. This corresponds to ~25 ng of total Hf consumed per analysis, roughly the same magnitude as that processed for the samples used in this study. The uptake rate of the ARIDUS® instrument was kept constant and verified on a regular basis; sweep gas settings were optimized to yield maximum ion signal intensity and minimize oxide levels. The level of Hf-oxide was typically at ≤0.1% of the ion signal for the metal. The intensity of the ion signal was typically 2.0×10^{-11} A of ^{180}Hf corresponding to an absolute sensitivity of ~120 volts/ppm. Data acquisition consisted of a 50 seconds "on-peak-zero" baseline measurement (i.e. gas and 2% HNO_3 blank) with the same 2% HNO_3 solution used to dilute the samples. Subsequent to sample introduction, two half-mass unit baseline measurements were obtained within the mass range 172.5 to 182.5, bracketing the mass range used for data acquisition. The JMC 475 standard and samples were analyzed for one block of 50 scans with a 10 seconds integration time per cycle. The measured Hf isotopic ratios were normalized to ^{179}Hf/^{177}Hf=0.7325 and corrected for mass bias using the exponential law [38]. Removal of "spike addition" was achieved using an iterative calculation [21]. Repeated measurements (n=22) of the JMC 475 standard (in 2% HNO_3) during the course of this study (April 2000 to May 2001) yielded the following results: ^{176}Hf/^{177}Hf=0.282158±23,

$^{178}Hf/^{177}Hf$=1.46727±13 and $^{180}Hf/^{177}Hf$=1.88669±21 (2σ standard deviation errors). Solutions made from high purity Lu and Yb metals from the Ames laboratory (20 and 10 ppb, respectively) and W (100 ppb) were analyzed prior to the measurement of samples in order to determine their mass bias and thus accurately correct for isobaric interferences, if present. However, intensities of ^{175}Lu, ^{173}Yb and ^{182}W were at or below the limit of detection for the majority of the samples. For spiked ^{176}Lu isotope dilution analyses, Yb is not separated from Lu in the chemical procedure. Thus careful evaluation of their respective mass biases are warranted in order to correct for the isobaric interference of ^{176}Yb on ^{176}Lu. Prior to sample analysis, the mass bias for Lu and Yb were determined by measuring the $^{176}Lu/^{175}Lu$ and $^{176}Yb/^{173}Yb$ for solutions of Ames Lu (20 ppb) and Yb (10 ppb) metals, and then compared to the recommended values of 0.02656 and 0.78761 [21], respectively. Evaluation of this correction was determined using a series (n=8) of Yb-doped and ^{176}Lu spiked gravimetrically prepared Ames Lu solutions. The quantity of Lu used in these solutions matched those for the peridotites; however, their Yb/Lu values were double those of the samples so as to purposely exaggerate the correction. The results indicate that the calculated Lu concentrations reproduce to better than 0.2% (2σ level). Moreover, the reproducibility for calculation of the isotopic compositions and concentrations of Hf were evaluated by a triplicate analysis (on three separate dissolutions of the same powder) of a fine-grained calc-alkaline basalt, which yielded $^{176}Hf/^{177}Hf$ values of 0.282633±11, 0.282638±8, 0.282636±8 and Hf concentrations of 3.47, 3.46, 3.48 ppm, respectively. The latter are identical to a Hf concentration of 3.42 ±0.17 ppm obtained by conventional ICP-MS analysis [39], despite the fact that the abundance of Ta

(0.4 ppm; [39]) in the basalt is more than four times the concentration of Ta measured in the Nikos peridotites.

4. Results

4.1. Kimberlite

The two kimberlite samples containing the least amounts of peridotite xenoliths (NK3-K3, NK3-K4) are characterized by low ^{176}Lu/^{177}Hf ratios (0.003) and have chondritic to slightly superchondritic [40] initial ^{176}Hf/^{177}Hf$_{(0.1Ga)}$ (0.282711 and 0.282852), corresponding to initial $\varepsilon_{Hf(0.1Ga)}$ values of 0 and +5.0 (Table 1; Fig. 2a). Two kimberlite samples (NK3-K1, NK3-K2) that contained abundant mantle xenoliths also have low ^{176}Lu/^{177}Hf ratios (0.004), but higher initial ^{176}Hf/^{177}Hf$_{(0.1Ga)}$ (0.283191 and 0.283307; initial $\varepsilon_{Hf(0.1Ga)}$=+17 and +21.1). Kimberlites from South Africa have been divided into two groups ("Group I" and "Group II") based on their distinct mineralogy and Sr-Nd-Pb isotopic signatures (e.g.; [41,42]). Recent studies have shown that both South African "Group I" and "Group II" kimberlites are characterized by low ^{176}Lu/^{177}Hf ratios similar to those of the Nikos kimberlite (Fig. 2a; [43]). The initial $\varepsilon_{Hf(0.1Ga)}$ values for two Nikos kimberlite samples plot within the field of initial $\varepsilon_{Hf(T)}$ values for South African "Group I" kimberlites, while those samples that containd abundant peridotite plot towards higher values. South African "Group II" kimberlites, in comparison, are characterized by negative initial $\varepsilon_{Hf(T)}$ values (Fig. 2a).

4.2. Mantle xenoliths

The low-temperature peridotites exhibit a significant range in ^{176}Lu/^{177}Hf ratios (0.027-0.048) and have radiogenic Hf isotopic compositions (^{176}Hf/^{177}Hf$_{(0.1Ga)}$=0.282963-0.284190; $\varepsilon_{Hf(0.1Ga)}$=+9.0 to +52.3) at the time of kimberlite emplacement (Table 1; Fig.

2b). In comparison, the high-temperature peridotites are characterized by lower $^{176}Lu/^{177}Hf$ ratios (0.004-0.016) and, in general, less radiogenic Hf isotopic compositions ($^{176}Hf/^{177}Hf_{(0.1Ga)}$=0.282654-0.283212; $\varepsilon_{Hf(0.1Ga)}$=-2.0 to +17.8; Fig. 2b). The Hf isotopic compositions of all Nikos peridotites (except one sample, NK3-25) are depleted relative a chondritic reservoir [40]. One high-temperature xenolith (NK1-7), which in contrast to most other samples is characterized by a porphyroclastic texture, has a $^{176}Lu/^{177}Hf$ and $^{176}Hf/^{177}Hf_{(0.1Ga)}$ ratio (0.035 and 0.283312, respectively; $\varepsilon_{Hf(0.1Ga)}$=+21.3; avg. of duplicate analyses; Fig. 2b) similar to those of the low-temperature peridotites.

In a $^{176}Lu/^{177}Hf$ versus $^{176}Hf/^{177}Hf$ diagram, the data for the low-temperature xenoliths show a positively sloped correlation. The regression line for the Lu-Hf data indicates that this array corresponds to an errorchron age of 2.8±0.8 Ga (n=6; MSWD=24) with an initial $^{176}Hf/^{177}Hf$ ratio of 0.28164±57 (ε_{Hf}=+23; Fig. 3). One low-temperature sample (NK1-2) is not included in the data regression as the presence of carbonate-rich veins suggest kimberlite contamination. Since the low-temperature peridotites were sampled over a large depth interval (80-150 km) and the errorchron age is associated with a large error, a 2.8 Ga reference isochron with a corresponding initial Hf isotopic ratio is plotted for comparison rather than the errorchron (Fig. 3). The majority of the high-temperature peridotites exhibit lower $^{176}Lu/^{177}Hf$ ratios and trend towards the composition of the Nikos kimberlite (Table 1; Fig. 2b). No data plot to the right of the reference isochron.

Duplicate analyses were obtained on separate dissolutions of the rock powders (not on sample splits after initial dissolution). The $^{176}Lu/^{177}Hf$ ratios vary by 5-8% and Hf isotope ratios by 4-8 ε_{Hf} units for the low-temperature peridotites (NK1-4, NK1-14, NK1-

2; Table 1). Although these variations are relatively large, in each case the parent-daughter ratio correlates with isotopic composition. The variations in the Lu/Hf ratios and Hf isotopic compositions are thus attributed to sample heterogeneity of the whole rock powders, resulting from the coarse-grained nature of the peridotites, in particular, the presence of large crystals of garnet (up to 5mm), and their (Archean) age. Duplicate analyses of Hf isotopic composition for two other low-temperature peridotites (NK1-23, NK1-3) are within error. For two high-temperature peridotites (NK1-19, NK1-7) parent-daughter ratios do not correlate with isotopic ratios, which is probably the result of kimberlite contamination (see later discussion). For samples with duplicate ^{176}Lu/^{177}Hf and Hf isotope ratios, these are plotted as average values in the figures.

4.3. Garnets

The garnets of the low-temperature xenoliths exhibit a large range in ^{176}Lu/^{177}Hf ratios (0.093-0.243) and their ^{176}Hf/^{177}Hf$_{(0.1Ga)}$ compositions (0.283096-0.286947; $\varepsilon_{Hf(0.1Ga)}$=+13.7 to +150) extend to extremely radiogenic values at the time of kimberlite emplacement (Table 2). In comparison, the garnets from the high-temperature peridotites have lower ^{176}Lu/^{177}Hf ratios (0.015-0.057) and less radiogenic ^{176}Hf/^{177}Hf$_{(0.1Ga)}$ compositions (0.282749-0.283407; $\varepsilon_{Hf(0.1Ga)}$=+1.4 to +24.7; Table 2). The garnets from the low-temperature peridotites are characterized by slightly higher Lu (avg. 0.30 ppm), but significantly lower Hf abundances (avg. 0.31 ppm) than garnets from the high-temperature peridotites (avg. Lu=0.25 ppm; Hf=0.95 ppm; Table 2). Tie lines for individual garnet-whole-rock pairs in the low-temperature peridotites are all positively sloped and correspond to internal isochrons "ages" ranging from 900 to 250 Ma (Table 2; Fig. 4). In contrast, the garnet-whole rock tie lines for most high-temperature peridotites (except porphyroclastic xenolith NK1-7; 330 Ma) define negative (or flat) trends (Fig. 4). Duplicate analyses of garnet separate NK1-7 yield a difference of ~0.9% for the ^{176}Lu/^{177}Hf value and identical ^{176}Hf/^{177}Hf compositions (Table 2), supporting our interpretation that sample heterogeneity is responsible for the variation exhibited by the replicate analyses of the whole rock powders.

5. Discussion

5.1. Kimberlite mantle source

Two Nikos kimberlite samples (NK3-K3, NK3-K4) are characterized by chondritic or slightly superchondritic initial Hf isotope compositions ($\varepsilon_{Hf(0.1Ga)}$=0 and +5.0), and these plot within the field of Lu-Hf isotope data for South African kimberlites (Fig. 2a; [43]). In comparison, initial $\varepsilon_{Hf(0.1Ga)}$ values (+17 and +21.1; NK3-K1, NK3-K2) for two kimberlite samples that contain abundant mantle xenoliths are much higher. The significant variation in Hf isotope ratios could be inherited from a (non-homogenous) kimberlite mantle source, or indicate the presence of xenocrysts (e.g.; garnet) in the kimberlite derived by fragmentation of peridotite xenoliths. It appears likely that xenocrystic garnet (as observed in thin sections) is responsible for the high $\varepsilon_{Hf(0.1Ga)}$ values of two kimberlite samples (NK3-K1, NK3-K2), since it has high ^{176}Lu/^{177}Hf and thus high time-integrated Hf isotopic ratios. This interpretation is supported by $\varepsilon_{Nd(0.1Ga)}$ values (+1.1 and +0.6, respectively; [36]) that correlate negatively with $\varepsilon_{Hf(0.1Ga)}$ values in these two samples, the opposite of what is observed for most terrestrial rocks [44].

The kimberlite samples that are characterized by low $\varepsilon_{Hf(0.1Ga)}$ values (NK3-K3, NK3-K4) are interpreted to represent the Hf isotopic composition of the Nikos kimberlite at the time of emplacement, and these are plotted in the figures. Since kimberlites represent low degree partial melts (1% or less; [45]), the small difference in their $\varepsilon_{Hf(0.1Ga)}$ values (0 and +5.0) may be attributed to the inhomogeneous composition of the mantle source. In a Hf-Nd diagram, the two Nikos kimberlite samples exhibit a positive correlation of these isotope ratios with chondritic to slightly superchondritic compositions, and plot within the terrestrial Hf-Nd array (Fig. 5).

5.2. Shallow versus deep lithosphere

The refractory major element compositions of the Nikos peridotites that sample the Somerset lithosphere indicate that these xenoliths are melt-depleted residues [29]. The Lu abundances of both the low and high-temperature peridotites show a good positive correlation with their bulk rock Al_2O_3 contents, which constitute a measure for the degree of major element depletion in residual peridotites (Fig. 6). These findings suggest that the Lu levels observed in these xenoliths were controlled by variable degrees of partial melting during lithosphere formation.

The low-temperature Nikos peridotites were sampled over a very large depth interval of about 70 km by their host kimberlite. These xenoliths are characterized by Lu-Hf isotopic compositions that plot close to a line corresponding to a reference isochron age of 2.8 Ga (Fig. 3). This reference isochron age is almost identical to Re depletion ages (2.7 Ga) that were recently reported for other Somerset Island peridotites [18]. A number of the low-temperature peridotites exhibit very radiogenic Hf isotopic compositions at the time of kimberlite magmatism ($^{176}Hf/^{177}Hf_{(0.1Ga)}$=0.2835-0.2841, $\varepsilon_{Hf(0.1Ga)}$=+30 to +50; Table 1; Figs. 2b, 5) compared to estimates for a typical "depleted" mantle (~0.2832, +18, respectively; [40, 46]. Long-term (billions of years) radiogenic ingrowth is required to produce the highly depleted Hf isotopic signatures. These results provide evidence for an ancient (Archean) depletion event that resulted in the stabilization of the mantle root beneath the northern Canadian craton to depths of about 150 km. The initial Hf isotopic value (^{176}Hf/^{177}Hf=0.28164±57) associated with this reference isochron corresponds to an ε_{Hf} value of +23 that within error could be as low as +3. These results suggest that the low-temperature Nikos peridotites were derived from a mantle having melt-depleted characteristics at the time of lithosphere stabilization rather than from a primitive mantle reservoir [40, 46]. A number of the low-temperature Nikos xenoliths are characterized by slightly subchondritic ^{176}Lu/^{177}Hf ratios (<0.033), while having superchondritic Hf isotopic compositions (^{176}Hf/^{177}Hf>0.282772; [40]), suggesting recent perturbation of their ^{176}Lu/^{177}Hf ratios. Since Lu levels correlate with other indices of melt depletion and thus appear to have been controlled by partial melting (Fig. 6), these xenoliths may have experienced minor Hf addition rather than Lu loss. The Nikos kimberlite is characterized by low ^{176}Lu/^{177}Hf ratios and high Hf abundances, and it appears likely that these xenoliths may have been affected by interaction with the host magma during sample transport. The addition of very small amounts of a kimberlite component (~0.5% bulk kimberlite or significantly less of a kimberlite-related Hf-bearing accessory mineral) as indicated by mass balance calculations, would produce slightly subchondritic ^{176}Lu/^{177}Hf ratios. In contrast to the low-temperature xenoliths, the majority of the high-temperature peridotites plot closer to the composition of the kimberlite (Fig. 2b, 3). This feature could be interpreted as the result of more extensive contamination with host kimberlite since these xenoliths resided closer to the area of kimberlite formation, and/or that these peridotites are younger and represent mantle of distinct origin.

The highly variable Hf isotopic compositions of the Nikos peridotites are predominantly superchondritic at the time of kimberlite magmatism (Fig. 5). A number of the peridotites extend to significantly higher Hf values compared to "depleted" mantle and plot above the terrestrial Hf-Nd array [44]. In comparison, the Nd isotopic compositions of the peridotites ($\varepsilon_{Nd(0.1Ga)}$=+1 to +4; [36]), which are distinctly lower than estimates for "depleted" mantle ($\varepsilon_{Nd(0.1Ga)}$ ~+10; Fig. 5; [8]), show little variation, and overlap those of the Nikos kimberlite ($\varepsilon_{Nd(0.1Ga)}$=+1 to +2; Fig. 5). The Nd isotope results have been interpreted to indicate that the xenoliths were contaminated with small amounts of host magma during sample transport [36]. In contrast to tightly constrained Nd isotopic signatures, the low-temperature peridotites are characterized by significantly less radiogenic Sr (Fig. 7) and higher Pb (not shown) isotopic compositions ($^{87}Sr/^{86}Sr_{(0.1Ga)}$=0.7051-0.7066; $^{206}Pb/^{204}Pb_{(0.1Ga)}$=17.82-19.03) than the high-temperature peridotites ($^{87}Sr/^{86}Sr_{(0.1Ga)}$=0.7064-0.7080; $^{206}Pb/^{204}Pb_{(0.1Ga)}$=17.18-18.30). In addition, the Sr isotope ratios of the Nikos peridotites, with the exception of one sample (NK1-23), differ from those of the host kimberlite (Fig. 7; [36]). The distinct Sr and Pb isotope compositions of low and high-temperature peridotites restrict the amount of interstitial kimberlite component to less than 1 wt% [36] as kimberlite contribution in excess of this amount would eradicate the observed isotopic differences. The Hf isotopic compositions of the Nikos peridotites are highly variable and the majority extend to significantly more radiogenic compositions than the host kimberlite (Figs. 2b, 5). As the average Hf abundance ratio (kimberlite/peridotite) of 20:1 is similar to that for Sr, but 3 times lower than for Nd (60:1), Hf is significantly less susceptible to kimberlite contamination than Nd. Since kimberlite addition was restricted to very small amounts, it is likely that the Hf isotopic differences observed for the Nikos peridotites existed prior to the kimberlite event (Figs. 2b, 5).

While all the Nikos xenoliths are refractory residues that were generated by extensive melt extraction, the low-temperature peridotites exhibit $\varepsilon_{Hf(0.1Ga)}$ values (+9 to +50) that are significantly higher and more variable than those of the high-temperature peridotites (-2 to +20). The distinct Hf isotopic compositions for low and high-temperature peridotites are in agreement with the previously reported differences in Sr and Pb isotope compositions [36] indicating that shallow and deep Somerset lithosphere do not share a common petrogenetic history. The depth stratification could have resulted from infiltration of the lower lithosphere with metasomatic melts or fluids. This model cannot be reconciled, however, with the significantly less enriched incompatible trace element signatures of the deep-seated peridotites (avg. La/Sm_N=3) relative to those of the shallow xenoliths (avg. La/Sm_N=6; [35]). Alternatively, the deep lithosphere could be younger and was added to the Archean subcratonic mantle by downward growth of the shallow lithosphere, an interpretation consistent with the isotopic and trace element record [35,36]. Mantle stratification and post-Archean lithosphere growth have previously been proposed for other cratonic areas such as the Kaapvaal craton beneath South Africa (e.g.; [10,16]) and appear to be a common feature for the lithospheric mantle root beneath the continents.

5.3. Garnet Hf isotope systematics

The garnets from the low-temperature peridotites are characterized by low Hf abundances (avg. 0.31 ppm) and their highly variable $^{176}Hf/^{177}Hf_{(0.1Ga)}$ compositions (0.28310-0.28695) extend to significantly more radiogenic values than those for garnets from the high-temperature peridotites (avg. Hf=0.95 ppm; $^{176}Hf/^{177}Hf_{(0.1Ga)}$=0.28275-0.28341; Table 2; Fig. 4). These signatures correlate with chemical characteristics such as TiO_2 contents that are lower for garnets from the shallow peridotites (0.08-0.09 wt%) relative to those for garnets from the deep-seated peridotites (0.1-0.3 wt%; [35]). The results indicate significant isotopic and chemical differences for garnets from low and high-temperature Nikos peridotites, and are consistent with the finding based on the whole rock Hf, Sr and Pb isotopic compositions that shallow and deep Somerset lithosphere represent mantle of distinct origin.

Internal Lu-Hf isochrons using garnet-whole rock pairs (Fig. 4) for the low-temperature peridotites yield "ages" ranging from 900 to 500 Ma, and 300 to 250 Ma for two samples that could have experienced minor kimberlite addition as suggested by the presence of carbonate-rich veins (NK1-2) and a slightly subchondritic $^{176}Lu/^{177}Hf$ ratio (NK1-3). The "dates" defined by the Lu-Hf whole rock-garnet isochrons decrease with increasing temperature (and thus depth), and the oldest "age" is obtained for the shallowest garnet-whole rock pair (870°C, 110 km; Fig. 8). No garnet-whole rock pair at any depth, however, defines an internal isochron corresponding to an Archean age. These findings indicate that lithospheric temperatures (870°C and higher) exceeded the closure temperatures for Hf (and Lu) diffusion in the garnet-whole rock system. The depth correlation of the Lu-Hf "ages" suggests that the extent of Hf isotope re-equilibration in the garnet-whole rock system varied as a function of temperature. In comparison, internal Sm-Nd isochrons for these same garnet-whole rock pairs yield "ages" of 200 to 90 Ma, and the youngest "date" essentially coincides with the age of kimberlite formation [36]. The Lu-Hf "date" for individual garnet-whole rock pairs is always older than that obtained using Sm-Nd systematics. Although Nd isotope systematics appear to be more susceptible to kimberlite contamination, these findings are also consistent with recent results based on high-grade metamorphic rocks suggesting that in garnet-whole rock systems the closure temperature of Lu-Hf is greater than or equal to that of Sm-Nd [28].

Tie lines joining garnet and corresponding whole rock for the low-temperature peridotites have positive slopes (Fig. 4), a feature consistent with Hf isotope re-equilibration in the garnet-whole rock system. In contrast, the tie lines joining garnet-whole rock pairs for the high-temperature samples (except porphyroclastic peridotite NK1-7) have negative (or flat) slopes, which could reflect recent Hf infiltration (Fig. 4). The fact that the whole rock Hf isotope compositions of the high-temperature xenoliths plot close to that of the Nikos kimberlite is consistent with an interpretation that these peridotites experienced Hf addition during sample transport.

5.4. Evolution of Archean lithosphere

The Hf isotopic composition of lithospheric mantle underlying Archean cratons has yet to be clearly established because of former difficulties with the analytical method prior to the development of MC-ICP-MS. Recent investigations have focused on Hf and Nd isotopic determinations for 3.8 Ga old supracrustal rocks from the Isua province of Greenland in order to characterize the isotopic composition of the early terrestrial mantle [46,47]. These samples exhibit a significant range in both initial Hf and Nd isotope ratios, which are dominantly more radiogenic than those of chondrites, suggestive of derivation from "depleted" mantle. The Lu/Hf and Sm/Nd ratios observed in these early Archean rocks, however, are distinct from those inferred for a "depleted" mantle reservoir [46-48], which as for most terrestrial rocks has been characterized by the covariant evolution of Hf and Nd isotopes [25,49,50]. This relationship has been interpreted to reflect the similar fractionation of Lu and Hf, and Sm and Nd during melt extraction from garnet-free residual peridotite assemblages [25,49,51]. In contrast, melting of mantle peridotite in the presence of garnet (i.e. depths >80 km) results in a significant fractionation of Lu/Hf and Sm/Nd ratios as garnet preferentially incorporates Lu relative to Hf, to a greater extent than Sm relative to Nd [24,46]. The data obtained from the 3.8 Ga old Isua samples suggest that elemental fractionation during partial melting in the early Archean mantle was much stronger than in the post-Archean "depleted" mantle reservoir and most likely occurred in the presence of garnet [46-48].

A number of the low-temperature Nikos peridotites, which represent the shallow lithosphere beneath the Canadian craton, are characterized by Hf isotopic signatures that are significantly higher compared to that estimated for "depleted" mantle [40,46]. These xenoliths exhibit superchondritic $^{176}Lu/^{177}Hf$ ratios (Figs. 2b, 3), indicative of strong fractionation of the Lu/Hf ratios during generation of the melt-depleted peridotites. The results can be interpreted as evidence that garnet was present as a residual phase during partial melting and that the Somerset lithosphere stabilized at a minimum depth of 80 km. Over billions of years, these fractionated $^{176}Lu/^{177}Hf$ ratios resulted in the very radiogenic $^{176}Hf/^{177}Hf$ compositions recorded by the low-temperature Nikos peridotites at the time of kimberlite emplacement.

6. Conclusions

The Hf isotopic compositions of the Nikos peridotites indicate significant differences exist between the low (shallow; <1100°C) and high-temperature (deep-seated; >1100°C) xenoliths. Although contamination with a kimberlite-related component may have been superimposed on the Hf isotope compositions of a number of xenoliths, it is likely that shallow and deep Somerset lithosphere do not share a common petrogenetic history. The Lu-Hf systematics of the low-temperature Nikos peridotites suggest that the Somerset lithosphere stabilized in the Archean to depths of at least 150 km.

A number of the low-temperature peridotites exhibit superchondritic $^{176}Lu/^{177}Hf$ ratios that suggest mantle root formation in the presence of residual garnet (depths >80 km). These fractionated $^{176}Lu/^{177}Hf$ ratios resulted in the radiogenic $^{176}Hf/^{177}Hf$ signatures observed at the time of kimberlite magmatism. These first Hf isotopic ratios for the subcontinental mantle indicate that at least part of the lithosphere beneath the North American craton is characterized by more radiogenic Hf isotope signatures than estimates for "depleted" mantle.

Acknowledgments

We thank Fabien Rasselet for assistance in the field and for handpicking separates of magmatic kimberlite for isotope analysis. S. Schmidberger and A. Simonetti are indebted to J. Blichert-Toft for introducing them to the secrets of Lu-Hf chemistry. The MC-ICP-MS facility is supported by a MFA grant from NSERC and the research was funded by a NSERC operating grant to D. Francis. S. Schmidberger is grateful for financial support in the form of a NSERC doctoral scholarship. The manuscript was greatly improved by comments from the reviewers, J. Blichert-Toft, J. Vervoort, and G. Nowell, and from discussions with the editor, Alex Halliday.

References

[1] T.H. Jordan, Structure and formation of the continental tectosphere, J. Petrol., Special Lithosphere Issue (1988) 11-37.

[2] S.P. Grand, Mantle shear structure beneath the Americas and surrounding oceans, J. Geophys. Res. 99 (1994) 11591-11621.

[3] F.R. Boyd, S.A. Mertzman, Composition and structure of the Kaapvaal lithosphere, southern Africa, in: B.O. Mysen (Ed.), Magmatic processes: physiochemical principles, Geological Society, Special Publications 1 (1987) pp. 13-24.

[4] P.H. Nixon, Kimberlitic xenoliths and their cratonic setting, in: P.H. Nixon (Ed.), Mantle xenoliths, John Wiley, Chichester, 1987, pp. 215-239.

[5] W.F. McDonough, Constraints on the composition of the continental lithospheric mantle, Earth Planet. Sci. Lett. 101 (1990) 1-18.

[6] T.H. Jordan, Mineralogies, densities and seismic velocities of garnet lherzolites and their geophysical implications, in: F.R. Boyd, H.O.A. Meyer (Eds.), The mantle sample: Inclusions in kimberlites and other volcanics, American Geophysical Union, Washington, 1979, pp. 1-13.

[7] H.N. Pollack, Cratonization and thermal evolution of the mantle, Earth Planet. Sci. Lett. 80 (1986) 175-182.

[8] A. Zindler, S. Hart, Chemical geodynamics, Ann. Rev. Earth Planet. Sci. 14 (1986) 493-571.

[9] A.J. Erlank, F.G. Waters, C.J. Hawkesworth, S.E. Haggerty, H.L. Allsopp, R.S. Rickard, M.A. Menzies, Evidence for mantle metasomatism in peridotite nodules from the Kimberley pipes, South Africa, in: M.A. Menzies, C.J. Hawkesworth (Eds.), Mantle metasomatism, Academic Press, London, 1987, pp. 221-311.

[10] M.A. Menzies, Archean, Proterozoic, and Phanerozoic lithospheres, in: M.A. Menzies (Ed.), Continental mantle, Oxford Univ. Press, Oxford, 1990, pp. 67-86.

[11] C. Brooks, D.E. James, S.R. Hart, Ancient lithosphere: its role in young continental volcanism, Science 139 (1976) 1086-1094.

[12] D.G. Pearson, The age of continental roots, Lithos 48 (1999) 171-194.

[13] G.M. Yaxley, A.J. Crawford, D.H. Green, Evidence for carbonatite metasomatism in spinel peridotite xenoliths from western Victoria, Earth Planet. Sci. Lett. 107 (1991) 305-317.

[14] R.L. Rudnick, W.F. McDonough, B.W. Chappell, Carbonatite metasomatism in the northern Tanzanian mantle, Earth Planet. Sci. Lett. 114 (1993) 463-475.

[15] R.W. Carlson, A.J. Irving, Depletion and enrichment history of subcontinental lithospheric mantle: Os, Sr, Nd and Pb evidence for xenoliths from the Wyoming Craton, Earth Planet. Sci. Lett. 126 (1994) 457-472.

[16] D.G. Pearson, R.W. Carlson, S.B. Shirey, F.R. Boyd, P.H. Nixon, Stabilisation of Archean lithospheric mantle: a Re-Os isotope study of peridotite xenoliths from the Kaapvaal craton, Earth Planet. Sci. Lett. 134 (1995a) 341-357.

[17] D.G. Pearson, S.B. Shirey, R.W. Carlson, F.R. Boyd, N.P. Pokhilenko, N. Shimizu, Re-Os, Sm-Nd, and Rb-Sr isotope evidence for thick Archean lithospheric mantle beneath the Siberian craton modified by multistage metasomatism, Geochim. Cosmochim. Acta 59 (1995b) 959-977.

[18] G.J. Irvine, M.G. Kopylova, R.W. Carlson, D.G. Pearson, S.B. Shirey, B.A. Kjarsgaard, Age of the lithospheric mantle beneath and around the Slave craton: a Rhenium-Osmium isotopic study of peridotite xenoliths from the Jericho and Somerset Island kimberlites, Ninth Annual V. M. Goldschmidt Conference, LPI Contribution No. 971 (1999) 134-135.

[19] J. Dalmasso, G. Barci-Funel, G.J. Ardisson, Reinvestigation of the decay of the long-lived odd-odd ^{176}Lu nucleus, Appl. Radiat. Isot. 43 (1992) 69-76.

[20] Y. Nir-El, N. Lavi, Measurement of half-life of ^{176}Lu, Appl. Radiat. Isot. 49 (1998) 1653-1655.

[21] J. Blichert-Toft, C. Chauvel, F. Albarède, Separation of Hf and Lu for high-precision isotope analysis of rock samples by magnetic sector-multiple collector ICP-MS, Contrib. Mineral. Petrol. 127 (1997) 248-260.

[22] R.M. Bedini, J.-L. Bodinier, Distribution of incompatible trace elements between the constituents of spinel peridotite xenoliths: ICP-MS data from the East African Rift, Geochim. Cosmochim. Acta 63 (1999) 3883-3900.

[23] S.R. Hart, T. Dunn, Experimental clinopyroxene-melt partitioning of 24 trace elements, Contrib. Mineral. Petrol. 113 (1993) 1-8.

[24] H. Fujimaki, M. Tatsumoto, K.I. Aoki, Partition coefficients of Hf, Zr, and REE between phenocrysts and groundmasses, J. Geophys. Res. 89 (1984) B662-B672.

[25] P.J. Patchett, M. Tatsumoto, Hafnium isotope variations in oceanic basalts, Geophys. Res. Lett. 7 (1980) 1077-1080.

[26] P.J. Patchett, M. Tatsumoto, Lu-Hf total-rock isochron for the eucrite meteorites, Nature 288 (1980) 571-574.

[27] S. Duchêne, J. Blichert-Toft, B. Luais, P. Télouk, J.-M. Lardeaux, F. Albarède, The Lu-Hf dating of garnets and the ages of the Alpine high-pressure metamorphism, Nature 387 (1997) 586-589.

[28] E.E. Scherer, K.L. Cameron, J. Blichert-Toft, Lu-Hf garnet geochronology: Closure temperature relative to the Sm-Nd system and the effects of trace mineral inclusions, Geochim. Cosmochim. Acta 64 (2000) 3413-3432.

[29] S.S. Schmidberger, D. Francis, Nature of the mantle roots beneath the North American craton: mantle xenolith evidence from Somerset Island kimberlites, Lithos 48 (1999) 195-216.

[30] J. Pell, New kimberlite discoveries on Somerset Island, in: Exploration Overview 1993, Yellowknife: NWT Geology Division, Department of Indian and Northern Affairs (1993) pp. 47.

[31] L.H. Heaman, The nature of the subcontinental mantle from Sr-Nd-Pb isotopic studies on kimberlite perovskite, Earth Planet. Sci. Lett. 92 (1989) 323-334.

[32] C.B. Smith, H.L. Allsopp, O.G.Garvie, J.D.Kramers, P.F.S. Jackson, C.R. Clement, Note on the U-Pb perovskite method for dating kimberlites: examples from the Wesselton and DeBeers mines, South Africa, and Somerset Island, Canada, Chem. Geol. (Isot. Geos.) 79 (1989) 137-145.

[33] T. Frisch, P.A. Hunt, Reconnaissance U-Pb geochronology of the crystalline core of the Boothia Uplift, District of Franklin, Northwest Territories, in: Radiogenic age and isotope studies: Report 7, Geological Survey of Canada, Paper 93-2 (1993) pp. 3-22.

[34] W.F. McDonough, S.S. Sun, The composition of the earth, Chem. Geol. 120 (1995) 223-253.

[35] S.S. Schmidberger, D. Francis, Constraints on the trace element composition of the Archean mantle root beneath Somerset Island, Arctic Canada, J. Petrol. 42 (2001) 1095-1117.

[36] S.S. Schmidberger, A. Simonetti, D. Francis, Sr-Nd-Pb isotope systematics of mantle xenoliths from Somerset Island kimberlites: Evidence for lithosphere stratification beneath Arctic Canada, Geochim. Cosmochim. Acta 65 (2001).

[37] N. Machado, A. Simonetti, U-Pb dating and the Hf isotope composition of zircon by laser-ablation-MC-ICP-MS, in: Laser-ablation-ICPMS in the Earth Sciences, Mineralogical Association of Canada, Short Course 29 (2001) pp. 121-146.

[38] W.A. Russell, D.A. Papanastassiou, T.A. Tombrello, Ca isotope fractionation on the Earth and other solar system materials, Geochim. Cosmochim. Acta 42 (1978) 1075-1090.

[39] S.S. Schmidberger, E. Hegner, Geochemistry and isotope systematics of calc-alkaline volcanic rocks from the Saar-Nahe basin (SW Germany) - implications for Late-Variscan orogenic development, Contrib. Mineral. Petrol. 135 (1999) 373-385.

[40] J. Blichert-Toft, F. Albarède, The Lu-Hf isotope geochemistry of chondrites and the evolution of the mantle-crust system, Earth Planet. Sci. Lett. 148 (1997) 243-258.

[41] J.B. Dawson, A review of the geology of kimberlite, in: P.J. Wyllie (Ed.), Ultramafic and related rocks, Wiley, New York, 1967, pp. 241-251.

[42] C.B Smith, Pb, Sr and Nd isotopic evidence for sources of southern African Cretaceous kimberlites, Nature 304 (1983) 51-54.

[43] G.M. Nowell, D.G. Pearson, P.D. Kempton, S.R. Noble, C.B. Smith, Origins of kimberlites: a Hf isotope perspective, in: Proceedings of the Seventh Int. Kimb. Conf., 1999, pp. 616-624.

[44] J.D. Vervoort, P.J. Patchett, F. Albarède, J. Blichert-Toft, R. Rudnick, H. Downes, Hf-Nd isotopic evolution of the lower crust, Earth Planet. Sci. Lett. 181 (2000) 115-129.

[45] J.A. Dalton, D.C. Presnall, The continuum of primary carbonatitic-kimberlitic melt compositions in equilibrium with lherzolite: data from the system CaO-MgO-Al_2O_3-SiO_2-CO_2 at 6 GPa, J. Petrol. 39 (1998) 1953-1964.

[46] J.D. Vervoort, J. Blichert-Toft, Evolution of the depleted mantle: Hf isotope evidence from juvenile rocks through time, Geochim. Cosmochim. Acta 63 (1999) 533-556.

[47] J. Blichert-Toft, F. Albarède, M. Rosing, R. Frei, D. Bridgwater, The Nd and Hf isotopic evolution of the mantle through the Archean. Results from the Isua supracrustals, West Greenland, and from the Birimian terranes of West Africa, Geochim. Cosmochim. Acta 63 (1999) 3901-3914.

[48] F. Albarède, J. Blichert-Toft, J.D. Vervoort, J.D. Gleason, M. Rosing, Hf-Nd isotope evidence for a transient dynamic regime in the early terrestrial mantle, Nature 404 (2000) 488-490.

[49] P.J. Patchett, Hafnium isotope results from mid-ocean ridges and Kerguelen, Lithos 16 (1983) 47-51.

[50] J.D. Vervoort, P.J. Patchett, J. Blichert-Toft, F. Albarède, Relationships between Lu-Hf and Sm-Nd isotopic systems in the global sedimentary system, Earth Planet. Sci. Lett. 168 (1999) 79-99.

[51] C.M. Johnson, B.L. Beard, Evidence from hafnium isotopes for ancient sub-oceanic mantle beneath the Rio Grande rift, Nature 362 (1993) 441-444.

[52] W.D. Steward, Late Proterozoic to Early Tertiary stratigraphy of Somerset Island and northern Boothia Peninsula, District of Franklin, Geological Survey of Canada, Paper 83-26 (1987) pp. 78.

Figure captions

Figure 5-1: Geological map of Somerset Island (after [52]) showing kimberlite locations. The mantle xenoliths from this study were collected from the Nikos kimberlite (black diamond). Legend: light gray, Paleozoic cover rocks; striped, Late Proterozoic cover rocks; dark gray, Precambrian basement; bold lines, normal faults.

Figure 5-2: (a) $^{176}Lu/^{177}Hf$ versus initial $\varepsilon_{Hf(T)}$ (100 Ma ago) for the Nikos kimberlite. Also shown are two samples that most likely experienced contamination by xenocrystic garnet (for further explanation see text). Data for South African "Group I" (90-110 Ma) and "Group II" (120-150 Ma) kimberlites are shown for comparison [43]. (b) $^{176}Lu/^{177}Hf$ versus $\varepsilon_{Hf(0.1Ga)}$ for Nikos peridotites at the time of kimberlite emplacement. For samples with duplicate analyses, the average composition is plotted.

Figure 5-3: $^{176}Lu/^{177}Hf$ versus $^{176}Hf/^{177}Hf$ diagram for Nikos peridotites. 2.8 Ga (billion years) Lu-Hf reference isochron is plotted, which corresponds to the regression line for data (and corresponding initial $^{176}Hf/^{177}Hf$) for the low-temperature peridotites (solid diamonds). See text for further details.

Figure 5-4: $^{176}Lu/^{177}Hf$ versus $^{176}Hf/^{177}Hf$ diagram for Nikos garnets and peridotites. Tie lines connect garnet with corresponding whole rock composition. Also shown are the "dates" (in million years) obtained for individual internal Lu-Hf isochrons using garnet-whole-rock pairs.

Figure 5-5: Hf-Nd variation diagram for Nikos peridotites at the time of kimberlite emplacement (Nd data from [36]). The Hf-Nd array for terrestrial samples

[44] and the composition of "depleted" mantle are plotted for comparison [8,40,46].

Figure 5-6: Lu (ppm) versus Al_2O_3 contents (wt%) for Nikos peridotites (Al_2O_3 data from [35]).

Figure 5-7: $\varepsilon_{Hf(0.1Ga)}$ versus $^{87}Sr/^{86}Sr_{(0.1Ga)}$ for Nikos peridotites (Sr data from [36]).

Figure 5-8: Lu-Hf and Sm-Nd internal isochron "dates" versus temperature (and depth) of last equilibration for low-temperature garnet-whole rock pairs (Sm-Nd data from [36]).

Table 5-1. Lu-Hf isotope data for Nikos peridotites and kimberlite.

Sample	Temp. °C	Press. kb	Lu ppm	Hf ppm	$^{176}Lu/^{177}Hf$	$^{176}Hf/^{177}Hf$ measured	$^{176}Hf/^{177}Hf_{(0.1Ga)}$	ε_{Hf}	$\varepsilon_{Hf(0.1Ga)}$
Low-temperature peridotites									
NK1-4	871	33.5	0.0227	0.0768	0.0422	0.283900 ±20	0.283821	39.9	39.3
NK1-4 Dup.			0.0289	0.0923	0.0446	0.284072 ±20	0.283988	46.0	45.2
NK2-3	887	34.6	0.0371	0.1389	0.0381	0.283566 ±23	0.283495	28.1	27.8
NK1-23	964	39.0	0.0349	0.1722	0.0289	0.283344 ±30	0.283290	20.2	20.5
NK1-23 Dup.				0.1905		0.283342 ±28		20.2	
NK1-14	1027	42.7	0.0198	0.0589	0.0480	0.284280 ±28	0.284190	53.3	52.3
NK1-14 Dup.			0.0209	0.0658	0.0452	0.284152 ±26	0.284068	48.8	48.0
NK1-2	1042	44.7	0.0160	0.0720	0.0316	0.283662 ±33	0.283603	31.5	31.6
NK1-2 Dup.			0.0167	0.0694	0.0343	0.283885 ±19	0.283820	39.3	39.3
NK1-3	1076	46.5	0.0182	0.0966	0.0269	0.283014 ±14	0.282963	8.5	9.0
NK1-3 Dup.				0.0905		0.282989 ±14		7.7	
NK2-9[a]	808		0.0028	0.0142	0.0284	0.283180 ±58	0.283127	14.4	14.7
High-temperature peridotites									
NK1-6	1149	48.8	0.0080	0.0718	0.0159	0.283164 ±16	0.283134	13.9	15.0
NK2-1	1216	51.5	0.0074	0.1080	0.0097	0.282884 ±30	0.282866	4.0	5.5
NK1-9	1219	53.4	0.0173	0.1624	0.0152	0.282834 ±07	0.282805	2.2	3.4
NK1-19	1228	51.9	0.0064	0.0588	0.0155	0.283012 ±13	0.282983	8.5	9.7
NK1-19 Dup.			0.0058	0.0589	0.0141	0.283139 ±15	0.283113	13.0	14.3
NK3-25	1256	54.0	0.0281	0.3038	0.0132	0.282679 ±51	0.282654	-3.3	-2.0
NK1-5	1262	54.6	0.0177	0.2091	0.0121	0.282805 ±14	0.282782	1.2	2.6
NK1-7[b]	1300	55.1	0.0164	0.0669	0.0349	0.283364 ±15	0.283298	20.9	20.8
NK1-7 Dup.			0.0187	0.0798	0.0334	0.283389 ±16	0.283326	21.8	21.8
NK2-2	1316	54.7	0.0220	0.1637	0.0191	0.283248 ±24	0.283212	16.8	17.8
NK1-10	1405	63.7	0.0043	0.1682	0.0037	0.282874 ±20	0.282867	3.6	5.6
Kimberlite									
NK3-K1			0.0751	2.973	0.0036	0.283197 ±25	0.283191	15.0	17.0
NK3-K2			0.0730	2.648	0.0039	0.283314 ±39	0.283307	19.2	21.1
NK3-K3			0.0899	3.751	0.0034	0.282858 ±13	0.282852	3.1	5.0
NK3-K4			0.0574	2.821	0.0029	0.282716 ±37	0.282711	-2.0	0

[a]spinel peridotite; [b]porphyroclastic texture. $\varepsilon_{Hf(0.1Ga)}$ values calculated for 100 Ma in-situ decay using present day ratios of $^{176}Hf/^{177}Hf_{(CHUR)}=0.282772$ and $^{176}Lu/^{177}Hf_{(CHUR)}=0.0332$ [40] and $\lambda=1.876\times10^{-11}$ yr^{-1} [19,20]. Precision for individual Hf isotope measurements is quoted at the 2σ level. Lu and Hf concentrations were determined by isotope dilution analysis; uncertainties for $^{176}Lu/^{177}Hf$ are ~2%.

Table 5-2. Lu-Hf isotope data for Nikos garnets.

Sample	Temp. °C	Press. kb	Lu ppm	Hf ppm	$^{176}Lu/^{177}Hf$	$^{176}Hf/^{177}Hf$ measured	$^{176}Hf/^{177}Hf_{(0.1Ga)}$	ε_{Hf}	$\varepsilon_{Hf(0.1Ga)}$	Date Ma
Low-temperature garnets										
NK1-4 Gt	871	33.5	0.2742	0.1609	0.2430	0.287403 ±59	0.286947	164	150	905
NK2-3 Gt	887	34.6	0.2812	0.2262	0.1774	0.285589 ±15	0.285256	99.6	90.1	769
NK2-10 Gt	1014	42.1	0.2636	0.4060	0.0926	0.283270 ±37	0.283096	17.6	13.7	499
NK1-14 Gt	1027	42.7	0.2741	0.2238	0.1747	0.285419 ±13	0.285091	93.6	84.2	
NK1-2 Gt	1042	44.7	0.3667	0.3479	0.1503	0.284465 ±18	0.284183	59.9	52.1	313
NK1-3 Gt	1076	46.5	0.3255	0.4952	0.0937	0.283309 ±11	0.283133	19.0	15.0	235
High-temperature garnets										
NK2-1 Gt	1216	51.5	0.1670	1.549	0.0154	0.282778 ±08	0.282749	0.2	1.4	
NK1-9 Gt	1219	53.4	0.2516	1.064	0.0337	0.282831 ±09	0.282768	2.1	2.1	
NK1-5 Gt	1262	54.6	0.2148	1.229	0.0249	0.282873 ±07	0.282826	3.6	4.1	
NK3-16 Gt	1280	53.5	0.3539	1.024	0.0493	0.282993 ±15	0.282900	7.8	6.7	
NK1-7 Gt	1300	55.1	0.2442	0.6252	0.0557	0.283512 ±13	0.283407	26.2	24.7	326
NK1-7 Gt Dup.			0.2411	0.6117	0.0562	0.283509 ±71	0.283403	26.1	24.5	
NK2-2 Gt	1316	54.7	0.2666	0.8145	0.0467	0.283165 ±74	0.283078	13.9	13.0	
NK3-4 Gt	1371	58.5	0.2702	0.6780	0.0568	0.283508 ±22	0.283401	26.0	24.5	

Analytical procedures as in Table 5-1. Date refers to internal isochron “age” using garnet-whole rock pairs.

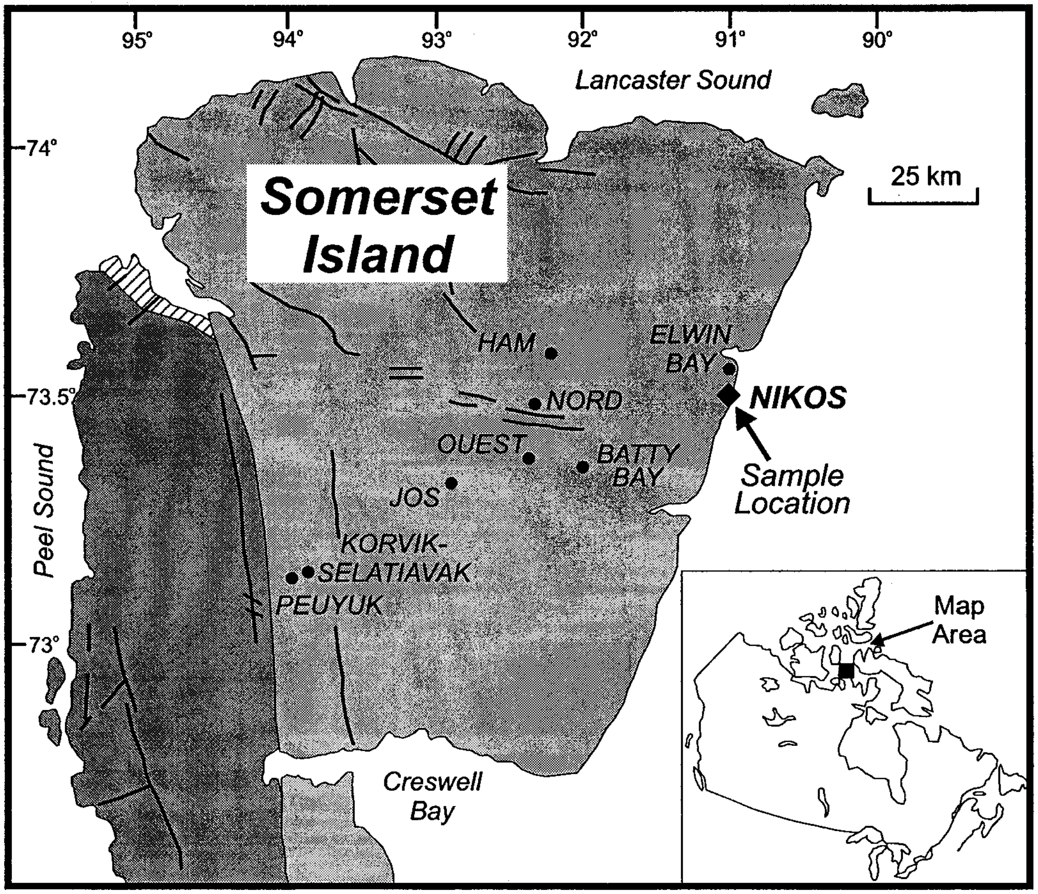

95°
94°
93°
92°
91°
90°
Lancaster Sound
-74°
25 km
Somerset Island
HAM
ELWIN BAY
-73.5°
NORD
NIKOS
OUEST
BATTY BAY
Sample Location
JOS
Peel Sound
KORVIK-SELATIAVAK
PEUYUK
-73°
Map Area
Creswell Bay

Figure 5-1

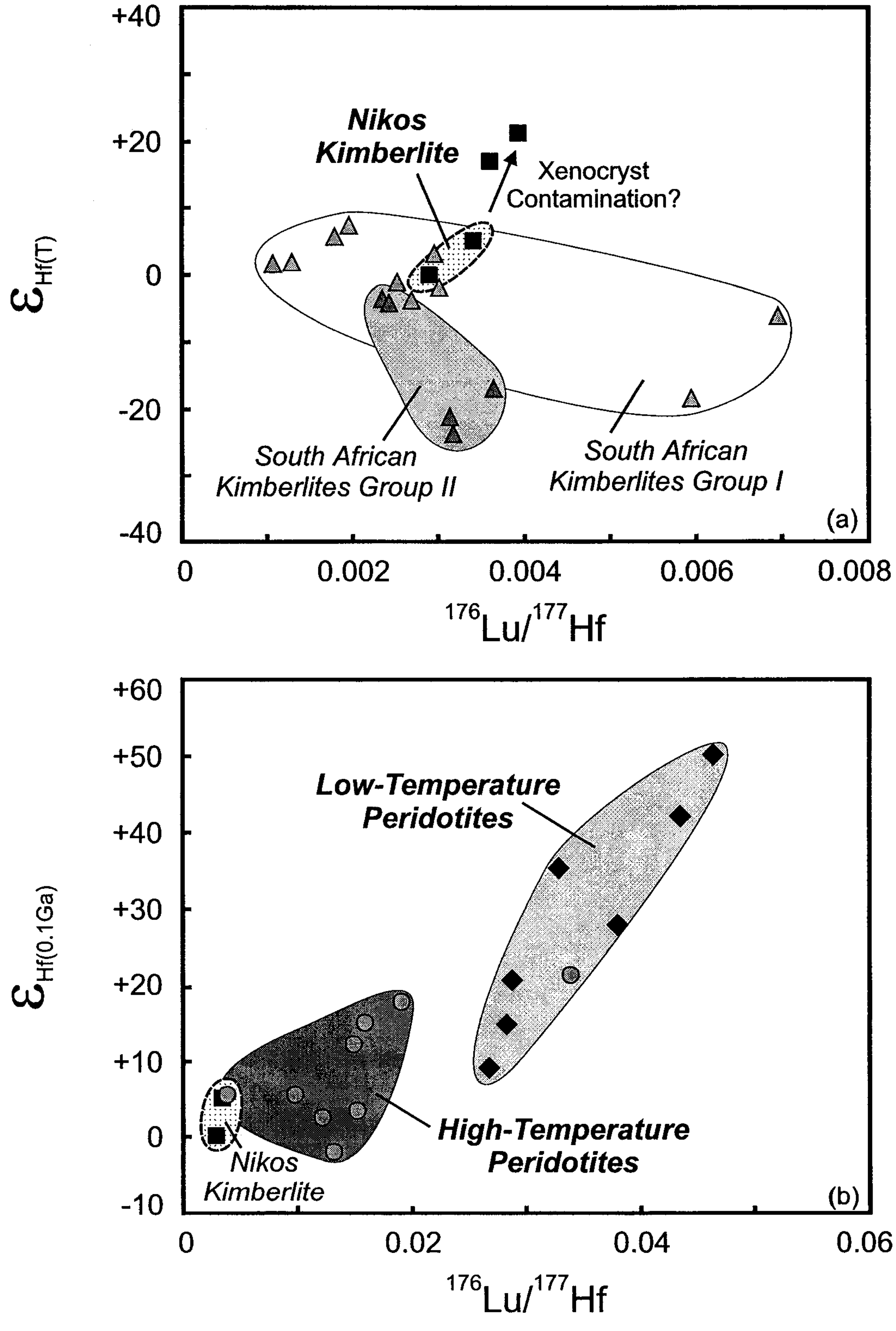
+40
+20
0
-20
-40
εHf(T)
Nikos Kimberlite
Xenocryst Contamination?
South African Kimberlites Group II
South African Kimberlites Group I
(a)
0
0.002
0.004
0.006
0.008
176Lu/177Hf
+60
+50
+40
+30
+20
+10
0
-10
εHf(0.1Ga)
Low-Temperature Peridotites
High-Temperature Peridotites
Nikos Kimberlite
(b)
0
0.02
0.04
0.06
176Lu/177Hf

Figure 5-2

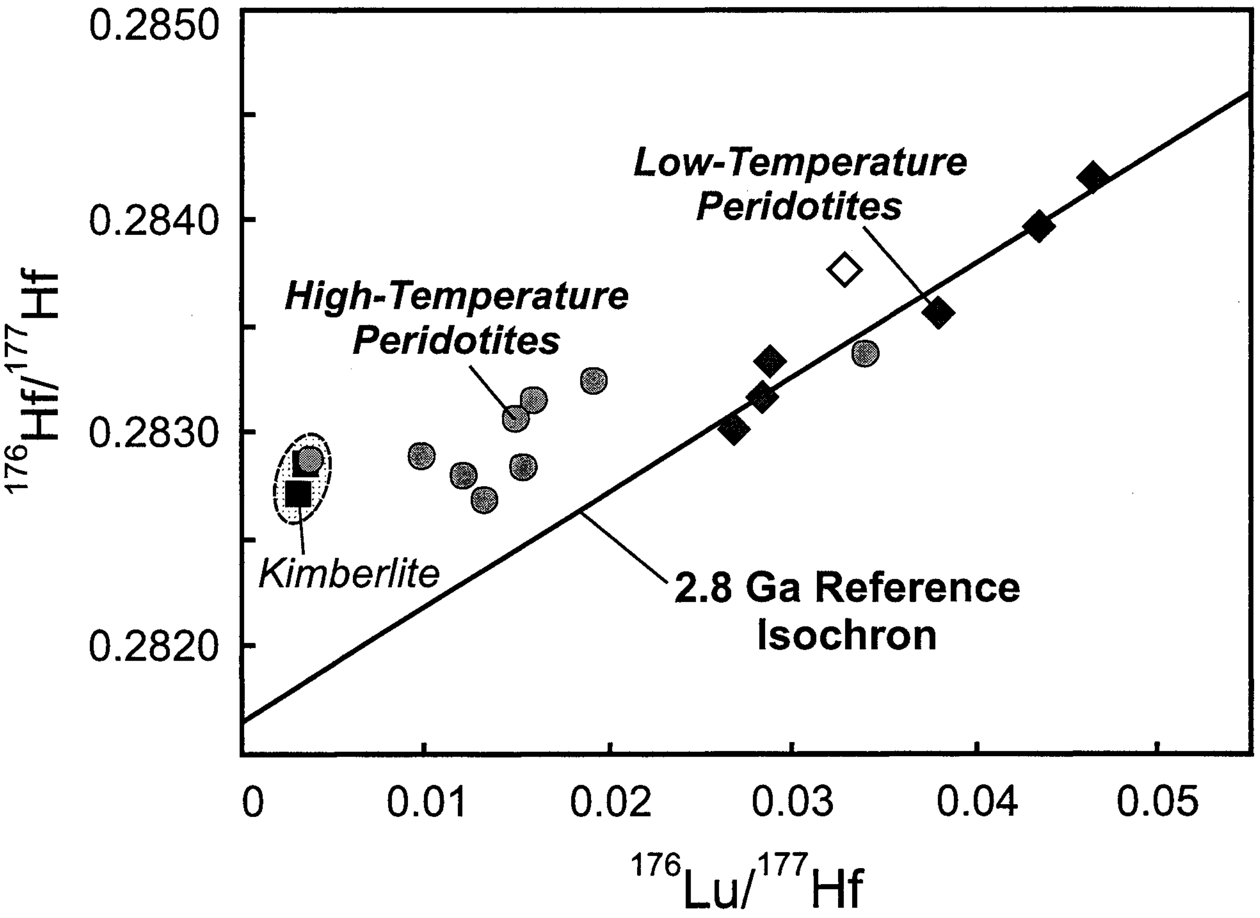
0.2850
0.2840
0.2830
0.2820
$^{176}Hf/^{177}Hf$
0
0.01
0.02
0.03
0.04
0.05
$^{176}Lu/^{177}Hf$
Low-Temperature Peridotites
High-Temperature Peridotites
Kimberlite
2.8 Ga Reference Isochron

Figure 5-3

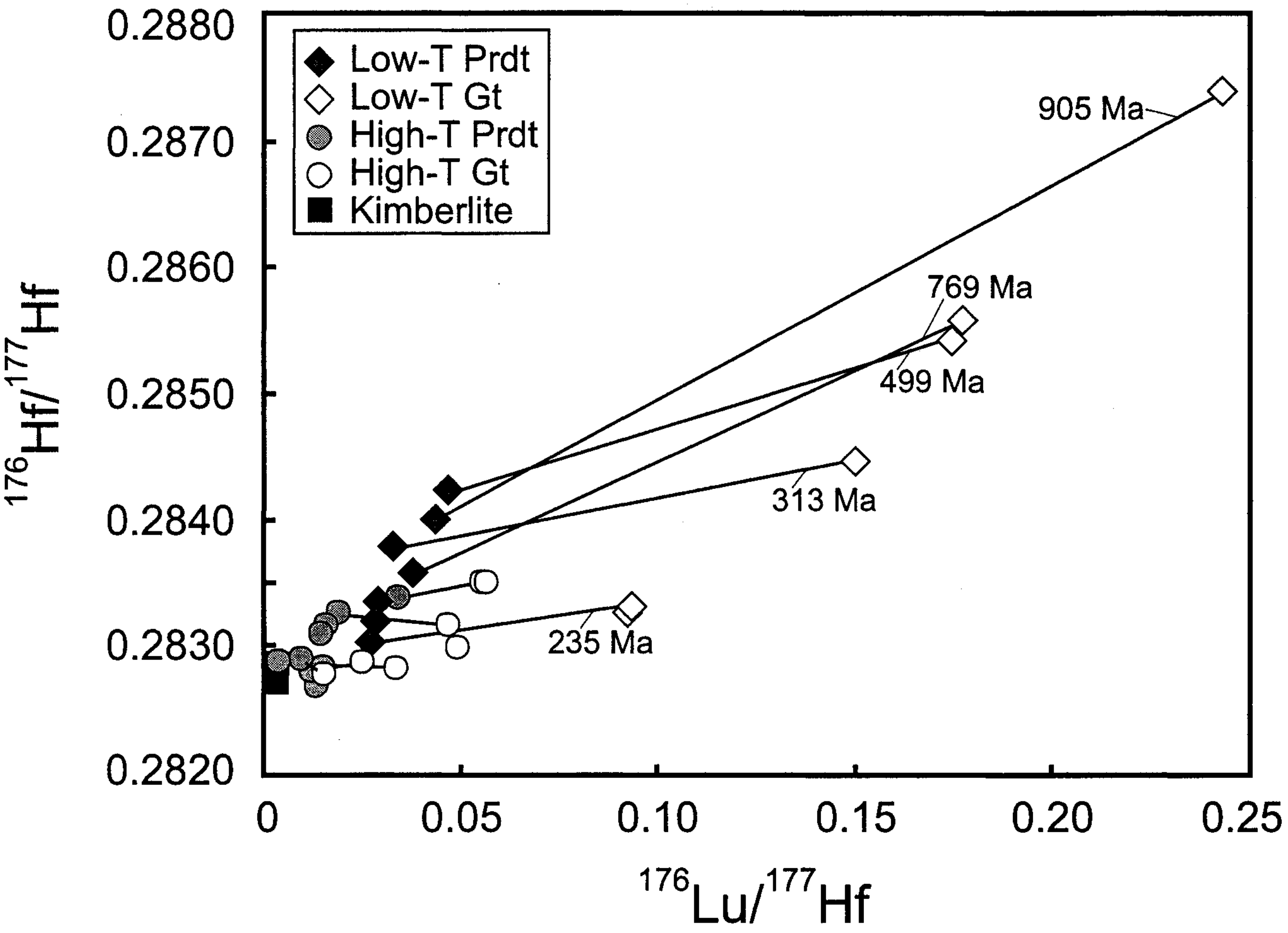

0.2880
0.2870
0.2860
0.2850
0.2840
0.2830
0.2820
0
0.05
0.10
0.15
0.20
0.25
176Hf/177Hf
176Lu/177Hf
◆ Low-T Prdt
◇ Low-T Gt
● High-T Prdt
○ High-T Gt
■ Kimberlite
905 Ma
769 Ma
499 Ma
313 Ma
235 Ma

Figure 5-4

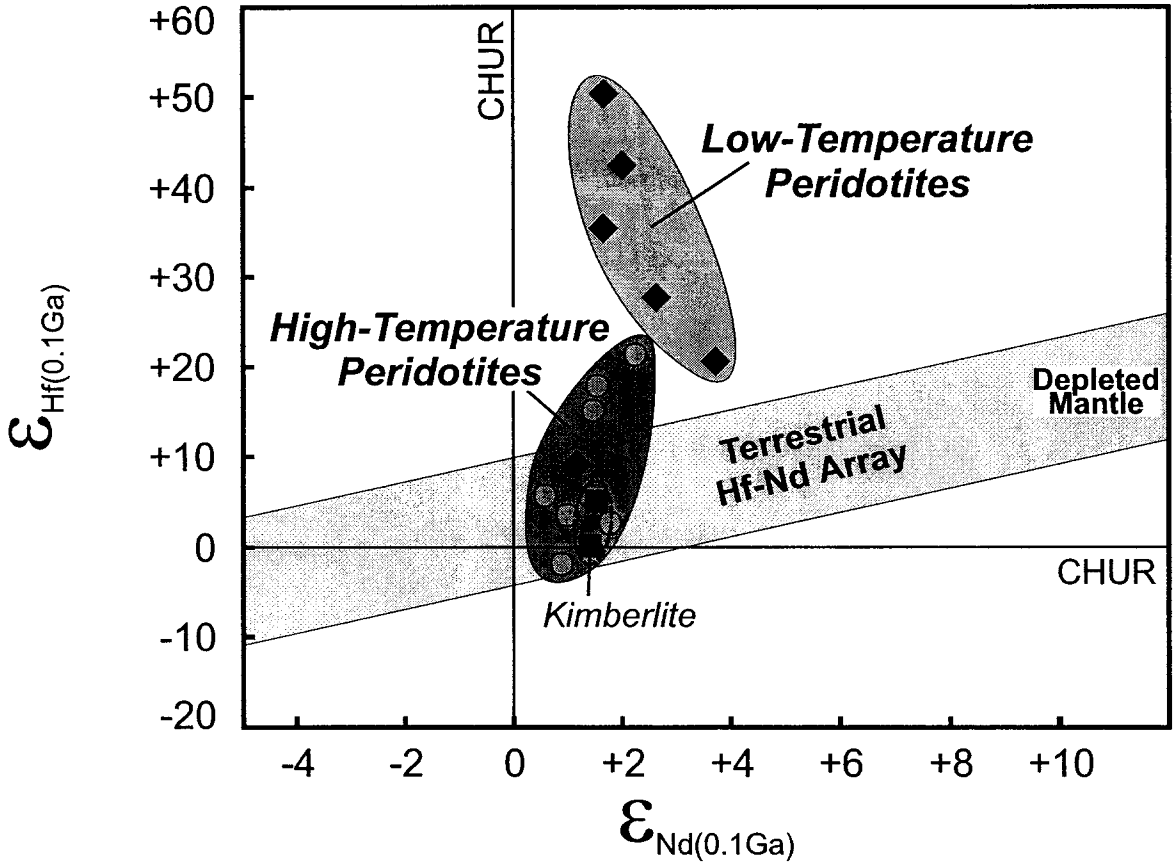

+60
+50
+40
+30
+20
+10
0
-10
-20
CHUR
Low-Temperature Peridotites
High-Temperature Peridotites
Depleted Mantle
Terrestrial Hf-Nd Array
CHUR
Kimberlite
-4
-2
0
+2
+4
+6
+8
+10
$\varepsilon_{Hf(0.1Ga)}$
$\varepsilon_{Nd(0.1Ga)}$

Figure 5-5

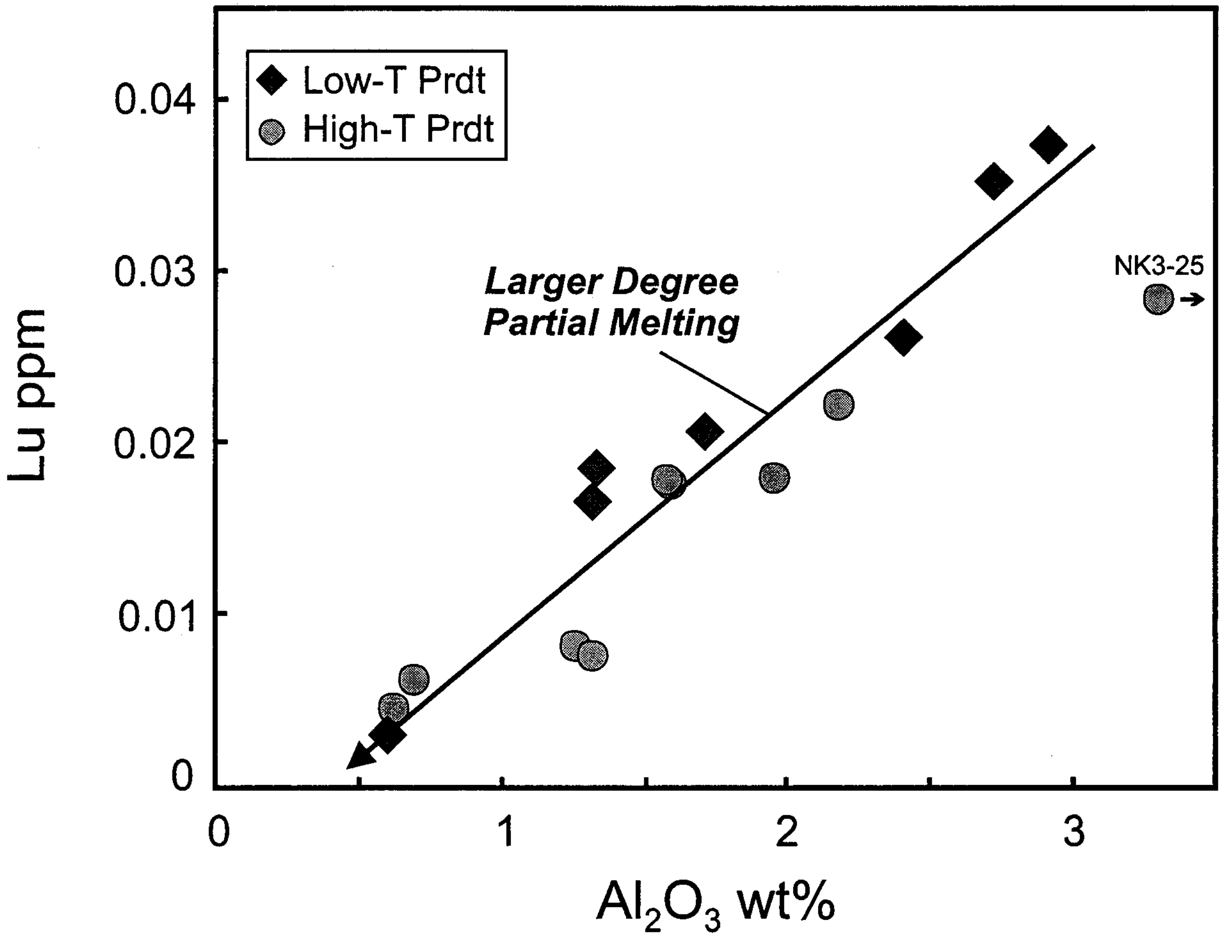

◆ Low-T Prdt
● High-T Prdt
Larger Degree Partial Melting
NK3-25
Lu ppm
0.04
0.03
0.02
0.01
0
0
1
2
3
Al_2O_3 wt%

Figure 5-6

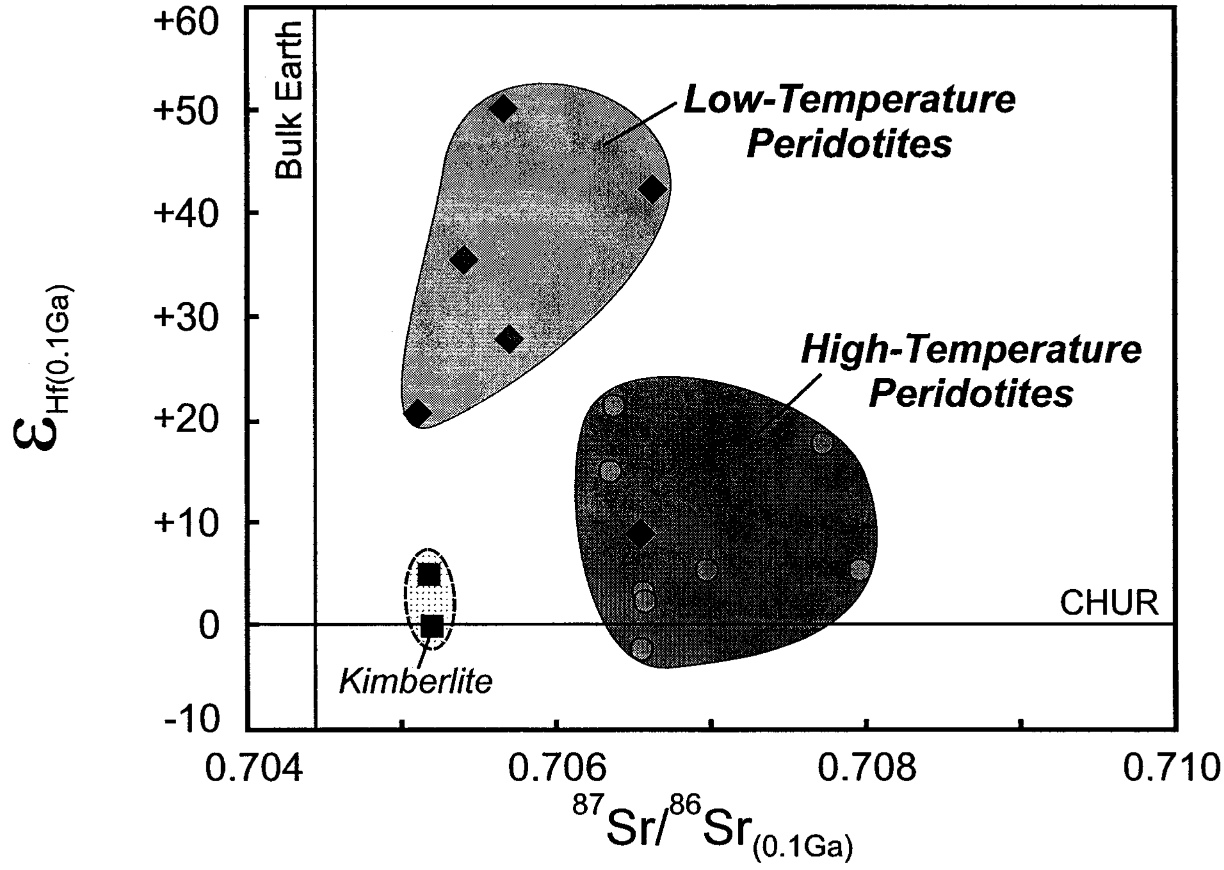

+60
+50
+40
+30
+20
+10
0
-10
$\varepsilon_{Hf(0.1Ga)}$
Bulk Earth
Low-Temperature Peridotites
High-Temperature Peridotites
CHUR
Kimberlite
0.704
0.706
0.708
0.710
$^{87}Sr/^{86}Sr_{(0.1Ga)}$

Figure 5-7

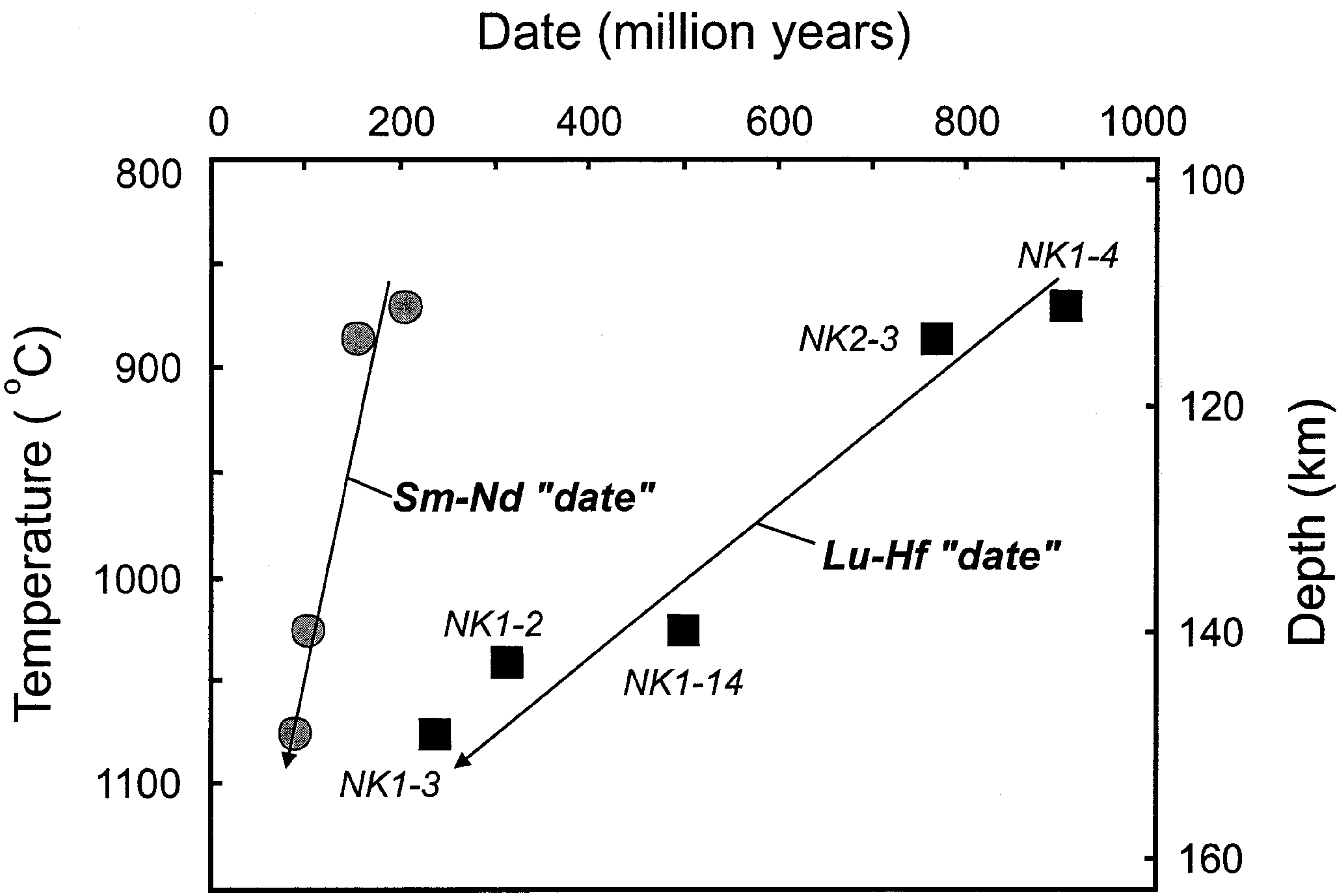
Date (million years)
0
200
400
600
800
1000
800
900
1000
1100
Temperature (°C)
100
120
140
160
Depth (km)
Sm-Nd "date"
Lu-Hf "date"
NK1-4
NK2-3
NK1-2
NK1-14
NK1-3

Figure 5-8

CHAPTER 6

GENERAL CONCLUSIONS

The subcratonic lithosphere beneath Somerset Island sampled by the Nikos kimberlite consists of refractory peridotites with minor occurrences of pyroxenites. The olivine-rich (avg. 80 wt.%) mineralogy and depleted major element compositions (e.g. Fe, Al, Ca) of the Nikos peridotites indicate formation and stabilization of the mantle root beneath the northern Canadian craton as the result of extensive melt extraction. The high abundances of large ion lithophile elements (LILE) and light rare earth elements (LREE) observed for the xenoliths provide evidence that these melt-depleted residues experienced metasomatism during residence in the mantle and/or sample transport. Nd isotopic compositions of the peridotites overlap those of the Nikos kimberlites and appear to reflect sample contamination with small amounts of kimberlite magma. These results indicate that metasomatic processes play an important role in modifying the chemical composition of the subcratonic lithospheric mantle.

The shallow low-temperature (<1100°C) and the deep-seated high-temperature (>1100°C) Nikos peridotites and their constituent clinopyroxene and garnet are characterized by distinct Sr, Pb and Hf isotopic compositions, which is in agreement with their differences in the abundances of trace and rare earth elements (REE). This provides evidence for a chemical and isotopic depth stratification of the Somerset lithosphere indicating that the shallow and deep subcontinental mantle do not share a common petrogenetic history. These results suggest a multi-stage evolution for the mantle root beneath the northern Canadian craton and the involvement of distinct magmatic processes.

The Lu-Hf isotope systematics for the shallow low-temperature peridotites plot along a 2.8 Ga reference isochron. A number of these xenoliths are characterized by highly radiogenic Hf isotopic compositions suggestive of billions of years of radiogenic ingrowth. These findings are consistent with an interpretation that the shallow Somerset lithosphere stabilized in the Archean to depth of ~150 km. The data indicate that part of the Canadian mantle root is characterized by a more radiogenic Hf isotope signature than that estimated for a typical "depleted" mantle. The majority of the high-temperature peridotites are probably younger and they could have been added to the shallow lithosphere by downward growth of the Archean mantle root. To date, the results presented in this thesis are the first Lu-Hf isotope data that have been reported for the subcontinental lithosphere. Comparing the Lu-Hf isotope results obtained for the Canadian mantle to those for other cratonic roots such as beneath South Africa, Siberia and North America would enable to obtain a better understanding of the origin and geochemical evolution of subcontinental lithosphere, which is an important reservoir in the Hf isotope budget of the Earth's mantle.

Dating peridotite sulfides using the Re-Os isotope technique, which appears to be little susceptible to metasomatic effects, can provide constraints on the stabilization age of the lithosphere. Investigating the Re-Os systematics of the Nikos peridotites and their accessory sulfides would offer the advantage of an integrated Hf, Os, Sr, Nd and Pb isotope study on a single peridotite xenolith suite. A combined Lu-Hf and Re-Os isotope investigation would for the first time enable a comparison of data obtained using silicate-hosted (Lu-Hf) and sulfide-hosted (Re-Os) elements, and help constrain the stabilization history of the Canadian mantle root.

APPENDIX A

^{180}Hf isotope tracer calibration

Isotope dilution analysis is used for accurate concentration determinations of an element by mass spectrometry (Moore et al., 1973; Faure, 1986). In this technique an isotope tracer ("spike") solution that is artificially enriched in one isotope of a particular element and of a precisely known concentration is added to a sample, the latter having a natural isotopic composition but unknown concentration of the element. The isotopic composition of the mixture can then be used to calculate the concentration of the element in question for the sample. The accuracy of the isotope dilution method depends on the accurate calibration of the isotope tracer solution, i.e. its isotopic composition and concentration have to be determined precisely and verified separately.

In order to obtain high-precision Hf concentration determinations, this study involved the calibration of a ^{180}Hf tracer (~98.2%) using the Micromass IsoProbe multicollector inductively coupled plasma mass spectrometer (MC-ICP-MS). The isotopic composition of the ^{180}Hf isotope tracer was determined by repeated measurements of a ~100 ppb spike solution in static, multicollection mode (Table A-1). As there are no certified values for the isotope ratios in the ^{180}Hf tracer, which may be used as a monitor for instrument-induced mass bias, a 50 ppb solution of the Hf standard JMC 475 was measured repeatedly prior to the spike analysis. The measured Hf isotopic ratios of the ^{180}Hf tracer were corrected using the mass discrimination coefficient based on the standard analyses and using the exponential law (Russell et al., 1978), which is expressed as follows:

$$R_{true} = R_{measured}(M_2/M_1)^f$$

where R is the ratio of the ion beams at masses M_2 and M_1 and f is the mass discrimination coefficient. The isotopic composition indicates a ^{180}Hf enrichment of 98.26% for the isotope tracer (Table A-1).

The ^{180}Hf tracer was diluted to an approximate concentration of 30 ppb from the stock solution (4000 ppm), and this was verified by isotope dilution against a solution of the JMC 475 Hf standard (~100 ppb). The concentration of the Hf standard was determined gravimetrically using a buoyancy correction calculation (Table A-1). A number of standard-Hf tracer mixtures with different ^{180}Hf proportions (mole fractions 0.95:0.05 to 0.05:0.95; n=6; Table A-1) were prepared and analyzed for their isotopic compositions by MC-ICP-MS. The Hf concentration of the ^{180}Hf tracer solution added to each mixture of Hf tracer (S) and standard (N) can be determined as follows (after Faure, 1986):

$$C_S = (C_N * W_S / W_N * wt_N/wt_S) / ((Ab180_S - R*Ab177_S)/(R*Ab177_N - Ab180_N))$$

where C_S and C_N are the Hf concentrations, W the atomic weights, wt the weights of the element, Ab the isotopic abundances of spike and standard, respectively. R is the fractionation corrected ^{180}Hf/^{177}Hf ratio of the mixture. The calculated concentrations of the ^{180}Hf tracer added to the individual mixtures yield an average value for ^{180}Hf of 30.436±0.070 ppb and total Hf content of 30.974±0.072 ppb (1SD; Table A-1). The total number of moles/g of ^{180}Hf in these mixtures when plotted versus their corresponding isotopic compositions fall on a mixing line ($R^2 = 0.999$) between the two endmembers compositions ^{180}Hf tracer and Hf standard JMC 475 (Table A-1; Fig. A-1).

References

Faure G. (1986) *Principles of isotope geology*. John Wiley & Sons, New York. pp. 589.

Moore L. J., Moody J. R., Barnes I. L., Gramich J. W., Murphy T. J., Paulsen P. J. and Shields W. R. (1973) Trace determination of rubidium and strontium in silicate glass standard reference materials. *Anal. Chem.* **45**, 2384-2387.

Russell W. A., Papanastassiou D. A. and Tombrello T. A. (1978) Ca isotope fractionation on the Earth and other solar system materials. *Geochim. Cosmochim. Acta* **42**, 1075-1090.

Table A-1. Hf isotope tracer calibration - parameters and calculations

^{180}Hf tracer and standard isotopic compositions

	^{174}Hf/^{177}Hf	^{176}Hf/^{177}Hf		^{178}Hf/^{177}Hf	^{179}Hf/^{177}Hf	^{180}Hf/^{177}Hf	# anal
Standard JMC 475	0.00867	0.282153		1.46731	0.7325	1.88677	12
^{180}Hf tracer	0.00859	0.241646		2.67303	2.85041	383.417	5

Abundance	^{174}Hf	^{176}Hf	^{177}Hf	^{178}Hf	^{179}Hf	^{180}Hf	atomic mass
Standard JMC 475	0.0016	0.0525	0.1860	0.2729	0.1362	0.3509	178.485
^{180}Hf tracer	0.00002	0.0006	0.0026	0.0069	0.0073	0.9826	179.915

Mixture standard-^{180}Hf tracer isotopic compositions

	mole fraction ^{180}Hf	^{176}Hf/^{177}Hf	^{178}Hf/^{177}Hf	^{179}Hf/^{177}Hf	^{180}Hf/^{177}Hf
Mixture1	0.95:0.05	0.282129	1.46747	0.732944	1.98409
Mixture1 Dup	0.95:0.05	0.282134	1.46749	0.733032	1.98421
Mixture2	0.60:0.40	0.282009	1.47132	0.739595	3.16882
Mixture2 Dup	0.60:0.40	0.281993	1.47138	0.739687	3.16892
Mixture3	0.40:0.60	0.281839	1.47609	0.748093	4.68133
Mixture3 Dup	0.40:0.60	0.281845	1.47610	0.748091	4.68147
Mixture4	0.20:0.80	0.281381	1.49054	0.773212	9.23102
Mixture4 Dup	0.20:0.80	0.281302	1.49051	0.773374	9.23189
Mixture5	0.10:0.90	0.280358	1.51845	0.822726	18.0688
Mixture5 Dup	0.10:0.90	0.280170	1.51803	0.822235	18.0654
Mixture6	0.05:0.95	0.278548	1.57078	0.914750	34.6600
Mixture6 Dup	0.05:0.95	0.278432	1.57020	0.914205	34.6429

Table A-1. Continued.

Isotope dilution calculation after Faure (1986)

Standard JMC 475 used for ^{180}Hf tracer calibration
Concentration calculation with buoyancy correction

	Weight (g)	Hf (ng)	Volume (ml)	Concentration (ppb)	(moles/g)
Standard stock solution	0.1711	101086		590801	
HNO$_3$ added	1000.92				
Standard dilution	1001.09		992.07		
Displaced air	1.2004				
Standard dilution buoyancy corrected	1002.29			100.855	1.98×10^{-10}

Mixture Standard-^{180}Hf tracer	^{180}Hf/^{177}Hf Average	Weight Standard (g)	^{180}Hf tracer (g)	Standard Hf total (ng)	^{180}Hf (ng)	^{180}Hf tracer Hf total (ng)	^{180}Hf (ng)	Hf total (ppb)	^{180}Hf (ppb)	Mixture ^{180}Hf (moles/g)
Mixture1	1.98415	5.05257	0.30733	509.575	178.795	9.515	9.350	30.961	30.424	1.95×10^{-10}
Mixture2	3.16887	1.95142	1.57410	196.810	69.055	48.537	47.694	30.835	30.299	1.84×10^{-10}
Mixture3	4.68140	1.00579	1.76298	101.439	35.592	54.747	53.797	31.054	30.515	1.79×10^{-10}
Mixture4	9.23145	1.00457	4.69620	101.316	35.549	145.456	142.931	30.973	30.435	1.74×10^{-10}
Mixture5	18.0671	0.50233	5.28655	50.662	17.776	164.109	161.260	31.043	30.504	1.72×10^{-10}
Mixture6	34.6514	0.24959	5.58345	25.172	8.832	172.968	169.965	30.979	30.441	1.70×10^{-10}
Average ^{180}Hf tracer								30.974	30.436	1.69×10^{-10}
Std deviation (1SD)								0.072	0.070	
Std error (%)								0.094	0.094	

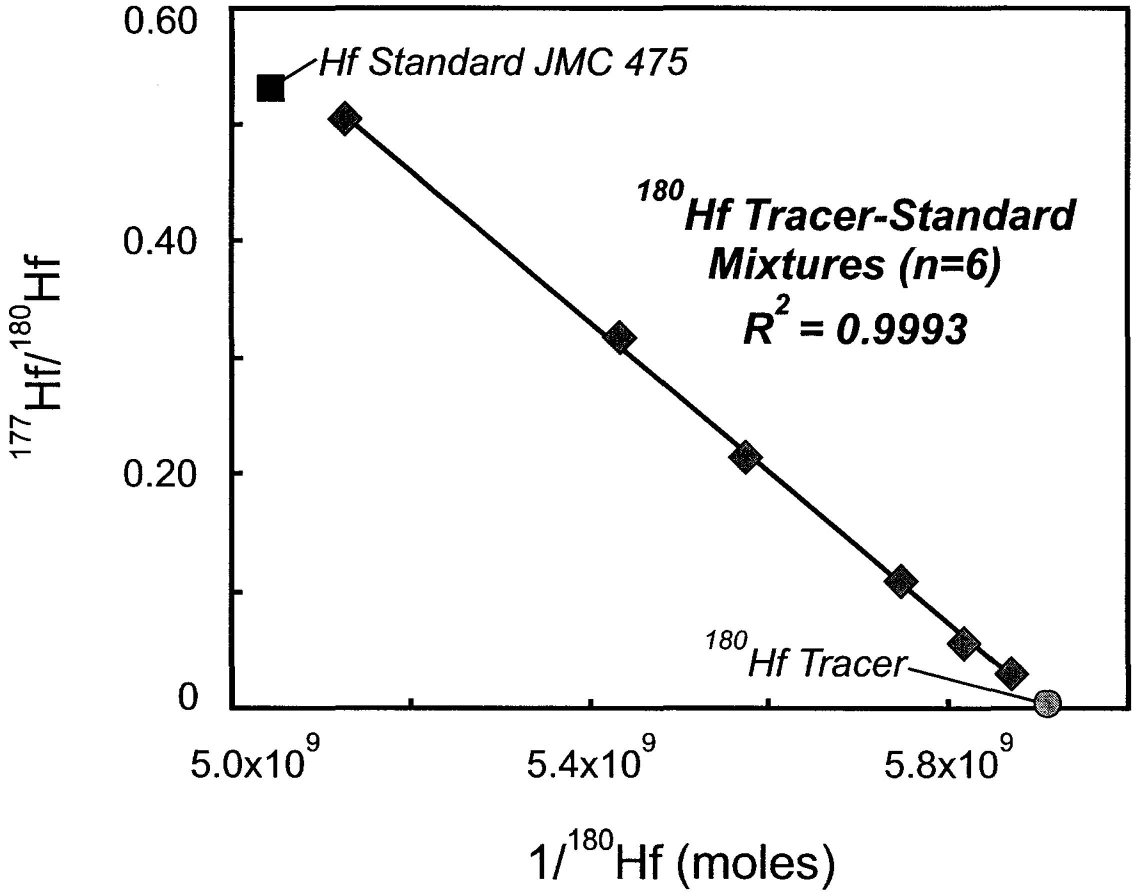
0.60
0.40
0.20
0
5.0x10^9
5.4x10^9
5.8x10^9
177Hf/180Hf
1/180Hf (moles)
Hf Standard JMC 475
180Hf Tracer-Standard Mixtures (n=6)
R2 = 0.9993
180Hf Tracer

Figure A-1

APPENDIX B

Table B-1. Major element analyses and calculated mineral modes for Nikos peridotites.

Sample	NK1-1	NK1-2	NK1-3	NK1-4	NK1-5	NK1-6	NK1-7	NK1-8	NK1-9	NK1-10	NK1-11	NK1-12	NK1-13	NK1-14
Rock	Prdt	Prdt	Prdt	Prdt	Prdt	Prdt	Prdt	Prdt	Prdt	Prdt	Prdt	Prdt	Prdt	Prdt
Texture	coarse	coarse	coarse	coarse	coarse	coarse	porphcl	coarse	coarse	coarse	coarse	coarse	coarse	coarse
SiO_2	41.25	41.77	40.81	41.60	42.28	40.37	41.24	43.34	41.88	41.09	42.60	40.80	42.20	42.02
TiO_2	0.07	0.03	0.03	0.06	0.07	0.02	0.03	0.03	0.04	0.02	0.05	0.03	0	0.03
Al_2O_3	1.00	1.31	1.33	2.43	1.95	1.25	1.57	1.01	1.59	0.62	0.49	0.56	0.20	1.71
FeO	7.49	7.39	7.42	7.09	7.74	7.10	7.06	6.89	7.29	6.93	7.21	7.76	6.90	7.27
MnO	0.11	0.11	0.11	0.13	0.12	0.10	0.10	0.10	0.11	0.10	0.10	0.11	0.10	0.11
MgO	43.30	44.44	44.03	40.90	41.49	43.41	43.55	44.37	43.48	44.81	45.17	45.32	44.60	42.92
CaO	0.58	1.11	0.82	1.20	1.44	0.41	0.72	0.49	0.96	0.20	0.40	0.57	0.30	1.13
Na_2O	0.02	0.10	0.01	0.01	0.06	0	0	0.08	0.03	0.08	0	0.12	0	0.15
K_2O	0.04	0.03	0.04	0.07	0.08	0.03	0.02	0.04	0.04	0.03	0.08	0.16	0.10	0.03
P_2O_5	0.01	0.02	0.02	0.01	0.01	0.01	0	0.01	0.01	0.01	0.02	0.03	0	0.02
Cr_2O_3	0.46	0.35	0.41	0.75	0.58	0.47	0.48	0.43	0.52	0.44	0.35	0.34	0.30	0.44
NiO	0.33	0.32	0.33	0.40	0.30	0.33	0.31	0.34	0.32	0.35	0.35	0.37	0.40	0.31
LOI	5.07	2.71	3.89	4.76	3.50	5.85	4.31	2.43	3.59	4.68	2.52	3.46	4.70	3.49
Total	99.73	99.69	99.25	99.41	99.62	99.35	99.37	99.56	99.87	99.36	99.33	99.63	99.80	99.63
mg-no.	0.912	0.915	0.914	0.911	0.905	0.916	0.917	0.920	0.914	0.920	0.918	0.912	0.921	0.913
Calculated modes in wt%														
Olivine	79	82	83	67	72	81	79	75	78	83	80	89	75	77
Opx	15	8	9	22	14	12	13	20	13	13	17	6	22	12
Cpx	1	4	2	5	5	1	1	1	2	1	1	4	2	4
Garnet	5	6	7	6	9	7	8	5	8	3	3	2		7
Spinel													1	
Temperatures and pressures														
Temp (ºC)	1222	1042	1076	871	1262	1149	1300	1409	1219	1405	1301	1054	n.a.	1027
Press (kb)	52.7	44.7	46.5	33.5	54.6	48.4	55.1	63.6	53.4	63.7	57.1	45.3	n.a.	42.7

Prdt: peridotite; H-Prxn: High-Mg pyroxenite; L-Prxn: Low-Mg pyroxenite; Opx: orthopyroxene; Cpx: clinopyroxene; porphcl: porphyroclastic. Major elements in wt%. Total Fe is given as FeO and mg-no.=Mg/(Mg+Fe). LOI: loss on ignition. For analytical techniques see Chapter 2. Mode calculation procedures and temperature and pressure calculations are discussed in Chapter 2.

Table B-1. Continued.

Sample Rock Texture	NK1-15 Prdt coarse	NK1-16 Prdt coarse	NK1-17 Prdt coarse	NK1-18 Prdt coarse	NK1-19 Prdt coarse	NK1-20 Prdt coarse	NK1-21 Prdt coarse	NK1-22 Prdt coarse	NK1-23 Prdt coarse	NK2-1 Prdt coarse	NK2-2 Prdt porphcl	NK2-3 Prdt coarse	NK2-5 Prdt porphcl	NK2-6 Prdt porphcl
SiO_2	42.29	41.17	41.22	42.94	43.60	42.34	41.44	39.97	41.01	45.66	42.69	42.46	43.22	41.50
TiO_2	0.06	0.03	0.01	0.03	0.06	0.06	0.02	0.02	0.10	0.09	0.08	0.09	0.15	0.10
Al_2O_3	1.09	0.93	0.81	0.79	0.69	0.70	0.81	0.93	2.71	1.31	2.17	2.90	1.06	0.30
FeO	7.30	7.27	7.05	6.97	7.17	7.02	6.98	7.24	7.81	7.08	7.69	7.21	8.07	7.70
MnO	0.11	0.10	0.11	0.10	0.11	0.10	0.10	0.10	0.12	0.12	0.12	0.13	0.12	0.10
MgO	42.69	43.95	45.40	44.93	42.78	42.94	44.78	43.01	40.25	42.09	42.80	41.87	44.14	48.20
CaO	0.88	0.67	0.49	0.54	0.70	0.82	0.27	0.91	1.79	0.93	2.21	1.98	1.01	0.30
Na_2O	0.01	0	0.08	0.05	0.08	0.08	0	0.02	0.16	0.40	0.19	0.15	0.04	0.10
K_2O	0.12	0.03	0.03	0.03	0.05	0.06	0.03	0.02	0.10	0.16	0.11	0.19	0.05	0.10
P_2O_5	0.03	0.01	0.03	0.01	0.01	0.02	0.01	0.01	0.02	0.01	0.01	0.02	0.01	0
Cr_2O_3	0.38	0.48	0.47	0.35	0.33	0.30	0.51	0.47	0.41	0.48	0.37	0.71	0.46	0.30
NiO	0.34	0.33	0.31	0.35	0.32	0.30	0.35	0.35	0.29	0.30	0.32	0.31	0.33	0.40
LOI	4.09	4.58	3.88	2.75	3.65	5.00	4.55	6.46	4.68	1.32	1.14	1.77	1.01	0.90
Total	99.39	99.52	99.89	99.84	99.55	99.73	99.82	99.50	99.46	99.94	99.89	99.80	99.67	99.80
mg-no.	0.913	0.915	0.920	0.920	0.914	0.916	0.920	0.914	0.902	0.914	0.908	0.912	0.907	0.918
Calculated modes in wt%														
Olivine	74	81	85	78	70	75	81	83	74	65	77	73	77	90
Opx	18	12	9	17	25	19	14	9	8	27	5	7	16	7
Cpx	3	1	1	1	2	3	0	3	7	5	10	8	3	2
Garnet	5	5	4	4	3	3	5	5	11	3	8	12	5	
Spinel														1
Temperatures and pressures														
Temp (ºC)	1131	n.a.	989	1223	1228	n.a.	n.a.	1265	964	1216	1316	887	1371	n.a.
Press (kb)	48.0	n.a.	40.6	52.1	51.9	n.a.	n.a.	53.5	39.0	51.5	54.7	34.6	57.9	n.a.

Table B-1. Continued.

Sample	NK2-8	NK2-9	NK2-10	NK3-2	NK3-3	NK3-4	NK3-5	NK3-6	NK3-7	NK3-10	NK3-11	NK3-12	NK3-13	NK3-15
Rock	Prdt	Prdt	Prdt	Prdt	Prdt	Prdt	Prdt	Prdt	Prdt	Prdt	Prdt	Prdt	Prdt	Prdt
Texture	coarse	coarse	coarse	fluidal	coarse	coarse	coarse	coarse	coarse	coarse	coarse	coarse	coarse	coarse
SiO_2	43.90	42.00	41.54	41.43	43.20	41.02	42.08	42.09	38.07	39.60	40.88	39.60	39.05	40.83
TiO_2	0	0	0.03	0.04	0	0.11	0.02	0.04	0.12	0.10	0.06	0.10	0.05	0.07
Al_2O_3	1.30	0.60	1.25	1.28	0.60	3.34	0.44	0.99	2.16	1.20	1.10	0.30	1.07	1.39
FeO	7.10	7.30	7.43	6.79	6.90	7.15	6.71	6.51	6.76	7.00	6.99	6.70	6.96	6.47
MnO	0.10	0.10	0.11	0.10	0.10	0.11	0.10	0.09	0.10	0.10	0.10	0.10	0.09	0.09
MgO	43.10	47.10	45.53	40.93	45.60	37.17	43.99	42.72	39.63	42.10	42.70	44.40	40.95	40.67
CaO	0.60	0.20	1.22	1.72	0.40	3.64	0.76	1.00	4.55	1.30	2.80	0.80	2.28	2.82
Na_2O	0	0.10	0.07	0	0.10	0.21	0.03	0.04	0.03	0	0.10	0	0.18	0.04
K_2O	0	0	0.05	0.08	0.10	0.32	0.07	0.08	0.28	0.20	0.05	0	0.07	0.07
P_2O_5	0	0	0.04	0.02	0	0.02	0.01	0.02	0.02	0	0.02	0	0.02	0.02
Cr_2O_3	0.50	0.50	0.36	0.43	0.50	0.43	0.34	0.31	0.45	0.50	0.54	0.30	0.59	0.38
NiO	0.30	0.40	0.32	0.31	0.30	0.28	0.34	0.30	0.31	0.30	0.31	0.30	0.30	0.34
LOI	3.00	1.60	1.84	6.54	2.20	5.57	4.88	5.55	6.75	7.40	3.88	6.70	8.11	6.32
Total	99.80	99.80	99.79	99.64	99.90	99.37	99.77	99.73	99.22	99.80	99.54	99.20	99.71	99.50
mg-no.	0.916	0.920	0.916	0.915	0.922	0.903	0.921	0.921	0.913	0.914	0.916	0.922	0.913	0.918
Calculated modes in wt%														
Olivine	65	84	86	72	75	68	78	74	74	78	82	85	84	75
Opx	31	14	4	15	22	2	17	18	0	14	0	10	0	6
Cpx	3	1	5	6	2	17	3	3	19	7	13	4	12	12
Garnet			6	7		13	2	5	8		5		5	6
Spinel	2	1			1					2		1		
Temperatures and pressures														
Temp (ºC)	n.a.	n.a.	1014	1023	n.a.	1371	1194	1253	1213	n.a.	1247	n.a.	830	1343
Press (kb)	n.a.	n.a.	42.1	34.3	n.a.	59.6	52.4	53.4	51.0	n.a.	53.1	n.a.	30.9	58.5

Table B-1. Continued.

Sample Rock Texture	NK3-16 Prdt coarse	NK3-18 Prdt coarse	NK3-20 Prdt coarse	NK3-22 Prdt porphcl	NK3-24 Prdt coarse	NK3-25 Prdt coarse	NK2-7 H-Prxn coarse	NK3-14 H-Prxn coarse	NK3-1 L-Prxn coarse	NK3-8 L-Prxn coarse	NK3-17 L-Prxn coarse
SiO_2	40.45	40.60	43.19	42.10	45.04	41.42	48.95	40.72	50.97	50.35	50.15
TiO_2	0.06	0.10	0.10	0	0.03	0.21	0.13	0.23	0.18	3.76	0.18
Al_2O_3	0.93	0.40	3.21	3.30	2.24	4.28	8.05	11.40	4.71	0.81	4.89
FeO	7.93	7.30	7.58	7.60	6.19	7.41	4.93	6.85	6.04	10.26	6.01
MnO	0.10	0.10	0.13	0.20	0.12	0.13	0.18	0.24	0.15	0.15	0.15
MgO	44.79	45.40	37.50	42.00	39.84	39.46	23.69	27.87	19.44	30.84	19.48
CaO	1.54	0.70	3.21	1.80	2.19	2.13	9.45	4.68	16.46	1.76	16.91
Na_2O	0.08	0	0.35	0	0.08	0.09	0.90	0.36	0.46	0.24	0.28
K_2O	0.04	0.20	0.14	0.10	0.05	0.52	0.11	1.13	0.11	0.15	0.09
P_2O_5	0.01	0	0.02	0	0.01	0.04	0.01	0.11	0.02	0.02	0.01
Cr_2O_3	0.30	0.40	0.46	0.70	0.66	0.75	1.16	1.50	0.54	0.02	0.50
NiO	0.32	0.30	0.28	0.30	0.24	0.25	0.38	0.22	0.09	0.03	0.09
LOI	3.01	4.50	3.30	1.70	3.10	2.81	1.90	4.07	0.52	1.24	0.58
Total	99.56	99.90	99.47	99.60	99.79	99.51	99.84	99.37	99.70	99.63	99.32
mg-no.	0.910	0.918	0.898	0.908	0.920	0.905	0.895	0.879	0.852	0.843	0.852
Calculated modes in wt%											
Olivine	89	84	62	68	57	70	4	9	0	n.a.	0
Opx	0	11	11	20	26	5	41	44	24	n.a.	22
Cpx	7	3	15	9	7	8	39	22	67	n.a.	68
Garnet	4		12		11	17	15	25	9	n.a.	10
Spinel		1		3						n.a.	
Temperatures and pressures											
Temp (ºC)	1280	n.a.	815	n.a.	770	1256	737	933	759	n.a.	720
Press (kb)	53.5	n.a.	29.8	n.a.	24.7	54.0	25.3	36.8	25.1	n.a.	22.2

Table B-2. Major element analyses of olivine.

Sample	NK1-1	NK1-2	NK1-3	NK1-4	NK1-5	NK1-6	NK1-7	NK1-8	NK1-9	NK1-10	NK1-11	NK1-12	NK1-13	NK1-14
Rock	Prdt	Prdt	Prdt	Prdt	Prdt	Prdt	Prdt	Prdt	Prdt	Prdt	Prdt	Prdt	Prdt	Prdt
# anal.	15	9	8	5	8	16	15	18	17	15	14	14	14	9
SiO_2	40.81	41.02	41.03	40.95	41.28	40.81	41.01	40.97	40.62	40.73	41.21	40.70	40.80	41.01
FeO	7.84	7.48	7.37	7.53	8.05	7.15	7.35	7.28	7.95	7.20	7.36	7.76	6.61	7.39
MnO	0.11	0.10	0.10	0.11	0.10	0.10	0.10	0.10	0.11	0.10	0.10	0.11	0.09	0.09
MgO	50.71	50.20	50.43	50.26	50.62	51.30	50.67	50.48	50.57	51.02	51.02	50.53	51.31	50.34
CaO	0.04	0.01	0.01	0.00	0.05	0.02	0.05	0.04	0.03	0.03	0.04	0.01	0.03	0.02
Cr_2O_3	0.03	0.01	0.01	0.01	0.03	0.02	0.04	0.04	0.03	0.03	0.03	0.01	0.04	0.01
NiO	0.38	0.35	0.35	0.39	0.37	0.38	0.37	0.41	0.38	0.40	0.39	0.39	0.41	0.36
Total	99.92	99.16	99.30	99.24	100.50	99.76	99.59	99.32	99.69	99.53	100.16	99.51	99.28	99.22
mg-no.	0.920	0.923	0.924	0.922	0.918	0.927	0.925	0.925	0.919	0.927	0.925	0.921	0.933	0.924
Cation proportions														
Si	0.993	1.003	1.002	1.001	0.999	0.992	0.999	1.000	0.992	0.993	0.998	0.994	0.994	1.002
Fe	0.159	0.153	0.150	0.154	0.163	0.145	0.150	0.149	0.162	0.147	0.149	0.159	0.135	0.151
Mn	0.002	0.002	0.002	0.002	0.002	0.002	0.002	0.002	0.002	0.002	0.002	0.002	0.002	0.002
Mg	1.841	1.831	1.836	1.832	1.827	1.859	1.840	1.838	1.841	1.855	1.842	1.841	1.864	1.834
Ca	0.001	0.000	0.000	0.000	0.001	0.000	0.001	0.001	0.001	0.001	0.001	0.000	0.001	0.001
Cr	0.001	0.000	0.000	0.000	0.001	0.000	0.001	0.001	0.001	0.001	0.001	0.000	0.001	0.000
Ni	0.007	0.007	0.007	0.008	0.007	0.007	0.007	0.008	0.007	0.008	0.008	0.008	0.008	0.007
Sum	3.005	2.996	2.997	2.998	3.000	3.007	3.000	2.998	3.007	3.006	3.000	3.005	3.005	2.997

Prdt: peridotite; H-Prxn: High-Mg pyroxenite; [a]porphyroclastic olivine; [b]olivine inclusion in garnet. Major elements in wt%. Total Fe is given as FeO and mg-no.=Mg/(Mg+Fe). For analytical techniques see Chapter 2.

Table B-2. Continued.

Sample	NK1-15	NK1-16	NK1-17	NK1-18	Nk1-19	NK1-20	NK1-22	NK1-23	NK2-1	NK2-2	NK2-3	NK2-5	NK2-5[a]	NK2-6
Rock	Prdt	Prdt	Prdt	Prdt	Prdt	Prdt	Prdt	Prdt	Prdt	Prdt	Prdt	Prdt	Prdt	Prdt
# anal.	10	14	17	9	15	10	15	16	14	15	10	11	7	11
SiO_2	40.94	41.01	40.94	41.26	41.10	41.35	41.24	40.78	41.27	40.41	41.43	41.13	40.98	41.15
FeO	7.37	7.36	7.09	7.21	7.88	7.21	7.34	8.53	7.84	8.14	7.07	8.31	8.22	7.39
MnO	0.10	0.10	0.10	0.10	0.11	0.10	0.10	0.09	0.11	0.10	0.10	0.12	0.11	0.10
MgO	50.52	50.84	51.04	50.88	50.34	50.98	50.97	50.47	50.57	50.46	51.04	50.06	50.01	50.60
CaO	0.03	0.05	0.02	0.03	0.05	0.02	0.05	0.01	0.05	0.06	0.01	0.07	0.07	0.05
Cr_2O_3	0.02	0.05	0.01	0.04	0.06	0.04	0.05	0.00	0.03	0.03	0.00	0.05	0.07	0.04
NiO	0.41	0.36	0.36	0.43	0.42	0.43	0.35	0.37	0.38	0.36	0.40	0.38	0.37	0.35
Total	99.39	99.78	99.55	99.96	99.95	100.13	100.10	100.25	100.27	99.56	100.05	100.13	99.83	99.68
mg-no.	0.924	0.925	0.928	0.926	0.919	0.927	0.925	0.913	0.920	0.917	0.928	0.915	0.916	0.924
Cation proportions														
Si	0.999	0.997	0.996	1.000	1.000	1.001	0.999	0.992	1.000	0.989	1.002	1.000	0.999	1.001
Fe	0.150	0.150	0.144	0.146	0.160	0.146	0.149	0.174	0.159	0.167	0.143	0.169	0.168	0.150
Mn	0.002	0.002	0.002	0.002	0.002	0.002	0.002	0.002	0.002	0.002	0.002	0.002	0.002	0.002
Mg	1.839	1.843	1.852	1.840	1.826	1.840	1.841	1.832	1.827	1.842	1.841	1.815	1.818	1.835
Ca	0.001	0.001	0.000	0.001	0.001	0.001	0.001	0.000	0.001	0.001	0.000	0.002	0.002	0.001
Cr	0.000	0.001	0.000	0.001	0.001	0.001	0.001	0.000	0.001	0.001	0.000	0.001	0.001	0.001
Ni	0.008	0.007	0.007	0.008	0.008	0.008	0.007	0.007	0.007	0.007	0.008	0.007	0.007	0.007
Sum	3.000	3.001	3.003	2.998	2.998	2.998	2.999	3.007	2.998	3.009	2.997	2.997	2.997	2.997

Table B-2. Continued.

Sample	NK2-6[a]	NK2-8	NK2-9	NK2-10	NK2-10[b]	NK3-3	NK3-4	NK3-5	NK3-6	NK3-7	NK3-10	NK3-11	NK3-12	NK3-13
Rock	Prdt	Prdt	Prdt	Prdt	Prdt	Prdt	Prdt	Prdt	Prdt	Prdt	Prdt	Prdt	Prdt	Prdt
# anal.	12	13	12	12	4	10	15	14	22	14	14	13	10	12
SiO_2	41.14	40.73	41.22	40.78	41.06	41.56	40.68	41.37	41.09	40.68	41.30	41.11	40.95	41.24
FeO	7.37	7.37	7.21	7.43	8.21	7.08	8.45	7.38	7.46	7.67	6.88	7.66	7.15	7.81
MnO	0.11	0.10	0.11	0.10	0.13	0.09	0.11	0.11	0.10	0.11	0.10	0.11	0.11	0.11
MgO	50.54	50.73	51.23	50.83	50.28	51.23	50.52	50.94	50.67	50.36	51.66	50.44	51.49	50.93
CaO	0.05	0.00	0.01	0.01	0.04	0.01	0.05	0.04	0.06	0.04	0.01	0.04	0.04	0.01
Cr_2O_3	0.04	0.00	0.00	0.01	0.03	0.00	0.02	0.03	0.03	0.02	0.00	0.04	0.04	0.00
NiO	0.35	0.42	0.37	0.36	0.36	0.38	0.29	0.42	0.40	0.37	0.35	0.37	0.37	0.35
Total	99.59	99.35	100.15	99.53	100.11	100.36	100.10	100.28	99.81	99.25	100.31	99.77	100.14	100.46
mg-no.	0.924	0.925	0.927	0.924	0.916	0.928	0.914	0.925	0.924	0.921	0.930	0.922	0.928	0.921
Cation proportions														
Si	1.001	0.995	0.998	0.995	0.998	1.002	0.991	1.000	0.999	0.996	0.996	1.000	0.992	0.998
Fe	0.150	0.151	0.146	0.152	0.167	0.143	0.172	0.149	0.152	0.157	0.139	0.156	0.145	0.158
Mn	0.002	0.002	0.002	0.002	0.003	0.002	0.002	0.002	0.002	0.002	0.002	0.002	0.002	0.002
Mg	1.834	1.848	1.849	1.849	1.823	1.843	1.835	1.837	1.837	1.839	1.859	1.830	1.859	1.837
Ca	0.001	0.000	0.000	0.000	0.001	0.000	0.001	0.001	0.001	0.001	0.000	0.001	0.001	0.000
Cr	0.001	0.000	0.000	0.000	0.001	0.000	0.000	0.001	0.001	0.000	0.000	0.001	0.001	0.000
Ni	0.007	0.008	0.007	0.007	0.007	0.007	0.006	0.008	0.008	0.007	0.007	0.007	0.007	0.007
Sum	2.997	3.004	3.002	3.005	3.000	2.997	3.008	2.998	3.000	3.003	3.003	2.998	3.007	3.002

Table B-2. Continued.

Sample	NK3-15	NK3-16	NK3-18	NK3-20	NK3-22	NK3-23	NK3-24	NK3-25	NK3-14	NK3-19
Rock	Prdt	Prdt	Prdt	Prdt	Prdt	Prdt	Prdt	Prdt	H-Prxn	H-Prxn
# anal.	14	18	15	15	12	16	10	10	8	17
SiO_2	40.38	41.13	41.19	40.81	40.63	40.82	40.45	41.29	40.75	41.48
FeO	7.16	8.26	7.56	8.23	7.68	7.83	7.13	8.47	8.01	7.62
MnO	0.10	0.10	0.11	0.10	0.10	0.10	0.09	0.11	0.12	0.12
MgO	51.08	50.26	51.26	50.42	50.83	50.87	51.33	50.48	50.12	51.15
CaO	0.04	0.05	0.04	0.02	0.01	0.04	0.01	0.05	0.01	0.02
Cr_2O_3	0.02	0.03	0.03	0.01	0.00	0.03	0.00	0.02	0.00	0.01
NiO	0.43	0.35	0.36	0.33	0.39	0.39	0.40	0.36	0.35	0.32
Total	99.21	100.18	100.55	99.91	99.64	100.07	99.41	100.79	99.36	100.71
mg-no.	0.927	0.916	0.924	0.916	0.922	0.921	0.928	0.914	0.918	0.923
Cation proportions										
Si	0.988	0.999	0.995	0.995	0.992	0.992	0.988	0.998	0.998	0.999
Fe	0.147	0.168	0.153	0.168	0.157	0.159	0.146	0.171	0.164	0.153
Mn	0.002	0.002	0.002	0.002	0.002	0.002	0.002	0.002	0.002	0.002
Mg	1.864	1.821	1.846	1.833	1.850	1.844	1.869	1.820	1.830	1.838
Ca	0.001	0.001	0.001	0.001	0.000	0.001	0.000	0.001	0.000	0.001
Cr	0.000	0.001	0.001	0.000	0.000	0.001	0.000	0.000	0.000	0.000
Ni	0.008	0.007	0.007	0.006	0.008	0.008	0.008	0.007	0.007	0.006
Sum	3.010	2.999	3.004	3.004	3.008	3.006	3.012	3.000	3.001	3.000

Table B-3. Major element analyses of orthopyroxene.

Sample	NK1-1	NK1-2	NK1-3	NK1-4	NK1-5	NK1-6	NK1-7	NK1-8	NK1-9	NK1-10	NK1-11	NK1-12	NK1-13	NK1-14
Rock	Prdt	Prdt	Prdt	Prdt	Prdt	Prdt	Prdt	Prdt	Prdt	Prdt	Prdt	Prdt	Prdt	Prdt
# anal.	10	5	7	11	10	5	12	20	8	16	13	22	17	11
SiO_2	57.25	57.11	57.18	56.76	56.69	56.49	57.44	57.82	57.76	57.83	57.25	58.01	57.19	58.06
TiO_2	0.14	0.04	0.05	0.05	0.09	0.04	0.04	0.03	0.08	0.02	0.05	0.05	0.07	0.04
Al_2O_3	1.18	0.95	0.97	0.98	1.22	1.17	1.36	1.21	1.11	1.19	1.20	1.00	0.69	1.02
FeO	5.09	4.72	4.65	4.70	5.00	4.54	4.42	4.39	5.18	4.37	4.61	4.74	4.29	4.58
MnO	0.12	0.12	0.13	0.13	0.13	0.11	0.11	0.10	0.12	0.11	0.12	0.13	0.11	0.11
MgO	34.98	35.80	35.89	36.08	35.00	35.89	34.99	35.23	35.11	35.43	35.57	35.45	35.81	35.64
CaO	0.63	0.34	0.30	0.26	0.71	0.39	0.93	0.67	0.57	0.58	0.63	0.33	0.49	0.36
Na_2O	0.12	0.09	0.08	0.06	0.14	0.14	0.18	0.14	0.13	0.11	0.13	0.15	0.10	0.08
Cr_2O_3	0.61	0.38	0.34	0.31	0.49	0.48	0.54	0.58	0.49	0.59	0.59	0.35	0.45	0.36
NiO	0.10	0.08	0.08	0.08	0.10	0.10	0.10	0.11	0.10	0.12	0.12	0.10	0.11	0.09
Total	100.23	99.62	99.68	99.39	99.57	99.34	100.10	100.30	100.65	100.34	100.26	100.30	99.31	100.34
mg-no.	0.925	0.931	0.932	0.932	0.926	0.934	0.934	0.935	0.924	0.935	0.932	0.930	0.937	0.933
Cation proportions														
Si	1.964	1.965	1.966	1.958	1.958	1.951	1.967	1.974	1.971	1.973	1.959	1.980	1.972	1.979
Ti	0.004	0.001	0.001	0.001	0.002	0.001	0.001	0.001	0.002	0.001	0.001	0.001	0.002	0.001
Al	0.048	0.038	0.039	0.040	0.049	0.047	0.055	0.049	0.045	0.048	0.049	0.040	0.028	0.041
Fe	0.146	0.136	0.134	0.136	0.144	0.131	0.127	0.125	0.148	0.125	0.132	0.135	0.124	0.130
Mn	0.004	0.003	0.004	0.004	0.004	0.003	0.003	0.003	0.003	0.003	0.003	0.004	0.003	0.003
Mg	1.789	1.837	1.839	1.856	1.803	1.849	1.787	1.793	1.787	1.802	1.816	1.804	1.841	1.812
Ca	0.023	0.013	0.011	0.009	0.026	0.014	0.034	0.024	0.021	0.021	0.023	0.012	0.018	0.013
Na	0.008	0.006	0.005	0.004	0.009	0.010	0.012	0.009	0.008	0.007	0.009	0.010	0.007	0.006
Cr	0.016	0.010	0.009	0.009	0.013	0.013	0.015	0.016	0.013	0.016	0.016	0.010	0.012	0.010
Ni	0.003	0.002	0.002	0.002	0.003	0.003	0.003	0.003	0.003	0.003	0.003	0.003	0.003	0.002
Sum	4.004	4.012	4.011	4.018	4.012	4.022	4.002	3.998	4.002	3.998	4.011	3.999	4.009	3.997

Prdt: peridotite; H-Prxn: High-Mg pyroxenite; L-Prxn: Low-Mg pyroxenite; [a]porphyroclastic orthopyroxene. Major elements in wt%. Total Fe is given as FeO and mg-no.=Mg/(Mg+Fe). For analytical techniques see Chapter 2.

Table B-3. Continued.

Sample	NK1-15	NK1-16	NK1-17	NK1-18	NK1-19	NK1-20	NK1-22	NK1-23	NK2-1	NK2-2	NK2-3	NK2-5	NK2-5[a]	NK2-6
Rock	Prdt	Prdt	Prdt	Prdt	Prdt	Prdt	Prdt	Prdt	Prdt	Prdt	Prdt	Prdt	Prdt	Prdt
# anal.	7	8	8	12	17	30	15	23	16	6	8	9	5	11
SiO_2	56.52	56.66	57.14	56.72	56.93	57.08	57.18	57.66	56.77	56.70	56.66	56.77	56.97	57.33
TiO_2	0.01	0.02	0.01	0.03	0.10	0.02	0.03	0.06	0.06	0.10	0.08	0.27	0.28	0.16
Al_2O_3	1.11	1.35	1.00	1.22	1.27	1.24	1.32	1.00	1.24	1.48	0.96	1.48	1.52	1.19
FeO	4.73	4.61	4.56	4.59	4.98	4.58	4.61	5.34	4.82	5.10	4.58	5.19	5.19	4.62
MnO	0.10	0.09	0.11	0.10	0.10	0.11	0.11	0.11	0.12	0.11	0.11	0.12	0.13	0.12
MgO	35.62	35.44	36.11	35.47	35.14	35.45	35.25	35.45	34.97	35.18	35.97	34.38	34.44	35.23
CaO	0.52	0.84	0.35	0.68	0.89	0.58	0.85	0.20	0.73	0.87	0.23	1.09	1.09	0.73
Na_2O	0.10	0.15	0.09	0.15	0.15	0.11	0.15	0.04	0.14	0.17	0.04	0.18	0.19	0.15
Cr_2O_3	0.49	0.68	0.36	0.59	0.60	0.60	0.68	0.23	0.55	0.33	0.27	0.64	0.66	0.61
NiO	0.11	0.10	0.08	0.11	0.12	0.11	0.10	0.07	0.11	0.11	0.09	0.11	0.11	0.10
Total	99.31	99.95	99.81	99.66	100.28	99.88	100.28	100.18	99.49	100.15	98.99	100.24	100.57	100.23
mg-no.	0.931	0.932	0.934	0.932	0.926	0.932	0.932	0.922	0.928	0.925	0.933	0.922	0.922	0.931
Cation proportions														
Si	1.955	1.949	1.962	1.954	1.954	1.960	1.958	1.975	1.960	1.949	1.961	1.952	1.952	1.963
Ti	0.000	0.001	0.000	0.001	0.003	0.001	0.001	0.002	0.002	0.003	0.002	0.007	0.007	0.004
Al	0.045	0.055	0.040	0.050	0.051	0.050	0.053	0.041	0.051	0.060	0.039	0.060	0.061	0.048
Fe	0.137	0.133	0.131	0.132	0.143	0.132	0.132	0.153	0.139	0.147	0.133	0.149	0.149	0.132
Mn	0.003	0.003	0.003	0.003	0.003	0.003	0.003	0.003	0.003	0.003	0.003	0.004	0.004	0.003
Mg	1.837	1.817	1.849	1.822	1.798	1.815	1.800	1.810	1.800	1.803	1.856	1.763	1.760	1.798
Ca	0.019	0.031	0.013	0.025	0.033	0.021	0.031	0.007	0.027	0.032	0.009	0.040	0.040	0.027
Na	0.007	0.010	0.006	0.010	0.010	0.007	0.010	0.002	0.009	0.011	0.002	0.012	0.012	0.010
Cr	0.013	0.019	0.010	0.016	0.016	0.016	0.018	0.006	0.015	0.009	0.007	0.017	0.018	0.017
Ni	0.003	0.003	0.002	0.003	0.003	0.003	0.003	0.002	0.003	0.003	0.002	0.003	0.003	0.003
Sum	4.019	4.019	4.016	4.017	4.014	4.009	4.010	4.001	4.009	4.020	4.015	4.008	4.007	4.005

Table B-3. Continued.

Sample	NK2-6[a]	NK2-8	NK2-9	NK2-10	NK3-2	NK3-3	NK3-4	NK3-5	NK3-6	NK3-7	NK3-10	NK3-11	NK3-12	NK3-13
Rock	Prdt	Prdt	Prdt	Prdt	Prdt	Prdt	Prdt	Prdt	Prdt	Prdt	Prdt	Prdt	Prdt	Prdt
# anal.	9	13	12	8	8	14	15	11	4	5	16	3	22	12
SiO_2	57.18	56.32	56.75	56.78	52.85	57.41	57.09	57.54	57.18	56.82	57.07	57.47	57.04	57.21
TiO_2	0.15	0.00	0.00	0.05	0.05	0.00	0.07	0.02	0.02	0.10	0.03	0.09	0.08	0.04
Al_2O_3	1.19	1.92	1.94	1.01	1.88	1.68	1.34	1.07	1.27	1.27	2.09	1.26	0.85	0.98
FeO	4.60	5.25	4.87	4.79	22.04	4.58	5.39	4.60	4.66	4.89	4.43	4.75	4.40	4.99
MnO	0.12	0.14	0.13	0.10	0.16	0.13	0.12	0.12	0.11	0.10	0.13	0.11	0.12	0.13
MgO	35.25	35.20	35.14	35.98	22.90	35.16	34.90	35.75	35.44	35.56	35.54	35.28	35.70	35.62
CaO	0.73	0.18	0.54	0.35	0.35	0.56	0.76	0.65	0.81	0.70	0.20	0.77	0.61	0.24
Na_2O	0.15	0.01	0.01	0.10	0.03	0.01	0.14	0.08	0.12	0.13	0.02	0.16	0.12	0.04
Cr_2O_3	0.63	0.27	0.50	0.33	0.03	0.45	0.27	0.53	0.46	0.38	0.25	0.61	0.54	0.25
NiO	0.10	0.07	0.08	0.10	0.02	0.07	0.11	0.11	0.11	0.10	0.07	0.11	0.10	0.07
Total	100.10	99.36	99.95	99.59	100.30	100.04	100.17	100.46	100.17	100.05	99.81	100.62	99.56	99.55
mg-no.	0.932	0.923	0.928	0.931	0.649	0.932	0.920	0.933	0.931	0.928	0.935	0.930	0.935	0.927
Cation proportions														
Si	1.961	1.946	1.948	1.957	1.954	1.964	1.961	1.964	1.959	1.952	1.954	1.961	1.964	1.970
Ti	0.004	0.000	0.000	0.001	0.001	0.000	0.002	0.000	0.001	0.003	0.001	0.002	0.002	0.001
Al	0.048	0.078	0.079	0.041	0.082	0.068	0.054	0.043	0.051	0.051	0.084	0.051	0.035	0.040
Fe	0.132	0.152	0.140	0.138	0.681	0.131	0.155	0.131	0.133	0.140	0.127	0.136	0.127	0.144
Mn	0.004	0.004	0.004	0.003	0.005	0.004	0.003	0.003	0.003	0.003	0.004	0.003	0.004	0.004
Mg	1.802	1.814	1.799	1.849	1.263	1.794	1.788	1.820	1.811	1.821	1.814	1.796	1.833	1.829
Ca	0.027	0.006	0.020	0.013	0.014	0.020	0.028	0.024	0.030	0.026	0.007	0.028	0.022	0.009
Na	0.010	0.001	0.000	0.006	0.002	0.001	0.010	0.005	0.008	0.009	0.001	0.011	0.008	0.002
Cr	0.017	0.007	0.013	0.009	0.001	0.012	0.007	0.014	0.013	0.010	0.007	0.017	0.015	0.007
Ni	0.003	0.002	0.002	0.003	0.001	0.002	0.003	0.003	0.003	0.003	0.002	0.003	0.003	0.002
Sum	4.007	4.011	4.006	4.020	4.004	3.996	4.011	4.009	4.012	4.019	4.000	4.007	4.012	4.007

Table B-3. Continued.

Sample	NK3-15	NK3-16	NK3-18	NK3-20	NK3-22	NK3-23	NK3-24	NK3-25	NK2-7	NK3-14	NK3-19	NK3-1	NK3-8	NK3-17
Rock	Prdt	Prdt	Prdt	Prdt	Prdt	Prdt	Prdt	Prdt	H-Prxn	H-Prxn	H-Prxn	L-Prxn	L-Prxn	L-Prxn
# anal.	19	13	9	10	15	8	11	7	7	4	18	8	12	5
SiO_2	57.73	56.56	56.70	57.07	57.58	56.81	57.82	56.79	57.02	57.59	57.33	56.16	57.00	55.64
TiO_2	0.07	0.16	0.11	0.06	0.03	0.03	0.02	0.09	0.06	0.07	0.04	0.03	0.24	0.02
Al_2O_3	1.29	1.40	0.85	0.99	1.45	1.14	1.22	1.24	0.95	1.03	0.94	1.11	0.76	1.17
FeO	4.36	5.12	4.80	5.73	4.87	4.76	4.55	5.34	4.97	4.98	4.92	9.68	7.94	9.66
MnO	0.10	0.12	0.12	0.11	0.12	0.10	0.11	0.12	0.11	0.11	0.13	0.14	0.14	0.12
MgO	35.23	34.61	35.19	35.31	35.34	35.21	35.97	34.78	35.70	35.74	35.57	32.66	33.43	32.55
CaO	0.74	0.79	0.64	0.21	0.37	0.66	0.21	0.68	0.22	0.28	0.34	0.20	0.84	0.22
Na_2O	0.13	0.17	0.12	0.02	0.03	0.11	0.02	0.13	0.03	0.11	0.10	0.01	0.11	0.00
Cr_2O_3	0.45	0.48	0.52	0.22	0.36	0.48	0.27	0.35	0.18	0.34	0.36	0.18	0.01	0.17
NiO	0.12	0.10	0.10	0.07	0.07	0.11	0.08	0.10	0.08	0.08	0.09	0.15	0.02	0.15
Total	100.22	99.51	99.15	99.79	100.22	99.41	100.26	99.62	99.33	100.33	99.82	100.32	100.48	99.71
mg-no.	0.935	0.923	0.929	0.917	0.928	0.930	0.934	0.921	0.928	0.928	0.928	0.857	0.882	0.857
Cation proportions														
Si	1.972	1.956	1.965	1.967	1.968	1.962	1.971	1.962	1.968	1.968	1.970	1.961	1.973	1.956
Ti	0.002	0.004	0.003	0.002	0.001	0.001	0.001	0.002	0.002	0.002	0.001	0.001	0.006	0.001
Al	0.052	0.057	0.035	0.040	0.058	0.047	0.049	0.050	0.039	0.041	0.038	0.046	0.031	0.048
Fe	0.125	0.148	0.139	0.165	0.139	0.137	0.130	0.154	0.144	0.142	0.141	0.283	0.230	0.284
Mn	0.003	0.003	0.004	0.003	0.003	0.003	0.003	0.004	0.003	0.003	0.004	0.004	0.004	0.004
Mg	1.794	1.785	1.818	1.815	1.801	1.813	1.829	1.792	1.837	1.822	1.823	1.701	1.725	1.706
Ca	0.027	0.029	0.024	0.008	0.014	0.024	0.008	0.025	0.008	0.010	0.013	0.008	0.031	0.008
Na	0.009	0.012	0.008	0.001	0.002	0.007	0.001	0.009	0.002	0.007	0.007	0.000	0.008	0.000
Cr	0.012	0.013	0.014	0.006	0.010	0.013	0.007	0.010	0.005	0.009	0.010	0.005	0.000	0.005
Ni	0.003	0.003	0.003	0.002	0.002	0.003	0.002	0.003	0.002	0.002	0.003	0.004	0.000	0.004
Sum	3.998	4.010	4.012	4.009	3.998	4.011	4.001	4.010	4.009	4.008	4.008	4.012	4.009	4.017

Table B-4. Major element analyses of clinopyroxene.

Sample	NK1-1	NK1-2	NK1-3	NK1-4	NK1-5	NK1-6	NK1-7	NK1-8	NK1-9	NK1-10	NK1-11	NK1-12	NK1-13	NK1-14
Rock	Prdt	Prdt	Prdt	Prdt	Prdt	Prdt	Prdt	Prdt	Prdt	Prdt	Prdt	Prdt	Prdt	Prdt
# anal.	7	9	5	10	15	5	9	5	14	11	6	13	9	8
SiO_2	53.73	53.89	54.19	54.21	54.72	54.07	54.11	55.45	54.36	54.62	54.48	55.22	53.76	53.86
TiO_2	0.29	0.13	0.13	0.10	0.17	0.13	0.08	0.42	0.15	0.87	0.69	0.16	0.45	0.12
Al_2O_3	2.28	2.74	2.98	2.93	2.52	3.70	2.36	1.07	2.64	1.46	0.94	3.76	0.64	2.67
FeO	2.45	2.25	2.31	1.61	2.65	2.35	2.34	2.73	2.45	3.17	2.93	2.57	2.41	2.19
MnO	0.07	0.08	0.09	0.06	0.10	0.07	0.08	0.09	0.09	0.12	0.13	0.08	0.09	0.07
MgO	17.12	16.07	15.84	15.94	17.52	14.91	18.07	19.73	16.58	19.19	19.03	14.97	19.44	16.06
CaO	18.91	19.67	19.14	20.54	18.87	17.20	18.68	18.51	18.82	18.28	19.71	17.39	20.46	19.59
Na_2O	1.92	2.20	2.46	2.19	1.93	3.36	1.61	0.85	2.07	1.14	1.06	3.48	0.68	2.27
Cr_2O_3	2.47	2.22	2.27	1.96	1.96	3.26	1.77	0.85	2.21	1.36	1.42	2.64	0.99	2.19
NiO	0.06	0.04	0.04	0.04	0.05	0.04	0.06	0.04	0.05	0.03	0.03	0.04	0.04	0.04
Total	99.29	99.30	99.45	99.59	100.48	99.10	99.18	99.75	99.41	100.26	100.40	100.30	98.98	99.06
mg-no.	0.926	0.927	0.924	0.946	0.922	0.919	0.932	0.928	0.923	0.915	0.921	0.912	0.935	0.929
Cation proportions														
Si	1.958	1.964	1.970	1.966	1.965	1.969	1.965	1.993	1.973	1.964	1.964	1.984	1.964	1.967
Ti	0.008	0.004	0.004	0.003	0.005	0.004	0.002	0.011	0.004	0.023	0.019	0.004	0.012	0.003
Al	0.098	0.118	0.128	0.125	0.107	0.159	0.101	0.046	0.113	0.062	0.040	0.159	0.028	0.115
Fe	0.075	0.069	0.070	0.049	0.080	0.072	0.071	0.082	0.074	0.095	0.088	0.077	0.074	0.067
Mn	0.002	0.003	0.003	0.002	0.003	0.002	0.003	0.003	0.003	0.004	0.004	0.002	0.003	0.002
Mg	0.930	0.873	0.859	0.862	0.939	0.810	0.978	1.057	0.897	1.029	1.023	0.802	1.059	0.874
Ca	0.738	0.768	0.745	0.798	0.726	0.671	0.727	0.713	0.732	0.705	0.761	0.670	0.801	0.766
Na	0.136	0.156	0.173	0.154	0.134	0.237	0.113	0.060	0.145	0.080	0.074	0.243	0.048	0.161
Cr	0.071	0.064	0.065	0.056	0.056	0.094	0.051	0.024	0.063	0.039	0.041	0.075	0.029	0.063
Ni	0.002	0.001	0.001	0.001	0.001	0.001	0.002	0.001	0.002	0.001	0.001	0.001	0.001	0.001
Sum	4.017	4.019	4.017	4.017	4.015	4.019	4.013	3.990	4.007	4.002	4.014	4.016	4.019	4.020

Prdt: peridotite; H-Prxn: High-Mg pyroxenite; L-Prxn: Low-Mg pyroxenite. Major elements in wt%. Total Fe is given as FeO and mg-no.=Mg/(Mg+Fe). For analytical techniques see Chapter 2.

Table B-4. Continued.

Sample	NK1-15	NK1-17	NK1-18	NK1-19	NK1-22	NK1-23	NK2-1	NK2-2	NK2-3	NK2-5	NK2-8	NK2-9	NK2-10	NK3-2
Rock	Prdt	Prdt	Prdt	Prdt	Prdt	Prdt	Prdt	Prdt	Prdt	Prdt	Prdt	Prdt	Prdt	Prdt
# anal.	10	9	5	3	11	21	16	7	8	10	9	6	5	6
SiO_2	53.84	54.28	53.93	52.82	54.35	54.57	53.87	54.21	53.92	54.35	53.49	54.09	53.99	52.68
TiO_2	0.05	0.02	0.07	0.86	0.05	0.26	0.10	0.21	0.18	0.48	0.01	0.00	0.14	0.39
Al_2O_3	2.21	2.38	2.31	1.02	2.09	3.32	2.31	2.89	2.65	2.33	1.81	1.32	2.91	3.86
FeO	2.21	2.17	2.31	3.15	2.41	2.24	2.44	2.80	1.99	3.05	1.20	1.33	2.34	8.29
MnO	0.07	0.06	0.07	0.10	0.09	0.06	0.08	0.09	0.06	0.11	0.06	0.05	0.06	0.06
MgO	16.99	16.31	17.28	18.39	18.02	15.54	17.45	18.07	16.15	18.54	17.25	18.29	15.82	13.15
CaO	19.68	20.13	19.09	20.25	19.25	20.09	19.31	18.35	20.92	18.18	24.10	23.57	19.45	20.65
Na_2O	1.84	2.12	1.81	0.89	1.56	2.31	1.74	1.78	1.90	1.55	0.60	0.26	2.43	1.61
Cr_2O_3	2.15	2.00	2.33	0.97	2.17	1.60	2.19	1.14	1.78	1.75	0.62	0.57	2.10	0.08
NiO	0.05	0.04	0.06	0.06	0.06	0.03	0.05	0.06	0.03	0.06	0.03	0.03	0.04	0.02
Total	99.07	99.52	99.26	98.51	100.05	100.00	99.55	99.60	99.59	100.40	99.17	99.53	99.29	100.79
mg-no.	0.932	0.931	0.930	0.912	0.930	0.925	0.927	0.920	0.935	0.916	0.962	0.961	0.923	0.739
Cation proportions														
Si	1.965	1.973	1.963	1.948	1.962	1.971	1.957	1.959	1.961	1.953	1.955	1.965	1.967	1.937
Ti	0.001	0.001	0.002	0.024	0.001	0.007	0.003	0.006	0.005	0.013	0.000	0.000	0.004	0.011
Al	0.095	0.102	0.099	0.044	0.089	0.141	0.099	0.123	0.114	0.099	0.078	0.057	0.125	0.167
Fe	0.067	0.066	0.070	0.097	0.073	0.068	0.074	0.085	0.061	0.092	0.037	0.041	0.071	0.255
Mn	0.002	0.002	0.002	0.003	0.003	0.002	0.003	0.003	0.002	0.003	0.002	0.002	0.002	0.002
Mg	0.925	0.884	0.938	1.012	0.970	0.837	0.945	0.973	0.876	0.994	0.940	0.991	0.860	0.721
Ca	0.770	0.784	0.745	0.800	0.744	0.777	0.752	0.711	0.815	0.700	0.944	0.917	0.759	0.814
Na	0.130	0.149	0.127	0.064	0.109	0.161	0.122	0.125	0.134	0.108	0.043	0.018	0.171	0.115
Cr	0.062	0.057	0.067	0.028	0.062	0.046	0.063	0.033	0.051	0.050	0.018	0.016	0.061	0.002
Ni	0.001	0.001	0.002	0.002	0.002	0.001	0.002	0.002	0.001	0.002	0.001	0.001	0.001	0.001
Sum	4.019	4.020	4.015	4.023	4.015	4.010	4.019	4.019	4.019	4.013	4.018	4.007	4.021	4.024

Table B-4. Continued.

Sample	NK3-3	NK3-4	NK3-5	NK3-6	NK3-7	NK3-11	NK3-12	NK3-13	NK3-15	NK3-16	NK3-18	NK3-20	NK3-22	NK3-23
Rock	Prdt	Prdt	Prdt	Prdt	Prdt	Prdt	Prdt	Prdt	Prdt	Prdt	Prdt	Prdt	Prdt	Prdt
# anal.	3	10	5	13	9	15	6	9	9	9	6	8	15	11
SiO_2	55.10	55.32	54.51	54.72	53.62	54.53	54.13	54.20	54.83	53.75	53.71	54.08	53.92	53.81
TiO_2	0.00	0.15	0.24	0.04	0.21	0.19	0.71	0.08	0.83	0.29	0.22	0.20	0.09	0.06
Al_2O_3	1.26	2.89	1.62	2.02	2.67	2.38	0.73	2.23	1.30	2.80	1.75	2.67	2.59	2.03
FeO	1.38	2.76	2.43	2.40	2.59	2.46	2.78	2.12	2.95	2.83	2.27	2.28	1.41	2.34
MnO	0.07	0.09	0.10	0.09	0.09	0.09	0.09	0.07	0.12	0.08	0.09	0.06	0.06	0.09
MgO	18.08	17.85	18.15	18.33	17.38	17.35	19.93	16.48	19.03	17.58	17.25	16.15	16.48	17.82
CaO	23.69	17.71	20.66	19.92	19.21	19.01	19.81	21.69	19.28	18.50	19.36	21.74	22.07	20.08
Na_2O	0.46	1.86	1.13	1.25	1.77	1.88	0.81	1.61	1.01	1.91	1.79	1.65	1.46	1.44
Cr_2O_3	0.75	1.01	1.59	1.42	1.49	2.35	0.98	1.51	0.68	1.85	2.82	1.46	1.31	1.79
NiO	0.04	0.05	0.07	0.06	0.05	0.05	0.03	0.03	0.03	0.05	0.05	0.04	0.03	0.06
Total	100.83	99.69	100.49	100.24	99.08	100.30	100.00	100.03	100.06	99.64	99.31	100.32	99.43	99.51
mg-no.	0.959	0.920	0.931	0.932	0.923	0.926	0.928	0.933	0.920	0.917	0.931	0.927	0.954	0.931
Cation proportions														
Si	1.975	1.988	1.963	1.968	1.955	1.964	1.957	1.965	1.974	1.949	1.960	1.956	1.961	1.957
Ti	0.000	0.004	0.006	0.001	0.006	0.005	0.019	0.002	0.022	0.008	0.006	0.005	0.002	0.002
Al	0.053	0.122	0.069	0.085	0.115	0.101	0.031	0.095	0.055	0.120	0.075	0.114	0.111	0.087
Fe	0.041	0.083	0.073	0.072	0.079	0.074	0.084	0.064	0.089	0.086	0.069	0.069	0.043	0.071
Mn	0.002	0.003	0.003	0.003	0.003	0.003	0.003	0.002	0.004	0.002	0.003	0.002	0.002	0.003
Mg	0.966	0.956	0.975	0.983	0.945	0.932	1.074	0.891	1.022	0.950	0.938	0.871	0.893	0.966
Ca	0.910	0.682	0.797	0.768	0.751	0.733	0.768	0.843	0.744	0.719	0.757	0.843	0.860	0.782
Na	0.032	0.130	0.079	0.087	0.125	0.131	0.057	0.113	0.070	0.134	0.127	0.116	0.103	0.101
Cr	0.021	0.029	0.045	0.041	0.043	0.067	0.028	0.043	0.019	0.053	0.081	0.042	0.038	0.052
Ni	0.001	0.001	0.002	0.002	0.002	0.002	0.001	0.001	0.001	0.001	0.002	0.001	0.001	0.002
Sum	4.003	3.997	4.012	4.010	4.022	4.012	4.022	4.020	4.001	4.023	4.018	4.018	4.014	4.022

Table B-4. Continued.

Sample	NK3-24	NK3-25	NK2-7	NK3-14	NK3-19	NK3-1	NK3-8	NK3-17
Rock	Prdt	Prdt	H-Prxn	H-Prxn	H-Prxn	L-Prxn	L-Prxn	L-Prxn
# anal.	5	5	4	9	8	8	11	4
SiO_2	54.13	53.85	53.65	54.56	54.68	53.99	54.66	53.02
TiO_2	0.05	0.16	0.16	0.17	0.09	0.08	0.53	0.09
Al_2O_3	1.77	2.61	2.70	4.04	2.80	1.73	1.32	1.80
FeO	1.71	2.75	1.95	3.03	2.45	3.12	4.66	3.04
MnO	0.06	0.09	0.05	0.12	0.08	0.06	0.12	0.05
MgO	16.75	17.65	16.02	14.26	16.07	16.82	18.20	16.60
CaO	22.68	19.00	21.86	18.38	19.45	23.61	19.96	23.59
Na_2O	1.05	1.71	1.58	3.38	2.49	0.63	1.07	0.50
Cr_2O_3	0.95	1.44	1.15	2.02	1.84	0.45	0.04	0.37
NiO	0.03	0.05	0.05	0.03	0.04	0.08	0.02	0.09
Total	99.17	99.32	99.17	100.00	100.00	100.57	100.58	99.16
mg-no.	0.946	0.920	0.936	0.894	0.921	0.906	0.874	0.907
Cation proportions								
Si	1.976	1.958	1.960	1.974	1.976	1.958	1.974	1.952
Ti	0.001	0.004	0.004	0.005	0.003	0.002	0.014	0.003
Al	0.076	0.112	0.116	0.172	0.119	0.074	0.056	0.078
Fe	0.052	0.084	0.060	0.092	0.074	0.095	0.141	0.094
Mn	0.002	0.003	0.002	0.004	0.002	0.002	0.004	0.002
Mg	0.912	0.957	0.873	0.769	0.866	0.909	0.980	0.911
Ca	0.887	0.740	0.856	0.713	0.753	0.918	0.772	0.931
Na	0.074	0.120	0.112	0.237	0.175	0.045	0.075	0.036
Cr	0.027	0.041	0.033	0.058	0.053	0.013	0.001	0.011
Ni	0.001	0.002	0.001	0.001	0.001	0.002	0.001	0.003
Sum	4.008	4.020	4.016	4.025	4.022	4.018	4.019	4.019

Table B-5. Major element analyses of garnet.

Sample	NK1-1	NK1-2	NK1-3	NK 1-4	NK1-5	NK1-6	NK1-7	NK1-9	NK1-10	NK1-11	NK1-12	NK1-14	NK1-15	NK1-16
Rock	Prdt	Prdt	Prdt	Prdt	Prdt	Prdt	Prdt	Prdt	Prdt	Prdt	Prdt	Prdt	Prdt	Prdt
# anal.	8	5	6	40	13	7	6	12	7	8	16	9	10	9
SiO_2	40.72	41.91	41.44	41.28	42.04	41.51	41.46	41.14	42.08	41.20	42.27	42.13	41.06	40.87
TiO_2	0.33	0.09	0.08	0.09	0.24	0.08	0.14	0.19	0.11	0.19	0.08	0.08	0.02	0.14
Al_2O_3	18.87	20.04	21.19	20.54	20.09	20.58	20.29	20.19	19.31	18.83	21.02	20.86	19.29	17.80
FeO	7.09	7.15	7.46	7.93	7.07	6.86	6.24	7.17	6.35	6.60	7.71	7.33	6.74	6.29
MnO	0.41	0.45	0.39	0.44	0.35	0.38	0.30	0.38	0.33	0.34	0.46	0.41	0.36	0.31
MgO	19.58	20.48	20.43	19.38	20.19	20.66	20.67	19.97	20.58	20.46	20.30	19.98	19.57	19.62
CaO	5.75	5.05	5.12	5.68	5.26	4.62	5.22	5.28	4.81	5.10	4.29	4.87	6.12	6.47
Na_2O	0.04	0.02	0.03	0.02	0.03	0.03	0.02	0.03	0.01	0.03	0.04	0.03	0.02	0.03
Cr_2O_3	6.54	3.99	4.13	4.41	4.80	4.42	4.76	4.97	6.09	6.26	3.77	4.04	6.16	7.65
NiO	0.01	0.00	0.00	0.00	0.01	0.01	0.02	0.01	0.01	0.01	0.00	0.00	0.01	0.00
Total	99.33	99.17	100.27	99.77	100.07	99.15	99.10	99.32	99.69	99.03	99.95	99.73	99.35	99.17
mg-no.	0.831	0.836	0.830	0.813	0.836	0.843	0.855	0.832	0.852	0.847	0.824	0.829	0.838	0.848
Cation proportions														
Si	2.966	3.022	2.961	2.980	3.009	2.989	2.987	2.975	3.021	2.992	3.018	3.017	2.981	2.986
Ti	0.018	0.005	0.004	0.005	0.013	0.004	0.008	0.010	0.006	0.011	0.004	0.004	0.001	0.008
Al	1.620	1.703	1.785	1.747	1.695	1.747	1.723	1.721	1.634	1.612	1.769	1.761	1.651	1.533
Fe	0.432	0.431	0.446	0.478	0.423	0.413	0.376	0.433	0.381	0.401	0.460	0.439	0.409	0.384
Mn	0.025	0.028	0.024	0.027	0.021	0.023	0.018	0.023	0.020	0.021	0.028	0.025	0.022	0.019
Mg	2.126	2.201	2.177	2.086	2.155	2.218	2.220	2.153	2.203	2.215	2.162	2.133	2.119	2.137
Ca	0.449	0.390	0.392	0.439	0.403	0.357	0.403	0.409	0.370	0.397	0.328	0.373	0.476	0.507
Na	0.005	0.001	0.004	0.003	0.004	0.004	0.003	0.004	0.002	0.004	0.006	0.004	0.003	0.004
Cr	0.378	0.227	0.233	0.251	0.272	0.252	0.271	0.284	0.346	0.360	0.213	0.229	0.353	0.442
Ni	0.000	0.000	0.000	0.000	0.001	0.001	0.001	0.000	0.001	0.001	0.000	0.000	0.000	0.000
Sum	8.019	8.008	8.027	8.017	7.997	8.008	8.009	8.014	7.984	8.013	7.989	7.986	8.016	8.020

Prdt: peridotite; H-Prxn: High-Mg pyroxenite; L-Prxn: Low-Mg pyroxenite; ^{a}garnet in clinopyroxene. Major elements in wt%. Total Fe is given as FeO and mg-no.=Mg/(Mg+Fe). For analytical techniques see Chapter 2.

Table B-5. Continued.

Sample	NK1-17	NK1-18	NK1-20	NK1-22	NK1-23	NK2-1	NK2-2	NK2-3	NK2-5	NK2-10	NK3-2	NK3-4	NK3-5	NK3-6
Rock	Prdt	Prdt	Prdt	Prdt	Prdt	Prdt	Prdt	Prdt	Prdt	Prdt	Prdt	Prdt	Prdt	Prdt
# anal.	8	6	5	12	14	9	5	8	12	6	11	12	6	15
SiO_2	41.38	41.13	41.24	41.25	41.47	41.17	42.08	41.34	41.20	41.42	38.08	42.22	41.10	41.92
TiO_2	0.02	0.13	0.10	0.14	0.09	0.23	0.29	0.08	0.87	0.09	0.05	0.25	0.08	0.10
Al_2O_3	20.78	18.93	19.27	18.05	22.46	19.35	21.57	21.44	18.13	21.27	21.47	22.30	18.24	20.10
FeO	7.01	6.46	6.51	6.34	9.26	7.08	6.87	7.85	6.84	7.57	24.45	7.16	6.59	6.46
MnO	0.42	0.31	0.32	0.32	0.49	0.36	0.31	0.48	0.32	0.41	0.44	0.32	0.36	0.30
MgO	19.88	20.38	20.95	19.66	19.07	19.63	21.16	19.53	19.44	20.01	9.06	21.15	18.92	20.29
CaO	5.45	5.90	5.11	6.28	4.84	5.67	4.50	5.28	6.61	5.07	5.61	4.01	7.09	5.76
Na_2O	0.04	0.01	0.02	0.02	0.02	0.02	0.03	0.03	0.05	0.03	0.05	0.03	0.02	0.01
Cr_2O_3	4.12	6.83	6.52	7.65	2.27	5.78	2.55	3.21	6.77	3.74	0.07	2.00	7.69	5.15
NiO	0.01	0.01	0.01	0.01	0.00	0.01	0.01	0.01	0.01	0.02	0.00	0.01	0.00	0.01
Total	99.10	100.07	100.05	99.72	99.97	99.29	99.37	99.25	100.23	99.62	99.30	99.48	100.10	100.10
mg-no.	0.835	0.849	0.851	0.847	0.786	0.832	0.846	0.816	0.835	0.825	0.398	0.840	0.837	0.849
Cation proportions														
Si	2.988	2.966	2.965	2.994	2.975	2.988	3.003	2.983	2.980	2.976	2.954	3.002	2.982	2.999
Ti	0.001	0.007	0.006	0.008	0.005	0.012	0.015	0.004	0.047	0.005	0.003	0.013	0.004	0.005
Al	1.769	1.609	1.633	1.544	1.899	1.655	1.814	1.823	1.545	1.801	1.963	1.869	1.561	1.695
Fe	0.423	0.389	0.392	0.385	0.555	0.430	0.410	0.474	0.414	0.455	1.586	0.426	0.400	0.386
Mn	0.026	0.019	0.020	0.020	0.030	0.022	0.019	0.029	0.020	0.025	0.029	0.020	0.022	0.018
Mg	2.140	2.191	2.246	2.127	2.040	2.124	2.251	2.101	2.096	2.144	1.048	2.243	2.048	2.164
Ca	0.422	0.456	0.394	0.489	0.372	0.441	0.344	0.408	0.512	0.391	0.467	0.306	0.551	0.442
Na	0.005	0.002	0.002	0.002	0.002	0.003	0.004	0.002	0.007	0.001	0.007	0.004	0.003	0.002
Cr	0.235	0.389	0.371	0.439	0.129	0.332	0.144	0.183	0.387	0.213	0.005	0.113	0.441	0.292
Ni	0.000	0.001	0.000	0.000	0.000	0.001	0.001	0.001	0.001	0.001	0.000	0.001	0.000	0.000
Sum	8.010	8.028	8.027	8.008	8.007	8.008	8.004	8.010	8.009	8.011	8.062	7.996	8.013	8.003

Table B-5. Continued.

Sample	NK3-7	NK3-11	NK3-13	NK3-15	NK3-16	NK3-20	NK3-24	NK3-25	NK2-7	NK3-14	NK3-19	NK3-1	NK3-1[a]	NK3-17
Rock	Prdt	Prdt	Prdt	Prdt	Prdt	Prdt	Prdt	Prdt	H-Prxn	H-Prxn	H-Prxn	L-Prxn	L-Prxn	L-Prxn
# anal.	6	11	5	12	16	14	7	20	6	26	5	27	10	3
SiO_2	41.48	41.43	41.04	42.22	41.43	42.01	41.53	41.84	41.67	42.18	41.43	40.67	40.79	40.53
TiO_2	0.27	0.30	0.04	0.10	0.39	0.07	0.02	0.32	0.04	0.10	0.07	0.05	0.01	0.09
Al_2O_3	21.58	18.73	21.58	20.36	19.84	22.56	23.02	20.76	23.35	22.42	21.09	22.00	22.04	22.49
FeO	6.99	6.88	8.52	6.28	7.00	9.38	8.07	7.23	8.11	8.10	7.43	14.89	14.64	14.88
MnO	0.34	0.36	0.54	0.29	0.30	0.46	0.49	0.33	0.48	0.43	0.43	0.60	0.55	0.56
MgO	20.71	19.76	18.85	20.63	20.28	19.03	20.01	20.11	20.11	20.46	20.41	14.63	15.80	14.97
CaO	4.96	5.93	5.43	5.04	5.40	4.80	4.93	5.02	4.65	4.22	5.32	5.88	5.79	6.07
Na_2O	0.03	0.03	0.01	0.01	0.04	0.01	0.01	0.03	0.01	0.04	0.02	0.01	0.01	0.01
Cr_2O_3	3.32	6.62	3.45	4.67	4.90	1.92	1.48	3.71	1.49	2.42	4.12	1.32	1.08	1.27
NiO	0.01	0.01	0.00	0.00	0.01	0.01	0.02	0.01	0.00	0.00	0.01	0.00	0.01	0.00
Total	99.70	100.05	99.45	99.61	99.57	100.26	99.55	99.36	99.91	100.36	100.33	100.04	100.72	100.87
mg-no.	0.841	0.837	0.798	0.854	0.838	0.783	0.815	0.832	0.815	0.818	0.830	0.637	0.658	0.642
Cation proportions														
Si	2.966	2.991	2.969	3.019	2.986	2.999	2.969	3.007	2.965	2.991	2.962	2.995	2.978	2.961
Ti	0.014	0.016	0.002	0.005	0.021	0.004	0.001	0.017	0.002	0.005	0.004	0.003	0.001	0.005
Al	1.818	1.594	1.840	1.716	1.685	1.898	1.940	1.759	1.958	1.874	1.777	1.909	1.896	1.937
Fe	0.418	0.415	0.516	0.376	0.422	0.560	0.483	0.434	0.483	0.480	0.444	0.917	0.894	0.909
Mn	0.021	0.022	0.033	0.018	0.018	0.028	0.030	0.020	0.029	0.026	0.026	0.037	0.034	0.035
Mg	2.208	2.128	2.033	2.200	2.179	2.026	2.133	2.154	2.134	2.163	2.175	1.606	1.720	1.632
Ca	0.380	0.459	0.421	0.386	0.417	0.367	0.377	0.387	0.355	0.321	0.407	0.464	0.453	0.475
Na	0.002	0.004	0.002	0.002	0.006	0.002	0.001	0.004	0.002	0.006	0.003	0.001	0.002	0.002
Cr	0.188	0.378	0.197	0.264	0.279	0.108	0.084	0.211	0.084	0.136	0.233	0.077	0.062	0.073
Ni	0.001	0.000	0.000	0.000	0.000	0.000	0.001	0.001	0.000	0.000	0.001	0.000	0.001	0.000
Sum	8.016	8.008	8.012	7.986	8.013	7.993	8.018	7.993	8.012	8.001	8.031	8.009	8.040	8.030